

INTRODUCTION TO INORGANIC CHEMISTRY



Wikibook
Penn State University

Book: Introduction to Inorganic Chemistry

This text is disseminated via the Open Education Resource (OER) LibreTexts Project (<https://LibreTexts.org>) and like the hundreds of other texts available within this powerful platform, it is freely available for reading, printing and "consuming." Most, but not all, pages in the library have licenses that may allow individuals to make changes, save, and print this book. Carefully consult the applicable license(s) before pursuing such effects.

Instructors can adopt existing LibreTexts texts or Remix them to quickly build course-specific resources to meet the needs of their students. Unlike traditional textbooks, LibreTexts' web based origins allow powerful integration of advanced features and new technologies to support learning.



The LibreTexts mission is to unite students, faculty and scholars in a cooperative effort to develop an easy-to-use online platform for the construction, customization, and dissemination of OER content to reduce the burdens of unreasonable textbook costs to our students and society. The LibreTexts project is a multi-institutional collaborative venture to develop the next generation of open-access texts to improve postsecondary education at all levels of higher learning by developing an Open Access Resource environment. The project currently consists of 14 independently operating and interconnected libraries that are constantly being optimized by students, faculty, and outside experts to supplant conventional paper-based books. These free textbook alternatives are organized within a central environment that is both vertically (from advance to basic level) and horizontally (across different fields) integrated.

The LibreTexts libraries are Powered by [NICE CXOne](#) and are supported by the Department of Education Open Textbook Pilot Project, the UC Davis Office of the Provost, the UC Davis Library, the California State University Affordable Learning Solutions Program, and Merlot. This material is based upon work supported by the National Science Foundation under Grant No. 1246120, 1525057, and 1413739.

Any opinions, findings, and conclusions or recommendations expressed in this material are those of the author(s) and do not necessarily reflect the views of the National Science Foundation nor the US Department of Education.

Have questions or comments? For information about adoptions or adaptations contact info@LibreTexts.org. More information on our activities can be found via Facebook (<https://facebook.com/Libretexts>), Twitter (<https://twitter.com/libretexts>), or our blog (<http://Blog.Libretexts.org>).

This text was compiled on 01/09/2024

TABLE OF CONTENTS

Licensing

1: Review of Chemical Bonding

- 1.1: Prelude to Chemical Bonding
- 1.2: Valence Bond Theory- Lewis Dot Structures, the Octet Rule, Formal Charge, Resonance, and the Isoelectronic Principle
- 1.3: The Shapes of Molecules (VSEPR Theory) and Orbital Hybridization
- 1.4: Bond Polarity and Bond Strength
- 1.5: Discussion Questions
- 1.6: Problems
- 1.7: References

2: Molecular Orbital Theory

- 2.1: Prelude to Molecular Orbital Theory
- 2.2: Constructing Molecular Orbitals from Atomic Orbitals
- 2.3: Orbital Symmetry
- 2.4: σ , π , and δ orbitals
- 2.5: Diatomic Molecules
- 2.6: Orbital Filling
- 2.7: Periodic Trends in π Bonding
- 2.8: Three-center Bonding
- 2.9: Building up the MOs of More Complex Molecules- NH_3 , P_4
- 2.10: Homology of σ and π orbitals in MO diagrams
- 2.11: Chains and Rings of π -Conjugated Systems
- 2.12: Discussion Questions
- 2.13: Problems
- 2.14: References

3: Acid-Base Chemistry

- 3.1: Prelude to Acid-Base Chemistry
- 3.2: Brønsted and Lewis Acids and Bases
- 3.3: Hard and Soft Acids and Bases
- 3.4: The Electrostatic-Covalent (ECW) Model for Acid-Base Reactions
- 3.5: Frustrated Lewis Pairs
- 3.6: Discussion Questions
- 3.7: Problems
- 3.8: References

4: Redox Stability and Redox Reactions

- 4.1: Prelude to Redox Stability and Redox Reactions
- 4.2: Balancing Redox Reactions
- 4.3: Electrochemical Potentials
- 4.4: Latimer and Frost Diagrams
- 4.5: Redox Reactions with Coupled Equilibria
- 4.6: Pourbaix Diagrams
- 4.7: Discussion Questions

- 4.8: Problems
- 4.9: References

5: Coordination Chemistry and Crystal Field Theory

- 5.1: Prelude to Coordination Chemistry and Crystal Field Theory
- 5.2: Counting Electrons in Transition Metal Complexes
- 5.3: Crystal Field Theory
- 5.4: Spectrochemical Series
- 5.5: π -Bonding between Metals and Ligands
- 5.6: Crystal Field Stabilization Energy, Pairing, and Hund's Rule
- 5.7: Non-octahedral Complexes
- 5.8: Jahn-Teller Effect
- 5.9: Tetrahedral Complexes
- 5.10: Stability of Transition Metal Complexes
- 5.11: Chelate and Macrocyclic Effects
- 5.12: Ligand Substitution Reactions
- 5.13: Discussion Questions
- 5.14: Problems
- 5.15: References

6: Metals and Alloys- Structure, Bonding, Electronic and Magnetic Properties

- 6.1: Prelude to Metals and Alloys
- 6.2: Unit Cells and Crystal Structures
- 6.3: Bravais Lattices
- 6.4: Crystal Structures of Metals
- 6.5: Bonding in Metals
- 6.6: Conduction in Metals
- 6.7: Atomic Orbitals and Magnetism
- 6.8: Ferro-, Ferri- and Antiferromagnetism
- 6.9: Hard and Soft Magnets
- 6.10: Discussion Questions
- 6.11: Problems
- 6.12: References

7: Metals and Alloys - Mechanical Properties

- 7.1: Defects in Metallic Crystals
- 7.2: Work Hardening, Alloying, and Annealing
- 7.3: Malleability of Metals and Alloys
- 7.4: Iron and Steel
- 7.5: Amorphous Alloys
- 7.6: Discussion Questions
- 7.7: Problems
- 7.8: References

8: Ionic and Covalent Solids - Structures

- 8.1: Prelude to Ionic and Covalent Solids - Structures
- 8.2: Close-packing and Interstitial Sites
- 8.3: Structures Related to NaCl and NiAs
- 8.4: Tetrahedral Structures

- 8.5: Layered Structures and Intercalation Reactions
- 8.6: Bonding in TiS_2 , MoS_2 , and Pyrite Structures
- 8.7: Spinel, Perovskite, and Rutile Structures
- 8.8: Discussion Questions
- 8.9: Problems
- 8.10: References

9: Ionic and Covalent Solids - Energetics

- 9.1: Ionic Radii and Radius Ratios
- 9.2: Structure Maps
- 9.3: Energetics of Crystalline Solids- The Ionic Model
- 9.4: Born-Haber Cycles for NaCl and Silver Halides
- 9.5: Kapustinskii Equation
- 9.6: Discovery of Noble Gas Compounds
- 9.7: Stabilization of High and Low Oxidation States
- 9.8: Alkalides and Electrides
- 9.9: Resonance Energy of Metals
- 9.10: Prelude to Ionic and Covalent Solids - Energetics
- 9.11: The Strange Case of the Alkali Oxides
- 9.12: Lattice Energies and Solubility
- 9.13: Discussion Questions
- 9.14: Problems
- 9.15: References

10: Electronic Properties of Materials - Superconductors and Semiconductors

- 10.1: Prelude to Electronic Properties of Materials - Superconductors and Semiconductors
- 10.2: Metal-Insulator Transitions
- 10.3: Superconductors
- 10.4: Periodic Trends- Metals, Semiconductors, and Insulators
- 10.5: Semiconductors- Band Gaps, Colors, Conductivity and Doping
- 10.6: Semiconductor p-n Junctions
- 10.7: Diodes, LEDs and Solar Cells
- 10.8: Amorphous Semiconductors
- 10.9: Discussion Questions
- 10.10: Problems
- 10.11: References

11: Basic Science of Nanomaterials

- 11.1: Prelude to Basic Science of Nanomaterials
- 11.2: Physics and Length Scales- Cavity Laser, Coulomb Blockade, Nanoscale Magnets
- 11.3: Semiconductor Quantum Dots
- 11.4: Synthesis of Semiconductor Nanocrystals
- 11.5: Surface Energy
- 11.6: Nanoscale Metal Particles
- 11.7: Applications of Nanomaterials
- 11.8: Discussion Questions
- 11.9: Problems
- 11.10: References

12: Resources for Students and Teachers

- [12.1: VIPER- Virtual Inorganic Pedagogical Electronic Resource- A Community for Teachers and Students of Inorganic Chemistry](#)
- [12.2: Beloit College/University of Wisconsin Video Lab Manual](#)
- [12.3: Atomic and Molecular Orbitals \(University of Liverpool\)](#)
- [12.4: Interactive 3D Crystal Structures \(University of Liverpool\)](#)
- [12.5: Appendix 1- Periodic Tables](#)
- [12.6: Appendix 2- Selected Thermodynamic Values](#)
- [12.7: Appendix 3- Bond Enthalpies](#)

13: Metals and Alloys - Mechanical Properties

- [13.1: Prelude to Metals and Alloys - Mechanical Properties](#)

[Index](#)

[Glossary](#)

[Detailed Licensing](#)

Licensing

A detailed breakdown of this resource's licensing can be found in [Back Matter/Detailed Licensing](#).

CHAPTER OVERVIEW

1: Review of Chemical Bonding

Learning Objectives

- Be able to draw Lewis dot structures, assign formal charges, predict molecular geometries (including bond angles), and calculate bond orders for molecules, including hypervalent molecules and ions.
- Describe hypervalent molecules using no-bond resonance.
- Understand and articulate how predictions of molecular structure and bonding can be experimentally verified.
- Learn to construct hybrid orbitals from s and p atomic orbitals.
- Use the isoelectronic principle to design new molecules and solids.
- Rationalize bond strength and chemical reactivity using bond polarity arguments.
- Interrelate bond length and bond strength.

There is no topic more fundamental to Chemistry than the nature of the chemical bond, and the introduction you find here will provide you with an overview of the fundamentals and a basis for further study.

[1.1: Prelude to Chemical Bonding](#)

[1.2: Valence Bond Theory- Lewis Dot Structures, the Octet Rule, Formal Charge, Resonance, and the Isoelectronic Principle](#)

[1.3: The Shapes of Molecules \(VSEPR Theory\) and Orbital Hybridization](#)

[1.4: Bond Polarity and Bond Strength](#)

[1.5: Discussion Questions](#)

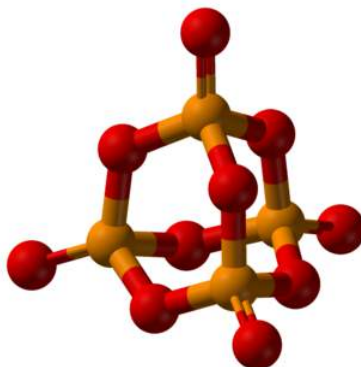
[1.6: Problems](#)

[1.7: References](#)

This page titled [1: Review of Chemical Bonding](#) is shared under a [CC BY-SA 4.0](#) license and was authored, remixed, and/or curated by [Chemistry 310 \(Wikibook\)](#) via [source content](#) that was edited to the style and standards of the LibreTexts platform; a detailed edit history is available upon request.

1.1: Prelude to Chemical Bonding

Molecules (and extended solids) are built from atoms that form chemical bonds. Theories of bonding seek to explain why molecules and solids form, what their structures are, why some are more stable than others, and how they react. As we will learn in Chapter 2, quantum mechanics gives us the most realistic picture of chemical bonding via molecular orbital (MO) theory. However, the MO description of bonding is conceptually difficult and mathematically intensive. This chapter will review less rigorous (but still useful) models such as Lewis dot structures and valence shell electron-pair repulsion (VSEPR) theory. When combined with a qualitative quantum mechanical description of bonding through the concepts of orbital hybridization and resonance, these simple models can help us understand a great deal about the structures, stabilities, and reactions of inorganic molecules.



Ball-and-stick representation of chemical bonding in the molecules P_4O_{10} and P_4S_{10} .

The theory of chemical bonding has a long history, dating back to ancient Greece and the atomists Democritus, Leucippus, and the Epicureans. They postulated the existence of immutable atoms moving through the void, and envisioned the physical properties of materials as arising from the kinds and shapes of atoms. In his epic poem *De rerum natura* (On the Nature of Things), the Roman poet Lucretius (c. 99 BC – c. 50 BC), drawing on his Epicurean beliefs, describes some atoms and chemical bonding in the following way:

*What seems to us the hardened and condensed
Must be of atoms among themselves more hooked,
Be held compacted deep within, as 'twere
By branch-like atoms -- of which sort the chief
Are diamond stones, despisers of all blows
And stalwart flint and strength of solid iron
And brazen bars, which, budging hard in locks,
Do grate and scream. But what are liquid, formed
Of fluid body, they indeed must be
Of elements more smooth and round -- because
Their globules severally will not cohere.*

Lucretius' poem is enjoyable reading and contains some remarkable insights into the microscopic world, given the tools available at the time. Modern analytical methods show that he was off base with his ideas about hooks and spheres, however. We will revisit the nature of chemical bonding in the substances Lucretius mentions (diamond, silicates, iron, brass, and water) in the context of modern chemical theories to understand why they have the special properties they do.

This page titled [1.1: Prelude to Chemical Bonding](#) is shared under a [CC BY-SA 4.0](#) license and was authored, remixed, and/or curated by [Chemistry 310 \(Wikibook\)](#) via [source content](#) that was edited to the style and standards of the LibreTexts platform; a detailed edit history is available upon request.

1.2: Valence Bond Theory- Lewis Dot Structures, the Octet Rule, Formal Charge, Resonance, and the Isoelectronic Principle

Atoms and Molecules

Atomism, because it was dismissed by Aristotle, enjoyed a long sleep in scientific discourse until it was reconsidered by Galileo, Decartes, and Gassendi in the 1600s. Dalton postulated the modern atomic theory in 1808 based on his observation that elements such as hydrogen and oxygen combined in specific ratios (the Law of Definite Proportions), but the atomic theory remained contentious throughout most of the 19th century. Thompson, Rutherford, Bohr, and others around the turn of the 20th century established that matter was indeed composed of atoms that contained heavy nuclei and light electrons, and that atoms could exist in excited states that could be interpreted as excitations of their electrons to different energy levels. However the atomic theory did not provide a ready explanation for the bonded states of atoms in molecules.

In 1916, still more than a decade before modern quantum theory would adequately describe the shapes of atomic orbitals, Lewis proposed the octet theory based on the empirically observed rules of valence, i.e., the combining ratios of atoms in molecules.^[1] This theory, in hindsight, can be rationalized for s- and p-block elements by observing that main-group atoms can use their four valence orbitals (s, p_x , p_y , and p_z) to accommodate up to eight electrons, some or all of which may be shared with other atoms. In Lewis' model, the valence electrons of an atom were situated at the corners of a cube, and the cubes could share edges or faces to complete their octets. Lewis developed a shorthand notation for these structures based on dots that represented the valence electrons, as illustrated in Fig. 1.2.1. A pair of electrons shared between atoms constitutes a chemical bond, and can also be represented as a line joining the atoms. Four electrons shared between atoms, represented by two lines, is a double bond, and so forth. Any pairs of electrons not involved in bonding form "lone pairs" that belong to one atom only and are thus not involved in bonding.

The Lewis picture is powerful in its simplicity. It can be readily used to rationalize or predict the combining ratios of atoms, to sort plausible and unlikely structures for molecules (including large ones), and to rationalize the acid-base properties of many molecules. It is important to remember that the model is built on a shaky, pre-quantum mechanical description of atoms and so with it, we will make mistakes. Nevertheless it is useful to see how far we can go with the Lewis model.

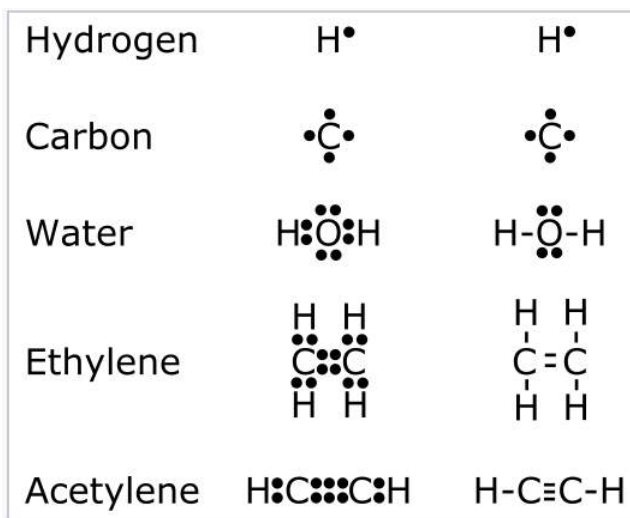


Figure 1.2.1: Examples of Lewis dot diagrams showing chemical bonds between carbon, hydrogen, and oxygen, and non-bonding electron pairs.

Constructing the octet valence bond picture for a molecule

We can construct an octet picture for any molecule using the **N-V method**:

Number of electrons *needed* to make separate octets around all atoms = N

(N = 8 for non-H atoms, N = 2 for H)

Number of *valence* electrons = **V** (add up using group numbers; don't forget to add or subtract for charges on ions)

Number of *shared* electrons = **S** = N-V; and therefore the number of bonds = S/2

Fill in lone pairs everywhere else to complete octets

Example: nitrate anion, NO_3^-

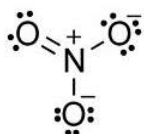
$N = 4 \text{ atoms} \times 8 \text{ electrons} = 32$

$V = 5 + 6 + 6 + 6 + 1 = 24$ (N + O + O + O + charge)

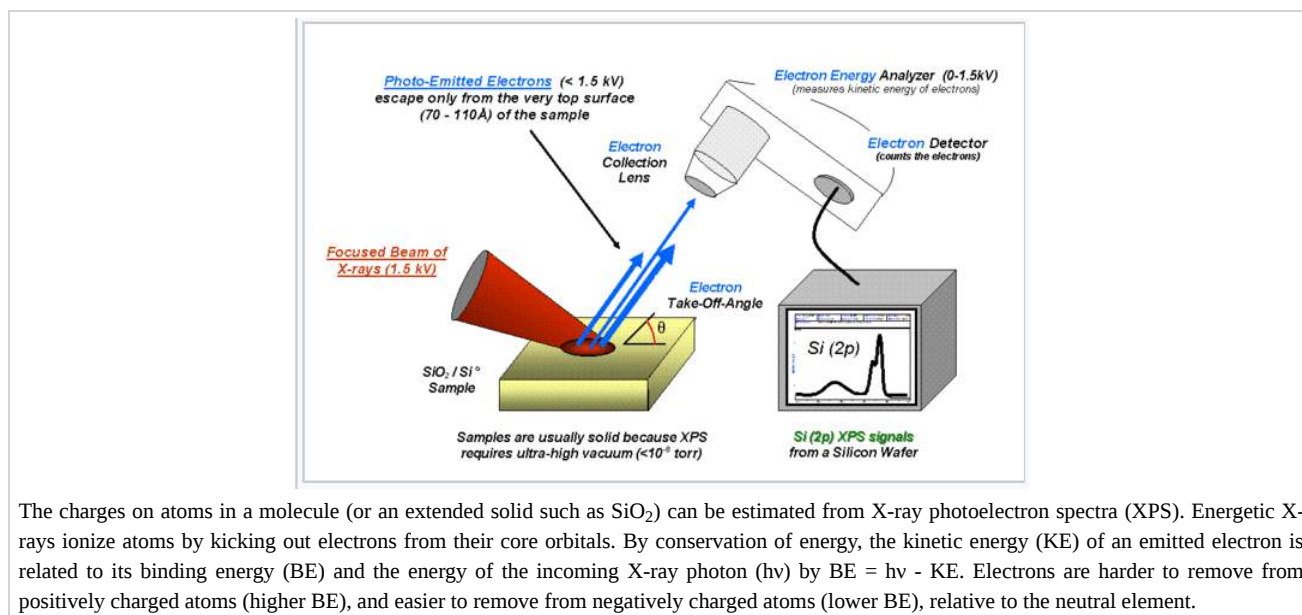
$S = 32 - 24 = 8$ shared electrons = **4 bonds**

The number of lone pairs is obtained by difference: $(V - S) / 2 = (24 - 8) / 2 = 8$

Now draw the molecule, starting with the four bonds and adding eight lone pairs to complete the octets:



Count the shared and unshared electrons around each atom in the nitrate ion and you will see that all atoms are **octet** and that the total number of valence electrons (V) is 24. If you do the N-V calculation according to the rules above, you should always get an octet structure.



The charges on atoms in a molecule (or an extended solid such as SiO_2) can be estimated from X-ray photoelectron spectra (XPS). Energetic X-rays ionize atoms by kicking out electrons from their core orbitals. By conservation of energy, the kinetic energy (KE) of an emitted electron is related to its binding energy (BE) and the energy of the incoming X-ray photon ($h\nu$) by $BE = h\nu - KE$. Electrons are harder to remove from positively charged atoms (higher BE), and easier to remove from negatively charged atoms (lower BE), relative to the neutral element.

The **formal charge** distribution is assigned by dividing the shared (bonding) electrons equally between atoms. Thus, the singly bonded O atoms each possess 7 electrons, and because O is in group 6, their formal charge is -1. The doubly bonded O has a formal charge of zero. The N atom has a formal charge of +1 because it "owns" 4 valence electrons and is in group 5.

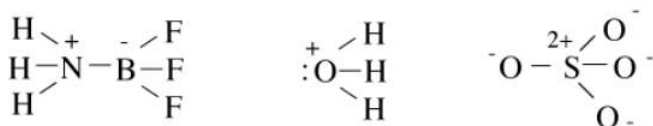
Note that the **formal charge** is **not** the same thing as the **oxidation number** (or **oxidation state**). In the nitrate ion, the oxidation state of nitrogen is +5 and the oxidation state of oxygen is -2. The formal charge is typically closer to the "real" charge on the atom (as measured, e.g., by X-ray photoelectron spectroscopy). Oxidation states are a useful bookkeeping device for keeping track of oxidation-reduction reactions, as we will discuss in Chapter 4. Like oxidation states, the formal charges on the atoms in a molecule or ion must *add up to its overall charge*.

We can similarly draw the Lewis structure for ammonia as shown below:



When we divide the shared electrons equally between the atoms, we see that the N atom has five electrons and each H atom has one. These are the same as their group numbers, and thus, all the formal charges in the ammonia molecule are zero.

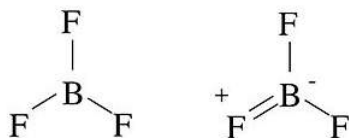
Octet structures of the Lewis acid-base adduct NH_3BF_3 , the hydronium ion H_3O^+ , and the sulfate anion SO_4^{2-} are shown below. In this case (and in many Lewis structures we will draw), we leave off the implied lone pairs around the peripheral atoms. Try calculating the number of bonds in each of these molecules using the N-V method, and fill in the lone pairs that are not explicitly drawn in.



In cases where more than one valence bond structure is possible, we can use formal charges to decide which structures should be more or less stable. The rules are:

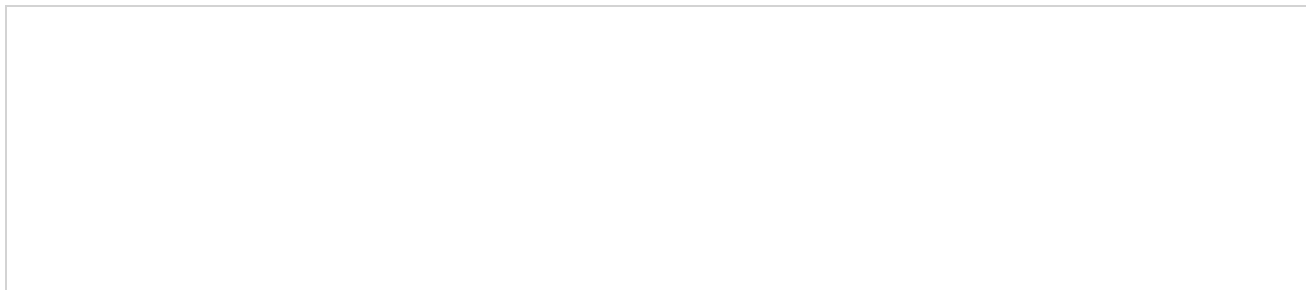
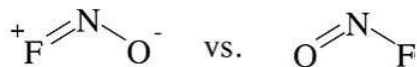
- The formal charges on atoms are minimized in stable structures, zero being the best case.
- Negative formal charges should be placed on the most electronegative atom(s).
- Positive formal charges should be placed on the least electronegative atom(s).
- It is unfavorable to place like charges (++) or (--) on neighboring atoms in a molecule.

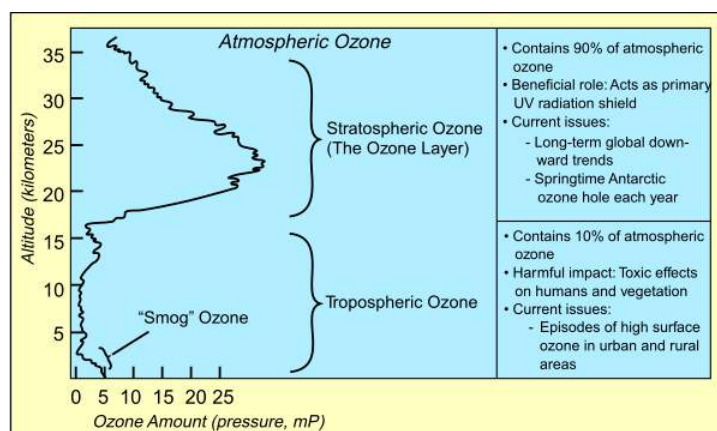
Examples of these rules are shown below for alternative structures of BF_3 and ONF .



In the BF_3 case, the structure on the left is non-octet, because there are only six electrons (three bonds) in the valence shell of B. Such structures are said to be *electron deficient*. An octet structure (right) can be drawn, but it places a positive formal charge on F, the most electronegative atom in the molecule. Thus, neither structure is completely "happy," but the formal charge rules tell us that the electron-deficient structure on the left is more stable. The electron deficiency of BF_3 makes it a powerful Lewis acid.

In the case of ONF , the structure on the left is unfavorable for two reasons. First, it places a positive formal charge on F, the most electronegative atom. Second, there is another possible structure (right) that has zero formal charge, which is preferable to one with non-zero charge. This means that the structure on the right, with a double bond between N and O, is more reasonable.

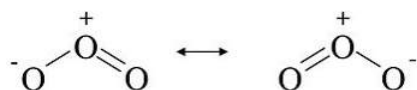




Life outside of the ocean owes its existence to the presence of ozone (O_3) in the stratosphere. Ozone absorbs the ultraviolet light in the solar spectrum, which otherwise would cause catastrophic damage to DNA and other biological molecules. Because ozone is produced photochemically from O_2 , which is itself generated by photosynthesis, the spectroscopic signature of ozone in the atmosphere of distant planets is one possible way to look for extraterrestrial life.

Resonance structures

The ozone (O_3) molecule has two equivalent octet structures, shown below:

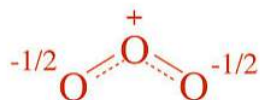


In both cases, the Lewis dot diagram suggests that there are three kinds of oxygen atoms in the molecule, with +1, 0, and -1 formal charges. These structures also suggest that ozone should have one single and one double bond. Experimentally (by electron diffraction), however, we find that the molecule is symmetric, with both O-O bond lengths the same. The real (instantaneous) structure is the average of the two forms, as shown below. In the classical Lewis picture of the molecule, we can rationalize resonance by observing that electrons, being thousands of times lighter than the nuclei of atoms, move very fast on the timescale of molecular vibrations. Thus, in the time it takes for the oxygen atoms to adjust their positions, the electrons can move back and forth many times. In the quantum mechanical MO picture (Chapter 2), we will see that resonance involves electrons that are fully delocalized over the atoms in the molecule. We represent resonance structures with a double-headed arrow to signify that the only difference between the Lewis structures is the distribution of electrons.

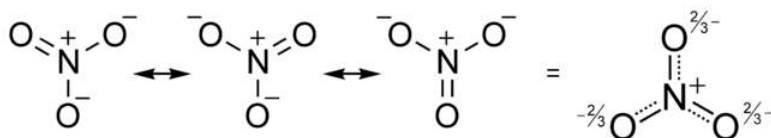


Susan Solomon discovered the heterogeneous catalytic mechanism whereby ozone is decomposed by chlorofluorocarbons (freons), creating the Antarctic ozone hole. Her work formed the basis of the U.N. Montreal Protocol, an international agreement to protect the ozone layer by regulating damaging chemicals.

In the instantaneous structure of ozone, the formal (-) charge is shared between the two terminal oxygen atoms and therefore each one has a formal charge of $-1/2$. The O-O bonds are the average of a single and a double bond, i.e., each O-O bond order is 1.5.

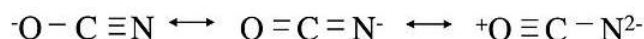


Similarly, the nitrate anion has three resonance structures, and experimentally (by X-ray crystallography of nitrate salts) we find that all the N-O bonds in the ion are the same. In this case, in the averaged structure, each O atom has a formal charge of $-2/3$ and the N-O bond order is $4/3$ ($=1.33\dots$).



Inequivalent resonance structures

The rules of resonance also apply to inequivalent structures, which in general will have different energies from each other. In this case the structure of the molecule represents a weighted average of the low energy structures. A good example is the cyanate ion, OCN^- . We can write three inequivalent octet structures for the molecule:



The first two are reasonable resonance structures, although we suspect the one on the left is the best because it puts the negative formal charge on the most electronegative atom. The last one is clearly a bad resonance structure, because the formal charges are high and there is a positive charge on the oxygen atom. The real structure is thus a weighted average of the first two.

No-bond resonance

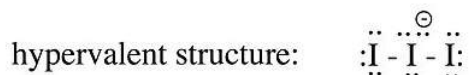
An interesting and useful kind of inequivalent resonance structure is one in which there is a bond order of *zero* between two of the atoms. This concept of **no-bond resonance** is important in understanding the bonding in many halogen- and hydrogen-containing compounds. The idea is illustrated below for the generic molecule X-Y-Z, where Z might be an electronegative halogen atom such as F. By moving the bonding electrons from the Y-Z bond onto the Z atom, and moving a lone pair from X into the X-Y bond, we generate the resonance structure shown on the right in which all atoms remain octet, but there is no bond between Y and Z.



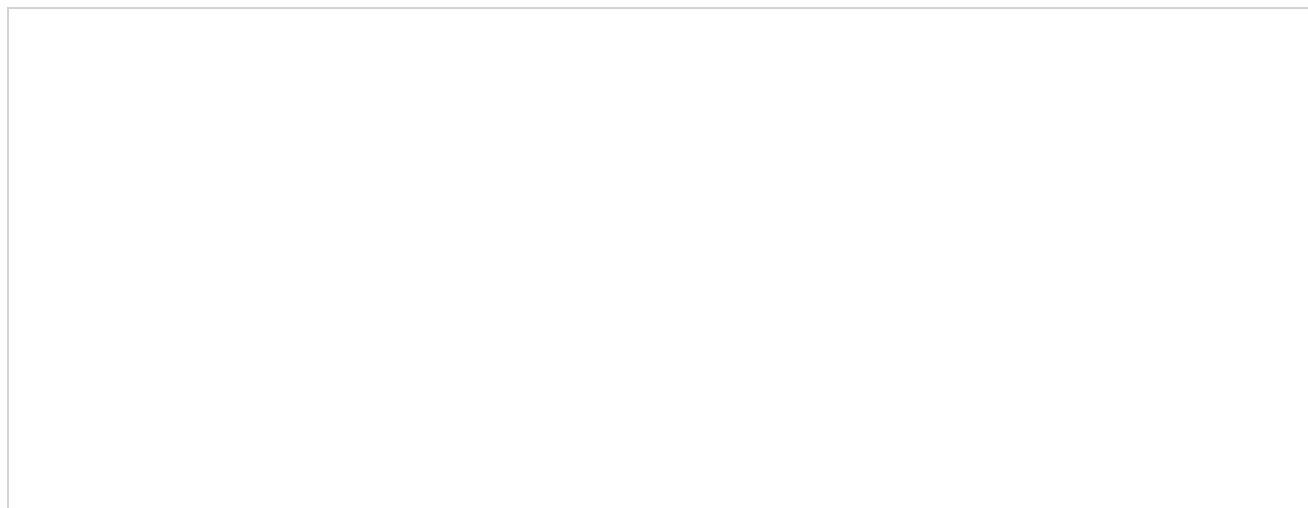
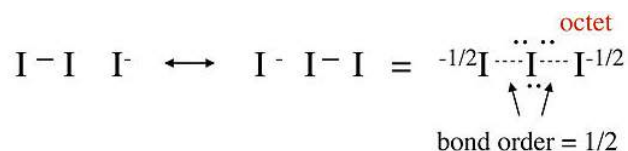
It is important to recognize in this example that the no-bond form is only one resonance structure, and therefore the Z atom is still bound to Y. If the two resonance structures in this example have the same energy, we would expect the X-Y bond order to be 1.5 and the Y-Z bond order to be 0.5. Therefore the Y-Z bond should be longer than it is in a compound where the bond order is one, and it should be relatively easy to break the Y-Z bond.

Some molecular examples of no-bond resonance are shown below. In the molecule ONF₃, the N-F bond is unusually long relative to the N-F bond in NF₃, in which the bond order is 1. This can be explained by the no-bond resonance forms shown on the right. Similarly, in the Lewis acid-base adduct formed by combining BH₃ with CO, we can explain the long B-H bonds using no-bond resonance forms that place a partial positive charge on the H atoms.

No-bond resonance is often used to provide an octet bonding picture for so-called **hypervalent compounds**, which are compounds that appear to have more than 8 valence electrons in the bonding shell of the central atom. For example, we can consider two different valence bond structures for the triiodide ion, I₃⁻, which is formed by reaction of I⁻ with I₂ in water:

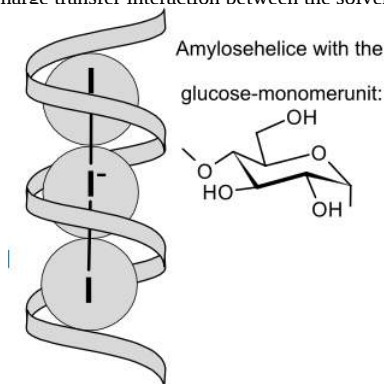


In this structure, the central iodine atom has 10 electrons in its valence shell, in violation of the octet rule. Raman spectra of the triiodide ion show that the I-I bond is weaker than the I-I single bond in I₂, suggesting that this picture is not an accurate description of the bonding. A better representation of I₃⁻ can be obtained with no-bond resonance structures, as shown below. We will see that this picture is consistent with the MO description of I₃⁻ in Chapter 2:

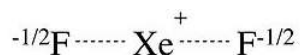




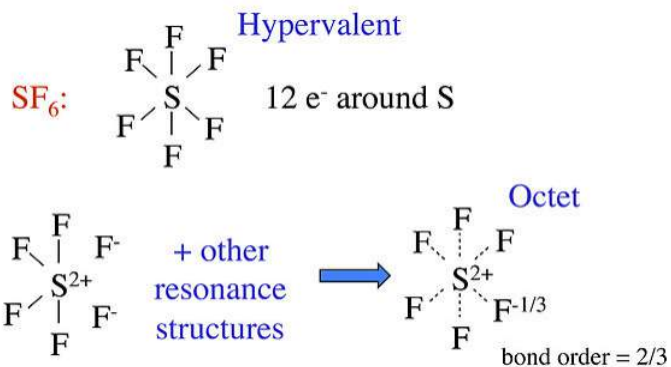
The deep blue color of starch-iodine solutions results from the complexation of linear polyiodide ions (I_n^-) by the starch (amylose) left-handed helix. The interior of the helix is hydrophobic. In electron donor solvents such as ethanol and water, I_2 and salts of I_3^- have a brown color, the result of a charge transfer interaction between the solvent and solute.^{[2][3]}

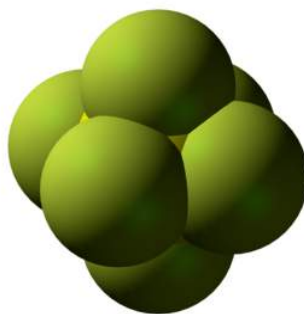


We can draw a similar picture for the XeF_2 molecule, which has the same number of valence electrons as I_3^- . This picture is consistent with XPS data, which show a partial negative charge on the F atoms, as well as vibrational spectra, which show that the Xe-F bond is weaker in XeF_2 than it is in the singly-bonded cation $Xe-F^+$.



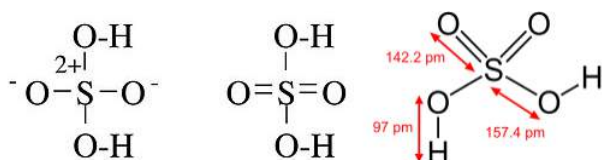
Other well known examples of hypervalent compounds are PF_5 , $P(CH_3)_5$, and SF_6 , as well as oxyacids such as H_2SO_4 and $HClO_4$. The hypervalent structure is often drawn for these molecules, with the explanation that d-orbitals on the central atom contribute to the bonding in dsp^3 and d^2sp^3 hybrids for 5- and 6-coordinate molecules, respectively. However, realistic molecular orbital calculations show that the phosphorus and sulfur 3d orbitals are too high in energy to contribute significantly to bonding in PF_5 and SF_6 . For these molecules, we can use no-bond resonance to make reasonable octet structures that predict polar bonds between the central atom and F.





Space-filling model of sulfur hexafluoride. SF_6 is surprisingly unreactive with water, relative to other compounds that contain S-F bonds. The tight packing of F atoms around S prevents nucleophilic attack by water.

In other cases, such as $\text{P}(\text{CH}_3)_5$, the octet structure is unreasonable because it suggests a polar bond between P and C, with a partial negative charge on C. Further, in the case of oxyacids such as H_2SO_4 and HClO_4 , X-ray crystallographic data establish that the S-O and Cl-O bonds are shorter for the oxygen atoms not bonded to hydrogen, which is more consistent with the hypervalent picture:

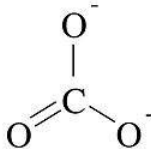
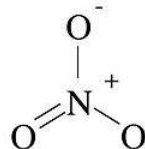
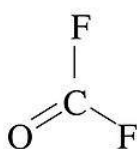
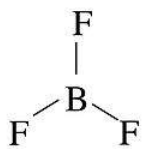
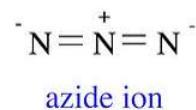
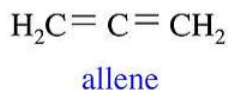
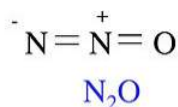
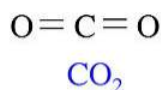


The question of whether hypervalency and the octet rule are really useful descriptions of the bonding in these compounds has been considered in a number of computational studies, which have used increasingly accurate quantum mechanical calculations to determine the number of electrons associated with the central atom. In a 2002 study, Gillespie and Silvi^[4] found that the population of the valence shell is greater than eight for compounds with electropositive ligands, such as $\text{P}(\text{CH}_3)_5$, and less than eight for compounds such as PF_5 . They concluded that these valence electron shell populations depend primarily on the coordination numbers and electronegativities of the central atoms and their ligands, and that there is no fundamental difference between the bonding in hypervalent and non-hypervalent (Lewis octet) molecules. This reminds us that the octet rule is not a law of nature, but rather an empirical rule that is useful within certain limits.

The isoelectronic principle

In calculating the octet structures of molecules using the N-V method, we needed to know only the number of atoms and the number of electrons, not the identities of the atoms themselves. This means that we will get the same answer (and the same set of octet and resonance structures) for *any* molecule or ion that contains (a) the same number of non-hydrogen atoms, and (b) the same total number of valence electrons. Such molecules are said to be *isoelectronic*. This is a powerful conclusion because, once we have determined the electronic structure of one molecule, we can write down the same solution for *all other molecules* that are isoelectronic. For example, we noted above that I_3^- and XeF_2 , which both have 22 valence electrons, have the same valence bond structure. We can further expect that isoelectronic molecules will have the same shapes and, very often, similar physical properties.

The four molecules and ions below all contain three non-hydrogen atoms and 16 valence electrons. All of them are linear molecules with two double bonds. The four molecules and ions shown below them all contain four non-hydrogen atoms and 24 valence electrons. These four have a trigonal planar shape. While BF_3 is a member of this isoelectronic series, we do not write it in the resonance form that contains a B=F double bond, because that would put a positive formal charge on F.



Similarly we can show that CH_4 , NH_3 , NH_4^+ , H_2O , H_3O^+ , HF , F^- , and OH^- are all isoelectronic with one non-H atom and eight valence electrons. In the next section we will see that this gives rise to nearly identical electronic shapes for these molecules.



Nitrous oxide (N_2O), or laughing gas, is isoelectronic with CO_2 . The two molecules have the same shape (linear) and similar physical properties. CO_2 sublimates at $-78\text{ }^\circ\text{C}$, whereas N_2O melts at $-91\text{ }^\circ\text{C}$ and boils at $-88\text{ }^\circ\text{C}$.

Isoelectronic solids

The isoelectronic principle works not just for molecules but for extended solids as well. One technologically important set of isoelectronic solids are the p-block semiconductors. The group 14 element Si is the most widely used semiconductor for electronics, but, as we will discuss later, it is not a good light emitter. Light-emitting diodes (LEDs), which are used in lasers, high efficiency lighting, and display technologies, are made from compounds that are isoelectronic with Si and Ge, especially GaAs, GaP, AlAs, and GaN (all contain four valence electrons per atom). CdTe and $\text{CuIn}_{1-x}\text{Ga}_x\text{Se}_2$ (CIGS) are promising solar cell materials that also have the same number of valence electrons per atom. Like Si and Ge, these compounds have tetrahedrally bonded structures in the solid state and absorb light across most of the solar spectrum, as we will discuss in more detail in Chapters 8 and 10.

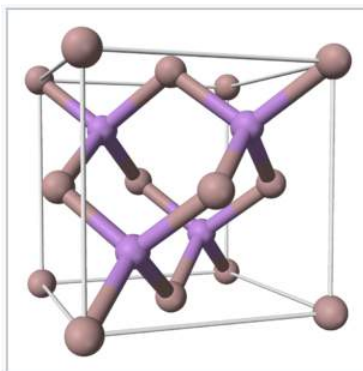


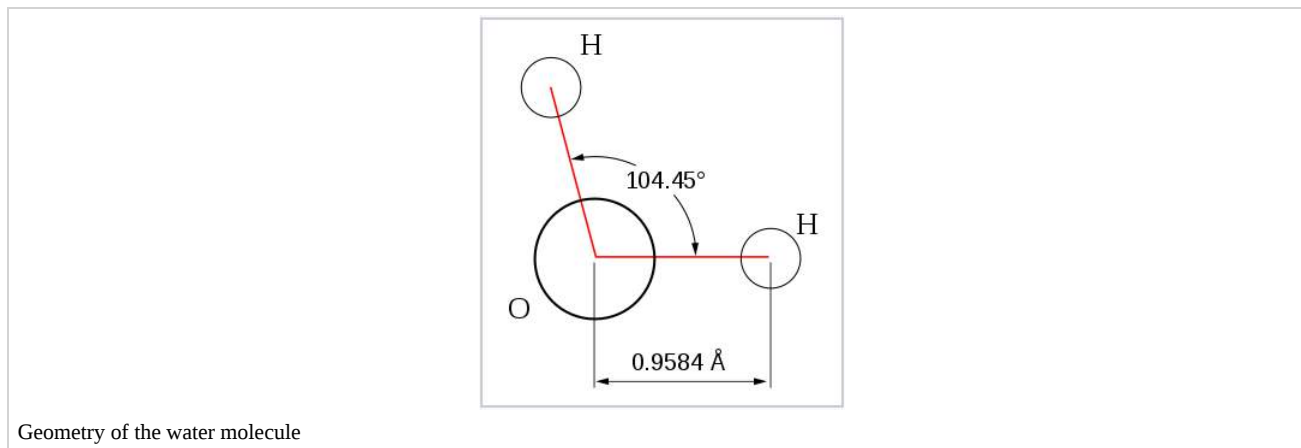
Figure 1.2.2: The tetrahedral bonding in crystals of GaAs, CdTe, $\text{CuIn}_{1-x}\text{Ga}_x\text{Se}_2$ and other semiconductors is similar to that in isoelectronic Si and Ge.

The isoelectronic principle is also a powerful tool in materials research, because it provides guidance about where to look for new materials with similar and perhaps improved properties. For example, the discovery that 8.5% efficient thin layer solar cells could be made with the compound CsSnI_3 ^[5] stimulated the exploration of many isoelectronic ABX_3 compounds with the same perovskite crystal structure. Very recently thin film solar cells based on light absorbers in this structural family $(\text{MA})\text{PbI}_{3-x}\text{Cl}_x$ and $\text{FA}_x\text{MA}_{1-x}\text{PbBr}_y\text{I}_{3-y}$ (MA^+ = methylammonium, CH_3NH_3^+ ; FA^+ = formamidinium, $\text{HC}(\text{NH}_2)_2^+$) have been reported with efficiencies as high as 22%.^{[6][7][8]}

This page titled [1.2: Valence Bond Theory- Lewis Dot Structures, the Octet Rule, Formal Charge, Resonance, and the Isoelectronic Principle](#) is shared under a [CC BY-SA 4.0](#) license and was authored, remixed, and/or curated by [Chemistry 310 \(Wikibook\)](#) via [source content](#) that was edited to the style and standards of the LibreTexts platform; a detailed edit history is available upon request.

1.3: The Shapes of Molecules (VSEPR Theory) and Orbital Hybridization

The Valence Shell Electron Pair Repulsion (VSEPR) theory is a simple and useful way to predict and rationalize the shapes of molecules. The theory is based on the idea of minimizing the electrostatic repulsion between electron pairs, as first proposed by Sidgwick and Powell in 1940,^[9] then generalized by Gillespie and Nyholm in 1957,^[10] and then broadly applied over the intervening 50+ years.^[11]

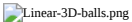




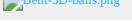


To use the VSEPR model, one begins with the Lewis dot picture to determine the number of lone pairs and bonding domains around a central atom. Because VSEPR considers all bonding domains equally (i.e., a single bond, a double bond, and a half bond all count as one electron domain), one can use either an octet or hypervalent structure, provided that the number of lone pairs (which should be the same in both) is calculated correctly. For example, in either the hypervalent or octet structure of the I_3^- ion above, there are three lone pairs on the central I atom and two bonding domains. We then follow these steps to obtain the **electronic geometry**:

- Determine the number of lone pairs on the central atom in the molecule, and add the number of bonded atoms (a.k.a. bonding domains)
- This number (the *steric number*) defines the electronic shape of the molecule by minimizing repulsion. For example a steric number of three gives a trigonal planar electronic shape.
- The angles between electron domains are determined primarily by the electronic geometry (e.g., 109.5° for a steric number of 4, which implies that the electronic shape is a tetrahedron)
- These angles are adjusted by the hierarchy of repulsions: (lone pair - lone pair) > (lone pair - bond) > (bond - bond)

The **molecular geometry** is deduced from the electronic geometry by considering the lone pairs to be present but invisible. The most commonly used methods to determine molecular structure - X-ray diffraction, neutron diffraction, and electron diffraction - have a hard time seeing lone pairs, but they can accurately determine the lengths of bonds between atoms and the bond angles.

The table below gives examples of electronic and molecular shapes for steric numbers between 2 and 9. We are most often concerned with molecules that have steric numbers between 2 and 6.

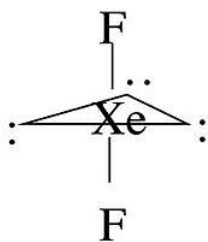
Bonding electron pairs	Lone pairs	Electron domains (Steric #)	Shape	Ideal bond angle (example's bond angle)	Example	Image
2	0	2	linear	180°	CO_2	
3	0	3	trigonal planar	120°	BF_3	
2	1	3	bent	120° (119°)	SO_2	
4	0	4	tetrahedral	109.5°	CH_4	
3	1	4	trigonal pyramidal	109.5° (107°)	NH_3	
2	2	4	bent	109.5° (104.5°)	H_2O	

Bonding electron pairs	Lone pairs	Electron domains (Steric #)	Shape	Ideal bond angle (example's bond angle)	Example	Image
5	0	5	trigonal bipyramidal	90°, 120°, 180°	PCl ₅	
4	1	5	seesaw	180°, 120°, 90° (173.1°, 101.6°)	SF ₄	
3	2	5	T-shaped	90°, 180° (87.5°, < 180°)	ClF ₃	
2	3	5	linear	180°	XeF ₂	
6	0	6	octahedral	90°, 180°	SF ₆	
5	1	6	square pyramidal	90° (84.8°), 180°	BrF ₅	
4	2	6	square planar	90°, 180°	XeF ₄	
7	0	7	pentagonal bipyramidal	90°, 72°, 180°	IF ₇	
6	1	7	pentagonal pyramidal	72°, 90°, 144°	XeOF ₅ ⁻	
5	2	7	planar pentagonal	72°, 144°	XeF ₅ ⁻	
8	0	8	square antiprismatic		XeF ₈ ²⁻	
9	0	9	tricapped trigonal prismatic		ReH ₉ ²⁻	

From the Table, we see that some of the molecules shown as examples have bond angles that depart from the ideal electronic geometry. For example, the H-N-H bond angle in ammonia is 107°, and the H-O-H angle in water is 104.5°. We can rationalize this in terms of the last rule above. The lone pair in ammonia repels the electrons in the N-H bonds more than they repel each other. This lone pair repulsion exerts even more steric influence in the case of water, where there are two lone pairs. Similarly, the axial F-S-F angle in the "seesaw" molecule SF₄ is a few degrees less than 180° because of repulsion by the lone pair in the molecule.

Geometrical isomers

For some molecules in the Table, we note that there is more than one possible shape that would satisfy the VSEPR rules. For example, the XeF₂ molecule has a steric number of five and a trigonal bipyramidal geometry. There are three possible stereoisomers: one in which the F atoms occupy axial sites, resulting in linear molecule, one in which the F atoms occupy one equatorial and one axial site (resulting in a 90° bond angle), and one in which the F atoms are both on equatorial sites, with a F-Xe-F bond angle of 120°.



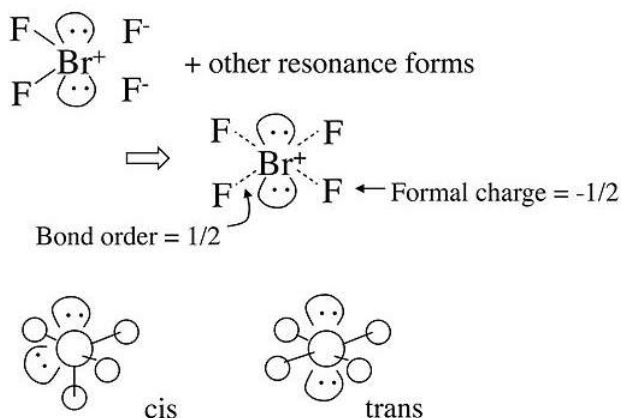
The observed geometry of XeF₂ is linear, which can be rationalized by considering the orbitals that are used to make bonds (or lone pairs) in the axial and equatorial positions. There are four available orbitals, s, p_x, p_y, and p_z. If we choose the z-axis as the axial direction, we can see that the p_x and p_y orbitals lie in the equatorial plane. We assume that the spherical s orbital is shared equally by the five electron domains in the molecule, the two axial bonds share the p_z orbital, and the three equatorial bonds share the p_x and p_y orbitals. We can then calculate the bond orders to axial and equatorial F atoms as follows:

axial : $\frac{1}{5} + \frac{1}{2}p_z = 0.7$ bond (formal charge = -0.3)

equatorial : $\frac{1}{5}s + \frac{1}{3}p_x + \frac{1}{3}p_y = 0.867$ bond (formal charge = -0.122)

Because fluorine is more electronegative than a lone pair, it prefers the axial site where it will have more negative formal charge. In general, by this reasoning, lone pairs and electropositive ligands such as CH_3 will always prefer the equatorial sites in the trigonal bipyramidal geometry. Electronegative ligands such as F will always go to the axial sites.

In the case of the BrF_4^- anion, which is isoelectronic with XeF_4 in the Table, the electronic geometry is octahedral and there are two possible isomers in which the two lone pairs are *cis* or *trans* to each other. In this case, lone pair - lone pair repulsion dominates and we obtain the *trans* arrangement of lone pairs, giving a square planar molecular geometry.



Orbital hybridization

The observation of molecules in the various electronic shapes shown above is, at first blush, in conflict with our picture of atomic orbitals. For an atom such as oxygen, we know that the $2s$ orbital is spherical, and that the $2p_x$, $2p_y$, and $2p_z$ orbitals are dumbbell-shaped and point along the Cartesian axes. The water molecule contains two hydrogen atoms bound to oxygen not at a 90° angle, but at an angle of 104.5° . Given the relative orientations of the atomic orbitals, how do we arrive at angles between electron domains of 104.5° , 120° , and so on? To understand this we will need to learn a little bit about the quantum mechanics of electrons in atoms and molecules.

The atomic orbitals ψ represent solutions to the **Schrödinger wave equation**,

$$E\psi = \hat{H}\psi \quad (1.3.1)$$

Here E is the energy of an electron in the orbital, and \hat{H} is the Hamiltonian operator.

By analogy with classical mechanics, the Hamiltonian is commonly expressed as the sum of operators corresponding to the kinetic and potential energies of a system in the form

$$\hat{H} = \hat{T} + \hat{V} \quad (1.3.2)$$

where $\hat{V} = V(\mathbf{r}, t)$ is the potential energy, and

$$\hat{T} = \frac{\hat{\mathbf{p}} \cdot \hat{\mathbf{p}}}{2m} = \frac{\hat{p}^2}{2m} = -\frac{\hbar^2}{2m} \nabla^2, \quad (1.3.3)$$

is the kinetic energy operator in which m is the mass of the particle and the momentum operator is:

$$\hat{p} = -i\hbar\nabla, \text{ where } \nabla = \frac{\delta}{\delta x} + \frac{\delta}{\delta y} + \frac{\delta}{\delta z} \quad (1.3.4)$$

Here \hbar is $h/2\pi$, where h is Planck's constant, and the Laplacian operator ∇^2 is:

$$\nabla^2 = \frac{\delta^2}{\delta x^2} + \frac{\delta^2}{\delta y^2} + \frac{\delta^2}{\delta z^2} \quad (1.3.5)$$

Although this is not the technical definition of the Hamiltonian in classical mechanics, it is the form it most commonly takes in quantum mechanics. Combining these together yields the familiar form used in the Schrödinger equation:

$$\hat{H} = \hat{T} + \hat{V} = \frac{\hat{\mathbf{p}} \cdot \hat{\mathbf{p}}}{2m} + V(\mathbf{r}, t) = -\frac{\hbar^2}{2m} \nabla^2 + V(\mathbf{r}, t) \quad (1.3.6)$$

For hydrogen-like (one-electron) atoms, the Schrödinger equation can be written as:

$$E\psi = -\frac{\hbar^2}{2\mu} \nabla^2 \psi - \frac{Ze^2}{4\pi\epsilon_0 r} \psi \quad (1.3.7)$$

where Z is the nuclear charge, e is the electron charge, and \mathbf{r} is the position of the electron. The radial potential term on the right side of the equation is due to the Coulomb interaction, i.e., the electrostatic attraction between the nucleus and the electron, in which ϵ_0 is the dielectric constant (permittivity of free space) and

$$\mu = \frac{m_e m_n}{m_e + m_n} \quad (1.3.8)$$

is the 2-body reduced mass of the nucleus of mass m_n and the electron of mass m_e . To a good approximation, $\mu \approx m_e$.



Erwin Schrödinger as a young scientist

This is the equation that Erwin Schrödinger famously derived in 1926 to solve for the energies and shapes of the s, p, d, and f atomic orbitals in hydrogen-like atoms. It was a huge conceptual leap for both physics and chemistry because it not only explained the quantized energy levels of the hydrogen atom, but also provided the theoretical basis for the octet rule and the arrangement of elements in the periodic table.

The Schrödinger equation can be used to describe chemical systems that are more complicated than the hydrogen atom (e.g., multi-electron atoms, molecules, infinite crystals, and the dynamics of those systems) if we substitute the appropriate potential energy function $V(\mathbf{r},t)$ into the Hamiltonian. The math becomes more complicated and the equation must be solved numerically in those cases, so for our purposes we will stick with the simplest case of time-invariant, one-electron, hydrogen-like atoms.

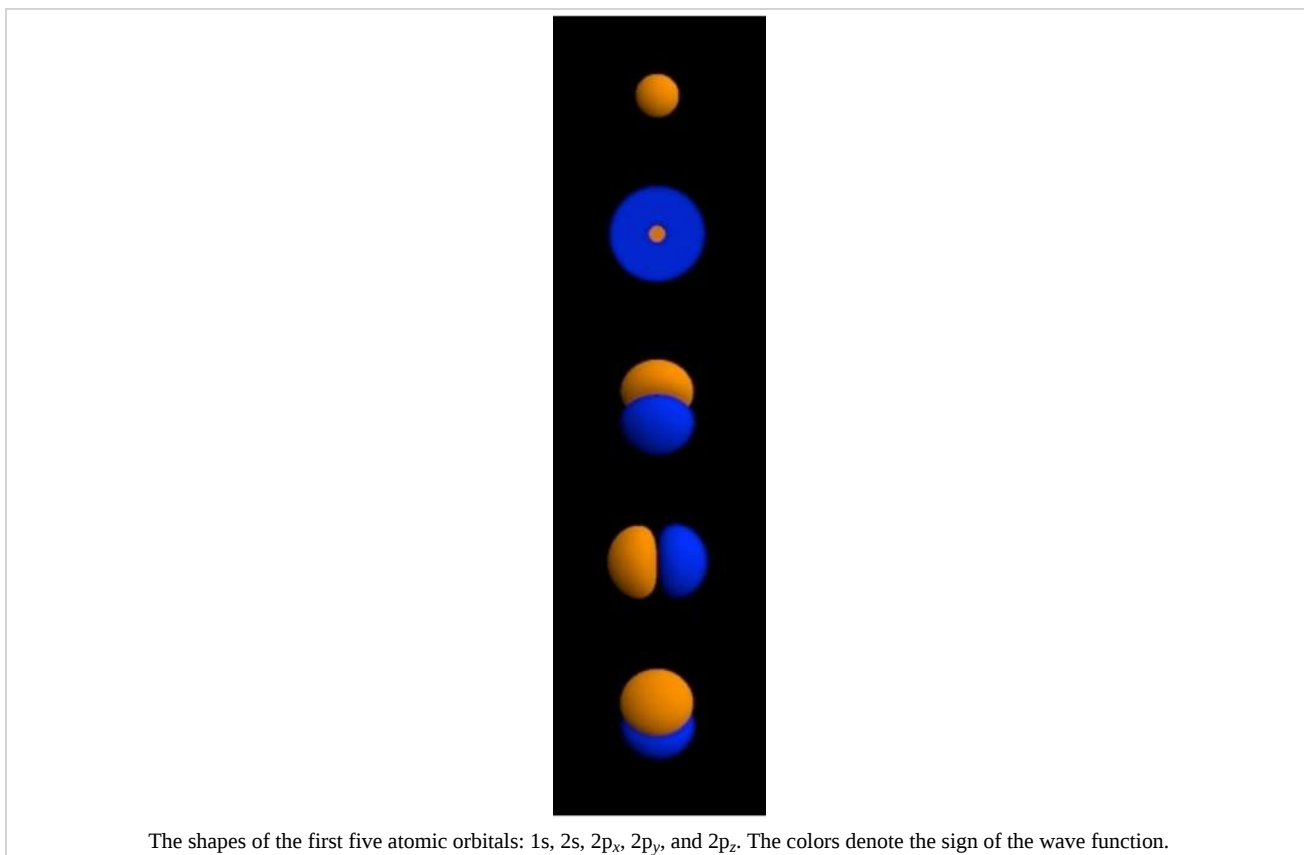
Without going into too much detail about the Schrödinger equation, we can point out some of its most important properties:

$$E\psi = -\frac{\hbar^2}{2\mu} \nabla^2 \psi - \frac{Ze^2}{4\pi\epsilon_0 r} \psi \quad (1.3.9)$$

- The equation derives from the fact that the total energy (E) is the sum of the kinetic energy (KE) and the potential energy (PE). These three quantities are represented mathematically as **operators** in the equation.
- On the left side of the equation, the total energy operator (E) is a scalar that is multiplied by the wavefunction ψ . ψ is a function of the spatial coordinates (x,y,z) and is related to the probability that the electron is at that point in space.
- The first term on the right side of the equation represents the kinetic energy (KE). The kinetic energy operator is proportional to ∇^2 (the Laplacian operator) which takes the second derivative (with respect to three spatial coordinates) of ψ . Thus, the Schrödinger equation is a **differential equation**.
- The second term on the right side of the equation represents the Coulomb potential (PE), i.e. the attractive energy between the positively charged nucleus and the negatively charged electron.
- The solutions to the Schrödinger equation are a set of **energies** E (which are scalar quantities) and **wavefunctions** (a.k.a. **atomic orbitals**) ψ , which are functions of the spatial coordinates. You will sometimes see the energies referred to as

eigenvalues and the orbitals as *eigenfunctions*, because mathematically the Schrödinger equation is an eigenfunction-eigenvalue equation. Although ψ is a function of the coordinates, E is not. So an electron in a $2p_z$ orbital has the same total energy E ($= PE + KE$) no matter where it is in space.

- These E values and their associated wavefunctions ψ are catalogued according to their **quantum numbers** n , l , and m_l . That is, there are many solutions to the differential equation, and each solution ($\psi(xyz)$ and E) has a unique set of quantum numbers. Some sets of orbitals are **degenerate**, meaning that they have the same energy (e.g., $2p_x$, $2p_y$, and $2p_z$).
- The solutions $\psi(xyz)$ to the Schrödinger equation (e.g., the $1s$, $2s$, $2p_x$, $2p_y$, and $2p_z$ orbitals) represent **probability amplitudes** for finding the electron at a particular point (x,y,z) in space. A probability amplitude can have either **+** or **- sign**. We typically represent the different signs by shading or by $+$ and $-$ signs on the two lobes of a $2p$ orbital.
- The square of the probability amplitude, ψ^2 , is always a positive number and represents the **probability** of finding the electron at a point x,y,z in space. Because the total probability of finding the electron somewhere is 1, the wavefunction must be **normalized** so that the integral of ψ^2 over the spatial coordinates (from $-\infty$ to $+\infty$) is 1.
- The solutions to the Schrödinger equation are **orthogonal**, meaning that the product of any two (integrated over all space) is zero. For example the product of the $2s$ and $2p_x$ orbitals, integrated over the spatial coordinates from $-\infty$ to $+\infty$, is zero.



Orbital hybridization involves making *linear combinations* of the atomic orbitals that are solutions to the Schrödinger equation. Mathematically, this is justified by recognizing that the Schrödinger equation is a *linear* differential equation. As such, any sum of solutions to the Schrödinger equation is also a valid solution. However, we still impose the constraint that our hybrid orbitals must be **orthogonal** and **normalized**.

Rules for orbital hybridization:

- Add and subtract atomic orbitals to get hybrid orbitals.
- We get the same number of orbitals out as we put in.
- The energy of a hybrid orbital is the weighted average of the atomic orbitals that make it up.
- The coefficients are determined by the constraints that the hybrid orbitals must be orthogonal and normalized.

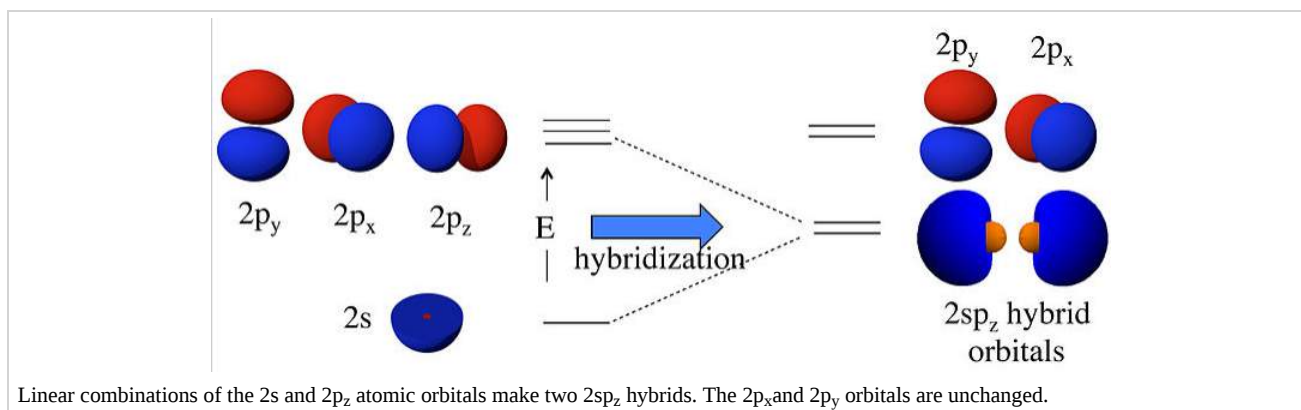
For **sp hybridization**, as in the BeF_2 or CO_2 molecule, we make two linear combinations of the $2s$ and $2p_z$ orbitals (assigning z as the axis of the Be-F bond):

$$\psi_1 = \frac{1}{\sqrt{2}}(2s) + \frac{1}{\sqrt{2}}(2p_z) \quad (1.3.10)$$

$$\psi_2 = \frac{1}{\sqrt{2}}(2s) - \frac{1}{\sqrt{2}}(2p_z) \quad (1.3.11)$$

Here we have simply added and subtracted the $2s$ and $2p_z$ orbitals; we leave it as an exercise for the interested student to show that both orbitals are normalized (i.e., $\int \psi_1^2 d\tau = \int \psi_2^2 d\tau = 1$) and orthogonal (i.e., $\int \psi_1 \psi_2 d\tau = 0$).

What this means physically is explained in the figure below. By combining the $2s$ and $2p_z$ orbitals we have created two new orbitals with large lobes (high electron probability) pointing along the z -axis. These two orbitals are degenerate and have an energy that is halfway between the energy of the $2s$ and $2p_z$ orbitals.



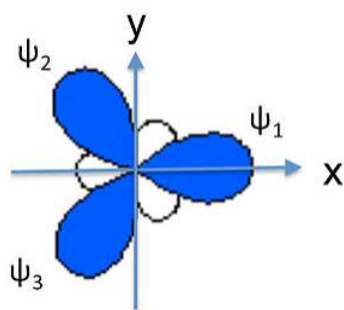
For an isolated Be atom, which has two valence electrons, the lowest energy state would have two electrons spin-paired in the $2s$ orbital. However, these electrons would not be available for bonding. By **promoting** these electrons to the degenerate $2sp_z$ hybrid orbitals, they become unpaired and are prepared for bonding to the F atoms in BeF_2 . This will occur if the **bonding energy** (in the promoted state) exceeds the promotion energy. The **overall bonding energy**, i.e., the energy released by combining a Be atom in its ground state with two F atoms, is the difference between the bonding and promotion energies.

We can similarly construct **sp² hybrids** (e.g., for the BF_3 molecule or the NO_3^- anion) from one $2s$ and two $2p$ atomic orbitals. Taking the plane of the molecule as the xy plane, we obtain three hybrid orbitals at 120° to each other. The three hybrids are:

$$\psi_1 = \frac{1}{\sqrt{3}}(2s) + \frac{\sqrt{2}}{\sqrt{3}}(2p_x) \quad (1.3.12)$$

$$\psi_2 = \frac{1}{\sqrt{3}}(2s) - \frac{1}{\sqrt{6}}(2p_x) + \frac{1}{\sqrt{2}}(2p_y) \quad (1.3.13)$$

$$\psi_3 = \frac{1}{\sqrt{3}}(2s) - \frac{1}{\sqrt{6}}(2p_x) - \frac{1}{\sqrt{2}}(2p_y) \quad (1.3.14)$$



These orbitals are again degenerate and their energy is the weighted average of the energies of the $2s$, $2p_x$, and $2p_y$ atomic orbitals.

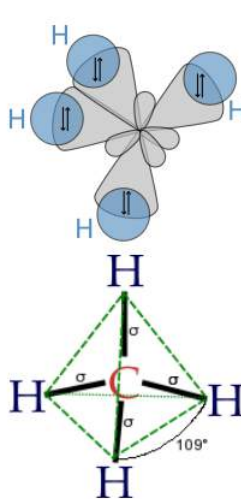
Finally, to make a sp^3 hybrid, as in CH_4 , H_2O , etc., we combine all four atomic orbitals to make four degenerate hybrids:

$$\psi_1 = \frac{1}{2}(2s + 2p_x + 2p_y + 2p_z) \quad (1.3.15)$$

$$\psi_2 = \frac{1}{2}(2s - 2p_x - 2p_y + 2p_z) \quad (1.3.16)$$

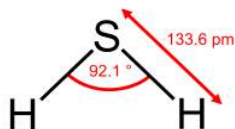
$$\psi_3 = \frac{1}{2}(2s + 2p_x - 2p_y - 2p_z) \quad (1.3.17)$$

$$\psi_4 = \frac{1}{2}(2s - 2p_x + 2p_y - 2p_z) \quad (1.3.18)$$



The lobes of the sp^3 hybrid orbitals point towards the vertices of a tetrahedron (or alternate corners of a cube), consistent with the tetrahedral bond angle in CH_4 and the nearly tetrahedral angles in NH_3 and H_2O . Similarly, we can show that we can construct the trigonal bipyramidal electronic shape by making sp and sp^2 hybrids, and the octahedral geometry from three sets of sp hybrids. The picture that emerges from this is that the atomic orbitals can hybridize as required by the shape that best minimizes electron pair repulsions.

Interestingly however, the bond angles in PH_3 , H_2S and H_2Se are close to 90° , suggesting that P, S, and Se primarily use their p-orbitals in bonding to H in these molecules. This is consistent with the fact that the energy difference between s and p orbitals stays roughly constant going down the periodic table, but the bond energy *decreases* as the valence electrons get farther away from the nucleus. In compounds of elements in the 3rd, 4th, and 5th rows of the periodic table, there thus is a *decreasing tendency to use s-p orbital hybrids in bonding*. For these heavier elements, the bonding energy is not enough to offset the energy needed to promote the s electrons to s-p hybrid orbitals.



This page titled [1.3: The Shapes of Molecules \(VSEPR Theory\) and Orbital Hybridization](#) is shared under a [CC BY-SA 4.0](#) license and was authored, remixed, and/or curated by [Chemistry 310 \(Wikibook\)](#) via [source content](#) that was edited to the style and standards of the LibreTexts platform; a detailed edit history is available upon request.

1.4: Bond Polarity and Bond Strength

Linus Pauling introduced the concept of electronegativity 1932 in order to explain the extra stability of molecules with polar bonds.^[12] The electronegativity of an atom, represented by the Greek letter χ , can be defined as the tendency of an atom to draw electrons to itself in a chemical bond. On the Pauling scale, the electronegativity difference between two atoms A and B was defined in terms of the dissociation energies E_d of the A-A, B-B, and A-B bonds:

$$\chi_A - \chi_B = \sqrt{E_d(AB) - [E_d(AA) + E_d(BB)]/2} \quad (1.4.1)$$

where the energies are expressed in electron volts.

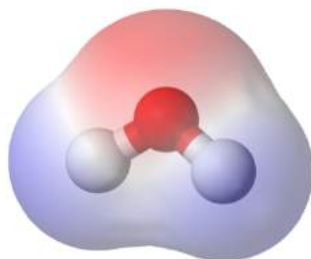


Figure 1.4.1: A water molecule, a commonly used example of polarity. The two charges are present with a negative charge in the middle (red), and a positive charge at the ends (blue).

This definition, while directly relevant to the strength of chemical bonds, requires thermochemical input data from many compounds, some of which were not available at the time. Mulliken^{[13][14]} and later Pearson^[15] developed a scale of electronegativities based on the average of the electron affinity and ionization energy of the free A and B atoms, which they correlated with thermochemical data and the Pauling scale.

On the Pauling scale, the least electronegative elements are the alkali metals ($\chi = 0.7-1.0$) and the most electronegative are oxygen (3.5) and fluorine (4.0) at the upper right of the periodic table. Carbon and hydrogen have intermediate electronegativities (2.6 and 2.2 on the Pauling scale, respectively). The general trend (see table below) is that electronegativities increase going up and to the right in the periodic table. There are some interesting exceptions to this behavior, most notably two islands of high electronegativity at the bottom of the transition series, peaking at tungsten ($\chi = 2.4$) and gold ($\chi = 2.5$). The first of these can be explained by the very high metal-metal bond energy of elements such as Mo and W, which can use all six of their valence electrons in bonding, as we will discuss in Chapter 6. The second however occurs with more weakly bonded noble metals such as Pt and Au, and is responsible for their low position in the activity series,^[16] as well as their extraordinary properties as catalysts.

Table of Pauling electronegativities

Periodic table of electronegativity using the Pauling scale

→ Atomic radius decreases → Ionization energy increases → Electronegativity increases →

Group →	1	2	3	4	5	6	7	8	9	10	11	12	13	14	15	16	17	18
↓ Period																		
1	H 2.20																	He
2	Li 0.98	Be 1.57											B 2.04	C 2.55	N 3.04	O 3.44	F 3.98	Ne
3	Na 0.93	Mg 1.31											Al 1.61	Si 1.90	P 2.19	S 2.58	Cl 3.16	Ar
4	K 0.82	Ca 1.00	Sc 1.36	Ti 1.54	V 1.63	Cr 1.66	Mn 1.55	Fe 1.83	Co 1.88	Ni 1.91	Cu 1.90	Zn 1.65	Ga 1.81	Ge 2.01	As 2.18	Se 2.55	Br 2.96	Kr 3.00
5	Rb 0.82	Sr 0.95	Y 1.22	Zr 1.33	Nb 1.6	Mo 2.16	Tc 1.9	Ru 2.2	Rh 2.28	Pd 2.20	Ag 1.93	Cd 1.69	In 1.78	Sn 1.96	Sb 2.05	Te 2.1	I 2.66	Xe 2.60
6	Cs 0.79	Ba 0.89	*	Hf 1.3	Ta 1.5	W 2.36	Re 1.9	Os 2.2	Ir 2.20	Pt 2.28	Au 2.54	Hg 2.00	Tl 1.62	Pb 1.87	Bi 2.02	Po 2.0	At 2.2	Rn 2.2
7	Fr 0.7	Ra 0.9	**	Rf	Db	Sg	Bh	Hs	Mt	Ds	Rg	Cn	Uut	Ff	Uup	Lv	Uus	Uuo
* Lanthanoids	La 1.1	Ce 1.12	Pr 1.13	Nd 1.14	Pm 1.13	Sm 1.17	Eu 1.2	Gd 1.2	Tb 1.1	Dy 1.22	Ho 1.23	Er 1.24	Tm 1.25	Yb 1.1	Lu 1.27			
** Actinoids	Ac 1.1	Th 1.3	Pa 1.5	U 1.38	Np 1.36	Pu 1.28	Am 1.13	Cm 1.28	Bk 1.3	Cf 1.3	Es 1.3	Fm 1.3	Md 1.3	No 1.3	Lr 1.3			

The polarity of bonds is determined by electronegativity differences. As a guideline we define bonds as:

- **ionic** if $\Delta\chi > 2.0$
- **polar** if $2.0 > \Delta\chi > 0.5$
- **nonpolar** if $0.5 > \Delta\chi$

The polarity of bonds helps us understand non-covalent forces between molecules, such as hydrogen bonding and dipole-dipole interactions. It also helps us interpret the reactivity of molecules. For example, the Si-H bond ($\chi_{\text{Si}} = 1.8$, $\chi_{\text{H}} = 2.1$) is more hydride-like than the C-H bond ($\chi_{\text{C}} = 2.5$, $\chi_{\text{H}} = 2.1$). Therefore silanes react with acids to make H_2 , whereas phosphines ($\chi_{\text{P}} = 2.1$) and hydrocarbons do not. Similarly, electrophilic substitution reactions occur more readily on Si-H and P-H compounds than they do on C-H compounds.

There is also a correlation between the strength of a chemical bond and the bond length, longer bonds being weaker because of weaker orbital overlap. Pauling introduced an empirical formula relating bond length to bond strength. For a given pair of atoms (for example, two carbon atoms):

$$D(n) = D(1) - 0.6 \log_{10}(n) \quad (1.4.2)$$

where $D(n)$ represents the bond length in Å and n is the bond order. $D(1)$ in this case would be the length of a C-C single bond, which we can obtain from the average bond length in alkanes (1.54 Å). Using this formula we can predict that the bond lengths in ethylene (C=C double bond) and acetylene (C≡C triple bond) should be 1.36 and 1.25 Å, respectively, which are close to the experimental values of 1.33 and 1.20 Å. In a related form the Pauling formula can be used to calculate bond lengths when the single bond length $D(1)$ is not available:

$$D(n) = D(m) - 0.6 \log_{10}(n/m) \quad (1.4.3)$$

Here n and m represent two different bond orders between the same kinds of atoms. This tells, for example, that the difference in length between a triple and double bond, $D(2)-D(3)$, should be $-0.6 \log_{10}(2/3) = 0.11$ Å. Some bond lengths and bond energies are anomalous. For example, the F-F bond length in F_2 is 1.43 Å, which is 0.15 Å longer than twice the covalent radius of the F atom (0.64 Å). The F-F bond is also quite weak (bond dissociation energy = 155 kJ/mol) relative to the Cl-Cl bond (242 kJ/mol). By putting the extra bond length into the Pauling formula, we calculate that the bond order in the F_2 molecule is only 0.6, i.e., substantially weaker than a F-F single bond. The physical reason for this is that the F-F bond is "stretched" by repulsion of the lone pairs on the F atoms. This crowding is caused by the fact that the [He] $1s^2$ core orbital, as well as the valence orbitals of the fluorine atoms, are contracted by the high nuclear charge. The Cl_2 atom, with its larger [Ne] ($1s^2 2s^2 2p^6$) core, in contrast, has a "normal" single bond length (1.98 Å) that is twice the covalent radius of the Cl atom (0.99 Å). A similar lone pair repulsion effect explains the anomalously long and weak N-N and O-O single bonds in hydrazine ($\text{H}_2\text{N-NH}_2$) and hydrogen peroxide (HO-OH), which are both highly reactive molecules.

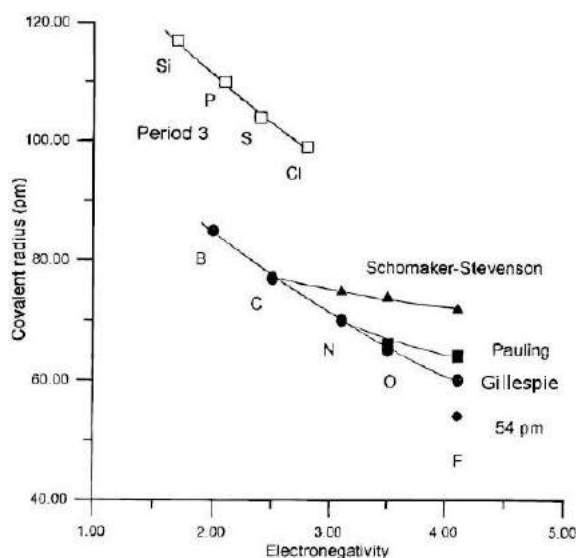


Figure 1.4.2: Trends in covalent radii for p-block elements. The covalent radius of F has been difficult to determine because of electron pair repulsion effects. Early reports (Shomaker and Stevenson, Pauling) overestimated the size of the F atom.^{[17][18]}
^[19]Accurate quantum chemical calculations place the F single-bond covalent radius at about 0.64 Å.^[20] (Public Domain; N4nojohn via Wikipedia)

The important roles of electronegativity differences and lone pair repulsion are evident when comparing trends in bond strengths. The table below shows the average single-bond enthalpies of p-block elements with H and F. H makes stronger bonds with 2nd row elements (C, N, O, F) than with third row elements (Si, P, S, Cl) because the 2p valence electrons are closer to the nucleus and thus make stronger bonds than electrons in 3p orbitals. The bonds to H also follow the expected trend of increasing bond strength with increasing electronegativity difference. Bonds between second row elements (C, N, O, F) and F are however anomalously weak because of lone pair repulsion. For this reason, the Si-F bond is substantially stronger than the C-F bond, whereas the C-H bond is much stronger than the Si-H bond. The strong Si-F bond is the reason that HF etches glass (to produce the SiF_6^{2-} anion), and the strong C-H bond is an important factor in the stability of hydrocarbons and other organic molecules.

Average E-H and E-F bond enthalpies (kJ/mol)

C-H 413	N-H 391	O-H 483	H-F 567
Si-H 323	P-H 322	S-H 339	H-Cl 431
C-F 485	N-F 272	O-F 190	F-F 155
Si-F 565	P-F 490	S-F 327	Cl-F 253

The anomalously weak bond in F_2 is responsible for the high electronegativity of fluorine, as well as the legendary reactivity of elemental fluorine gas, which reacts explosively with hydrogen and powdered metals. Because of the instability of elemental fluorine and the polar nature of its bonds with more electropositive elements, fluorine compounds tend to be very stable. For example, the noble gases Xe and Kr react with fluorine to make covalent compounds, whereas other halogens do not react. Fluorocarbon compounds contain strong C-F bonds and have high thermal and chemical stability. Perfluorocarbons such as Teflon (poly(tetrafluoroethylene), $-(\text{CF}_2\text{CF}_2)_n-$, PTFE) are also highly hydrophobic. The extraordinary hydrophobicity of perfluorocarbons arises from the fact that $-\text{CF}_2-$ and $-\text{CF}_3$ groups are "fatter" than $-\text{CH}_2-$ and $-\text{CH}_3$ groups; dissolving them in water is therefore more disruptive to the hydrogen bonding network than is dissolving a hydrocarbon.^[21]



Figure 1.4.2: Fabric treated with fluorosurfactant

This page titled [1.4: Bond Polarity and Bond Strength](#) is shared under a [CC BY-SA 4.0](#) license and was authored, remixed, and/or curated by [Chemistry 310 \(Wikibook\)](#) via [source content](#) that was edited to the style and standards of the LibreTexts platform; a detailed edit history is available upon request.

1.5: Discussion Questions

Group essay project:

Join a group of classmates from your inorganic chemistry course. Each group should have 3 or 4 students. Arrange a time to meet for an hour or so. Prior to the meeting, read part I (pp. 1367-1391) as well as the summary at the end of Linus Pauling's article (J. Am. Chem. Soc. 1931, 53, 1367-1400) on the nature of the chemical bond.

This paper was published only a few years after Schrödinger developed the quantum mechanical theory of atomic orbitals and is considered one of the most important papers in the history of modern chemistry. At the meeting, discuss the following questions: (1) What was understood about chemical bonding in molecules before Pauling published this work? (2) What new concepts did the paper introduce that we still use today? (3) Why were these ideas important? and (4) What, if anything, did Pauling get wrong, and why?

Together with your classmates, write a 1-2 page essay addressing these questions. Please include the names of all students in your group on the first page; all of you will receive the same grade on this assignment. Anonymous excerpts from a few of these essays will be shared with the class.

In-class discussion questions from this chapter:

- What are inequivalent resonance structures? Illustrate with some new examples not covered above.
- Explain no-bond resonance and hypervalency, using some new examples.
- What are the limitations of valence bond theory for molecules that contain an odd number of electrons? Illustrate with one or two examples.

This page titled [1.5: Discussion Questions](#) is shared under a [CC BY-SA 4.0](#) license and was authored, remixed, and/or curated by [Chemistry 310 \(Wikibook\)](#) via [source content](#) that was edited to the style and standards of the LibreTexts platform; a detailed edit history is available upon request.

1.6: Problems

- Write octet structures (including formal charges, bond order, and molecular shape) for SeO_3^{2-} , SeF_4 , XeF_4 , HClO_3 (= HOClO_2), NO_3^- , and ClO_2^+ .
- Write octet structures (including formal charges, bond order, and molecular shape) for Al_2Cl_6 , SnCl_3^- , BrF_4^- , HOClO , SO_3 , and NO_2^+ .
- Show using resonance why the S-O bond is slightly shorter in SO_2F_2 than in SO_2 .
- Give the formulas for five stable molecules and/or ions that are isoelectronic with ammonia.
- Name three well known molecules or ions that are isoelectronic with (a) O_3 , (b) BF , (c) CO_3^{2-} , and (d) N_3^- .
- Name three well known molecules or ions that are isoelectronic with (a) CN^- , (b) H_2O , (c) BF_3 , and (d) CO_2 .
- The N-N bond distance is 1.10 Å in N_2 . Using the Pauling bond length – bond strength formula, $D(n) = D(1) - 0.6 \log(n)$, calculate the bond distance in the N_2^+ cation.
- In hydroxylamine, H_2NOH , the N-O bond distance is 1.46 Å. Using the Pauling bond length - bond strength formula, estimate the N-O bond distances in NO_2 and NO_3^- .
- While PF_5 and SF_6 are stable molecules, NF_5 and OF_6 are unknown. Can you draw octet structures for these compounds? Why would these molecules be unstable?
- Consider the compounds NH_3 and PH_3 . The H-N-H bond angle in ammonia is 108° (close to the tetrahedral angle, 109.5°), but the analogous angle in PH_3 is 93° . Why is the angle in PH_3 closer to 90° than it is to the tetrahedral angle?
- Two hypothetical structures for the N_2F_3^+ ion are $[\text{N}-\text{NF}_3]^+$ and $[\text{F}-\text{N}-\text{NF}_2]^+$. Which one is more stable? Explain. (Note: lines in the formulas can represent either single or multiple bonds)
- Krypton difluoride, KrF_2 , decomposes at dry ice temperature to Kr and F_2 . However, several salts of the $[\text{KrF}]^+$ ion are relatively stable. Draw valence bond pictures for KrF_2 and $[\text{KrF}]^+$, showing lone pairs, possible resonance structures, formal charges, bond orders, and bond angles. Why is $[\text{KrF}]^+$ more stable than KrF_2 ?
- Consider the molecule ClF_3O_2 (with Cl the central atom). How many isomers are possible? Which is the most stable?
- The Br-F bond distance in the interhalogen compound BrF is 1.76 Å. Use this information to estimate the average bond lengths in BrF_3 and BrF_5 .
- The B-H bond distances are about the same in BH_3 and BH_4^- . however, the B-F bond distance in BF_3 is shorter than that in the BF_4^- ion. Explain.
- The N-N bond dissociation energy in hydrazine ($\text{H}_2\text{N}-\text{NH}_2$) is 159 kJ/mol. The dissociation energy of the N-N triple bond in N_2 is 941 kJ/mol, i.e., much greater than three times the N-N single bond dissociation energy in hydrazine. Explain why the N-N bond in hydrazine is so weak, and why this effect is not seen in N_2 .
- Show that a set of three sp^2 hybrid orbitals satisfies the following criteria: (a) any two orbitals in the sp^2 set are orthogonal, and (b) the orbitals are properly normalized.
- Quantum mechanically, the momentum (p) of a particle traveling in a specific direction (e.g., the x direction) can be obtained by operating on its wavefunction ψ with the **momentum operator**:

$$\hat{p}\psi = p\psi, \text{ where } \hat{p} = -i\hbar \frac{\delta}{\delta x} \quad (1.6.1)$$

Knowing the correct form of this operator was the key to Schrödinger's formulation of the Hamiltonian operator, $\hat{H} = \frac{\hat{p}^2}{2m} + V$, which operates on a wavefunction to give the total energy. The momentum operator must also be consistent with the **de Broglie relation**, $p = \frac{h}{\lambda}$, which relates the momentum to the particle wavelength.

By analogy to electromagnetic waves, Schrödinger knew that a wavelike particle (such as an electron) traveling in free space in the x-direction could be described by the wavefunction:

$$\psi(x, t) = Ae^{i(kx - \omega t + \varphi)} \quad (1.6.2)$$

where the **wavenumber** k is inversely related to the particle's **de Broglie wavelength** λ by $k = \frac{2\pi}{\lambda}$. Here A is a normalization constant, ω is the frequency of the wave, and φ represents its phase.

Show using the momentum operator \hat{p} that the value of the momentum p we obtain for a free particle from $\hat{p}\psi = p\psi$ is consistent with the de Broglie relation, $p = \frac{h}{\lambda}$.

(Hint: k , ω , and φ are independent of x)

19. Which S-N bonds in the cyclic $S_4N_3^+$ ion would you predict to be the shortest? The atomic connectivity in the ring is: -S-S-N-S-N-S-N-. [Hint: determine the number of π -bonds in the molecule by electron counting and then find the most stable resonance structures].

20. F has a higher electronegativity than Cl, and F_2 is a much stronger oxidizing agent than Cl_2 , despite the fact that the electron affinity of fluorine (-328 kJ/mol) is weaker than that of chlorine (-349 kJ/mol). Explain this apparent contradiction.

21. (a) Explain why C-H, N-H, and O-H bonds in chemical compounds are stronger than Si-H, P-H, and S-H bonds, respectively. (b) Explain why C-F, N-F, and O-F single bonds follow the opposite trend, namely, they are weaker than Si-F, P-F, and S-F single bonds, respectively.

This page titled [1.6: Problems](#) is shared under a [CC BY-SA 4.0](#) license and was authored, remixed, and/or curated by [Chemistry 310 \(Wikibook\)](#) via [source content](#) that was edited to the style and standards of the LibreTexts platform; a detailed edit history is available upon request.

1.7: References

1. G. N. Lewis, "The atom and the molecule," *J. Am. Chem. Soc.* 1916, 38, 762-785
2. W. Saenger, "The structure of the blue starch-iodine complex," *Naturwissenschaften* 71, 31-36 (1984).
3. R. D. Hancock and B. J. Tarbet, "The other double helix - the fascinating chemistry of starch," *J. Chem. Ed.* 77, 988-992 (2000).
4. R. J. Gillespie and B. Silvi, "The octet rule and hypervalence: two misunderstood concepts," *Coord. Chem. Rev.* 233-234, 53-62 (2002).
5. I. Chung, B. Lee, J. He, R. P. H. Chang and M. G. Kanatzidis, All-solid-state dye-sensitized solar cells with high efficiency, *Nature* 485, 486-489 (2012). doi:10.1038/nature11067
6. S.D. Stranks, G. E. Eperon, G. Grancini, C. Menelaou, M. J. P. Alcocer, T. Leijtens, L. M. Herz, A. Petrozza, and H. J. Snaith, Electron-Hole Diffusion Lengths Exceeding 1 Micrometer in an Organometal Trihalide Perovskite Absorber, *Science* 342, 341-344 (2013). DOI: 10.1126/science.1243982
7. G. Xing, N. Mathews, S. Sun, S. S. Lim, Y. M. Lam, M. Grätzel, S. Mhaisalkar, and T. C. Sum, Long-Range Balanced Electron- and Hole-Transport Lengths in Organic-Inorganic CH₃NH₃PbI₃, *Science* 342, 344-347 (2013). DOI: 10.1126/science.1243167
8. J.-P. Correa-Baena, A. Abate, M. Saliba, W. Tress, T. J. Jacobsson, M. Grätzel, and A. Hagfeldt, The rapid evolution of highly efficient perovskite solar cells, *Energy Environ. Sci.*, 10, 710-727 (2017). DOI: 10.1039/C6EE03397K
9. N. V. Sidgwick and H. M. Powell, *Proc. Roy. Soc. A* 176, 153 (1940),
10. R. J. Gillespie and R. S. Nyholm, *Quart. Rev. Chem. Soc.*, 11, 339 (1957).
11. R. J. Gillespie, "Fifty years of the VSEPR model," *Coord. Chem. Rev.* 252, 1315-1327 (2008). DOI: 10.1016/j.ccr.2007.07.007
12. Pauling, L. (1932). "The Nature of the Chemical Bond. IV. The Energy of Single Bonds and the Relative Electronegativity of Atoms". *J. Am. Chem. Soc.* **54** (9): 3570–3582. doi:10.1021/ja01348a011.
13. Mulliken, R. S. (1934). "A New Electroaffinity Scale; Together with Data on Valence States and on Valence Ionization Potentials and Electron Affinities". *J. Chem. Phys.* **2** (11): 782–793. doi:10.1063/1.1749394. Bibcode: 1934JChPh...2..782M.
14. Mulliken, R. S. (1935). "Electronic Structures of Molecules XI. Electroaffinity, Molecular Orbitals and Dipole Moments". *J. Chem. Phys.* **3** (9): 573–585. doi:10.1063/1.1749731. Bibcode: 1935JChPh...3..573M.
15. Pearson, R. G. (1985). "Absolute electronegativity and absolute hardness of Lewis acids and bases". *J. Am. Chem. Soc.* **107** (24): 6801. doi:10.1021/ja00310a009.
16. B. Hammer and J. K. Nørskov, "Why gold is the noblest of all the metals," *Nature* **376**, 238 - 240 (2002). doi:10.1038/376238a0
17. Schomaker, Verner; Stevenson, D. P. (1941). "Some Revisions of the Covalent Radii and the Additivity Rule for the Lengths of Partially Ionic Single Covalent Bonds *". *Journal of the American Chemical Society* **63**: 37–40. doi:10.1021/ja01846a007.
18. Pauling, L. *The Nature of the Chemical Bond*, 3rd ed.; Cornell University Press: Ithaca, NY, 1960; p. 224.
19. Robinson, Edward A.; Johnson, Samuel A.; Tang, Ting-Hua; Gillespie, Ronald J. (1997). "Reinterpretation of the Lengths of Bonds to Fluorine in Terms of an Almost Ionic Model". *Inorganic Chemistry* **36** (14): 3022–3030. doi:10.1021/ic961315b. PMID 11669953.
20. Pyykkö, Pekka; Atsumi, Michiko (2009). "Molecular Double-Bond Covalent Radii for Elements Li–E112". *Chemistry: A European Journal* **15** (46): 12770–12779. doi:10.1002/chem.200901472.
21. V. H. Dalvi and P. J. Rosicky, Molecular origins of fluorocarbon hydrophobicity, *Proc. Natl. Acad. Sci. USA* 107,13603–13607 (2010). DOI: 10.1073/pnas.0915169107.

This page titled [1.7: References](#) is shared under a [CC BY-SA 4.0](#) license and was authored, remixed, and/or curated by [Chemistry 310 \(Wikibook\)](#) via [source content](#) that was edited to the style and standards of the LibreTexts platform; a detailed edit history is available upon request.

CHAPTER OVERVIEW

2: Molecular Orbital Theory

Learning Objectives

- Be able to construct molecular orbital diagrams for homonuclear diatomic, heteronuclear diatomic, homonuclear triatomic, and heteronuclear triatomic molecules.
- Understand and be able to articulate how molecular orbitals form – conceptually, visually, graphically, and (semi)mathematically.
- Interrelate bond order, bond length, and bond strength for diatomic and triatomic molecules, including neutral and ionized forms.
- Use molecular orbital theory to predict molecular geometry for simple triatomic systems
- Rationalize molecular structure for several specific systems in terms of orbital overlap and bonding.
- Understand the origin of aromaticity and anti-aromaticity in molecules with π -bonding.

Valence bond (VB) theory gave us a qualitative picture of chemical bonding, which was useful for predicting the shapes of molecules, bond strengths, etc. It fails to describe some bonding situations accurately because it ignores the wave nature of the electrons. Molecular orbital (MO) theory has the potential to be more quantitative. With it we can also get a picture of where the electrons are in the molecule, as shown in the image at the right. This can help us understand patterns of bonding and reactivity that are otherwise difficult to explain.

[2.1: Prelude to Molecular Orbital Theory](#)

[2.2: Constructing Molecular Orbitals from Atomic Orbitals](#)

[2.3: Orbital Symmetry](#)

[2.4: \$\sigma\$, \$\pi\$, and \$\delta\$ orbitals](#)

[2.5: Diatomic Molecules](#)

[2.6: Orbital Filling](#)

[2.7: Periodic Trends in \$\pi\$ Bonding](#)

[2.8: Three-center Bonding](#)

[2.9: Building up the MOs of More Complex Molecules- \$\text{NH}_3\$, \$\text{P}_4\$](#)

[2.10: Homology of \$\sigma\$ and \$\pi\$ orbitals in MO diagrams](#)

[2.11: Chains and Rings of \$\pi\$ -Conjugated Systems](#)

[2.12: Discussion Questions](#)

[2.13: Problems](#)

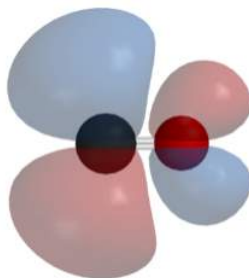
[2.14: References](#)

This page titled [2: Molecular Orbital Theory](#) is shared under a [CC BY-SA 4.0](#) license and was authored, remixed, and/or curated by [Chemistry 310 \(Wikibook\)](#) via [source content](#) that was edited to the style and standards of the LibreTexts platform; a detailed edit history is available upon request.

2.1: Prelude to Molecular Orbital Theory

Valence bond (VB) theory gave us a qualitative picture of chemical bonding, which was useful for predicting the shapes of molecules, bond strengths, etc. It fails to describe some bonding situations accurately because it ignores the wave nature of the electrons. Molecular orbital (MO) theory has the potential to be more quantitative. With it we can also get a picture of where the electrons are in the molecule, as shown in the image at the right. This can help us understand patterns of bonding and reactivity that are otherwise difficult to explain.

Although MO theory in principle gives us a way to calculate the energies and wavefunctions of electrons in molecules very precisely, usually we settle for simplified models here too. These simple models do not give very accurate orbital and bond energies, but they do explain concepts such as resonance (e.g., in the ferrocene molecule) that are hard to represent otherwise. We can get more accurate energies from MO theory by computational "number crunching." While MO theory is more correct than VB theory and can be very accurate in predicting the properties of molecules, it is also rather complicated even for fairly simple molecules. For example, you should have no trouble drawing the VB pictures for CO, NH₃, and benzene, but we will find that these are increasingly challenging with MO theory.



The lowest unoccupied molecular orbital of the carbon monoxide molecule is a π antibonding orbital that derives from the 2p orbitals of carbon (left) and oxygen (right)

This page titled [2.1: Prelude to Molecular Orbital Theory](#) is shared under a [CC BY-SA 4.0](#) license and was authored, remixed, and/or curated by [Chemistry 310 \(Wikibook\)](#) via [source content](#) that was edited to the style and standards of the LibreTexts platform; a detailed edit history is available upon request.

2.2: Constructing Molecular Orbitals from Atomic Orbitals

Molecular orbital theory involves solving (approximately) the Schrödinger equation for the electrons in a molecule. To review from Chapter 1, this is a differential equation in which the first and second terms on the right represent the kinetic and potential energies:

$$E\psi = -\frac{\hbar^2}{2\mu}\nabla^2\psi + V\psi \quad (2.2.1)$$

While the Schrödinger equation can be solved analytically for the hydrogen atom, the potential energy function V becomes more complicated - and the equation can then only be solved numerically - when there are many (mutually repulsive) electrons in a molecule. So as a first approximation we will assume that the s, p, d, f, etc. orbitals of the atoms that make up the molecule are good solutions to the Schrödinger equation. We can then allow these wavefunctions to interfere constructively and destructively as we bring the atoms together to make bonds. In this way, we use the atomic orbitals (AO) as our basis for constructing MO's.

LCAO-MO = **linear combination of atomic orbitals**. In physics, this is called this the tight binding approximation.

We have actually seen linear combinations of atomic orbitals before when we constructed hybrid orbitals in Chapter 1. The basic rules we developed for hybridization also apply here: orbitals are added with scalar coefficients (c) in such a way that the resulting orbitals are **orthogonal** and **normalized**. The difference is that in the MO case, the atomic orbitals come from different atoms.

The linear combination of atomic orbitals always gives back the *same number of molecular orbitals*. So if we start with two atomic orbitals (e.g., an s and a p_z orbital as shown in Fig. 2.2.1), we end up with two molecular orbitals. When atomic orbitals add in phase, we get constructive interference and a lower energy orbital. When they add out of phase, we get a node and the resulting orbital has higher energy. The lower energy MOs are *bonding* and higher energy MOs are *antibonding*.

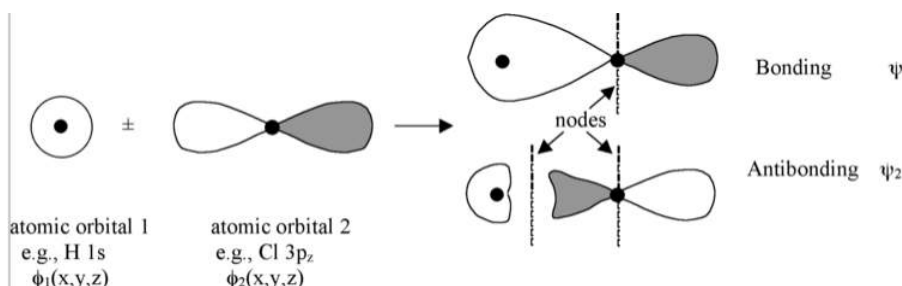


Figure 2.2.1: Sigma bonding and antibonding combinations of an s and p orbital

Molecular orbitals are also called **wavefunctions** (ψ), because they are solutions to the Schrödinger equation for the molecule. The atomic orbitals (also called basis functions) are labeled as ϕ 's, for example, ϕ_{1s} and ϕ_{3p_z} or simply as ϕ_1 and ϕ_2 .

In principle, we need to solve the Schrödinger equation for all the orbitals in a molecule, and then fill them up with pairs of electrons as we do for the orbitals in atoms. In practice we are really interested only in the MOs that derive from the valence orbitals of the constituent atoms, because these are the orbitals that are involved in bonding. We are especially interested in the **frontier orbitals**, i.e., the highest occupied molecular orbital (the **HOMO**) and the lowest unoccupied molecular orbital (the **LUMO**). Filled orbitals that are much lower in energy (i.e., core orbitals) do not contribute to bonding, and empty orbitals at higher energy likewise do not contribute. Those orbitals are however important in photochemistry and spectroscopy, which involve electronic transitions from occupied to empty orbitals. The fluorescent dyes that stain the cells shown in Fig. 2.2.2 absorb light by promoting electrons in the HOMO to empty MOs and give off light when the electrons drop back down to their original energy levels.

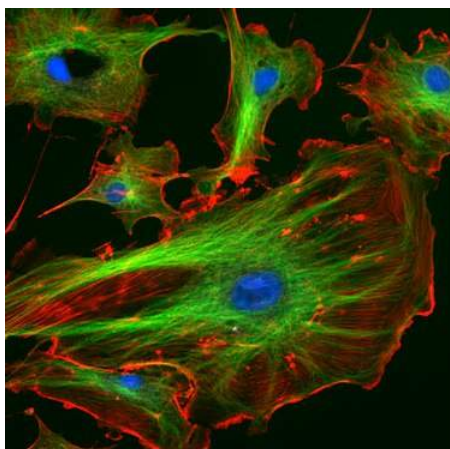


Figure 2.2.2: Different components of endothelial cells are stained by blue, green, and red fluorescent dyes. For each dye the color of emitted light corresponds to the energy given off when an electron drops from the LUMO to the HOMO of the molecule.

As an example of the LCAO-MO approach we can construct two MO's (ψ_1 and ψ_2) of the HCl molecule from two AO's ϕ_1 and ϕ_2 (Fig. 2.1.1). To make these two linear combinations, we write:

$$\Psi_1 = c_1\phi_1 + c_2\phi_2 \quad (2.2.2)$$

and

$$\Psi_2 = c_1\phi_1 - c_2\phi_2 \quad (2.2.3)$$

The coefficients c_1 and c_2 will be equal (or nearly so) when the two AOs from which they are constructed are the same, e.g., when two hydrogen 1s orbitals combine to make bonding and antibonding MOs in H_2 . They will be unequal when there is an energy difference between the AOs, for example when a hydrogen 1s orbital and a chlorine 3p orbital combine to make a polar H-Cl bond.

Nodes:

The wavefunctions ϕ and ψ are **amplitudes** that are related to the probability of finding the electron at some point in space. They have lobes with (+) or (-) signs, which we indicate by shading or color. Wherever the wavefunction changes sign we have a node. As you can see in Fig. 2.2.1, nodes in MOs result from destructive interference of (+) and (-) wavefunctions. Generally, the more nodes, the higher the energy of the orbital.

In the example above we have drawn a simplified picture of the Cl 3p_z orbital and the resulting MOs, leaving out the radial node. Recall that 2p orbitals have no radial nodes, 3p orbitals have one, as illustrated in Fig. 2.2.3. 4p orbitals have two radial nodes, and so on. The MOs we make by combining the AOs have these nodes too.



Figure 2.2.3: Nodal structure of 2p and 3p orbitals

Normalization:

We square the wave functions to get probabilities, which are always positive or zero. So if an electron is in orbital ϕ_1 , the probability of finding it at point xyz is the square^[1] of $\phi_1(x,y,z)$. The total probability does not change when we combine AOs to make MOs, so for the simple case of combining ϕ_1 and ϕ_2 to make ψ_1 and ψ_2 ,

$$\Psi_1^2 + \Psi_2^2 = \phi_1^2 + \phi_2^2 \quad (2.2.4)$$

Overlap integral:

The spatial overlap between two atomic orbitals ϕ_1 and ϕ_2 is described by the overlap integral S,

$$S_{12} = \int \varphi_1 * \varphi_2 d\tau \quad (2.2.5)$$

where the integration is over all space $d\tau = dx dy dz$.

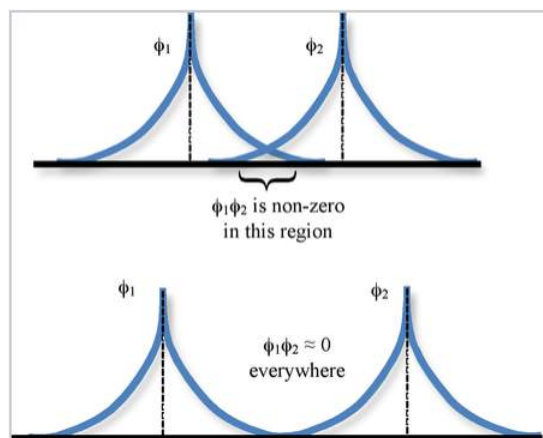


Figure 2.2.4: The wavefunctions of atomic orbitals decrease exponentially with distance. Orbital overlap is non-zero when two atoms are close together, as illustrated for 1s orbitals in the upper figure. The lower figure shows orbitals that are too far away to interact. In this case both S and β are close to zero.

Energies of bonding and antibonding MOs:

The energies of bonding and antibonding orbitals depend strongly on the distance between atoms. This is illustrated in Fig. 2.1.5 for the hydrogen molecule, H_2 . At very long distances, there is essentially no difference in energy between the in-phase and out-of-phase combinations of H 1s orbitals. As they get closer, the in-phase (bonding) combination drops in energy because electrons are shared between the two positively charged nuclei. The energy reaches a minimum at the equilibrium bond distance (0.74 \AA) and then rises again as the nuclei get closer together. The antibonding combination has a node between the nuclei so its energy rises continuously as the atoms are brought together.

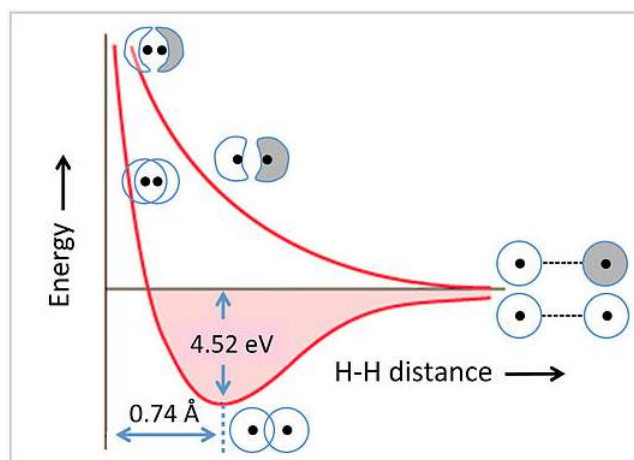


Figure 2.2.5: Energy as a function of distance for the bonding and antibonding orbitals of the H_2 molecule

At the equilibrium bond distance, the energies of the bonding and antibonding molecular orbitals (ψ_1, ψ_2) are lower and higher, respectively, than the energies of the atomic basis orbitals φ_1 and φ_2 . This is shown in Fig. 2.2.6 for the MO's of the H_2 molecule.

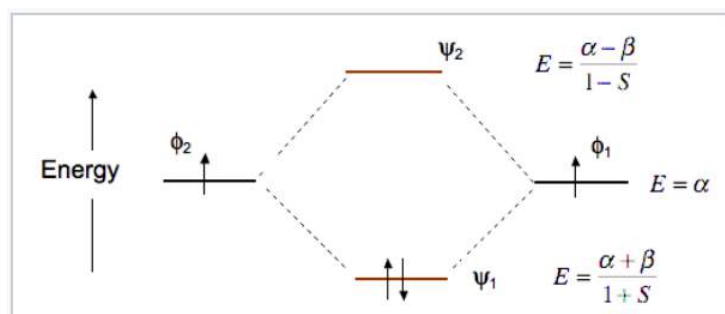


Figure 2.2.6: Molecular orbital energy diagram for the H₂ molecule

The energy of an electron in one of the atomic orbitals is α , the **Coulomb integral**.

$$\alpha = \int \varphi_1 H \varphi_1 d\tau \quad (2.2.6)$$

where **H** is the **Hamiltonian operator**. Essentially, α represents the *ionization energy* of an electron in atomic orbital φ_1 or φ_2 .

The energy difference between an electron in the AO's and the MO's is determined by the **exchange integral β** ,

$$\beta = \int \varphi_1 H \varphi_2 d\tau \quad (2.2.7)$$

β is an important quantity, because it tells us about the bonding energy of the molecule, and also the difference in energy between bonding and antibonding orbitals. Calculating β is not straightforward for multi-electron molecules because we cannot solve the Schrödinger equation analytically for the wavefunctions. We can however make some approximations to calculate the energies and wavefunctions numerically. In the Hückel approximation, which can be used to obtain approximate solutions for π molecular orbitals in organic molecules, we simplify the math by taking $S=0$ and setting $H=0$ for any p-orbitals that are not adjacent to each other. The extended Hückel method,^[2] developed by Roald Hoffmann, and other semi-empirical methods can be used to rapidly obtain relative orbital energies, approximate wavefunctions, and degeneracies of molecular orbitals for a wide variety of molecules and extended solids. More sophisticated ab initio methods are now readily available in software packages and can be used to compute accurate orbital energies for molecules and solids.

We can get the coefficients c_1 and c_2 for the hydrogen molecule by applying the normalization criterion:

$$\Phi_1 = (\varphi_1 + \varphi_2) / (\sqrt{2(1+S)}) \text{ (bonding orbital)} \quad (2.2.8)$$

and

$$\Phi_2 = (\varphi_1 - \varphi_2) / (\sqrt{2(1-S)}) \text{ (antibonding orbital)} \quad (2.2.9)$$

In the case where $S \approx 0$, we can eliminate the $1-S$ terms and both coefficients become $1/\sqrt{2}$

Note that the bonding orbital in the MO diagram of H₂ is stabilized by an energy $\beta/1+S$ and the antibonding orbital is destabilized by $\beta/1-S$. That is, the antibonding orbital goes up in energy more than the bonding orbital goes down. This means that H₂ ($\psi_1^2\psi_2^0$) is energetically more stable than two H atoms, but He₂ with four electrons ($\psi_1^2\psi_2^2$) is *unstable* relative to two He atoms.

Bond order: In any MO diagram, the bond order can be calculated as $\frac{1}{2}$ (# of bonding electrons - # of antibonding electrons). For H₂ the bond order is 1, and for He₂ the bond order is zero.

Heteronuclear case (e.g., HCl) - Polar bonds

Here we introduce an electronegativity difference between the two atoms making the chemical bond. The energy of an electron in the H 1s orbital is higher (it is easier to ionize) than the electron in the chlorine 3p_z orbital. This results in a larger energy difference between the resulting molecular orbitals ψ_1 and ψ_2 , as shown in Fig. 2.2.7. The bigger the electronegativity difference between atomic orbitals (the larger $\Delta\alpha$ is) the more " φ_2 character" the bonding orbital has, i.e., the more it resembles the Cl 3p_z orbital in this case. This is consistent with the idea that H-Cl has a polar single bond: the two electrons reside in a bonding molecular orbital that is primarily localized on the Cl atom.

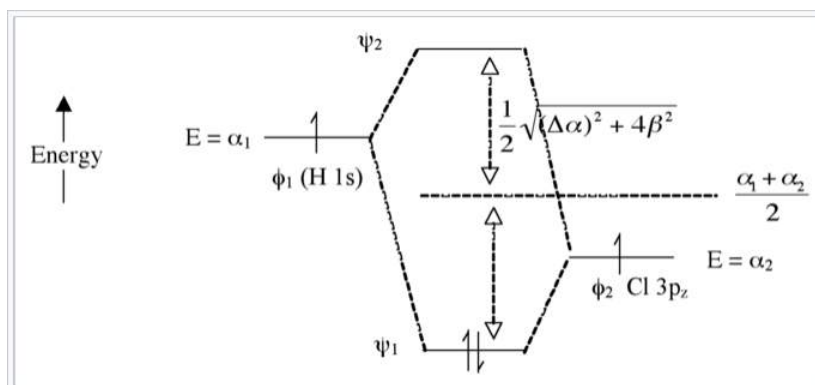


Figure 2.2.7: Molecular orbital energy diagram for the HCl molecule

The antibonding orbital (empty) has more H-character. The bond order is again 1 because there are two electrons in the bonding orbital and none in the antibonding orbital.

Extreme case - Ionic bonding (NaF): very large $\Delta\alpha$

In this case, there is not much mixing between the AO's because their energies are far apart (Fig. 2.2.8). The two bonding electrons are localized on the F atom, so we can write the molecule as Na^+F^- . Note that if we were to excite an electron from ψ_1 to ψ_2 using light, the resulting electronic configuration would be $(\psi_1^1\psi_2^1)$ and we would have Na^0F^0 . This is called a charge transfer transition.

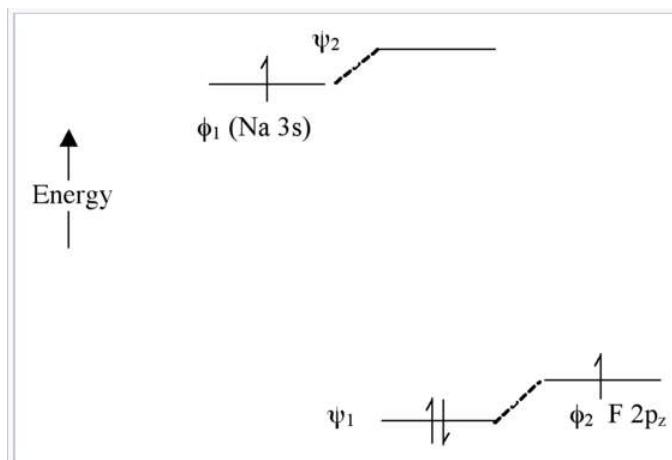


Figure 2.2.8: Molecular orbital energy diagram illustrating ionic bonding in the NaF molecule

Summary of molecular orbital theory so far:

- **Add and subtract** AO wavefunctions to make MOs. Two AOs \rightarrow two MOs. More generally, the *total number of MOs equals the number of AO basis orbitals*.
- We showed the simplest case (only two basis orbitals). More accurate calculations use a much larger basis set (more AOs) and solve for the matrix of c 's that gives the lowest total energy, using mathematically friendly approximations of the potential energy function that is part of the Hamiltonian operator H .
- **More nodes** \rightarrow **higher energy MO**
- **Bond order** = $\frac{1}{2}$ (# of bonding electrons - # of antibonding electrons)
- **Bond polarity** emerges in the MO picture as orbital “character.”
- AOs that are **far apart in energy** do not interact much when they combine to make MOs.

This page titled [2.2: Constructing Molecular Orbitals from Atomic Orbitals](#) is shared under a [CC BY-SA 4.0](#) license and was authored, remixed, and/or curated by [Chemistry 310 \(Wikibook\)](#) via [source content](#) that was edited to the style and standards of the LibreTexts platform; a detailed edit history is available upon request.

2.3: Orbital Symmetry

The MO picture for a molecule gets complicated when many valence AOs are involved. We can simplify the problem enormously by noting (without proof here) that orbitals of different symmetry with respect to the molecule do not interact. The symmetry operations of a molecule (which can include rotations, mirror planes, inversion centers, etc.), and the symmetry classes of bonds and orbitals in molecules, can be rigorously defined according to **group theory**. Here we will take a simple approach to this problem based on our intuitive understanding of the symmetry of three-dimensional objects as illustrated in Fig. 2.3.1.



Figure 2.3.1: Example of σ symmetry.

AO's must have the same **nodal symmetry** (as defined by the molecular symmetry operations), or their overlap is zero.

For example, in the HCl molecule, there is a unique symmetry axis \rightarrow , which is typically defined as the Cartesian z-axis, as shown in Fig. 2.3.2

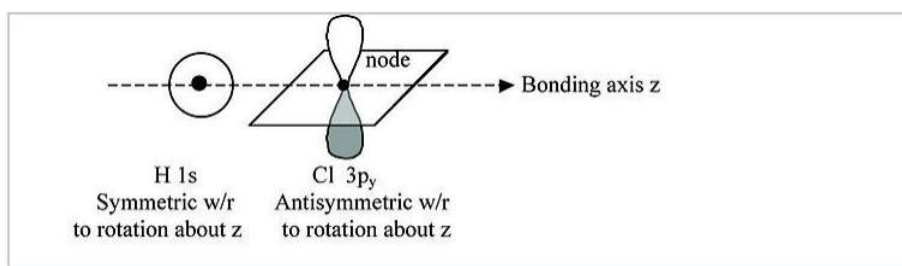


Figure 2.3.2: Orbitals of σ and π symmetry do not interact.

We can see from this figure that the H 1s orbital is unchanged by a 180° rotation about the bond axis. However, the same rotation inverts the sign of the Cl $3p_y$ wavefunction. Because these two orbitals have different symmetries, the Cl $3p_y$ orbital is **nonbonding** and doesn't interact with the H 1s. The same is true of the Cl $3p_x$ orbital. The p_x and p_y orbitals have π symmetry (nodal plane containing the bonding axis) and are labeled π_{nb} in the MO energy level diagram, Fig. 2.3.3. In contrast, the H 1s and Cl $3p_z$ orbitals both have σ symmetry, which is also the symmetry of the clay pot shown in Fig. 2.3.1. Because these orbitals have the same symmetry (in the point group of the molecule), they can make the bonding and antibonding combinations shown in Fig. 2.1.1.

The MO diagram of HCl that includes all the valence orbitals of the Cl atom is shown in Fig. 2.3.3. Two of the Cl valence orbitals ($3p_x$ and $3p_y$) have the wrong symmetry to interact with the H 1s orbital. The Cl 3s orbital has the same (σ) symmetry as H 1s, but it is much lower in energy so there is little orbital interaction. The energy of the Cl 3s orbital is thus affected only slightly by forming the molecule. The pairs of electrons in the π_{nb} and σ_{nb} orbitals are therefore **non-bonding**.

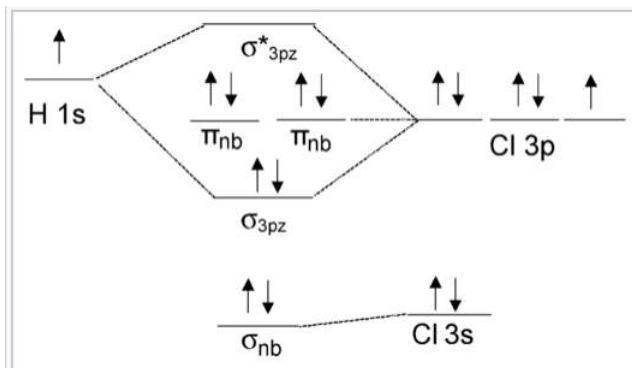


Figure 2.3.3: Energy level diagram of the HCl molecule showing MOs derived from the valence AOs.

Note that the MO result in Fig. 2.3.3 (1 bond and three pairs of nonbonding electrons) is the same as we would get from valence bond theory for HCl. The nonbonding orbitals are localized on the Cl atom, just as we would surmise from the valence bond picture.

In order to differentiate it from the σ bonding orbital, the σ antibonding orbital, which is empty in this case, is designated with an asterisk.

This page titled [2.3: Orbital Symmetry](#) is shared under a [CC BY-SA 4.0](#) license and was authored, remixed, and/or curated by [Chemistry 310 \(Wikibook\)](#) via [source content](#) that was edited to the style and standards of the LibreTexts platform; a detailed edit history is available upon request.

2.4: σ , π , and δ orbitals

Inorganic compounds use s, p, and d orbitals (and more rarely f orbitals) to make bonding and antibonding combinations. These combinations result in σ , π , and δ bonds (and antibonds).

You are already familiar with σ and π bonding in organic compounds. In inorganic chemistry, π bonds can be made from p- and/or d-orbitals. δ bonds are more rare and occur by face-to-face overlap of d-orbitals, as in the ion $\text{Re}_2\text{Cl}_8^{2-}$. The fact that the Cl atoms are eclipsed in this anion is evidence of δ bonding.

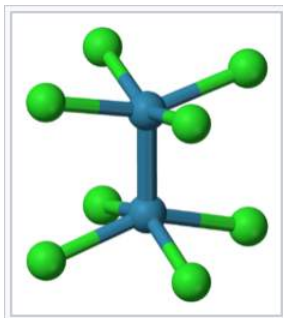
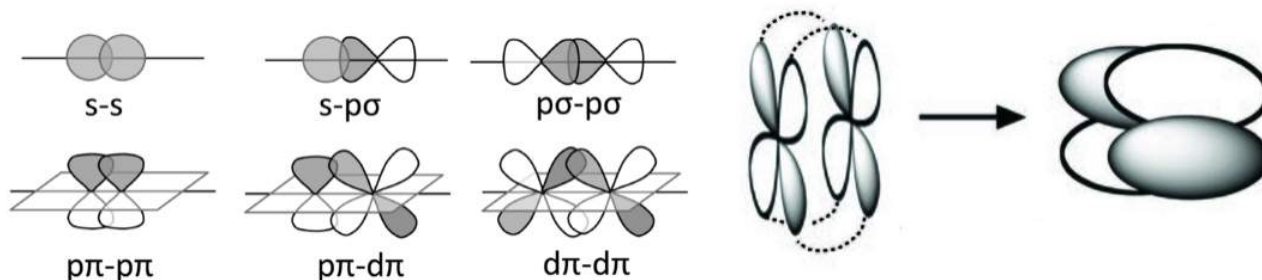
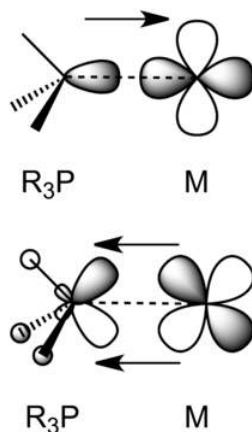


Figure 2.4.1: The octachlorodirhenate(III) anion, $[\text{Re}_2\text{Cl}_8]^{2-}$, which has a quadruple Re-Re bond.^[3]

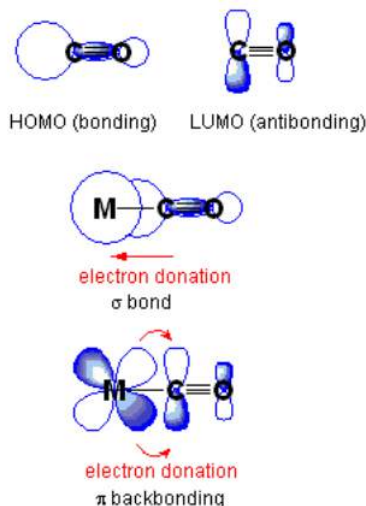
Some possible σ (top row), π (bottom row), and δ bonding combinations (right) of s, p, and d orbitals are sketched below. In each case, we can make bonding or antibonding combinations, depending on the signs of the AO wavefunctions. Because π - π bonding involves sideways overlap of p-orbitals, it is most commonly observed with second-row elements (C, N, O). π -bonded compounds of heavier elements are rare because the larger cores of the atoms prevent good π -overlap. For this reason, compounds containing C=C double bonds are very common, but those with Si=Si bonds are rare. δ bonds are generally quite weak compared to σ and π bonds. Compounds with metal-metal δ bonds occur in the middle of the transition series.



Transition metal d-orbitals can also form σ bonds, typically with s-p hybrid orbitals of appropriate symmetry on ligands. For example, phosphines (R_3P) are good σ donors in complexes with transition metals, as shown below.



π - $d\pi$ bonding is also important in transition metal complexes. In metal carbonyl complexes such as $\text{Ni}(\text{CO})_4$ and $\text{Mo}(\text{CO})_6$, there is sideways overlap between filled metal d-orbitals and the empty π -antibonding orbitals (the LUMO) of the CO molecule, as shown in the figure below. This interaction strengthens the metal-carbon bond but weakens the carbon-oxygen bond. The C-O infrared stretching frequency is diagnostic of the strength of the bond and can be used to estimate the degree to which electrons are transferred from the metal d-orbital to the CO π -antibonding orbital.

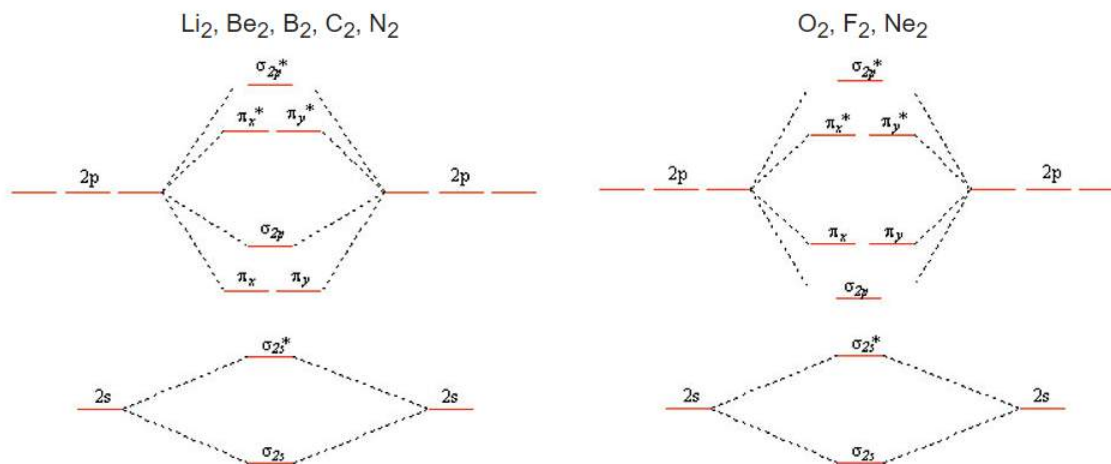


The same kind of backbonding occurs with phosphine complexes, which have empty π orbitals, as shown at the right. Transition metal complexes containing halide ligands can also have significant π - $d\pi$ bonding, in which a filled $p\pi$ orbital on the ligand donates electron density to an unfilled metal $d\pi$ orbital. We will encounter these bonding situations in Chapter 5.

This page titled [2.4: \$\sigma\$, \$\pi\$, and \$\delta\$ orbitals](#) is shared under a [CC BY-SA 4.0](#) license and was authored, remixed, and/or curated by [Chemistry 310 \(Wikibook\)](#) via [source content](#) that was edited to the style and standards of the LibreTexts platform; a detailed edit history is available upon request.

2.5: Diatomic Molecules

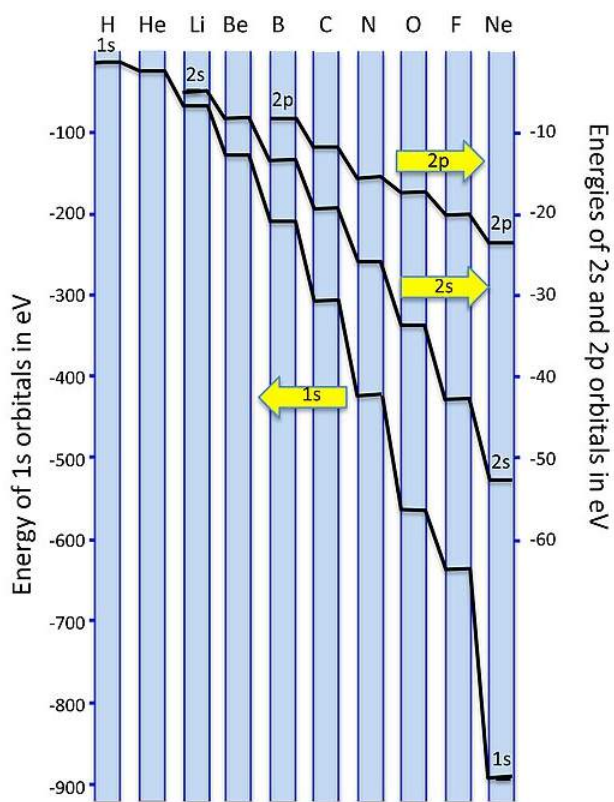
Valence bond theory fails for a number of the second row diatomics, most famously for O_2 , where it predicts a diamagnetic, doubly bonded molecule with four lone pairs. O_2 does have a double bond, but it has two unpaired electrons in the ground state, a property that can be explained by the MO picture. We can construct the MO energy level diagrams for these molecules as follows



We get the simpler diatomic MO picture on the right when the 2s and 2p AOs are well separated in energy, as they are for O, F, and Ne. The picture on the left results from mixing of the σ_{2s} and σ_{2p} MO's, which are close in energy for Li_2 , Be_2 , B_2 , C_2 , and N_2 . The effect of this mixing is to push the σ_{2s}^* down in energy and the σ_{2p} up, to the point where the π orbitals are below the σ_{2p} . Asymmetric diatomic molecules and ions such as CO, NO, and NO^+ also have the ordering of energy levels shown on the left because of sp mixing. A good animation of the molecular orbitals in the CO molecule can be found on the University of Liverpool [Structure and Bonding](#) website.

Why don't we get sp-orbital mixing for O_2 and F_2 ? The reason has to do with the energies of the orbitals, which are not drawn to scale in the simple picture above. As we move across the second row of the periodic table from Li to F, we are progressively adding protons to the nucleus. The 2s orbital, which has finite amplitude at the nucleus, "feels" the increased nuclear charge more than the 2p orbital. This means that as we progress across the periodic table (and also, as we will see later, when we move down the periodic table), the **energy difference between the s and p orbitals increases**. As the 2s and 2p energies become farther apart in energy, there is less interaction between the orbitals (i.e., less mixing).

A plot of orbital energies is shown below. Because of the very large energy difference between the 1s and 2s/2p orbitals, we plot them on different energy scales, with the 1s to the left and the 2s/2p to the right. For elements at the left side of the 2nd period (Li, Be, B) the 2s and 2p energies are only a few eV apart. The energy difference becomes very large - more than 20 electron volts - for O and F. Since single bond energies are typically about 3-4 eV, this energy difference would be very large on the scale of our MO diagrams. For all the elements in the 2nd row of the periodic table, the 1s (core) orbitals are very low in energy compared to the 2s/2p (valence) orbitals, so we don't need to consider them in drawing our MO diagrams.



This page titled [2.5: Diatomic Molecules](#) is shared under a [CC BY-SA 4.0](#) license and was authored, remixed, and/or curated by [Chemistry 310 \(Wikibook\)](#) via [source content](#) that was edited to the style and standards of the LibreTexts platform; a detailed edit history is available upon request.

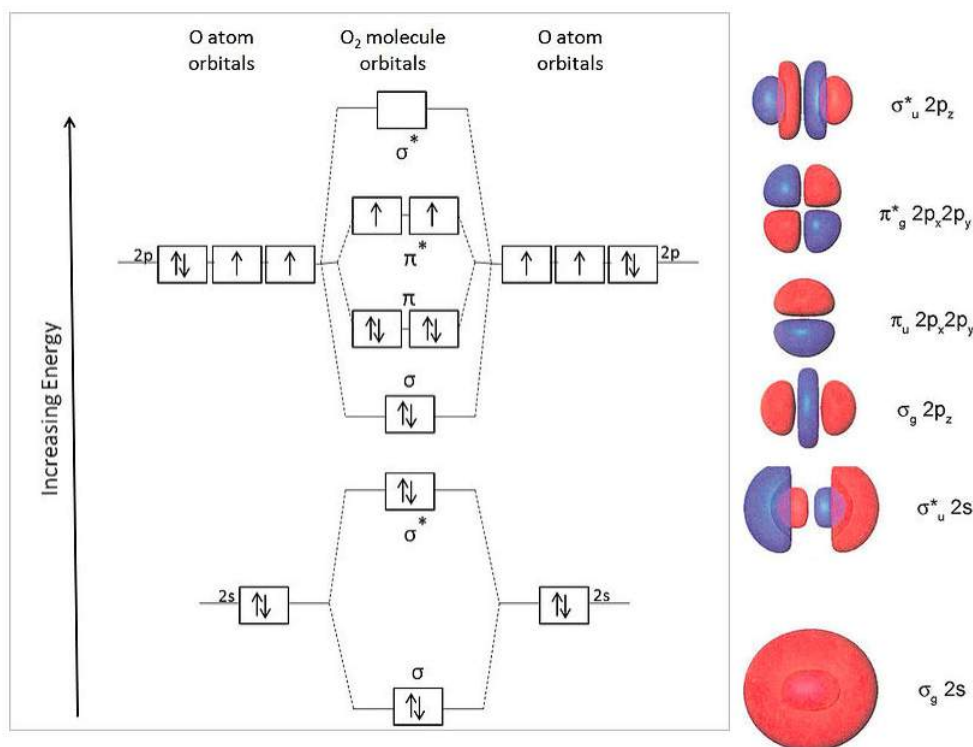
2.6: Orbital Filling

MO's are filled from the bottom according to the **Aufbau principle** and **Hund's rule**, as we learned for atomic orbitals.

Question: what is the quantum mechanical basis of Hund's rule?

Consider the case of two degenerate orbitals, such as the π or π^* orbitals in a second-row diatomic molecule. If these orbitals each contain one electron, their spins can be parallel (as preferred by Hund's rule) or antiparallel. The Pauli exclusion principle says that no two electrons in an orbital can have the same set of quantum numbers (n , l , m_l , m_s). That means that, in the parallel case, the Pauli principle prevents the electrons from ever visiting each other's orbitals. In the antiparallel case, they are free to come and go because they have different m_s quantum numbers. However, having two electrons in the same orbital is energetically unfavorable because like charges repel. Thus, the parallel arrangement, thanks to the Pauli principle, has lower energy.

For O_2 (12 valence electrons), we get the MO energy diagram below. The shapes of the molecular orbitals are shown at the right.



This energy ordering of MOs correctly predicts **two unpaired electrons** in the π^* orbital and a net **bond order of two** (8 bonding electrons and 4 antibonding electrons). This is consistent with the experimentally observed paramagnetism of the oxygen molecule.

Other interesting predictions of the MO theory for second-row diatomics are that the C_2 molecule has a bond order of 2 and that the B_2 molecule has two unpaired electrons (both verified experimentally).

We can also predict (using the O_2 , F_2 , Ne_2 diagram above) that NO has a bond order of 2.5, and CO has a bond order of 3.

The symbols "g" and "u" in the orbital labels, which we only include in the case of centrosymmetric molecules, refer to their symmetry with respect to inversion. *Gerade* (g) orbitals are symmetric, meaning that inversion through the center leaves the orbital unchanged. *Ungerade* (u) means that the sign of the orbital is reversed by the inversion operation. Because g and u orbitals have different symmetries, they have zero overlap with each other. As we will see below, factoring orbitals according to g and u symmetry simplifies the task of constructing molecular orbitals in more complicated molecules, such as butadiene and benzene.

The orbital shapes shown above were computed using a *one-electron model* of the molecule, as we did for hydrogen-like AOs to get the shapes of s, p, and d-orbitals. To get accurate MO energies and diagrams for *multi-electron* molecules (i.e. all real molecules), we must include the fact that electrons are "correlated," i.e. that they avoid each other in molecules because of their negative charge. This problem cannot be solved analytically, and is solved approximately in numerical calculations by using

density functional theory (DFT). We will learn about the consequences of electron correlation in solids (such as superconductors) in Chapter 10.



Red giant stars are characterized by the presence of C_2 molecules in their atmospheres. Since C_2 has a net bond order of two, it reacts rapidly as it cools from the gas phase to make other forms of carbon such as **fullerenes**, **graphite**, and **diamond**, all of which have four bonds for every two carbon atoms.

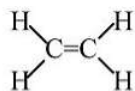
This page titled [2.6: Orbital Filling](#) is shared under a [CC BY-SA 4.0](#) license and was authored, remixed, and/or curated by [Chemistry 310 \(Wikibook\)](#) via [source content](#) that was edited to the style and standards of the LibreTexts platform; a detailed edit history is available upon request.

2.7: Periodic Trends in π Bonding

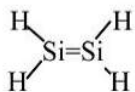
As we noted in Section 2.3, *p π -bonding almost always involves a second-row element.*

We encounter π -bonding from the sideways overlap of p-orbitals in the MO diagrams of second-row diatomics ($B_2 \dots O_2$). It is important to remember that π -bonds are weaker than σ bonds made from the same AOs, and are especially weak if they involve elements beyond the second row.

Example:



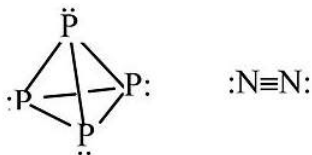
Ethylene: Stable molecule, doesn't polymerize without a catalyst.



Silylene: Never isolated, spontaneously polymerizes. Calculations indicate 117 kJ/mol stability in the gas phase relative to singly-bonded (triplet) $H_2Si-SiH_2$.

The large Ne core of Si atoms inhibits sideways overlap of 3p orbitals \rightarrow weak π -bond.

Other examples: P_4 vs. N_2



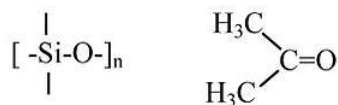
P cannot make π -bonds with itself, so it forms a tetrahedral molecule with substantial ring strain. This allotrope of P undergoes spontaneous combustion in air. Solid white phosphorus very slowly converts to red phosphorus, a more stable allotrope that contains sheets of pyramidal P atoms, each with bonds to three neighboring atoms and one lone pair.



White phosphorus (P_4) is a soft, waxy solid that ignites spontaneously in air, burning with a bright flame and generating copious white P_4O_{10} smoke. The sample shown here is photographed under water to prevent the oxidation reaction

N can make π -bonds, so N_2 has a very strong triple bond and is a relatively inert diatomic gas.

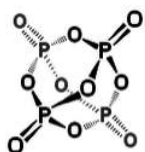
$(CH_3)_2SiO$ vs. $(CH_3)_2CO$



"RTV" silicone polymer (4 single bonds to Si) vs. acetone ($C=O$ double bond). Silicones are soft, flexible polymers that can be heated to high temperatures ($>300^\circ C$) without decomposing. Acetone is a flammable molecular liquid that boils at $56^\circ C$.



Silicone polymers $(R_2SiO)_n$ are used in non-stick cookware like these muffin cups, in Silly Putty, soft robotics, and many other applications.



Exceptions:

2nd row elements can form reasonably strong π -bonds with the *smallest* of the 3rd row elements, P, S, and Cl. Thus we find S=N bonds in sulfur-nitrogen compounds such as S_2N_2 and $S_3N_3^-$; P=O bonds in phosphoric acid and P_4O_{10} (shown above), and a delocalized π -molecular orbital in SO_2 (as in ozone).

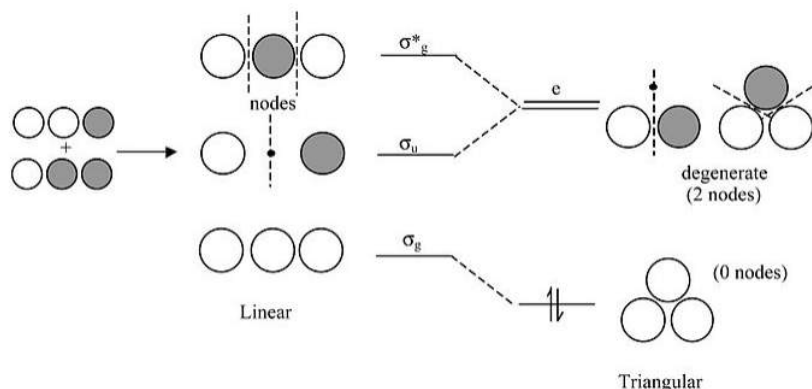
This page titled [2.7: Periodic Trends in \$\pi\$ Bonding](#) is shared under a [CC BY-SA 4.0](#) license and was authored, remixed, and/or curated by [Chemistry 310 \(Wikibook\)](#) via [source content](#) that was edited to the style and standards of the LibreTexts platform; a detailed edit history is available upon request.

2.8: Three-center Bonding

Many (but not all) of the problems we will solve with MO theory derive from the MO diagram of the H_2 molecule (Fig. 2.1.5), which is a case of two-center bonding. The rest we will solve by analogy to the H_3^+ ion, which introduces the concept of three-center bonding.

We can draw the H_3^+ ion (and also H_3 and H_3^-) in either a **linear** or **triangular** geometry.

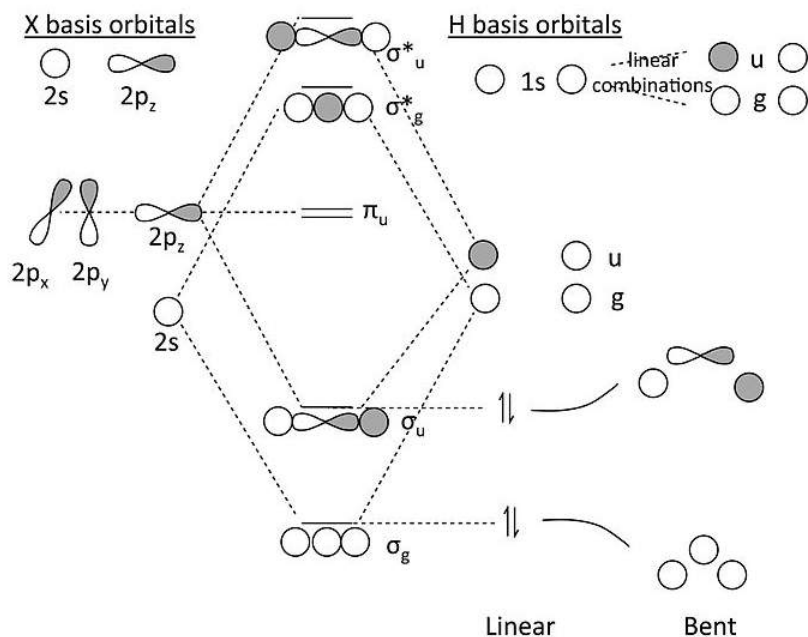
Walsh correlation diagram for H_3^+ :



A few important points about this diagram:

- For the linear form of the ion, the highest and lowest MO's are symmetric with respect to the inversion center in the molecule. Note that the central 1s orbital has **g symmetry**, so by symmetry it has **zero overlap** with the **u combination** of the two 1s orbitals on the ends. This makes the σ_u orbital a **nonbonding** orbital.
- In the triangular form of the molecule, the orbitals that derive from σ_u and σ_g^* become degenerate (i.e., they have identically the same energy by symmetry). The term symbol "e" means **doubly degenerate**. We will see later that "t" means triply degenerate. Note that we drop the "g" and "u" for the triangular orbitals because a triangle does not have an inversion center.
- The **triangular form is most stable** because the two electrons in H_3^+ have lower energy in the lowest orbital. Bending the molecule creates a third bonding interaction between the 1s orbitals on the ends.

MO diagram for XH_2 ($X = Be, B, C...$):



Some key points about this MO diagram:

- In the linear form of the molecule, which has inversion symmetry, the 2s and 2p orbitals of the X atom factor into three symmetry classes:

$$2s = \sigma_g$$

$$2p_z = \sigma_u$$

$$2p_x, 2p_y = \pi_u$$

- Similarly, we can see that the two H 1s orbitals make two linear combinations, one with σ_g symmetry and one with σ_u symmetry. They look like the bonding and antibonding MO's of the **H₂ molecule** (which is why we say we use that problem to solve this one).
- The π_u orbitals must be **non-bonding** because there is no combination of the H 1s orbitals that has π_u symmetry.
- In the MO diagram, we make bonding and antibonding combinations of the σ_g 's and the σ_u 's. For BeH₂, we then populate the lowest two orbitals with the four valence electrons and discover (not surprisingly) that the molecule has **two bonds** and can be written **H-Be-H**. The correlation diagram shows that a bent form of the molecule should be **less stable**.

An interesting story about this MO diagram is that it is difficult to predict a priori whether CH₂ should be linear or bent. In 1970, Charles Bender and Henry Schaefer, using quantum chemical calculations, predicted that the ground state should be a bent triplet with an H-C-H angle of 135°. [4] The best experiments at the time suggested that methylene was a linear singlet, and the theorists argued that the experimental result was wrong. *Later experiments proved them right!*

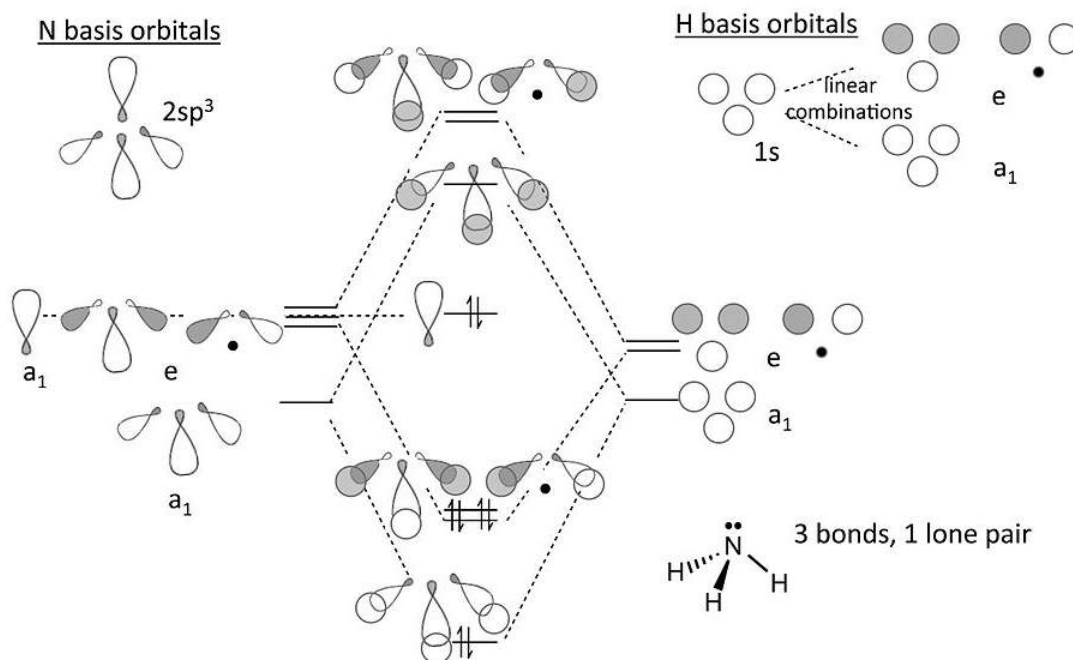
“A theory is something nobody believes, except the person who made it. An experiment is something everybody believes, except the person who made it.” – Einstein

This page titled [2.8: Three-center Bonding](#) is shared under a [CC BY-SA 4.0](#) license and was authored, remixed, and/or curated by [Chemistry 310 \(Wikibook\)](#) via [source content](#) that was edited to the style and standards of the LibreTexts platform; a detailed edit history is available upon request.

2.9: Building up the MOs of More Complex Molecules- NH₃, P₄

MO diagram for NH₃

We can now attempt the MO diagram for NH₃, building on the result we obtained with triangular H₃⁺.

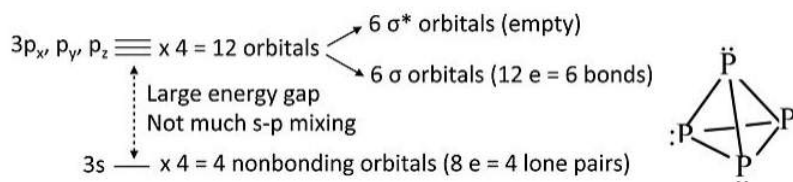


Notes on the MO diagram for ammonia:

- Viewed end-on, a p-orbital or an sp_x hybrid orbital looks just like an s-orbital. Hence we can use the solutions we developed with s-orbitals (for H₃⁺) to set up the σ bonding and antibonding combinations of nitrogen sp³ orbitals with the H 1s orbitals.
- We now construct the sp³ hybrid orbitals of the nitrogen atom and orient them so that one is "up" and the other three form the triangular base of the tetrahedron. The latter three, by analogy to the H₃⁺ ion, transform as one totally symmetric orbital ("a₁") and an e-symmetry pair. The hybrid orbital at the top of the tetrahedron also has a₁ symmetry.
- The three hydrogen 1s orbitals also make one a₁ and one (doubly degenerate) e combination. We make bonding and antibonding combinations with the nitrogen orbitals of the same symmetry. The remaining a₁ orbital on N is non-bonding. The dotted lines show the correlation between the basis orbitals of a₁ and e symmetry and the molecular orbitals
- The result in the 8-electron NH₃ molecule is **three N-H bonds** and **one lone pair** localized on N, the **same as the valence bond picture** (but much more work!).

P₄ molecule and P₄²⁺ ion:

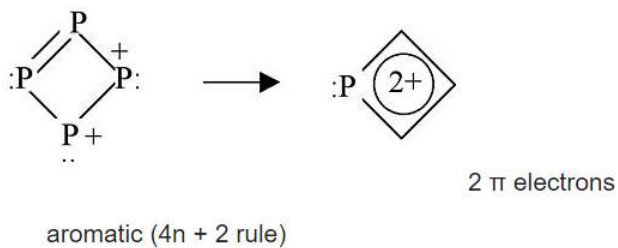
By analogy to NH₃ we can construct the MO picture for one vertex of the P₄ tetrahedron, and then multiply the result by 4 to get the bonding picture for the molecule. An important difference is that there is relatively little s-p hybridization in P₄, so the lone pair orbitals have more s-character and are lower in energy than the bonding orbitals, which are primarily pσ.



Take away 2 electrons to make P₄²⁺

Highest occupied MO is a bonding orbital → *break one bond, 5 bonds left*

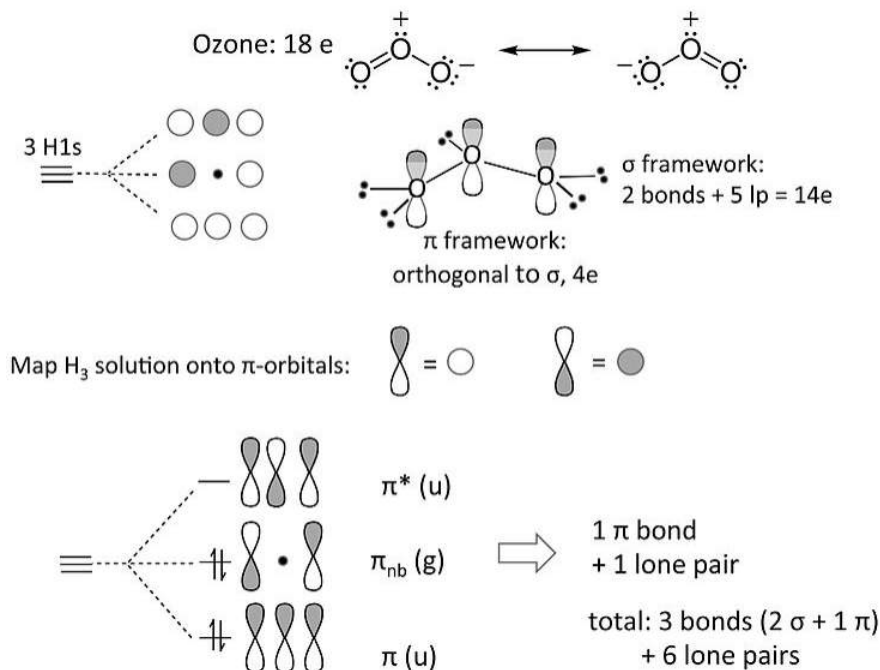
Square form relieves ring strain, ($60^\circ \rightarrow 90^\circ$)



This page titled [2.9: Building up the MOs of More Complex Molecules- NH₃, P₄](#) is shared under a [CC BY-SA 4.0](#) license and was authored, remixed, and/or curated by [Chemistry 310 \(Wikibook\)](#) via [source content](#) that was edited to the style and standards of the LibreTexts platform; a detailed edit history is available upon request.

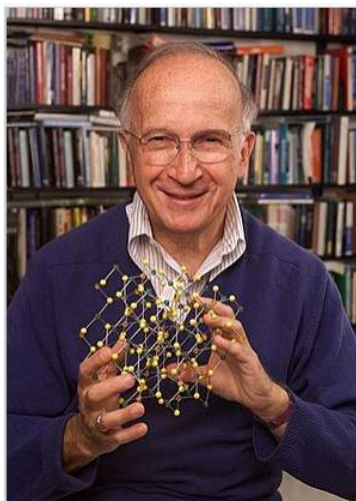
2.10: Homology of σ and π orbitals in MO diagrams

The **ozone molecule** (and related 18e molecules that contain three non-H atoms, such as NO_2^- and the allyl anion $[\text{CH}_2\text{-CH-CH}_2]^-$) is an example of **3-center 4-electron** π -bonding. Our MO treatment of ozone is entirely analogous to the 4-electron H_3^- anion. We map that solution onto this one as follows:



The nonbonding π -orbital has a node at the central O atom. This means that the non-bonding electron pair in the π -system is shared by the two terminal O atoms, i.e., that the formal charge is shared by those atoms. This is consistent with the octet resonance structure of ozone.

This trick of mapping the solution for a set of s-orbitals onto a π -bonding problem is a simple example of a broader principle called the **isolobal analogy**. This idea, developed extensively by Roald Hoffmann at Cornell University, has been used to understand bonding and reactivity in organometallic compounds.^[5] In the isolobal analogy, symmetry principles (as illustrated above in the analogy between H_3^- and ozone) are used to construct MO diagrams of complex molecules containing d-frontier orbitals from simpler molecular fragments.



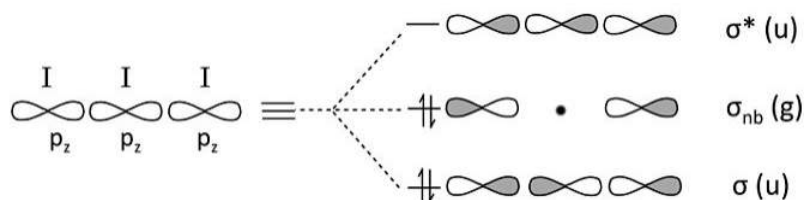
Professor Roald Hoffmann's ideas about orbital symmetry have helped explain the bonding and reactivity of organic and organometallic molecules, and also the structures and properties of extended solids.

The triiodide ion. An analogous (and seemingly more complicated) case of 3-center 4-electron bonding is I_3^- . Each I atom has 4 valence orbitals (5s, 5p_x, 5p_y, 5p_z), making a total of 12 frontier orbitals, and the I_3^- anion has 22 electrons.

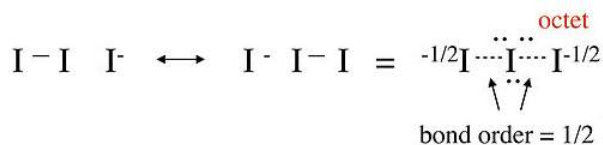
We can simplify the problem by recalling two periodic trends:

- The s-p orbital splitting is large, relative to the bond energy, after the second row of the periodic table. Thus, the 5s orbital is low in energy and too contracted to make bonds with its neighbors.
- π -overlap of 5p orbitals is very weak, so the 5p_x and 5p_y orbitals will also be non-bonding.

This leaves only the three 5p_z orbitals to make bonding/nonbonding/antibonding combinations. Again, the problem is entirely analogous to ozone or H₃⁺.

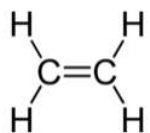


Counting orbitals we obtain 9 lone pairs from the nonbonding 5s, 5p_x, and 5p_y orbitals, as well as one bond and one lone pair from the 5p_z orbital combinations above. The total of 10 nonbonding pairs and one bond accounts for the 22 electrons in the ion. The non-bonding 5p_z pair is localized on the terminal I atoms, giving each a -1/2 formal charge. This MO description is entirely consistent with the octet no-bond resonance picture of I_3^- that we developed in Chapter 1.

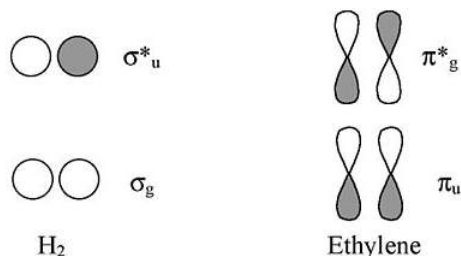


This page titled [2.10: Homology of \$\sigma\$ and \$\pi\$ orbitals in MO diagrams](#) is shared under a [CC BY-SA 4.0](#) license and was authored, remixed, and/or curated by [Chemistry 310 \(Wikibook\)](#) via [source content](#) that was edited to the style and standards of the LibreTexts platform; a detailed edit history is available upon request.

2.11: Chains and Rings of π -Conjugated Systems

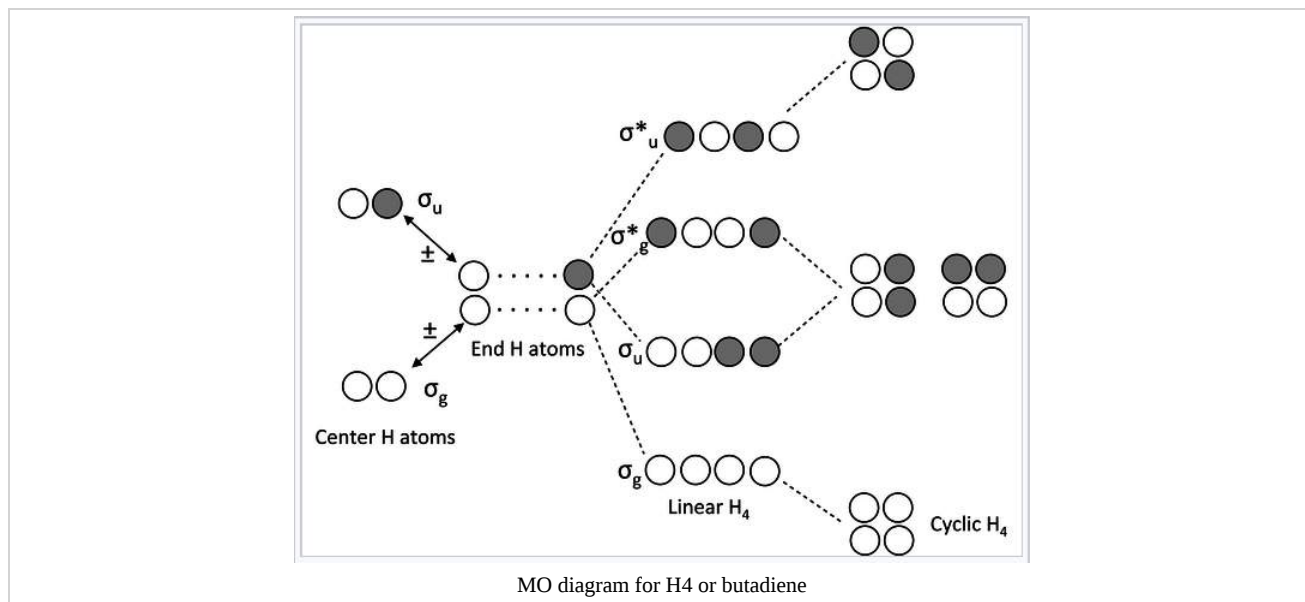


Ethylene: The π system is analogous to σ -bonding in H_2



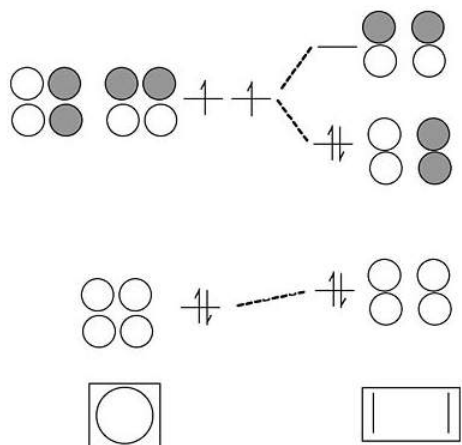
Viewed from the top or bottom, the ethylene π -orbitals look like the H_2 σ orbitals. Thus we can map solutions from chains and rings of H atoms onto chains and rings of π -orbitals (as we did for the three-orbital case of O_3).

Chains and rings of four H atoms or π -orbitals (H_4 or butadiene):



A few notes about this MO diagram:

- In the linear form of the molecule, the combination of AOs makes a *ladder* of evenly spaced energy levels that alternate $g - u - g - u \dots$. Each successive orbital has one more node. This is a general rule for linear chains of σ or π orbitals with even numbers of atoms.
- In the cyclic form of the molecule, there is one non-degenerate orbital at the bottom, one at the top, and a ladder of doubly degenerate orbitals in between. This is also a general rule for cyclic molecules with even numbers of atoms. This is the origin of the **$4n+2$ rule** for aromatics.
- H_4 has four valence electrons, and by analogy butadiene has four π -electrons. These electrons fill the lowest two MOs in the linear form of the molecule, corresponding to two conjugated π -bonds in butadiene ($H_2C=CH-CH=CH_2$).
- In the cyclic form of the molecule, the degenerate orbitals are singly occupied. The molecule can break the degeneracy (and lower its energy) by distorting to a puckered rectangle. This is a general rule for **anti-aromatic** cyclic molecules ($4n$ rule). Thus *cyclobutadiene should be anti-aromatic* and have two single and two double bonds that are not delocalized by resonance.

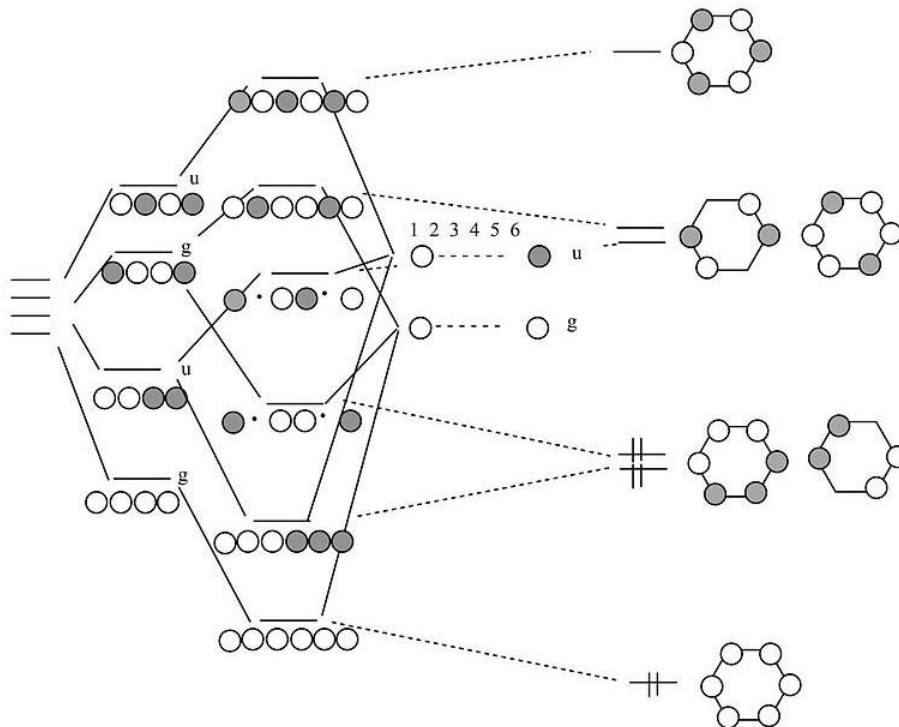


Cyclobutadiene is actually a very unstable molecule because it polymerizes to relieve ring strain. Sterically hindered derivatives of the molecule do have the puckered rectangular structure predicted by MO theory.

Benzene π -orbitals:

How do we get from a 4-atom to 6-atom chain?

By analogy to the process we used to go from a 2-atom chain to a 4-atom chain, we now go from 4 to 6. We start with the orbitals of the 4-atom chain, which form a ladder of g and u orbitals. Then we make g and u combinations of the two atoms that we are adding at the ends. By combining g's with g's and u's with u's, we end up with the solutions for a string of 6 atoms. Closing these orbitals into a loop gives us the π molecular orbitals of the benzene molecule. The result is three π bonds, as we expected. Benzene fits the $4n+2$ rule ($n=2$) and is therefore aromatic.



Here we have used the isolobal analogy to construct MO diagrams for π -bonded systems, such as ethylene and benzene, from combinations of s-orbitals. It raises the interesting question of whether the aromatic $4n+2$ rule might apply to s-orbital systems, i.e.,

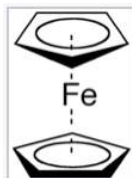
if three molecules of H_2 could get together to form an aromatic H_6 molecule. In fact, recent studies of hydrogen under ultra-high pressures in a diamond anvil cell show that such structures do form. A solid hydrogen phase exists that contains sheets of distorted six-membered rings, analogous to the fully connected 2D network of six-membered rings found in graphite or graphene.^[6]

It should now be evident from our construction of MO diagrams for four- and six-orbital molecules that we can keep adding atomic orbitals to make chains and rings of 8, 10, 12... atoms. In each case, the g and u orbitals form a ladder of MOs. At the bottom rung of the ladder of an N-atom chain, there are no nodes in the MO, and we add one node for every rung until we get to the top, where there are N-1 nodes. Another way of saying this is that the *wavelength* of an electron in orbital x, counting from the bottom (1,2,3...x,...N), is $2Na/x$, where a is the distance between atoms. We will find in Chapters 6 and 10 that we can learn a great deal about the electronic properties of metals and semiconductors from this model, using the infinite chain of atoms as a model for the crystal.

This page titled [2.11: Chains and Rings of \$\pi\$ -Conjugated Systems](#) is shared under a [CC BY-SA 4.0](#) license and was authored, remixed, and/or curated by [Chemistry 310 \(Wikibook\)](#) via [source content](#) that was edited to the style and standards of the LibreTexts platform; a detailed edit history is available upon request.

2.12: Discussion Questions

- Derive the molecular orbital diagrams for linear and bent H_2O .
- Explain why the bond angles in H_2O and H_2S are different.
- We have derived the MO diagrams for the pi-systems of four- and six-carbon chains and rings. Repeat this exercise for a 5-carbon chain and 5-carbon ring (e.g., the cyclopentadienide anion), starting from the MO pictures for H_2 and H_3 . This tricky problem helps us understand the electronic structure of ferrocene, and was the subject of a Nobel prize in 1973.



Ferrocene

This page titled [2.12: Discussion Questions](#) is shared under a [CC BY-SA 4.0](#) license and was authored, remixed, and/or curated by [Chemistry 310 \(Wikibook\)](#) via [source content](#) that was edited to the style and standards of the LibreTexts platform; a detailed edit history is available upon request.

2.13: Problems

- The ionization energy of a hydrogen atom is 1312 kJ/mol and the bond dissociation energy of the H_2^+ molecular ion is 256 kJ/mol. The overlap integral S for the H_2^+ molecular ion is given by the expression $S = (1 + R/a_0 + R^2/3a_0^2)\exp(-R/a_0)$, where R is the bond distance (1.06 Å) and a_0 is the Bohr radius, 0.529 Å. What are the values of α and β (in units of kJ/mol) for H_2^+ ?
- Compare the bond order in H_2^+ and H_2 using the molecular orbital energy diagram for H_2 . The bond dissociation energy of the H_2 molecule is 436 kJ/mol. Explain why this energy is less than twice that of H_2^+ .
- What is the bond order in HHe ? Why has this compound never been isolated?
- Would you expect the Be_2 molecule to be stable in the gas phase? What is the total bond order, and how many net σ and π bonds are there?
- Give a plausible explanation for the following periodic trend in F-M-F bond angles for gas-phase alkali difluoride (MF_2) molecules. (Hint - it has something to do with a trend in s- and p-orbital energies; see Chapter 1, section 1.2)

Compound	F-M-F angle (degrees)
BeF_2	180
MgF_2	158
CaF_2	140
SrF_2	108
BaF_2	100

- The most stable allotrope of nitrogen is N_2 , but the analogous phosphorus molecule (P_2) is unknown. Explain.
- Using molecular orbital theory, show why the H_3^+ ion has a triangular rather than linear shape.
- Use MO theory to determine the bond order and number of unpaired electrons in (a) O_2^- , (b) O_2^+ , (c) gas phase BN , and (d) NO^- . Estimate the bond lengths in O_2^- and O_2^+ using the Pauling formula, and the bond length in the O_2 molecule (1.21 Å).
- Compare the results of MO theory and valence bond theory for describing the bonding in (a) CN^- and (b) neutral CN . Is it possible to have a bond order greater than 3 in a second-row diatomic molecule?
- The C_2 molecule, which is a stable molecule only in the gas phase, is the precursor to fullerenes and carbon nanotubes. Its luminescence is also responsible for the green glow of comet tails. Draw the molecular orbital energy diagram for this molecule. Determine the bond order and the number of unpaired electrons.
- Use the Pauling formula to estimate the bond order in C_2 from the bond distance, 1.31 Å. The C-C single bond distance in ethane is 1.54 Å. Does your calculation agree with your answer to problem 11? What bond order would valence bond theory predict for C_2 ?
- Draw the MO diagram for the linear $[\text{FHF}]^-$ ion. The only orbitals you need to worry about are the frontier orbitals, i.e., the H 1s and the two F sp_z hybrid orbitals that lie along the bonding (z) axis. What is the order of the HF bonds? What are the formal charges on the atoms?
- The cyclooctatetraene (cot) molecule (picture a stop sign with four double bonds) has a puckered ring structure. However in $\text{U}(\text{cot})_2$, where the oxidation state of uranium is 4+ and the cot ligand has a formal charge of 2-, the 8-membered rings are planar. Why is cot^{2-} planar?

This page titled [2.13: Problems](#) is shared under a [CC BY-SA 4.0](#) license and was authored, remixed, and/or curated by [Chemistry 310 \(Wikibook\)](#) via [source content](#) that was edited to the style and standards of the LibreTexts platform; a detailed edit history is available upon request.

2.14: References

1. More precisely, in the case of a complex wavefunction ϕ , the probability is the product of ϕ and its complex conjugate ϕ^*
 2. Hoffmann, R. (1963). "An Extended Hückel Theory. I. Hydrocarbons." *J. Chem. Phys.* **39** (6): 1397–1412.
doi:[10.1063/1.1734456](https://doi.org/10.1063/1.1734456). Bibcode: [1963JChPh..39.1397H](https://doi.org/10.1063/1.1734456).
 3. Cotton, F. A.; Harris, C. B. *Inorg. Chem.*, 1965, 4 (3), 330-333. DOI|[10.1021/ic50025a015](https://doi.org/10.1021/ic50025a015)
 4. C. F. Bender and H. F. Schaefer III, New theoretical evidence for the nonlinearity of the triplet ground state of methylene, *J. Am. Chem. Soc.* 92, 4984–4985 (1970).
 5. Hoffmann, R. (1982). "Building Bridges Between Inorganic and Organic Chemistry (Nobel Lecture)". *Angew. Chem. Int. Ed.* **21** (10): 711–724. doi:[10.1002/anie.198207113](https://doi.org/10.1002/anie.198207113).
 6. I. Naumov and R. J. Hemley, *Acc. Chem. Res.* 47, 3551–3559 (2014) [dx.doi.org/10.1021/ar5002654](https://doi.org/10.1021/ar5002654).
-

This page titled [2.14: References](#) is shared under a [CC BY-SA 4.0](#) license and was authored, remixed, and/or curated by [Chemistry 310 \(Wikibook\)](#) via [source content](#) that was edited to the style and standards of the LibreTexts platform; a detailed edit history is available upon request.

CHAPTER OVERVIEW

3: Acid-Base Chemistry

Learning Objectives

- Understand the Brønsted and Lewis definitions of acids and bases.
- Identify conjugate acids and bases, and rules for strong & weak acids/bases, in both Brønsted and Lewis acid-base systems.
- Use Pauling's rules to predict the pK_a s of oxoacids.
- Understand the periodic trends of acidic, basic, and amphoteric compounds
- Predict, describe, and rationalize acid/base chemistry in non-aqueous systems, including acidic and basic solvents, aprotic solvents, and molten salts.
- Apply the principles of acid-base chemistry to the design of molecules and Lewis acids with target functions.
- Understand the connection between acid-base chemistry and the stabilization of oxidation states.
- Predict favorable and stable compounds using hard-soft acid-base (HSAB) theory.
- Understand the applications of the ECW model.

Acid-base reactions form the basis of the most common kinds of equilibrium problems which you will encounter in almost any application of chemistry. There are three major classifications of acids and bases: (1) The Arrhenius definition states that an acid produces H^+ in solution and a base produces OH^- and the (2) Brønsted-Lowry and (3) Lewis definitions of acids and bases. Of particular importance in inorganic chemistry is the "hard and soft (Lewis) acids and bases" (HSAB) theory that is widely used for explaining stability of compounds, reaction mechanisms, and reaction pathways.

[3.1: Prelude to Acid-Base Chemistry](#)

[3.2: Brønsted and Lewis Acids and Bases](#)

[3.3: Hard and Soft Acids and Bases](#)

[3.4: The Electrostatic-Covalent \(ECW\) Model for Acid-Base Reactions](#)

[3.5: Frustrated Lewis Pairs](#)

[3.6: Discussion Questions](#)

[3.7: Problems](#)

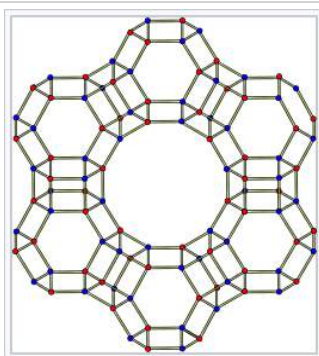
[3.8: References](#)

This page titled [3: Acid-Base Chemistry](#) is shared under a [CC BY-SA 4.0](#) license and was authored, remixed, and/or curated by [Chemistry 310 \(Wikibook\)](#) via [source content](#) that was edited to the style and standards of the LibreTexts platform; a detailed edit history is available upon request.

3.1: Prelude to Acid-Base Chemistry

Acids and bases are important for a number reasons in inorganic chemistry.

- Many industrially useful catalytic reactions involve inorganic acids and superacids, such as zeolites, anhydrous hydrogen fluoride, and sulfated zirconia. These acids are sufficiently strong in anhydrous media that they can protonate olefins and alcohols to produce carbocations. Carbocations are key intermediates in the transformations of hydrocarbons.
- Inorganic compounds are sometimes synthesized in strongly acidic or basic media. For example, ternary metal oxides can be synthesized and crystallized in molten NaOH or KOH, which are strongly basic. Organic fluorination reactions are often done in strongly acidic media, such as anhydrous HF. Understanding the familiar chemistry of acids and bases in water helps us understand how these non-aqueous media work.
- The acidic or basic environment of metal ions affects the stability of their oxidation states. We will learn more about this in Chapter 4.
- Transition metal complexes (coordination compounds and organometallic compounds) are essentially Lewis acid-base complexes. We can understand a great deal about their stability and reactivity by considering the acid-base character of metals and ligands. We will learn about this in Chapter 5.



Solid acid catalysts, such as zeolite Y, are used to isomerize hydrocarbons in the processing of crude oil into gasoline. Edith Flanigen (below with President Barack Obama) received the 2014 National Medal of Technology for her research on the synthesis of zeolite Y.

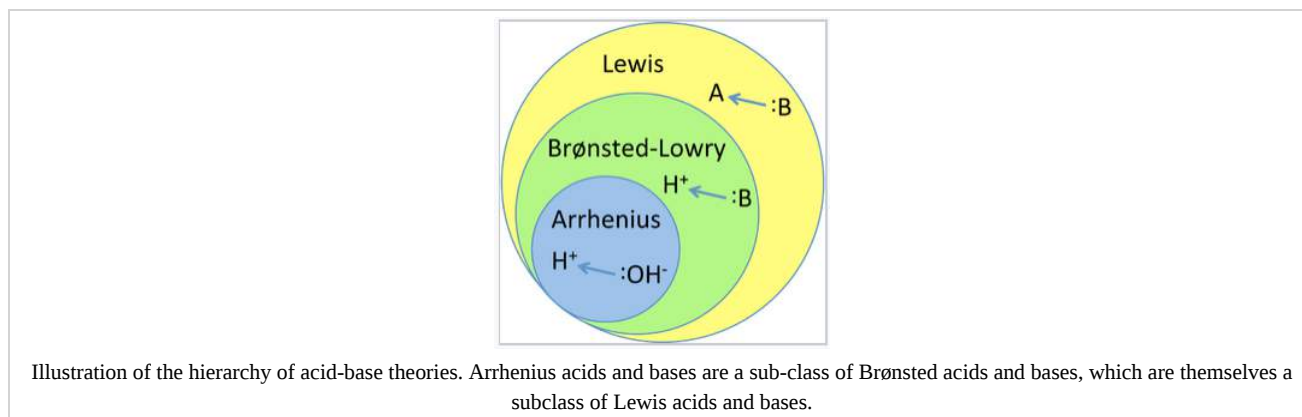


This page titled [3.1: Prelude to Acid-Base Chemistry](#) is shared under a [CC BY-SA 4.0](#) license and was authored, remixed, and/or curated by [Chemistry 310 \(Wikibook\)](#) via [source content](#) that was edited to the style and standards of the LibreTexts platform; a detailed edit history is available upon request.

3.2: Brønsted and Lewis Acids and Bases

Three theories of acids and bases

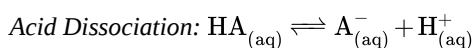
There are three major classifications of substances known as acids or bases. The Arrhenius definition states that an acid produces H^+ in solution and a base produces OH^- . This theory was developed by Svante Arrhenius in 1883. Later, two more sophisticated and general theories were proposed. These are the Brønsted-Lowry and the Lewis definitions of acids and bases. The relationship between these theories is illustrated in the figure below.



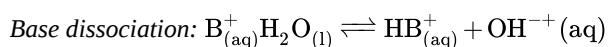
The Arrhenius theory, which is the simplest and least general description of acids and bases, includes acids such as $HClO_4$ and bases such as $NaOH$ or $Mg(OH)_2$. This theory successfully describes how acids and bases react with each other to make water and salts. However, it does not explain why some substances that do not contain hydroxide ions, for example F^- and NO_2^- , can make basic solutions in water. The Brønsted-Lowry definition of acids and bases addresses this problem. In this theory an **acid is a substance that can release a proton** (like in the Arrhenius theory) and a **base is a substance that can accept a proton**. A basic salt such as Na^+F^- generates OH^- ions in water by taking protons from water itself (to make HF):



When a Brønsted acid dissociates, it increases the concentration of hydrogen ions in the solution, $[H^+]$; conversely, Brønsted bases dissociate by taking a proton from the solvent (water) to generate $[OH^-]$.



$$K_a = \frac{[A^-][H^+]}{[HA]} \quad (3.2.2)$$



$$K_b = \frac{[HB^+][OH^-]}{[B]} \quad (3.2.3)$$

Conjugate acids and bases

One important consequence of these equilibria is that every **acid** (HA) has a **conjugate base** (A^-), and vice-versa. In the base dissociation equilibrium above the conjugate acid of base B is HB^+ .

For a given acid or base, these equilibria are linked by the water dissociation equilibrium:

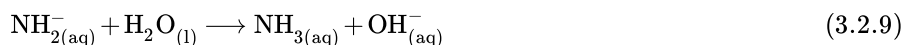
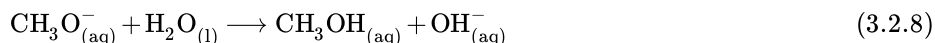
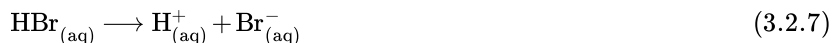


$$K_w = [H^+][OH^-] \quad (3.2.5)$$

for which the equilibrium constant K_w is 1.00×10^{-14} at $25^\circ C$. It can be easily shown that the product of the acid and base dissociation constants K_a and K_b is K_w .

Strong and weak acids and bases

Acids and bases that dissociate completely are said to be strong:



Here the right-handed arrow (\longrightarrow) implies that the reaction goes to completion. That is, a 1.0 M solution of HClO_4 in water actually contains 1.0 M H^+ (aq) and 1.0 M ClO_4^- (aq), and very little undissociated HClO_4 .

Conversely, weak acids such as acetic acid (CH_3COOH) and weak bases such as ammonia (NH_3) dissociate only slightly in water - typically a few percent, depending on their concentration and the values of K_a and K_b - and exist mostly as the undissociated molecules.



Antacid tablets typically contain calcium salts of the bicarbonate ion (HCO_3^-), a weak base. Its conjugate acid, carbonic acid (H_2CO_3) is a weak acid. The acid-base equilibrium between carbonic acid and bicarbonate is important in maintaining blood pH.

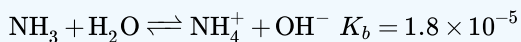
Example

Household ammonia is a solution of NH_3 in water that ranges from about 5-10% by weight. Let's calculate the percent ionization and the pH of the solution.

Solution

For a solution that is 8% ammonia by weight, assuming that the density is about the same as that of liquid water, the analytical concentration of ammonia is $(80 \text{ g/L}) / (17 \text{ g/mol}) = 4.7 \text{ M}$.

The other thing we need to know to solve this problem is the base dissociation constant, K_b .



We can solve this problem rigorously by invoking both charge balance ($[\text{H}^+] + [\text{NH}_4^+] = [\text{OH}^-]$) and mass balance ($4.7 \text{ M} = [\text{NH}_3] + [\text{NH}_4^+]$) and using $K_w = [\text{H}^+][\text{OH}^-]$. But because the algebra becomes complicated with that method - leading to a cubic equation that is hard to solve - we'll invoke two simplifying assumptions:

$$[\text{NH}_4^+] \approx [\text{OH}^-] \gg [\text{H}^+] \quad (\text{which is a reasonable assumption for a basic solution})$$

and

$$[\text{NH}_3] \gg [\text{NH}_4^+] \quad (\text{also reasonable if the percent ionization is small})$$

Now we can write:

$$[\text{NH}_4^+][\text{OH}^-] \approx [\text{OH}^-]^2 = (4.7 \text{ M})(K_b) = 8.4 \times 10^{-5}$$

$$[\text{OH}^-] = 9.2 \times 10^{-3} \text{ M} (\approx [\text{NH}_4^+]), \quad [\text{H}^+] = \frac{K_w}{[\text{OH}^-]} = 1.1 \times 10^{-12} \text{ M}, \quad \text{pH} = 11.97$$

The percent ionization is:

$$100\% \times 9.2 \times 10^{-3} M / 4.7 M = \mathbf{0.19\%}$$

This example illustrates that it is technically incorrect to label a bottle of aqueous ammonia as “ammonium hydroxide,” since only about 2/10 of one percent of the weak base exists in that form.

Conjugate acids and bases

A common misconception is that strong acids have weak conjugate bases, and that weak acids have strong conjugate bases. It is easy to see that this is incorrect by remembering that $K_a K_b = K_w$. Our definition of a strong acid or base is that $K \gg 1$, i.e., that the substance dissociates completely. Our definition of a weak acid or base is $1 > K > K_w$. It follows that if $K_a \gg 1$ (strong) then K_b cannot be $> K_w$ (weak).

In fact, **strong acids** such as HCl dissociate to produce **spectator ions** such as Cl^- as conjugate bases, whereas **weak acids** produce **weak conjugate bases**. This is illustrated below for acetic acid and its conjugate base, the acetate anion. Acetic acid is a weak acid ($K_a = 1.8 \times 10^{-5}$) and acetate is a weak base ($K_b = \frac{K_w}{K_a} = 5.6 \times 10^{-10}$)



The strength of a conjugate acid/base varies inversely with the strength or weakness of its parent acid or base. Any acid or base is technically a conjugate acid or conjugate base also; these terms are simply used to identify species in solution (i.e. acetic acid is the conjugate acid of the acetate anion, a base, while acetate is the conjugate base of acetic acid, an acid).

Neutral oxyacids (H_2SO_4 , H_3PO_4 , HNO_3 , HClO_2 , etc.) can be classified as strong or weak following a simple rule first noted by Linus Pauling. If the number of oxygen atoms exceeds the number of hydrogen atoms by two or more, then the acid is strong; otherwise it is weak. For example HClO_4 and HClO_3 , where the difference is 3 and 2, respectively, are both strong acids. HNO_2 and HClO_2 are both weak because the difference is 1 in both cases. For weak acids, the relative strength depends on this difference (i.e., HClO_2 is a stronger weak acid than HOCl) and on the electronegativity of the central atom (HOCl is stronger than HOI).

Acids that can donate more than one proton are called **polyprotic acids**. For example, sulfuric acid, H_2SO_4 , is a strong acid that has a conjugate base that actually happens to be a weak acid itself. This means that every mole of H_2SO_4 in aqueous solution donates more than 1 mole of protons. Carbonic acid (H_2CO_3) and phosphoric acid (H_3PO_4) are weak polyprotic acids. Typically, the sequential $\text{p}K_a$'s of polyprotic acid are separated by about 5 pH units, because it becomes progressively more difficult to remove protons as the ion becomes more negatively charged. For example, the three $\text{p}K_a$'s of phosphoric acid are 2.15, 7.20, and 12.35.

Amphoteric compounds

Some substances can act either as an acid and as a base. An example is water. H_2O molecules may either donate a hydrogen ion or accept one. This property makes water an **amphoteric** solvent. In the situation where an acid dissociates in solution, water is acting as a base. Conversely, water acts as an acid when bases dissociate. The strongest acid we can make in H_2O is H^+ (aq), and the strongest base we can make in H_2O is OH^- (aq).

Other examples of amphoteric compounds are oxides and hydroxides of elements that lie on the border between the metallic and non-metallic elements in the periodic table. For example, aluminum hydroxide ($\text{Al}(\text{OH})_3$) is insoluble at neutral pH, but can accept protons in acid to make $[\text{Al}(\text{H}_2\text{O})_6]^{3+}$ or accept an OH^- ion in base to form $\text{Al}(\text{OH})_4^-$ ions. Consequently, aluminum oxide is soluble in acid and in base, but not neutral water. Other examples of amphoteric oxides are BeO , ZnO , Ga_2O_3 , Sb_2O_3 , and PbO . Increasing the oxidation state of a metal increases the acidity of its oxide by withdrawing electron density from the oxygen atoms. Thus, Sb_2O_5 is acidic, but Sb_2O_3 is amphoteric.

Group 1	2	13	14	15	16	17
Li ₂ O	BeO	B ₂ O ₃	CO ₂	N ₂ O ₃ N ₂ O ₅	O	OF ₂
Na ₂ O	MgO	Al ₂ O ₃	SiO ₂	P ₂ O ₃ P ₂ O ₅	SO ₂ SO ₃	Cl ₂ O Cl ₂ O ₇
K ₂ O	CaO	Ga ₂ O ₃	GeO ₂	As ₂ O ₅ As ₂ O ₃	SeO ₂ SeO ₃	Br ₂ O
Rb ₂ O	SrO	In ₂ O ₃ In ₂ O	SnO ₂	Sb ₂ O ₅ Sb ₂ O ₃	TeO ₂	I ₂ O ₅
Cs ₂ O	BaO	Tl ₂ O	PbO ₂ PbO	Bi ₂ O ₃	Po	At

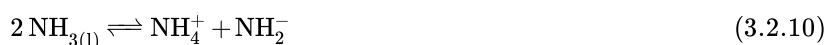
Periodic table showing basic (blue), amphoteric (green) and acidic (red) oxides. The metal-nonmetal boundary is indicated by the gray staircase line.

Solvent leveling

Solvent leveling is an effect that occurs when a strong acid is placed in a solvent such as (but not limited to) H₂O. Because strong acids donate their protons to the solvent, the strongest possible acid that can exist is the conjugate acid of the solvent. In aqueous solution, this is H₃O⁺. This means that the strength of acids such as HCl and HBr cannot be differentiated in water as they both are dissociated 100% to H₃O⁺. In the context of our discussion of conjugate bases above, we would say that both Cl⁻ and Br⁻ are spectator ions in water: neither one is a strong enough base to accept a proton from H₃O⁺. In order to differentiate the acidities of strong acids such as HClO₄ and HCl, or the basicities of strong bases such as CH₃O⁻ and NH₂⁻, we must typically work in non-aqueous solvents, as explained below.

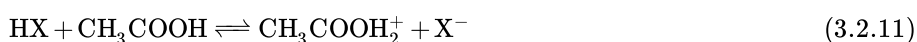
Nonaqueous solutions

The Brønsted theory encompasses any type of solvent that can donate and accept H⁺ ions, not just aqueous solutions. The strength of an acid or a base varies depending on the solvent. Non-aqueous acid-base chemistry follows similar rules to those developed for acids and bases in water. For example in liquid ammonia, the solvent autodissociates in the reaction:



This equilibrium is analogous to the autodissociation of water, but has a smaller equilibrium constant ($K \approx 10^{-30}$). It follows by analogy to water that NH₄⁺ is the strongest acid and NH₂⁻ is the strongest base that can exist in liquid ammonia. Because ammonia is a basic solvent, it enhances the acidity and suppresses the basicity of substances dissolved in it. For example, the ammonium ion (NH₄⁺) is a weak acid in water ($K_a = 6 \times 10^{-10}$), but it is a strong acid in ammonia. Similarly, acetic acid is weak in water but strong in ammonia. Solvent leveling in fact makes HCl, CH₃COOH, and NH₄Cl all strong acids in ammonia, where they have equivalent acid strength.

Strong acids that are leveled in water have different acid strengths in acidic solvents such as HF or anhydrous acetic acid. For example, acid dissociation of HX in acetic acid (CH₃COOH) involves protonating the solvent to make its conjugate acid (CH₃COOH₂⁺) and the X⁻ anion. Because CH₃COOH₂⁺ is a stronger acid than H₃O⁺, the anion X⁻ (which is a spectator in water) can become a weak base in CH₃COOH:



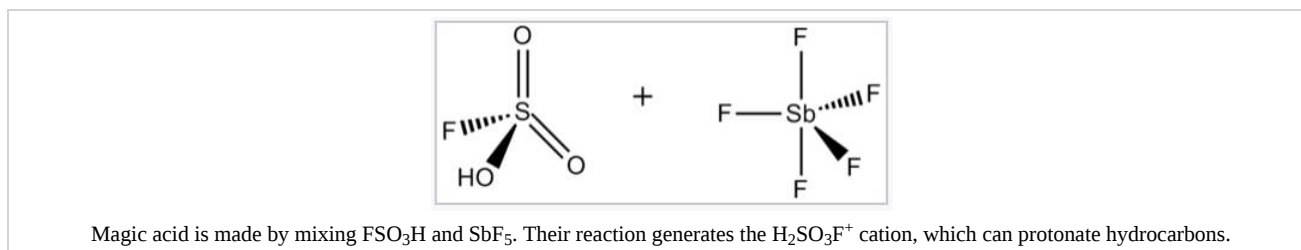
It follows that acidic solvents magnify the Brønsted basicities of substances that cannot accept protons in water. Conversely, basic solvents magnify the acidity of substances that cannot donate a proton to OH⁻.

The acidity and basicity of non-aqueous solvents is difficult to quantify precisely, but one good relative measure is the Hammett acidity function, H_0 . H_0 is defined analogously to pH according to the Henderson-Hasselbach equation:

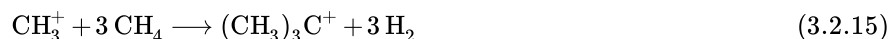
$$H_0 = pK_a + \log\left(\frac{[base]}{[conjugate\ acid]}\right) \quad (3.2.12)$$

For non-aqueous solvents, or for acidic or basic compounds dissolved in solvents that do not themselves dissociate, H_0 is a rough measure of the pH of the solvent or compound in question. Anhydrous HF and H_2SO_4 have H_0 values of approximately -10 and -12 respectively.

Superacids and superbases. The term *superacid* was originally coined by James Bryant Conant in 1927 to describe acids that were stronger than conventional mineral acids.^[1] George A. Olah prepared the so-called magic acid, so-named for its ability to attack hydrocarbons, by mixing antimony pentafluoride (SbF_5) and fluorosulfonic acid (FSO_3H). The name was coined after a candle was placed in a sample of magic acid. The candle dissolved, showing the ability of the acid to protonate hydrocarbons, which under aqueous acidic conditions cannot be protonated.



At 140 °C, FSO_3H-SbF_5 converts methane into the tertiary-butyl carbocation, a reaction that begins with the protonation of methane:^[2]



Fluoroantimonic acid, $HSbF_6$, can produce solutions with H_0 down to -28.^[3] Fluoroantimonic acid is made by combining HF and SbF_5 . In this system, HF releases its proton (H^+) concomitant with the binding of F^- by antimony pentafluoride, which (as described below) is a Lewis acid. The resulting anion (SbF_6^-) is both a weak nucleophile and an extraordinarily weak base.

Superacids are useful in reactions such as the isomerization of alkanes. Industrially, anhydrous acid-exchanged zeolites, which are superacid catalysts, are used on a massive scale to isomerize hydrocarbons in the processing of crude oil to gasoline. Superbases such as lithium diethylamide ($LiNEt_2$), alkyllithium compounds (RLi), and Grignard reagents ($RMgX$) useful in a broad range of organic reactions. $LiNEt_2$ deprotonates C-H bonds to generate reactive carbanions. RLi and $RMgX$ are powerful nucleophiles.

The use of superbases in nonaqueous media allows us to rank the acidities (and measure the pK_a 's) of different classes of molecules. This ranking is particularly important in understanding the reactions of organic molecules. Note that the order of acidities for hydrocarbons is alkynes \gg alkenes, aromatics \gg alkanes. This ordering has to do with the hybridization of the carbon atom that forms the carbanion. The negatively charged lone pair of the carbanion is stabilized in orbitals that have high s character (e.g., sp vs. sp^2 or sp^3). This is because s orbitals have finite probability density at the nucleus and "feel" the positive nuclear charge (thereby stabilizing the extra negative charge on carbon) more than p orbitals. Resonance effects also stabilize carbanions. Thus, cyclopentadiene is more acidic than even an alkyne because the negative charge is delocalized over the entire (aromatic) $C_5H_5^-$ ring when the C_5H_6 is deprotonated.





name	formula	structural formula	pKa
Methane	CH_4		56
Propene	C_3H_6		44
Benzene	C_6H_6		43
Acetylene	C_2H_2		25

Table 1. Carbon acid acidities in pKa in DMSO [4].

Acid-base equilibria in molten salts

When a solid salt melts, it forms a solution of the cations and anions. For example, KOH melts at temperatures above 400 °C and dissociates into K⁺ and OH⁻ ions which can act as a solvent for chemical reactions. Because of the autodissociation of the OH⁻ solvent, water is always present in a molten KOH flux, according to the acid-base equilibrium:

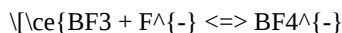


It follows that in this very basic solvent, water (the conjugate acid of the solvent) is the strongest acid that can exist. The conjugate base of the solvent, O²⁻, is the strongest base. This autodissociation equilibrium allows for the acidity of a flux to be easily tuned through the addition or boiling off of water. A "wet" flux is more acidic, and can dissolve metal oxides that contain the basic O²⁻ anion. Conversely a "dry" flux is more basic and will cause oxides to precipitate. Molten hydroxide fluxes can thus be used in the synthesis of oxide crystals, such as the perovskite superconductor (K_{1-x}Ba_xBiO₃).^[5] Eutectic mixtures of NaOH and KOH are relatively low melting (≈ 200 °C) and can be used as solvents for crystallizing a variety of basic oxides.

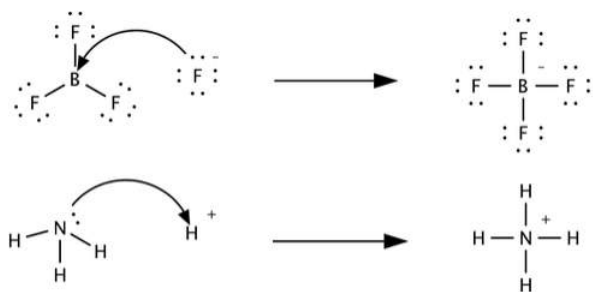
Lewis Acids and Bases

The Lewis classification of acids and bases is broader than the Brønsted-Lowry definition, and encompasses many more substances. Whereas the Brønsted-Lowry and the Arrhenius classifications are based on transfer of protons, Lewis acidity and basicity are based on the sharing of an electron pair. **Lewis acids** can accept an electron pair, while **Lewis bases** can donate an electron pair. This definition encompasses the Brønsted-Lowry definition, in that H⁺ is an electron pair acceptor (when interacting with a base), and a base is an electron pair donor in its interaction with H⁺. This is illustrated below for the protonation of ammonia.

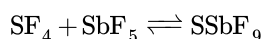
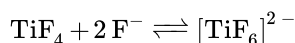
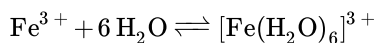
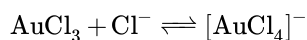
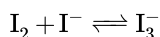
Boron trifluoride, BF₃ acts as a Lewis acid when it combines with a basic ion or molecule that can donate an electron pair. Such a reaction is shown below.



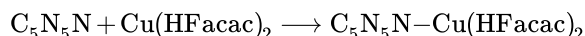
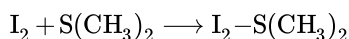
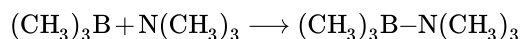
Here, the acid is BF₃ and the base is F⁻. This acid-base reaction allows boron (which is electron-deficient in BF₃) to complete its octet. Similarly, AlCl₃ is a Lewis acid that can react with Cl⁻ (a Lewis base) to make the Lewis "salt" AlCl₄⁻. Note that in water Cl⁻ is a spectator ion (a weaker base than the solvent) in Brønsted acid-base reactions.



Additional examples of Lewis acid base reactions. In each, try to identify the acid, the base, and the salt, based on the concept that the base is the molecule or ion that donates an electron pair. In cases where you are not sure, it may help to draw the VSEPR structures of the molecules:



In other Lewis acid base reactions both acid and base are molecules and the product is referred to as an adduct.



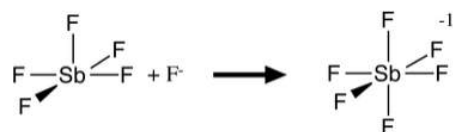
Lewis acidity is the basis for coordination chemistry, a topic we will discuss in more detail in Chapter 5. This is because coordination chemistry involves **metal ions** that are Lewis acids, which bond to ligands that are Lewis bases.

Determining the strength of metal ion Lewis acids

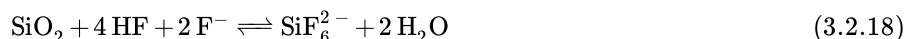
There are three determining factors in the Lewis acid strength of a metal ion:

1. The higher positive charge on the metal, the more acidic it is. For example, Al^{3+} and Fe^{3+} are good Lewis acids and their salts make acidic solutions in water, but K^+ and Na^+ are not.
2. The smaller the atomic radius of the metal ion, the more acidic it is. Going down the periodic table, the Lewis acidity of metal ions decreases (e.g., $\text{Al}^{3+} > \text{Ga}^{3+} > \text{In}^{3+}$) because the ionic radius increases.
3. For transition metal ions, more electronegative metals tend to make stronger Lewis acids. The electronegativity has maxima at W and Au in the 5d series, so metal ions near in that part of the periodic table are good Lewis acids.

Molecules with five coordinate geometries (e.g., PCl_5 , AsF_5 , SbF_5) are typically strong Lewis acids, because when accepting another pair of electrons from a base, they form an octahedral molecule or anion. Neither of the common five-coordinate geometries (trigonal bipyramidal or square pyramidal) is efficient in terms of packing. The Lewis acid-base reaction forms an additional bond with a relatively small energetic penalty of stretching the existing bonds:

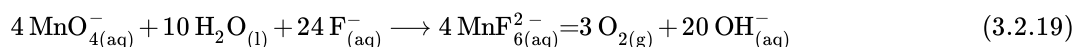


Because F^- is a good Lewis base, and also a small anion, it can form stable octahedral anions with both main group elements and transition metals. For this reason, TiO_2 and SiO_2 dissolve in HF (but are unreactive with aqueous HCl and other strong acids):

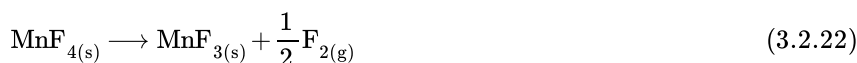


Lewis bases stabilize high oxidation states.

An interesting example of using Lewis acid-base chemistry to drive reactions is the chemical synthesis of fluorine gas, which was devised by Karl O. Christe in 1986.^[6] Christe at the time was organizing a symposium to commemorate the 100th anniversary of the isolation of elemental fluorine by Henri Moissan, which Moissan did in 1886 by electrolyzing a solution of anhydrous HF. 100 years later, there was still no direct (non-electrochemical) synthesis of F_2 . Christe's reaction scheme followed two steps. The first was the known synthesis of K_2MnF_6 from KMnO_4 :



The second step involved reacting K_2MnF_6 with the powerful Lewis acid SbF_5 , to make metastable MnF_4 , which decomposes spontaneously to MnF_3 and fluorine gas:



This reaction teaches us something interesting and important about the connection between acid-base and redox chemistry. Acids tend to stabilize low oxidation states, and bases stabilize high oxidation states (We will see this again soon in Chapter 4, in the context of Pourbaix diagrams). Mn is stable in the +4 oxidation state in K_2MnF_6 , where it is surrounded by six basic F^- anions.

However, the highest stable neutral fluoride of Mn is MnF_3 , and MnF_4 (transiently formed from K_2MnF_6) spontaneously decomposes to generate fluorine.

Oxide is a better base than fluoride. Interestingly, Mn can lose all its valence electrons to form Mn^{7+} in the permanganate ion, MnO_4^- . Here the $7+$ oxidation state is stabilized electrostatically by coordination to four O^{2-} ions, and by the overall -1 charge on the MnO_4^- anion. Because of its $2-$ charge, O^{2-} is a stronger base and a better ion for stabilizing high oxidation states than F^- . This is a general trend among transition metals: the highest oxidation state is usually reached in the oxide, not in the fluoride, despite the fact that F is a more electronegative element than O. For example, Cr^{6+} is stable in the CrO_4^{2-} and $\text{Cr}_2\text{O}_7^{2-}$ anions, but not in any neutral fluoride or fluoroanion. The $+8$ oxidation state occurs in RuO_4 and OsO_4 , but not in any fluoride of Ru or Os.

This page titled [3.2: Brønsted and Lewis Acids and Bases](#) is shared under a [CC BY-SA 4.0](#) license and was authored, remixed, and/or curated by [Chemistry 310 \(Wikibook\)](#) via [source content](#) that was edited to the style and standards of the LibreTexts platform; a detailed edit history is available upon request.

3.3: Hard and Soft Acids and Bases

Lewis acids and bases can be classified by designating them as hard or soft.

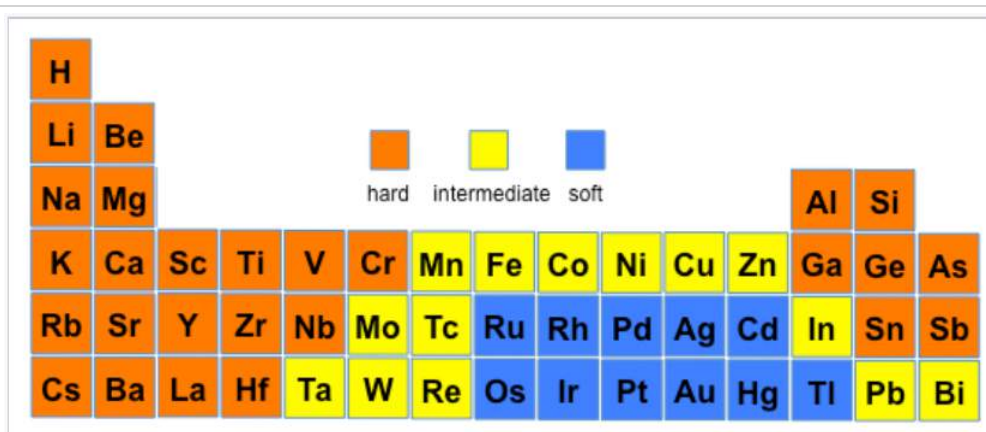
Hard Acids/Bases:

"Hard" acids and bases have a high charge (positive for acids, negative for bases) to ionic radius ratio along with higher oxidation states. Hard acids are not very polarizable and have high charge densities. Thus metal ions with high positive charges and smaller ionic sizes tend to be hard acids. Early transition metal ions in the 3d series tend to be hard Lewis acids. Hard bases are typically small anions and neutral molecules. Some examples of hard acids and bases include: H⁺, O²⁻, OH⁻, F⁻, Fe³⁺, and Al³⁺.

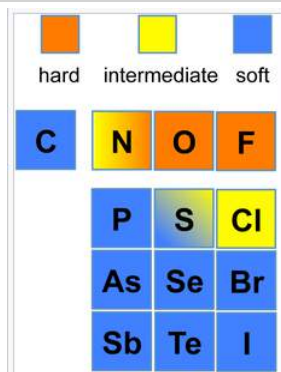
Soft Acids/Bases:

"Soft" acids or bases have a low charge to radius ratio, with low oxidation states. They are normally larger ions that are polarizable. For example, I⁻ and S²⁻ are soft bases and low charge density transition metals, such as Ag⁺, are considered soft acids. Soft acids often include transition metals in the second and third row of the periodic table that have a +1 or +2 charge, as well as late transition metals (especially those in the 4d and 5d series) with filled or almost completely filled *d* orbitals.

Acids and bases are not strictly hard or soft, with many ions and compounds being classified as intermediate. For example, trimethylborane, Fe²⁺, and Pb²⁺ cations are intermediate acids, and pyridine and aniline are examples of intermediate bases. An element can also change its hard/soft character depending on its oxidation state. The most extreme example is hydrogen, where H⁺ is a hard acid and H⁻ is a soft base. Ni³⁺ (as in the layered compound NiOOH) is a hard acid, but Ni⁰ (as in Ni(CO)₄) is a soft acid. The figures below show hard/soft trends for acids (left) and bases (right) in the periodic table. For bases, the major hard/soft discontinuity is between the 2nd row (N,O,F) and the rows below.



Hard-soft trends for acids



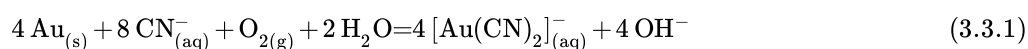
Hard-soft trends for bases

Like binds with Like

Hard acids interact more strongly with hard bases than they do with soft bases, and soft acids interact more strongly with soft bases than hard bases. Thus, the most stable complexes are those with hard-hard and soft-soft interactions. This tendency is illustrated in the table below, which shows the trend in formation constants for hard and soft acids. Hard acids bind halides in the order $F^- > Cl^- > Br^- > I^-$, whereas soft acids follow the opposite trend.

Log K_1	fluoride	chloride	bromide	iodide	acid classification
Fe^{3+}	6.0	1.4	0.5	-	Hard
Pb^{2+}	1.3	0.9	1.1	1.3	Intermediate
Ag^+	0.4	3.3	4.7	6.6	Soft
Hg^{2+}	1.0	6.7	8.9	12.9	Soft

The softest metal ion in the periodic table is $Au^+(aq)$. It forms stable complexes with soft bases such as phosphines and CN^- , but not with hard bases such as O^{2-} or F^- . The affinity of Au^+ for the soft base CN^- is high, and the resulting $[Au(CN)_2]^-$ complex is so stable that gold (which is normally very difficult to oxidize) can be oxidized by oxygen in the air:



This reaction is used in gold mining to separate small flakes of Au from large volumes of sand and other oxides. Ag is similarly dissolved by air oxidation in cyanide solutions. The precious metals are then isolated from the solution using chemical reducing agents or by electroplating. The use of cyanide ion on a large scale in mining, however, creates a potentially serious environmental hazard. In 2000, a spill at Baia Mare, Romania resulted in the worst environmental disaster in Europe since Chernobyl. Cyanide, which is highly toxic, is gradually oxidized by air to the less toxic cyanate (OCN^-) ion. On the laboratory scale, cyanide plating solutions are typically disposed of by using bleach to oxidize CN^- to OCN^- , and the metal is recovered as an insoluble chloride salt.



Netted solution pond next to cyanide heap leaching of gold ore near Elko, Nevada (1992).

The Au^{3+} ion, because of its higher positive charge, is a harder acid than Au^+ and can form complexes with harder bases such as H_2O and amines. In keeping with the "like binds like" principle, the compound AuI (soft-soft) is stable, but AuI_3 (hard-soft) is unknown. Conversely, AuF has never been isolated but AuF_3 (hard-hard) is stable.

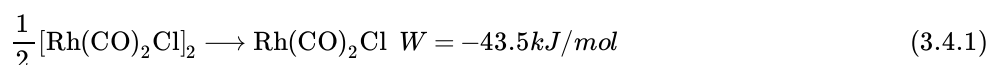
This page titled [3.3: Hard and Soft Acids and Bases](#) is shared under a [CC BY-SA 4.0](#) license and was authored, remixed, and/or curated by [Chemistry 310 \(Wikibook\)](#) via [source content](#) that was edited to the style and standards of the LibreTexts platform; a detailed edit history is available upon request.

3.4: The Electrostatic-Covalent (ECW) Model for Acid-Base Reactions

The classification of Lewis acids and bases as hard and soft is a useful qualitative approach to rationalize their behavior. The ECW Model is a more quantitative model that describes and predicts the strength of Lewis acid – Lewis base interactions. The strength of the acid-base interaction is measured as the enthalpy of adduct formation, ΔH . Each acid is characterized by an E_A and a C_A . Each base is likewise characterized by its own E_B and C_B . The E and C parameters refer, respectively, to the electrostatic and covalent contributions to the strength of the bonds that the acid and base will form. These parameters have been empirically obtained by using enthalpies for adducts that *form only σ bonds between the acid and base as well as adducts that have no steric repulsion between the acid and base.*

$$-\Delta H = E_A E_B + C_A C_B + W$$

This equation reproduces and predicts the enthalpy change, ΔH , of a reaction between many acids and a bases. ΔH is a measure of strength of the bond between the acid and the base, both in the gas phase and in weakly solvating media. The W term represents a constant energy for cleavage of a dimeric acid or base. For example, the enthalpy of cleavage of $[\text{Rh}(\text{CO})_2\text{Cl}]_2$ by base B involves two steps. The first step is cleavage of the dimer, which is W:



The second step is the binding of B to the $\text{RhCl}(\text{CO})_2$ monomer. In another case, W is the enthalpy needed to cleave the internal hydrogen bonding of the H-bonding acid $(\text{CF}_3)_3\text{COH}$.

The calculation of the enthalpy of adduct formation for the reaction of pyridine, $\text{C}_5\text{H}_5\text{N}$ and bis(hexafluoroacetylacetonato)copper (II), $\text{Cu}(\text{HFacac})_2$, shows how these parameters are used. In this case $W = 0$ since neither the acid nor the base is a dimer. Selected parameters can be found at the Wikipedia page for the **ECW Model**

$$-\Delta H = E_A E_B + C_A C_B = (1.82)(1.78) + (2.86)(3.54) = 13.4 \text{ kcal/mol} = -56.1 \text{ kJ/mol}$$

$$\Delta H = -56.1 \text{ kJ/mol}, \quad \Delta H_{\text{measured}} = -56.1 \text{ kJ/mol}$$

However, the ΔH calculated for the reaction of Me_3B with Me_3N is less negative than that observed. This discrepancy is attributed to steric repulsion between the methyl groups on the B and N atoms. The difference between the calculated and observed values can then be taken as the amount of the steric effect, a value otherwise not attainable. Steric effects have also been identified with $(\text{CH}_3)_3\text{SnCl}$ and with $\text{Cu}(\text{HFacac})_2$. When π bonding contributes to the measured enthalpy, the enthalpy calculated from the E and C parameters will be less than the measured enthalpy and the difference provides a measure of the extent of the π bonding contribution.

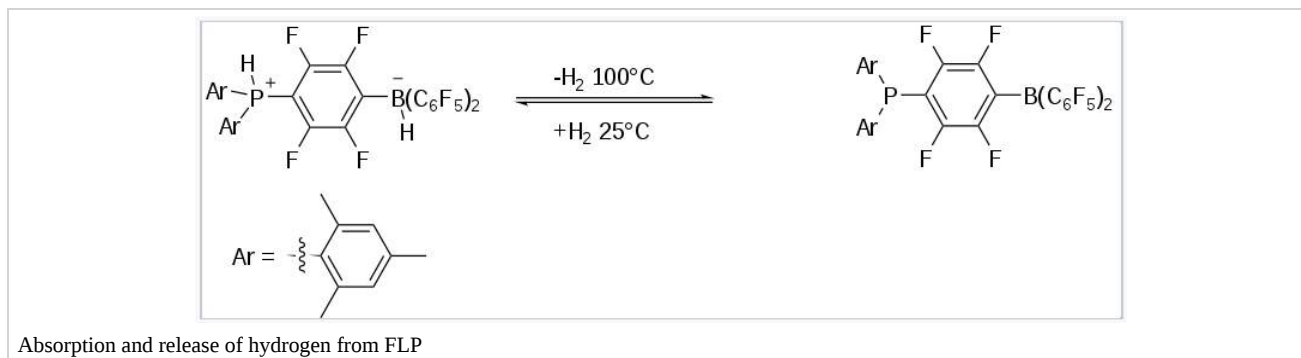
A graphical presentation of this model clearly shows that *there is no single ranking order of Lewis acid or Lewis base strengths*, a point often overlooked, and emphasizes that the magnitude of acid and base interactions requires two parameters (E & C) to account for the interactions. A **Cramer-Bopp plot**^[7] using the three Lewis bases: acetonitrile, ammonia, and dimethyl sulfide illustrates that there is no unique ordering of Lewis base strengths. The Cramer-Bopp plot is a visual tool for comparing Lewis base strengths with the range of possible Lewis acid partners, and similar plots can be constructed to examine selected Lewis acids against the range of possible Lewis bases. These plots show that two properties are needed to completely define acid and base strength and that any attempt to define strength with one property or parameter is limited in its utility. For Drago's quantitative ECW model the two properties are electrostatic and covalent while for Pearson's qualitative HSAB theory the two properties are hardness and strength.

This page titled [3.4: The Electrostatic-Covalent \(ECW\) Model for Acid-Base Reactions](#) is shared under a [CC BY-SA 4.0](#) license and was authored, remixed, and/or curated by [Chemistry 310 \(Wikibook\)](#) via [source content](#) that was edited to the style and standards of the LibreTexts platform; a detailed edit history is available upon request.

3.5: Frustrated Lewis Pairs

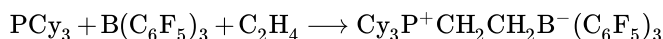
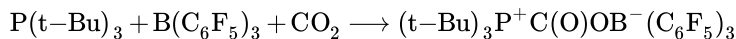
A **frustrated Lewis pair (FLP)** is a compound or mixture that contains a Lewis acid and a Lewis base which, because of steric hindrance, cannot combine to form a classical adduct.^[8] Many kinds of FLPs have been devised, and their reactivity towards other molecules has been broadly developed.^{[9][10]}

The hydrogen adduct of the original FLP, a phosphonium-borate salt, can be prepared by combining a phenylene bridged phosphinoborane and dihydrogen. The salt, which is colorless, is stable in the presence of air and moisture. It releases molecular H₂ when heated above 100 °C. This reactivity is remarkable considering the strength of the H-H bond, 432 kJ/mol.



The discovery that some FLPs can split H₂^[11] triggered the rapid growth of research into FLP's. Because of their "unquenched" reactivity, such systems are reactive toward substrates that can undergo heterolysis. For example, many FLP's split the hydrogen molecule. This reactivity suggested that FLP's can be useful for hydrogenation reactions. A sizable range of homogeneous and heterogeneous catalytic reactions have now been developed using FLP's.

Mixtures of sterically hindered Lewis acids and bases also can act as FLPs. One successful strategy is to mix sterically hindered triarylphosphines with triarylboranes. Small molecules such as CO₂ and ethylene can then form a bridge between the phosphine Lewis base and borane Lewis acid, e.g.,



Because FLPs behave at the same time as both nucleophiles and electrophiles, they can effect the ring-opening of cyclic ethers such as THF, 2,5-dihydrofuran, coumaran, and dioxane.^[12]

This page titled [3.5: Frustrated Lewis Pairs](#) is shared under a [CC BY-SA 4.0](#) license and was authored, remixed, and/or curated by [Chemistry 310 \(Wikibook\)](#) via [source content](#) that was edited to the style and standards of the LibreTexts platform; a detailed edit history is available upon request.

3.6: Discussion Questions

- Discuss periodic trends in the Lewis acidity of metal ions.
 - Explain what we mean by hard and soft acids and bases, using specific examples.
 - Explain why hard and soft should not be equated with electrostatic and covalent.
 - According to HSAB theory Cu and Zn are classified as intermediate acids while Cd is classified as soft. The base $(\text{CH}_2)_4\text{O}$ is considered hard while $(\text{CH}_2)_4\text{S}$ is soft. Using E and C numbers for $\text{Cd}[\text{N}(\text{Si}(\text{CH}_3)_3)_2]$ and ZnTPP calculate the enthalpies for these two acids interacting with $(\text{CH}_2)_4\text{O}$ and $(\text{CH}_2)_4\text{S}$ and show that the HSAB model correctly predicts which base interacts more strongly with which acid. Do the same comparison using $\text{Cu}(\text{HFacac})_2$ as the acid and show that HSAB fails to predict which base interacts more strongly. How are these results related to the Cramer-Bopp plot that show one property or one parameter cannot be used to rank Lewis acid or base strength?
-

This page titled [3.6: Discussion Questions](#) is shared under a [CC BY-SA 4.0](#) license and was authored, remixed, and/or curated by [Chemistry 310 \(Wikibook\)](#) via [source content](#) that was edited to the style and standards of the LibreTexts platform; a detailed edit history is available upon request.

3.7: Problems

1. Classify each of the substances below as an acid or base, and as strong or weak or as a spectator in the solvent listed. For each case, write out the dissociation reaction.

(a) H_3AsO_4 in water

(b) HCl in glacial acetic acid

(c) CH_3COOH in liquid ammonia

(d) H_2O in molten NaOH

(e) Cl^- in liquid ammonia

2. Write out the dissociation reactions for an acid HA and its conjugate base A^- in water. Use the equilibrium expressions for K_a and K_b to prove that $K_a K_b = K_w$.

3. Calculate the percent ionization of 1 M acetic acid ($K_a = 1.8 \times 10^{-5}$) in water.

4. For each pair of compounds below, indicate which one is a stronger acid and explain your choice:

(a) $[\text{Fe}(\text{H}_2\text{O})_6]^{3+}$ or $[\text{Fe}(\text{H}_2\text{O})_6]^{2+}$

(b) H_3BO_3 or H_3PO_3

(c) $[\text{Ga}(\text{H}_2\text{O})_6]^{3+}$ or $[\text{Al}(\text{H}_2\text{O})_6]^{3+}$

(d) HIO_3 or HIO_4

(e) H_3PO_4 or H_2SeO_4

5. The Mg^{2+} and Cu^{2+} cations have similar ionic radii, but the acidities of aqueous nitrate solutions containing the two ions are different. Explain which ion is more acidic and why.

6. Cobalt reacts with excess fluorine to make CoF_3 , but higher oxidation states of cobalt do not exist in binary fluorides. However, Co(IV) is stable in oxides such as CoO_2 and BaCoO_3 . Explain why these oxides can stabilize a higher oxidation state of cobalt than fluorides.

7. (a) When solutions of the hydrosulfide (SH^-) salts of As^{3+} , Sb^{3+} , and Sn^{4+} are reacted with aqueous solutions of ammonium hydrosulfide ($\text{NH}_4^+ \text{SH}^-$), the sulfide salts As_2S_3 , Sb_2S_3 , and SnS_2 precipitate. When excess aqueous Na_2S is added, however, these sulfides re-dissolve to form soluble anionic complexes. In contrast, solutions of Cu^{2+} , Pb^{2+} , Hg^{2+} , Bi^{3+} and Cd^{2+} precipitate as solid sulfides but do not re-dissolve in solutions that contain excess sulfide. We may consider the first group of ions to be amphoteric for soft acid-base reactions that involve SH^- instead of OH^- . The second group is more basic (less acidic) in the sense that it does not react with excess soft base. Use this information to locate the amphoteric diagonal in the periodic table for sulfides. Compare this with the diagonal that defines the amphoteric oxides, which dissolve in either acidic or basic solutions. Does your analysis agree with the description of S^{2-} as a softer base than O^{2-} ?

(b) Au^+ is also precipitated by SH^- ions, and the sulfide Au_2S redissolves to form a soluble complex in excess SH^- . Does this fit the trend you discovered in part (a)? Does it make sense in terms of the electronegativity of Au ? Explain.

8. Calculate the enthalpy for the adduct $(\text{CH}_3)_3\text{B-N}(\text{CH}_3)_3$ and compare it to the measured value of -73.6 kJ/mol. Parameters can be found at ECW Model.

9. Calculate the enthalpy for the adduct formation for the Lewis acid $(\text{CH}_3)_3\text{SnCl}$ with each of the following Lewis bases $(\text{C}_2\text{H}_5)_2\text{O}$, $(\text{CH}_2)_4\text{O}$, and CH_3CN . Their respective measured enthalpies are -9.2 , -21.3 and -20.1 kJ/mol. Explain the any differences between the calculated and measured enthalpies. Parameters can be found at ECW Model.

10. Refer to the Cramer-Bopp plot found at ECW Model and indicate the order of Lewis base strength for

(a) An acid with $R_a = -0.5$

(b) An acid with $R_a = 0.33$

(c) An acid with $R_a = -0.9$

11. The Lewis acid $[\text{Rh}(\text{CO})_2\text{Cl}]_2$ has a W value of -43.47 kJ/mol

- (a) What does W refer to?
- (b) The E, C, and W parameters found at ECW Model give the enthalpy for forming one mole adduct, that is,
 $B + \frac{1}{2} [\text{Rh}(\text{CO})_2\text{Cl}]_2 \longrightarrow B-\text{RhCl}(\text{CO})_2$
- (1) What is the heat of dissociation of one mole of $[\text{Rh}(\text{CO})_2\text{Cl}]_2$?
- (2) What is the enthalpy of $2 B + [\text{Rh}(\text{CO})_2\text{Cl}]_2 \longrightarrow 2 B-\text{RhCl}(\text{CO})_2$
- (3) Calculate the enthalpy per mol of B- $\text{RhCl}(\text{CO})_2$ for $\text{C}_5\text{H}_5\text{N}$, $(\text{CH}_3)_2\text{CO}$

This page titled [3.7: Problems](#) is shared under a [CC BY-SA 4.0](#) license and was authored, remixed, and/or curated by [Chemistry 310 \(Wikibook\)](#) via [source content](#) that was edited to the style and standards of the LibreTexts platform; a detailed edit history is available upon request.

3.8: References

1. Hall NF, Conant JB (1927). "A Study of Superacid Solutions". *Journal of the American Chemical Society* **49** (12): 3062–70. doi:[10.1021/ja01411a010](https://doi.org/10.1021/ja01411a010).
2. George A. Olah, Schlosberg RH (1968). "Chemistry in Super Acids. I. Hydrogen Exchange and Polycondensation of Methane and Alkanes in FSO₃H–SbF₅ ("Magic Acid") Solution. Protonation of Alkanes and the Intermediacy of CH₅⁺ and Related Hydrocarbon Ions. The High Chemical Reactivity of "Paraffins" in Ionic Solution Reactions". *Journal of the American Chemical Society* **90** (10): 2726–7. doi:[10.1021/ja01012a066](https://doi.org/10.1021/ja01012a066).
3. Herlem, Michel (1977). "Are reactions in superacid media due to protons or to powerful oxidising species such as SO₃ or SbF₅?". *Pure & Applied Chemistry* **49**: 107–113. doi:[10.1351/pac197749010107](https://doi.org/10.1351/pac197749010107).
4. *Equilibrium acidities in dimethyl sulfoxide solution* Frederick G. Bordwell Acc. Chem. Res.; **1988**; 21(12) pp 456 - 463; DOI:[10.1021/ar00156a004](https://doi.org/10.1021/ar00156a004)
5. R. J. Cava, et al. (1988). "Superconductivity near 30 K without copper: the Ba_{0.6}K_{0.4}BiO₃ perovskite". *Nature* **332**: 814–6. doi:[10.1038/332814a0](https://doi.org/10.1038/332814a0).
6. Christe, Karl O. (1986). "Chemical synthesis of elemental fluorine". *Inorganic Chemistry* **25** (21): 3721. doi:[10.1021/ic00241a001](https://doi.org/10.1021/ic00241a001).
7. Cramer RE, Bopp TT (1977). "Great E and C plot. Graphical display of the enthalpies of adduct formation for Lewis acids and bases". *Journal of Chemical Education* **54** (10): 612–613. doi:[10.1021/ed054p612](https://doi.org/10.1021/ed054p612).
8. Stephan, D. W. (2008). "Frustrated Lewis pairs: a concept for new reactivity and catalysis". *Org. Biomol. Chem.* **6**: 1535–1539. doi:[10.1039/b802575b](https://doi.org/10.1039/b802575b).
9. Stephan, D. W.; Erker, G. (2010). "Frustrated Lewis Pairs: Metal-free Hydrogen Activation and More". *Angewandte Chemie International Edition* **49** (1): 46–76. doi:[10.1002/anie.200903708](https://doi.org/10.1002/anie.200903708). ISSN [1433-7851](https://doi.org/10.1002/anie.200903708).
10. Stephan, D. W.; Erker, G. (2017). "Frustrated Lewis pair chemistry". *Philosophical Transactions of the Royal Society A: Mathematical, Physical and Engineering Sciences* (Royal Society) **375** (2101): 20170239. doi:[10.1098/rsta.2017.0239](https://doi.org/10.1098/rsta.2017.0239). ISSN [1364-503X](https://doi.org/10.1098/rsta.2017.0239). PMID [28739971](https://pubmed.ncbi.nlm.nih.gov/28739971/). Bibcode: [2017RSPTA.37570239S](https://pubmed.ncbi.nlm.nih.gov/28739971/).
11. Welch, G. C.; San Juan, R. R.; Masuda, J. D.; Stephan, D. W. (2006). "Reversible, Metal-Free Hydrogen Activation". *Science* **314** (5802): 1124–1126. doi:[10.1126/science.1134230](https://doi.org/10.1126/science.1134230). ISSN [0036-8075](https://doi.org/10.1126/science.1134230). PMID [17110572](https://pubmed.ncbi.nlm.nih.gov/17110572/). Bibcode: [2006Sci...314.1124W](https://pubmed.ncbi.nlm.nih.gov/17110572/).
12. Birkmann, B., et al. (2010). "Frustrated Lewis Pairs and Ring-Opening of THF, Dioxane, and Thioxane". *Organometallics* **29**: 5310–5319. doi:[10.1021/om1003896](https://doi.org/10.1021/om1003896).

This page titled [3.8: References](#) is shared under a [CC BY-SA 4.0](#) license and was authored, remixed, and/or curated by [Chemistry 310 \(Wikibook\)](#) via [source content](#) that was edited to the style and standards of the LibreTexts platform; a detailed edit history is available upon request.

CHAPTER OVERVIEW

4: Redox Stability and Redox Reactions

Learning Objectives

- Balance complex oxidation-reduction reactions by the ion-electron method.
- Understand periodic trends in the activity series and electrochemical series.
- Use the Nernst equation to determine half-cell and cell potentials.
- Derive the stability field of water and use this to rationalize aqueous redox chemistry.
- Construct and be proficient with Latimer diagrams, using them to determine unknown reduction potential values and to quickly identify stable and unstable species.
- Construct and be proficient with Frost diagrams, using them to identify stable and unstable species, as well as those that are strong oxidizers.
- Construct and be proficient with Pourbaix diagrams, using them to identify redox and non-redox reactions, reactions that are and are not pH-dependent, and ultimately to predict and rationalize stability, reactivity, corrosion, and passivation.

In redox reactions, one element or compound is reduced (gains electrons) and another is oxidized (loses electrons). In terms of everyday life, redox reactions occur all of the time around us. For example, the metabolism of sugars to CO_2 , which stores energy in the form of ATP, is a redox reaction. Another example of redox is fire or combustion, such as in a car engine. In a car engine, hydrocarbons in the fuel are oxidized to carbon dioxide and water, while oxygen is reduced to water. Corrosion (i.e. the formation of rust on iron) is a redox reaction involving oxidation of a metal.

[4.1: Prelude to Redox Stability and Redox Reactions](#)

[4.2: Balancing Redox Reactions](#)

[4.3: Electrochemical Potentials](#)

[4.4: Latimer and Frost Diagrams](#)

[4.5: Redox Reactions with Coupled Equilibria](#)

[4.6: Pourbaix Diagrams](#)

[4.7: Discussion Questions](#)

[4.8: Problems](#)

[4.9: References](#)

This page titled [4: Redox Stability and Redox Reactions](#) is shared under a [CC BY-SA 4.0](#) license and was authored, remixed, and/or curated by [Chemistry 310 \(Wikibook\)](#) via [source content](#) that was edited to the style and standards of the LibreTexts platform; a detailed edit history is available upon request.

4.1: Prelude to Redox Stability and Redox Reactions

In redox reactions, one element or compound is reduced (gains electrons) and another is oxidized (loses electrons). In terms of everyday life, redox reactions occur all of the time around us. For example, the metabolism of sugars to CO_2 , which stores energy in the form of ATP, is a redox reaction. Another example of redox is fire or combustion, such as in a car engine. In a car engine, hydrocarbons in the fuel are oxidized to carbon dioxide and water, while oxygen is reduced to water. Corrosion (i.e. the formation of rust on iron) is a redox reaction involving oxidation of a metal.



Oxidation states of vanadium in acidic solution. From left to right the oxidation state goes from +5 to +2. These four oxidation states form the basis of the vanadium flow battery, a storage device for electricity generated from sunlight and wind.^[1]

Oxidation-reduction reactions are important to understanding inorganic chemistry for several reasons:

- Transition metals can have multiple oxidation states
- Main group elements (N, halogens, O, S...) also have multiple oxidation states and important redox chemistry
- Many inorganic compounds catalyze redox reactions (which are especially useful in industrial and biological applications)
- Energy conversion and storage technologies (solar water splitting, batteries, electrolyzers, fuel cells) rely on inorganic redox reactions and catalysis
- Electrochemistry provides a way to measure equilibrium constants for dissolution/precipitation, complexation, and other reactions.
- Reaction mechanisms in organometallic chemistry (oxidative addition, reductive elimination) involve changes in the oxidation states of metals.

Not all oxidizers and reducers are created equal. The electrochemical series ranks substances according to their oxidizing and reducing power, i.e., their standard electrode potential. Strong oxidizing agents are typically compounds with elements in high oxidation states or with high electronegativity, which gain electrons in the redox reaction. Examples of strong oxidizers include hydrogen peroxide, permanganate, and osmium tetroxide. Reducing agents are typically electropositive elements such as hydrogen, lithium, sodium, iron, and aluminum, which lose electrons in redox reactions. Hydrides (compounds that contain hydrogen in the formal -1 oxidation state), such as sodium hydride, sodium borohydride and lithium aluminum hydride, are often used as reducing agents in organic and organometallic reactions.

This page titled [4.1: Prelude to Redox Stability and Redox Reactions](#) is shared under a [CC BY-SA 4.0](#) license and was authored, remixed, and/or curated by [Chemistry 310 \(Wikibook\)](#) via [source content](#) that was edited to the style and standards of the LibreTexts platform; a detailed edit history is available upon request.

4.2: Balancing Redox Reactions

In studying redox chemistry, it is important to begin by learning to balance electrochemical reactions. Simple redox reactions (for example, $\text{H}_2 + \text{I}_2 \rightarrow 2 \text{HI}$) can be balanced by inspection, but for more complex reactions it is helpful to have a foolproof, systematic method. The **ion-electron method** allows one to balance redox reactions regardless of their complexity. We illustrate this method with two examples.

Example 1:

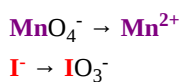
I^- is oxidized to IO_3^- by MnO_4^- , which is reduced to Mn^{2+} .

How can this reaction be balanced? In the ion-electron method we follow a series of four steps:

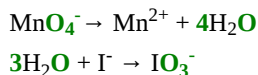
Step 1A: Write out the (unbalanced) reaction and identify the elements that are undergoing redox.



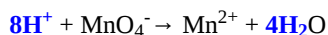
Step 1B: Separate the reaction into two **half reactions**, balancing the element undergoing redox in each.



Step 2A: Balance the **oxygen** atoms by adding water to one side of each half reaction.



Step 2B: Balance the **hydrogen** atoms by adding H^+ ions.

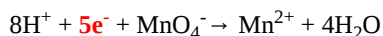


The left side has a net charge of +7 and the right side has a net charge of +2



The left side has a net charge of -1 and the right side has a net charge of +5

Step 2C: Balance the overall charge by adding **electrons**



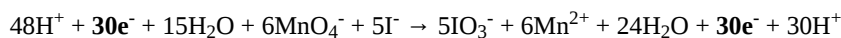
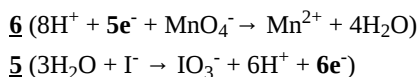
The left side has a charge of +2 while the right side has a charge of +2. They are balanced.



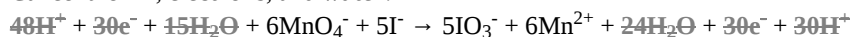
The left side has a charge of -1 while the right side has a charge of -1. They are balanced.

Note: We did not need to explicitly determine the oxidation states of Mn or I to arrive at the correct number of electrons in each half reaction.

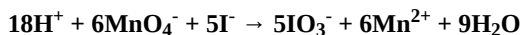
Step 3: Combine the half reactions so that there are equal numbers of electrons on the left and right sides



Cancel the H^+ , **electrons**, and **water**:

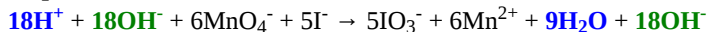


The overall balanced reaction is therefore:

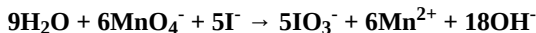


Check your work by making sure that all **elements** and **charges** are balanced.

Step 4: If the reaction occurs under basic conditions, we add OH^- to each side to cancel H^+



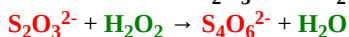
The $18\text{H}^+ + 18\text{OH}^-$ will become $18\text{H}_2\text{O}$ so the overall balanced reaction is:



Again, it is a good idea to check and make sure that all of the elements are balanced, and that the charge is the same on both sides. If this is not the case, you need to find the error in one of the earlier steps.

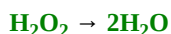
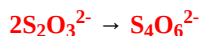
Example 2:

Redox reaction of $\text{S}_2\text{O}_3^{2-}$ and H_2O_2



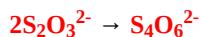
Which elements are undergoing redox? **S** and **O**

Step 1: Write out half reactions, balancing the element undergoing redox

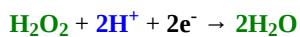
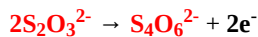


Step 2A: Balance oxygen (already balanced)

Step 2B: Balance hydrogen:

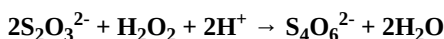


Step 2C: Balance charge by adding electrons:



Step 3: Combine the half reactions so that there are equal numbers of electrons on the left and right sides (already equal)

Overall balanced reaction:



Note that again, we did not need to know the formal oxidation states of S or O in the reactants and products in order to balance the reaction. In this case, assigning the oxidation states would be rather complex, because $\text{S}_2\text{O}_3^{2-}$ and $\text{S}_4\text{O}_6^{2-}$ both contain sulfur in more than one oxidation state.

This page titled [4.2: Balancing Redox Reactions](#) is shared under a [CC BY-SA 4.0](#) license and was authored, remixed, and/or curated by [Chemistry 310 \(Wikibook\)](#) via [source content](#) that was edited to the style and standards of the LibreTexts platform; a detailed edit history is available upon request.

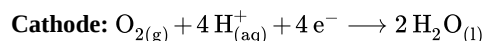
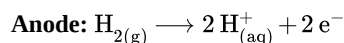
4.3: Electrochemical Potentials

In electrochemical cells, or in redox reactions that happen in solution, the thermodynamic driving force can be measured as the **cell potential**. Chemical reactions are spontaneous in the direction of $-\Delta G$, which is also the direction in which the cell potential (defined as $E_{\text{cathode}} - E_{\text{anode}}$) is positive. A cell operating in the **spontaneous** direction (for example, a battery that is discharging) is called a **galvanic cell**. A cell that is being driven in the **non-spontaneous** direction is called an **electrolytic cell**. For example, let us consider the reaction of hydrogen and oxygen to make water:



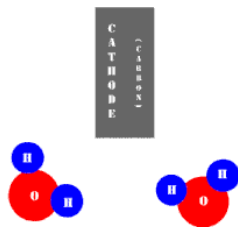
Thermodynamically, this reaction is spontaneous in the direction shown and has an overall standard free energy change (ΔG°) of -237 kJ per mole of water produced.

When this reaction occurs electrochemically in the spontaneous direction (e.g., in a hydrogen-air fuel cell), the two half cell reactions that occur are:



Here the anode is the negative electrode and the cathode is the positive electrode; under conditions of very low current density (where there are minimal resistive losses and kinetic overpotentials), the potential difference we would measure between the two electrodes would be 1.229 V.

In an **electrolytic cell**, this reaction is run in reverse. That is, we put in electrical energy to split water into hydrogen and oxygen molecules. In this case, the half reactions (and their standard potentials) reverse. $\text{O}_2(\text{g})$ bubbles form at the anode and $\text{H}_2(\text{g})$ is formed at the cathode. Now the **anode** is the **positive** electrode and the **cathode** is **negative**. Electrons are extracted from the substance at the anode (water) and pumped into the solution at the cathode to make hydrogen. An animation of the cathode half reaction is shown below.



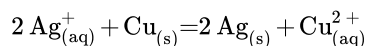
In both galvanic and electrolytic cells, **oxidation** occurs at the **anode** and **reduction** occurs at the **cathode**.

Half-cell potentials

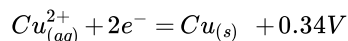
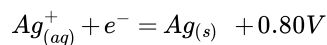
As noted above, the equilibrium voltage of an electrochemical cell is proportional to the free energy change of the reaction. Because electrochemical reactions can be broken up into two half-reactions, it follows that the potentials of half reactions (like free energies) can be added and subtracted to give an overall value for the reaction. If we take the **standard hydrogen electrode** as our reference, i.e., if we assign it a value of zero volts, we can measure all the other half cells against it and thus obtain the voltage of each one. This allows us to rank redox couples according to their **standard reduction potentials** (or more simply their **standard potentials**), as shown in the table below.

	Half Reaction	Standard Potential (V)
↑ stronger oxidizing agent	$F_2 + 2e^- \rightleftharpoons 2F^-$	+2.87
	$Pb^{4+} + 2e^- \rightleftharpoons Pb^{2+}$	+1.67
	$Cl_2 + 2e^- \rightleftharpoons 2Cl^-$	+1.36
	$O_2 + 4H^+ + 4e^- \rightleftharpoons 2H_2O$	+1.23
	$Ag^+ + 1e^- \rightleftharpoons Ag$	+0.80
	$Fe^{3+} + 1e^- \rightleftharpoons Fe^{2+}$	+0.77
	$Cu^{2+} + 2e^- \rightleftharpoons Cu$	+0.34
	$2H^+ + 2e^- \rightleftharpoons H_2$	0.00
	$Pb^{2+} + 2e^- \rightleftharpoons Pb$	-0.13
	$Fe^{2+} + 2e^- \rightleftharpoons Fe$	-0.44
↓ stronger reducing agent	$Zn^{2+} + 2e^- \rightleftharpoons Zn$	-0.76
	$Al^{3+} + 3e^- \rightleftharpoons Al$	-1.66
	$Mg^{2+} + 2e^- \rightleftharpoons Mg$	-2.36
	$Li^+ + 1e^- \rightleftharpoons Li$	-3.05

Note that when we construct an electrochemical cell and calculate the voltage, we simply take the difference between the half cell potentials and do not worry about the number of electrons in the reaction. For example, for the displacement reaction in which silver ions are reduced by copper metal, the reaction is:



The two half-cell reactions are:



and the standard potential $E^o = +0.80 - 0.34V = +0.46V$

The reason we don't need to multiply the Ag potential by 2 is that E^o is a measure of the free energy change **per electron**. Dividing the free energy change by the number of electrons (see below) makes E^o an **intensive property** (like pressure, temperature, etc.).

Relationship between E and ΔG. For systems that are in equilibrium, $\Delta G^o = -nFE^o_{cell}$, where n is number of moles of electrons per mole of products and F is the Faraday constant, ~ 96485 C/mol. Here the o symbol indicates that the substances involved in the reaction are in their standard states. For example, for the water electrolysis reaction, the standard states would be pure liquid water, H^+ at 1M concentration (or more precisely, at unit activity), and O_2 and $H_2(g)$ at 1 atmosphere pressure.

More generally (at any concentration or pressure), $\Delta G = -nFE$, where

$$E = E^o - \frac{RT}{nF} * \ln Q \quad (4.3.2)$$

or at 298 K

$$E = E^o - \frac{0.0592}{n} * \log Q \quad (4.3.3)$$

where Q is the concentration ratio of products over reactants, raised to the powers of their coefficients in the reaction. This equation (in either form) is called the Nernst equation. The second term in the equation, when multiplied by $-nF$, is $RT * \ln Q$. This is the free energy difference between ΔG and ΔG^o . We can think of this as an entropic term that takes into account the positive entropy change of dilution, or the negative entropy change of concentrating a reactant or product, relative to its standard state.

Using the Nernst equation

Example 1:

For the half reaction $2 H^+ + 2 e^- = H_2$, $E^o_{1/2} = 0.000$ V (by definition)

What is $E_{1/2}$ at pH 5 and $P_{H_2} = 1 \text{ atm}$?

$pH = -\log[H^+] = 5$, so $[H^+] = 10^{-5} \text{ M}$

$$E = E^\circ - \frac{0.0592}{2} * \log \frac{P_{H_2}}{(H^+)^2} = E^\circ - \frac{0.0592}{2} * \log(10^5)^2 = E^\circ - \frac{0.0592}{2}(10) = 0.000 - 0.296 = -0.296V \quad (4.3.4)$$

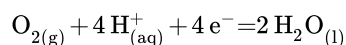
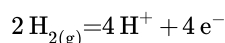
Example 2:

What is the potential of a fuel cell (a galvanic H_2/O_2 cell) operating at pH 5?

Overall reaction: $2 H_{2(g)} + O_{2(g)} = 2 H_2O_{(l)}$

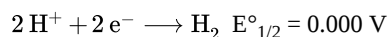
In this reaction, H_2 is oxidized to H^+ and O_2 is reduced to H_2O . According to our convention, we write out and balance both half-cell reactions as reductions. For convenience, we do this in acid. (It is left as an exercise to the interested reader to try to work the problem in base)

Half cell reactions:

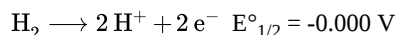


Toyota fuel cell hybrid bus. The bus runs on electrical energy obtained directly from the H_2/O_2 reaction. Individual fuel cells are connected in series to make a power train that charges a battery pack and drives an electric motor. Although the standard potential of the reaction is 1.23 V, because of kinetic overpotentials each fuel cell in the power train operates at a voltage of about 0.70 V. Despite this energy loss, the fuel cell system is still about twice as efficient as a combustion engine performing the same reaction.

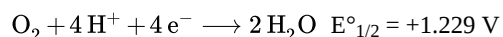
To solve this problem we need to find the difference between the H_2/H^+ and O_2/H_2O half cell potentials at pH 5.



Like all standard potentials, this is written as a reduction. We need to reverse it and change the sign of E° since H_2 is being oxidized:



and add the standard potential of the substance being reduced at the cathode:



The difference between the two standard half cell potentials is $+1.229 - 0.000 = +1.229 \text{ V}$

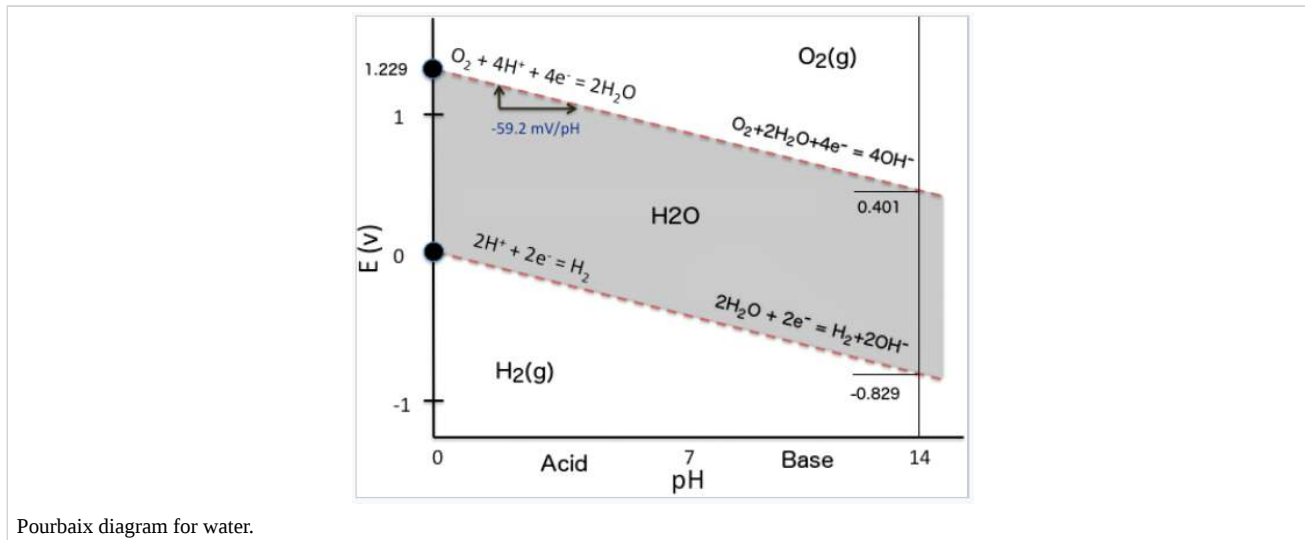
$$E^\circ_{\text{cell}} = +1.229 \text{ Volts}$$

We now use the Nernst equation to account for the fact that H^+ is not in its standard state:

$$E_{\text{cell}} = E^\circ - \frac{0.0592}{4} * \log \frac{[H^+]^4}{P_{O_2} P_{H_2}^2 [H^+]^4} = E^\circ - \frac{0.0592}{4} * \log(1) = E^\circ = +1.229V \quad (4.3.5)$$

Note that the value of E_{cell} **does not change** with pH since **both couples shift -59.2 mV/pH** according to the Nernst equation. This is the consequence of the fact that the number of electrons equals the number of protons in each of the half cell reactions. Another way to rationalize this result is to remember that the overall reaction ($2\text{H}_2 + \text{O}_2 = 2\text{H}_2\text{O}$) does not involve H^+ as a reactant or product, so ΔG and E should be independent of pH.

We can plot the shift in the H_2/H^+ and $\text{O}_2/\text{H}_2\text{O}$ half-cell potentials with pH on a potential-pH diagram (also called a Pourbaix diagram) as shown below. The pH-dependent potentials of the H_2 and O_2 couples are shown as dotted lines. Notice that the potential difference between them is always 1.23 V. The dark circles represent the standard potentials.



Pourbaix diagrams are essentially electrochemical **phase diagrams**, which plot regions of thermodynamic stability for redox-active substances. As in other kinds of phase diagrams, the lines represent conditions under which two phases coexist in equilibrium. The shaded area in the water Pourbaix diagram represents the conditions of potential and pH where liquid water is stable relative to hydrogen or oxygen. Outside the shaded region, water is thermodynamically unstable and is reduced to $\text{H}_2(\text{g})$ or oxidized to $\text{O}_2(\text{g})$. Although these processes are spontaneous in the thermodynamic sense (for example, water is unstable in the presence of Pb^{4+} , Cl_2 , Fe, Zn, or Al), they are kinetically slow and require catalysis to proceed.

This page titled [4.3: Electrochemical Potentials](#) is shared under a [CC BY-SA 4.0](#) license and was authored, remixed, and/or curated by [Chemistry 310 \(Wikibook\)](#) via [source content](#) that was edited to the style and standards of the LibreTexts platform; a detailed edit history is available upon request.

4.4: Latimer and Frost Diagrams

In addition to Pourbaix diagrams, there are two other kinds of redox stability diagrams known as Latimer and Frost diagrams. Each of these diagrams contains similar information, but one representation may be more useful in a given situation than the others.

Latimer and Frost diagrams help predict stability relative to higher and lower oxidation states, usually at one fixed pH. Pourbaix diagrams help understand pH-dependent equilibria, which are often coupled to solubility equilibria and corrosion (which will be talked about more later).



Manganese nodules on the sea floor contain Mn in oxidation states 2+, 3+, and 4+.

Latimer diagrams:

Latimer diagrams are the oldest and most compact way to represent electrochemical equilibria for substances that have multiple oxidation states. Electrochemical potential values are written for successive redox reactions (from highest to lowest oxidation state), typically under standard conditions in either strong acid ($[H^+] = 1 \text{ M}$, pH 0) or strong base ($[OH^-] = 1 \text{ M}$, pH 14). The oxidation states of successive substances in a Latimer diagram can differ by one or more electrons. Oxidation states for the element undergoing redox are typically determined by difference; we assign the oxygen atoms an oxidation state of -2 and the hydrogen atoms an oxidation state of +1.

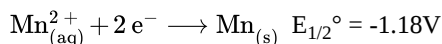
Example:

Mn in Acid

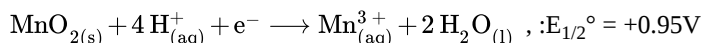


The Latimer diagram for Mn illustrates its standard reduction potentials (in 1 M acid) in oxidation states from +7 to 0.

The Latimer diagram compresses into shorthand notation all the standard potentials for redox reactions of the element Mn. For example, the entry that connects Mn^{2+} and Mn gives the potential for the half-cell reaction:



and the entry connecting Mn^{4+} and Mn^{3+} represents the reaction:



We can also calculate values for **multi-electron reactions** by first adding $\Delta G^\circ (= -nFE^\circ)$ values and then dividing by the total number of electrons

For example, for the 5-electron reduction of MnO_4^- to Mn^{2+} , we write

$$E^\circ = \frac{1(0.564) + 1(0.274) + 1(4.27) + 1(0.95) + 1(1.51)}{5} = +1.51\text{V} \quad (4.4.1)$$

and for the three-electron reduction of $\text{MnO}_4^-(\text{aq})$ to $\text{MnO}_2(\text{s})$,

$$E^\circ = \frac{1(0.564) + 1(0.274) + 1(4.27)}{3} = +1.70\text{V} \quad (4.4.2)$$

Remember to divide by the number of electrons involved in the oxidation number change (5 and 3 for the above equations).

Thermodynamically stable and unstable oxidation states

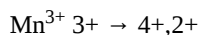
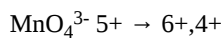
An unstable species on a Latimer diagram will have a lower standard potential to the left than to the right.

Example:

$\text{MnO}_4^{3-} \rightarrow \text{MnO}_2 + \text{MnO}_4^{2-}$ the MnO_4^{3-} species is unstable

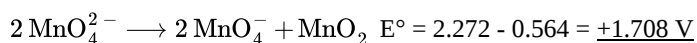
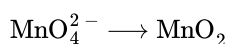
$$E^\circ = +4.27 - 0.274 = 3.997\text{V} \text{ (spontaneous disproportionation)}$$

Which Mn species are unstable with respect to disproportionation?



So stable species are: MnO_4^- , MnO_4^{2-} , MnO_2 , Mn^{2+} , and Mn^0 .

But MnO_4^{2-} is also unstable - why?



Moral: All possible disproportionation reactions must be considered in order to determine stability (this is often more convenient with a Frost diagram).

Note

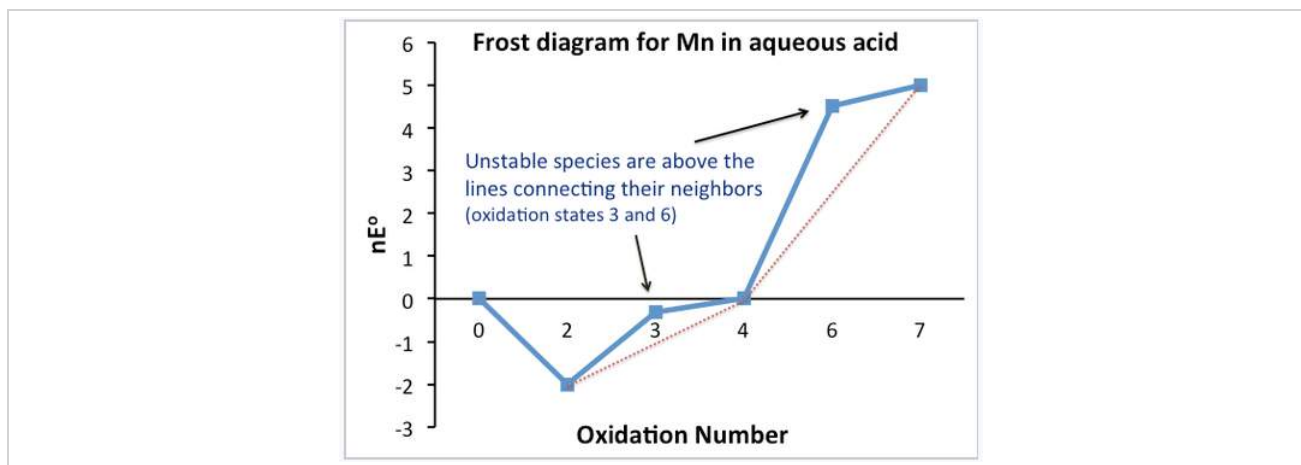
Thermodynamically unstable ions can be quite stable kinetically. For example, most N-containing molecules (NO_2 , NO , N_2H_4) are unstable relative to the elements (O_2 , N_2 , H_2), but they are still quite stable kinetically.

Frost diagrams:

In a Frost diagram, we plot $\Delta G^\circ F (= nE^\circ)$ vs. oxidation number. The zero oxidation state is assigned a nE° value of zero.^[2]

Stable and **unstable oxidation states** can be easily identified in the plot. Unstable compounds are higher on the plot than the line connecting their neighbors. Note that this is simply a graphical representation of what we did with the Latimer diagram to determine which oxidation states were stable and unstable.

The **standard potential** for any electrochemical reaction is given by the **slope** of the line connecting the two species on a Frost diagram. For example, the line connecting Mn^{3+} and MnO_2 on the Frost diagram has a slope of +0.95, the standard potential of MnO_2 reduction to Mn^{3+} . This is the number that is written above the arrow in the Latimer diagram for Mn. Multielectron potentials can be calculated easily by connecting the dots in a Frost diagram.



A Frost diagram:

Contains the same information as in a Latimer diagram, but graphically shows stability and oxidizing power.

The lowest species on the diagram are the most stable (Mn^{2+} , MnO_2)

The highest species on diagram are the strongest oxidizers (MnO_4^-)

This page titled [4.4: Latimer and Frost Diagrams](#) is shared under a [CC BY-SA 4.0](#) license and was authored, remixed, and/or curated by [Chemistry 310 \(Wikibook\)](#) via [source content](#) that was edited to the style and standards of the LibreTexts platform; a detailed edit history is available upon request.

4.5: Redox Reactions with Coupled Equilibria

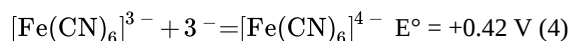
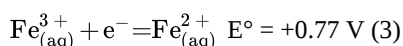
Redox Reactions with Coupled Equilibria

Coupled equilibria (solubility, complexation, acid-base, and other reactions) change the value of E° , effectively by changing the concentrations of free metal ions. We can use the Nernst equation to calculate the value of E° from the equilibrium constant for the coupled reaction. Alternatively, we can measure the half-cell potential with and without the coupled reaction to get the value of the equilibrium constant. This is one of the best ways to measure K_{sp} , K_a , and K_d values.

As an example, we consider the complexation of Fe^{2+} and Fe^{3+} by CN^- ions:



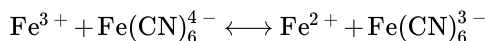
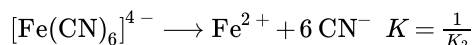
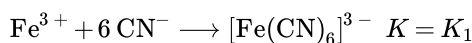
Which oxidation state of Fe is more strongly complexed by CN^- ? We can answer this question by measuring the standard half-cell potential of the $[Fe(CN)_6]^{3-/4-}$ couple and comparing it to that of the $Fe^{3+/2+}$ couple:



Iron(III) is **harder to reduce** (i.e., E° is **less positive**) when it is complexed to CN^-

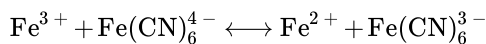
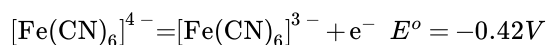
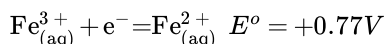
This implies that the equilibrium constant for complexation reaction (Equation 4.5.1) should be **smaller** than that for reaction (Equation 4.5.2). How much smaller?

We can calculate the ratio of equilibrium constants by adding and subtracting reactions:



The equilibrium constant for this reaction is the product of the two reactions we added, i.e., $K = K_1/K_2$.

But we can make the same overall reaction by combining reactions (3) and (4)



In this case, we can calculate $E^\circ = 0.77 - 0.42 = +0.35 \text{ V}$

It follows from $nFE^\circ = -\Delta G^\circ = RT \ln K$ that

$$E^\circ = \frac{RT}{nF} \ln \frac{K_1}{K_2}$$

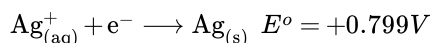
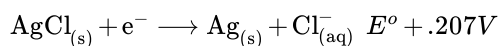
$$\frac{K_1}{K_2} = \exp\left(\frac{nFE^\circ}{RT}\right) = \exp[(1 \text{ equiv/mol})(96,500 \text{ C/equiv})(0.35 \text{ J/C})(8.314 \text{ J/molK})(298)] = \exp(13.63) = 8 \times 10^5$$

Thus we find that $Fe(CN)_6^{3-}$ is about a million times more stable as a complex than $Fe(CN)_6^{4-}$.

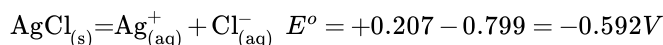
Solubility Equilibria

We can use a similar procedure to measure K_{sp} values electrochemically.

For example, the silver halides ($AgCl$, $AgBr$, AgI) are sparingly soluble. We can calculate the K_{sp} of $AgCl$ by measuring the standard potential of the $AgCl/Ag$ couple. This can be done very simply by measuring the potential of a silver wire, which is in contact with solid $AgCl$ and 1 M $Cl^-(aq)$, against a hydrogen reference electrode. That value is then compared to the standard potential of the Ag^+/Ag couple:



Subtracting the second reaction from the first one we obtain:



and again using $nFE^{\circ} = RT\ln K$, we obtain $K = K_{sp} = 9.7 \times 10^{-11} \text{ M}^2$.



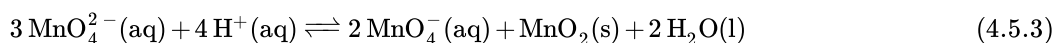
Because the solubility of the silver halides is so low, this would be a very difficult number to measure by other methods, e.g., by measuring the concentration of Ag^{+} spectroscopically, or by gravimetry. In practice almost all K_{sp} values involving electroactive substances are measured potentiometrically.

Acid-Base Equilibria

Many electrochemical reactions involve H^{+} or OH^{-} . For these reactions, the half-cell potentials are **pH-dependent**.

Example: Recall that the disproportionation reaction $3 \text{MnO}_{4(a)}^{2-} \longrightarrow 2 \text{MnO}_{4(a)}^{-} + \text{MnO}_{2(s)}$ is **spontaneous** at $\text{pH}=0$ ($[\text{H}^{+}] = 1\text{M}$), from the Latimer diagram or Frost plot.

However, when we properly balance this half reaction we see that it involves **protons as a reactant**:



By Le Chatelier's principle, it follows that **removing protons** (increasing the pH) should **stabilize** the reactant, MnO_4^{2-} . Thus we would expect the +6 oxidation state of Mn, which is unstable in acid, to be stabilized in basic media. We will examine these proton-coupled redox equilibria more thoroughly in the context of Pourbaix diagrams below.



Acid mine drainage occurs when sulfide rocks such as pyrite (FeS_2) are exposed to the air and oxidized. The reaction produces aqueous Fe^{3+} and H_2SO_4 . When the acidic effluent of the mine meets a stream or lake at higher pH, solid $\text{Fe}(\text{OH})_3$ precipitates, resulting in the characteristic orange muddy color downstream of the mine. The acidic effluent is toxic to plants and animals.

This page titled [4.5: Redox Reactions with Coupled Equilibria](#) is shared under a [CC BY-SA 4.0](#) license and was authored, remixed, and/or curated by [Chemistry 310 \(Wikibook\)](#) via [source content](#) that was edited to the style and standards of the LibreTexts platform; a detailed edit history is available upon request.

4.6: Pourbaix Diagrams

Pourbaix Diagrams plot electrochemical stability for different redox states of an element as a function of pH.^[3] As noted above, these diagrams are essentially phase diagrams that map the conditions of potential and pH (most typically in aqueous solutions) where different redox species are stable. We saw a simple example of such a diagram in section 4.2 for H₂O. Typically, the water redox reactions are plotted as dotted lines on these more complicated diagrams for other elements.

The lines in Pourbaix diagrams represent redox and acid-base reactions, and are the parts of the diagram where two species can exist in equilibrium. For example, in the Pourbaix diagram for Fe below, the horizontal line between the Fe³⁺ and Fe²⁺ regions represents the reaction $\text{Fe}_{(\text{aq})}^{3+} + \text{e}^- = \text{Fe}_{(\text{aq})}^{2+}$, which has a standard potential of +0.77 V. While we could use standard potentials for all these lines, in practice Pourbaix diagrams are usually plotted for lower ion concentrations (often 1 mM) that are more relevant to corrosion and electrochemical experiments.

Example: Iron Pourbaix diagram

Areas in the Pourbaix diagram mark regions where a single species (Fe²⁺(aq), Fe₃O₄(s), etc.) is stable. More stable species tend to occupy larger areas.

Lines mark places where two species exist in equilibrium.

- **Pure redox** reactions are **horizontal** lines - these reactions are not pH-dependent
- **Pure acid-base** reactions are **vertical** lines - these do not depend on potential
- Reactions that are **both** acid-base and redox have a slope of $-0.0592 \text{ V/pH} \times \# \text{H}^+/\# \text{e}^-$

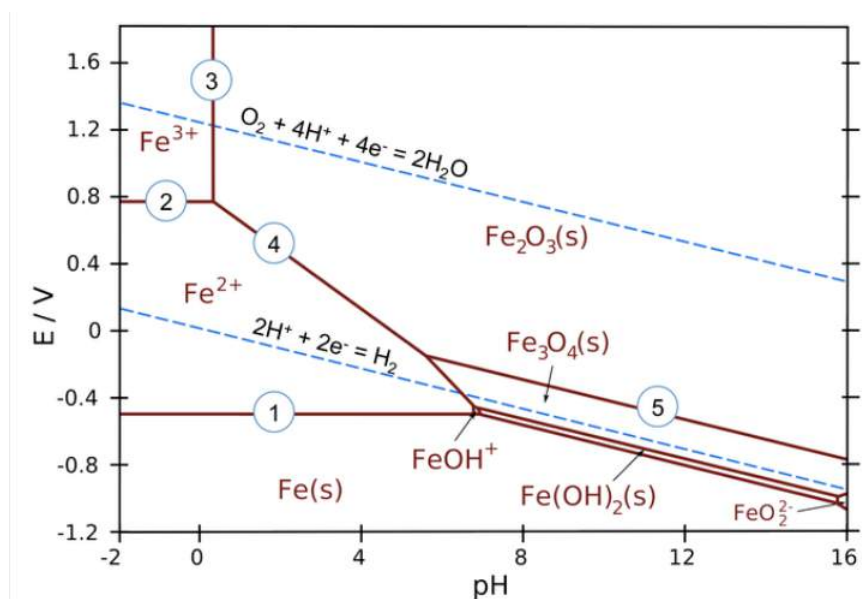
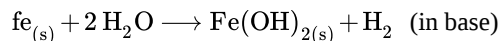
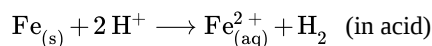


Figure 4.6.1: Pourbaix diagram for iron at ionic concentrations of 1.0 mM. (CC BY-SA 3.0 Unported; Metallos via [Wikipedia](#))

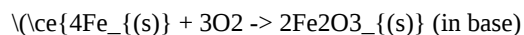
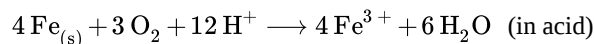
Examples of equilibria in the iron Pourbaix diagram (numbered on the plot):

1. $\text{Fe}^{2+} + 2 \text{e}^- \longrightarrow \text{Fe}_{(\text{s})}$ (pure redox reaction - no pH dependence)
2. $\text{Fe}^{3+} + \text{e}^- \longrightarrow \text{Fe}^{2+}$ (pure redox reaction - no pH dependence)
3. $2 \text{Fe}^{3+} + 3 \text{H}_2\text{O} \longrightarrow \text{Fe}_2\text{O}_3(\text{s}) + 6 \text{H}^+$ (pure acid-base, no redox)
4. $2 \text{Fe}^{2+} + 3 \text{H}_2\text{O} \longrightarrow \text{Fe}_2\text{O}_3(\text{s}) + 6 \text{H}^+ + 2 \text{e}^-$ (slope = $-59.2 \times 6/2 = -178 \text{ mV/pH}$)
5. $2 \text{Fe}_3\text{O}_4(\text{s}) + \text{H}_2\text{O} \longrightarrow 2 \text{H}^+ + 2 \text{e}^-$ (slope = $-59.2 \times 2/2 = -59.2 \text{ mV/pH}$)

The water redox lines have special significance on a Pourbaix diagram for an element such as iron. Recall that liquid water is stable *only* in the region between the dotted lines. Below the H₂ line, water is unstable relative to hydrogen gas, and above the O₂ line, water is unstable with respect to oxygen. For active metals such as Fe, the region where the pure element is stable is typically below the H₂ line. This means that iron metal is unstable in contact with water, undergoing reactions:



Iron (and most other metals) are also thermodynamically unstable in air-saturated water, where the potential of the solution is close to the O_2 line in the Pourbaix diagram. Here the spontaneous reactions are:



Corrosion and passivation. It certainly sounds bad for our friend Fe: unstable in water, no matter what the pH or potential. Given enough time, it will all turn into rust. But iron (and other active metals) can corrode, or can be stabilized against corrosion, depending on the conditions. Because our civilization is dependent on the use of active metals such as Fe, Al, Zn, Ti, Cr... for practically everything, it is important to understand this, and we can do so by referring to the Pourbaix diagram.

The **corrosion** of iron (and other active metals such as Al) is indeed rapid in parts of the Pourbaix diagram where the element is oxidized to a soluble, ionic product such as $\text{Fe}^{3+}(\text{aq})$ or $\text{Al}^{3+}(\text{aq})$. However, solids such as Fe_2O_3 , and especially Al_2O_3 , form a protective coating on the metal that greatly impedes the corrosion reaction. This phenomenon is called **passivation**.

Draw a vertical line through the iron Pourbaix diagram at the pH of tap water (about 6) and you will discover something interesting: at slightly acidic pH, iron is quite unstable with respect to corrosion by the reaction:

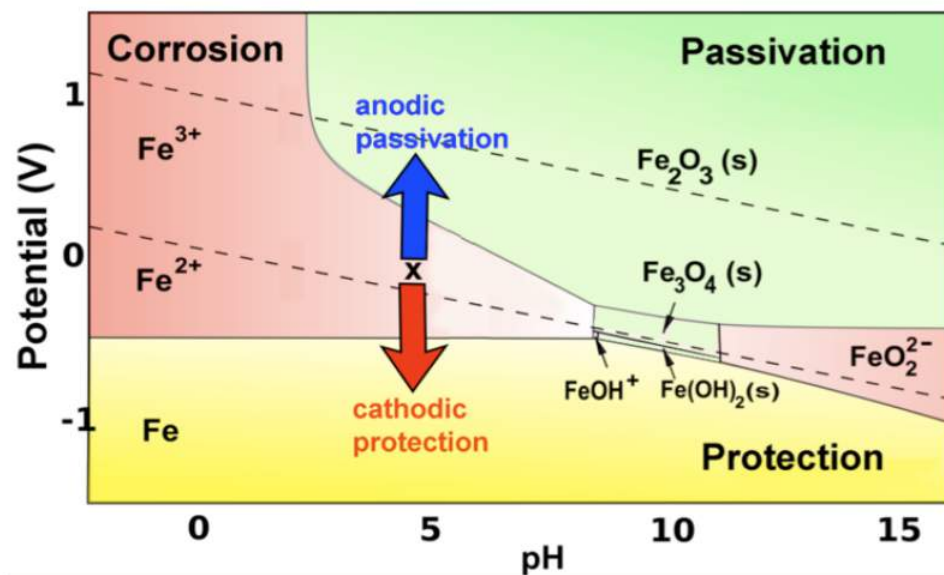


but *only in water that contains relatively little oxygen*, i.e., in solutions where the potential is near the H_2 line. Saturating the water with air or oxygen moves the system closer to the O_2 line, where the most stable species is Fe_2O_3 and the corrosion reaction is:



This oxidation reaction is orders of magnitude slower because the oxide that is formed *passivates* the surface. Therefore iron corrodes much more slowly in oxygenated solutions.

More generally, iron (and other active metals) are passivated whenever they oxidize to produce a solid product, and corrode whenever the product is ionic and soluble. This behavior can be summed up on the color-coded Pourbaix diagram below. The red and green regions represent conditions under which oxidation of iron produces soluble and insoluble products, respectively.



In the yellow part of the diagram, an active metal such as iron can be **protected** by a second mechanism, which is to bias it so that its potential is below the oxidation potential of the metal. This **cathodic protection** strategy is most frequently carried out by

connecting a more active metal such as Mg or Zn to the iron or steel object (e.g., the hull of a ship, or an underground gas pipeline) that is being protected. The active metal (which must be higher than Fe in the activity series) is also in contact with the solution and slowly corrodes, so it must eventually be replaced. In some cases a battery or DC power supply - the anode of which oxidizes water to oxygen in the solution - is used instead to apply a negative bias.



The white patches visible on the ship's hull are zinc block sacrificial anodes.

Another common mode of corrosion of iron and carbon steel is **differential aeration**. In this case, part of the iron object - e.g., the base of a bridge, or the drill in an oil rig - is under water or in an anoxic environment such as mud or soil. The potential of the solution is close to the H_2 line in the Pourbaix diagram, where Fe can corrode to Fe^{2+} (aq). Another part of the iron object is in the air, or near the surface where water is well oxygenated. At that surface oxygen can be reduced to water, $O_2 + 4H^+ + 4e^- = 2 H_2O$. The conductive iron object completes the circuit, carrying electrons from the anode (where Fe is oxidized) to the cathode (where O_2 is reduced). Corrosion by differential aeration can be rapid because soluble ions are produced, and the reaction has a driving force of over 1 V. Iron or carbon steel that is subjected to frequent weathering, such as the cast iron bridge and lamppost shown below, is corroded on the surface by differential aeration.



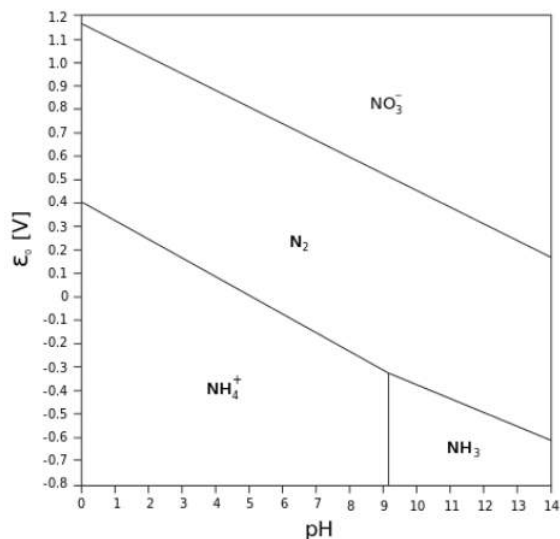
Rusty cast iron bridge and lamppost, North Ayrshire, Scotland

Differential aeration is involved in the formation of a rust ring around wet areas of cast iron, e.g., an iron frying pan left partially submerged in water for a day or more. (You may have seen this mechanism of corrosion in action when you did not get to the dirty dishes right away). Under the water, Fe is oxidized to soluble Fe^{2+} , and at the water line O_2 is reduced to H_2O . As Fe^{2+} ions diffuse towards the water surface, they encounter oxygen molecules and are oxidized to Fe^{3+} . However Fe^{3+} is insoluble at neutral pH and deposits as rust, typically just below the water line, forming the rust ring.

This page titled [4.6: Pourbaix Diagrams](#) is shared under a [CC BY-SA 4.0](#) license and was authored, remixed, and/or curated by [Chemistry 310 \(Wikibook\)](#) via [source content](#) that was edited to the style and standards of the LibreTexts platform; a detailed edit history is available upon request.

4.7: Discussion Questions

- Explain the simplified Pourbaix diagram for nitrogen, shown below. Discuss the reactions that are implied by the lines, and explain why they have the slopes they do.

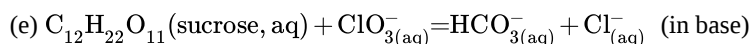
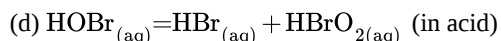
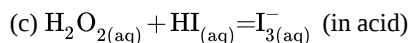
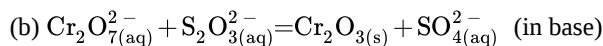
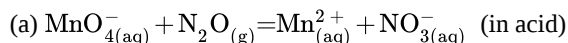


- Use the information in the Pourbaix diagram to construct a Frost diagram for nitrogen at pH 7.

This page titled [4.7: Discussion Questions](#) is shared under a [CC BY-SA 4.0](#) license and was authored, remixed, and/or curated by [Chemistry 310 \(Wikibook\)](#) via [source content](#) that was edited to the style and standards of the LibreTexts platform; a detailed edit history is available upon request.

4.8: Problems

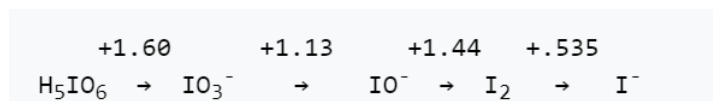
1. Balance the following redox reactions, adding H_2O and H^+ (or OH^-) as needed. Predict for each one whether the reaction would become more or less spontaneous at higher pH.



2. Silver metal is not easily oxidized, and does not react with oxygen-saturated water. However, when excess NaCN is added to a suspension of silver particles, some silver dissolves. If oxygen is removed (e.g., by bubbling nitrogen through the solution), the dissolution reaction stops. Write a balanced equation for the dissolution reaction (hint: it is a redox reaction).

3. The standard potentials for the $\text{Fe}^{3+}/\text{Fe}^{2+}$ and Cl^-/Cl_2 couples are +0.77 and +1.36 V. Calculate the cell potential of a redox flow battery that has $\text{Fe}^{3+}/\text{Fe}^{2+}$ and Cl^-/Cl_2 solutions on the two sides (both containing 1.0 M HCl as the electrolyte). The pressure of Cl_2 gas on the chlorine side is 0.2 atm, and the concentrations of Fe^{2+} and Fe^{3+} on the iron side are both 0.10 M.

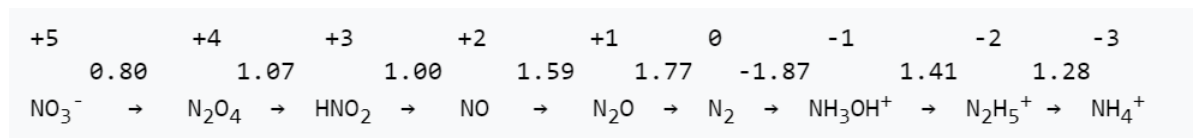
4. The Latimer potential diagram for iodine (in acidic solutions) is given below.



(a) What is the potential for the IO_3^-/I^- redox couple?

(b) Construct a Frost diagram and identify any species that are unstable with respect to disproportionation.

5. The Latimer diagram for nitrogen in acidic solutions is shown below:



(a) Write a balanced half reaction for reduction of NO to NH_4^+ in acid.

(b) What is the value of E° for the half reaction in part (a)?

(c) Is this half reaction more thermodynamically favorable in acid or in base? Explain.

(d) All the nitrogen-containing molecules and ions listed above are kinetically stable, but only three are *thermodynamically* stable with respect to disproportionation in acid. Which ones are they?

6. Referring to the Pourbaix diagram for Mn below:

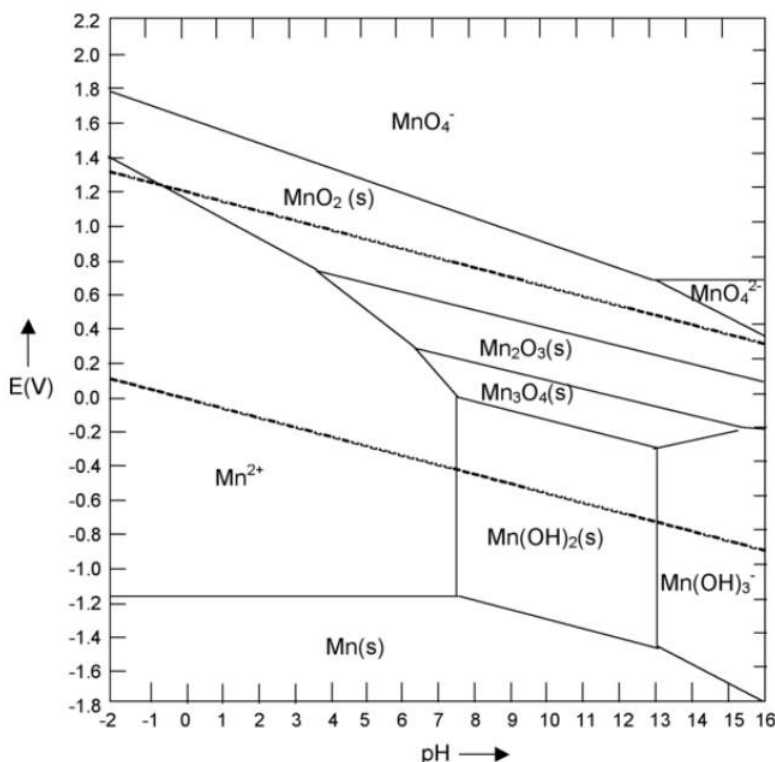
(a) Write out the balanced half reaction corresponding to the line separating Mn^{2+} and Mn_2O_3 . Use your answer to calculate the slope of the line (give units).

(b) Is Mn metal stable in water at any pH? If so, in what range of pH?

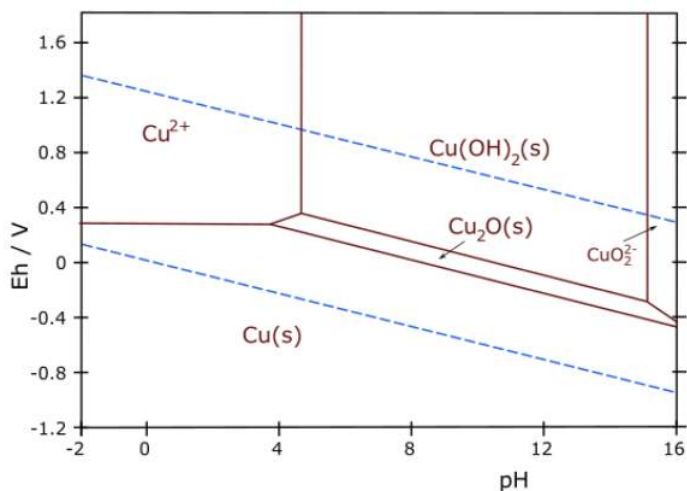
(c) What spontaneous reaction would you expect for an aqueous solution of MnO_4^- at pH 6?

(d) Describe an electrochemical procedure (specifying pH and potential) for making $\text{Mn}_3\text{O}_4(\text{s})$ from aqueous Mn^{2+} .

(e) Label the regions of the diagram that correspond to corrosion and passivation of Mn metal.



7. The Pourbaix diagram for copper is shown below.



- Write a balanced half-reaction that corresponds to the boundary between the Cu₂O(s) and Cu(OH)₂(s) regions of the diagram.
- What is the slope of the line (do not try to measure it from the graph!) that connects the Cu²⁺(aq) and Cu₂O(s) regions? Explain your reasoning.
- Over what pH range (if any) is copper metal stable in contact with pure water?
- Thermodynamically, the reaction between copper and oxygen is spontaneous at pH 7. Would you expect copper to corrode or to be passivated against corrosion in aerated water at neutral pH? Explain your reasoning.
- Some recent studies have suggested the use of Cu₂O as a water splitting photocatalyst. Would you expect Cu₂O to be stable in the presence of the oxygen formed in the reaction? Explain your reasoning.

This page titled [4.8: Problems](#) is shared under a [CC BY-SA 4.0](#) license and was authored, remixed, and/or curated by [Chemistry 310 \(Wikibook\)](#) via [source content](#) that was edited to the style and standards of the LibreTexts platform; a detailed edit history is available upon request.

4.9: References

1. Alotto, P.; Guarnieri, M.; Moro, F. (2014). "Redox Flow Batteries for the storage of renewable energy: a review". *Renewable & Sustainable Energy Reviews* **29**: 325–335. doi:[10.1016/j.rser.2013.08.001](https://doi.org/10.1016/j.rser.2013.08.001).
 2. Frost, Arthur (1951). "Oxidation Potential–Free Energy Diagrams". *Journal of the American Chemical Society* **73** (6): 2680–2682. doi:[10.1021/ja01150a074](https://doi.org/10.1021/ja01150a074).
 3. Pourbaix, M., Atlas of electrochemical equilibria in aqueous solutions. 2d English ed. 1974, Houston, Tex.: National Association of Corrosion Engineers.
-

This page titled [4.9: References](#) is shared under a [CC BY-SA 4.0](#) license and was authored, remixed, and/or curated by [Chemistry 310 \(Wikibook\)](#) via [source content](#) that was edited to the style and standards of the LibreTexts platform; a detailed edit history is available upon request.

CHAPTER OVERVIEW

5: Coordination Chemistry and Crystal Field Theory

Learning Objectives

- Determine oxidation states and assign d-electron counts for transition metals in complexes.
- Derive the d-orbital splitting patterns for octahedral, elongated octahedral, square pyramidal, square planar, and tetrahedral complexes.
- For octahedral and tetrahedral complexes, determine the number of unpaired electrons and calculate the crystal field stabilization energy.
- Know the spectrochemical series, rationalize why different classes of ligands impact the crystal field splitting energy as they do, and use it to predict high vs. low spin complexes, and the colors of transition metal complexes.
- Use the magnetic moment of transition metal complexes to determine their spin state.
- Understand the origin of the Jahn-Teller effect and its consequences for complex shape, color, and reactivity.
- Understand the extra stability of complexes formed by chelating and macrocyclic ligands.

Coordination compounds (or complexes) are molecules and extended solids that contain bonds between a transition metal ion and one or more ligands. In forming these coordinate covalent bonds, the metal ions act as Lewis acids and the ligands act as Lewis bases. Typically, the ligand has a lone pair of electrons, and the bond is formed by overlap of the molecular orbital containing this electron pair with the d-orbitals of the metal ion.

[5.1: Prelude to Coordination Chemistry and Crystal Field Theory](#)

[5.2: Counting Electrons in Transition Metal Complexes](#)

[5.3: Crystal Field Theory](#)

[5.4: Spectrochemical Series](#)

[5.5: \$\pi\$ -Bonding between Metals and Ligands](#)

[5.6: Crystal Field Stabilization Energy, Pairing, and Hund's Rule](#)

[5.7: Non-octahedral Complexes](#)

[5.8: Jahn-Teller Effect](#)

[5.9: Tetrahedral Complexes](#)

[5.10: Stability of Transition Metal Complexes](#)

[5.11: Chelate and Macrocyclic Effects](#)

[5.12: Ligand Substitution Reactions](#)

[5.13: Discussion Questions](#)

[5.14: Problems](#)

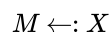
[5.15: References](#)

This page titled [5: Coordination Chemistry and Crystal Field Theory](#) is shared under a [CC BY-SA 4.0](#) license and was authored, remixed, and/or curated by [Chemistry 310 \(Wikibook\)](#) via [source content](#) that was edited to the style and standards of the LibreTexts platform; a detailed edit history is available upon request.

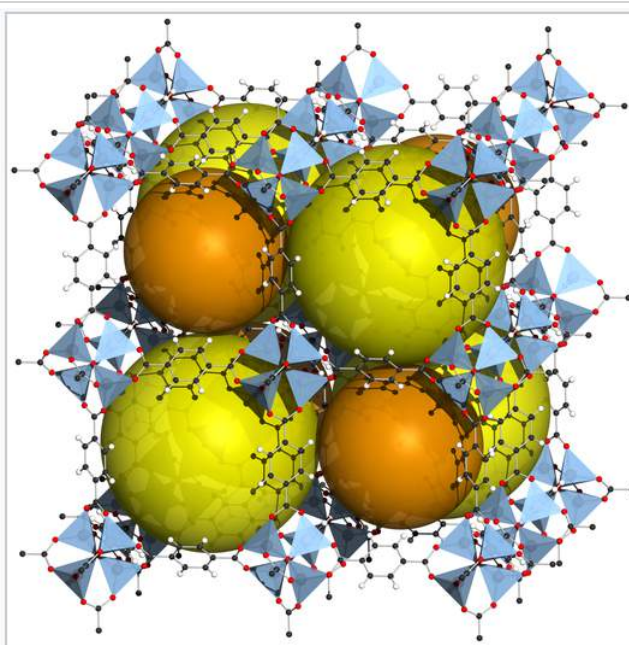
5.1: Prelude to Coordination Chemistry and Crystal Field Theory

Coordination compounds (or **complexes**) are molecules and extended solids that contain bonds between a **transition metal** ion and one or more **ligands**. In forming these **coordinate covalent bonds**, the metal ions act as Lewis acids and the ligands act as Lewis bases. Typically, the ligand has a lone pair of electrons, and the bond is formed by overlap of the molecular orbital containing this electron pair with the d-orbitals of the metal ion. Ligands that are commonly found in coordination complexes are neutral molecules (H_2O , NH_3 , organic bases such as pyridine, CO , NO , H_2 , ethylene, and phosphines PR_3) and anions (halides, CN^- , SCN^- , cyclopentadienide (C_5H_5^-), H^- , etc.). The resulting complexes can be cationic (e.g., $[\text{Cu}(\text{NH}_3)_4]^{2+}$), neutral ($[\text{Pt}(\text{NH}_3)_2\text{Cl}_2]$) or anionic ($[\text{Fe}(\text{CN})_6]^{4-}$). As we will see below, ligands that have weak or negligible strength as Brønsted bases (for example, CO , CN^- , H_2O , and Cl^-) can still be potent Lewis bases in forming transition metal complexes.

With ligands that are Lewis bases, coordinate covalent bonds (also called dative bonds) are typically drawn as lines, or sometimes as arrows to indicate that the electron pair "belongs" to the ligand X:



In counting electrons on the metal (described below), the convention is to assign both electrons in the dative bond to the ligand, although in reality the bonds are typically polar covalent and electrons are shared between the metal and the ligand.



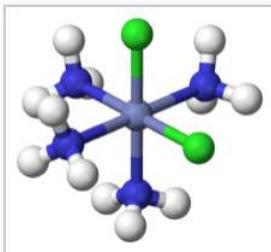
$\text{Zn}_4\text{O}(\text{BDC})_3$, also called MOF-5, is a metal-organic framework in which 1,4-benzenedicarboxylate (BDC) anions bridge between cationic Zn_4O clusters.^[1] The rigid framework contains large voids, represented by orange spheres. MOFs can be made from many different transition metal ions and bridging ligands, and are being developed for practical applications in storing gases, especially H_2 and CO_2 . MOF-5 has a volumetric storage density of 66 g H_2/L , close to that of liquid H_2 .

When writing out the formulas of coordination compounds, we use square brackets [...] around the metal ions and ligands that are directly bonded to each other. Thus the compound $[\text{Co}(\text{NH}_3)_5\text{Cl}]\text{Cl}_2$ contains octahedral $[\text{Co}(\text{NH}_3)_5\text{Cl}]^{2+}$ ions, in which five ammonia molecules and one chloride ion are directly bonded to the metal, and two Cl^- anions that are not coordinated to the metal.

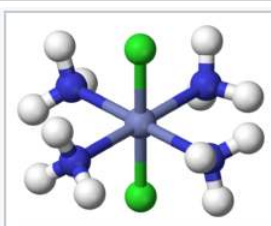
History

Coordination compounds have been known for centuries, but their structures were initially not understood. For example, Prussian Blue, which has an empirical formula $\text{Fe}_7(\text{CN})_{18} \cdot x\text{H}_2\text{O}$, is an insoluble, deep blue solid that has been used as a pigment since its accidental discovery by Diesbach in 1704. Prussian Blue actually contains Fe^{3+} cations and $[\text{Fe}(\text{CN})_6]^{4-}$ anions, and a more descriptive formulation is $(\text{Fe}^{3+})_4([\text{Fe}(\text{CN})_6]^{4-})_3 \cdot x\text{H}_2\text{O}$. Simpler compounds such as the ammonia complex of Co^{3+} were known to chemists but did not fit the expected behavior of ionic solids. For example, cobalt(III)hexammine chloride, $[\text{Co}(\text{NH}_3)_6]\text{Cl}_3$ was formulated as $\text{CoCl}_3 \cdot 6\text{NH}_3$. It had mysterious properties, in that it dissolved in water like an ionic solid, but it retained its six ammonia molecules when recrystallized. Even more intriguing was the observation that chemically different forms (isomers) of

transition metal complexes such as $[\text{Co}(\text{NH}_3)_4\text{Cl}_2]\text{Cl}$ could be made. The puzzle was solved by Alfred Werner, who proposed in 1893 that these Co complexes contained octahedrally coordinated metal ions that made primary (covalent) bonds to six ligands. Werner showed through conductivity measurements that solutions of $\text{CoCl}_3 \cdot 6\text{NH}_3$ contained three free Cl^- anions and one $[\text{Co}(\text{NH}_3)_6]^{3+}$ cation per formula unit. Magnetic susceptibility measurements later confirmed the presence of diamagnetic Co^{3+} in both the salt and its solutions. Werner's theory also explained the existence of two (and only two) structural isomers for $[\text{Co}(\text{NH}_3)_4\text{Cl}_2]^+$.



cis- $[\text{Co}(\text{NH}_3)_4\text{Cl}_2]^+$



trans- $[\text{Co}(\text{NH}_3)_4\text{Cl}_2]^+$

Like organic compounds, transition metal complexes can vary widely in size, shape, charge and stability. We will see that bonds formed from the d-orbitals of the metal largely control these properties.



Alfred Werner was a Swiss chemist who received the Nobel prize in 1913 for elucidating the bonding in coordination compounds.

This page titled [5.1: Prelude to Coordination Chemistry and Crystal Field Theory](#) is shared under a [CC BY-SA 4.0](#) license and was authored, remixed, and/or curated by [Chemistry 310 \(Wikibook\)](#) via [source content](#) that was edited to the style and standards of the LibreTexts platform; a detailed edit history is available upon request.

5.2: Counting Electrons in Transition Metal Complexes

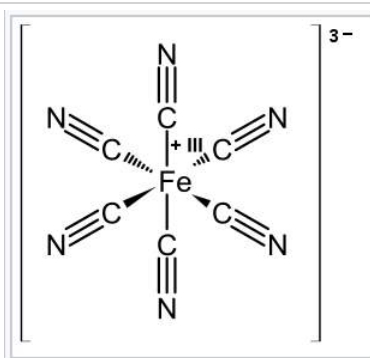
The d-orbitals are the frontier orbitals (the HOMO and LUMO) of transition metal complexes. Many of the important properties of complexes - their shape, color, magnetism, and reactivity - depend on the electron occupancy of the metal's d-orbitals. To understand and rationalize these properties it is important to know how to count the d-electrons.

Because transition metals are generally less electronegative than the atoms on the ligands (C, N, O, Cl, P...) that form the metal-ligand bond, our convention is to assign **both electrons** in the bond to the **ligand**. For example, in the ferricyanide complex $[\text{Fe}(\text{CN})_6]^{3-}$, if the cyanide ligand keeps both of its electrons it is formulated as CN^- . By difference, iron must be Fe^{3+} because the charges ($3^+ + 6(1^-)$) must add up to the overall -3 charge on the complex.

The next step is to determine how many d-electrons the Fe^{3+} ion has. The rule is to count **all** of iron's valence electrons as **d-electrons**. Iron is in group 8, so

$$\text{group } 8 - 3^+ \text{ charge} = d^5 \text{ (or } 3d^5\text{)}$$

$$8 - 3 = 5$$

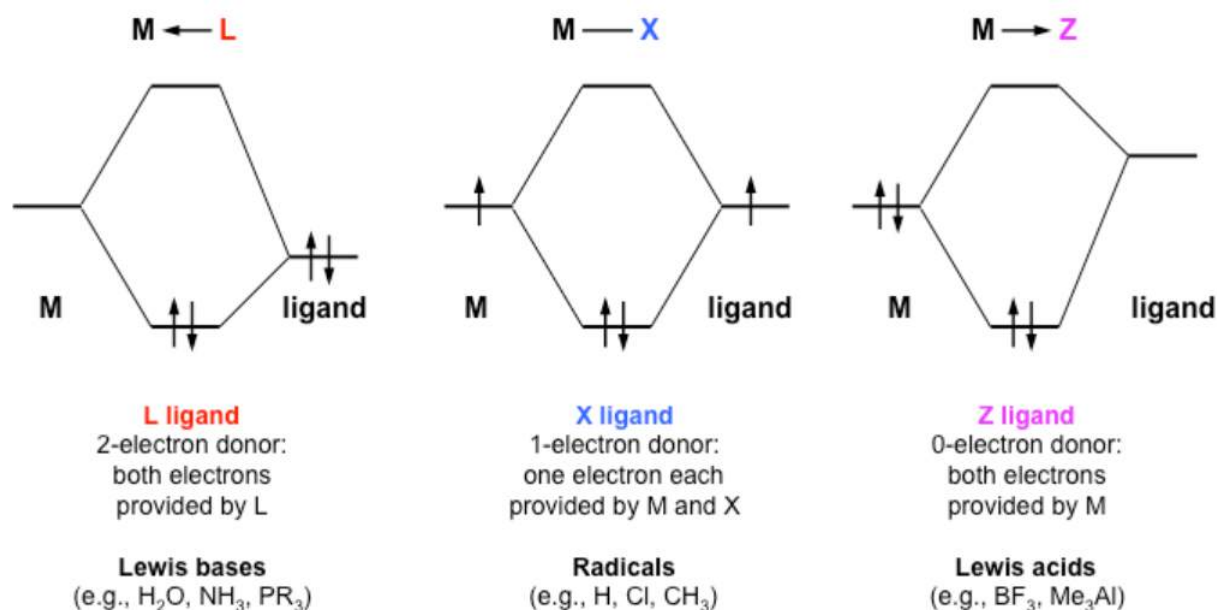


Structure of the octahedral ferricyanide anion. Because the overall charge of the complex is 3^- , Fe is in the $+3$ oxidation state and its electron count is $3d^5$.

The same procedure can be applied to any transition metal complex. For example, consider the complex $[\text{Cu}(\text{NH}_3)_4]^{2+}$. Because ammonia is a neutral ligand, Cu is in the 2^+ oxidation state. Copper (II), in group 11 of the periodic table has 11 electrons in its valence shell, minus two, leaving it with 9 d-electrons ($3d^9$). In the neutral complex $[\text{Rh}(\text{OH})_3(\text{H}_2\text{O})_3]$, Rh is in the $+3$ oxidation state and is in group 9, so the electron count is $4d^6$. Zinc(II) in group 12 would have 10 d-electrons in $[\text{Zn}(\text{NH}_3)_4]^{2+}$, a full shell, and manganese (VII) has zero d-electrons in MnO_4^- . Nickel carbonyl, $\text{Ni}(\text{CO})_4$, contains the neutral CO ligand and Ni in the zero oxidation state. Since Ni is in group 10, we count the electrons on Ni as $3d^{10}$.

A frequent source of confusion about electron counting is the fate of the s-electrons on the metal. For example, our electron counting rules predict that Ti is $3d^1$ in the octahedral complex $[\text{Ti}(\text{H}_2\text{O})_6]^{3+}$. But the electronic configuration of a free Ti atom, according to the Aufbau principle, is $4s^23d^2$. Why is the Ti^{3+} ion $3d^1$ and not $4s^1$? Similarly, why do we assign Mn^{2+} as $3d^5$ rather than $4s^23d^3$? The short answer is that the metal s orbitals are higher in energy in a metal complex than they are in the free atom because they have antibonding character. We will justify this statement with a MO diagram in Section 5.2.

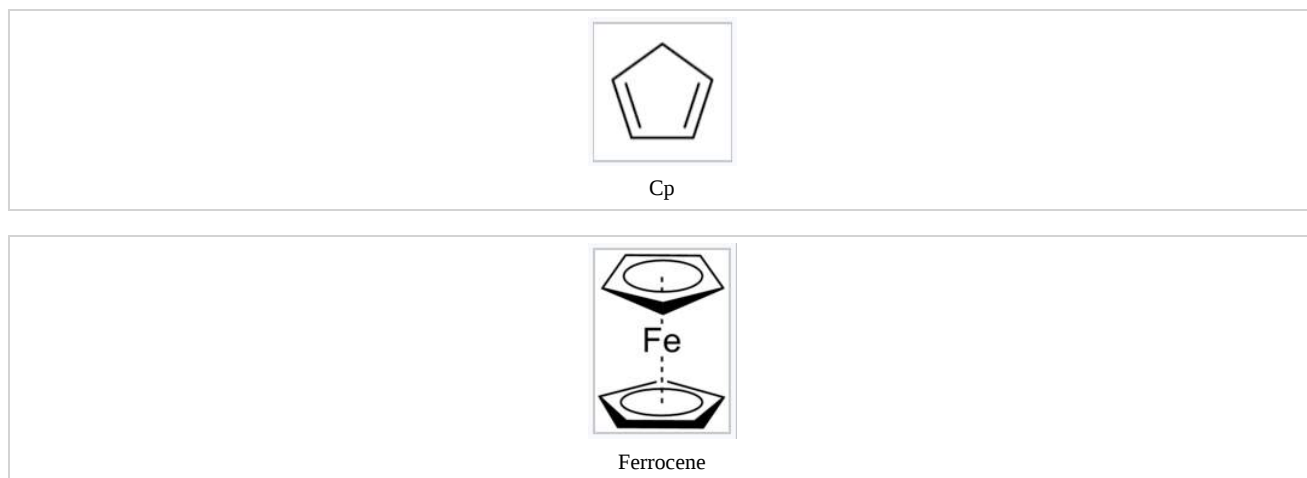
Covalent Bond Classification (CBC) Method. Although the electron counting rule we have developed above is useful and works reliably for all kinds of complexes, the assignment of all the shared electrons in the complex to the ligands does not always represent the true bonding picture. This picture would be most accurate in the case of ligands that are much more electronegative than the metal. But in fact, there are all kinds of ligands, including those such as H, alkyl, cyclopentadienide, and others where the metal and ligand have comparable electronegativity. In those cases, especially with late transition metals that are relatively electropositive, we should regard the metal-ligand bond as covalent. The CBC method, also referred to as LXZ notation, was introduced in 1995 by M. L. H. Green^[2] in order to better describe the different kinds of metal-ligand bonds. The molecular orbital pictures below summarize the difference between L, X, and Z ligands.^[3] Of these, L and X are the most common types.



L-type ligands are Lewis bases that donate two electrons to the metal center regardless of the electron counting method being used. These electrons can come from lone pairs, pi or sigma donors. The bonds formed between these ligands and the metal are dative covalent bonds, which are also known as coordinate bonds. Examples of this type of ligand include CO , PR_3 , NH_3 , H_2O , carbenes ($=\text{CRR}'$), and alkenes.

X-type ligands are those that donate one electron to the metal and accept one electron from the metal when using the neutral ligand method of electron counting, or donate two electrons to the metal when using the donor pair method of electron counting.^[4] Regardless of whether it is considered neutral or anionic, these ligands yield normal covalent bonds. A few examples of this type of ligand are H , CH_3 , halogens, and NO (bent).

Z-type ligands are those that accept two electrons from the metal center as opposed to the donation occurring with the other two types of ligands. However, these ligands also form dative covalent bonds like the L-type. This type of ligand is not usually used, because in certain situations it can be written in terms of L and X. For example, if a Z ligand is accompanied by an L type, it can be written as X_2 . Examples of these ligands are Lewis acids, such as BR_3 .



Some multidentate ligands can act as a combination of ligand types. A famous example is the cyclopentadienyl (or Cp) ligand, C_5H_5 . We would classify this neutral ligand as $[\text{L}_2\text{X}]$, with the two L functionalities corresponding to the two "olefinic" fragments while the X functionality corresponds to the CH "radical" carbon in the ring. The addition of one electron makes the Cp^- anion, which has six pi electrons and is thus planar and aromatic. In the ferrocene complex, Cp_2Fe , using the "standard" donor pair counting method we can regard the two Cp^- ligands as each possessing six pi electrons, and by difference Fe is in the +2 oxidation

state. The Fe^{2+} ion is d^6 . Thus the iron atom in the complex (regardless of the counting method) has $6+6+6=18$ electrons in its coordination environment, which is a particularly stable electron count for transition metal complexes.

This page titled [5.2: Counting Electrons in Transition Metal Complexes](#) is shared under a [CC BY-SA 4.0](#) license and was authored, remixed, and/or curated by [Chemistry 310 \(Wikibook\)](#) via [source content](#) that was edited to the style and standards of the LibreTexts platform; a detailed edit history is available upon request.

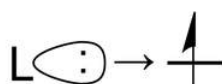
5.3: Crystal Field Theory

Crystal field theory is one of the simplest models for explaining the structures and properties of transition metal complexes. The theory is based on the electrostatics of the metal-ligand interaction, and so its results are only approximate in cases where the metal-ligand bond is substantially covalent. But because the model makes effective use of molecular symmetry, it can be surprisingly accurate in describing the magnetism, colors, structure, and relative stability of metal complexes.

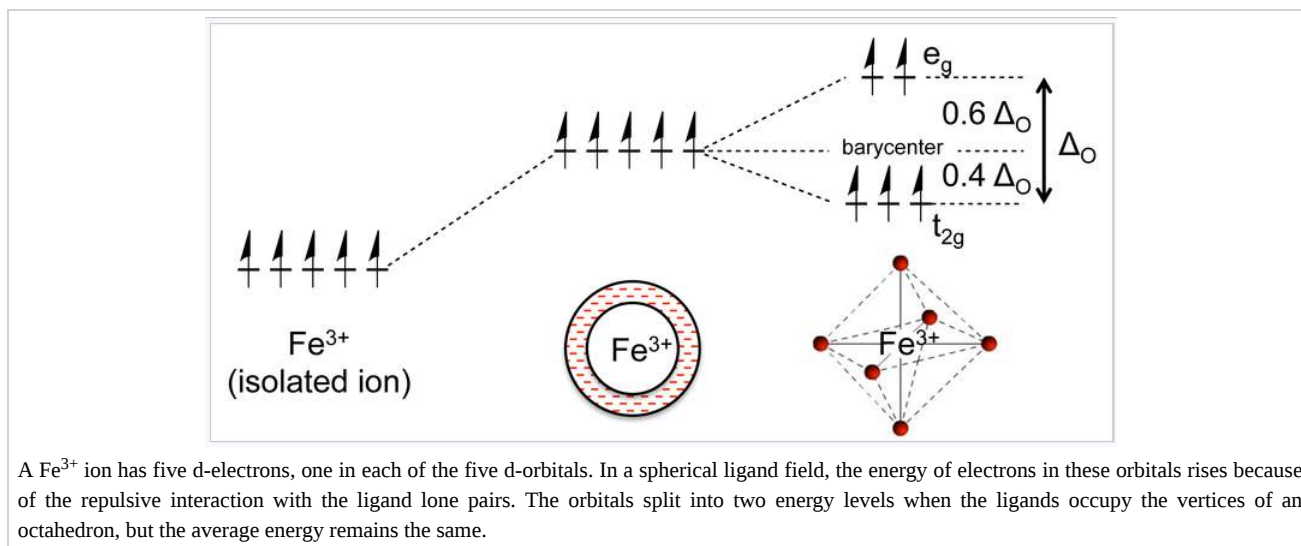
Consider a positively charged metal ion such as Fe^{3+} in the "field" of six negatively charged ligands, such as CN^- . There are two energetic terms we need to consider. The first is the **electrostatic attraction** between the metal and ligands, which is inversely proportional to the distance between them:

$$E_{elec} = \frac{1}{4\pi\epsilon_0} \sum_{\text{ligands}} \frac{q_M q_L}{r_{ML}} \quad (5.3.1)$$

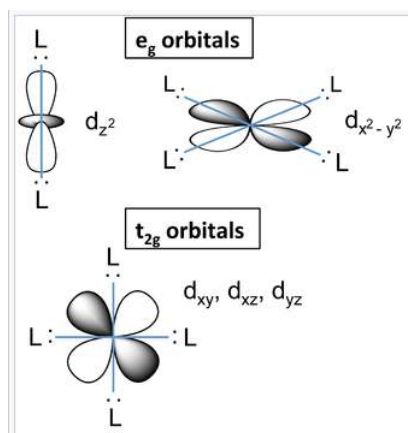
The second term is the **repulsion** that arises from the Pauli exclusion principle when a third electron is added to a filled orbital. There is no place for this third electron to go except to a higher energy antibonding orbital. This is the situation when a ligand lone pair approaches an occupied metal d-orbital:



Now let us consider the effect of these attractive and repulsive terms as the metal ion and ligands are brought together. We do this in two steps, first forming a ligand "sphere" around the metal and then moving the six ligands to the vertices of an octahedron. Initially all five d-orbitals are degenerate, i.e., they have the same energy by symmetry. In the first step, the antibonding interaction drives up the energy of the orbitals, but they remain degenerate. In the second step, the d-orbitals split into two symmetry classes, a lower energy, triply-degenerate set (the t_{2g} orbitals) and a higher energy, doubly degenerate set (the e_g orbitals).



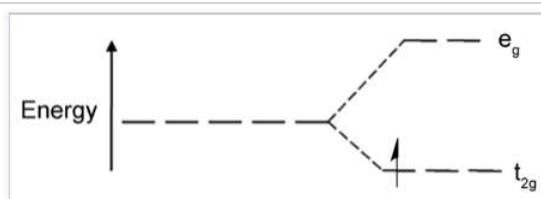
The **energy difference** between the e_g and t_{2g} orbitals is given the symbol Δ_O , where the "O" stands for "octahedral." We will see that this splitting energy is sensitive to the degree of orbital overlap and thus depends on both the metal and the ligand. Relative to the midpoint energy (the **barycenter**), the t_{2g} orbitals are stabilized by $2/5 \Delta_O$ and the e_g orbitals are destabilized by $3/5 \Delta_O$ in an octahedral complex.



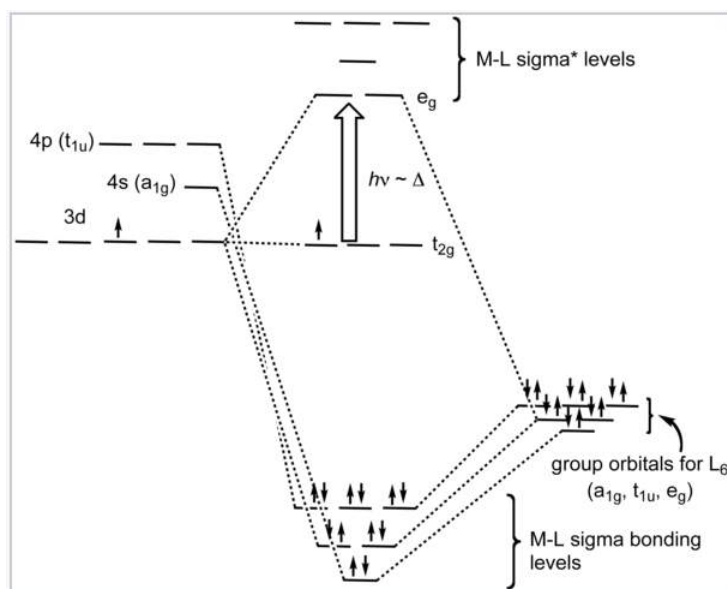
d-orbitals and their orientation with relation to ligands in an octahedral complex.

What causes the d-orbitals to split into two sets? Recall that the d-orbitals have a specific orientation with respect to the Cartesian axes. The lobes of the d_{xy} , d_{xz} , and d_{yz} orbitals (the **t_{2g} orbitals**) lie in the xy -, xz -, and yz -planes, respectively. These three d-orbitals have **nodes** along the x -, y -, and z -directions. The orbitals that contain the ligand lone pairs are oriented along these axes and therefore have **zero overlap with the metal t_{2g} orbitals**. It is easy to see that these three d-orbitals must be degenerate by symmetry. On the other hand, the lobes of the d_{z^2} and $d_{x^2-y^2}$ orbitals (the **e_g orbitals**) point directly along the bonding axes and have strong overlap with the ligand orbitals. While it is less intuitively obvious, these orbitals are also degenerate by symmetry and have antibonding character.

It is informative to compare the results of **crystal field theory** and **molecular orbital theory** (also called **ligand field theory** in this context) for an octahedral transition metal complex. The energy level diagrams below make this comparison for the d^1 octahedral ion $[\text{Ti}(\text{H}_2\text{O})_6]^{3+}$. In the MO picture below, the frontier orbitals are derived from the metal d-orbitals. The lower t_{2g} set, which contains one electron, is non-bonding by symmetry, and the e_g orbitals are antibonding. The metal 4s orbital, which has a_{1g} symmetry, makes a low energy bonding combination that is ligand-centered, and an antibonding combination that is metal-centered and above the e_g levels. This is the reason that our d-electron counting rules do not need to consider the metal 4s orbital. The important take-home message is that crystal field theory and MO theory give **very similar results** for the frontier orbitals of transition metal complexes.



Crystal field energy diagram for the d^1 octahedral complex $[\text{Ti}(\text{H}_2\text{O})_6]^{3+}$.



Ligand-field diagram for the octahedral complex $[\text{Ti}(\text{H}_2\text{O})_6]^{3+}$.

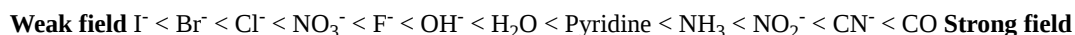
This page titled [5.3: Crystal Field Theory](#) is shared under a [CC BY-SA 4.0](#) license and was authored, remixed, and/or curated by [Chemistry 310 \(Wikibook\)](#) via [source content](#) that was edited to the style and standards of the LibreTexts platform; a detailed edit history is available upon request.

5.4: Spectrochemical Series

Strong and weak field ligands. The spectrochemical series ranks ligands according to the **energy difference Δ_0** between the t_{2g} and e_g orbitals in their octahedral complexes. This energy difference is measured in the spectral transition between these levels, which often lies in the visible part of the spectrum and is responsible for the colors of complexes with partially filled d-orbitals. Ligands that produce a large splitting are called **strong field** ligands, and those that produce a small splitting are called **weak field** ligands.

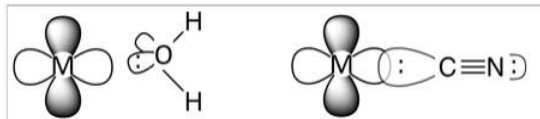


An abbreviated spectrochemical series is:

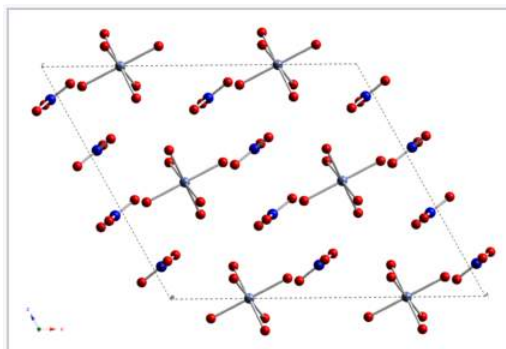


Orbital overlap

Referring to the molecular orbital diagram above, we see that the splitting between d-electron levels reflects the antibonding interaction between the e_g metal orbitals and the ligands. Thus, we expect ligand field strength to correlate with metal-ligand orbital overlap. Ligands that bind through very electronegative atoms such as **O and halogens** are thus expected to be **weak field**, and ligands that bind through **C or P** are typically **strong field**. Ligands that bind through **N** are **intermediate** in strength. Another way to put this is that hard bases tend to be weak field ligands and soft bases are strong field ligands.



Water is a weak field ligand. The electronegative O atom is strongly electron-withdrawing, so there is poor orbital overlap between the electron pair on O and a metal d-orbital. The more electropositive C atom in the strong field ligand CN^- allows better orbital overlap and sharing of the electron pair. Note that CN^- typically coordinates metal ions through the C atom rather than the N atom.



Cobalt (II) complexes have different colors depending on the nature of the ligand. In crystals of the red compound cobalt(II) nitrate dihydrate, each cobalt ion is coordinated by six water molecules. The $[\text{Co}(\text{H}_2\text{O})_6]^{2+}$ cations and NO_3^- anions crystallize to make a salt. When the complex is dissolved in water, Co(II) retains its coordination shell of six water molecules and the solution has the same red color as the crystal.

Energy units

Energy can be calculated in a number of ways and it is useful to try to relate the splitting energy Δ_O to more familiar quantities like bond energies.

$$E = h\nu = h \frac{c}{\lambda} = hc\tilde{\nu} \quad (5.4.1)$$

Here ν is the frequency of the electromagnetic radiation, h is Planck's constant (6.626×10^{-34} J*s), and c is the speed of light. $\tilde{\nu}$ is called the "wavenumber" and is the inverse of the wavelength, usually measured in cm^{-1} . Energy gaps are often expressed by spectroscopists in terms of wavenumbers.

For example, a red photon has a wavelength of about 620 nm and a wavenumber of about $16,000 \text{ cm}^{-1}$. In other energy units, the same red photon has an energy of 2.0 eV (1 eV = 1240 nm) or 193 kJ/mol (1 eV = 96.5 kJ/mol). If we compare this to the dissociation energy of a carbon-carbon single bond (350 kJ/mol), we see that the C-C bond has about twice the energy of a red photon. We would need an ultraviolet photon ($E > 350 \text{ kJ/mol} = 3.6 \text{ eV} = 345 \text{ nm} = 29,000 \text{ cm}^{-1}$) to break a C-C bond.

We will see that Δ_O varies widely for transition metal complexes, from near-infrared to ultraviolet wavelengths. Thus the energy difference between the t_{2g} and e_g orbitals can range between the energy of a rather weak to a rather strong covalent bond.

Δ_O depends on both the metal and the ligand. We can learn something about trends in Δ_O by comparing a series of d^6 metal complexes

Complex	Δ_O (cm^{-1})
$[\text{Co}(\text{H}_2\text{O})_6]^{2+}$	9,300
$[\text{Co}(\text{H}_2\text{O})_6]^{3+}$	18,200
$[\text{Co}(\text{CN})_6]^{3-}$	33,500
$[\text{Rh}(\text{H}_2\text{O})_6]^{3+}$	27,000
$[\text{Rh}(\text{CN})_6]^{3-}$	45,500

Important trends in Δ_O :

- Co^{3+} complexes have larger Δ_O than Co^{2+} complexes with the same ligand. This reflects the **electrostatic** nature of the crystal field splitting.
- Rh^{3+} complexes have larger Δ_O than Co^{3+} complexes. In general, elements in the 2nd and 3rd transition series (the **4d and 5d elements**) have **larger splitting** than those in the 3d series.

For a given metal in one oxidation state (e.g., Co^{3+}), the trend in Δ_O follows the **spectrochemical series**. Thus Δ_O is larger for $[\text{Co}(\text{CN})_6]^{3-}$, which contains the strong field CN^- ligand, than it is for $[\text{Co}(\text{H}_2\text{O})_6]^{3+}$ with the weak field ligand H_2O .

The 4d and 5d elements are similar in their size and their chemistry. In comparing Δ_O values for complexes in the 3d, 4d, and 5d series (e.g., comparing elements in the triads Co,Rh,Ir or Fe,Ru,Os), we always find $3d \ll 4d \lesssim 5d$. This trend reflects the spatial extent of the d-orbitals and thus their overlap with ligand orbitals. The 3d orbitals are smaller, and they are less effective in bonding than the 4d or 5d. The 4d and 5d orbitals are similar to each other because of the lanthanide contraction. At the beginning of the 5d series (between ^{56}Ba and ^{72}Hf) are the fourteen lanthanide elements ($^{57}\text{La} - ^{71}\text{Lu}$).

Although the valence orbitals of the 5d elements are in a higher principal quantum shell than those of the 4d elements, the addition of 14 protons to the nucleus in crossing the lanthanide series contracts the sizes of the atomic orbitals. The important result is that **the valence orbitals of the 4d and 5d elements have similar sizes** and thus the elements resemble each other in their chemistry much more than they resemble their cousins in the 3d series. For example, the chemistry of Ru is very similar to that of Os, as illustrated below, but quite different from that of Fe.

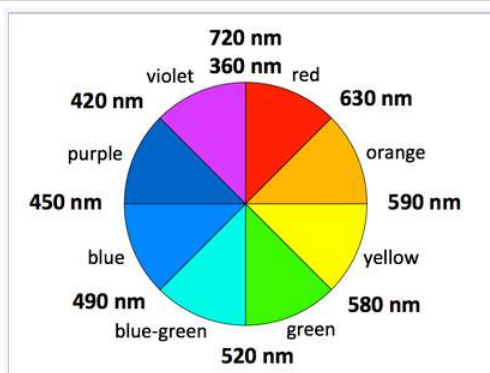




Both Os and Ru form volatile, molecular tetroxides MO_4 . OsO_4 is used in epoxidation reactions and as a stain in electron microscopy. In contrast, the highest binary oxide of iron is Fe_2O_3 .

Colors of transition metal complexes

A simple, qualitative way to see the relative crystal field splitting energy, Δ_O , is to observe the color of a transition metal complex. The higher the energy of the absorbed photon, the larger the energy gap. However, the color a complex absorbs is **complementary** to the color it appears (i.e., the color of light it reflects), which is **opposite** the absorbed color on the color wheel.



Complementary colors are across the color wheel from each other

Examples: (all d^7 Co^{2+} complexes)

$[Co(H_2O)_6]^{2+}$ looks purple in its salts and in concentrated solution because it absorbs in the green range.

$[Co(NH_3)_6]^{2+}$ is straw-colored because it absorbs in the blue range.

$[Co(CN)_6]^{4-}$, looks red, absorbs in the violet and ultra-violet part of the spectrum. This is consistent with the idea that CN^- is a stronger field ligand than NH_3 , because the energy of a UV photon is higher than that of a red-orange photon.

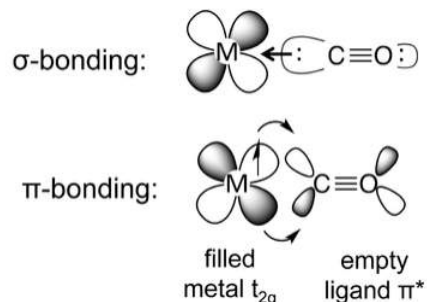
This method is applicable to most transition metal complexes, as the majority of them absorb somewhere in the visible range (400-700 nm = 25,000 to 14,300 cm^{-1}), or have UV transitions that tail into the visible, making them appear yellow; however there are complexes such as $[Rh(CN)_6]^{3-}$ that appear colorless because their d-d transitions are in the ultraviolet. Other complexes such as $[Mn(H_2O)_6]^{2+}$ are weakly colored because their d-d transitions involve a change in the spin state of the complex.

This page titled [5.4: Spectrochemical Series](#) is shared under a [CC BY-SA 4.0](#) license and was authored, remixed, and/or curated by [Chemistry 310 \(Wikibook\)](#) via [source content](#) that was edited to the style and standards of the LibreTexts platform; a detailed edit history is available upon request.

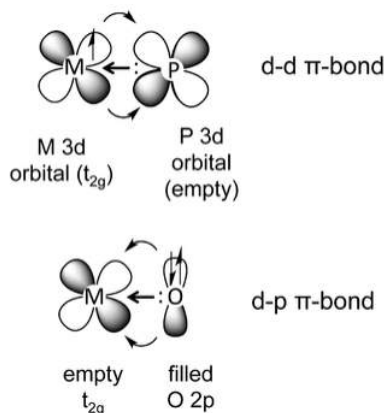
5.5: π -Bonding between Metals and Ligands

An important factor that contributes to the high ligand field strength of ligands such as CO, CN⁻, and phosphines is **π -bonding** between the metal and the ligand. There are three types of pi-bonding in metal complexes:

The most common situation is when a ligand such as carbon monoxide or cyanide donates its sigma (nonbonding) electrons to the metal, while accepting electron density from the metal through overlap of a metal t_{2g} orbital and a ligand π^* orbital. This situation is called "**back-bonding**" because the ligand donates σ -electron density to the metal and the metal donates π -electron density to the ligand. The ligand is thus acting as a **σ -donor and a π -acceptor**. In π -backbonding, the metal donates π electrons to the ligand π^* orbital, adding electron density to an *antibonding* molecular orbital. This results in weakening of the C-O bond, which is experimentally observed as lengthening of the bond (relative to free CO in the gas phase) and lowering of the C-O infrared stretching frequency.



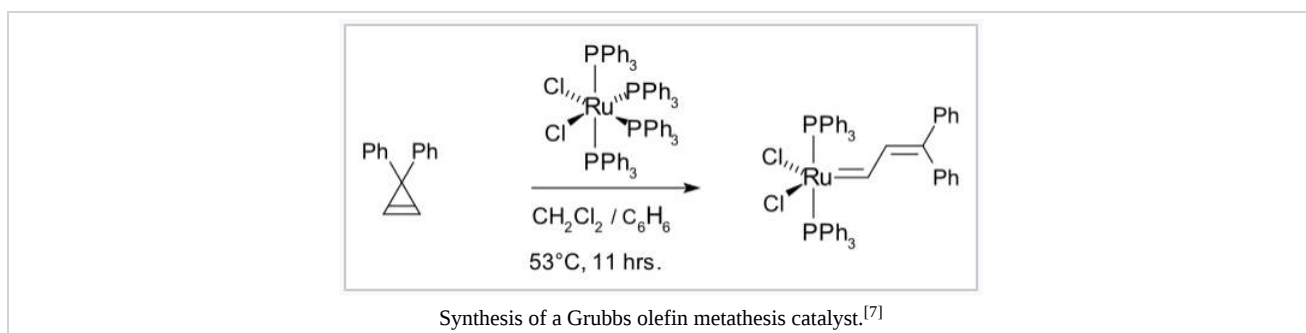
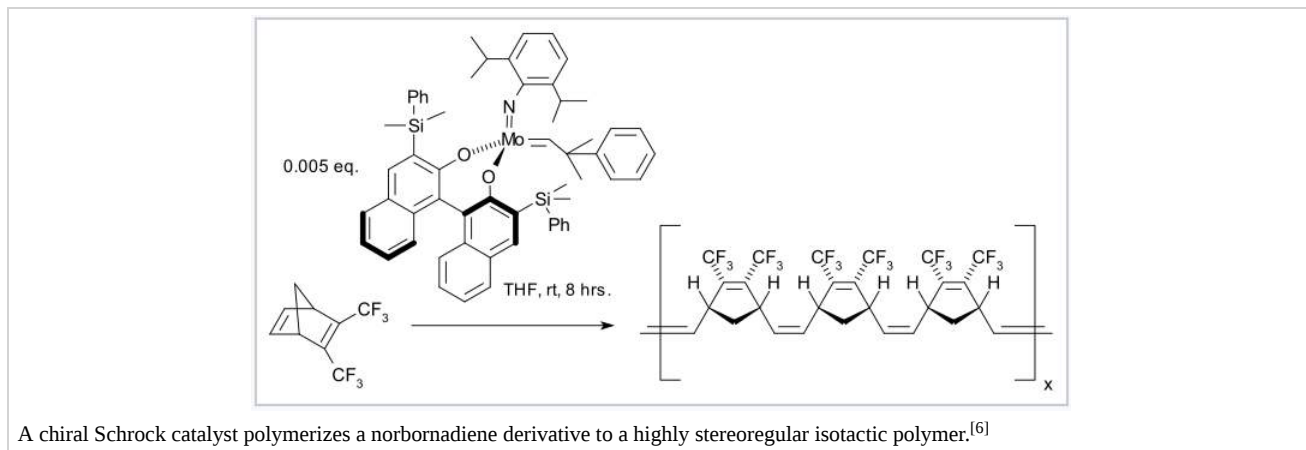
d-d π bonding occurs when an element such as phosphorus, which has a σ -symmetry lone pair and an empty metal 3d orbital, binds to a metal that has electrons in a t_{2g} orbital. This is a common situation for phosphine complexes (e.g., triphenylphosphine) bound to low-valent, late transition metals. The backbonding in this case is analogous to the CO example, except that the acceptor orbital is a phosphorus 3d orbital rather than a ligand π^* orbital. Here the phosphine ligand acts as a σ -donor and a π -acceptor, forming a $d\pi$ - $d\pi$ bond.



The third kind of metal-ligand π -bonding occurs when a **π -donor ligand** - an element with both a σ -symmetry electron pair and a filled orthogonal p-orbital - bonds to a metal, as shown above at the right for an O^{2-} ligand. This occurs in early transition metal complexes. In this example, O^{2-} is acting as both a **σ -donor and a π -donor**. This interaction is typically drawn as a metal-ligand multiple bond, e.g., the V=O bond in the vanadyl cation $[VO]^{2+}$. Typical π -donor ligands are oxide (O^{2-}), nitride (N^{3-}), imide (RN^{2-}), alkoxide (RO^-), amide (R_2N^-), and fluoride (F^-). For late transition metals, strong π -donors form anti-bonding interactions with the filled d-levels, with consequences for spin state, redox potentials, and ligand exchange rates. π -donor ligands are low in the spectrochemical series.^[5]

Carbon-containing ligands that are π -donors and their complexes with transition metal ions are very important in **olefin metathesis**, a reaction in which carbon-carbon double bonds are interchanged. Using these catalysts, cyclic olefins can be transformed into linear polymers in high yield through ring-opening metathesis polymerization (ROMP). Catalysts of this kind were developed by the groups of Richard Schrock and Robert Grubbs, who shared the 2005 Nobel Prize in Chemistry with Yves Chauvin for their

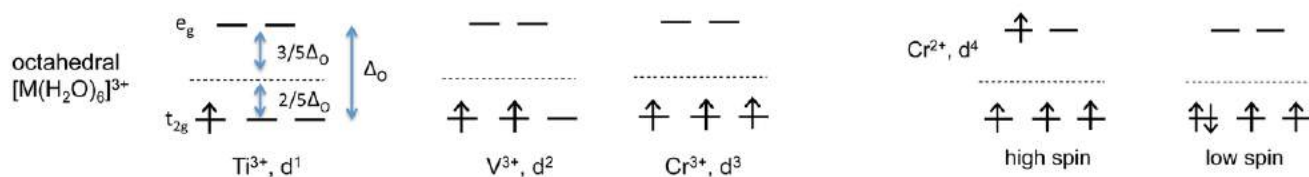
discoveries. The Schrock catalysts are based on early transition metals such as Mo; they are more reactive but less tolerant of different organic functional groups and protic solvents than the Grubbs catalysts, which are based on Ru complexes.



This page titled [5.5: \$\pi\$ -Bonding between Metals and Ligands](#) is shared under a [CC BY-SA 4.0](#) license and was authored, remixed, and/or curated by [Chemistry 310 \(Wikibook\)](#) via [source content](#) that was edited to the style and standards of the LibreTexts platform; a detailed edit history is available upon request.

5.6: Crystal Field Stabilization Energy, Pairing, and Hund's Rule

The splitting of the d-orbitals into different energy levels in transition metal complexes has important consequences for their stability, reactivity, and magnetic properties. Let us first consider the simple case of the octahedral complexes $[M(H_2O)_6]^{3+}$, where $M = Ti, V, Cr$. Because the complexes are octahedral, they all have the same energy level diagram:



The Ti^{3+} , V^{3+} , and Cr^{3+} complexes have one, two and three d-electrons respectively, which fill the degenerate t_{2g} orbitals singly. The spins align parallel according to Hund's rule, which states that the lowest energy state has the highest spin angular momentum.

For each of these complexes we can calculate a **crystal field stabilization energy, CFSE**, which is the energy difference between the complex in its ground state and in a hypothetical state in which all five d-orbitals are at the energy barycenter.

For Ti^{3+} , there is one electron stabilized by $2/5 \Delta_o$, so $CFSE = -(1)(\frac{2}{5})(\Delta_o) = -\frac{2}{5} \Delta_o$

Similarly, $CFSE = -4/5 \Delta_o$ and $-6/5 \Delta_o$ for V^{3+} and Cr^{3+} , respectively.

For Cr^{2+} complexes, which have four d-electrons, the situation is more complicated. Now we can have a high spin configuration $(t_{2g}^3)(e_g)^1$, or a low spin configuration $(t_{2g}^4)(e_g)^0$ in which two of the electrons are paired. What are the energies of these two states?

High spin: $CFSE = (-3)(\frac{2}{5})\Delta_o + (1)(\frac{3}{5})\Delta_o = -\frac{3}{5} \Delta_o$

Low spin: $CFSE = (-4)(\frac{2}{5})\Delta_o + P = -\frac{8}{5} \Delta_o + P$, where P is the **pairing energy**

Energy difference = $-\Delta_o + P$

The **pairing energy P** is the energy penalty for putting two electrons in the same orbital, resulting from the electrostatic repulsion between electrons. For 3d elements, a typical value of P is about $15,000 \text{ cm}^{-1}$.

The important result here is that a complex will be **low spin** if $\Delta_o > P$, and **high spin** if $\Delta_o < P$.

Because Δ_o depends on both the metals and the ligands, it determines the spin state of the complex.

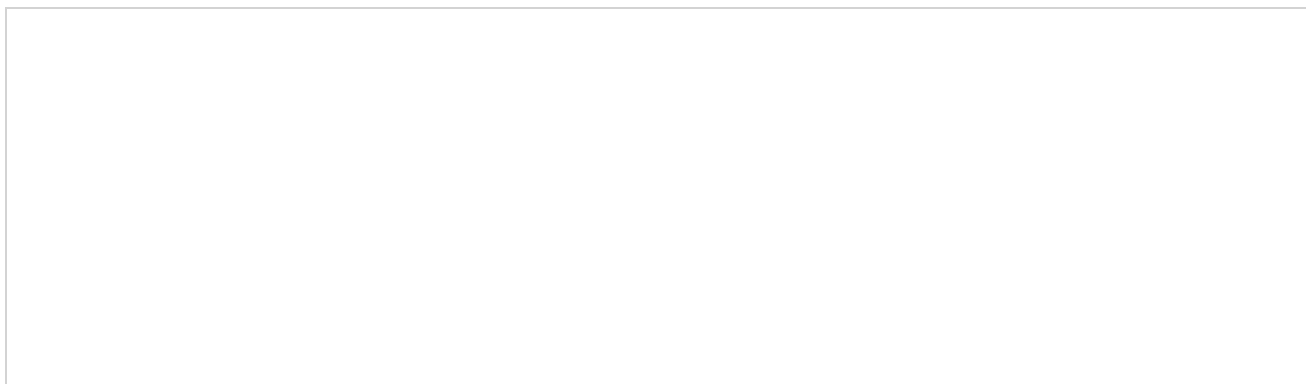
Rules of thumb:

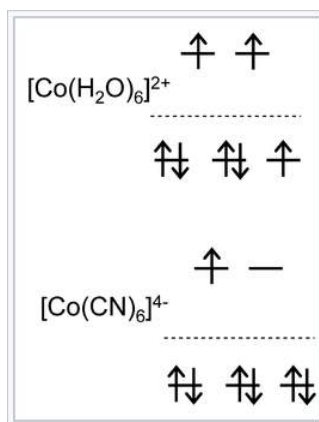
3d complexes are **high spin** with **weak field** ligands and **low spin** with **strong field** ligands.

High valent 3d complexes (e.g., Co^{3+} complexes) tend to be **low spin** (large Δ_o)

4d and 5d complexes are **always low spin** (large Δ_o)

Note that high and low spin states occur only for 3d metal complexes with between 4 and 7 d-electrons. Complexes with 1 to 3 d-electrons can accommodate all electrons in individual orbitals in the t_{2g} set. Complexes with 8, 9, or 10 d-electrons will always have completely filled t_{2g} orbitals and 2-4 electrons in the e_g set.





d-orbital energy diagrams for high and low spin Co^{2+} complexes, d^7

Examples of high and low spin complexes:

$[\text{Co}(\text{H}_2\text{O})_6]^{2+}$ contains a d^7 metal ion with a weak field ligand. This complex is known to be high spin from magnetic susceptibility measurements, which detect three unpaired electrons per molecule. Its orbital occupancy is $(t_{2g})^5(e_g)^2$.

We can calculate the CFSE as $-(5)(\frac{2}{5})\Delta_o + (2)(\frac{3}{5})\Delta_o = -\frac{4}{5}\Delta_o$

$[\text{Co}(\text{CN})_6]^{4-}$ is also an octahedral d^7 complex but it contains CN^- , a strong field ligand. Its orbital occupancy is $(t_{2g})^6(e_g)^1$ and it therefore has one unpaired electron.

In this case the CFSE is $-(6)(\frac{2}{5})\Delta_o + (1)(\frac{3}{5})\Delta_o + P = -\frac{9}{5}\Delta_o + P$.

Magnetism of transition metal complexes

Compounds with **unpaired electrons** have an inherent magnetic moment that arises from the **electron spin**. Such compounds interact strongly with applied magnetic fields. Their **magnetic susceptibility** provides a simple way to measure the number of unpaired electrons in a transition metal complex.

If a transition metal complex has no unpaired electrons, it is **diamagnetic** and is weakly repelled from the high field region of an inhomogeneous magnetic field. Complexes with unpaired electrons are typically **paramagnetic**. The spins in paramagnets align independently in an applied magnetic field but do not align spontaneously in the absence of a field. Such compounds are attracted to a magnet, i.e., they are drawn into the high field region of an inhomogeneous field. The attractive force, which can be measured with a **Guoy balance** or a **SQUID magnetometer**, is proportional to the **magnetic susceptibility** (χ) of the complex.

The effective **magnetic moment** of an ion (μ_{eff}), in the absence of spin-orbit coupling, is given by the sum of its spin and orbital moments:

$$\mu_{\text{eff}} = \mu_{\text{spin}} + \mu_{\text{orbital}} = \mu_s + \mu_L \quad (5.6.1)$$

In octahedral 3d metal complexes, the orbital angular momentum is largely "quenched" by symmetry, so we can approximate:

$$\mu_{\text{eff}} \approx \mu_s \quad (5.6.2)$$

We can calculate μ_s from the number of unpaired electrons (n) using:

$$\mu_{\text{eff}} = \sqrt{n(n+2)}\mu_B \quad (5.6.3)$$

Here μ_B is the **Bohr magneton** ($= eh/4\pi m_e$) $= 9.3 \times 10^{-24}$ J/T. This spin-only formula is a good approximation for first-row transition metal complexes, especially high spin complexes. The table below compares calculated and experimentally measured values of μ_{eff} for octahedral complexes with 1-5 unpaired electrons.

Ion	Number of unpaired electrons	Spin-only moment / μ_B	observed moment / μ_B

Ti ³⁺	1	1.73	1.73
V ⁴⁺	1		1.68–1.78
Cu ²⁺	1		1.70–2.20
V ³⁺	2	2.83	2.75–2.85
Ni ²⁺	2		2.8–3.5
V ²⁺	3	3.87	3.80–3.90
Cr ³⁺	3		3.70–3.90
Co ²⁺	3		4.3–5.0
Mn ⁴⁺	3		3.80–4.0
Cr ²⁺	4	4.90	4.75–4.90
Fe ²⁺	4		5.1–5.7
Mn ²⁺	5	5.92	5.65–6.10
Fe ³⁺	5		5.7–6.0

The small deviations from the spin-only formula for these octahedral complexes can result from the neglect of orbital angular momentum or of spin-orbit coupling. Tetrahedral d³, d⁴, d⁸ and d⁹ complexes tend to show larger deviations from the spin-only formula than octahedral complexes of the same ion because quenching of the orbital contribution is less effective in the tetrahedral case.

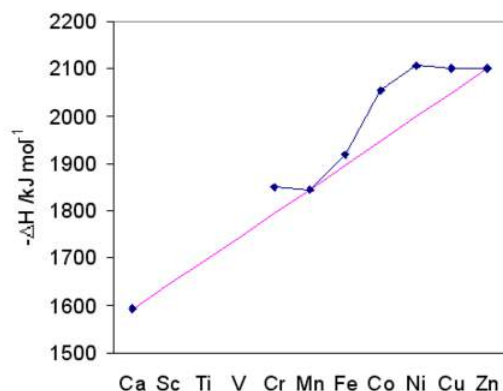
Summary of rules for high and low spin complexes:

3d complexes: Can be high or low spin, depending on the ligand (d⁴, d⁵, d⁶, d⁷)

4d and 5d complexes: Always low spin, because Δ_O is large

Maximum CFSE is for d³ and d⁸ cases (e.g., Cr³⁺, Ni²⁺) with weak field ligands (H₂O, O²⁻, F⁻,...) and for d³-d⁶ with strong field ligands (Fe²⁺, Ru²⁺, Os²⁺, Co³⁺, Rh³⁺, Ir³⁺,...)

Irving-Williams series. For M²⁺ complexes, the stability of the complex follows the order Mg²⁺ < Mn²⁺ < Fe²⁺ < Co²⁺ < Ni²⁺ < Cu²⁺ > Zn²⁺. This trend represents increasing Lewis acidity as the ions become smaller (going left to right in the periodic table) as well as the trend in CFSE. This same trend is reflected in the hydration enthalpy of gas-phase M²⁺ ions, as illustrated in the graph at the right. Note that Ca²⁺, Mn²⁺, and Zn²⁺, which are d⁰, d⁵(high spin), and d¹⁰ aquo ions, respectively, all have zero CFSE and fall on the same line. Ions that deviate the most from the line such as Ni²⁺ (octahedral d⁸) have the highest CFSE.



Colors and spectra of transition metal complexes

Transition metal complexes often have beautiful colors because, as noted above, their d-d transition energies can be in the visible part of the spectrum. With octahedral complexes these colors are faint (the transitions are weak) because they violate the Laporte

selection rule. According to this rule, $g \rightarrow g$ and $u \rightarrow u$ transitions are forbidden in centrosymmetric complexes. d-orbitals have g (gerade) symmetry, so d-d transitions are Laporte-forbidden. However octahedral complexes can absorb light when they momentarily distort away from centrosymmetry as the molecule vibrates. Spin flips are also forbidden in optical transitions by the spin selection rule, so the excited state will always have the same spin multiplicity as the ground state.

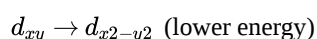
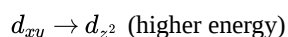
The spectra of even the simplest transition metal complexes are rather complicated because of the many possible ways in which the d-electrons can fill the t_{2g} and e_g orbitals. For example, if we consider a d^2 complex such as $V^{3+}(aq)$, we know that the two electrons can reside in any of the five d-orbitals, and can either be spin-up or spin-down. There are actually 45 different such arrangements (called **microstates**) that do not violate the Pauli exclusion principle for a d^2 complex. Usually we are concerned only with the six of lowest energy, in which both electrons occupy individual orbitals in the t_{2g} set and all their spins are aligned either up or down.



From left: $[V(H_2O)_6]^{2+}$ (lilac), $[V(H_2O)_6]^{3+}$ (green), $[VO(H_2O)_5]^{2+}$ (blue) and $[VO(H_2O)_5]^{3+}$ (yellow).

We can see how these microstates play a role in electronic spectra when we consider the d-d transitions of the $[Cr(NH_3)_6]^{3+}$ ion. This ion is d^3 , so each of the three t_{2g} orbitals contains one unpaired electron. We expect to see a transition when one of the three electrons in the t_{2g} orbitals is excited to an empty e_g orbital. Interestingly, we find not one but **two** transitions in the visible.

The reason that we see two transitions is that the electron can come from any one of the t_{2g} orbitals and end up in either of the e_g orbitals. Let us assume for the sake of argument that the electron is initially in the d_{xy} orbital. It can be excited to either the d_{z^2} or the $d_{x^2-y^2}$ orbital:



The first transition is at higher energy (shorter wavelength) because in the excited state the configuration is $(d_{yz}^1 d_{xz}^1 d_{z^2}^1)$. All three of the excited state orbitals have some z-component, so the d-electron density is "piled up" along the z-axis. The energy of this transition is thus increased by **electron-electron repulsion**. In the second case, the excited state configuration is $(d_{yz}^1 d_{xz}^1 d_{x^2-y^2}^1)$, and the d-electrons are more symmetrically distributed around the metal. This effect is responsible for a splitting of the d-d bands by about $8,000 \text{ cm}^{-1}$. We can show that all other possible transitions are equivalent to one of these two by symmetry, and hence we see only two visible absorption bands for Cr^{3+} complexes.

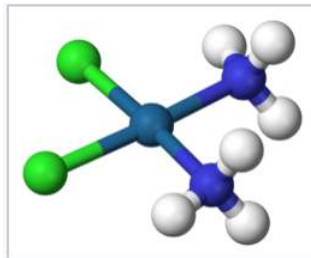
This page titled [5.6: Crystal Field Stabilization Energy, Pairing, and Hund's Rule](#) is shared under a [CC BY-SA 4.0](#) license and was authored, remixed, and/or curated by [Chemistry 310 \(Wikibook\)](#) via [source content](#) that was edited to the style and standards of the LibreTexts platform; a detailed edit history is available upon request.

5.7: Non-octahedral Complexes

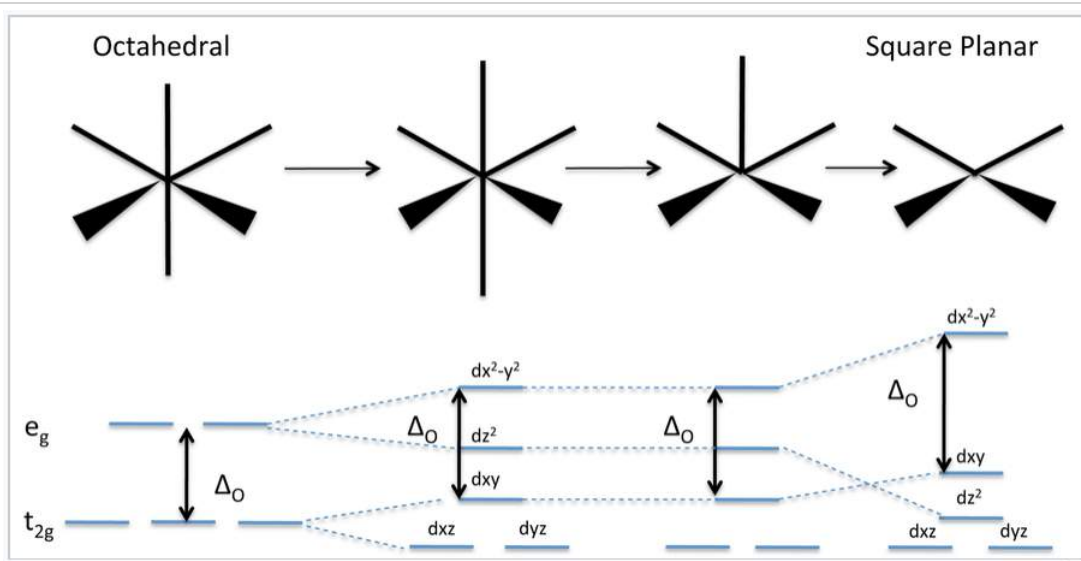
The most important non-octahedral geometries for transition metal complexes are:

4-coordinate: square planar and tetrahedral

5-coordinate: square pyramidal and trigonal bipyramidal



cis-Pt(NH₃)₂Cl₂, a 5d⁸ square planar complex



Crystal field energy diagram showing the transition from octahedral to square planar geometry

Energies of the d-orbitals in non-octahedral geometries

The figure above shows what happens to the d-orbital energy diagram as we progressively distort an octahedral complex by elongating it along the z-axis (a **tetragonal distortion**), by removing one of its ligands to make a **square pyramid**, or by removing both of the ligands along the z-axis to make a **square planar** complex. In all cases, we keep the total bond order the same by making the bonds in the xy plane shorter as the bonds in the z-direction are stretched and/or broken.



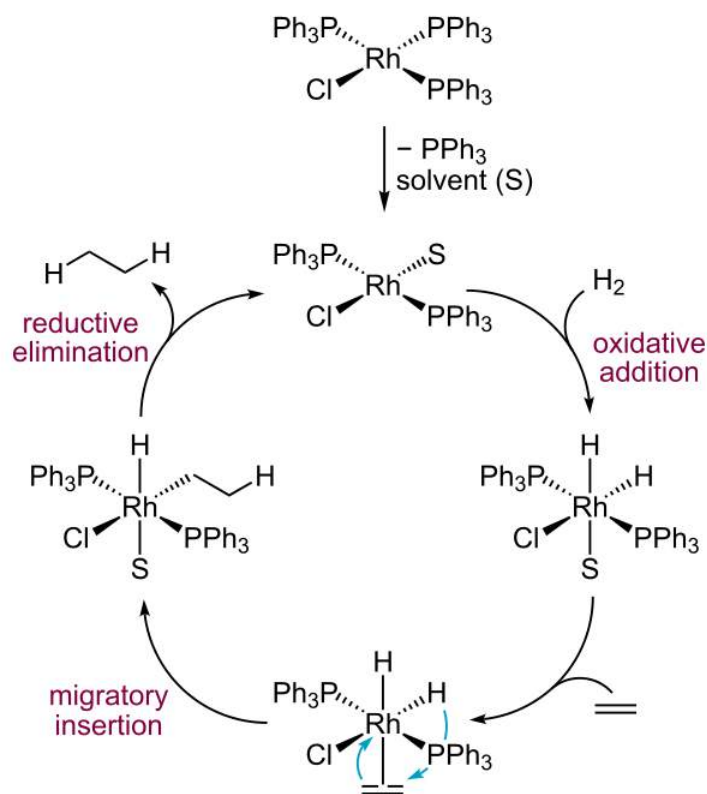
Barnett Rosenberg (Michigan State University) accidentally discovered the biological effects of square planar $\text{cis-Pt}(\text{NH}_3)_2\text{Cl}_2$ while researching bacterial growth in electric fields.^[8] The Pt electrode he used reacted with chloride and ammonium ions in the electrolyte to produce the compound at 1-10 ppm concentration. Further experiments revealed that the cis-isomer (but not the trans-isomer) is a potent anti-cancer drug which is especially effective against testicular cancer. The drug works by cross-linking guanine-cytosine rich regions of DNA, thus inhibiting cell division.

The distortion away from octahedral symmetry breaks the degeneracy of the t_{2g} and e_g orbitals. d-orbitals with a z-component (d_{xz} , d_{yz} , d_{z^2}) go down in energy as orbitals that reside in the xy plane (d_{xy} , $d_{x^2-y^2}$) rise in energy. The barycenter (the weighted average orbital energy) remains constant. Also, it is important to note that the splitting between the d_{xy} and $d_{x^2-y^2}$ orbitals stays constant at Δ_O regardless of the nature of the distortion.

Why would a "happy" octahedral complex want to lose two of its ligands to make a **square planar** complex? This occurs frequently in d^8 and sometimes in d^9 complexes with large Δ_O , i.e., **$3d^8$ complexes with strong field ligands and $4d^8$, $5d^8$ complexes with any ligands**. Examples of such d^8 complexes are $[\text{Ni}(\text{CN})_4]^{2-}$, the anti-cancer drug cisplatin ($\text{cis-Pt}(\text{NH}_3)_2\text{Cl}_2$), $[\text{Pd}(\text{H}_2\text{O})_4]^{2+}$, and $[\text{AuCl}_4]^-$. At the d^8 electron count, the lowest four orbitals are filled and the highest orbital (the $d_{x^2-y^2}$) is empty, resulting in a large CFSE. These complexes are diamagnetic and tend to be quite stable. With weak field ligands, $3d^8$ complexes are octahedral and paramagnetic (e.g., $[\text{Ni}(\text{H}_2\text{O})_6]^{2+}$, which has two unpaired electrons in the e_g orbitals).

Square planar complexes in catalysis:

Square planar d^8 complexes can be oxidized by two electrons to become octahedral (low spin) d^6 complexes, which also have a large CFSE. Because the loss of two electrons is accompanied by the gain of two ligands, this process is called **oxidative addition**. The reverse process is called **reductive elimination**. Both processes function together in catalytic cycles, such as the hydrogenation of olefins using **Wilkinson's catalyst**.^{[10][11]} The catalytic cycle is shown below.



The catalyst cycles between 4-coordinate Rh(I) ($4d^8$) and 6-coordinate Rh(III) ($4d^6$). The complex first adds H_2 oxidatively, to give a six-coordinate complex in which the hydrogen is formally H^- . An olefin molecule displaces a solvent molecule, using its π -electrons to coordinate the metal. The complex rearranges by inserting the olefin into the metal-hydrogen bond, a process called **migratory insertion**. Finally, the complex returns to the square planar geometry by eliminating the hydrogenated olefin (reductive elimination). Wilkinson's catalyst is highly active and is widely used for homogeneous hydrogenation, hydroboration, and hydrosilation reactions.^{[12][13]} With chiral phosphine ligands, the catalyst can hydrogenate prochiral olefins to give enantiomerically pure products.^[14]

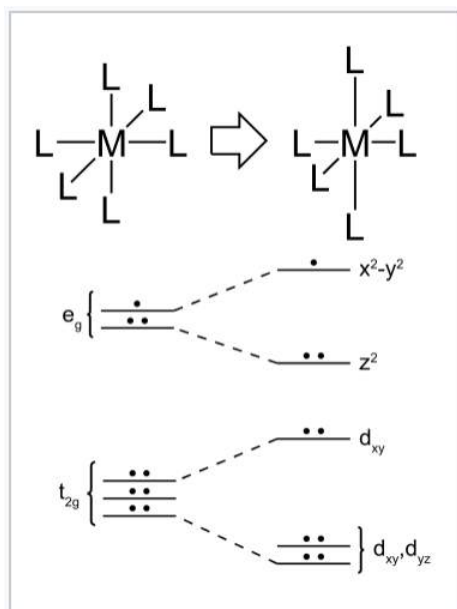


Sir Geoffrey Wilkinson, an inorganic chemist at Imperial College London, developed Wilkinson's catalyst in 1966. Earlier, as an Assistant Professor at Harvard University, he had elucidated the sandwich structure of ferrocene,^[9] which had been discovered a few years before but not understood. Wilkinson was awarded the Nobel Prize in Chemistry in 1973 for his contributions to organometallic chemistry.

This page titled [5.7: Non-octahedral Complexes](#) is shared under a [CC BY-SA 4.0](#) license and was authored, remixed, and/or curated by [Chemistry 310 \(Wikibook\)](#) via [source content](#) that was edited to the style and standards of the LibreTexts platform; a detailed edit history is available upon request.

5.8: Jahn-Teller Effect

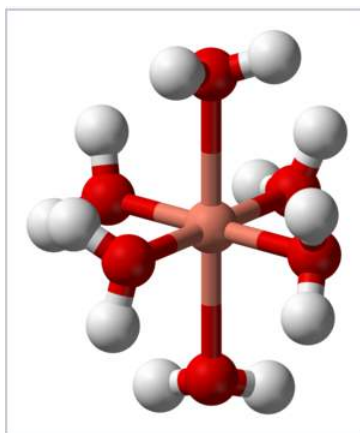
The **Jahn–Teller effect**, sometimes also known as **Jahn–Teller distortion**, describes the geometrical distortion of molecules and ions that is associated with certain electron configurations. This electronic effect is named after Hermann Arthur Jahn and Edward Teller, who proved, using group theory, that orbitally degenerate molecules *cannot* be stable.^[15] The **Jahn–Teller theorem** essentially states that any non-linear molecule with a spatially degenerate electronic ground state will undergo a geometrical distortion that removes that degeneracy, because the distortion lowers the overall energy of the molecule.



Jahn-Teller distortion of a d^9 octahedral transition metal complex. The tetragonal distortion lengthens the bonds along the z-axis as the bonds in the x-y plane become shorter. This change lowers the overall energy, because the two electrons in the d_{z^2} orbital go down in energy as the one electron in the $d_{x^2-y^2}$ orbital goes up.

We can understand this effect in the context of octahedral metal complexes by considering d-electron configurations in which the e_g orbital set contains **one or three electrons**. The most common of these are high spin d^4 (e.g., CrF_2), low spin d^7 (e.g., NaNiO_2), and d^9 (e.g., Cu^{2+}). If the complex can distort to break the symmetry, then one of the (formerly) degenerate e_g orbitals will go down in energy and the other will go up. More electrons will occupy the lower orbital than the upper one, resulting in an overall lowering of the electronic energy. A similar distortion can occur in tetrahedral complexes when the t_2 orbitals are partially filled. Such geometric distortions that lower the electronic energy are said to be **electronically driven**. Similar electronically driven distortions occur in one-dimensional chain compounds, where they are called Peierls distortions, and in two-dimensionally bonded sheets, where they are called charge density waves.

The Jahn–Teller effect is most often encountered in octahedral complexes, especially six-coordinate copper(II) complexes.^[16] The d^9 electronic configuration of this ion gives three electrons in the two degenerate e_g orbitals, leading to a doubly degenerate electronic ground state. Such complexes distort along one of the molecular fourfold axes (always labelled the z axis), which has the effect of removing the orbital and electronic degeneracies and lowering the overall energy. The distortion normally takes the form of elongating the bonds to the ligands lying along the z axis, but occasionally occurs as a shortening of these bonds instead (the Jahn–Teller theorem does not predict the direction of the distortion, only the presence of an unstable geometry). When such an elongation occurs, the effect is to lower the electrostatic repulsion between the electron-pair on the Lewis basic ligand and any electrons in orbitals with a z component, thus lowering the energy of the complex. If the undistorted complex would be expected to have an inversion center, this is preserved after the distortion.



The Jahn–Teller effect is responsible for the tetragonal distortion of the hexaquaquacopper(II) complex ion, $[\text{Cu}(\text{OH}_2)_6]^{2+}$, which might otherwise possess octahedral geometry. The two axial Cu–O distances are 2.38 Å, whereas the four equatorial Cu–O distances are ~ 1.95 Å.

In octahedral complexes, the Jahn–Teller effect is most pronounced when an odd number of electrons occupy the e_g orbitals. This situation arises in complexes with the configurations d^9 , low-spin d^7 or high-spin d^4 complexes, all of which have doubly degenerate ground states. In such compounds the e_g orbitals involved in the degeneracy point directly at the ligands, so distortion can result in a large energetic stabilization. Strictly speaking, the effect also occurs when there is a degeneracy due to the electrons in the t_{2g} orbitals (*i.e.* configurations such as d^1 or d^2 , both of which are triply degenerate). In such cases, however, the effect is much less noticeable, because there is a much smaller lowering of repulsion on taking ligands further away from the t_{2g} orbitals, which do not point *directly* at the ligands (see the table below). The same is true in tetrahedral complexes (e.g. manganate: distortion is very subtle because there is less stabilisation to be gained because the ligands are not pointing directly at the orbitals).

The expected effects for octahedral coordination are given in the following table:

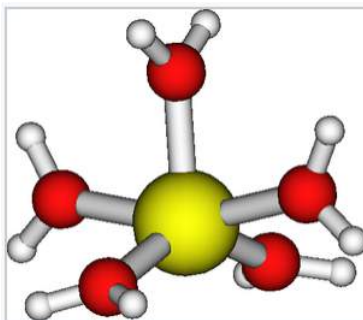
		Jahn–Teller effect												
Number of d electrons		1	2	3	4	5	6	7	8	9	10			
High/Low Spin					HS	LS	HS	LS	HS	LS				
Strength of J-T Effect		w	w		s	w		w	w		w	s		s
...														

w: weak Jahn–Teller effect (t_{2g} orbitals unevenly occupied)

s: strong Jahn–Teller effect expected (e_g orbitals unevenly occupied)

blank: no Jahn–Teller effect expected.

The Jahn–Teller effect is manifested in the UV-VIS absorbance spectra of some compounds, where it often causes splitting of bands. It is readily apparent in the structures of many copper(II) complexes.^[17] Additional, detailed information about the anisotropy of such complexes and the nature of the ligand binding can be obtained from the fine structure of the low-temperature electron spin resonance spectra.

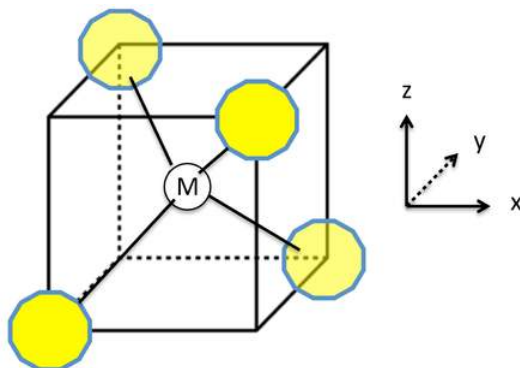


The Cu(II) ion can also coordinate five water molecules in an elongated square pyramid with four Cu-O_{eq} bonds (2x1.98 Å and 2x1.95 Å) and a long Cu-O_{ax} bond (2.35 Å). The four equatorial ligands are distorted from the mean equatorial plane by $\pm 17^\circ$.

This page titled [5.8: Jahn-Teller Effect](#) is shared under a [CC BY-SA 4.0](#) license and was authored, remixed, and/or curated by [Chemistry 310 \(Wikibook\)](#) via [source content](#) that was edited to the style and standards of the LibreTexts platform; a detailed edit history is available upon request.

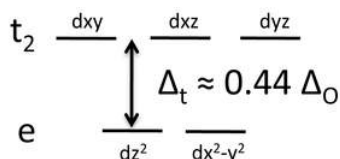
5.9: Tetrahedral Complexes

Tetrahedral complexes are formed with late transition metal ions (Co^{2+} , Cu^{2+} , Zn^{2+} , Cd^{2+}) and some early transition metals (Ti^{4+} , Mn^{2+}), especially in situations where the ligands are large. In these cases the small metal ion cannot easily accommodate a coordination number higher than four. Examples of tetrahedral ions and molecules are $[\text{CoCl}_4]^{2-}$, $[\text{MnCl}_4]^{2-}$, and TiX_4 (X = halogen). Tetrahedral coordination is also observed in some oxo-anions such as $[\text{FeO}_4]^{4-}$, which exists as discrete anions in the salts Na_4FeO_4 and Sr_2FeO_4 , and in the neutral oxides RuO_4 and OsO_4 . The metal carbonyl complexes $\text{Ni}(\text{CO})_4$ and $[\text{Co}(\text{CO})_4]^-$ are also tetrahedral.

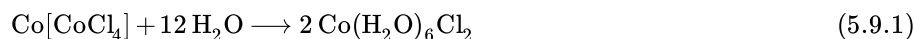


The splitting of the d-orbitals in a tetrahedral crystal field can be understood by connecting the vertices of a tetrahedron to form a cube, as shown in the picture at the left. The tetrahedral M-L bonds lie along the body diagonals of the cube. The d_{z^2} and $d_{x^2-y^2}$ orbitals point along the cartesian axes, i.e., towards the faces of the cube, and have the least contact with the ligand lone pairs. Therefore these two orbitals form a low energy, doubly degenerate e set. The d_{xy} , d_{yz} , and d_{xz} orbitals point at the edges of the cube and form a triply degenerate t_2 set. While the t_2 orbitals have more overlap with the ligand orbitals than the e set, they are still weakly interacting compared to the e_g orbitals of an octahedral complex.

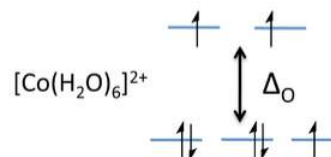
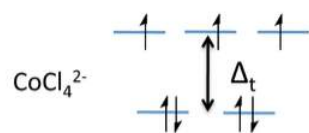
The resulting crystal field energy diagram is shown at the right. The splitting energy, Δ_t , is about 4/9 the splitting of an octahedral complex formed with the same ligands. For 3d elements, Δ_t is thus small compared to the pairing energy and their tetrahedral complexes are always high spin. Note that we have dropped the "g" subscript because the tetrahedron does not have a center of symmetry.



Tetrahedral complexes often have **vibrant colors** because they **lack the center of symmetry** that forbids a d-d* transition. Because the low energy transition is allowed, these complexes typically absorb in the visible range and have extinction coefficients that are 1-2 orders of magnitude higher than the those of the corresponding octahedral complexes. An illustration of this effect can be seen in Drierite, which contains particles of colorless, anhydrous calcium sulfate (gypsum) that absorbs moisture from gases. The indicator dye in Drierite is cobalt (II) chloride, which is a light pink when wet (octahedral) and deep blue when dry (tetrahedral). The reversible hydration reaction is:



(**deep blue**, tetrahedral CoCl_4^{2-}) (**light pink**, octahedral $[\text{Co}(\text{H}_2\text{O})_6]^{2+}$)



This page titled [5.9: Tetrahedral Complexes](#) is shared under a [CC BY-SA 4.0](#) license and was authored, remixed, and/or curated by [Chemistry 310 \(Wikibook\)](#) via [source content](#) that was edited to the style and standards of the LibreTexts platform; a detailed edit history is available upon request.

5.10: Stability of Transition Metal Complexes

The crystal field stabilization energy (**CFSE**) is an important factor in the stability of transition metal complexes. Complexes with high CFSE tend to be **thermodynamically** stable (i.e., they have high values of K_a , the equilibrium constant for metal-ligand association) and are also **kinetically** inert. They are kinetically inert because ligand substitution requires that they *dissociate* (lose a ligand), *associate* (gain a ligand), or *interchange* (gain and lose ligands at the same time) in the transition state. These distortions in coordination geometry lead to a large **activation energy** if the CFSE is large, even if the product of the ligand exchange reaction is also a stable complex. For this reason, complexes of Pt^{4+} , Ir^{3+} (both low spin $5d^6$), and Pt^{2+} (square planar $5d^8$) have very slow ligand exchange rates.

There are two other important factors that contribute to complex stability:

- **Hard-soft interactions** of metals and ligands (which relate to the **energy** of complex formation)
- The **chelate effect**, which is an **entropic** contributor to complex stability.

Hard-soft interactions

Hard acids are typically small, high charge density cations that are weakly polarizable such as H^+ , Li^+ , Na^+ , Be^{2+} , Mg^{2+} , Al^{3+} , Ti^{4+} , and Cr^{6+} . *Electropositive metals in high oxidation states* are typically hard acids. These elements are predominantly found in oxide minerals, because O^{2-} is a hard base.

Some hard bases include H_2O , OH^- , O^{2-} , F^- , NO_3^- , Cl^- , and NH_3 .

The hard acid-base interaction is primarily **electrostatic**. Complexes of hard acids with hard bases are stable because of the electrostatic component of the CFSE.

Soft acids are large, polarizable, *electronegative metal ions in low oxidation states* such as Ni^0 , Hg^{2+} , Cd^{2+} , Cu^+ , Ag^+ , and Au^+ .

Soft bases are anions/neutral bases such as H^- , C_2H_4 , CO , PR_3 , R_2S , and CN^- . Soft acids typically occur in nature as sulfide or arsenide minerals.

The bonding between soft acids and soft bases is predominantly **covalent**. For example, metal carbonyls bind through a covalent interaction between a zero- or low-valent metal and neutral CO to form $\text{Ni}(\text{CO})_4$, $\text{Fe}(\text{CO})_5$, $\text{Co}(\text{CO})_4^-$, $\text{Mn}_2(\text{CO})_{10}$, $\text{W}(\text{CO})_6$, and related compounds.

The preference for hard-hard and soft-soft interactions ("like binds like") is nicely illustrated in the properties of the copper halides:

- CuF : unstable
- **CuI : stable**
- **CuF_2 : stable**
- CuI_2 : unstable

The compounds CuF and CuI_2 have never been isolated, and are thermodynamically unstable to disproportionation:

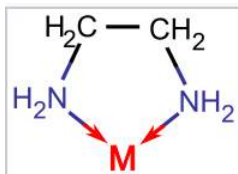


We will learn more about quantifying the energetics of these compounds in Chapter 9.

This page titled [5.10: Stability of Transition Metal Complexes](#) is shared under a [CC BY-SA 4.0](#) license and was authored, remixed, and/or curated by [Chemistry 310 \(Wikibook\)](#) via [source content](#) that was edited to the style and standards of the LibreTexts platform; a detailed edit history is available upon request.

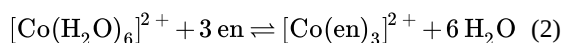
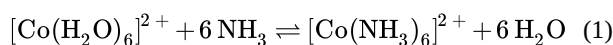
5.11: Chelate and Macrocyclic Effects

Ligands that contain more than one binding site for a metal ion are called **chelating** ligands (from the Greek word *χηλή*, *chēlē*, meaning "claw"). As the name implies, chelating ligands have **high affinity** for metal ions relative to ligands with only one binding group (which are called monodentate = "single tooth") ligands.



Ethylenediamine (en) is a bidentate ligand that forms a five-membered ring in coordinating to a metal ion M

Consider the two complexation equilibria in aqueous solution, between the cobalt (II) ion, $\text{Co}^{2+}(\text{aq})$ and ethylenediamine (en) on the one hand and ammonia, NH_3 , on the other.



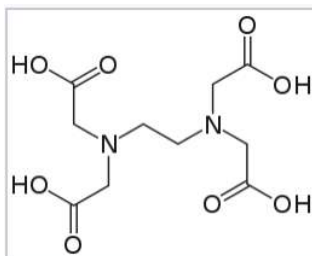
Electronically, the ammonia and en ligands are very similar, since both bind through N and since the Lewis base strengths of their nitrogen atoms are similar. This means that ΔH° must be very similar for the two reactions, since six Co-N bonds are formed in each case. Interestingly however, we observe that the equilibrium constant is *100,000 times larger* for the second reaction than it is for the first.

The big difference between these two reactions is that the second one involves "condensation" of *fewer particles* to make the complex. This means that the **entropy changes** for the two reactions are different. The first reaction has a ΔS° value close to zero, because there are the same number of molecules on both sides of the equation. The second one has a positive ΔS° because four molecules come together but seven molecules are produced. The difference between them ($\Delta\Delta S^\circ$) is about $+100 \text{ J/mol}\cdot\text{K}$. We can translate this into a ratio of equilibrium constants using:

$$K_f(\text{en})/K_f(\text{NH}_3) = e^{-\Delta\Delta G^\circ/RT} \approx e^{+\Delta\Delta S^\circ/R} \approx e^{12} \approx 10^5$$

$$\frac{K_f(\text{en})}{K_f(\text{NH}_3)} = e^{\frac{-\Delta\Delta G^\circ}{RT}} \approx e^{\frac{+\Delta\Delta S^\circ}{R}} \approx e^{12} \approx 10^5 \quad (5.11.1)$$

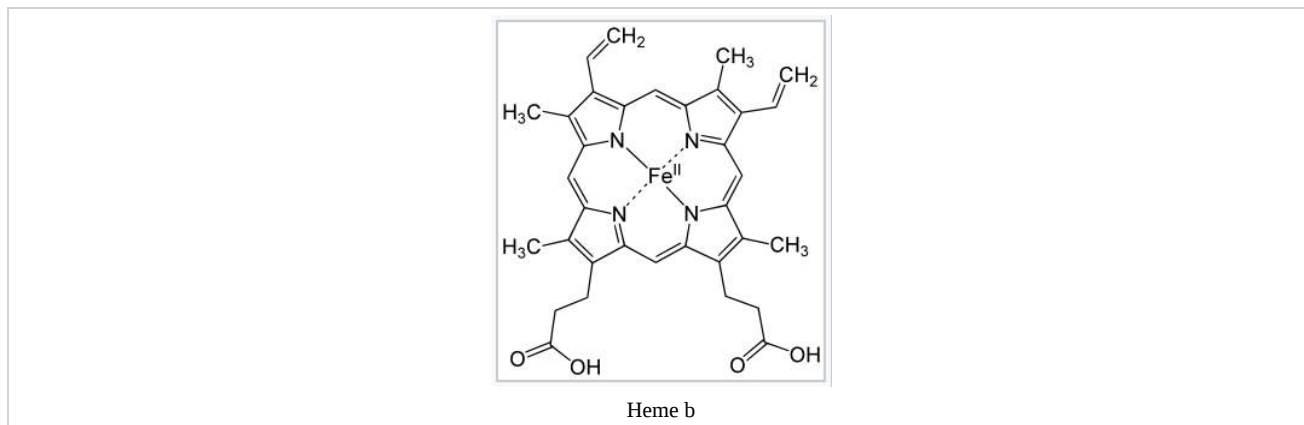
The bottom line is that the chelate effect is **entropy-driven**. It follows that the more binding groups a ligand contains, the more positive the ΔS° and the higher the K_f will be for complex formation. In this regard, the hexadentate ligand ethylenediamine tetraacetic acid (EDTA) is an optimal ligand for making octahedral complexes because it has six binding groups. In basic solutions where all four of the COOH groups are deprotonated, the **chelate effect** of the EDTA^{4-} ligand is approximately 10^{15} . This means, for a given metal ion, K_f is 10^{15} times larger for EDTA^{4-} than it would be for the relevant monodentate ligands at the same concentration. EDTA^{4-} tightly binds essentially any 2+, 3+, or 4+ ion in the periodic table, and is a very useful ligand for both analytical applications and separations.



Ethylenediaminetetraacetic acid (EDTA), a hexadentate ligand

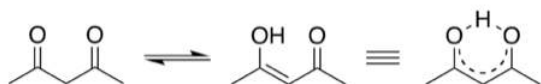
The **macrocyclic effect** follows the same principle as the chelate effect, but the effect is further enhanced by the cyclic conformation of the ligand. Macrocyclic ligands are not only multi-dentate, but because they are covalently constrained to their cyclic form, they allow less conformational freedom. The ligand is said to be "**pre-organized**" for binding, and there is little

entropy penalty for wrapping it around the metal ion. For example heme b is a tetradentate cyclic ligand which is strongly complexes transition metal ions, including (in biological systems) Fe^{+2} .



Some other common chelating and cyclic ligands are shown below:

Acetylacetonate (acac^- , right) is an anionic bidentate ligand that coordinates metal ions through two oxygen atoms. Acac^- is a hard base so it prefers hard acid cations. With divalent metal ions, acac^- forms neutral, volatile complexes such as $\text{Cu}(\text{acac})_2$ and $\text{Mo}(\text{acac})_2$ that are useful for chemical vapor deposition (CVD) of metal thin films.



2,2'-Bipyridine and related bidentate ligands such as 1,10-phenanthroline (below, center left) form propeller-shaped complexes with metals such as Ru^{2+} . The $[\text{Ru}(\text{bpy})_3]^{2+}$ complex (below left) is photoluminescent and can also undergo photoredox reactions, making it an interesting compound for both photocatalysis and artificial photosynthesis. The chiral propeller shapes of metal polypyridyl complexes such as $[\text{Ru}(\text{bpy})_3]^{2+}$ coincidentally match the size and helicity of the major groove of DNA. This has led to a number of interesting studies of electron transfer reactions along the DNA backbone, initiated by photoexcitation of the metal complex.

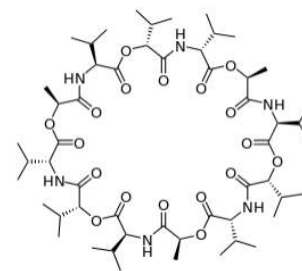
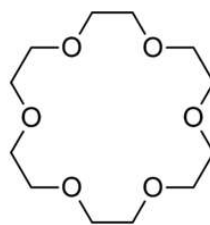
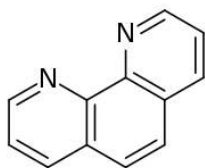
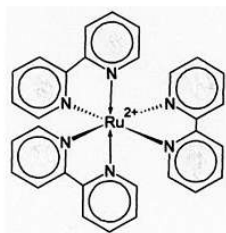


Prof. Jacqueline Barton (Caltech) has used metal polypyridyl complexes to study electron transfer reactions that are implicated in the biological sensing and repair of damage in DNA molecules.

Crown ethers such as 18-crown-6 (below, center right) are cyclic hard bases that can complex alkali metal cations. Crowns can selectively bind Li^+ , Na^+ , or K^+ depending on the number of ethylene oxide units in the ring.

The chelating properties of crown ethers are mimetic of the natural antibiotic **valinomycin** (below right), which selectively transports K^+ ions across bacterial cell membranes, killing the bacterium by dissipating its membrane potential. Like crown

ethers, valinomycin is a cyclic hard base.

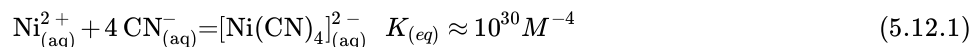


This page titled [5.11: Chelate and Macrocyclic Effects](#) is shared under a [CC BY-SA 4.0](#) license and was authored, remixed, and/or curated by [Chemistry 310 \(Wikibook\)](#) via [source content](#) that was edited to the style and standards of the LibreTexts platform; a detailed edit history is available upon request.

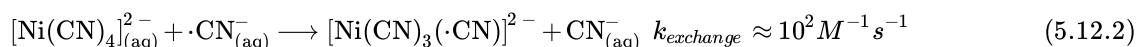
5.12: Ligand Substitution Reactions

Transition metal complexes can exchange one ligand for another, and these reactions are important in their synthesis, stereochemistry, and catalytic chemistry. The mechanisms of chemical reactions are intimately connected to reaction kinetics. As in organic chemistry, the mechanisms of transition metal reactions are typically inferred from experiments that examine the concentration dependence of the incoming and outgoing ligands on the reaction rate, the detection of intermediates, and the stereochemistry of the reactants and products.

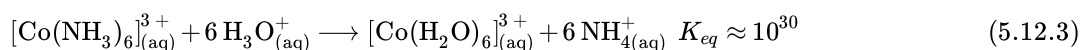
Thermodynamic vs. kinetics. When we think about the reactions of transition metal complexes, it is important to recall the distinction between their *thermodynamics* and *kinetics*. Take for example the formation of the square planar tetracyanonickelate complex:



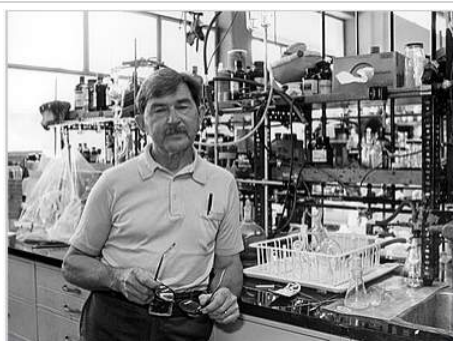
Thermodynamically, $[\text{Ni}(\text{CN})_4]^{2-}$ is very **stable**, meaning that the equilibrium above lies very far to the right. Kinetically, however, the complex is **labile**, meaning that it can exchange its ligands rapidly. For example the exchange between a ^{13}C labeled CN^{-} ion and a bound CN^{-} ligand occurs on the timescale of tens of milliseconds:



Conversely, a compound can be thermodynamically **unstable** but kinetically **inert**, meaning that it takes a relatively long time to react. For example, the $[\text{Co}(\text{NH}_3)_6]^{3+}$ ion is unstable in acid, but its hydrolysis reaction with concentrated HCl takes about one week to go to completion at room temperature:

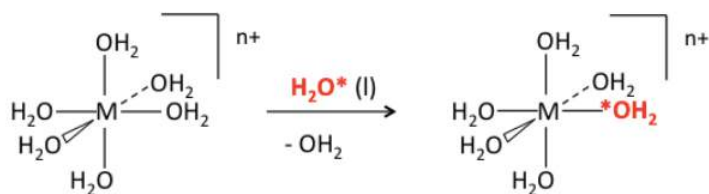


Henry Taube, who studied the mechanisms of ligand exchange reactions in simple test tube experiments, classified transition metal complexes as **labile** if their reaction half-life was one minute or less, and **inert** if they took longer to react. The dynamic range of ligand substitution rates is enormous, spanning at least 15 orders of magnitude. On the timescale of most laboratory experiments, the Taube definition of lability is a useful one for classifying reactions into those that have low and high activation energies. As we will see, the **crystal field stabilization energy (CFSE)** plays a key role in determining the activation energy and therefore the rate of ligand substitution.



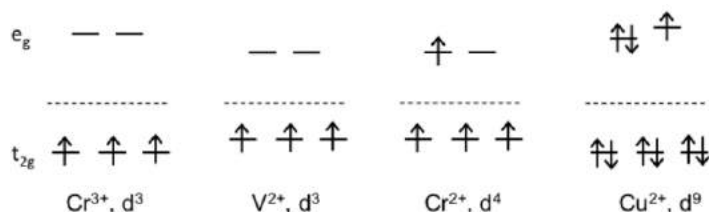
Henry Taube (Stanford University) received the 1983 Nobel Prize for his work on the electron transfer and ligand exchange reactions of transition metal complexes

Crystal field stabilization energy and ligand exchange rates. Let's consider a very common and simple ligand exchange reaction, which is the substitution of one water molecule for another in an octahedral $[\text{M}(\text{H}_2\text{O})_6]^{n+}$ complex. Since the products (except for the label) are the same as the reactants, we know that $\Delta G^\circ = 0$ and $K_{\text{eq}} = 1$ for this reaction. The progress of the reaction can be monitored by NMR by using isotopically labeled water (typically containing ^{17}O or ^{18}O):



The most striking thing about this (otherwise boring) reaction is the vast difference in rate constants - about 14 orders of magnitude - for different metal ions and oxidation states:

M^{n+}	$\log k \text{ (sec}^{-1}\text{)}$
Cr^{3+}	-6
V^{2+}	-2
Cr^{2+}	8
Cu^{2+}	8



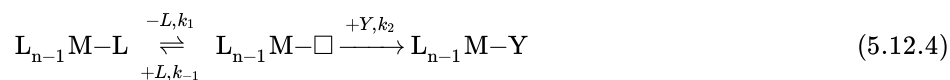
While at first it may seem strange that the same ion in two different oxidation states (Cr^{3+} vs. Cr^{2+}) would be inert or labile, respectively, we can begin to rationalize the difference by drawing d-orbital splitting diagrams for the complexes. What we find is that octahedral complexes that have **high CFSE** (Cr^{3+} , V^{2+}) tend to be **inert**. Conversely, ions with electrons in high energy e_g orbitals (Cr^{2+} , Cu^{2+}) tend to be labile. In the case of Cr^{3+} and V^{2+} , the energy penalty for distorting the complex away from octahedral symmetry - to make, for example, a 5- or 7-coordinate intermediate - is particularly high. This activation energy for ligand substitution is lower for Cr^{2+} and Cu^{2+} , which already have electrons in antibonding e_g orbitals.

Based on the rules we developed for calculating the CFSE of transition metal complexes, we can now predict the trends in ligand substitution rates:

- Octahedral complexes with **d^3 and d^6 (low spin)** configurations, such as Cr^{3+} (d^3), Co^{3+} (d^6), Rh^{3+} (d^6), Ru^{2+} (d^6), and Os^{2+} (d^6) tend to be **substitution-inert** because of their high CFSE.
- Square planar d^8** complexes, especially those in the 4d and 5d series, are also **substitution-inert**. Examples are complexes of Pd^{2+} , Pt^{2+} , and Au^{3+} .
- Intermediate cases are complexes of Fe^{3+} , V^{3+} , V^{2+} , Ni^{2+} , and of main group ions (Be^{2+} , Al^{3+}) that are hard Lewis acids. These complexes make strong metal-oxygen bonds and have water exchange rates in the range of 10^1 - 10^6 s^{-1} .
- Ions with zero CFSE** exchange water molecules on a timescale of nanoseconds ($k \approx 10^8$ - 10^9 s^{-1}). These include ions with d^0 , d^5 (high spin), and d^{10} electron counts, including alkali metal (Li^+ , Na^+ , K^+ , Rb^+ , Cs^+) and alkali earth (Mg^{2+} , Ca^{2+} , Sr^{2+} , Ba^{2+}) cations, Zn^{2+} , Cd^{2+} , Hg^{2+} , and Mn^{2+} . In these cases the CFSE is zero and the energetic cost of breaking octahedral symmetry is relatively low.
- For p-block elements, faster exchange occurs with larger ions (e.g., $Ba^{2+} > Ca^{2+}$ and $Ga^{3+} > Al^{3+}$), because Lewis acid strength decreases with increasing ion size.
- The Cu^{2+} ion (d^9), as a **Jahn-Teller ion**, is already distorted away from octahedral symmetry and is therefore quite **labile**, exchanging water ligands at a rate of about 10^8 s^{-1} .

Ligand Substitution Mechanisms. For an ML_n complex undergoing ligand substitution, there are essentially three different reaction mechanisms:

- In the **dissociative mechanism**, a ML_n complex first **loses a ligand** to form an ML_{n-1} intermediate, and the incoming ligand Y reacts with the ML_{n-1} fragment:



This mechanism is illustrated below for ligand substitution on an octahedral ML_6 complex. The intermediate state in this example involves a trigonal bipyramidal ML_5 fragment as well as free L and Y ligands.

If the rate determining step is the dissociation of L from the complex, then the concentration of Y does not affect the rate of reaction, leading to the first-order rate law:

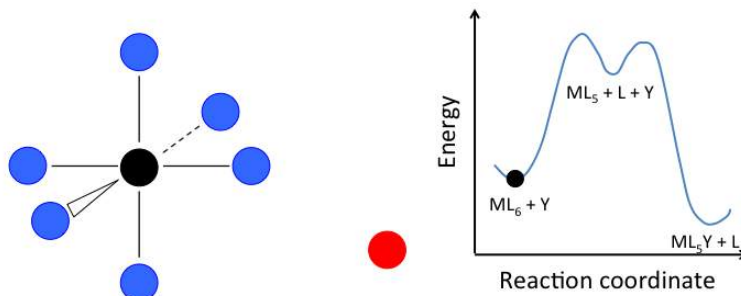


Illustration of the dissociative ligand substitution mechanism for an ML_6 complex. The reaction energy profile is shown at the right.

$$Rate = k_1[ML_n] \quad (5.12.5)$$

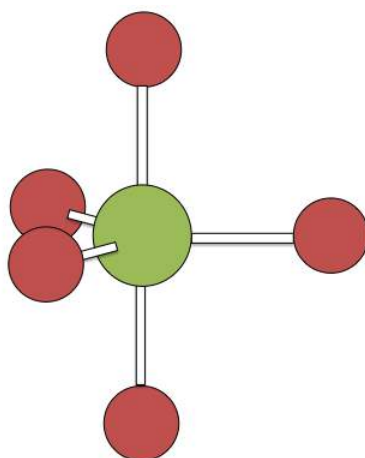
In the case of an octahedral complex, this reaction would be first order in ML_6 and zero order in Y, but only if the highest energy transition state is the one that precedes the formation of the ML_5 intermediate. If the two transition states are close in energy (as in the case of the animation at the right), then the rate law becomes more complicated. In this case, we can simplify the problem by assuming a low steady-state concentration of the ML_n intermediate. The resulting rate law is:

$$Rate = \frac{k_1 k_2 [Y][ML_n]}{k_{-1}[L] + k_2[Y]} \quad (5.12.6)$$

which reduces to the simpler first-order rate law when $k_2[Y] \gg k_{-1}[L]$. Because the formation of the transition state involves dissociation of a ligand, the entropy of activation is always positive in the dissociative mechanism.

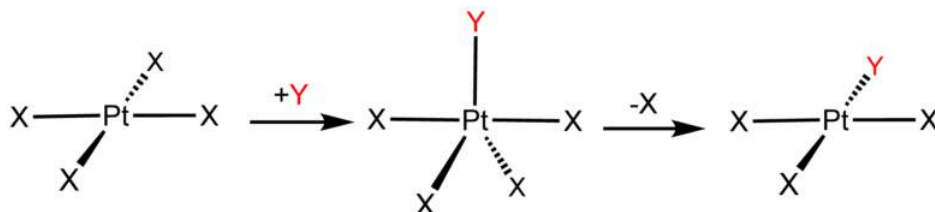
- In the **associative mechanism**, the incoming ligand Y attacks the ML_n complex, transiently forming an ML_nY intermediate, and the intermediate then loses a ligand L forming the $ML_{n-1}Y$ product

Complexes that undergo associative substitution are typically either coordinatively unsaturated or contain a ligand that can change its bonding to the metal, e.g. a change in the hapticity or bending of a nitric oxide ligand (NO). In homogeneous catalysis, the associative pathway is desirable because the binding event, and hence the selectivity of the reaction, depends not only on the nature of the metal catalyst but also on the molecule that is involved in the catalytic cycle.



Berry pseudorotation mechanism

Examples of associative mechanisms are commonly found in the chemistry of d^8 square planar metal complexes, e.g. Vaska's complex ($\text{IrCl}(\text{CO})[\text{P}(\text{C}_6\text{H}_5)_3]_2$) and tetrachloroplatinate(II). These compounds (ML_4) bind the incoming (substituting) ligand Y to form pentacoordinate intermediates ML_4Y , which in a subsequent step dissociate one of their ligands. Although the incoming ligand is initially bound at an equatorial site, the **Berry pseudorotation** provides a low energy pathway for all ligands to sample both the equatorial and axial sites. Ligand dissociation must occur from an equatorial site according to the principle of microscopic reversibility. Dissociation of Y results in no reaction, but dissociation of L results in net substitution, yielding the d^8 complex ML_3Y . The first step is typically rate determining. Thus, the entropy of activation is negative, which indicates an increase in order in the transition state. Associative reactions follow second order kinetics: the rate of the appearance of product depends on the concentration of both ML_4 and Y .



The Trans Effect, which is connected with the associative mechanism, controls the stereochemistry of certain ligand substitution reactions.

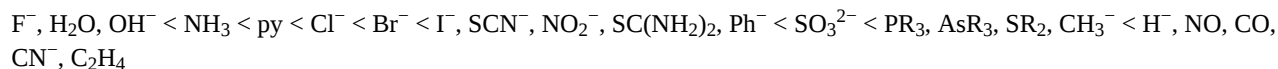
The trans effect refers to the labilization (making more reactive) of ligands that are **trans** to certain other ligands, the latter being

referred to as **trans-directing ligands**. The labilization of trans ligands is attributed to electronic effects and is most notable in square planar complexes, but it can also be observed with octahedral complexes.^[18] The cis effect is most often observed in octahedral complexes.

In addition to the *kinetic trans effect*, trans ligands also have an influence on the ground state of the molecule, the most notable ones being bond lengths and stability. Some authors prefer the term **trans influence** to distinguish this from the kinetic effect,^[19] while others use more specific terms such as **structural trans effect** or **thermodynamic trans effect**.^[18]

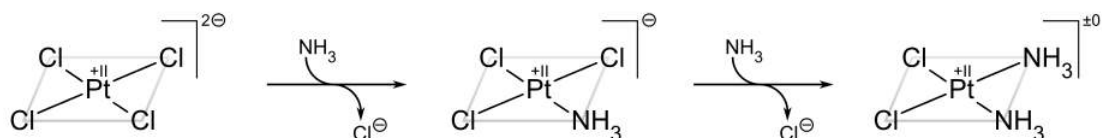
The discovery of the trans effect is attributed to Ilya Ilich Chernyaev,^[20] who recognized it and gave it a name in 1926.^[21]

The intensity of the trans effect (as measured by the increase in the rate of substitution of the trans ligand) follows this sequence:

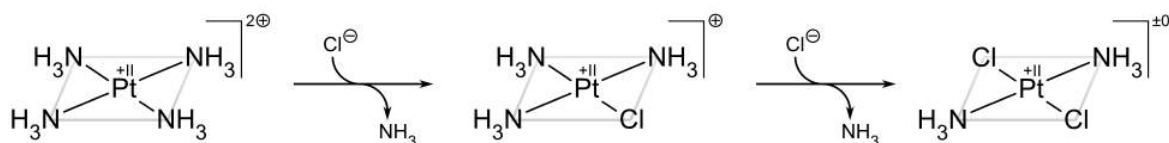


Note that weak field ligands tend to be poor trans-directing ligands, whereas strong field ligands are strongly trans-directing.

The classic example of the trans effect is the synthesis of cisplatin and its trans isomer.^[22] Starting from PtCl_4^{2-} , the first NH_3 ligand is added to any of the four equivalent positions at random. However, since Cl^- has a greater trans effect than NH_3 , the second NH_3 is added trans to a Cl^- and therefore cis to the first NH_3 .



If, on the other hand, one starts from $\text{Pt}(\text{NH}_3)_4^{2+}$, the *trans* product is obtained instead:

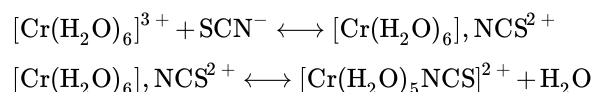


The trans effect in square complexes can be explained in terms of the associative mechanism, described above, which goes through a trigonal bipyramidal intermediate. Ligands with a high kinetic trans effect are in general those with high π acidity (as in the case of phosphines) or low-ligand lone-pair- d_π repulsions (as in the case of hydride), which prefer the more π -basic equatorial sites in the intermediate. The second equatorial position is occupied by the incoming ligand. The third and final equatorial site is occupied by the departing trans ligand, so the net result is that the kinetically favored product is the one in which the ligand trans to the one with the largest trans effect is eliminated.^[19]

- The **interchange mechanism** is similar to the associative and dissociative pathways, except that no distinct ML_nY or ML_{n-1} intermediate is formed. This concerted mechanism can be thought of as analogous to nucleophilic substitution via the $\text{S}_{\text{N}}2$ pathway at a tetrahedral carbon atom in organic chemistry. The interchange mechanism is further classified as associative (I_a) or dissociative (I_d) depending on the relative importance of $\text{M}-\text{Y}$ and $\text{M}-\text{L}$ bonding in the transition state. If the transition state is characterized by the formation of a strong $\text{M}-\text{Y}$ bond, then the mechanism is I_a . Conversely, if weakening of the $\text{M}-\text{L}$ bond is more important in reaching the transition state, then the mechanism is I_d .

An example of the I_a mechanism is the interchange of bulk and coordinated water in $[\text{V}(\text{H}_2\text{O})_6]^{2+}$. In contrast, the slightly more compact ion $[\text{Ni}(\text{H}_2\text{O})_6]^{2+}$ ion exchanges water via the I_d mechanism.^[23]

Effects of ion pairing. Highly charged cationic complexes tend to form ion pairs with anionic ligands, and these ion pairs often undergo reactions via the I_a pathway. The electrostatically held nucleophilic incoming ligand can exchange positions with a ligand in the first coordination sphere, resulting in net substitution. An illustrative process is the "anation" (reaction with an anion) of the chromium(III) hexaaquo complex:



This page titled [5.12: Ligand Substitution Reactions](#) is shared under a [CC BY-SA 4.0](#) license and was authored, remixed, and/or curated by [Chemistry 310 \(Wikibook\)](#) via [source content](#) that was edited to the style and standards of the LibreTexts platform; a detailed edit history is available upon request.

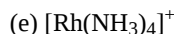
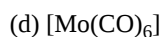
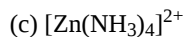
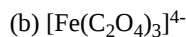
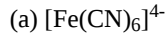
5.13: Discussion Questions

- Discuss chelating ligands and what they do, using some new examples.
 - Explain (using some new examples) how we know if an octahedral complex of a metal ion will be high spin or low spin, and what measurements we can do to confirm it.
-

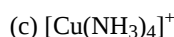
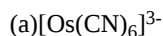
This page titled [5.13: Discussion Questions](#) is shared under a [CC BY-SA 4.0](#) license and was authored, remixed, and/or curated by [Chemistry 310 \(Wikibook\)](#) via [source content](#) that was edited to the style and standards of the LibreTexts platform; a detailed edit history is available upon request.

5.14: Problems

1. Predict the shape of the following complexes, and determine whether each will be diamagnetic or paramagnetic:



2. For each of the following transition metal complexes, give (i) the d-electron count, (ii) the approximate shape of the complex, and (iii) an energy level diagram showing the splitting and filling of the d-orbitals.

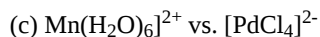
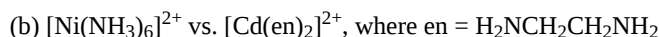
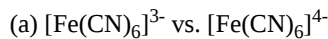


3. Tetrahedral complexes are almost always high spin, whereas octahedral complexes can be either high or low spin. Explain.

4. For each of the Mn complexes in the table below, give electronic configurations (within the t_{2g} and e_g sets of 3d orbitals) that are consistent with the observed magnetic moments.

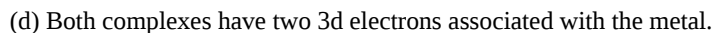
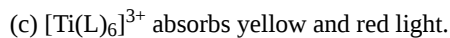
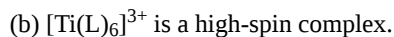
Compound	μ (BM)
$[\text{Mn}(\text{CN})_6]^{4-}$	1.8
$[\text{Mn}(\text{CN})_6]^{3-}$	3.2
$[\text{Mn}(\text{NCS})_6]^{4-}$	6.1
$[\text{Mn}(\text{acac})_3]$	5.0

5. For each of the following pairs, identify the complex with the higher crystal field stabilization energy (and show your work).



6. In a solution made by combining FeCl_3 with excess ethylenediaminetetraacetic acid (EDTA) at neutral pH, the concentration of $\text{Fe}^{3+}(\text{aq})$ ions is on the order of 10^{-17} M. However, in a solution of ethylenediamine and acetic acid at comparable concentration, the $\text{Fe}^{3+}(\text{aq})$ concentration is about 10^{-7} , i.e., 10^{10} times higher. Explain.

7. The complex $[\text{Ti}(\text{H}_2\text{O})_6]^{3+}$ is violet, while the analogous complex with another monodentate neutral ligand L, $[\text{Ti}(\text{L})_6]^{3+}$ is orange. How many of the following statements are true? Explain briefly.



8. OH^- and CN^- are both Brønsted bases, and both can form complexes with metal ions. Explain how OH^- can be a much stronger Brønsted base than CN^- , and at the same time much lower in the spectrochemical series.

9. A solution of $[\text{Ni}(\text{H}_2\text{O})_6]^{2+}$ is faint green and paramagnetic ($\mu = 2.90$ BM), whereas a solution of $[\text{Ni}(\text{CN})_4]^{2-}$ is yellow and diamagnetic.

(a) Draw the molecular geometry and the d-orbital energy level diagrams for each complex, showing the electronic occupancy of the d-orbitals.

(b) Explain the differences in magnetism and color.

10. W. Deng and K. W. Hipps (J. Phys. Chem. B 2003, 107, 10736-10740) reported an STM study of the electronic properties of Ni(II)tetraphenyl porphyrin (NiTPP), a red-purple, neutral diamagnetic complex that is made by reacting Ni(II) perchlorate with tetraphenylporphine. When NiTPP is reacted with sodium thiocyanate it forms another complex that is paramagnetic. Draw the structures of NiTPP and the product complex, and the crystal field energy level diagram that explains each. What value of the magnetic moment (in units of μ_B) would you expect for the paramagnetic complex?

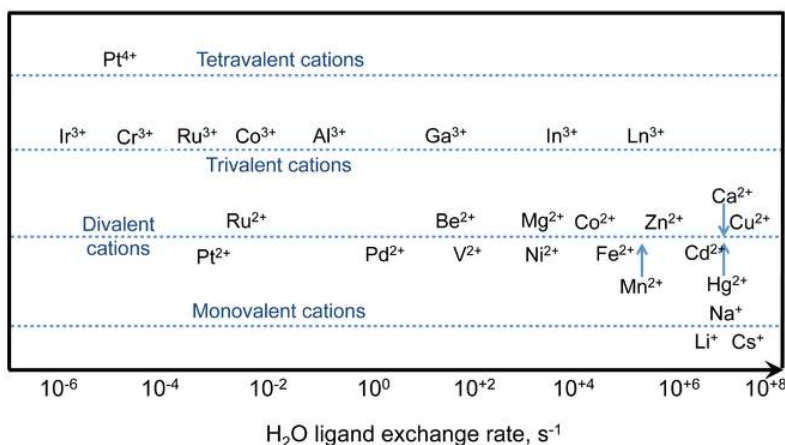
11. One of the simplest reactions a coordination complex can do is **ligand exchange**. For example, metal aquo complexes can exchange a coordinated water molecule with a free (solvent) water molecule, and the rate of the reaction can be measured by isotope labeling, NMR, and other techniques. Interestingly, these rates vary widely for water exchange with different metal ions - over a range of *14 orders of magnitude* - as shown in the figure below. For some metal ions, the rate is so slow that it takes weeks for one water molecule to exchange for another. In other cases, the timescale of the exchange is nanoseconds.

(a) There is an overall trend in which the rate of exchange decreases as the oxidation state of the metal increases. Explain this trend in terms of crystal field stabilization energy (CFSE). How is the CFSE related to the activation energy of the water exchange reaction?

(b) Explain any trends you observe for the rate of water exchange among divalent metal ions.

(c) Cu^{2+} has an anomalously fast ligand exchange rate. Why?

(d) What are the geometries and d-electron counts of the aquo complexes of the slowest divalent, trivalent, and tetravalent metal ions in the figure? Do they have particularly high or low CFSE's? Explain.



12. Ligand exchange rates for main group ions increase going down a group, e.g., $\text{Al}^{3+} < \text{Ga}^{3+} < \text{In}^{3+}$. For transition metal ions, we see the opposite trend, e.g., $\text{Fe}^{2+} > \text{Ru}^{2+} > \text{Os}^{2+}$. Explain why these trends are different.

13. Seppelt and coworkers reported the very unusual ion $[\text{AuXe}_4]^{2+}$ in the salt $[\text{AuXe}_4]^{2+} (\text{Sb}_2\text{F}_{11}^-)_2$ (Science 2000, 290, 117-118). This was the first report of a compound containing a bond between a metal and a noble gas atom. Draw a d-orbital energy diagram for this ion and predict whether it should be diamagnetic or paramagnetic. Would you expect to be able to form a similar complex using Cu in place of Au, or Kr in place of Xe? Why or why not?

14. For the reaction $\text{cis-Mo}(\text{CO})_4\text{L}_2 + \text{CO} \rightarrow \text{Mo}(\text{CO})_5\text{L} + \text{L}$, the reaction rate is found to vary by a factor of 500 for two different ligands L, but it is relatively insensitive to the pressure of CO gas. (a) What kind of mechanism does this reaction have? (b) What are the signs of the activation volume and the activation entropy?

15. In Rosenberg's initial discovery of the biological effects of *cis*-Pt(NH₃)₂Cl₂, the compound was made accidentally by partial dissolution of a Pt anode in an electrolyte solution that contained glucose and magnesium chloride.^[24] The electrolysis reaction also produced small amounts of ammonium ions. Explain mechanistically why the *cis*-isomer is formed selectively under these conditions.

This page titled 5.14: Problems is shared under a CC BY-SA 4.0 license and was authored, remixed, and/or curated by Chemistry 310 (Wikibook) via source content that was edited to the style and standards of the LibreTexts platform; a detailed edit history is available upon request.

5.15: References

- Rosi, Nathaniel L.; Eckert, Juergen; Eddaoudi, Mohamed; Vodak, David T.; Kim, Jaheon; O'Keefe, Michael; Yaghi, Omar M. (2003). "Hydrogen storage in microporous metal-organic frameworks". *Science* **300** (5622): 1127–1129. doi:[10.1126/science.1083440](https://doi.org/10.1126/science.1083440). PMID [12750515](https://pubmed.ncbi.nlm.nih.gov/12750515/). Bibcode: [2003Sci...300.1127R](https://ui.adsabs.org/abs/2003Sci...300.1127R).
- Green, M.L.H. (1995). "A new approach to the formal classification of covalent compounds of the elements". *Journal of Organometallic Chemistry* **500**: 127–148. doi:[10.1016/0022-328X\(95\)00508-N](https://doi.org/10.1016/0022-328X(95)00508-N).
- [The CBC Method](#), Parkin group, Columbia University.
- Crabtree, Robert. *The Organometallic Chemistry of the Transition Metals*: 4th edition. Wiley-Interscience, 2005
- "Metal–Ligand Multiple Bonds: The Chemistry of Transition Metal Complexes Containing Oxo, Nitrido, Imido, Alkylidene, or Alkylidyne Ligands" W. A. Nugent and J. M. Mayer; Wiley-Interscience, New York, 1988.
- McConville, David H.; Wolf, Jennifer R.; Schrock, Richard R. (1993). "Synthesis of chiral molybdenum ROMP initiators and all-cis highly tactic poly(2,3-(R)2norbornadiene) (R = CF₃ or CO₂Me)". *J. Am. Chem. Soc.* **115** (10): 4413–4414. doi:[10.1021/ja00063a090](https://doi.org/10.1021/ja00063a090).
- Nguyen, Sonbinh T.; Johnson, Lynda K.; Grubbs, Robert H.; Ziller, Joseph W. (1992). "Ring-opening metathesis polymerization (ROMP) of norbornene by a Group VIII carbene complex in protic media". *J. Am. Chem. Soc.* **114** (10): 3974–3975. doi:[10.1021/ja00036a053](https://doi.org/10.1021/ja00036a053).
- Rosenberg B, Vancamp L, Troscio JE, Mansour VH (1969). "Platinum compounds - a new class of potent antitumour agents". *Nature* **222** (5191): 385–386. doi:[10.1038/222385a0](https://doi.org/10.1038/222385a0).
- G. Wilkinson, M. Rosenblum, M. C. Whiting, R. B. Woodward (1952). "The Structure of Iron Bis-Cyclopentadienyl". *Journal of the American Chemical Society* **74** (8): 2125–2126. doi:[10.1021/ja01128a527](https://doi.org/10.1021/ja01128a527).
- Osborn, J. A.; Jardine, F. H.; Young, J. F.; Wilkinson, G. (1966). "The Preparation and Properties of Tris(triphenylphosphine)halogenorhodium(I) and Some Reactions Thereof Including Catalytic Homogeneous Hydrogenation of Olefins and Acetylenes and Their Derivatives". *Journal of the Chemical Society A*: 1711–1732. doi:[10.1039/J19660001711](https://doi.org/10.1039/J19660001711).
- "Tris(triphenylphosphine)halorhodium(I)" J. A. Osborn, G. Wilkinson, *Inorganic Syntheses*, 1967, Volume 10, p. 67. DOI [10.1002/9780470132418.ch12](https://doi.org/10.1002/9780470132418.ch12)
- D. A. Evans, G. C. Fu and A. H. Hoveyda (1988). "Rhodium(I)-catalyzed hydroboration of olefins. The documentation of regio- and stereochemical control in cyclic and acyclic systems". *J. Am. Chem. Soc.* **110** (20): 6917–6918. doi:[10.1021/ja00228a068](https://doi.org/10.1021/ja00228a068).
- I. Ojima, T. Kogure (1972). "Selective reduction of α,β -unsaturated terpene carbonyl compounds using hydrosilane-rhodium(I) complex combinations". *Tetrahedron Lett.* **13** (49): 5035–5038. doi:[10.1016/S0040-4039\(01\)85162-5](https://doi.org/10.1016/S0040-4039(01)85162-5).
- W. S. Knowles (2003). "Asymmetric Hydrogenations (Nobel Lecture 2001)". *Advanced Synthesis and Catalysis* **345** (12): 3–13. doi:[10.1002/adsc.200390028](https://doi.org/10.1002/adsc.200390028).
- H. Jahn and E. Teller (1937). "Stability of Polyatomic Molecules in Degenerate Electronic States. I. Orbital Degeneracy". *Proceedings of the Royal Society A* **161**(905): 220–235. doi:[10.1098/rspa.1937.0142](https://doi.org/10.1098/rspa.1937.0142). Bibcode: [1937RSPSA.161..220J](https://ui.adsabs.org/abs/1937RSPSA.161..220J).
- Rob Janes and Elaine A. Moore (2004). [Metal-ligand bonding](#). Royal Society of Chemistry. ISBN [0-85404-979-7](https://www.rsc.org/books/9780854049797).
- Patrick Frank, Maurizio Benfatto, Robert K. Szilagyi, Paola D'Angelo, Stefano Della Longa, and Keith O. Hodgson "The Solution Structure of [Cu(aq)]²⁺ and Its Implications for Rack-Induced Bonding in Blue Copper Protein Active Sites" *Inorganic Chemistry* 2005, vol 44, pp 1922–1933. DOI [10.1021/ic0400639](https://doi.org/10.1021/ic0400639)
- Coe, B. J.; Glenwright, S. J. Trans-effects in octahedral transition metal complexes. *Coordination Chemistry Reviews* **2000**, 203, 5–80.
- Robert H. Crabtree (2005). *The Organometallic Chemistry of the Transition Metals* (4th ed.). New Jersey: Wiley-Interscience. ISBN [0-471-66256-9](https://www.wiley.com/9780471662569).
- Kauffmann, G. B. I'lya I'lich Chernyaev (1893-1966) and the Trans Effect. *J. Chem. Educ.* **1977**, 54, 86–89.
- Chernyaev, I. I. The mononitrites of bivalent platinum. I. *Ann. inst. platine (USSR)* **1926**, 4, 243–275.
- George B. Kauffman, Dwaine O. Cowan (1963). "cis- and trans-Dichlorodiammineplatinum(II)". *Inorg. Synth.* **7**: 239–245. doi:[10.1002/9780470132388.ch63](https://doi.org/10.1002/9780470132388.ch63).
- Helm, Lothar; Merbach, André E. (2005). "Inorganic and Bioinorganic Solvent Exchange Mechanisms". *Chem. Rev.* **105** (6): 1923–1959. doi:[10.1021/cr030726o](https://doi.org/10.1021/cr030726o). PMID [15941206](https://pubmed.ncbi.nlm.nih.gov/15941206/).
- Rosenberg, B.; Van Camp, L.; Krigas, T. (1965). "Inhibition of Cell Division in Escherichia coli by Electrolysis Products from a Platinum Electrode". *Nature* **205**(4972): 698–9. doi:[10.1038/205698a0](https://doi.org/10.1038/205698a0). PMID [14287410](https://pubmed.ncbi.nlm.nih.gov/14287410/).

This page titled [5.15: References](#) is shared under a [CC BY-SA 4.0](#) license and was authored, remixed, and/or curated by [Chemistry 310 \(Wikibook\)](#) via [source content](#) that was edited to the style and standards of the LibreTexts platform; a detailed edit history is available upon request.

CHAPTER OVERVIEW

6: Metals and Alloys- Structure, Bonding, Electronic and Magnetic Properties

Learning Objectives

- Identify and assign unit cells, coordination numbers, asymmetric units, numbers of atoms contained within a unit cell, and the fraction of space filled in a given structure.
- Relate molecular orbital theory to the delocalization of valence electrons in metals.
- Understand the concepts of electron wavelength and density of states.
- Understand the consequences of the nearly free electron model for the band structure of metals and their conductivity.
- Explain why some metals are magnetic and others are diamagnetic, and how these phenomena relate to bonding and orbital overlap.
- Use the Curie-Weiss law to explain the temperature dependence of magnetic ordering.
- Acquire a physical picture of different kinds of magnetic ordering and the magnetic hysteresis loops of ferro- and ferrimagnets.

It should come as no surprise that the properties of extended solids are also connected to their structures, and so to understand what they do we should begin with their crystal structures. Most of the metals in the periodic table have relatively simple structures and so this is a good place to begin.

[6.1: Prelude to Metals and Alloys](#)

[6.2: Unit Cells and Crystal Structures](#)

[6.3: Bravais Lattices](#)

[6.4: Crystal Structures of Metals](#)

[6.5: Bonding in Metals](#)

[6.6: Conduction in Metals](#)

[6.7: Atomic Orbitals and Magnetism](#)

[6.8: Ferro-, Ferri- and Antiferromagnetism](#)

[6.9: Hard and Soft Magnets](#)

[6.10: Discussion Questions](#)

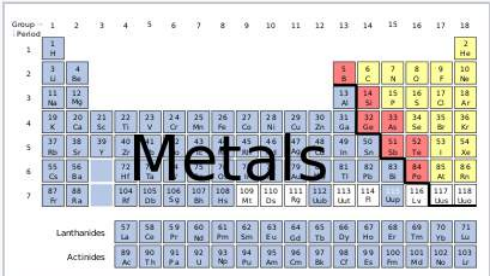
[6.11: Problems](#)

[6.12: References](#)

This page titled [6: Metals and Alloys- Structure, Bonding, Electronic and Magnetic Properties](#) is shared under a [CC BY-SA 4.0](#) license and was authored, remixed, and/or curated by [Chemistry 310 \(Wikibook\)](#) via [source content](#) that was edited to the style and standards of the LibreTexts platform; a detailed edit history is available upon request.

6.1: Prelude to Metals and Alloys

In the chemistry of molecular compounds, we are accustomed to the idea that properties depend strongly on structure. For example we can rationalize the polarity of the water molecule based on its shape. We also know that two molecules with the same composition (e.g., ethanol and dimethyl ether) have very different properties based on the bonding arrangements of atoms. It should come as no surprise that the properties of extended solids are also connected to their structures, and so to understand what they do we should begin with their crystal structures. Most of the metals in the periodic table have relatively simple structures and so this is a good place to begin. We will see in Chapter 8 that the structures of more complex compounds are also in many cases related to the simple structures of metals and alloys.



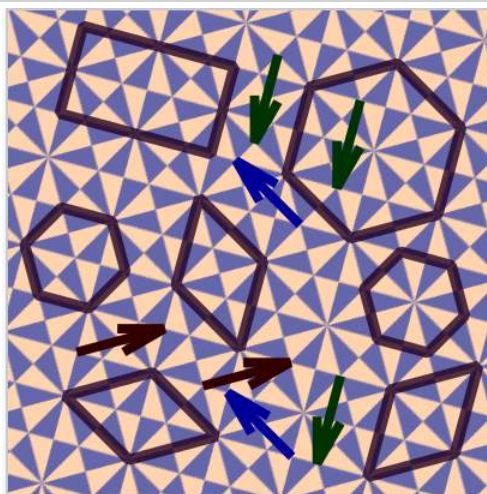
Over 2/3 of the elements in the periodic table exist in their pure form as metals. All elemental metals (except the three - Cs, Ga, Hg - that are liquid) are crystalline solids at room temperature, and most have one of three simple crystal structures.

This page titled [6.1: Prelude to Metals and Alloys](#) is shared under a [CC BY-SA 4.0](#) license and was authored, remixed, and/or curated by [Chemistry 310 \(Wikibook\)](#) via [source content](#) that was edited to the style and standards of the LibreTexts platform; a detailed edit history is available upon request.

6.2: Unit Cells and Crystal Structures


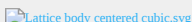


Crystals can be thought of as repeating patterns, much like wallpaper or bathroom tiles, but in three dimensions. The fundamental repeating unit of the crystal is called the **unit cell**. It is a three dimensional shape that can be repeated over and over by unit translations to fill space (and leave minimal gaps) in the structure. Some possible unit cells are shown in the tiling pattern at the right, along with arrows that indicate **unit translation vectors**. In three dimensions, the hexagonal or rhombic unit cells of this pattern would be replaced by three dimensional boxes that would stack together to fill all space. As shown in the figure, the origin of the unit cell is arbitrary. The same set of boxes will fill all space no matter where we define the origin of the lattice. We will see that pure metals typically have very simple crystal structures with cubic or hexagonal unit cells. However the crystal structures of alloys can be quite complicated.

When considering the crystal structures of metals and alloys, it is not sufficient to think of each atom and its neighboring ligands as an isolated system. Instead, think of the entire metallic crystal as a network of atoms connected by a sea of shared valence electrons. The **electrons are delocalized** because there are **not enough of them** to fill each "bond" between atoms with an electron pair. For example, in the crystal structures of s-block and p-block metals, each atom has either 8 or 12 nearest neighbors, but the maximum number of s + p electrons is 8. Thus, there are not enough to put two electrons between each pair of atoms. Transition metals can also use their d-orbitals in bonding, but again there are never enough electrons to completely fill all the "bonds."



Possible unit cells in a periodic tile pattern. The arrows connect translationally equivalent points (lattice points) in the pattern.

The atoms in a metal lattice arrange themselves in a certain pattern which can be represented as a 3D box structure known as the **unit cell** which repeats across the entire metal.

Simple Cubic	Body Centered Cubic	Face Centered Cubic	Hexagonal Close Packed
			
1 atom/cell	2 atoms/cell	4 atoms/cell	2 atoms/cell

Metal atoms can be approximated as spheres, and therefore are not 100 % efficient in packing, the same way a stack of cannonballs has some empty spaces between the balls. Different unit cells have different packing efficiencies. The number of atoms that is included in the unit cell only includes the fractions of atoms *inside* of the box. Atoms on the corners of the unit cell count as $\frac{1}{8}$ of an atom, atoms on a face count as $\frac{1}{2}$, an atom in the center counts as a full atom. Using this, let's calculate the number of atoms in a simple cubic unit cell, a face centered cubic (fcc) unit cell, and a body centered cubic (bcc) unit cell.

Simple Cubic:

8 corner atoms $\times \frac{1}{8} = 1$ atom/cell. The packing in this structure is not efficient (52%) and so this structure type is very rare for metals.

Body Centered Cubic, bcc:

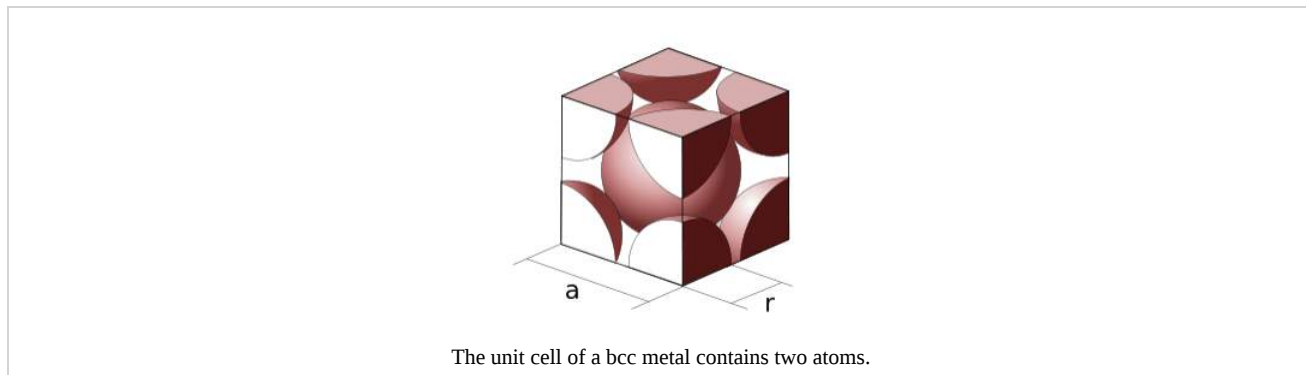
$(8 \text{ corner atoms} \times \frac{1}{8}) + (1 \text{ center atom} \times 1) = 2 \text{ atoms/cell}$. The packing is more efficient (68%) and the structure is a common one for alkali metals and early transition metals. Alloys such as brass (CuZn) also adopt these structures.

Face Centered Cubic, fcc (also called Cubic Close Packed, ccp):

$(8 \text{ corner atoms} \times \frac{1}{8}) + (6 \text{ face atoms} \times \frac{1}{2}) = 4 \text{ atoms/cell}$. This structure, along with its hexagonal relative (hcp), has the most efficient packing (74%). Many metals adopt either the fcc or hcp structure.

Hexagonal Close Packed, hcp:

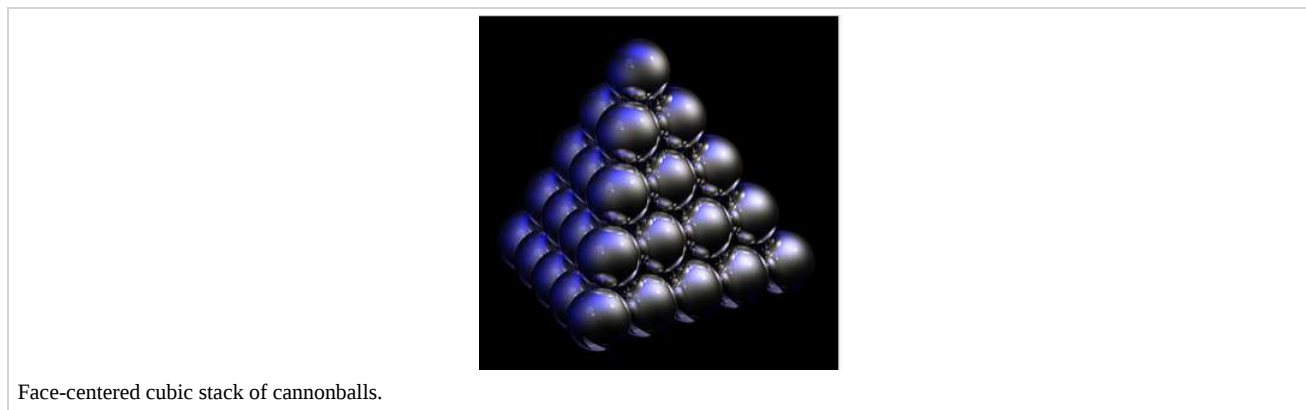
Like the fcc structure, the packing density of hcp is 74%.



Calculating the packing fraction. The packing fractions of the crystal structures shown above can be calculated by dividing the volume of the atoms in the cell by the volume of the cell itself. The volume of the atoms in the cell is equal to the number of atoms/cell times the volume of a sphere, $(\frac{4}{3})\pi r^3$. The volume of the cubic cells is found by cubing the side length. As an example, let's calculate the packing efficiency of a simple cubic unit cell. As we saw earlier in the section, a simple cubic unit cell contains one atom. The side length of the simple cubic unit cell is $2r$, since the centers of each atom occupy the corners of the unit cell.

$$\text{Packing efficiency} = \frac{(1 \text{ atom}) \times (\frac{4}{3})\pi r^3}{(2r)^3} = 0.523 \quad (6.2.1)$$

The same method can be applied to bcc and fcc structures.



This page titled [6.2: Unit Cells and Crystal Structures](#) is shared under a [CC BY-SA 4.0](#) license and was authored, remixed, and/or curated by [Chemistry 310 \(Wikibook\)](#) via [source content](#) that was edited to the style and standards of the LibreTexts platform; a detailed edit history is available upon request.

6.3: Bravais Lattices

Crystal lattices can be classified by their **translational** and **rotational symmetry**. In three-dimensional crystals, these symmetry operations yield 14 distinct lattice types which are called **Bravais lattices**. In these lattice diagrams (shown below) the dots represent lattice points, which are places where the whole structure repeats by translation. For example, in the body-centered cubic (**bcc**) structure of sodium metal, which is discussed below, we put one atom at the corner lattice points and another in the center of the unit cell. In the NaCl structure, which is discussed in Chapter 8, we place one NaCl formula unit on each lattice point in the face-centered cubic (**fcc**) lattice. That is, one atom (Na or Cl) would be placed on the lattice point and the other one would be placed halfway between. Similarly, in the cubic diamond structure, we place one C_2 unit around each lattice point in the fcc lattice.

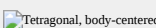
The fourteen Bravais lattices fall into seven **crystal systems** that are defined by their rotational symmetry. In the lowest symmetry system (**triclinic**), there is no rotational symmetry. This results in a unit cell in which none of the edges are constrained to have equal lengths, and none of the angles are 90° . In the **monoclinic** system, there is one two-fold rotation axis (by convention, the b-axis), which constrains two of the angles to be 90° . In the **orthorhombic** system, there are three mutually perpendicular two-fold axes along the three unit cell directions. **Orthorhombic** unit cells have three unequal unit cell edges that are mutually perpendicular. **Tetragonal** unit cells have a four-fold rotation axis which constrains all the angles to be 90° and makes the a and b axes equivalent. The **rhombohedral** system has a three-fold axis, which constrains all the unit cell edges and angles to be equal, and the **hexagonal** system has a six-fold axis, which constrains the a and b lattice dimensions to be equal and the angle between them to be 120° . The **cubic** system has a three-fold axis along the body diagonal of the cube, as well as two-fold axes along the three perpendicular unit cell directions. In the cubic system, all unit cell edges are equal and the angles between them are 90° .

The translational symmetry of the Bravais lattices (the lattice **centerings**) are classified as follows:

- Primitive (P): lattice points on the cell corners only (sometimes called simple)
- Body-Centered (I): lattice points on the cell corners with one additional point at the center of the cell
- Face-Centered (F): lattice points on the cell corners with one additional point at the center of each of the faces of the cell
- Base-Centered (A, B, or C): lattice points on the cell corners with one additional point at the center of each face of one pair of parallel faces of the cell (sometimes called end-centered)

Not all combinations of the crystal systems and lattice centerings are unique. There are in total $7 \times 6 = 42$ combinations, but it can be shown that several of these are in fact equivalent to each other. For example, the monoclinic I lattice can be described by a monoclinic C lattice by different choice of crystal axes. Similarly, all A- or B-centred lattices can be described either by a C- or P-centering. This reduces the number of combinations to 14 conventional Bravais lattices, shown in the table below.

When the fourteen Bravais lattices are combined with the **32 crystallographic point groups**, we obtain the **230 space groups**. These space groups describe all the combinations of symmetry operations that can exist in unit cells in three dimensions. For two-dimensional lattices there are only 17 possible plane groups, which are also known as wallpaper groups.

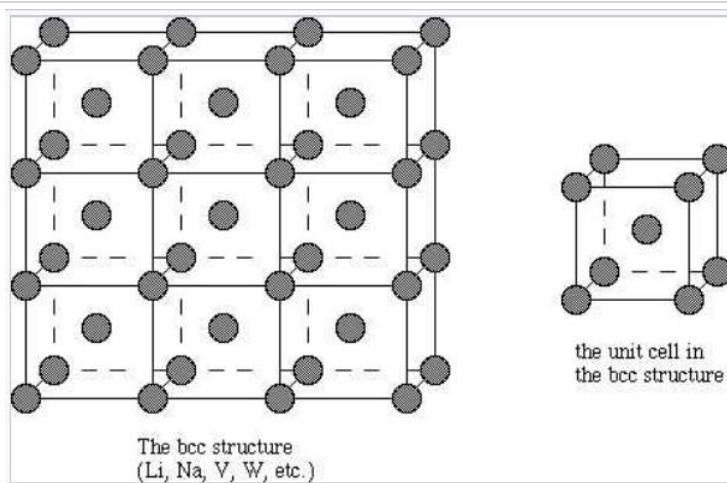
Crystal family	Lattice system	Schönflies	14 Bravais Lattices			
			Primitive	Base-centered	Body-centered	Face-centered
Triclinic		C_i				
Monoclinic		C_{2h}				
Orthorhombic		D_{2h}				
Tetragonal		D_{4h}				
Hexagonal	rhombohedral	D_{3d}				
	hexagonal	D_{6h}				
Cubic		O_h				

This page titled [6.3: Bravais Lattices](#) is shared under a [CC BY-SA 4.0](#) license and was authored, remixed, and/or curated by [Chemistry 310 \(Wikibook\)](#) via [source content](#) that was edited to the style and standards of the LibreTexts platform; a detailed edit history is available upon request.

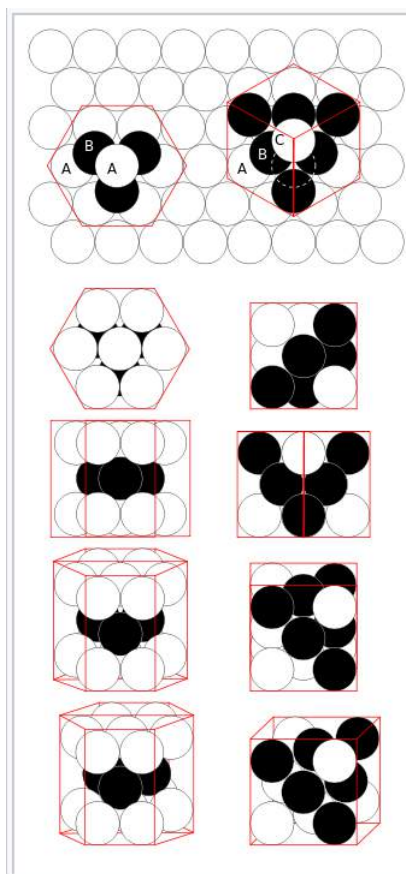
6.4: Crystal Structures of Metals

The Crystalline Nature of Metals

All metallic elements (except Cs, Ga, and Hg) are crystalline solids at room temperature. Like ionic solids, metals and alloys have a very strong tendency to crystallize, whether they are made by thermal processing or by other techniques such as solution reduction or electroplating. Metals crystallize readily and it is difficult to form a glassy metal even with very rapid cooling. Molten metals have low viscosity, and the identical (essentially spherical) atoms can pack into a crystal very easily. Glassy metals can be made, however, by rapidly cooling alloys, particularly if the constituent atoms have different sizes. The different atoms cannot pack in a simple unit cell, sometimes making crystallization slow enough to form a glass.



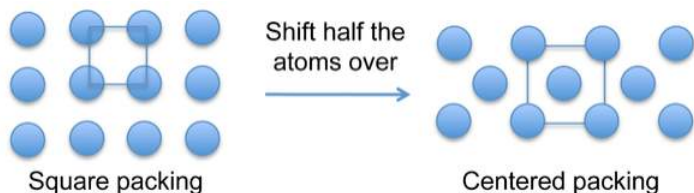
Body-centered cubic



hcp (left) and fcc (right) close-packing of spheres

Crystal structures

Most metals and alloys crystallize in one of three very common structures: body-centered cubic (bcc), hexagonal close packed (hcp), or cubic close packed (ccp, also called face centered cubic, fcc). In all three structures the coordination number of the metal atoms (i.e., the number of equidistant nearest neighbors) is rather high: 8 for bcc, and 12 for hcp and ccp. We can contrast this with the low coordination numbers (i.e., low valences - like 2 for O, 3 for N, or 4 for C) found in nonmetals. In the bcc structure, the nearest neighbors are at the corners of a cube surrounding the metal atom in the center. In the hcp and ccp structures, the atoms pack like stacked cannonballs or billiard balls, in layers with a six-coordinate arrangement. Each atom also has six more nearest neighbors from layers above and below. The stacking sequence is ABCABC... in the ccp lattice and ABAB... in hcp. In both cases, it can be shown that the spheres fill 74% of the volume of the lattice. This is the highest volume fraction that can be filled with a lattice of equal spheres.



Atoms in metallic crystals have a tendency to pack in dense arrangements that fill space efficiently. The simple square packing (above) upon which the simple cubic structure is based is inefficient and thus rare among metallic crystal structures. Body- or face-centered structures fill space more efficiently and more common.

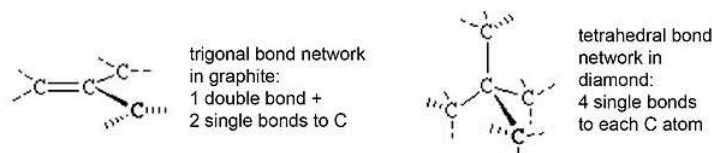
Periodic trends in structure and metallic behavior

Remember where we find the metallic elements in the periodic table - everywhere except the upper right corner. This means that as we go down a group in the p-block (let's say, group IVA, the carbon group, or group VA, the nitrogen group), the properties of the elements gradually change from nonmetals to metalloids to metals. The carbon group nicely illustrates the transition. Starting at the top, the element carbon has two stable allotropes - graphite and diamond. In each one, the valence of carbon atoms is exactly satisfied by making four electron pair bonds to neighboring atoms. In graphite, each carbon has three nearest neighbors, and so there are two single bonds and one double bond. In diamond, there are four nearest neighbors situated at the vertices of a tetrahedron, and so there is a single bond to each one.

The two elements right under carbon (silicon and germanium) in the periodic table also have the diamond structure (recall that these elements cannot make double bonds to themselves easily, so there is no graphite allotrope for Si or Ge). While diamond is a good insulator, both silicon and germanium are semiconductors (i.e., metalloids). Mechanically, they are hard like diamond. Like carbon, each atom of Si and Ge satisfies its valence of four by making single bonds to four nearest neighbors.

The next element under germanium is tin (Sn). Tin has two allotropes, one with the diamond structure, and one with a slightly distorted bcc structure. The latter has metallic properties (metallic luster, malleability), and conductivity about 10^9 times higher than Si. Finally, lead (Pb), the element under Sn, has the ccp structure, and also is metallic. Note the trends in coordination number and conducting properties:

Element	Structure	Coord. no.	Conductivity
C	graphite, diamond	3, 4	semimetal, insulator
Si	diamond	4	semiconductor
Ge	diamond	4	semiconductor
Sn	diamond, distorted bcc	4, 8	semiconductor, metal
Pb	ccp	12	metal

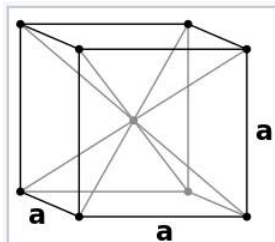


The elements C, Si, and Ge obey the octet rule, and we can easily identify the electron pair bonds in their structures. Sn and Pb, on the other hand, adopt structures with high coordination numbers. They *do not have enough valence electrons* to make electron pair bonds to each neighbor (this is a common feature of metals). What happens in this case is that the valence electrons become "smeared out" or delocalized over all the atoms in the crystal. It is best to think of the bonding in metals as a crystalline arrangement of positively charged cores with a "sea" of shared valence electrons gluing the structure together. Because the electrons are not localized in any particular bond between atoms, they can move in an electric field, which is why metals conduct electricity well. Another way to describe the bonding in metals is nondirectional. That is, an atom's nearest neighbors surround it in every direction, rather than in a few particular directions (like at the corners of a tetrahedron, as we found for diamond). Nonmetals (insulators and semiconductors), on the other hand, have directional bonding. Because the bonding is non-directional and coordination numbers are high, it is relatively easy to deform the coordination sphere (i.e., break or stretch bonds) than it is in the case of a nonmetal. This is why elements like Pb are much more malleable than C, Si, or Ge.

This page titled [6.4: Crystal Structures of Metals](#) is shared under a [CC BY-SA 4.0](#) license and was authored, remixed, and/or curated by [Chemistry 310 \(Wikibook\)](#) via [source content](#) that was edited to the style and standards of the LibreTexts platform; a detailed edit history is available upon request.

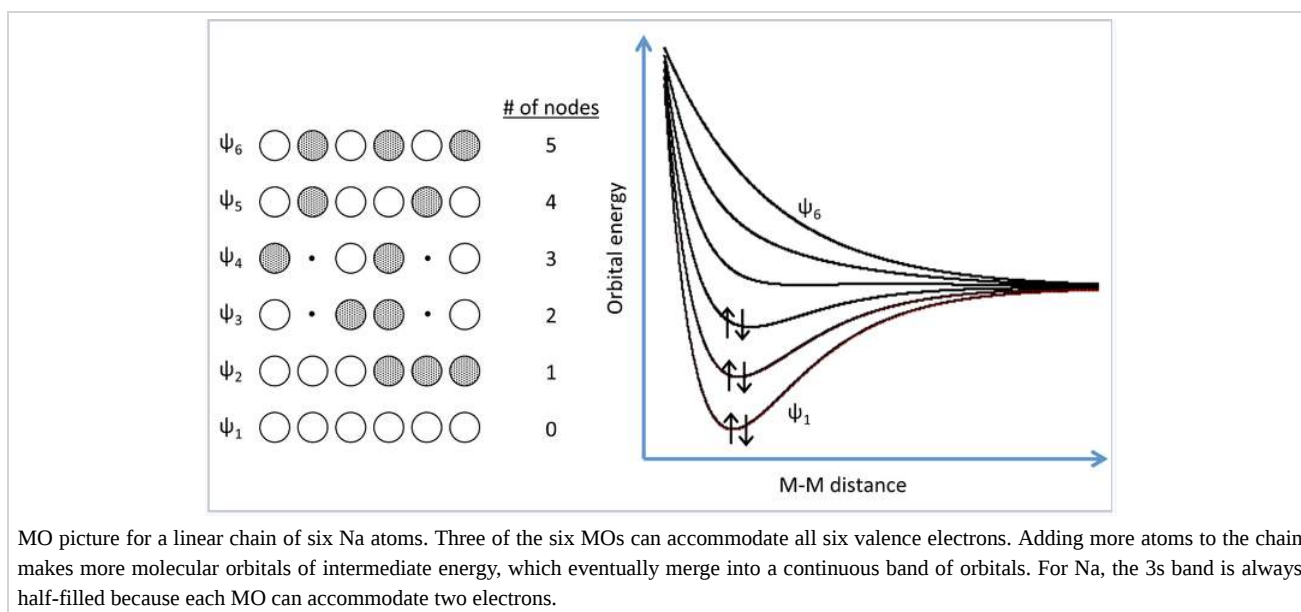
6.5: Bonding in Metals

The electron pair description of chemical bonds, which was the basis of the octet rule for p-block compounds, breaks down for metals. This is illustrated well by Na metal, the structure of which is shown at the left. Na has too few valence electrons to make electron pair bonds between each pair of atoms. We could think of the Na unit cell as having eight no-bond resonance structures in which only one Na-Na bond per cell contains a pair of electrons. This means that the Na-Na bond order is 1/8 in Na metal.

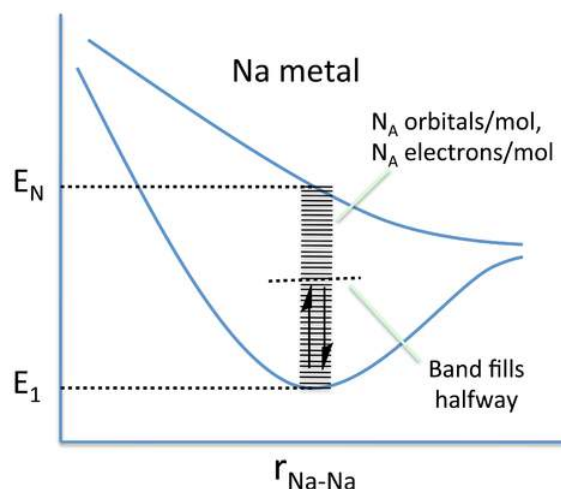


Sodium metal crystallizes in the body-centered cubic structure, in which each atom has eight nearest neighbors. Since the electronic configuration of Na is $[\text{Ar}]3s^1$, there are only two valence electrons per unit cell that are shared among eight Na-Na bonds. This means that the Na-Na bond order is 1/8 in Na metal.

A more realistic way to describe the bonding in metals is through **band theory**. The evolution of energy bands in solids from simple MO theory (Chapter 2) is illustrated at the right for a chain of six Na atoms, each of which has one 3s valence orbital and contributes one valence electron. In general, n atomic orbitals (in this case the six Na 3s orbitals) will generate n molecular orbitals with $n-1$ possible nodes. In Chapter 2, we showed that the energy versus internuclear distance graph for a two hydrogen atom system has a low energy level and a high energy level corresponding to the bonding and antibonding molecular orbitals, respectively. These two energy levels were well separated from each other, and the two electrons in H_2 energetically prefer the lower energy level. If more atoms are introduced to the system, there will be a number of additional levels between the lowest and highest energy levels.



In band theory, the atom chain is extrapolated to a very large number - on the order of 10^{22} atoms in a crystal - so that the different combinations of bonding and anti-bonding orbitals create "bands" of possible energy states for the metal. In the language of physics, this approach of building the bands from discrete atomic orbitals is called the "tight-binding" approximation. The number of atoms is so large that the energies can be thought of as a continuum rather than a series of distinct levels. A metal will only partially fill this band, as there are fewer valence electrons than there are energy states to fill. In the case of Na metal, this results in a half-filled 3s band.



Nearly free electron model

In metals, the valence electrons are delocalized over many atoms. The total energy of each electron is given by the sum of its kinetic and potential energy:

$$E = KE + PE$$

$$E \approx p^2/2m + V$$

where \mathbf{p} is the momentum of the electron (a vector quantity), m is its mass, and V is an average potential that the electron feels from the positive cores of the atoms. This potential holds the valence electrons in the crystal but, in the free electron model, is essentially uniform across the crystal.

Electron wavelength and wavenumber

What are the consequences of this model for band theory? For a hypothetical infinite chain (i.e., a 1D crystal) of Na atoms, the molecular orbitals at the bottom of the 3s band are fully bonding and the *wavelength* of electrons (2x the distance between nodes) in these orbitals is very long. At the top of the band, the highest orbital is fully antibonding and the wavelength is 2 times the distance between atoms ($2a$), since there is one node per atom. Remember that the **wavelength of an electron (λ)** is inversely proportional to its momentum p , according to the de Broglie relation $\lambda = h/p$.

For a (nearly) free electron, the kinetic energy can be expressed in terms of its wavelength, using $KE = p^2/2m$ and the de Broglie relation:

$$KE = \frac{p^2}{2m} = \frac{h^2}{2m\lambda^2} \quad (6.5.1)$$

We can think of the wavelength of an electron in a molecular orbital as twice the distance between nodes. If there are N atoms in a linear chain, the wavelength of the n th orbital is given by $\lambda = 2Na/n$, where a is the distance between atoms.

At this point, it is convenient to define the **wavenumber** of the electron as \mathbf{k} , which has units of inverse length and is inversely proportional to λ . \mathbf{k} is also directly proportional to the momentum \mathbf{p} . Like \mathbf{p} , \mathbf{k} is a vector quantity. In a 1D crystal, \mathbf{k} can be either positive or negative, corresponding to an electron moving to the left or right along the chain.

$$k = \frac{2\pi}{\lambda} = \frac{2\pi p}{h} \quad \text{where } h \text{ is Planck's constant} \quad (6.5.2)$$

The most important property of \mathbf{k} is that it is *directly proportional to the number of nodes \mathbf{n}* in a molecular orbital within the band. For a 1D crystal of sodium atoms that contains \mathbf{N} unit cells, each separated by a distance \underline{a} , a molecular orbital with n nodes has a wavelength $\lambda = 2Na/n$ and the wavenumber $k = \pi n/Na$. We can see from this definition that $k = 0$ at the bottom of the band (where λ is infinite) and $k = \pi/a$ at the top of the band where the MO contains \mathbf{N} nodes and $\lambda = 2a$.

Energies of orbitals in a metallic crystal

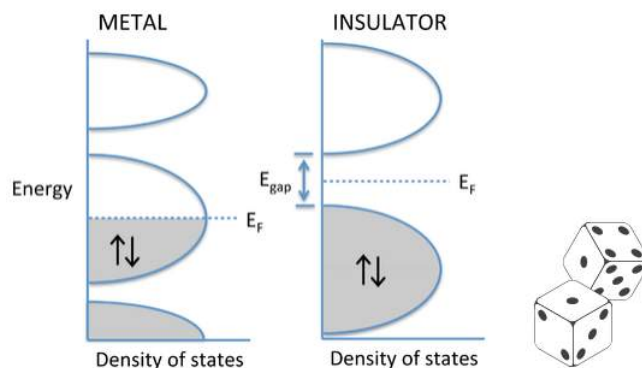
Electrons with long wavelengths do not "feel" the individual atoms in the lattice and so they behave as if they are *nearly free* (but confined to the crystal). Near the bottom of the band, the electron energy increases *parabolically* with the number of nodes ($KE \propto \mathbf{n}^2$), since the momentum \mathbf{p} is directly proportional to \mathbf{n} . Because \mathbf{p} is also directly proportional to \mathbf{k} , we can write:

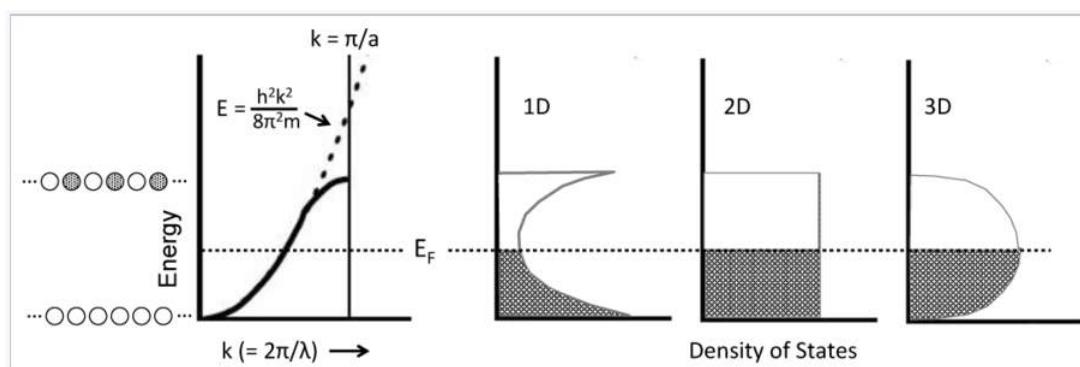
$$KE = \frac{p^2}{2m} = \frac{h^2 k^2}{8\pi^2 m} \quad (6.5.3)$$

This parabolic relationship is followed as long as the electron wavelength is long compared to the distance between atoms. Near the top of the band, the wavelength becomes shorter and the electrons start to feel the positively charged atomic cores. In particular, the electrons prefer to have the maxima in their wavefunctions line up with the atomic cores, which is the most electrostatically favorable situation. The electron-atom attraction lowers the energy and causes the E vs. k curve to deviate from the parabolic behavior of a "free" electron as shown in the figure below.

Density of States (DOS)

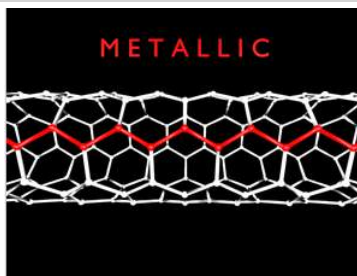
The density of states is defined as the number of orbitals per unit of energy within a band. Because of the parabolic relation between E and k , the density of states for a 1D metallic crystal is highest near the bottom and top of the energy band where the slope of the E vs. k curve is closest to zero. The shape of the DOS curve is different in crystals of higher dimensionality as shown in the figure in the left, because statistically there are more ways to make an orbital with $N/2$ nodes than there are with zero or N nodes. The situation is analogous to the numbers you can make by rolling dice. With one die, the numbers 1-6 have equal probability. However, with two dice there is only one way to make a two (snake eyes) or a twelve (boxcars), but many ways to make a seven (a winner!).





Electrons in metals follow a parabolic dispersion curve, where the energy increases with the square of the wavenumber, k . Near the top of the band, the dispersion curve deviates from the parabolic dotted line. Because there is one MO for each value of k , the number of orbitals per unit energy (the density of states, DOS) is highest at the bottom and top of the band for a 1D chain of atoms. The density of states is constant with energy for a 2D crystal, and has a maximum in the middle of the band for a 3D crystal. At low temperature, all the MOs below the Fermi level E_F are occupied, and all the MOs above it are empty.

While most of the time we will talk about 3D crystals that have their maximum DOS near the middle of the energy band, there are examples of quasi-1D systems, such as carbon nanotubes. Metallic carbon nanotubes have strong optical absorption bands that correspond to transitions between the two regions of high DOS (the van Hove singularities) near the bottom and top of the bands.



Single-walled carbon nanotubes with "armchair" chirality are metallic and have characteristic sharp absorption bands in the infrared. Prof. Millie Dresselhaus (below) did foundational research on the electronic properties of carbon nanotubes and other low-dimensional conductors.

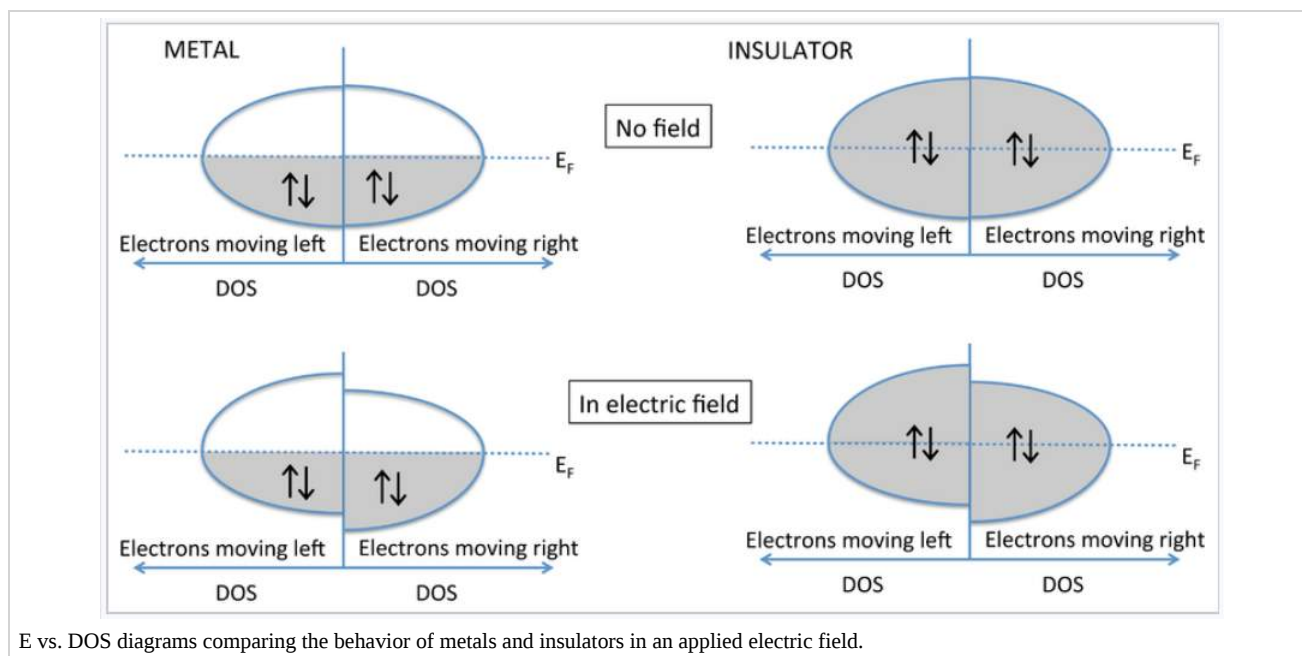


Metals, semiconductors, and insulators

The degree to which bands fill determines whether a crystalline solid is a metal, semiconductor, or insulator. If the highest occupied molecular orbitals lie within a band - i.e., if the Fermi level E_F cuts through a band of orbitals - then the electrons are free to change their speed and direction in an electric field and the solid is metallic. However, if the solid contains just enough electrons to completely fill a band, and the next highest set of molecular orbitals is empty, then it is a semiconductor or insulator. In this case, there is an energy gap between the filled and empty bands, which are called the valence and conduction bands, respectively. Although the distinction is somewhat arbitrary, materials with a large gap (> 3 eV) are called insulators, and those with smaller gaps are called semiconductors. We will learn more about the properties of semiconductors in Chapter 10.

Why don't insulators conduct electricity? The energy vs. DOS diagram below shows what happens when an electric field is applied to a metal or an insulator. In this case we have changed the diagram to show explicitly the energies of electrons moving left and right. These energies are the same in the absence of an electric field. Once we apply a field (e.g., by putting a voltage across a metal wire), the electrons moving in the direction of the field have lower energy than those moving in the opposite direction. In the case of the metal, the populations of electrons moving with and against the electric field are different, and there is a net flow of current.

Note that this can happen only when the Fermi level cuts through a partially filled band. With a semiconductor or insulator, the valence band is filled and the conduction band is empty. Applying an electric field changes the energies of electrons traveling with and against the field, but because the band is filled, the same number are going in both directions and there is no net current flow.



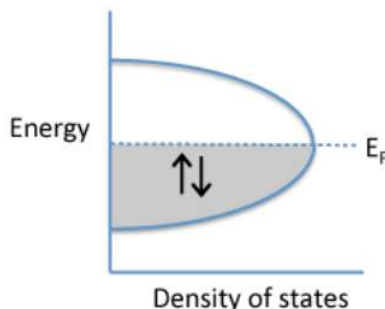
E vs. DOS diagrams comparing the behavior of metals and insulators in an applied electric field.

Note that in this picture, all the molecular orbitals extend over the entire crystal. The valence electrons are *delocalized*, even in the case of a semiconductor or insulator. However, there can be no net movement of electrons unless the band is partially filled.

This page titled [6.5: Bonding in Metals](#) is shared under a [CC BY-SA 4.0](#) license and was authored, remixed, and/or curated by [Chemistry 310 \(Wikibook\)](#) via [source content](#) that was edited to the style and standards of the LibreTexts platform; a detailed edit history is available upon request.

6.6: Conduction in Metals

In metals, the valence electrons are in molecular orbitals that extend over the entire crystal lattice. As we will learn in Chapter 7, metals are almost always crystalline and the individual crystal grains are typically micron size. This means that the spatial extent of the orbitals is *very large* compared to the size of the atoms or the unit cell. The diagram at the left shows a generic plot of electron energy vs. density of states for a metal such as Na, Cu, or Ag. In these cases, there are N orbitals for N electrons, and each orbital can accommodate two electrons. Therefore the Fermi level, which corresponds to the energy of the highest occupied MO at zero temperature, is somewhere in the middle of the band of orbitals. The energy level spacing between orbitals is very small compared to the thermal energy kT , so we can think of the orbitals as forming a continuous band.



Classically, if the electrons in this band were free to be thermally excited, we would expect them to have a specific heat of $3R$ per mole of electrons. However, experimentally we observe that C_p is only about $0.02 R$ per mole. This suggests that *only about 1%* of the electrons in the metal can be thermally excited at room temperature. However, essentially *all* of the valence electrons are free to move in the crystal and contribute to electrical conduction. To understand this apparent paradox, we need to recall that the electrons exist in *quantized energy levels*.

Because of quantization, electrons in metals have a Fermi-Dirac distribution of energies. In this distribution, most of the electrons are spin-paired, although the individual electrons in these pairs can be quite far apart since the orbitals extend over the entire crystal. A relatively small number of electrons at the top of the Fermi sea are unpaired by thermal excitation. This is the origin of the Pauli paramagnetism of metals.

How fast are electrons traveling in a typical metal? Because of the bell shape of the E vs. DOS curve, most of the electrons have $E \approx E_F$. At the midpoint energy (E_F) of the band, the MO's have one node for every two atoms. We can calculate the de Broglie wavelength as twice the distance between nodes and thus:

$$\lambda = 4a \text{ at the midpoint of the band.}$$

where a is the interatomic spacing. Since a typical value of a is about 2 \AA , we obtain the **de Broglie wavelength** $\lambda \approx 8 \text{ \AA}$.

Using the de Broglie relation $p = h/\lambda$, we can write:

$$\mathbf{p} = \frac{\mathbf{h}}{\lambda} = \mathbf{m}_e \mathbf{v}_F \quad (6.6.1)$$

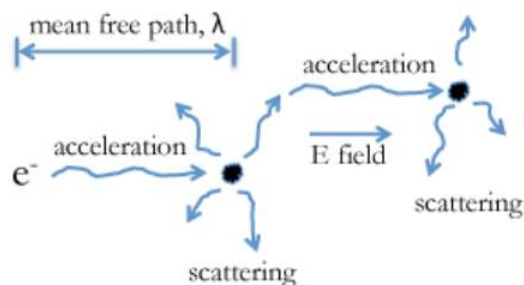
where \mathbf{m}_e is the mass of the electron and \mathbf{v}_F is the velocity of electrons with energy E_F .

$$\text{Solving for } v_F = \frac{h}{m_e \lambda} \text{ we obtain } \mathbf{v}_F = \frac{(6.62 \times 10^{-34} \text{ Js})}{(9.1 \times 10^{-31} \text{ kg})(8 \times 10^{-10} \text{ m})} = \mathbf{1.0} \times \mathbf{10^6} \text{ m/s}$$

Experimental values of v_F are 1.07×10^6 and 1.39×10^6 m/s for Na and Ag, respectively, so our approximations are pretty good.

How fast are electrons moving in metals? Really, really fast!! **1,000,000 meters per second!** This is about $1/300$ the speed of light, and about 3000 times the speed of sound in air (3×10^2 m/s).

However, the **drift velocity** of electrons in metals - the speed at which electrons move in applied electric field - is quite slow, on the order of 0.0001 m/s, or $.01$ cm/s. You can easily outrun an electron drifting in a metal, even if you have been drinking all night and have been personally reduced to a very slow crawl.



In order to understand the great disparity between the Fermi velocity and the drift velocity of electrons in metals, we need to consider a picture for the scattering of electrons, and their acceleration in an electric field, as shown at the left. If we apply a voltage across a metal (e.g., a metal wire), the electrons are subjected to an electric field E , which is the voltage divided by the length of the wire. This electric field exerts a force on the electron, causing it to accelerate. However, the electron is frequently scattered, mostly by phonons (lattice vibrations). Each time the electron is scattered its acceleration starts all over again. The time between scattering events is τ and the distance the electrons travel between scattering events is the **mean free path**, λ . (Note that this is NOT the same λ as the de Broglie wavelength, they just unfortunately have the same symbol!)

We can write the force on the electron as:

$$\mathbf{F} = e\mathbf{E} = m_e \mathbf{a} = \frac{m_e \mathbf{v}_{\text{drift}}}{\tau} \quad (6.6.2)$$

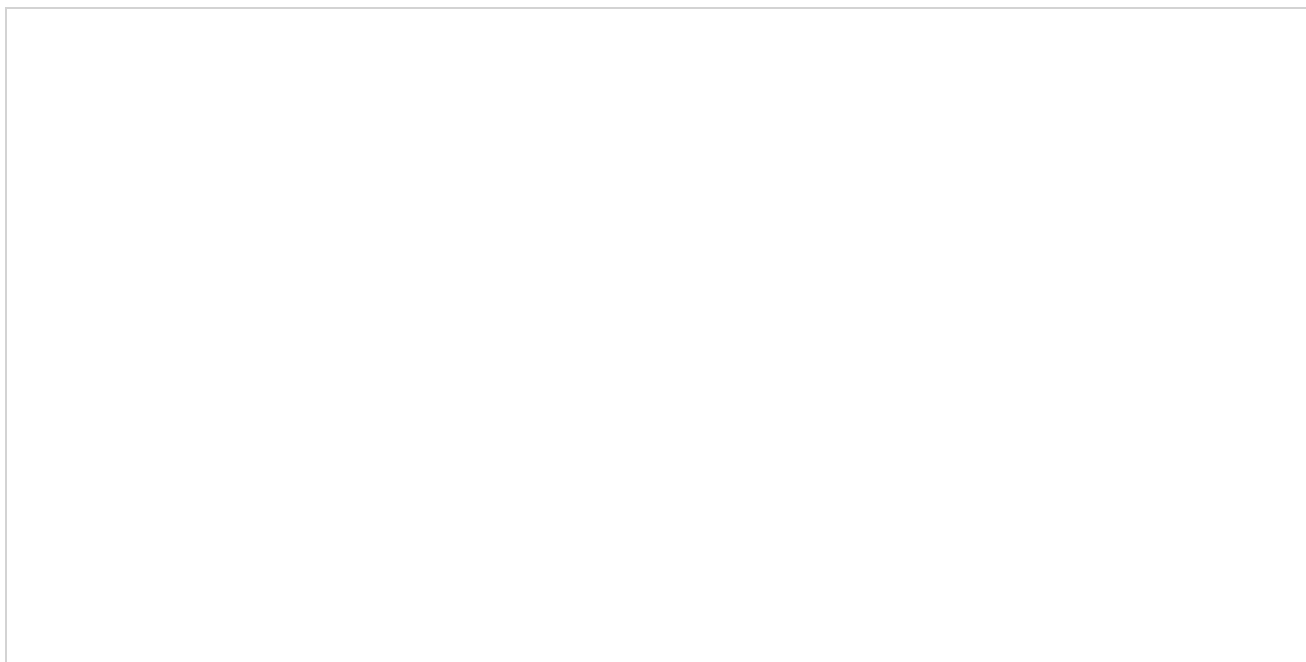
In this equation, \mathbf{a} is the acceleration in the electric field, m_e is the mass, and $\mathbf{v}_{\text{drift}}$ is the **drift velocity** of the electron.

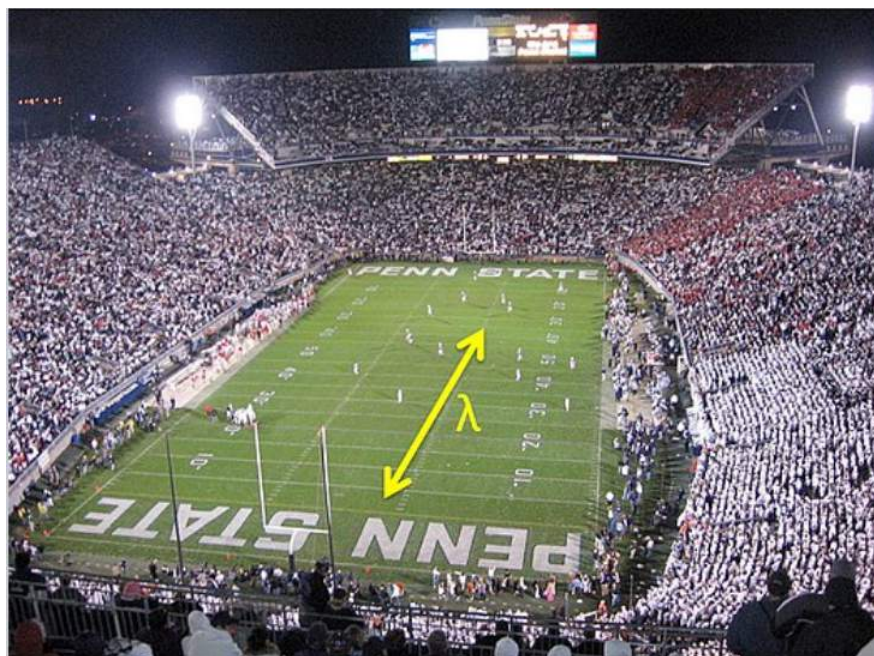
Experimentally, the mean free path is typically obtained by measuring the scattering time. For an electron in Cu metal at 300 K, the scattering time τ is about 2×10^{-14} s. From this we can calculate the mean free path as:

$$\lambda = \mathbf{v}_{\text{avg}} \tau \approx \mathbf{v}_F \tau = (1 \times 10^6 \text{ m/s})(2 \times 10^{-14}) = \mathbf{40 \text{ nm}} \quad (6.6.3)$$

The mean free path (40 nm = 400 Å) is quite long compared to the interatomic spacing (2 Å). To put it in perspective, if the interatomic spacing were scaled to the length of a football (0.3 m), the mean free path would be over half the length of the football field (60 m). Thus an electron travels a fairly long way between scattering events and scarcely notices the atomic structure of the metal in which it is traveling.

To summarize, electrons are traveling in metals at the Fermi velocity v_F , which is very, very fast (10^6 m/s), but the flux of electrons is the same in all directions. That is, they are *going nowhere fast*. In an electric field, a very small but directional *drift velocity* is superimposed on this fast random motion of valence electrons.





For ordinary metals, the mean free path of a valence electron (λ) is quite long relative to the interatomic spacing, represented in this analogy as the length of a football.

We can calculate the drift velocity of electrons as the acceleration in the electric field times the scattering time:

From $F = ma$, we obtain the acceleration (a) as:

$$\mathbf{a} = \frac{\mathbf{F}}{m_e} = \frac{e\mathbf{E}}{m_e} \quad (6.6.4)$$

And thus,

$$\mathbf{v}_{\text{drift}} = \mathbf{a}\tau = \frac{e\mathbf{E}\tau}{m_e} \quad (6.6.5)$$

If we divide both sides of this equation by the magnitude of the electric field (\mathbf{E}), we obtain the **mobility** (μ):

$$\mu = \frac{\mathbf{v}_{\text{drift}}}{\mathbf{E}} = \frac{e\tau}{m_e} \quad (6.6.6)$$

μ has units of velocity/field = $\text{cm/s} / \text{V/cm} = \text{cm}^2/\text{Vs}$

An important consequence of the calculation of $\mathbf{v}_{\text{drift}}$ is **Ohm's Law**, $V = iR$. From the equations above, we can see that the drift velocity increases linearly with the applied electric field. The drift velocity (cm/s) is proportional to the current (i , coul/s), and the electric field (\mathbf{E} , V/cm) is proportional to the voltage (V):

$$\mathbf{Current (i)} = n\mathbf{e}\mathbf{v}_{\text{drift}} \times \mathbf{area} \quad (6.6.7)$$

$$\mathbf{Voltage (V)} = \mathbf{E} \times \mathbf{length} \quad (6.6.8)$$

Here n is the density of valence electrons ($\#/\text{cm}^3$) and e is the charge of the electron (coul). Combining these equations with our equation for $\mathbf{v}_{\text{drift}}$ we obtain:

$$V = i \left(\frac{m_e}{ne^2\tau} \right) \frac{(\text{area})}{\text{length}} = iR \quad (6.6.9)$$

Thus, $V = iR$, where R is the combination of the two terms in parentheses. The first of these is the **resistivity**, ρ , and the second is a geometrical factor.

The **conductivity** (σ) of a metal, which is the inverse of ρ , is proportional to μ , which in turn is proportional to τ (and λ):

$$\sigma = \mathbf{n}e\mu = \frac{\mathbf{n}e^2\tau}{\mathbf{m}_e} \quad (6.6.10)$$

We can use this equation to work out the conductivity of a specific metal (Cu), for which $n = 8.5 \times 10^{22} \text{ cm}^{-3}$ and $\tau = 2 \times 10^{-14} \text{ s}$. Putting in the numbers for m_e and e , we obtain $\sigma = 7 \times 10^5 \text{ } \Omega^{-1} \text{ cm}^{-1}$ for Cu, in good agreement with the measured value ($6 \times 10^5 \text{ } \Omega^{-1} \text{ cm}^{-1}$).

This page titled [6.6: Conduction in Metals](#) is shared under a [CC BY-SA 4.0](#) license and was authored, remixed, and/or curated by [Chemistry 310 \(Wikibook\)](#) via [source content](#) that was edited to the style and standards of the LibreTexts platform; a detailed edit history is available upon request.

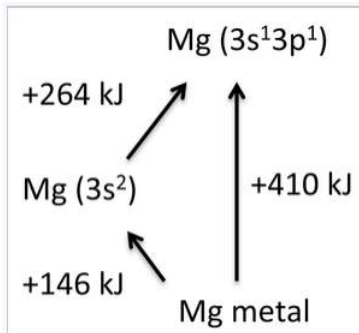
6.7: Atomic Orbitals and Magnetism

The MO picture we developed in Section 6.4 helps us rationalize the electrical conductivity of Na ($3s^1$), but what about Mg, which (as an atom in the gas phase) has a $3s^2$ electronic configuration? The two valence electrons are spin-paired in atomic Mg, as they are in the helium atom ($1s^2$). When the 3s orbitals of Mg combine to form a band, we would expect the band to be completely filled, since Mg has two electrons per orbital. By this reasoning, solid Mg should be an insulator. But Mg has all the properties of a metal: high electrical and thermal conductivity, metallic luster, malleability, etc. In this case the 3s and 3p bands are sufficiently broad (because of strong orbital overlap between Mg atoms) that they form a continuous band. This band, which contains a total of four orbitals (one 3s and three 3p) per atom, is only partially filled by the two valence electrons.



Mg crystals

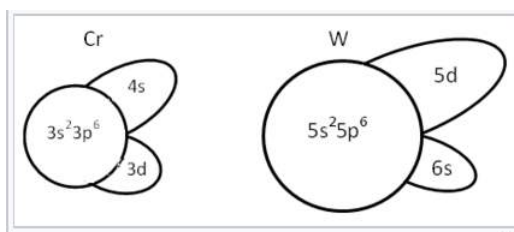
Another way to think about this is to consider the **hybridization** of the 3s and 3p electrons in Mg. Hybridization requires promotion from the $3s^2 3p^0$ ground state of an Mg atom to a $3s^1 3p^1$ excited state. The **promotion energy** (+264 kJ/mol) is more than offset by the **bonding energy** (-410 kJ/mol), the energy released when gaseous atoms in the excited state condense to form the metallic solid. The heat of vaporization, or the cohesive energy of a metal, is the difference between the bonding energy and the promotion energy. Experimentally, we can measure the vaporization energy (+146 kJ/mol) and the promotion energy and use them to calculate the bonding energy. From this we learn that each s or p electron is worth about 200 kJ/mol in bonding energy. The concepts of promotion energy and bonding energy are very useful in rationalizing periodic trends in the bond strengths and magnetic properties of metals, which are described below.



The cohesive energy of Mg metal is the difference between the bonding and promotion energies. The ground state of a gas phase Mg atom is $[\text{Ar}]3s^2$, but it can be promoted to the $[\text{Ar}]3s^1 3p^1$ state, which is 264 kJ/mol above the ground state. Mg uses two electrons per atom to make bonds, and the sublimation energy of the metal is 146 kJ/mol.

Periodic trends in d-electron bonding

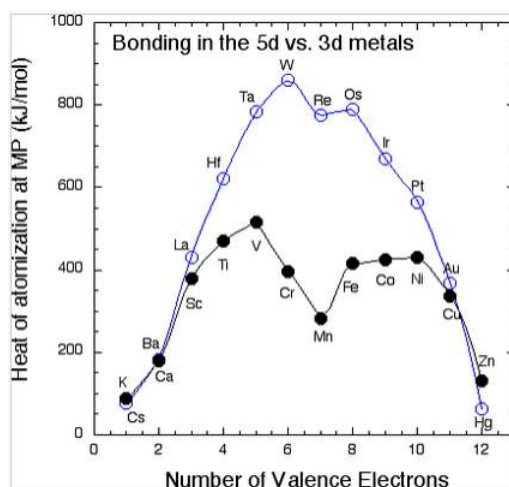
While electrons in s and p orbitals tend to form strong bonds, d-electron bonds can be strong or weak. There are two important periodic trends that are related to orbital size and orbital overlap. As we move *across the periodic table* (Sc - Ti - V - Cr - Fe), the *d orbitals contract* because of increasing nuclear charge. Moving *down the periodic table* (V - Nb - Ta), the *d orbitals expand* because of the increase in principal quantum number. These trends explain the distinct behavior of the 3d elements relative to those in the 4d and 5d series. In the 3d series, the contraction of orbitals affects the ability of the d electrons to contribute to bonding. Past V in the first row of the transition metals, the 3d electrons become much less effective in bonding because they overlap weakly with their neighbors. Weak overlap of 3d orbitals gives narrow d-bands and results in the emergence of magnetic properties as discussed below.



Schematic representation of the sizes of different orbitals of Cr and W. In the first transition series, shielding of the 3d orbitals is poor. Therefore the 4s and 4p orbitals are more effective in bonding than the 3d. In the third transition series, the situation is reversed. The increased nuclear charge is felt most strongly by the 6s, which takes on the character of an inert electron pair. The 5d orbitals are well shielded by the complete $n=4$ shell so they have good orbital overlap with neighboring atoms.

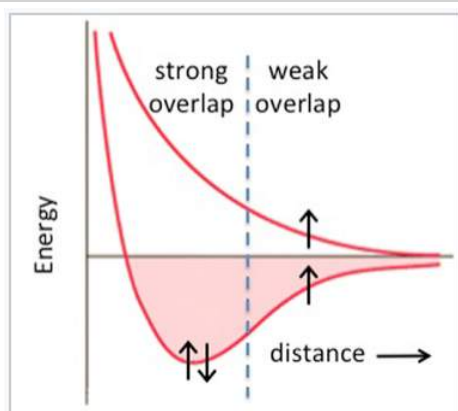
Group →	1	2	3	4	5	6	7	8	9	10	11	12	13	14	15	16	17	18	
↓Period																			
1	1 H																		2 He
2	3 Li	4 Be											5 B	6 C	7 N	8 O	9 F	10 Ne	
3	11 Na	12 Mg											13 Al	14 Si	15 P	16 S	17 Cl	18 Ar	
4	19 K	20 Ca	21 Sc	22 Ti	23 V	24 Cr	25 Mn	26 Fe	27 Co	28 Ni	29 Cu	30 Zn	31 Ga	32 Ge	33 As	34 Se	35 Br	36 Kr	
5	37 Rb	38 Sr	39 Y	40 Zr	41 Nb	42 Mo	43 Tc	44 Ru	45 Rh	46 Pd	47 Ag	48 Cd	49 In	50 Sn	51 Sb	52 Te	53 I	54 Xe	
6	55 Cs	56 Ba	*	72 Hf	73 Ta	74 W	75 Re	76 Os	77 Ir	78 Pt	79 Au	80 Hg	81 Tl	82 Pb	83 Bi	84 Po	85 At	86 Rn	
7	87 Fr	88 Ra	**	104 Rf	105 Db	106 Sg	107 Bh	108 Hs	109 Mt	110 Ds	111 Rg	112 Cn	113 Nh	114 Fl	115 Mc	116 Lv	117 Ts	118 Og	
			*	57 La	58 Ce	59 Pr	60 Nd	61 Pm	62 Sm	63 Eu	64 Gd	65 Tb	66 Dy	67 Ho	68 Er	69 Tm	70 Yb	71 Lu	
			**	89 Ac	90 Th	91 Pa	92 U	93 Np	94 Pu	95 Am	96 Cm	97 Bk	98 Cf	99 Es	100 Fm	101 Md	102 No	103 Lr	

In the **4d and 5d series**, a plot of cohesive energy vs. number of valence electrons (below left) has a "volcano" shape that is peaked at the elements Mo and W ($5s^14d^5$ and $6s^15d^5$, respectively). The number of bonding electrons, and therefore the bonding energy, increases steadily going from Rb to Mo in the 4d series, and from Cs to W in the 5d series. Mo and W have the most bonding energy because they can use all six of their valence electrons in bonding without promotion. Elements past Mo and W have more d electrons, but some of them are spin paired and so some promotion energy is needed to prepare these electrons for bonding. For example, Pt metal must be promoted from the $6s^15d^9$ atomic ground state to $6s^15d^76p^2$ in order to make six bonds per atom, and the energy cost of promoting electrons from the 5d to the 6p orbitals is reflected in the net bonding energy. Because of their strong bonding energy, elements in the middle of the 4d and 5d series have very high melting points. We do not see magnetism in the 4d or 5d metals or their alloys because orbital overlap is strong and the bonding energy exceeds the electron pairing energy.



The heat of vaporization (the cohesive energy) of metals in the 3d and 5d series, measured at the melting point of the metal.

The **3d elements** (Sc through Zn) are distinctly different from the 4d and 5d elements in their bonding (and consequently in their magnetic properties). In the 3d series, we see the expected increase in cohesive energy going from Ca ($4s^2$) to Sc ($4s^23d^1$) to Ti ($4s^23d^2$) to V ($4s^23d^3$), but then something very odd happens. The 3d series has a "crater" in the cohesive energy plot where there was a peak in the 5d series. The cohesive energy actually *decreases* going from V to Mn, even though the number of valence electrons is increasing. We can explain this effect by remembering that the 3d orbitals are progressively contracting as more protons are added to the nucleus. For elements beyond V, the orbital overlap is so poor that the 3d electrons are no longer effective in bonding, and the valence electrons begin to unpair. At this point the elements become **magnetic**. Depending on the way the spins order, metals and alloys in this part of the periodic table can be ferromagnetic (spins on neighboring atoms aligned parallel, as in the case of Fe or Ni) or antiferromagnetic (spins on neighboring atoms antiparallel, as in the case of Mn). We have seen the trade-off between orbital overlap and magnetism before (in Chapter 5) in the context of paramagnetic transition metal complexes. It is worth recalling that this behavior is predicted in the energy vs. distance diagram of the hydrogen atom (from Chapter 2). At short interatomic distances (or with strong overlap between atomic orbitals), the spins of the electrons pair and a bond is formed. Unpairing the electrons becomes favorable at larger interatomic distances where the overlap between orbitals is poor.



With strong overlap between orbitals of neighboring atoms, the bonding energy exceeds the pairing energy and electrons spin-pair. With weaker overlap, bonding is weak and spins unpair, resulting in magnetic behavior.

Interestingly, many alloys of the **4f elements** (the lanthanides) are also magnetic because the 4f orbitals, like the 3d orbitals, are poorly shielded from the nuclear charge and are ineffective in bonding. Strong permanent magnets often contain alloys of Nd, Sm, or Y, usually with magnetic 3d elements such as Fe and Co.

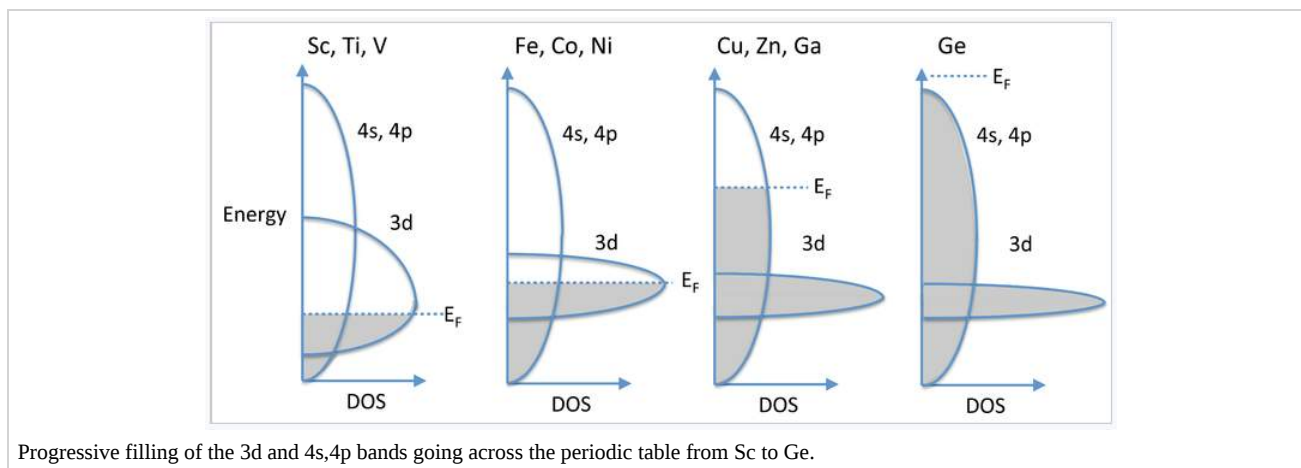
Because the 4f orbitals are contracted and not very effective in bonding, other physical properties of the lanthanides can also be affected. For example, it has been proposed that oxides of the 4f elements have weak surface interactions with polar molecules such as water because of f-orbital contraction. Experimentally, CeO_2 , Er_2O_3 , and Ho_2O_3 are observed to be hydrophobic, whereas main group and early transition metal oxides (e.g., Al_2O_3 , SiO_2 , TiO_2) are quite hydrophilic.^[1]

Late transition metal alloys

Although the bonding in the 5d series follows a "normal" volcano plot, the situation is a bit more complex for alloys of Re, Os, Ir, Pt, and Au. There is strong overlap between the 5d orbitals, but because these elements contain more than five d-electrons per atom, they cannot make as many bonds as 4d or 5d elements with half-filled d-shells such as Mo or W. This progressive filling of the d-band explains the steady decrease in bonding energy going from Os to Au. Pt and Au are both soft metals with relatively low heats of vaporization. However, these metals (especially Ir, Pt, and Au) can combine with early transition metals to form stable alloys with very negative heats of formation and high melting points. For example, ZrC and Pt react to form a number of stable alloys (ZrPt , $\text{Zr}_9\text{Pt}_{11}$, Zr_3Pt_4 , ZrPt_3)^[2] plus carbon. This reactivity is unusual because we normally think of Pt as a "noble" (i.e., unreactive) metal, and because ZrC is a very stable, refractory metal carbide. The favorable combination of early and late transition metals has been interpreted as arising from a d-electron "acid-base" interaction.^[3] For example, in HfPt_3 , Hf is the "acid" with an electron configuration of $6s^25d^2$, while Pt is the "base" with the electron configuration of $6s^15d^9$. They combine to create a stable "salt" product with a filled 5d electron configuration without promoting any electrons to higher orbitals. The implication is that Pt donates d-electrons to the "d-acid," Zr or Hf. However, electronic structure calculations on model compounds show that much of the bonding energy in ZrPt and ZrPt_3 arises from electron transfer from Zr to Pt (not the other way around) and the polarity of the resulting metal-metal bonds.^[4] Regardless of the source of their stability, some early-late transition metal alloys are of particular interest for use in catalysis. For example, the alloy ScPt_3 is a good catalyst for oxygen reduction in fuel cells. Even though Sc is an active metal that is easily oxidized, it is stabilized in the aqueous acid environment of the fuel cell by its strong interaction with Pt.^[5]

Filling of the 3d and 4s,4p bands

In the 3d series, we see magnetic behavior for elements and alloys between Cr and Ni. Past Ni, the elements (Cu, Zn, Ga,...) are no longer magnetic and they are very good electrical conductors, implying that their valence electrons are highly delocalized. We can understand this behavior by considering the overlap of 4s, 4p, and 3d orbitals, all of which are close in energy. The 4s and 4p have strong overlap and form a broad, continuous band. On the other hand, the 3d electrons are contracted and form a relatively narrow band. Progressing from the early 3d elements (Sc, Ti, V), we begin to fill the 3d orbitals, which are not yet so contracted that they cannot contribute to bonding. Thus, the valence electrons in Sc, Ti, and V are all spin-paired, except for a small number near the Fermi level that give rise to a weak Pauli paramagnetism. Moving across the 3d series to the magnetic elements (Fe, Co, Ni), the d-orbitals are now so contracted that their electrons unpair and we see cooperative ordering of spins (ferromagnetism and antiferromagnetism). Referring to the band diagram at the right, the 3d band is only partially filled and the Fermi level cuts through it. For Cu, Zn, and Ga, the 3d orbitals are even more contracted and the 3d band is thus more narrow, but now it is completely filled and the Fermi level is in the 4s,4p band. The strong orbital overlap in these bands results in spin pairing and a high degree of electron delocalization. Consequently, metals in this part of the periodic table (Cu, Ag) are diamagnetic and are among the best electrical conductors at room temperature. Finally, at Ge, the 4s,4p band is completely filled and the solid is a semiconductor.







Materials are classified as diamagnetic if they contain no unpaired electrons. Diamagnetic substances are very weakly repelled from an inhomogeneous magnetic field. As we learned in Chapter 5, molecules or ions that have unpaired spins are paramagnetic and are attracted to a magnet, i.e., they move towards the high field region of an inhomogeneous field. This attractive force results

from the alignment of spins with the field, but in the case of paramagnetism each molecule acts independently. In metals, alloys, oxides, and other solid state compounds, the unpaired spins interact strongly with each other and can order spontaneously, resulting in the cooperative magnetic phenomena described below.

This page titled [6.7: Atomic Orbitals and Magnetism](#) is shared under a [CC BY-SA 4.0](#) license and was authored, remixed, and/or curated by [Chemistry 310 \(Wikibook\)](#) via [source content](#) that was edited to the style and standards of the LibreTexts platform; a detailed edit history is available upon request.

6.8: Ferro-, Ferri- and Antiferromagnetism

The magnetism of metals and other materials are determined by the orbital and spin motions of the unpaired electrons and the way in which unpaired electrons align with each other. All magnetic substances are **paramagnetic** at sufficiently high temperature, where the thermal energy (kT) exceeds the interaction energy between spins on neighboring atoms. Below a certain critical temperature, spins can adopt different kinds of ordered arrangements.

Ferromagnetic 	Below T_C , spins are aligned parallel in magnetic domains
Antiferromagnetic 	Below T_N , spins are aligned antiparallel in magnetic domains
Ferrimagnetic 	Below T_C , spins are aligned antiparallel but do not cancel
Paramagnetic 	Spins are randomly oriented (any of the others above T_C or T_N)

A pictorial description of the ordering of spins in ferromagnetism, antiferromagnetism, ferrimagnetism, and paramagnetism

Let's begin by considering an individual atom in the bcc structure of iron metal. Fe is in group VIIIb of the periodic table, so it has eight valence electrons. The atom is promoted to the $4s^13d^7$ state in order to make bonds. A localized picture of the d-electrons for an individual iron atom might look like this:



Since each unpaired electron has a spin moment of $1/2$, the total spin angular momentum, S , for this atom is:

$$S = 3\frac{1}{2} = \frac{3}{2} \text{ (in units of } h/2\pi\text{)}$$

We can think of each Fe atom in the solid as a little bar magnet with a spin-only moment S of $3/2$. The spin moments of neighboring atoms can align in parallel ($\uparrow \uparrow$), antiparallel ($\uparrow \downarrow$), or random fashion. In bcc Fe, the tendency is to align parallel because of the positive sign of the exchange interaction. This results in **ferromagnetic** ordering, in which all the spins within a magnetic domain (typically hundreds of unit cells in width) have the same orientation, as shown in the figure at the right. Conversely, a negative exchange interaction between neighboring atoms in bcc Cr results in **antiferromagnetic** ordering. A third arrangement, **ferrimagnetic** ordering, results from an antiparallel alignment of spins on neighboring atoms when the magnetic moments of the neighbors are unequal. In this case, the spin moments do not cancel and there is a net magnetization. The ordering mechanism is like that of an antiferromagnetic solid, but the magnetic properties resemble those of a ferromagnet. Ferrimagnetic ordering is most common in metal oxides, as we will learn in Chapter 7.

Magnetization and susceptibility

The **magnetic susceptibility**, χ , of a solid depends on the ordering of spins. Paramagnetic, ferromagnetic, antiferromagnetic, and ferrimagnetic solids all have $\chi > 0$, but the magnitude of their susceptibility varies with the kind of ordering and with temperature. We will see these kinds of magnetic ordering primarily among the **3d** and **4f** elements and their alloys and compounds. For example, Fe, Co, Ni, $\text{Nd}_2\text{Fe}_{14}\text{B}$, SmCo_5 , and YCo_5 are all ferromagnets, Cr and MnO are antiferromagnets, and Fe_3O_4 and CoFe_2O_4 are ferrimagnets. Diamagnetic compounds have a weak *negative* susceptibility ($\chi < 0$).

Definitions

- H = applied magnetic field (units: Henry (H))
- B = induced magnetic field in a material (units: Tesla (T))
- M = magnetization, which represents the magnetic moments within a material in the presence of an external field H.

Magnetic susceptibility $\chi = M/H$

Usually, χ is given in *molar* units in the *cgs* system:

$$\chi_M = \text{molar susceptibility (units: cm}^3/\text{mol)}$$

Typical values of χ_M :

Compound	Type of Magnetism	χ at 300K (cm ³ /mol)
SiO ₂	Diamagnetic	- 3 x 10 ⁻⁴
Pt metal	Pauli paramagnetic	+ 2 x 10 ⁻⁴
Gd ₂ (SO ₄) ₃ ·8H ₂ O	Paramagnetic	+ 5 x 10 ⁻²
Ni-Fe alloy	Ferromagnetic	+ 10 ⁴ - 10 ⁶

To correlate χ with the number of unpaired electrons in a compound, we first correct for the small diamagnetic contribution of the core electrons:

$$\chi^{corr} = \chi^{obs} - \chi^{diamagnetic\ cores} \quad (6.8.1)$$

Susceptibility of paramagnets

For a paramagnetic substance,

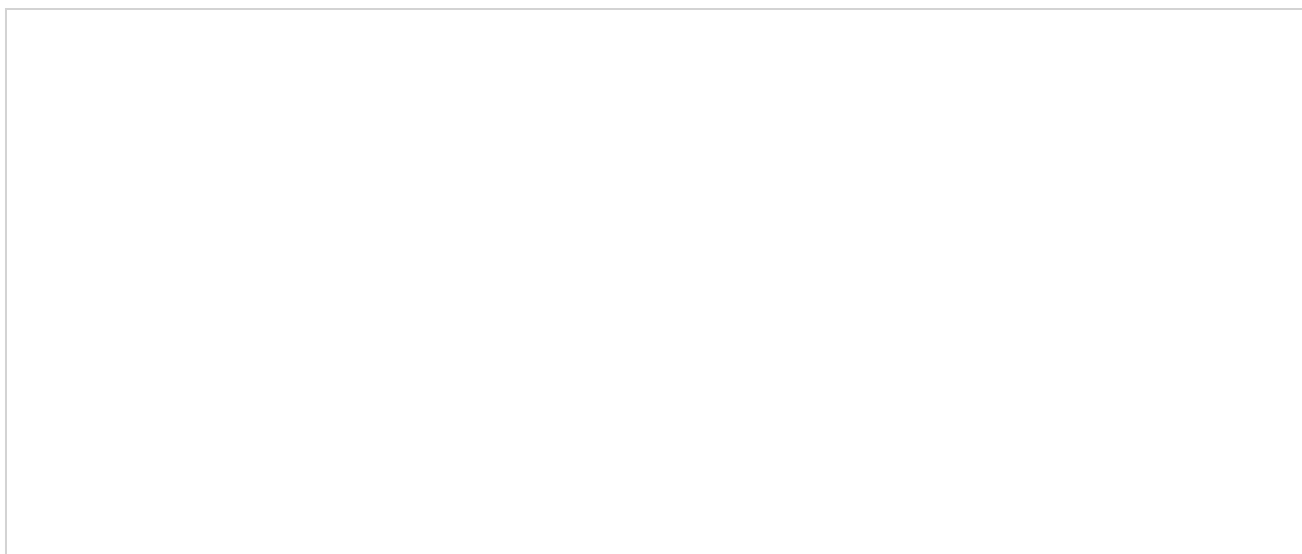
$$\chi_M^{corr} = \frac{C}{T} \quad (6.8.2)$$

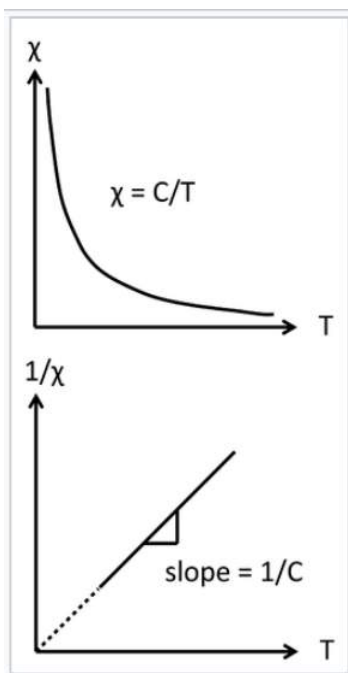
The inverse relationship between the magnetic susceptibility and T, the absolute temperature, is called **Curie's Law**, and the proportionality constant C is the **Curie constant**:

$$C = \frac{N_A}{3k_B} \mu_{eff}^2 \quad (6.8.3)$$

Note that C is not a "constant" in the usual sense, because it depends on μ_{eff} , the **effective magnetic moment** of the molecule or ion, which in turn depends on its number of unpaired electrons:

$$\mu_{eff} = \sqrt{n(n+2)} \mu_B \quad (6.8.4)$$





Curie law behavior of a paramagnet. A plot of $1/\chi$ vs. absolute temperature is a straight line, with a slope of $1/C$ and an intercept of zero.

Here μ_B is the Bohr magneton, a physical constant defined as $\mu_B = eh/4\pi m_e = 9.274 \times 10^{-21}$ erg/gauss (in cgs units).

In cgs units, we can combine physical constants,

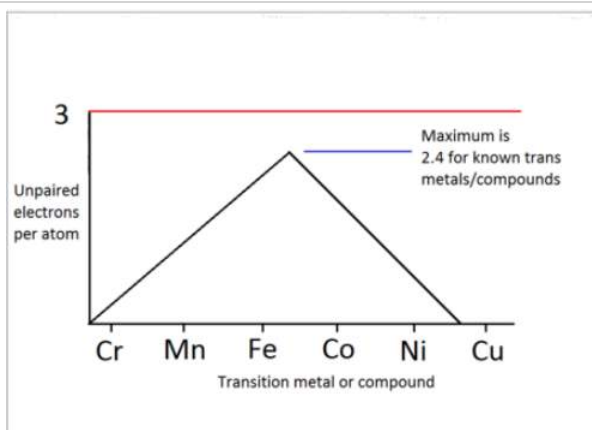
$$\frac{N_A}{3k_B} \mu_B^2 = .125 \quad (6.8.5)$$

Combining these equations, we obtain

$$\chi_M^{corr} = \frac{.125}{T} \left(\frac{\mu_{eff}}{\mu_B} \right)^2 \quad (6.8.6)$$

These equations relate the molar susceptibility, a bulk quantity that can be measured with a magnetometer, to μ_{eff} , a quantity that can be calculated from the number of unpaired electrons, n . Two important points to note about this formula are:

- The magnetic susceptibility is inversely proportional to the absolute temperature, with a proportionality constant C (Curie's Law)
- So far we are talking only about paramagnetic substances, where there is no interaction between neighboring atoms.



Number of unpaired electrons per atom, determined from Curie constants of transition metals and their 1:1 alloys.

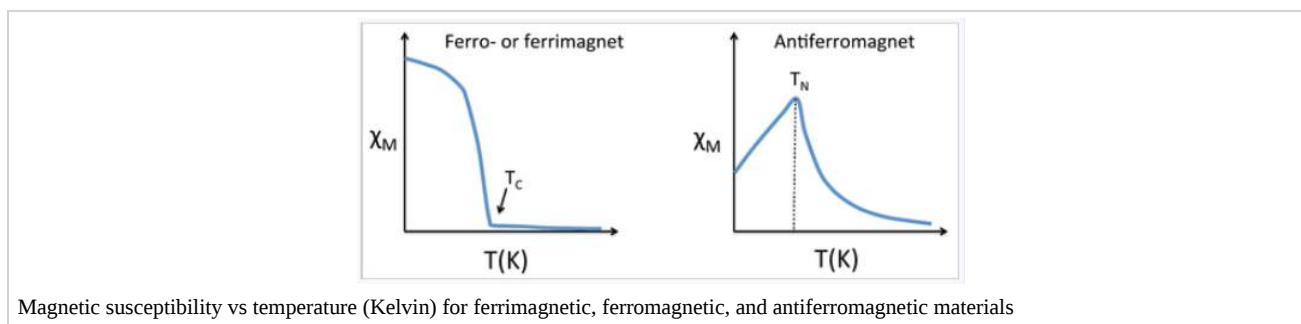
Returning to the isolated Fe atom with its three unpaired electrons, we can measure the Curie constant for iron metal (above the temperature of its transition to a paramagnetic solid) and compare it to the calculation of μ_{eff} . Since $n = 3$, we calculate:

$$\mu_{eff} = \sqrt{(3)(5)}\mu_B = 3.87\mu_B \quad (6.8.7)$$

The plot at the right shows the number of unpaired electrons per atom, calculated from measured Curie constants, for the magnetic elements and 1:1 alloys in the 3d series. The plot peaks at a value of 2.4 spins per atom, slightly lower than we calculated for an isolated iron atom. This reflects that fact that there is some pairing of d-electrons, i.e., that they do contribute somewhat to bonding in this part of the periodic table.

Susceptibility of ferro-, ferri-, and antiferromagnets

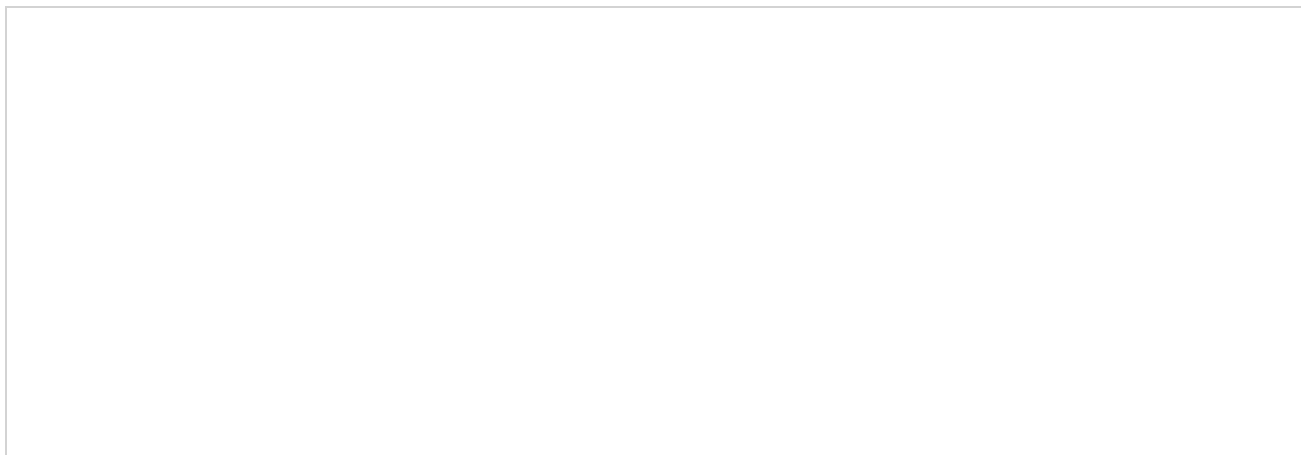
Below a certain critical temperature, the spins of a solid paramagnetic substance order and the susceptibility deviates from simple Curie-law behavior. Because the ordering depends on the short-range exchange interaction, this critical temperature varies widely. Metals and alloys in the 3d series tend to have high critical temperatures because the atoms are directly bonded to each other and the interaction is strong. For example, Fe and Co have critical temperatures (also called the Curie temperature, T_C , for ferromagnetic substances) of 1043 and 1400 K, respectively. The Curie temperature is determined by the strength of the magnetic exchange interaction and by the number of unpaired electrons per atom. The number of unpaired electrons peaks between Fe and Co as the d-band is filled, and the exchange interaction is stronger for Co than for Fe. In contrast to ferromagnetic metals and alloys, paramagnetic salts of transition metal ions typically have critical temperatures below 1K because the magnetic ions are not directly bonded to each other and thus their spins are very weakly coupled in the solid state. For example, in gadolinium sulfate, the paramagnetic Gd^{3+} ions are isolated from each other by SO_4^{2-} ions.

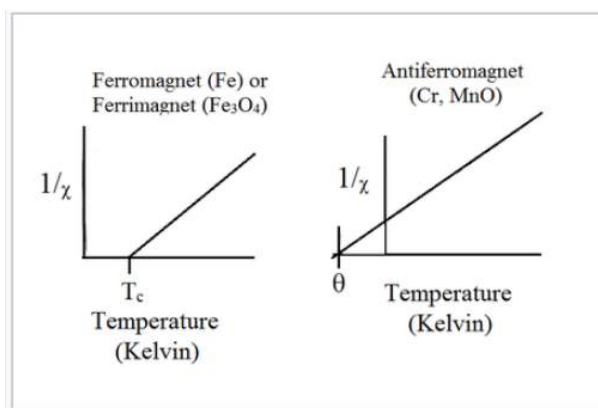


Above the critical temperature T_C , **ferromagnetic** compounds become paramagnetic and obey the **Curie-Weiss law**:

$$\chi = \frac{C}{T - T_c} \quad (6.8.8)$$

This is similar to the Curie law, except that the plot of $1/\chi$ vs. T is shifted to a positive intercept T_C on the temperature axis. This reflects the fact that ferromagnetic materials (in their paramagnetic state) have a greater tendency for their spins to align in a magnetic field than an ordinary paramagnet in which the spins do not interact with each other. Ferrimagnets follow the same kind of ordering behavior. Typical plots of χ vs. T and $1/\chi$ vs. T for ferro-/ferrimagnets are shown above and below.





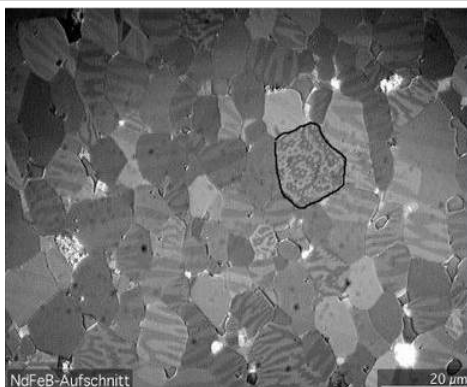
Plots of $1/\chi$ vs. T for ferromagnets, ferrimagnets, and antiferromagnets.

Antiferromagnetic solids are also paramagnetic above a critical temperature, which is called the Néel temperature, T_N . For antiferromagnets, χ reaches a maximum at T_N and is smaller at higher temperature (where the paramagnetic spins are further disordered by thermal energy) and at lower temperature (where the spins pair up). Typically, antiferromagnets retain some positive susceptibility even at very low temperature because of canting of their paired spins. However the maximum value of χ is much lower for an antiferromagnet than it is for a ferro- or ferrimagnet. The Curie-Weiss law is also modified for an antiferromagnet, reflecting the tendency of spins (in the paramagnetic state above T_N) to resist parallel ordering. A plot of $1/\chi$ vs. T intercepts the temperature axis at a negative temperature, $-\theta$, and the Curie-Weiss law becomes:

$$\chi = \frac{C}{T + \theta} \quad (6.8.9)$$

Ordering of spins below T_C

Below T_C , the spins align spontaneously in ferro- and ferrimagnets. Complex magnetization behavior is observed that depends on the history of the sample. For example, if a ferromagnetic material is cooled in the absence of an applied magnetic field, it forms a mosaic structure of magnetic domains that each have internally aligned spins. However, neighboring domains tend to align the opposite way in order to minimize the total energy of the system. This is illustrated in the figure at the left for a Nd-Fe-B magnet. The sample consists of 5-10 μm wide crystal grains that can be easily distinguished by the sharp boundaries in the image. Within each grain are a series of lighter and darker stripes (imaged by using the optical Kerr effect) that are ferromagnetic domains with opposite orientations. Averaged over the whole sample, these domains have random orientation so the net magnetization is zero.



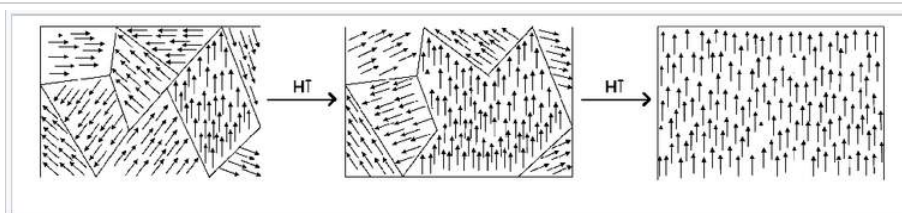
Microcrystalline grains within a piece of $\text{Nd}_2\text{Fe}_{14}\text{B}$ (the alloy used in neodymium magnets) with magnetic domains made visible with a Kerr microscope. The domains are the light and dark stripes visible within each grain.

When a sample like this one is magnetized (i.e., exposed to a strong magnetic field), the domain walls move and the favorably aligned domains grow at the expense of those with the opposite orientation. This transformation can be seen in real time in the Kerr microscope. The domain walls are typically hundreds of atoms wide, so movement of a domain wall involves a cooperative tilting of spin orientation (analogous to "the wave" in a sports stadium) and is a relatively low energy process.



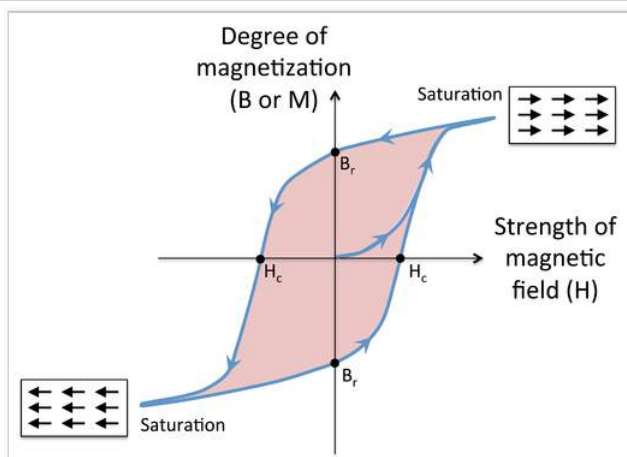
The movement of domain walls in a grain of silicon steel is driven in this movie by increasing the external magnetic field in the "downward" direction, and is imaged using a Kerr microscope. White areas are domains with their magnetization directed up, dark areas - which eventually comprise the entire grain - are domains with their magnetization directed down.

The process of magnetization moves the solid away from its lowest energy state (random domain orientation), so magnetization involves input of energy. When the external magnetic field is removed, the domain walls relax somewhat, but the solid (especially in the case of a "hard" magnet) can retain much of its magnetization. If you have ever magnetized a nail or a paper clip by using a permanent magnet, what you were doing was moving the walls of the magnetic domains inside the ferromagnet. The object thereafter retains the "memory" of its magnetization. However, annealing a permanent magnet destroys the magnetization by returning the system to its lowest energy state in which all the magnetic domains cancel each other.



Rotation of orientation and increase in size of magnetic domains in response to an externally applied magnetic field.

Magnetic hysteresis. Cycling a ferro- or ferrimagnetic material in a magnetic field results in hysteresis in the magnetization of the material, as shown in the figure at the left. At the beginning, the magnetization is zero, but it begins to rise rapidly as the magnetic field is applied. At high field, the magnetic domains are aligned and the magnetization is said to be saturated. When the field is removed, a certain **remanent magnetization** (indicated as the point B_r on the graph) is retained, i.e., the material is magnetized. Applying a field in the opposite direction begins to orient the magnetic domains in the other direction, and at a field H_c (the **coercive field**), the magnetization of the sample is reduced to zero. Eventually the material reaches saturation in the opposite direction, and when the field is removed again, it has remanent magnetization B_r , but in the opposite direction. As the field continues to reverse, the magnet follows the hysteresis loop as indicated by the arrows. The area of colored region inside the loop is proportional to the magnetic work done in each cycle. When the field cycles rapidly (for example, in the core of a transformer, or in read-write cycles of a magnetic disk) this work is turned into heat.



Magnetization of a ferro- or ferrimagnet vs. applied magnetic field H . Starting at the origin, the upward curve is the initial magnetization curve. The downward curve after saturation, along with the lower return curve, form the main loop. The intercepts H_c and B_r are the coercivity and remanent magnetization.

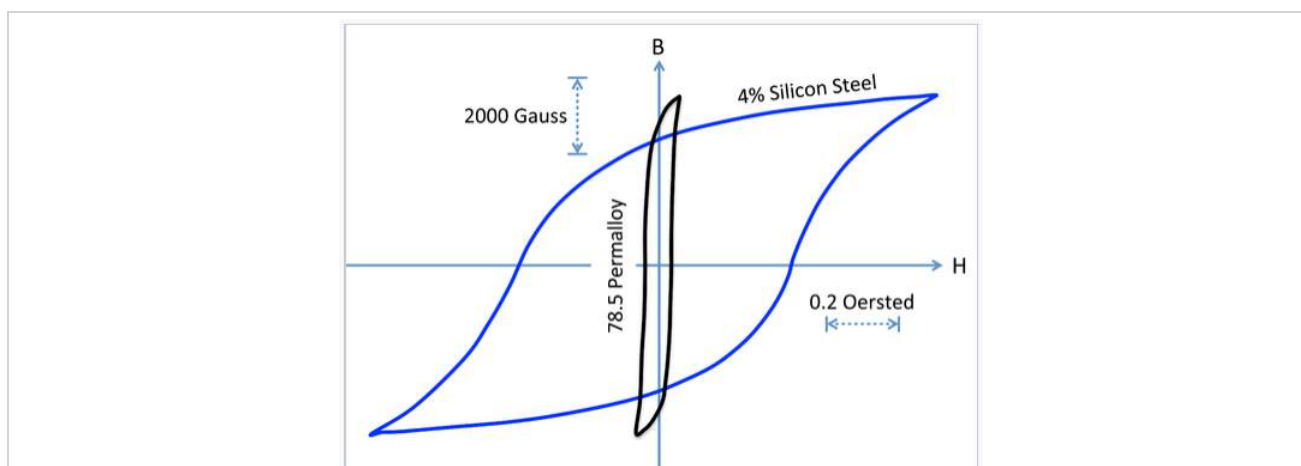
This page titled [6.8: Ferro-, Ferri- and Antiferromagnetism](#) is shared under a [CC BY-SA 4.0](#) license and was authored, remixed, and/or curated by [Chemistry 310 \(Wikibook\)](#) via [source content](#) that was edited to the style and standards of the LibreTexts platform; a detailed edit history is available upon request.

6.9: Hard and Soft Magnets

Whether a ferro- or ferrimagnetic material is a **hard** or a **soft magnet** depends on the strength of the magnetic field needed to align the magnetic domains. This property is characterized by H_c , the coercivity. Hard magnets have a high coercivity (H_c), and thus retain their magnetization in the absence of an applied field, whereas soft magnets have low values.

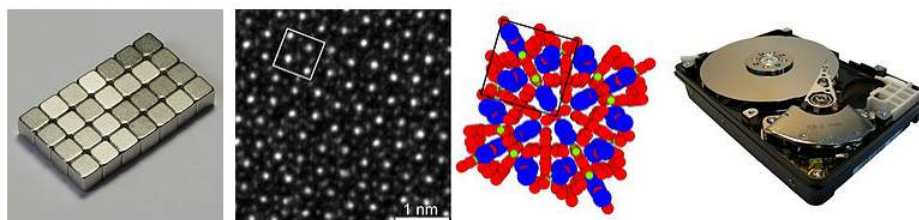
The figure at the right compares hysteresis loops for hard and soft magnets. Recall that the energy dissipated in magnetizing and demagnetizing the material is proportional to the area of the hysteresis loop. We can see that soft magnets, while they can achieve a high value of B_{sat} , dissipate relatively little energy in the loop. This makes **soft magnets** preferable for use in **transformer cores**, where the field is switched rapidly. **Permalloy**, an alloy consisting of about 20% Fe and 80% Ni, is a soft magnet that has very high magnetic permeability μ (i.e., a large maximum slope of the B vs. H curve) and a very narrow hysteresis loop.

Some materials, such as iron metal, can exist as either hard or soft magnets. Whether bcc iron is a hard or soft magnet depends on the crystal grain size. When crystal grains in iron are sub-micron size, and comparable to the size of the magnetic domains, then the magnetic domains are pinned by crystal grain boundaries. When the magnetic domains are pinned a stronger coercive magnetic field needs to be applied to cause them to re-align. When iron is annealed, the crystal grains grow and the magnetic domains become more free to align with applied magnetic fields. This decreases the coercive field and the material becomes a soft magnet.



Hysteresis loops comparing a hard magnet (iron-silicon steel) to a soft magnet (permalloy) on the same scale. H_c for permalloy is 0.05 Oe, about 10 times lower than that of the hard magnet. The remanent magnetizations of the two materials are comparable.

Hard magnets such as CrO_2 , $\gamma\text{-Fe}_2\text{O}_3$, and cobalt ferrite (CoFe_2O_4) are used in magnetic recording media, where the high coercivity allows them to retain the magnetization state (read as a logical 0 or 1) of a magnetic bit over long periods of time. Hard magnets are also used in disk drives, refrigerator magnets, electric motors and other applications. Drive motors for hybrid and electric vehicles such as the Toyota Prius use the hard magnet $\text{Nd}_2\text{Fe}_{14}\text{B}$ (also used to make strong refrigerator magnets) and require 1 kilogram (2.2 pounds) of neodymium.^[6] A high-resolution transmission electron microscope image of $\text{Nd}_2\text{Fe}_{14}\text{B}$ is shown below and compared to the crystal structure with the unit cell marked.



This page titled [6.9: Hard and Soft Magnets](#) is shared under a [CC BY-SA 4.0](#) license and was authored, remixed, and/or curated by [Chemistry 310 \(Wikibook\)](#) via [source content](#) that was edited to the style and standards of the LibreTexts platform; a detailed edit history is available upon request.

6.10: Discussion Questions

- Discuss the relationship between the trends in bonding energy of the transition metals and their magnetic properties.
 - Draw the hcp unit cell in sections and show how you would calculate (a) the number of atoms in the unit cell and (b) the fraction of space filled by equal spheres.
-

This page titled [6.10: Discussion Questions](#) is shared under a [CC BY-SA 4.0](#) license and was authored, remixed, and/or curated by [Chemistry 310 \(Wikibook\)](#) via [source content](#) that was edited to the style and standards of the LibreTexts platform; a detailed edit history is available upon request.

6.11: Problems

1. C-centered Bravais lattices exist in the monoclinic and orthorhombic systems but not in the tetragonal system. That is because the C-centered tetragonal lattice is equivalent to one of the other Bravais lattices. Which one is it? Show with a drawing how that lattice is related to the C-centered tetragonal lattice. How many atoms are in the unit cell of that lattice?

2. Which of the following sequences of close packed layers fills space most efficiently? Explain your answer.

(a) ABACCABA...

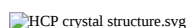
(b) ABABAB...

(c) AABBAABB...

(d) ABACABAC...

3. Calculate the fraction of space that is occupied by packing spheres in the (a) simple cubic, (b) body-centered cubic structure, (c) face-centered cubic (cubic close packed) structures. Assume that nearest neighbor spheres are in contact with each other.

4. The hexagonal close packed (hcp) structure is shown below. If the radius of the spheres is R , what is the vertical distance between layers in units of R ? What fraction of space is filled by the spheres in the hcp lattice?



5. Consider a one-dimensional chain of sodium atoms that contains N atoms, where N is a large number. The distance between atoms in the chain is the lattice constant a . In the highest occupied molecular orbital of the chain, what is the distance between nodes (in units of a)?

6. Starting from the left side of the periodic table, the melting and boiling points of the elements first increase, and then decrease. For example, the order of boiling points is $\text{Rb} < \text{Sr} < \text{Y} < \text{Zr} < \text{Nb} < \text{Mo} > \text{Tc} \approx \text{Ru} > \text{Rh} > \text{Pd} > \text{Ag}$. Briefly explain the reason for this trend.

7. Going across the periodic table from left to right starting from potassium, the bonding energies and heats of vaporization increase in the order $\text{K} < \text{Ca} < \text{Sc} < \text{Ti} < \text{V}$, but then decrease going from V to Mn ($\text{V} > \text{Cr} > \text{Mn}$). The heats of vaporization of V , Cr , and Mn are much less than those of Nb , Mo , and Tc , respectively. Explain these trends.

8. Some alloys of early and late transition metals (e.g., ZrPt_3) have much higher enthalpies of vaporization (per metal atom) than either pure metal. Why are such alloys unusually stable, relative to the pure metals?

9. Graphite is a semimetal composed of sheets of fused benzene rings. There are no bonds between sheets, only van der Waals interactions. What is the C-C bond order in graphite? Show why the C-C distance (1.42 \AA) is different from that of benzene (1.40 \AA).

10. Fe, Co, and Ni are ferromagnetic, whereas Ru, Ir, and Pt are diamagnetic. Explain why magnetic metals are found only among the 3d and 4f elements. Why are Sc and Ti, which are also 3d elements, diamagnetic?

11. The Curie temperature of cobalt is 1127°C , which is higher than that of Fe (770°C) or Ni (358°C). Why does Co have the highest Curie temperature?

12. Iron metal comes in magnetically “soft” and “hard” forms. Briefly explain the structural differences between them and draw magnetic hysteresis curves for each, indicating on your curves the coercive field and the remanent magnetization.

13. Aluminum metal has the fcc structure, a lattice constant of 4.046 \AA , three valence electrons per atom, and an electron scattering time (at room temperature) of 11.8 fs . Use these values to calculate the room temperature resistivity (in ohm-cm) of Al metal.

This page titled [6.11: Problems](#) is shared under a [CC BY-SA 4.0](#) license and was authored, remixed, and/or curated by [Chemistry 310 \(Wikibook\)](#) via [source content](#) that was edited to the style and standards of the LibreTexts platform; a detailed edit history is available upon request.

6.12: References

1. G. Azimi et al., *Nature Materials* **12**,315–320 (2013), doi:10.1038/nmat3545
 2. Stalick, J. K.; Waterstrat, R. J. *J. Alloys Compounds* **430**, 123-131 (2007).
 3. Brewer, L.; Wengert, P. R. *Metall. Trans.* 1973, **4**, 83.
 4. Wang, H.; Carter, E. A.; *J. Am. Chem. Soc.* 1993, **115**, 2357-2362.
 5. Greeley, J. et al., Alloys of platinum and early transition metals as oxygen reduction electrocatalysts, *Nature Chem.* **1**, 552 - 556 (2009)
 6. www.reuters.com/article/2009/08/31/us-mining-toyota-idUSTRE57U02B20090831
-

This page titled [6.12: References](#) is shared under a [CC BY-SA 4.0](#) license and was authored, remixed, and/or curated by [Chemistry 310 \(Wikibook\)](#) via [source content](#) that was edited to the style and standards of the LibreTexts platform; a detailed edit history is available upon request.

CHAPTER OVERVIEW

7: Metals and Alloys - Mechanical Properties

Learning Objectives

- Understand the structure of dislocations and grain boundaries and their role in controlling the mechanical properties of solids.
- Explain why the mechanical properties of bcc metals and alloys differ from those with close packed structures.
- Explain the effects of work hardening and annealing on structure and mechanical properties.
- Explain the mechanical properties of steel in terms of its phase behavior.
- Understand the structure and mechanical properties of amorphous metals.

How much do the mechanical properties of metals and alloys vary with processing? The answer is, a great deal.

[7.1: Defects in Metallic Crystals](#)

[7.2: Work Hardening, Alloying, and Annealing](#)

[7.3: Malleability of Metals and Alloys](#)

[7.4: Iron and Steel](#)

[7.5: Amorphous Alloys](#)

[7.6: Discussion Questions](#)

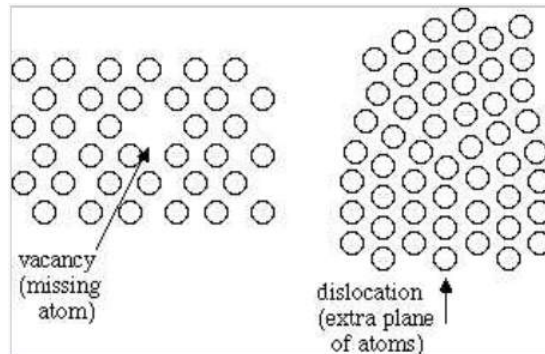
[7.7: Problems](#)

[7.8: References](#)

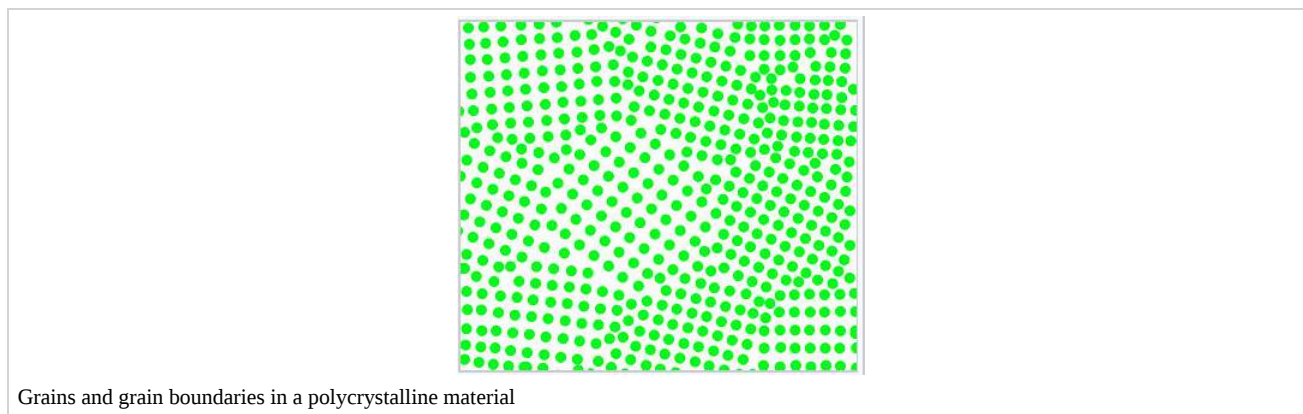
This page titled [7: Metals and Alloys - Mechanical Properties](#) is shared under a [CC BY-SA 4.0](#) license and was authored, remixed, and/or curated by [Chemistry 310 \(Wikibook\)](#) via [source content](#) that was edited to the style and standards of the LibreTexts platform; a detailed edit history is available upon request.

7.1: Defects in Metallic Crystals

“Crystals are like people, it is the defects in them which tend to make them interesting!” - *Colin Humphreys*.



Metals, by virtue of their non-directional bonding, are more energetically tolerant of **defects** than are covalent network or ionic solids. Because there is no strong preference for one atomic position over another, the energy of a metallic crystal is not greatly impaired by the vacancy of a single atom or by the dislocation of a group of atoms. These kinds of "mistakes" in the packing of metal atoms within crystals are collectively called defects. The deformability of metals is the direct result of defects in the crystal structure. Defects in metals such as Al and Fe are responsible for the three orders of magnitude difference between the yield stress of annealed polycrystalline samples (i.e., normal articles of commerce) and perfect single crystals.

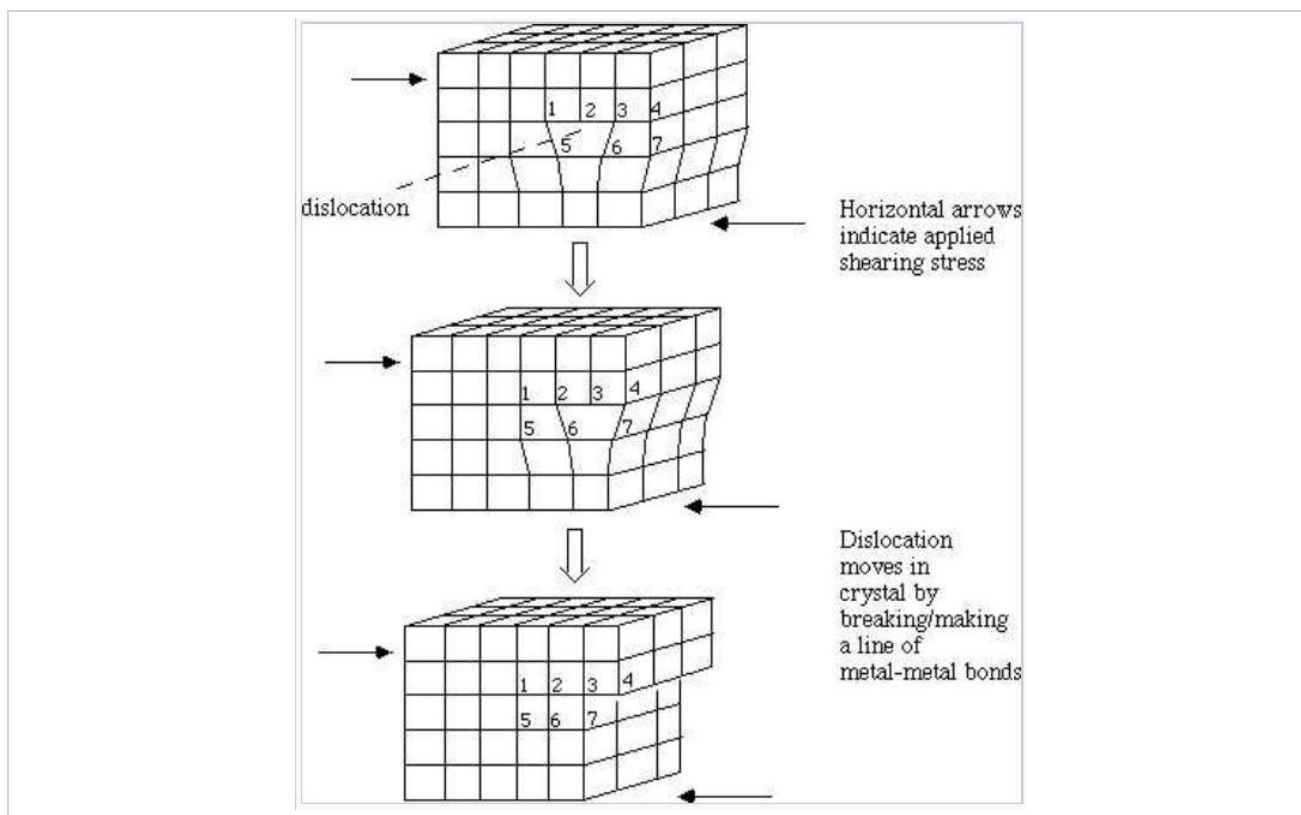


This page titled [7.1: Defects in Metallic Crystals](#) is shared under a [CC BY-SA 4.0](#) license and was authored, remixed, and/or curated by [Chemistry 310 \(Wikibook\)](#) via [source content](#) that was edited to the style and standards of the LibreTexts platform; a detailed edit history is available upon request.

7.2: Work Hardening, Alloying, and Annealing

One of the questions we would like to ask is, why are the yield stresses of normal (polycrystalline) metal samples so much lower (by a factor of 1000) than they are in perfect single crystals? The answer has to do with the motion of dislocations. Consider the picture below, which shows planes of metal atoms near a dislocation (the individual atoms are numbered to help you see which bonds are broken and which are formed). The arrows indicate force applied under shear stress. Notice how the dislocation moves by breaking/making metal-metal bonds.

The key point here is that we can induce plastic deformation (shear) by breaking only one line of metal-metal bonds at a time along the dislocation line. This involves far less force than breaking an entire plane of bonds, as we would need to do to shear a perfect crystal. In a given polycrystalline sample, there are many dislocation lines that run perpendicular to all possible shear directions, so their motion can be used to "tear" the metal apart. Turbine rotors on large jets are made of very expensive **single crystal** nickel-titanium alloys, so that these shearing deformations can be avoided.^[1]



We can see that motion of dislocations is basically bad news if we want a metal to be strong and hard (e.g., if we want a structural material, or a knife that can hold a decent edge). There are several ways we can overcome (to some extent) this problem:

1. Use **single crystals** and anneal out all the dislocations (expensive - especially with large items like turbine blades, and impossible with very large items like airplane wings or bridges).
2. **Work hardening** of the metal - this moves all dislocations to grain boundaries (the dislocation essentially becomes part of the grain boundary). Since a grain boundary is a planar defect, it is much less responsive to stress than a line defect.
3. Introduce **impurity atoms** (that is alloying elements) or impurity phases that "pin" the motion of defects. An impurity atom stops the motion because it is a different size, or makes stronger bonds, than the other metal atoms; the line defect has a hard time moving away from rows of such atoms. An impurity phase (like Fe_3C in iron) makes extra grain boundaries that can stop the motion of defects. This effect is analogous to the graphite fibers in fiber-reinforced cross-linked polymers (used, e.g., in tennis rackets) that stop the propagation of cracks.

A simple illustration of work hardening can be done with a piece of copper wire. When struck many times with a hammer, the copper wire becomes stiffer, and it is possible to hang a weight from it. Dislocations move to the crystal grain boundaries during

work hardening, effectively halting their motion and at the same time making the individual crystal grains smaller. Because the crystal grains are now smaller, the amount of grain boundary area has increased, and with it the free energy of the material. Annealing reverses the process by lowering the free energy. When the wire is annealed in a flame (heated so that atoms can move and rearrange), the crystal grains grow, and the dislocations reappear. The copper again becomes ductile, and bends easily. Cold-working (work hardening) of metals is important for strengthening structural materials (e.g., iron beams) and for making brittle, hard edges (this is why blacksmiths hammer on knives and swords when they are making them. If you have ever watched them, they do the same thing to horseshoes, when they cool down, to make them stiff).

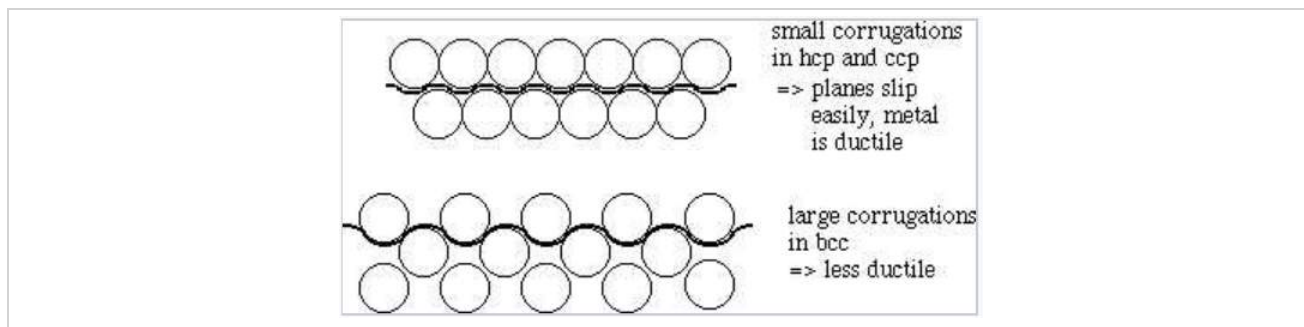


Blacksmith, 1606

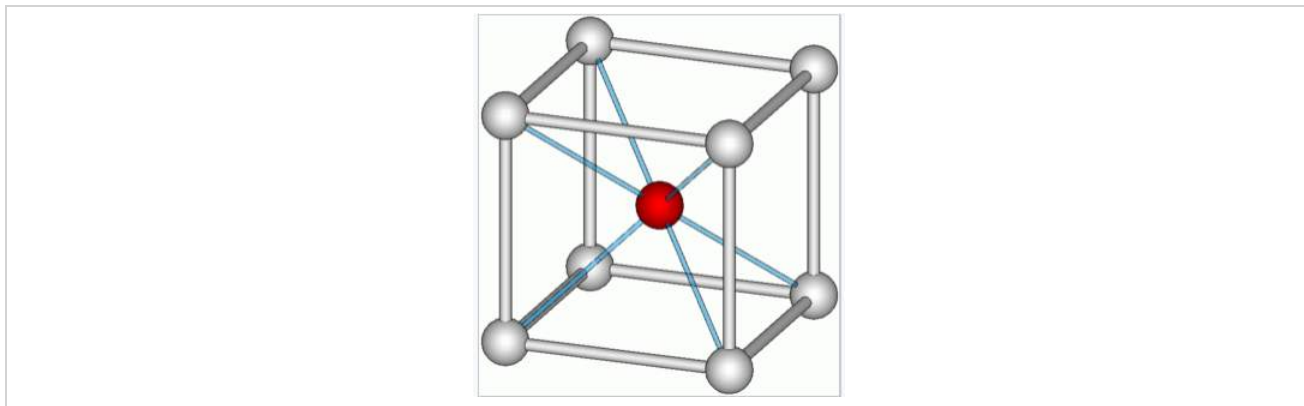
This page titled [7.2: Work Hardening, Alloying, and Annealing](#) is shared under a [CC BY-SA 4.0](#) license and was authored, remixed, and/or curated by [Chemistry 310 \(Wikibook\)](#) via [source content](#) that was edited to the style and standards of the LibreTexts platform; a detailed edit history is available upon request.

7.3: Malleability of Metals and Alloys

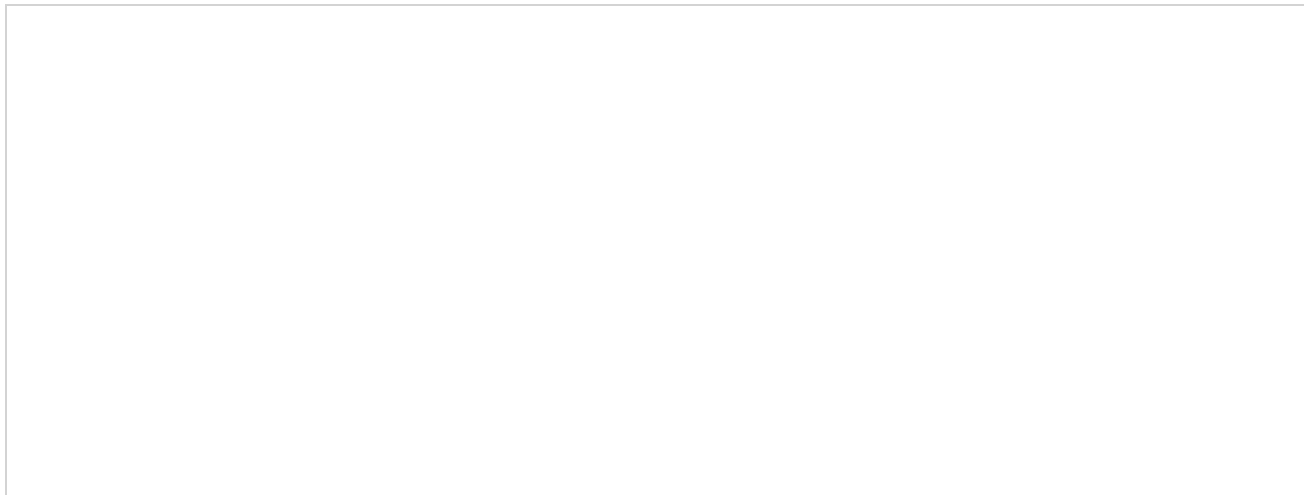
Metals with close-packed structures (HCP and FCC) such as copper, gold, silver, zinc, magnesium, etc. are in general more malleable than those with the BCC structure (tungsten, vanadium, chromium, etc.). Why? In the close-packed structure, there is relatively little corrugation between sheets of metal atoms. This means that these planes can slip past each other relatively easily. In the BCC structure, there are no close-packed planes, and much greater corrugation between atoms at different levels. This makes it much harder for one row to slide past another.



This effect explains the hardness of alloys like brass (CuZn, which has the BCC structure), which are made by combining two soft metals (Cu and Zn, which are respectively FCC and HCP as pure metals, are both soft and ductile). Bronzes - originally made as alloys of copper and arsenic, but later as alloys of copper and tin - are harder than either of the constituent metals for the same reason.



The history of bronzes and brass dates to pre-historic times, with the earliest bronzes made by smelting copper-zinc ores. In the Bronze Age, possession of these hard alloys provided a tactical advantage in warfare (see image at right), that was later supplanted when the technology for smelting iron was developed.



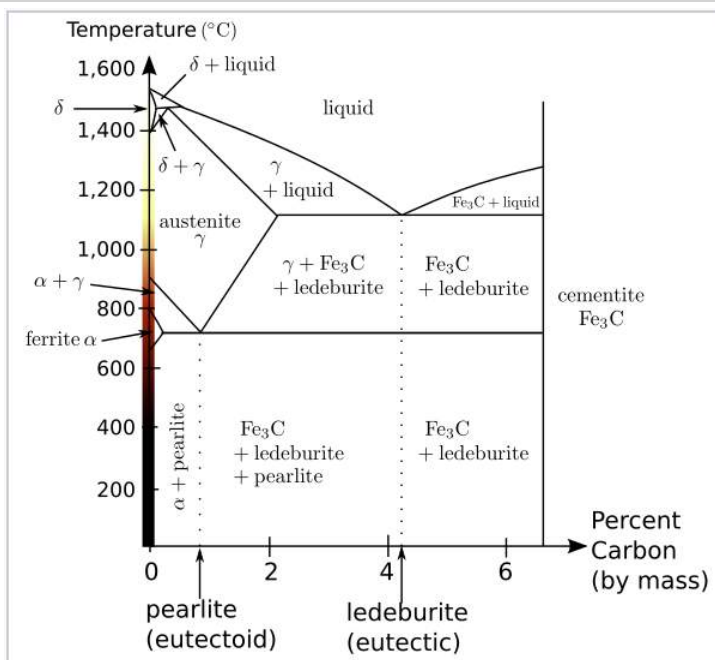


Bronze age weapons from Romania.

This page titled [7.3: Malleability of Metals and Alloys](#) is shared under a [CC BY-SA 4.0](#) license and was authored, remixed, and/or curated by [Chemistry 310 \(Wikibook\)](#) via [source content](#) that was edited to the style and standards of the LibreTexts platform; a detailed edit history is available upon request.

7.4: Iron and Steel

One other very important place where the difference between the hardness of a BCC and a close-packed metal is important is in steelmaking. Between room temperature and 912°C, iron has the BCC structure, and is a tough, hard metal ("tough as nails"). Above 912°C, pure iron switches over to the FCC (austenite) structure, which is much more ductile. So hot iron can be bent and worked into a variety of shapes when it is very hot but still solid (it melts at 1535°C). Rapid quenching of hot iron - e.g., when the blacksmith plunges a red hot piece directly into cold water - cools it to room temperature, but doesn't allow time for the FCC → BCC phase transition to occur; therefore, such pieces are still relatively malleable and can be shaped.



The iron-iron carbide (Fe-Fe₃C) phase diagram. Below 912 °C, pure iron exists as the alpha phase, ferrite, which has the BCC structure. Between 912 and 1,394 °C, pure iron exists as the gamma phase, austenite, which has the FCC structure. Carbon is more soluble in the FCC phase, which occupies area "γ" on the phase diagram, than it is in the BCC phase. The percent carbon determines the type of iron alloy that is formed upon cooling from the FCC phase, or from liquid iron: alpha iron, carbon steel (pearlite), or cast iron.

Carbon is added (about 1% by weight) to iron to make "carbon steel", which is a very hard material. Carbon is rather soluble in the FCC phase of iron, but not in the BCC phase. Therefore, when the ductile FCC phase cools and turns into BCC ("tempering" the steel, which means cooling it slowly enough so the FCC to BCC transformation can occur), the iron can no longer dissolve the excess carbon. The carbon forms layers or grains of an extra phase, Fe₃C ("cementite" - a very hard material) which are layered or dotted throughout the matrix of BCC iron grains. The effect of all these little grains of Fe₃C is to stop the motion of dislocations, making for a harder but (with higher carbon content) increasingly brittle material. This is why knives and swords are quenched from the FCC phase, cold worked into the appropriate shapes, and then heated up again and tempered (before they are sharpened) when they are made. Cast iron objects (frying pans, radiators, etc) have a higher carbon content and are therefore very strong, but tend to fracture rather than bend because of the larger fraction of the brittle Fe₃C phase in the alloy.



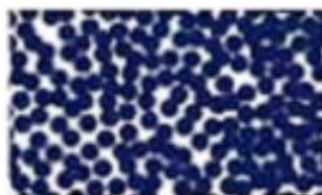
Upon cooling, high carbon steels phase segregate into a mixture of bcc iron (light gray) and Fe₃C (dark gray) microscopic grains.

This page titled [7.4: Iron and Steel](#) is shared under a [CC BY-SA 4.0](#) license and was authored, remixed, and/or curated by [Chemistry 310 \(Wikibook\)](#) via [source content](#) that was edited to the style and standards of the LibreTexts platform; a detailed edit history is available upon request.

7.5: Amorphous Alloys

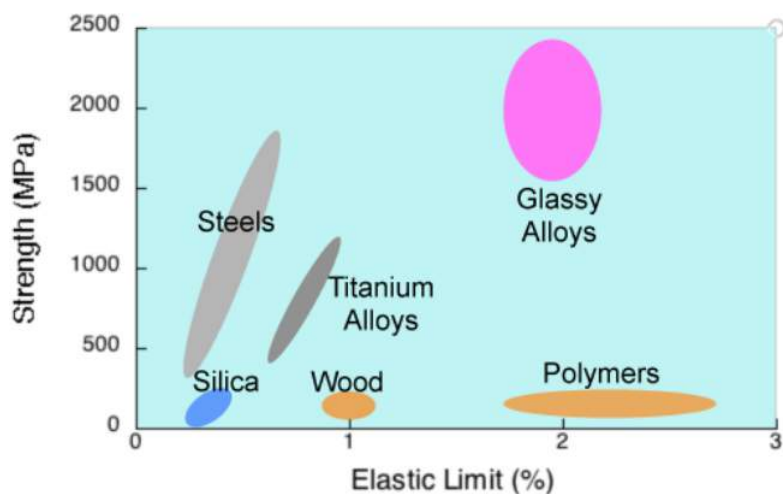


Polycrystalline



Liquid or Glass

Alloys of metals with more complex stoichiometries can be made in amorphous form by slower cooling from the melt. These alloys have been prepared and studied since the 1960s, and since the 1990s amorphous alloys have been discovered that can be prepared in bulk form at cooling rates on the order of 1 deg/s, similar to the cooling rates of other kinds of glasses.



Currently amorphous metals (marketed under the tradenames Vitreloy and Liquidmetal) are used commercially in golf clubs, watches, USB flash drives, and other applications where very high elasticity, yield strength, and/or wear resistance are needed.

Year	Alloy	Cooling Rate (K/s)
1960	Au ₇₅ Si ₂₄	10 ⁶ - thin films & ribbons ^[3]
1969	Pd-Cu-Si	100-1000
1980s	La-Al-Cu & others	1-100
1990s	Zr-Ti-Cu-Ni-Be	~1 (similar to oxide glasses)

This page titled [7.5: Amorphous Alloys](#) is shared under a [CC BY-SA 4.0](#) license and was authored, remixed, and/or curated by [Chemistry 310 \(Wikibook\)](#) via [source content](#) that was edited to the style and standards of the LibreTexts platform; a detailed edit history is available upon request.

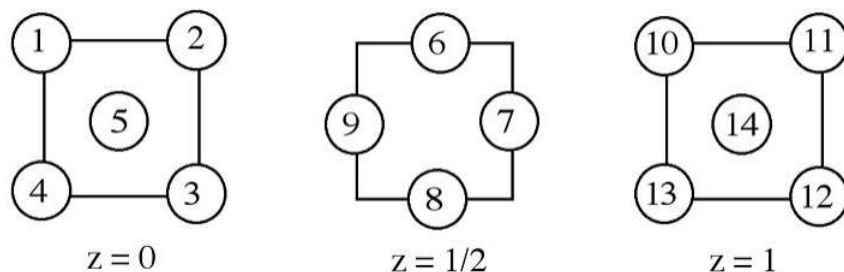
7.6: Discussion Questions

- Discuss the thermodynamics of work hardening and annealing in terms of the microscopic picture of defects in metallic crystals.
 - In your pocket or purse, you may have a brass key, which is an alloy of Cu and Zn. How do the mechanical properties of this alloy depend on its structure, and why don't we make keys out of pure Cu or Zn?
 - Cooling carbon steels along the eutectic lines (A and B) in the iron-carbon phase diagram above results in the formation of pearlite and ledeburite. How does the microstructure of these two iron alloys differ, and how does the microstructure affect their mechanical properties?
-

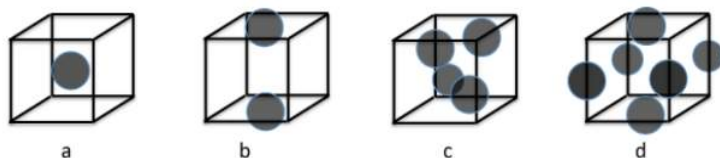
This page titled [7.6: Discussion Questions](#) is shared under a [CC BY-SA 4.0](#) license and was authored, remixed, and/or curated by [Chemistry 310 \(Wikibook\)](#) via [source content](#) that was edited to the style and standards of the LibreTexts platform; a detailed edit history is available upon request.

7.7: Problems

1. Show in a drawing how a planar dislocation moves through a solid under stress.
2. Why is a metal sample that has been annealed more malleable than one that has been work hardened? Explain which state of the metal has smaller crystal grains and why.
3. Explain (on the basis of structure) why alloys such as bronze make better structural materials than the constituent metals (copper and tin). How did the discovery of these alloys change civilization?
4. A layer sequence for an FCC = CCP metal is shown below. A body diagonal passes through the centers of atoms numbered 1 and 12. A close-packed plane perpendicular to this diagonal contains the centers of atoms numbered 3, 7, 8, 11, 13, and 14.



- (a) Other close-packed planes of atoms parallel to this one pass through the cell. Segregate the remaining eight numbered atoms (not contained by this plane) into groups by the parallel plane that contains the center of the atom.
 - (b) Identify the other body diagonals by the numbered atoms that the diagonals pass through, and also identify one representative face diagonal by numbered atoms.
5. Identify the Bravais lattices that go with cubic unit cells (a) - (d). Remember that the origin of the unit cell is arbitrary.



This page titled [7.7: Problems](#) is shared under a [CC BY-SA 4.0](#) license and was authored, remixed, and/or curated by [Chemistry 310 \(Wikibook\)](#) via [source content](#) that was edited to the style and standards of the LibreTexts platform; a detailed edit history is available upon request.

7.8: References

1. P. Caron and T. Khan (1999), Evolution of Ni-based superalloys for single crystal gas turbine blade applications, *Aerospace Science and Technology*, 3, 513–523. [http://dx.doi.org/10.1016/S1270-9638\(99\)00108-X](http://dx.doi.org/10.1016/S1270-9638(99)00108-X)
 2. Libermann H. and Graham C. (1976). "Production Of Amorphous Alloy Ribbons And Effects Of Apparatus Parameters On Ribbon Dimensions". *IEEE Transactions on Magnetics* **12** (6): 921. doi:[10.1109/TMAG.1976.1059201](https://doi.org/10.1109/TMAG.1976.1059201). Bibcode: [1976ITM....12..921L](https://ui.adsabs.org/abs/1976ITM....12..921L).
 3. Klement, W.; Willens, R. H.; Duwez, POL (1960). "Non-crystalline Structure in Solidified Gold-Silicon Alloys". *Nature* **187** (4740): 869–870. doi:[10.1038/187869b0](https://doi.org/10.1038/187869b0). Bibcode: [1960Natur.187..869K](https://ui.adsabs.org/abs/1960Natur.187..869K).
-

This page titled [7.8: References](#) is shared under a [CC BY-SA 4.0](#) license and was authored, remixed, and/or curated by [Chemistry 310 \(Wikibook\)](#) via [source content](#) that was edited to the style and standards of the LibreTexts platform; a detailed edit history is available upon request.

CHAPTER OVERVIEW

8: Ionic and Covalent Solids - Structures

Learning Objectives

- Describe many crystal structures in terms of close-packed frameworks with systematic filling of octahedral and tetrahedral holes.
- Represent crystal structures by drawing them in sections.
- Rationalize, using chemical principles, why certain crystal structures are stable for certain compounds but not for others, as well as why certain structural and bonding motifs are preferred for certain compounds relative to others.
- Predict which crystal structures are most favorable for a given composition based on ionicity and periodic trends.
- Explain structure-dependent properties such as ferroelectricity and magnetic ordering based on crystal structures.
- Understand intercalation reactions in layered and open framework solids.
- Predict the preferred formation of normal or inverse spinels using arguments from transition metal chemistry (e.g. crystal field stabilization energies).

Inorganic solids often have simple crystal structures, and some of these structures are adopted by large families of ionic or covalent compounds. Examples of the most common structures include NaCl, CsCl, NiAs, zincblende, wurtzite, fluorite, perovskite, rutile, and spinel. We will develop these structures systematically from the close packed and non-close packed lattices shown below. Some layered structures, such as CdCl_2 and CdI_2 , can be thought of as relatives of simple ionic lattices with some atoms "missing."

[8.1: Prelude to Ionic and Covalent Solids - Structures](#)

[8.2: Close-packing and Interstitial Sites](#)

[8.3: Structures Related to NaCl and NiAs](#)

[8.4: Tetrahedral Structures](#)

[8.5: Layered Structures and Intercalation Reactions](#)

[8.6: Bonding in \$\text{TiS}_2\$, \$\text{MoS}_2\$, and Pyrite Structures](#)

[8.7: Spinel, Perovskite, and Rutile Structures](#)

[8.8: Discussion Questions](#)

[8.9: Problems](#)

[8.10: References](#)

This page titled [8: Ionic and Covalent Solids - Structures](#) is shared under a [CC BY-SA 4.0](#) license and was authored, remixed, and/or curated by [Chemistry 310 \(Wikibook\)](#) via [source content](#) that was edited to the style and standards of the LibreTexts platform; a detailed edit history is available upon request.

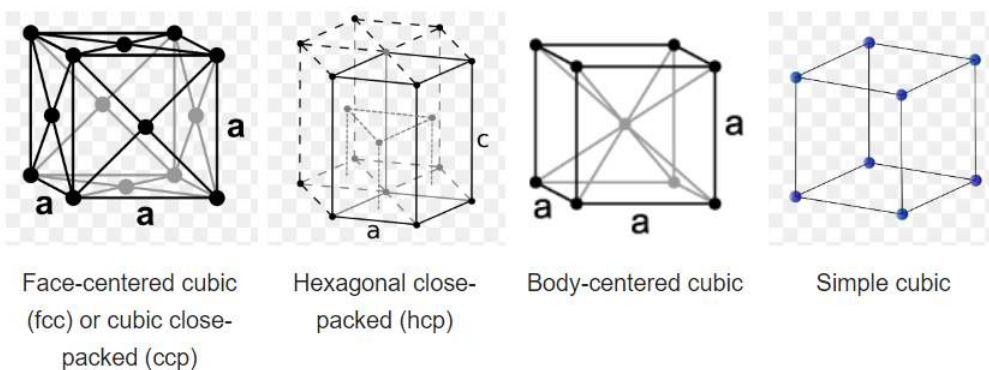
8.1: Prelude to Ionic and Covalent Solids - Structures

As we noted in our discussion of metal and alloy structures in Chapter 6, there is an intimate connection between the structures and the physical properties of materials. As we "graduate" from simple metal structures based on sphere packings to more complex structures, we find that this is still true. In this chapter we will try to systematize the structures of inorganic solids - metal oxides, halides, sulfides, and related compounds - and develop some rules for which structures to expect based on electronegativity differences, hard-soft acid-base rules, and other periodic trends. We will see that many of these structures are related to the sphere packings that we learned about in Chapter 6.



The morphology of twinned crystals of iron pyrite (FeS_2) is related to the underlying cubic symmetry of the unit cell. Like NaCl, the pyrite crystal structure can be thought of as a face-centered cubic array of anions (S_2^{2-}) with cations (Fe^{2+}) occupying all the octahedral holes.

Inorganic solids often have simple crystal structures, and some of these structures are adopted by large families of ionic or covalent compounds. Examples of the most common structures include NaCl, CsCl, NiAs, zinblende, wurtzite, fluorite, perovskite, rutile, and spinel. We will develop these structures systematically from the close packed and non-close packed lattices shown below. Some layered structures, such as CdCl_2 and CdI_2 , can be thought of as relatives of simple ionic lattices with some atoms "missing."



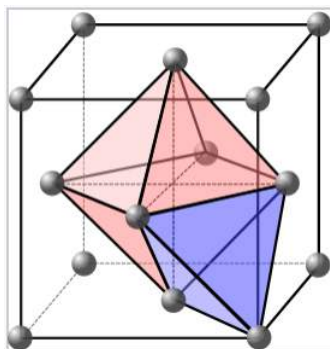
This page titled [8.1: Prelude to Ionic and Covalent Solids - Structures](#) is shared under a [CC BY-SA 4.0](#) license and was authored, remixed, and/or curated by [Chemistry 310 \(Wikibook\)](#) via [source content](#) that was edited to the style and standards of the LibreTexts platform; a detailed edit history is available upon request.

8.2: Close-packing and Interstitial Sites

Many common inorganic crystals have structures that are related to cubic close packed (face-centered cubic) or hexagonal close packed sphere packings. These packing lattices contain two types of sites or "holes" that the interstitial atoms fill, and the coordination geometry of these sites is either **tetrahedral** or **octahedral**. An interstitial atom filling a tetrahedral hole is coordinated to four packing atoms, and an atom filling an octahedral hole is coordinated to six packing atoms. In both the hexagonal close packed and cubic close packed lattices, there is one octahedral hole and two tetrahedral holes per packing atom.

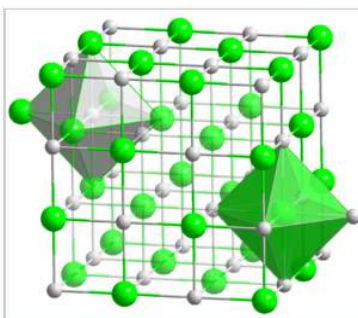
Question: Would anions or cations be better as packing atoms?

We might expect that anions, which are often larger than cations, would be better suited to the positions of packing atoms. While this is often true, there are many examples of structures in which cations are the packing atoms, and others in which the distinction is arbitrary. The NaCl structure is a good example of the latter.



One octahedral and one tetrahedral site in a face-centered cubic unit cell. Each cell contains four packing atoms (gray), four octahedral sites (pink), and eight tetrahedral sites (blue).

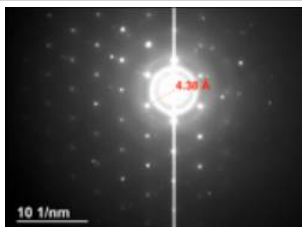
In the NaCl structure, shown on the right, the green spheres are the Cl^- ions and the gray spheres are the Na^+ ions. The octahedral holes in a face-centered cubic lattice can be found at fractional coordinates $(1/2 \ 1/2 \ 1/2)$, $(1/2 \ 0 \ 0)$, $(0 \ 1/2 \ 0)$, and $(0 \ 0 \ 1/2)$. There are four of these holes per cell, and they are filled by the chloride ions. The packing atoms (Na^+) have coordinates $(0 \ 0 \ 0)$, $(0 \ 1/2 \ 1/2)$, $(1/2 \ 1/2 \ 0)$, and $(1/2 \ 0 \ 1/2)$. Note that each of the Na^+ positions is related to a Cl^- position by a translation of $(1/2 \ 0 \ 0)$. Another way of stating this is that the structure consists of **two interpenetrating fcc lattices**, which are related to each other by a translation of half the unit cell along any of the three Cartesian axes. We could have equivalently placed the Cl ions at the fcc lattice points and the Na ions in the octahedral holes by simply translating the origin of the unit cell by $(1/2 \ 0 \ 0)$. Thus the distinction between packing and interstitial atoms in this case is arbitrary.



Crystal structure of NaCl. Both the Na^+ and Cl^- ions are octahedrally coordinated.

NaCl is interesting in that it is a three-dimensional checkerboard, and thus there are no NaCl "molecules" that exist in the structure. When this structure was originally solved (in 1913 by using X-ray diffraction) by W. L. Bragg, his interpretation met resistance by chemists who thought that precise integer stoichiometries were a consequence of the valency of atoms in molecules. The German chemist P. Pfeiffer noted in 1915 that 'the ordinary notion of valency didn't seem to apply', and fourteen years later, the influential chemist H. E. Armstrong still found Bragg's proposed structure of sodium chloride 'more than repugnant to the common sense, not chemical cricket'! Nevertheless, Bragg and his father, W. H. Bragg, persevered and used the then-new technique of X-ray diffraction to determine the structures of a number of other compounds, including diamond, zincblende, calcium fluoride, and other

alkali halides. These experiments gave chemists their first real look at the atomic structure of solids, and laid the groundwork for X-ray diffraction experiments that later elucidated the structures of DNA, proteins, and many other compounds. For their work on X-ray diffraction the Braggs received the Nobel prize in Physics in 1915.

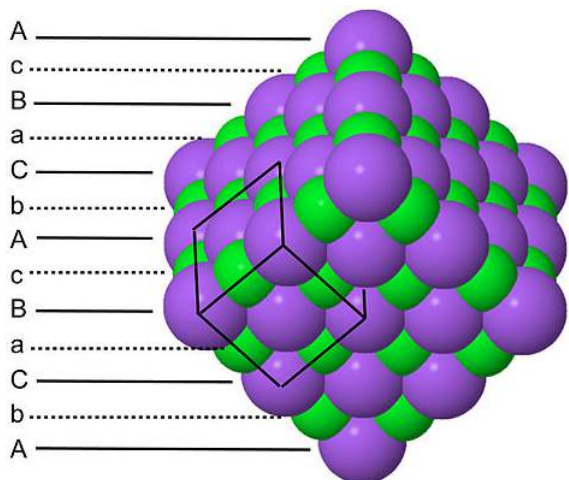


The lattice dimensions and positions of atoms in crystals such as NaCl are inferred from diffraction patterns.

Since each type of atom in the NaCl structure forms a face-centered cubic lattice, there are four Na and four Cl atoms per NaCl unit cell. It is because of this ratio that NaCl has a 1:1 stoichiometry. The shaded green and gray bipyramidal structures in the NaCl lattice show that the Na^+ ions are coordinated to six Cl^- ions, and vice versa. The NaCl structure can be alternatively drawn as a stacking of close-packed layer planes, AcBaCbAcBa... along the body diagonal of the unit cell. Here the uppercase letters represent the packing atoms, and the lower case letters are the interstitial atoms. This layered packing is illustrated below:

NaCl structure

- ----- A
- ---c---
- ----- B
- ---a---
- ----- C
- ---b---
- ----- A
- ---c---
- ----- B
- ---a---
- ----- C
- ---b---
- ----- A

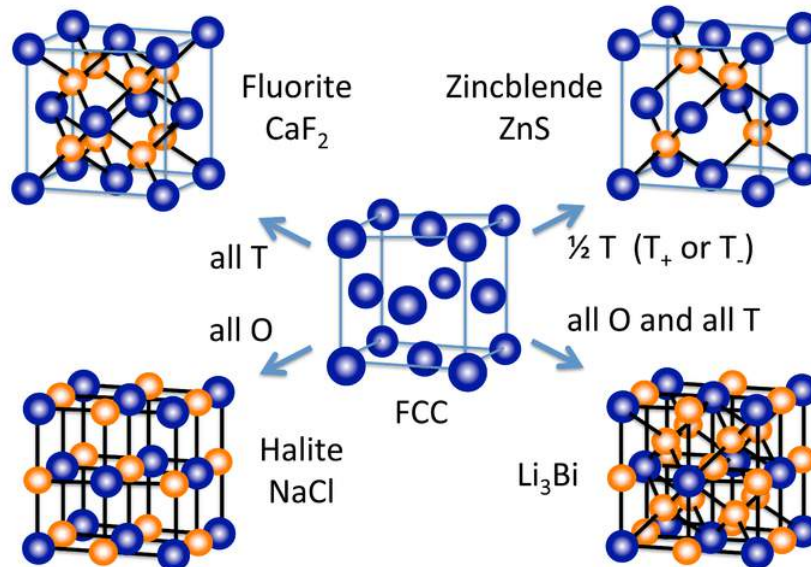


Note that both the packing atoms and interstitials are stacked in the sequence A-B-C-A-B-C..., in keeping with the fact that each forms a cubic close-packed lattice.

The NaCl structure is fairly common among ionic compounds:

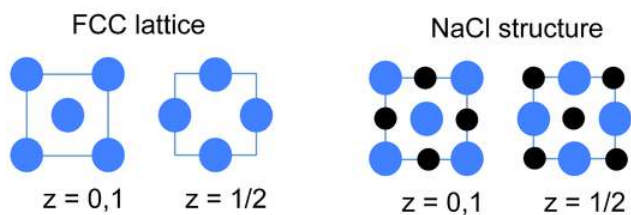
- Alkali Halides (except CsCl, CsBr, and CsI)

- Transition Metal Monoxides (TiO, VO, ..., NiO)
- Alkali Earth Oxides and Sulfides (MgO, CaO, BaS... except BeO and MgTe)
- Carbides and Nitrides (TiC, TiN, ZrC, NbC) -these are very stable refractory, interstitial alloys (metallic)



A number of other inorganic crystal structures are formed (at least conceptually) by filling octahedral and/or tetrahedral holes in close-packed lattices. The figure at the right shows some of the most common structures (fluorite, halite, zincblende) as well as a rather rare one (Li_3Bi) that derive from the fcc lattice. From the hcp lattice, we can make the NiAs and wurzite structures, which are the hexagonal relatives of NaCl and zincblende, respectively.

An alternative and very convenient way to represent inorganic crystal structures (especially complex structures such as Li_3Bi) is to draw the unit cell in slices along one of the unit cell axes. This kind of representation is shown at the left for the fcc lattice and the NaCl structure. Since all atoms in these structures have z-coordinates of either 0 or 1/2, only those sections need to be drawn in order to describe the contents of the unit cell. It is a useful exercise to draw some of the fcc compound structures (above) in sections.

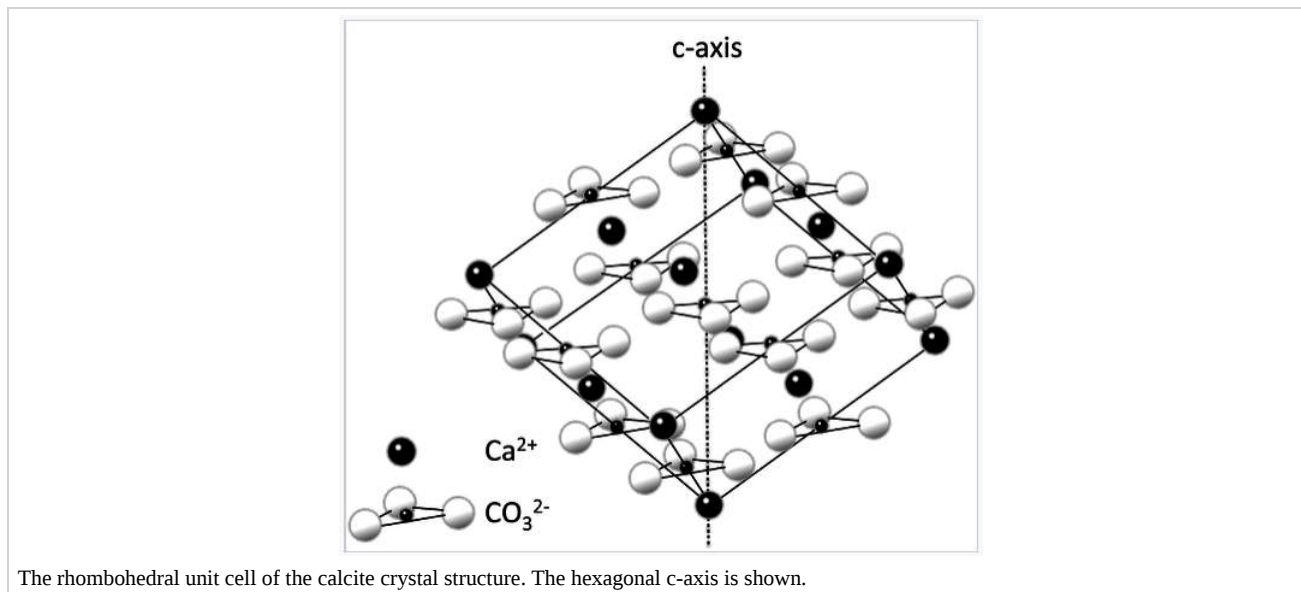


This page titled [8.2: Close-packing and Interstitial Sites](#) is shared under a [CC BY-SA 4.0](#) license and was authored, remixed, and/or curated by [Chemistry 310 \(Wikibook\)](#) via [source content](#) that was edited to the style and standards of the LibreTexts platform; a detailed edit history is available upon request.

8.3: Structures Related to NaCl and NiAs

There are a number of compounds that have structures similar to that of NaCl, but have a lower symmetry (usually imposed by the geometry of the anion) than NaCl itself. These compounds include:

- FeS₂ (pyrite, "fools gold"): S₂²⁻ (disulfide) and Fe²⁺
- CaC₂ (a salt-like carbide): Ca²⁺ and linear C₂²⁻ anions
- CaCO₃ (calcite, limestone, marble): Ca²⁺ and triangular CO₃²⁻.



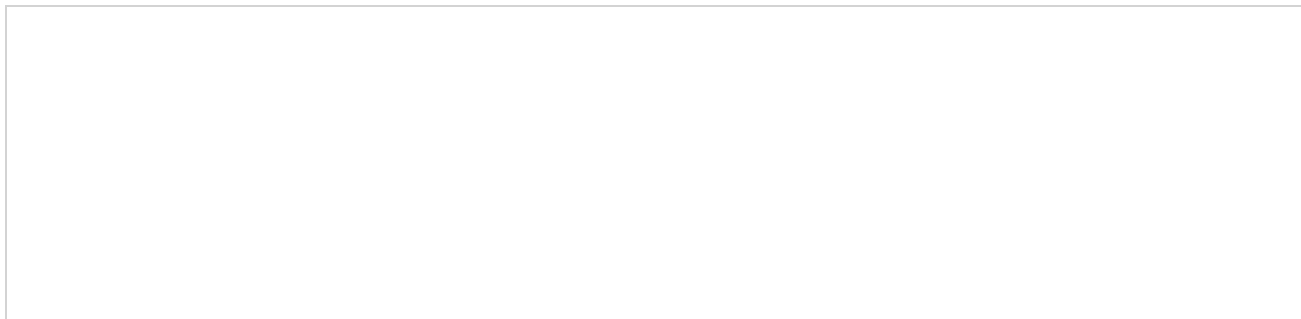
The **calcite** (CaCO₃) crystal structure is shown above. Triangular CO₃²⁻ ions fill octahedral holes between the Ca²⁺ ions (black spheres) in a distorted NaCl lattice. As in NaCl, each ion is coordinated by six of the other kind. From this image we can see why the CaCO₃ structure has a lower symmetry than that of NaCl. The fourfold rotation symmetry of the NaCl unit cell is lost when the spherical Cl⁻ ions are replaced by triangular CO₃²⁻ ions. Because of this symmetry lowering, transparent crystals calcite are birefringent, as illustrated below.

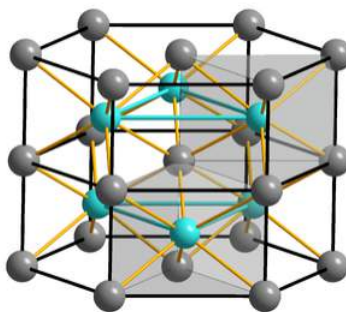


Calcite crystals are birefringent, meaning that their refractive indices are different along the two principal crystal directions. This gives rise to the phenomenon of double refraction.

NiAs structure

The NaCl structure can be described a face-centered cubic lattice with all of the octahedral holes filled. What if we start with a hexagonal-close packed lattice rather than a face-centered cubic lattice?





Nickel arsenide crystal structure. The Ni_6As trigonal prisms are shaded gray. One octahedron of six As atoms surrounding a Ni atom is shown in the center of the figure.

This is the structure adopted by **NiAs** and many other transition metal sulfides, phosphides, and arsenides. The cations are shown in gray while the anions are light blue in the figure at the right. The cations are in octahedral coordination, so each cation is coordinated to six anions. The anions are also coordinated to six cations, but they occupy trigonal prismatic sites. In terms of layer stacking, the NiAs structure is AcBcAcBc..., where the A and B sites (the hcp lattice) are occupied by the As atoms, and the c sites, which are eclipsed along the layer stacking axis, are occupied by Ni. Unlike the NaCl structure, where the anion and cation sites are interchangeable, NiAs has unique anion and cation sites. The layer stacking sequence for NiAs is shown below:

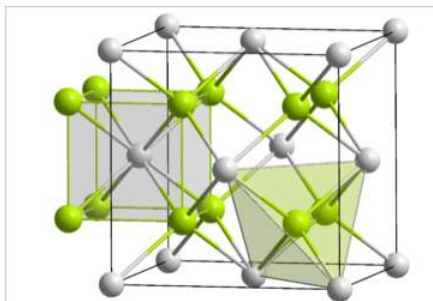
- ----- A
- ---c---
- ----- B
- ---c---
- ----- A
- ---c---
- ----- B
- ---c---

The NiAs structure cannot be adopted by ionic compounds because of the eclipsing cations, because the cation-cation repulsions would be internally destabilizing for an ionic compound. This structure is mainly adopted by covalent and polar covalent MX compounds, typically with "soft" X anions (S, Se, P, As,...) and low-valent transition metal cations. For example, some compounds with the NiAs structure are: MS, MSe, MTe (M=Ti, V, Fe, Co, Ni). Often these are nonstoichiometric or complex stoichiometries with ordered vacancies (Cr_7S_8 , Fe_7S_8).

This page titled [8.3: Structures Related to NaCl and NiAs](#) is shared under a [CC BY-SA 4.0](#) license and was authored, remixed, and/or curated by [Chemistry 310 \(Wikibook\)](#) via [source content](#) that was edited to the style and standards of the LibreTexts platform; a detailed edit history is available upon request.

8.4: Tetrahedral Structures

In ccp and hcp lattices, there are two tetrahedral holes per packing atom. A stoichiometry of either M_2X or MX_2 gives a structure that fills all tetrahedral sites, while an MX structure fills only half of the sites. An example of an MX_2 structure is **fluorite**, CaF_2 , whose structure is shown in the figure at the left. The packing atom in fluorite is Ca^{2+} and the structure is composed of three interpenetrating fcc lattices. It should be noted that the Ca^{2+} ion (gray spheres) as a packing atom defies our "rule" that anions are larger than cations and therefore must be the packing atoms. The fluorite structure is common for ionic MX_2 (MgF_2 , ZrO_2 , etc.) and M_2X compounds (Li_2O). In contrast, the hcp relative of the fluorite structure is quite rare because of unfavorable close contacts between like-charged ions.

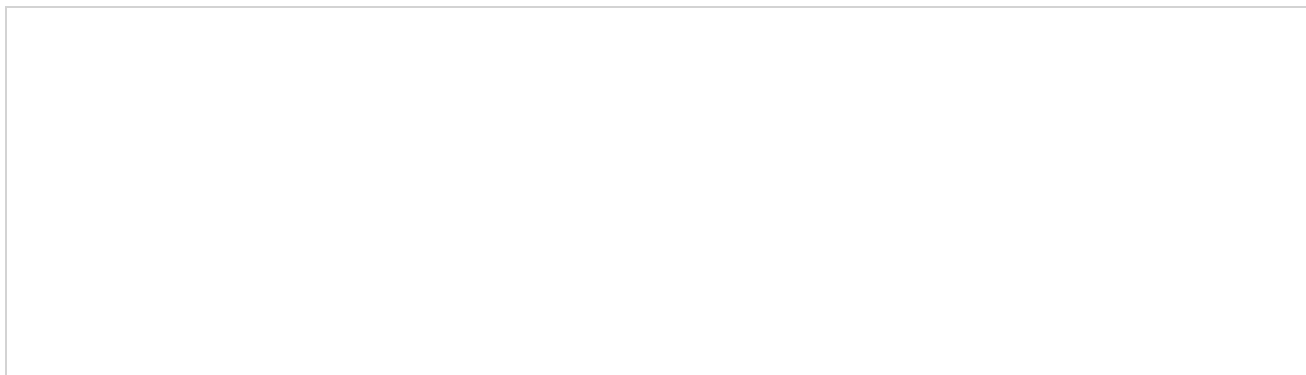


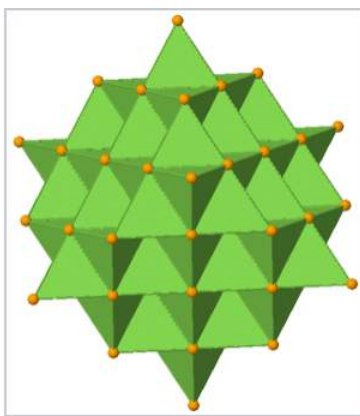
The fluorite (CaF_2) crystal structure showing the coordination environments of the Ca and F atoms

In terms of geometry, Ca^{2+} is in cubic coordination with eight F^- neighbors, and the fluoride ions are tetrahedrally coordinated by four Ca^{2+} ions. The 8:4 coordination geometry is consistent with the 1:2 Ca:F stoichiometry; in all crystal structures the ratio of the coordination numbers is the inverse of the stoichiometric ratio. The three interpenetrating fcc lattices have Ca at $0,0,0$, $1/2,1/2,0$, etc... F at $1/4,1/4,1/4$, $3/4,3/4,1/4$, etc... and F at $3/4,3/4,3/4$, $1/4,1/4,3/4$, etc.

Looking more closely at the tetrahedral sites in fluorite, we see that they fall into two distinct groups: T_+ and T_- . If a tetrahedron is oriented with a vertex pointing upwards along the stacking axis, the site is T_+ . Likewise, a tetrahedron with a vertex oriented downward is T_- . The alternation of T_+ and T_- sites allows for efficient packing of ions in the structure. The layer stacking sequence in this structure (including fluoride ions in the T_+ and T_- sites) is:

- ----- A
- ---b--- T_+
- ---a--- T_-
- ----- B
- ---c--- T_+
- ---b--- T_-
- ----- C
- ---a--- T_+
- ---c--- T_-
- ----- A
- ---b--- T_+
- ---a--- T_-

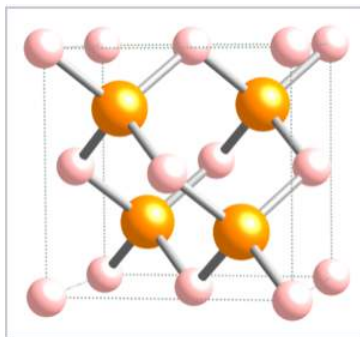




Polyhedral view of the fluorite crystal structure, showing T_+ and T_- Ca_4F tetrahedra. The Ca^{2+} ions are stacked ABCABC... along the body diagonal of the unit cell, which is the vertical direction in this image.

Tetrahedrally bonded compounds with a 1:1 stoichiometry (MX compounds) have only **half** of the tetrahedral sites (either the T_+ or T_- sites) filled. In this case, both the M and the X atoms are tetrahedrally coordinated. The **zincblende** and **wurtzite** structures are 1:1 tetrahedral structures based on fcc and hcp lattices, respectively. Both structures are favored by p-block compounds that follow the octet rule, and these compounds are usually semiconductors or insulators. The zincblende structure, shown below, can be thought of as two interpenetrating fcc lattices, one of anions and one of cations, offset from each other by a translation of $1/4$ along the body diagonal of the unit cell. Examples of compounds with the zincblende structure include CuCl, CuI, ZnSe, HgS, BeS, CdTe, AlP, GaP, SnSb, CSi, and diamond. Additionally, the compound $CuInSe_2$ is zincblende in an ordered, doubled unit cell (the chalcopyrite structure). The solid solution compounds $CuIn_{1-x}Ga_xSe_2$ with this structure are among the most widely studied materials for use in efficient thin film photovoltaic cells. Using ZnS as a representative of zincblende, the coordination of both Zn and S atoms is tetrahedral. The layer sequence, which is AbBcCaAbBcC..., results in six-membered ZnS rings that have the same geometry as the "chair" version of cyclohexane. The chair conformation allows for a relatively long distance between opposite atoms in the ring and, as a result, it is more sterically favorable than the boat form. The sequence of close-packed layers in zincblende, filling only the T_+ sites and leaving the T_- sites empty, is shown below:

- ----- A
- ---b--- T_+
- ----- T_-
- ----- B
- ---c--- T_+
- ----- T_-
- ----- C
- ---a--- T_+
- ----- T_-

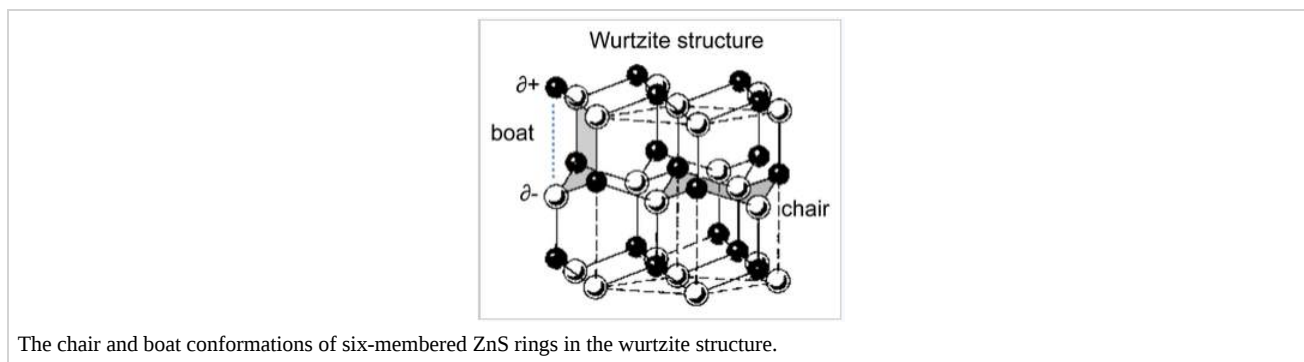


The zincblende unit cell

The wurtzite structure is a close relative of zinc blende, based on filling half the tetrahedral holes in the hcp lattice. Like zincblende, wurtzite contains planes of fused six-membered rings in the chair conformation. Unlike zincblende, however, the rings

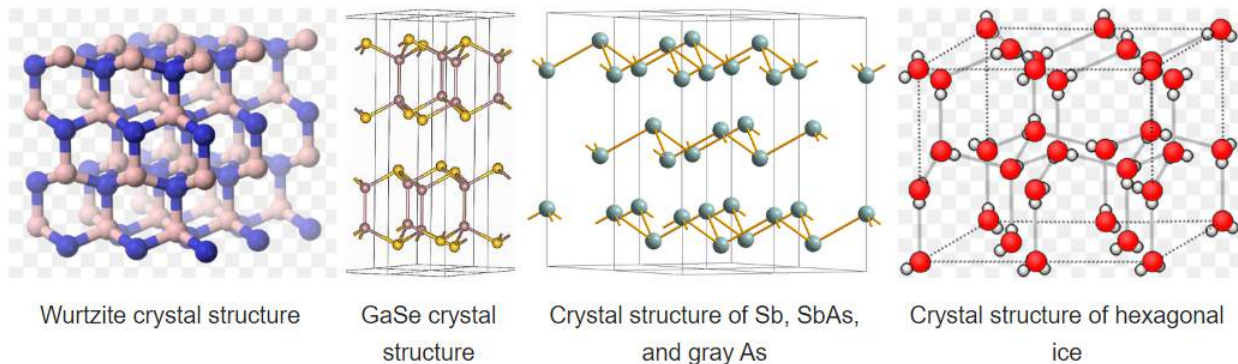
joining these planes contain six-membered "boat" rings. The boat aligns the anions so that they are directly above the cations in the structure, a less favorable situation sterically but a more favorable one in terms of electrostatics. As a result, the wurtzite structure tends to favor more polar or ionic compounds (e.g., ZnO, NH_4^+F^-) than the zincblende structure. As with zincblende, both ions are in tetrahedral (4:4) coordination and there are typically eight valence electrons in the MX compound. Examples of compounds with this structure include: BeO, ZnO, MnS, CdSe, MgTe, AlN, and NH_4F . The layered structure of wurtzite is AbBaAbB and the layer sequence with T_+ sites filled is illustrated below:

- ----- A
- --b--- T_+
- ----- T_-
- ----- B
- --a--- T_+
- ----- T_-
- ----- A
- --b--- T_+
- ----- T_-
- ----- B



An interesting consequence of the layer stacking in the wurtzite structure is that the crystals are polar. When cleaved along the c -axis (the stacking axis), crystals of ZnO, ZnS, and GaN have one negatively charged face and an opposite positively charged face. An applied electric field interacts with the crystal dipole, resulting in compression or elongation of the lattice along this direction. For this reason crystals of compounds in the wurtzite structure are typically piezoelectric.

Some compounds are diamorphic and can have either the zincblende or wurtzite structure. Examples of these compounds that have intermediate polarities include CdS and ZnS. SiO_2 exists in polymorphs (cristobalite and tridymite) that resemble zincblende and wurtzite with O atoms midway between each of the Si atoms. The zincblende and wurtzite structures have efficient packing arrangements for tetrahedrally bonded networks and are commonly found in compounds that have tetrahedral bonding. Water, for example, has a tetrahedral hydrogen bonding network and is wurtzite-type. The undistorted wurtzite and zinc blende structures are typically found for AX compounds with eight valence electrons, which follow the octet rule. AX compounds with nine or ten electrons such as GaSe and GaAs crystallize in distorted variants of the wurtzite structure. In GaSe, the extra electrons form lone pairs and this creates layers in the structure, as can be seen in the figure below. To the right of GaSe, the structures of As, Sb, and SbAs show an ever further breakdown of the structure into layers as more valence electrons are added.



Hexagonal ice is the most stable polymorph of ice, which is obtained upon freezing at 1 atmosphere pressure. This polymorph (ice-I) has a hcp wurtzite-type structure. Looking at the structure shown at the right, we see that there are irregular arrangements of the O-H---O bonds. In the structure, hydrogen bonding enforces the tetrahedral coordination of each water molecule, resulting in a relatively open structure that is less dense than liquid water. For this reason, ice floats in water.

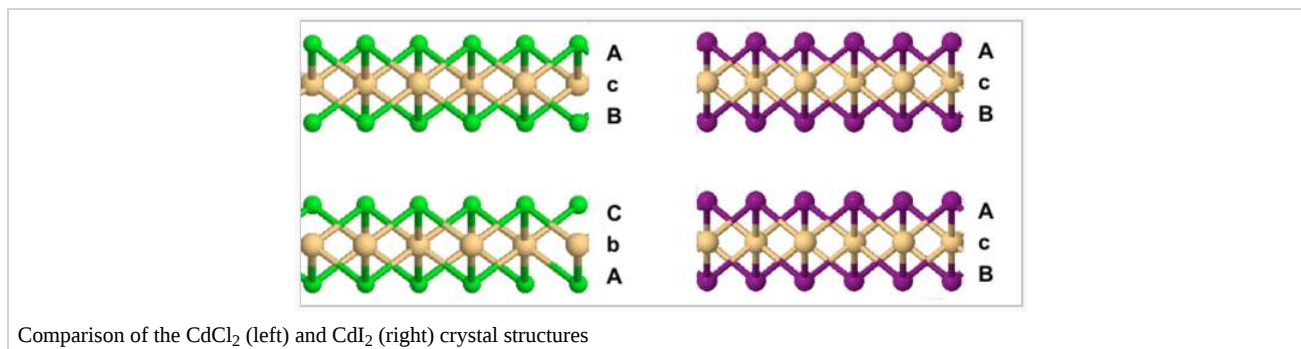
This page titled [8.4: Tetrahedral Structures](#) is shared under a [CC BY-SA 4.0](#) license and was authored, remixed, and/or curated by [Chemistry 310 \(Wikibook\)](#) via [source content](#) that was edited to the style and standards of the LibreTexts platform; a detailed edit history is available upon request.

8.5: Layered Structures and Intercalation Reactions

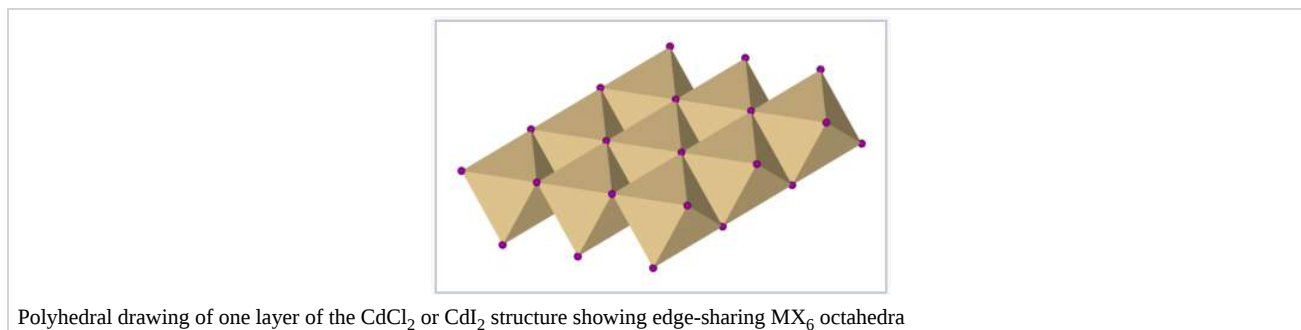
Layered structures are characterized by strong (and typically covalent) bonding between atoms in two dimensions and weaker bonding in the third. A broad range of compounds including metal halides, oxides, sulfides, selenides, borides, nitrides, carbides, and allotropes of some pure elements (B, C, P, As) exist in layered forms. Structurally, the simplest of these structures (for example binary metal halides and sulfides) can be described as having some fraction of the octahedral and/or tetrahedral sites are filled in the fcc and hcp lattices. For example, the CdCl_2 structure is formed by filling all the octahedral sites in alternate layers of the fcc lattice, and the CdI_2 structure is the relative of this structure in the hcp lattice.

In the **CdCl_2 structure**, the stacking sequence of anion layers is ABCABC...

In the **CdI_2 structure**, the anion stacking sequence is ABAB..., and all the cations are eclipsed along the stacking axis.



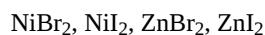
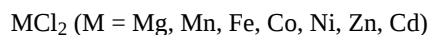
These are examples of **6-3 structures**, because the cations are coordinated by an octahedron of six anions, and the anions are coordinated by three cations to make a trigonal pyramid (like NH_3). Another way to describe these structures is to say that the MX_6 octahedra each share six edges in the MX_2 sheets.



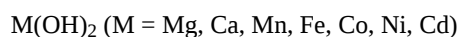
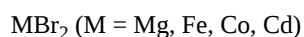
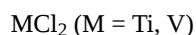
Because these structures place the packing atoms (the anions) in direct van der Waals contact, they are most stable for relatively **covalent** compounds. Otherwise, the electrostatic repulsion between contacting anions would destabilize the structure energetically. More ionic MX_2 compounds tend to adopt the fluorite (CaF_2) or rutile (TiO_2) structures, which are not layered.

Despite the fact that these two structure types are the same at the level of nearest and next-nearest neighbor ions, the CdI_2 structure is much more common than the CdCl_2 structure.

CdCl_2 structure:



CdI_2 structure:



MS_2 (M = Ti, Zr, Sn, Ta, Pt)

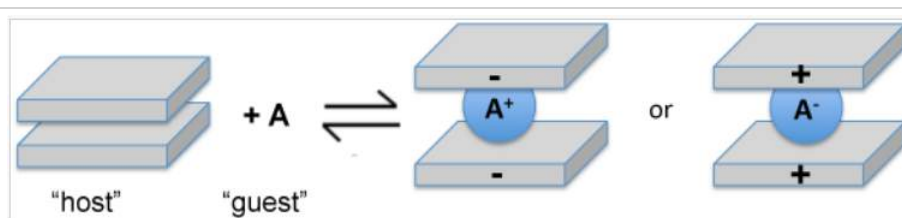
MSe_2 (M = Ti, Zr, Sn, V, Pt)

MTe_2 (M = Ti, Co, Ni, Rh, Pd, Pt)

Physically, layered compounds are **soft** and **slippery**, because the layer planes slide past each other easily. For example, graphite, MoS_2 , and talc (a silicate) are layered compounds that are used widely as **lubricants** and lubricant additives.

An important reaction of layered compounds is **intercalation**. In intercalation reactions, guest molecules and ions enter the galleries that separate the sheets, usually with expansion of the lattice along the stacking axis. This reaction is typically reversible if it does not perturb the bonding within the sheets. Often the **driving force for intercalation is a redox reaction**, i.e., electron transfer between the host and guest. For example, lithium metal reacts with TiS_2 , MoS_2 , and graphite to produce $LiTiS_2$, Li_xMoS_2 ($x < 1$), and LiC_6 . In these compounds, lithium is ionized to Li^+ and the sheets are negatively charged. Oxidizing agents such as Br_2 , $FeCl_3$, and AsF_5 also react with graphite. In the resulting intercalation compounds, the sheets are positively charged and the intercalated species are anionic.

Intercalation reactions are especially important for electrochemical energy storage in **secondary batteries**, such as **lithium ion** batteries, **nickel-metal hydride** batteries, and **nickel-cadmium** batteries. The reversible nature of the intercalation reaction allows the electrodes to be charged and discharged up to several thousand times without losing their mechanical integrity. In lithium ion batteries, the negative electrode material is typically graphite, which is intercalated by lithium to make LiC_6 . Several different oxides and phosphates containing redox active transition metal ions (Mn, Fe, Co, Ni) are used as the positive electrode materials.



Oxidative or reductive intercalation involves the placement of anions or cations between sheets.

Lithium ion batteries based on CoO_2 were first described in 1980^[1] by John B. Goodenough's research group at Oxford. In batteries based on CoO_2 , which has the CdI_2 structure, the positive electrode half-reaction is:



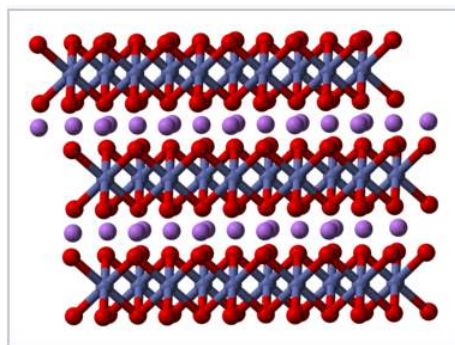
The negative electrode half reaction is:



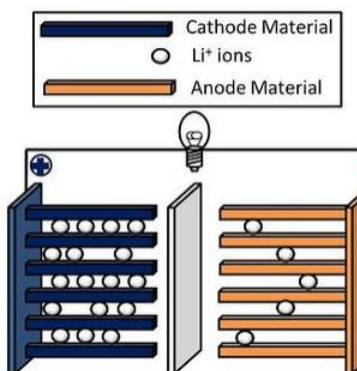
The battery is fully charged when the positive electrode is in the CoO_2 form and the negative electrode is in the LiC_6 form. Discharge involves the motion of Li^+ ions through the electrolyte, forming Li_xCoO_2 and graphite at the two electrodes.



Blue plaque erected by the Royal Society of Chemistry commemorating the development of cathode materials for the lithium-ion battery



Crystal structure of LiCoO_2 ^[2]



The lithium ion battery is a "rocking chair" battery, so named because charging and discharging involve moving Li^+ ions from one side to the other. CoO_2 is one example of a positive electrode material that has been used in lithium ion batteries. It has a high energy density, but batteries based on CoO_2 have poor thermal stability. Safer materials include lithium iron phosphate (LiFePO_4), and LiMO_2 (M = a mixture of Co, Mn, and Ni). These batteries are used widely in laptop computers, portable electronics, cellular telephones, cordless tools, and electric and hybrid vehicles.

A similar intercalation reaction occurs in nickel-cadmium batteries and nickel-metal hydride batteries, except in this case the reaction involves the movement of protons in and out of the Ni(OH)_2 lattice, which has the CdI_2 structure:

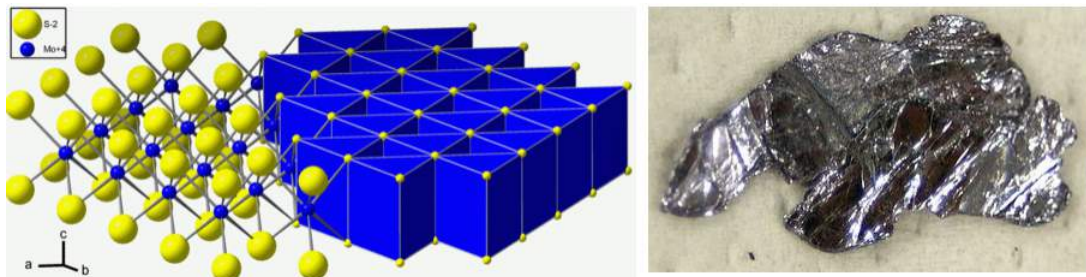


There are many layered compounds that cannot be intercalated by redox reactions, typically because some other stable product is formed. For example, the reaction of layered CdI_2 with Li produces LiI (NaCl structure) and Cd metal.

This page titled [8.5: Layered Structures and Intercalation Reactions](#) is shared under a [CC BY-SA 4.0](#) license and was authored, remixed, and/or curated by [Chemistry 310 \(Wikibook\)](#) via [source content](#) that was edited to the style and standards of the LibreTexts platform; a detailed edit history is available upon request.

8.6: Bonding in TiS_2 , MoS_2 , and Pyrite Structures

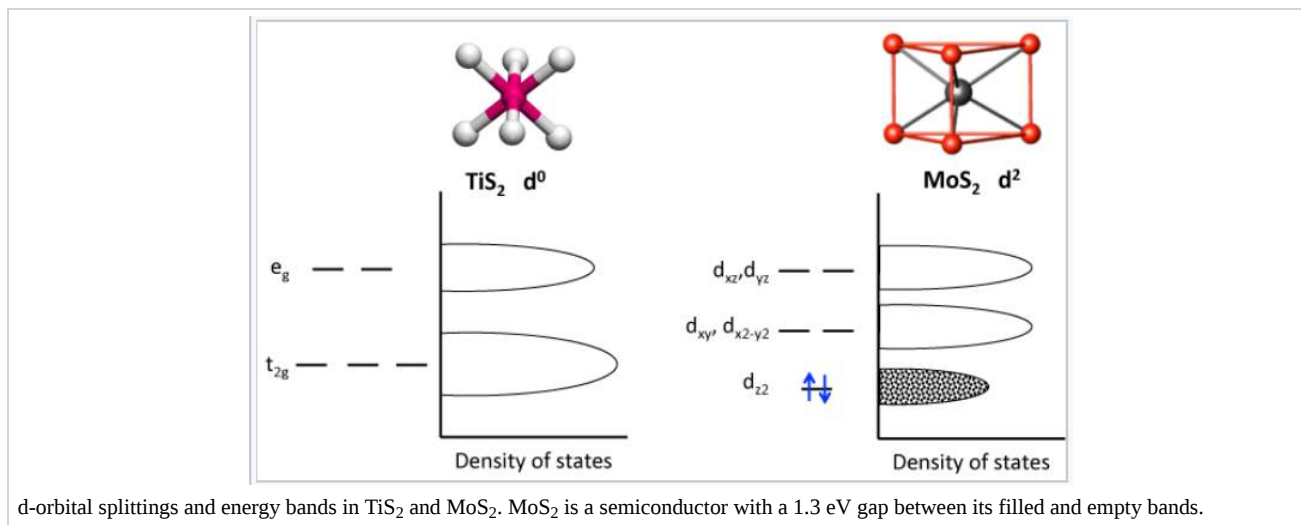
Many layered dichalcogenides, such as TiS_2 and ZrS_2 , have the CdI_2 structure. In these compounds, as we have noted above, the metal ions are octahedrally coordinated by S. Interestingly, the structures of MoS_2 and WS_2 , while they are also layered, are different. In these cases, the metal is surrounded by a **trigonal prism** of sulfur atoms. NbS_2 , TaS_2 , MoSe_2 , MoTe_2 , and WSe_2 also have the trigonal prismatic molybdenite structure, which is shown below alongside a platy crystal of MoS_2 .



The coordination of the metal ions by a trigonal prism of chalcogenide ions is **sterically unfavorable** relative to octahedral coordination. There are close contacts between the chalcogenide ions, which are eclipsed in the stacking sequence **AbA/BaB/AbA/BaB...** (where "/" indicates the van der Waals gap between layers). What stabilizes this structure?

The molybdenite structure occurs most commonly in MX_2 compounds with a **d^1 or d^2 electron count**. The figure below compares the splitting of d-orbital energies in the octahedral and trigonal prismatic coordination environments:

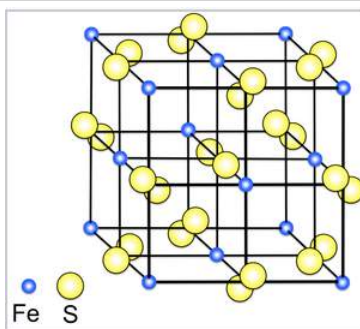
The trigonal prismatic structure is stabilized in MoS_2 by filling the lowest energy band, the d_{z^2} . The d_{z^2} orbital which points vertically through the triangular top and bottom faces of the trigonal prism, has the least interaction with the sulfide ligands and therefore the lowest energy. The d_{xz} and d_{yz} orbitals, which point at the ligands, have the highest energy. The d_{z^2} orbital is lower in energy in this structure than the t_{2g} orbitals are in the octahedral structure of TiS_2 .



Because it has an unfilled t_{2g} band, TiS_2 is relatively easy to reduce by intercalation with Li. For this reason, LiTiS_2 was one of the first intercalation compounds studied by Stanley Whittingham, who developed the concept of the non-aqueous lithium ion battery in the early 1970's.^[3] Because it has a filled d_{z^2} band, MoS_2 is harder to reduce, but it can be intercalated by reaction with the powerful reducing agent n-butyllithium to make Li_xMoS_2 ($x < 1$). Atoms in the van der Waals planes of these compounds are relatively unreactive, which gives MoS_2 its good oxidative stability and enables its application as a high temperature lubricant. Atoms at the edges of the crystals are however more reactive and in fact are catalytic. High surface area MoS_2 , which has a high density of exposed edge planes, is used as a hydrodesulfurization catalyst and is also of increasing interest as an electrocatalyst for the reduction of water to hydrogen.

Layered metal dichalcogenides, including MoS_2 , WS_2 , and SnS_2 , can form closed nanostructures that take the shape of multiwalled onions and multiwalled tubes. These materials were discovered by the group of Reshef Tenne in 1992, shortly after the discovery of

carbon nanotubes. Since then nanotubes have been synthesized from many other materials, including vanadium and manganese oxides.



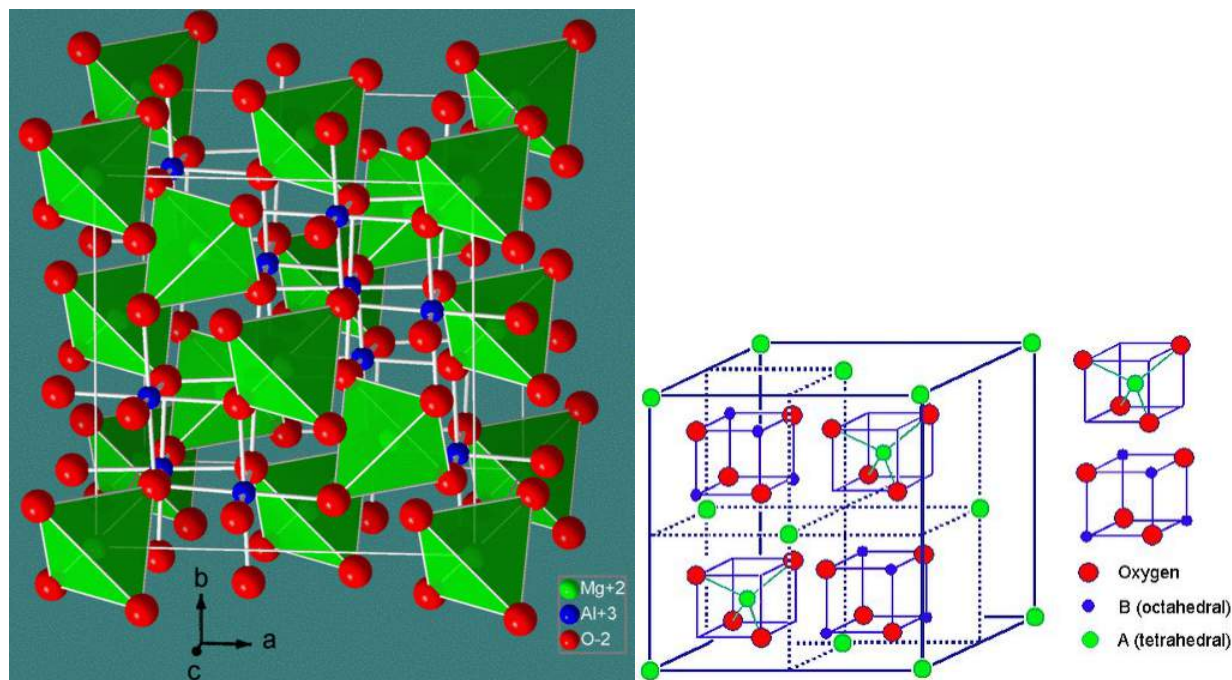
The pyrite (FeS_2) crystal structure. The structure is related to NaCl, with Fe^{2+} and S_2^{2-} ions occupying the cation and anion sites.

Although early (TiS_2) and late (PtS_2) transition metal disulfides have layered structures, a number of MS_2 compounds in the middle of the transition series, such as MnS_2 , FeS_2 and RuS_2 , have three-dimensionally bonded structures. For example, FeS_2 has the **pyrite structure**, which is related to the NaCl structure. The reason is that FeS_2 is not $\text{Fe}^{4+}(\text{S}^{2-})_2$, but is actually $\text{Fe}^{2+}(\text{S}_2^{2-})$, where S_2^{2-} is the disulfide anion (which contains a single bond like the peroxide anion O_2^{2-}). S^{2-} is too strong a reducing agent to exist in the same compound with Fe^{4+} , which is a strong oxidizing agent. Because FeS_2 is actually $\text{Fe}^{2+}(\text{S}_2^{2-})$, it is a 1:1 compound and adopts a 1:1 structure.

This page titled [8.6: Bonding in \$\text{TiS}_2\$, \$\text{MoS}_2\$, and Pyrite Structures](#) is shared under a [CC BY-SA 4.0](#) license and was authored, remixed, and/or curated by [Chemistry 310 \(Wikibook\)](#) via [source content](#) that was edited to the style and standards of the LibreTexts platform; a detailed edit history is available upon request.

8.7: Spinel, Perovskite, and Rutile Structures

There are three more structures, which are derived from close-packed lattices, that are particularly important because of the material properties of their compounds. These are the **spinel** structure, on which ferrites and other magnetic oxides are based, the **perovskite** structure, which is adopted by ferroelectric and superconducting oxides, and the **rutile** structure, which is a common binary 6:3 structure adopted by oxides and fluorides.

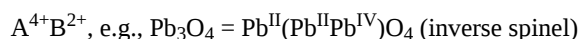
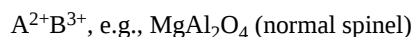


The **spinel structure** is formulated MM'_2X_4 , where M and M' are tetrahedrally and octahedrally coordinated cations, respectively, and X is an anion (typically O or F). The structure is named after the mineral $MgAl_2O_4$, and oxide spinels have the general formula AB_2O_4 .

In the **normal spinel** structure, there is a close-packed array of anions. The A-site cations fill 1/8 of the tetrahedral holes and the B-site cations fill 1/2 of the octahedral holes. A polyhedral view of the normal spinel unit cell is shown at the left, and a simplified view (with the contents of the back half of the cell removed for clarity) is shown above. Each unit cell contains eight formula units and has a composition $A_8B_{16}O_{32}$.

Inverse spinels have a closely related structure (with the same large unit cell) in which the A-site ions and half of the B-site ions switch places. Inverse spinels are thus formulated $B(AB)O_4$, where the AB ions in parentheses occupy octahedral sites, and the other B ions are on tetrahedral sites. There are also mixed spinels, which are intermediate between the **normal** and **inverse** spinel structure.

Some spinel and inverse spinel AB combinations are:

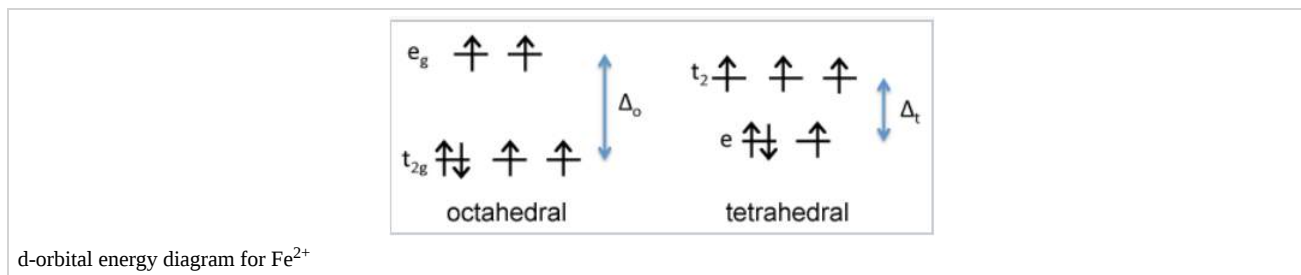


Many magnetic oxides, such as Fe_3O_4 and $CoFe_2O_4$, are spinels.

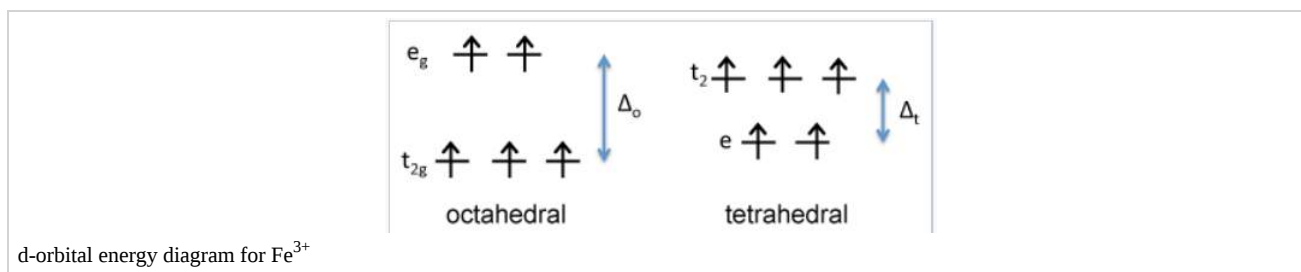
Normal vs. inverse spinel structure

For transition metal oxide spinels, the choice of the normal vs. inverse spinel structure is driven primarily by the **crystal field stabilization energy** (CFSE) of ions in the tetrahedral and octahedral sites. For spinels that contain 3d elements such as Cr, Mn, Fe, Co, and Ni, the electron configuration is typically **high spin** because O^{2-} is a **weak field ligand**.

As an example, we can consider magnetite, Fe_3O_4 . This compound contains one Fe^{2+} and two Fe^{3+} ions per formula unit, so we could formulate it as a normal spinel, $\text{Fe}^{2+}(\text{Fe}^{3+})_2\text{O}_4$, or as an inverse spinel, $\text{Fe}^{3+}(\text{Fe}^{2+}\text{Fe}^{3+})\text{O}_4$. Which one would have the lowest energy?



First we consider the crystal field energy of the Fe^{2+} ion, which is d^6 . Comparing the tetrahedral and high spin octahedral diagrams, we find that the CFSE in an **octahedral** field of O^{2-} ions is $[(4)(\frac{2}{5}) - (2)(\frac{3}{5})]\Delta_o - P = 0.4\Delta_o - P$. In the **tetrahedral** field, the CFSE is $[(3)(\frac{3}{5}) - (3)(\frac{2}{5})]\Delta_t - P = 0.6\Delta_t - P$. Since Δ_o is about 2.25 times larger than Δ_t , the octahedral arrangement has a larger CFSE and is preferred for Fe^{2+} .



In contrast, it is easy to show that Fe^{3+} , which is d^5 , would have a CFSE of zero in either the octahedral or tetrahedral geometry. This means that Fe^{2+} has a preference for the octahedral site, but Fe^{3+} has no preference. Consequently, we place Fe^{2+} on octahedral sites and **Fe_3O_4 is an inverse spinel**, $\text{Fe}^{3+}(\text{Fe}^{2+}\text{Fe}^{3+})\text{O}_4$.

Ferrites are compounds of general formula $\text{M}^{\text{II}}\text{Fe}_2\text{O}_4$. We can see that magnetite is one example of a ferrite (with $\text{M} = \text{Fe}$). Other divalent metals ($\text{M} = \text{Mg}, \text{Mn}, \text{Co}, \text{Ni}, \text{Zn}$) also form ferrites. Ferrites can be normal or inverse spinels, or mixed spinels, depending on the CFSE of the M^{II} ion. Based on their CFSE, Fe^{2+} , Co^{2+} , and Ni^{2+} all have a strong preference for the octahedral site, so those compounds are all inverse spinels. ZnFe_2O_4 is a normal spinel because the small Zn^{2+} ion (d^{10}) fits more easily into the tetrahedral site than Fe^{3+} (d^5), and both ions have zero CFSE. MgFe_2O_4 and MnFe_2O_4 , in which all ions have zero CFSE and no site preference, are mixed spinels. **Chromite** spinels, $\text{M}^{\text{III}}\text{Cr}_2\text{O}_4$, are always **normal spinels** because the d^3 Cr^{3+} ion has a strong preference for the octahedral site.

Examples of normal and inverse spinel structures:

MgAl_2O_4 is a **normal spinel** since both Mg^{2+} and Al^{3+} are non-transition metal ions and thus $\text{CFSE} = 0$. The more highly charged Al^{3+} ion prefers the octahedral site, where it is surrounded by six negatively charged oxygen atoms.

Mn_3O_4 is a **normal spinel** since the Mn^{2+} ion is a high spin d^5 system with zero CFSE. The two Mn^{3+} ions are high spin d^4 with higher CFSE on the octahedral sites ($3/5 \Delta_o$) than on the tetrahedral site ($2/5 \Delta_t \sim 1/5 \Delta_o$).

Fe_3O_4 is an **inverse spinel** since the Fe^{3+} ion is a high spin d^5 system with zero CFSE. Fe^{2+} is a high spin d^6 system with more CFSE on an octahedral site than on a tetrahedral one.

NiFe_2O_4 is again an **inverse spinel** since Ni^{2+} (a d^8 ion) prefers the octahedral site and the CFSE of Fe^{3+} (a d^5 ion) is zero.

FeCr_2O_4 is a **normal spinel** since Fe^{2+} is high spin d^6 ion with $\text{CFSE} = [4(\frac{2}{5}) - 2(\frac{3}{5})]\Delta_o = \frac{2}{5}\Delta_o$ on an octahedral site, and Cr^{3+} is a d^3 ion with $\text{CFSE} = 3(2/5)\Delta_o = 6/5\Delta_o$. Hence it is more energetically favorable for Cr^{3+} to occupy both of the octahedral sites.

Co_3O_4 is a **normal spinel**. Even in the presence of weak field oxo ligands, Co^{3+} is a low spin d^6 ion with very high CFSE on the octahedral sites, because of the high charge and small size of the Co^{3+} ion. Hence the Co^{3+} ions occupy both octahedral sites, and Co^{2+} occupies the tetrahedral site.

Magnetism of ferrite spinels

Ferrite spinels are of technological interest because of their magnetic ordering, which can be ferrimagnetic or antiferromagnetic depending on the structure (normal or inverse) and the nature of the metal ions. Fe_3O_4 , CoFe_2O_4 , and NiFe_2O_4 are all inverse spinels and are ferrimagnets. The latter two compounds are used in magnetic recording media and as deflection magnets, respectively.

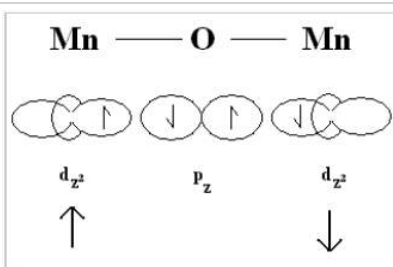
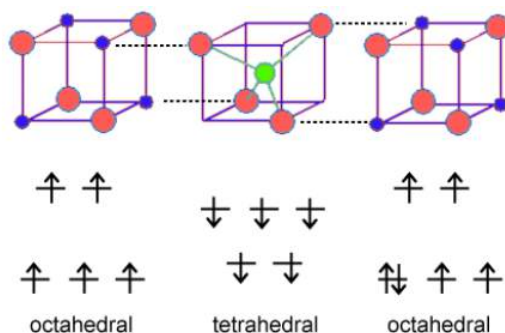


Illustration of antiferromagnetic superexchange between two transition metal cations through a shared oxygen atom.

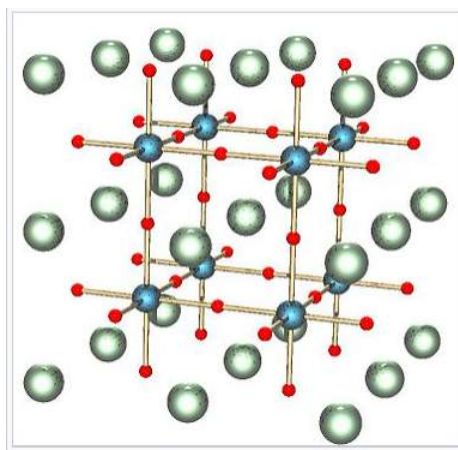
In order to understand the magnetism of ferrites, we need to think about how the unpaired spins of metal ions are coupled in oxides. If an oxide ion is shared by two metal ions, it can mediate the coupling of spins by superexchange as shown at the right. The coupling can be antiferromagnetic, as shown, or ferromagnetic, depending on the orbital filling and the symmetry of the orbitals involved. The **Goodenough-Kanamori rules** predict the local magnetic ordering (ferromagnetic vs. antiferromagnetic) that results from superexchange coupling of the electron spins of transition metal ions. For ferrites, the strongest coupling is between ions on neighboring **tetrahedral and octahedral sites**, and the ordering of spins between these two sites is reliably **antiferromagnetic**.



Because all the tetrahedral and octahedral sites in a spinel or inverse spinel crystal are coupled together identically, it works out that ions on the tetrahedral sites will all have one orientation (e.g., spin down) and ions on all the octahedral sites will have the opposite orientation (e.g., spin up). If the number of spins on the two sites is the same, then the solid will be antiferromagnetic. However, if the **number of spins is unequal** (as in the case of Fe_3O_4 , CoFe_2O_4 , and NiFe_2O_4) then the solid will be **ferrimagnetic**. This is illustrated above for Fe_3O_4 . The spins on the Fe^{3+} sites cancel, because half of them are up and half are down. However, the four unpaired electrons on the Fe^{2+} ions are all aligned the same way in the crystal, so the compound is ferrimagnetic.

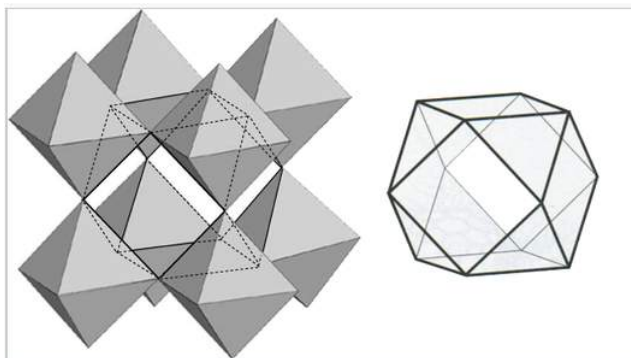
Perovskites are **ternary oxides** of general formula ABO_3 . More generally, the perovskite formula is ABX_3 , where the anion X can be **O, N, or halogen**. The A ions are typically large ions such as Sr^{2+} , Ba^{2+} , Rb^+ , or a lanthanide $3+$ ion, and the B ions are smaller transition metal ions such as Ti^{4+} , Nb^{5+} , Ru^{4+} , etc. The mineral after which the structure is named has the formula CaTiO_3 .

The perovskite structure has simple cubic symmetry, but is related to the fcc lattice in the sense that the A site cations and the three O atoms comprise a fcc lattice. The B-site cations fill 1/4 of the octahedral holes and are surrounded by six oxide anions.



ABX₃ perovskite structure. A, B, and X are white, blue, and red, respectively.

The coordination of the A ions in perovskite and the arrangement of BO₆ octahedra is best understood by looking at the ReO₃ structure, which is the same structure but with the A-site cations removed. In the polyhedral representation of the structure shown at the right, it can be seen that the octahedra share all their vertices but do not share any octahedral edges. This makes the ReO₃ and perovskite structures flexible, like three-dimensional wine racks, in that the octahedra can **rotate and tilt cooperatively**. Eight such octahedra surround a large **cuboctahedral cavity**, which is the site of the A ions in the perovskite structure. Cations in these sites are coordinated by 12 oxide ions, as expected from the relationship between the perovskite and fcc lattices.



Polyhedral representation of the ReO₃ structure showing the large cuboctahedral cavity that is surrounded by 12 oxygen atoms

Because the A-site is empty in the ReO₃ structure, compounds with that structure can be reversibly **intercalated** by small ions such as **Li⁺ or H⁺**, which then occupy sites in the cuboctahedral cavity. For example, smart windows that darken in bright sunlight contain the **electrochromic** material WO₃, which has the ReO₃ structure. In the sunlight, a photovoltaic cell drives the reductive intercalation of WO₃ according to the reaction:

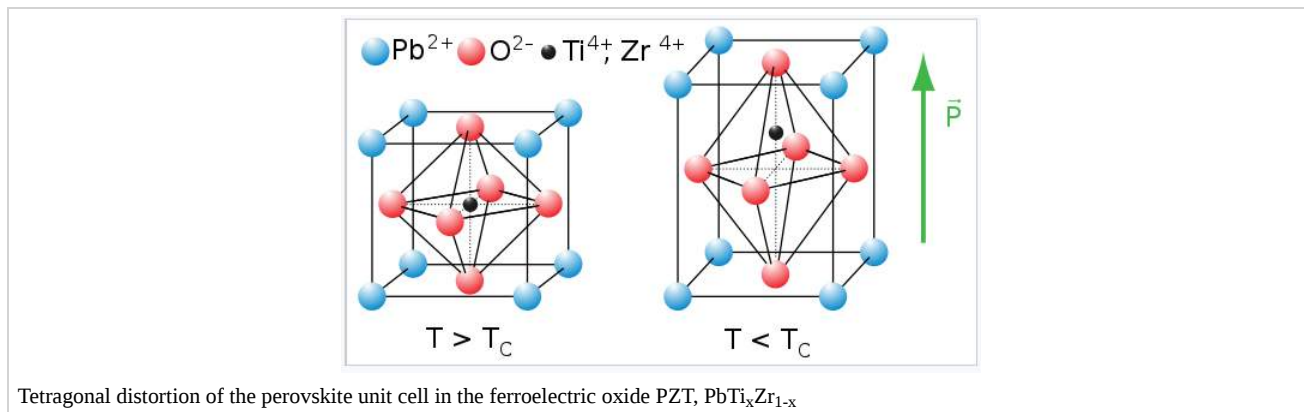


WO₃ is a light yellow compound containing d⁰ W(VI). In contrast, H_xWO₃, which is mixed-valent W(V)-W(VI) = d¹-d⁰, has a deep blue color. Such coloration is typical of mixed-valence transition metal complexes because their d-electrons can be excited to delocalized conduction band levels by red light. Because the electrochemical intercalation-deintercalation process is powered by a solar cell, the tint of the windows can adjust automatically to the level of sunlight.

Ferroelectric perovskites

The flexibility of the network of corner-sharing BO₆ octahedra is also very important in ferroelectric oxides that have the perovskite structure. In some perovskites with small B-site cations, such as Ti⁴⁺ and Nb⁵⁺, the cation is too small to fit symmetrically in the BO₆ octahedron. The octahedron distorts, allowing the cation to move off-center. These distortions can be **tetragonal** (as in the example shown at the right), **rhombohedral**, or **orthorhombic**, depending on whether the cation moves towards a vertex, face, or edge of the BO₆ octahedron. Moving the cation off-center in the octahedron creates an **electric dipole**. In

ferroelectrics, these dipoles align in neighboring unit cells through cooperative rotation and tilting of octahedra. The crystal thus acquires a net electrical polarization.

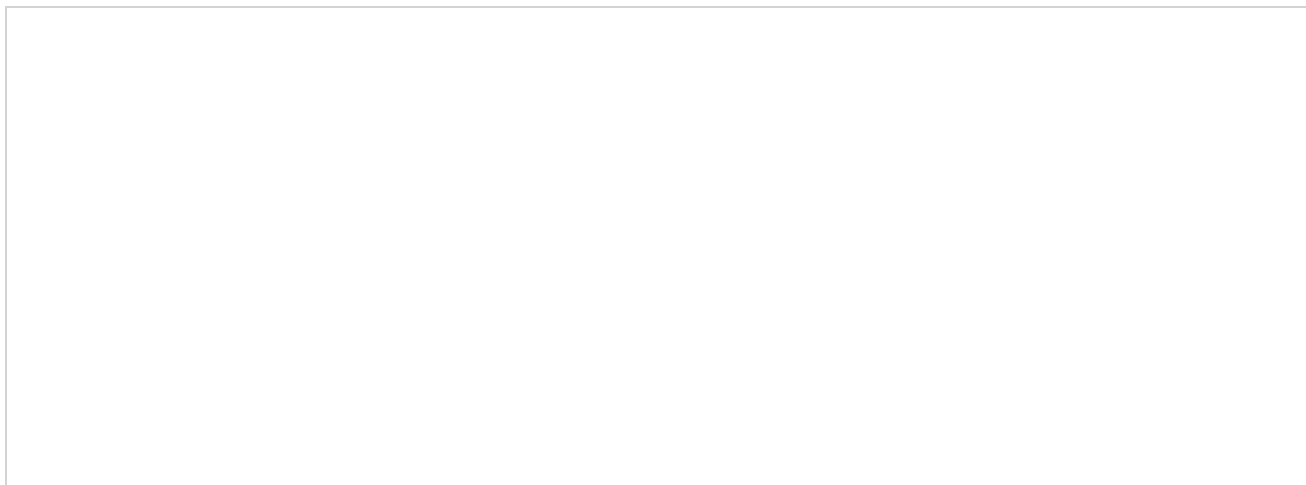


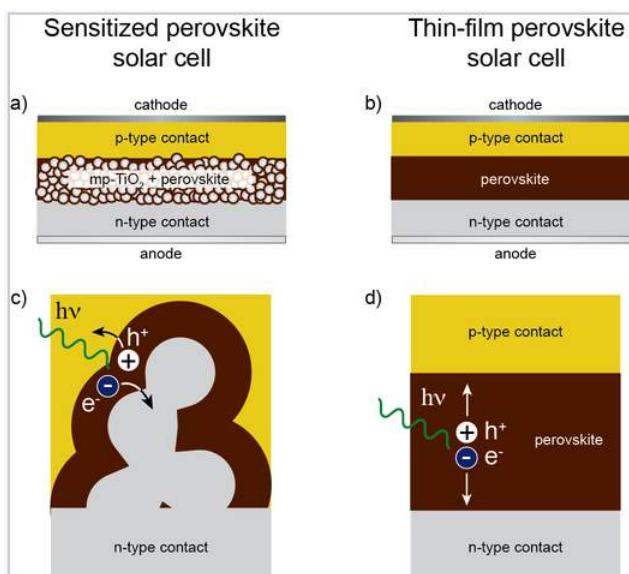
Ferroelectricity behaves analogously to **ferromagnetism**, except that the polarization is electrical rather than magnetic. In both cases, there is a **critical temperature** (T_c) above which the **spontaneous polarization** of the crystal disappears. Below T_c , the electric polarization of a ferroelectric can be switched with a coercive field, and hysteresis loop of polarization vs. field resembles that of a ferromagnet. Above T_c , the crystal is **paraelectric** and has a high dielectric permittivity.

Ferroelectric and paraelectric oxides (along with piezoelectrics and pyroelectrics) have a wide variety of applications as switches, actuators, transducers, and dielectrics for capacitors. **Ferroelectric capacitors** are important in memory devices (FRAM) and in the tuning circuits of cellular telephones. **Multiferroics**, which are materials that are simultaneously ferroelectric and ferromagnetic, are rare and are being now intensively researched because of their potential applications in electrically addressable magnetic memory.

Halide perovskites (ABX_3 , $X = \text{Cl}, \text{Br}, \text{I}$) can be made by combining salts of monovalent A ions ($A^+ = \text{Cs}^+, \text{NH}_4^+, \text{RNH}_3^+$) and divalent metal salts such as PbCl_2 or PbI_2 . These compounds have sparked recent interest as light absorbers for **thin film solar cells** that produce electricity from sunlight. Lead and tin halide perovskites can be grown as thin films from solution precursors or by thermal evaporation at relatively low temperatures. In some lead halide perovskites, the mobility of electrons and holes is very high, comparable to that of more expensive III-V semiconductors such as GaAs, which must be grown as very pure single crystals at high temperatures for use in solar cells. Because of their high carrier mobility, some lead halide perovskites are also electroluminescent and are of interest as inexpensive materials for light-emitting diodes (LEDs).

Tin and lead halide perovskites were first studied in the 1990s as materials for thin film electronics,^[4] and more recently as light absorbers in dye-sensitized solar cells. Soon after the results on dye-sensitized perovskite cells were reported, it was discovered that halide perovskites could also be used in thin film solid state solar cells. The structures of these solar cells are shown schematically at the right. The highest reported solar power conversion efficiencies of perovskite solar cells have jumped from 3.8% in 2009^[5] to 10.2% in 2012^[6] and a certified 20.1% in 2014.^[7] The highest performing cells to date contain divalent lead in the perovskite B cation site and a mixture of methylammonium and formamidinium ions in the perovskite A cation site.

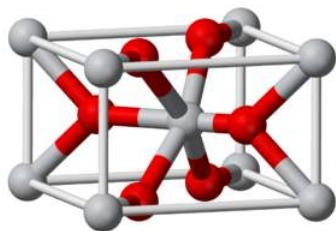




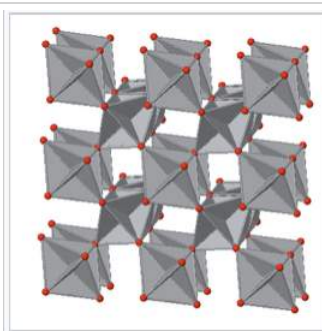
a) Solar cell architecture in which a lead halide perovskite absorber coats a layer of nanocrystalline anatase TiO_2 . b) Thin-film solar cell, with a layer of lead halide perovskite sandwiched between two selective contacts. c) Charge generation and extraction in the sensitized architecture and d) in the thin-film architecture.

Despite their very impressive efficiency, perovskite solar cells are stable for relatively short periods of time and are sensitive to air and moisture. Current research is focused on understanding the degradation mechanisms of these solar cells and improving their stability under operating conditions.

The **rutile structure** is an important MX_2 ($X = \text{O}, \text{F}$) structure. It is a 6:3 structure, in which the cations are octahedrally coordinated by anions, and as such is intermediate in polarity between the CaF_2 (8:4) and SiO_2 (4:2) structures. The mineral rutile is one of the polymorphs of TiO_2 , the others (anatase and brookite) also being 6:3 structures.



The rutile structure can be described as a distorted version of the NiAs structure with half the cations removed. Recall that compounds with the NiAs structure were typically metallic because the metal ions are eclipsed along the stacking axis and thus are in relatively close contact. In rutile, the MO_6 **octahedra share edges** along the tetragonal c-axis, and so some rutile oxides, such as **NbO_2 , RuO_2 and IrO_2** , are also **metallic** because of **d-orbital overlap** along that axis. These compounds are important as electrolyzer catalysts and catalyst supports because they combine high catalytic activity with good electronic conductivity.



View down the tetragonal c-axis of the rutile lattice, showing edge-sharing MO_6 octahedra.

Rutile TiO_2 , because of its high refractive index, is the base pigment for white paint. It is a wide bandgap semiconductor that has also been extensively researched as an electrode for water splitting solar cells and as a photocatalyst (primarily as the anatase polymorph) for degradation of pollutants in air and water. Self-cleaning glass exploits the photocatalytic properties of a thin film of TiO_2 to remove oily substances from the glass surface and improve the wetting properties of the glass.

This page titled [8.7: Spinel, Perovskite, and Rutile Structures](#) is shared under a [CC BY-SA 4.0](#) license and was authored, remixed, and/or curated by [Chemistry 310 \(Wikibook\)](#) via [source content](#) that was edited to the style and standards of the LibreTexts platform; a detailed edit history is available upon request.

8.8: Discussion Questions

- Using the Liverpool 3D visualization website (http://www.chemtube3d.com/solidstate/_table.htm) determine the anion and cation coordination geometries in cadmium chloride and anatase. Describe the arrangement of octahedra (in terms of whether they share edges, faces, etc.) in these structures.
 - Count the number of atoms in the Li_3Bi and ReO_3 unit cells, and determine the coordination environments of each of the ions.
 - Silicon, germanium, and many other semiconductors adopt the diamond (or zincblende) structure. Assuming that all the atoms are the same size, calculate the volume fraction of the unit cell that is occupied by the atoms. How does the filling fraction of diamond compare to simple cubic and close-packed structures, and what does this tell us about the relationship between coordination number and density?
 - Describe the structural basis of ferroelectricity in barium titanate.
-

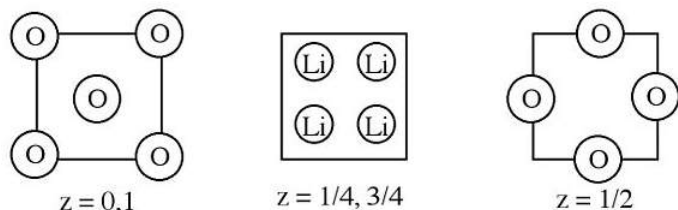
This page titled [8.8: Discussion Questions](#) is shared under a [CC BY-SA 4.0](#) license and was authored, remixed, and/or curated by [Chemistry 310 \(Wikibook\)](#) via [source content](#) that was edited to the style and standards of the LibreTexts platform; a detailed edit history is available upon request.

8.9: Problems

1. For each of the following close packed layer sequences, indicate the name of the structure (structure type), the coordination environment of the cations (represented by lower case letters), and the coordination environment of the anions (upper case letters). Give two additional examples (apart from the structure type itself) of compounds with the same structure.

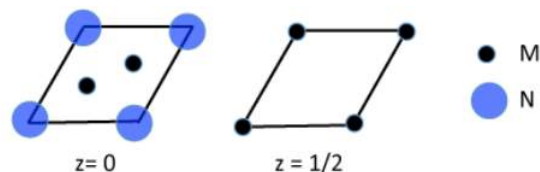
- AbBaAbBaAbB.....
- AaBbCcAaBbCc.....
- AcBaCbAcBaCb.....
- AcB | AcB | AcB | ("|" = van der Waals gap)

2. Below are sections of the lithium oxide unit cell.



- Describe how to obtain (and do obtain) the empirical formula.
- What is the coordination number and geometry for each type of ion?
- Which atom is close-packed?
- What type and fraction of holes are filled by the other ion?

3. The hexagonal unit cell of a metal nitride is shown below in sections.

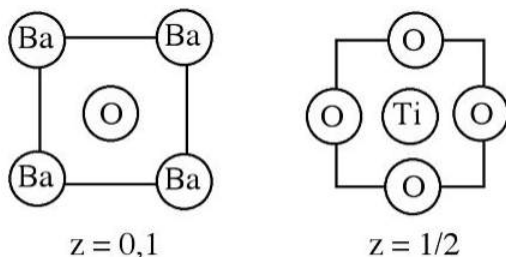


- What is the empirical formula of the compound?
- How many M atoms are coordinated to each N atom?
- In what group of the periodic table would you expect to find M?

4. Draw the cubic Li_3Bi unit cell in sections.

5. If half the cesium is removed from the CsCl structure, such that each Cl atom is then tetrahedrally coordinated, what structure type is generated?

6. The crystal structure of barium titanate is shown below.



- What is the empirical formula of the compound?
- Which atoms (if any) are close packed?

(c) How many oxygen atoms coordinate (i) Ti^{4+} and (ii) Ba^{2+} ?

(d) Why are the coordination numbers are different?

7. The structures of the disulfides (MS_2) show an apparently unusual trend, proceeding from left to right across the transition series. On the left side (TiS_2 , ZrS_2 , MoS_2 , etc.), one finds layered structures, whereas in the middle (ReS_2 , FeS_2 , RuS_2) there are three-dimensional pyrite- and marcasite-type structures. On the right (PtS_2 , SnS_2), there are again layered structures. Briefly explain these trends.

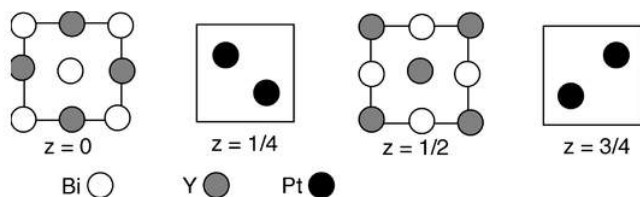
8. Explain why ionic compounds rarely have layered crystal structures.

9. Draw the zinblende structure in sections.

10. The zinblende structure is rarely found with very polar or ionic compounds. However, some polar and ionic compounds (BeO , NH_4F , etc.) have the wurtzite structure.

(a) Describe the similarities and the differences between the zinblende and wurtzite structures (in terms of coordination numbers, stacking sequence of cations and anions, etc.) (b) Why is wurtzite more ionic than zinblende?

11. A recent article by R. Cava and co-workers (*Nature Materials* 2010, 9, 546-9) describes the unusual electronic properties of a Y-Pt-Bi alloy, the structure of which is shown in sections below:



(a) What is the stoichiometry of the compound?

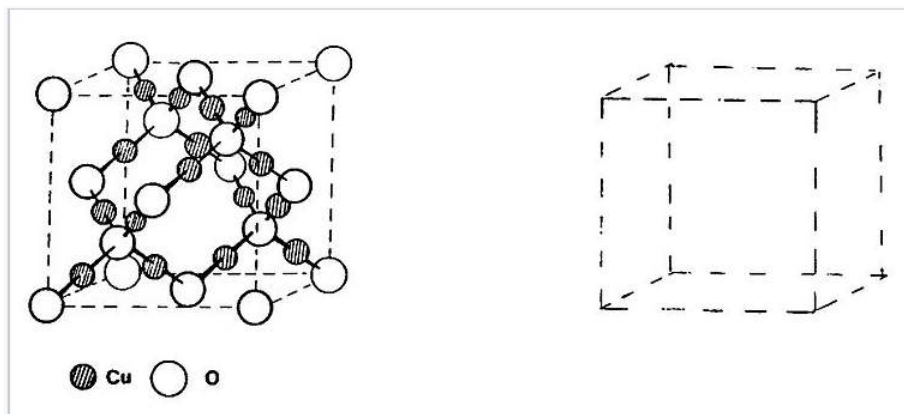
(b) How many Y and how many Pt atoms coordinate each Bi atom?

12. The fluorite structure, CaF_2 , which is generated by filling all the tetrahedral holes in a FCC array, is a common MX_2 structure type.

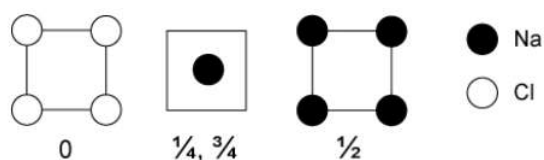
(a) What is the coordination environment of F in a hypothetical relative of CaF_2 , in which Ca forms a hcp array and F occupies all the tetrahedral sites?

(b) Suggest a reason why the structure described in (a) is very rare.

13. The cuprite (Cu_2O) structure is related to zinblende (or diamond) in that oxygen occupies both the Zn and S positions, with copper in between. This is shown schematically at the right. Actually, in cuprite there are two such interpenetrating networks with no bonds between them. Draw the second network in the empty cell. If you put the two halves together and take out the copper, what cubic packing lattice do you get? Is it a closest packing lattice? (*Hint #1*: start with an O atom at $1/2, 1/2, 1/2$) (*Hint #2*: try this in pencil first)



14. Draw the rutile structure in sections of the unit cell, and verify that the stoichiometry is MX_2 . What are the coordination numbers of Ti and O?
15. Stishovite is a high pressure form of SiO_2 found in meteorite craters. While normal SiO_2 has the quartz structure, in which each Si is coordinated by four O atoms, stishovite has the rutile structure. Would you expect the Si-O bond to be longer in stishovite, or in quartz? What is the bond order in each polymorph?
16. Na and Cl combine in a 1:1 ratio to make the ionic NaCl lattice. Interestingly, recent theoretical predictions (confirmed by high pressure synthesis and crystallography) have identified several other stoichiometries that form stable crystals at high pressure. These include Na_3Cl , Na_2Cl , Na_3Cl_2 , NaCl_3 , and several others.^[8] The structure of one of these new sodium chlorides is shown below in sections.



- a) What is the stoichiometry of this compound?
- b) What are the coordination numbers of Na and Cl, and how do they compare to the coordination numbers in NaCl and Na metal?
- c) Based on your answer to (b), explain why high pressure should stabilize this phase.
17. One of the new compounds discovered in the study described in problem 16 is NaCl_3 . There are two polymorphs of this compound, one of which contains linear Cl_3^- ions. Accurate molecular orbital calculations indicate that the charge on the central Cl atom in these linear anions is close to zero. Draw a valence bond structure for the Cl_3^- ion that is consistent with these observations. Would you expect the Cl-Cl bond to be longer or shorter than the bond in Cl_2 ?
18. Some MX salts can exist in either the CsCl or NaCl structure. Use the Pauling formula to predict the M-X bond length in the CsCl structure of a compound that has a bond length of 3.5 Å in the NaCl structure. Would applying a high pressure stabilize the CsCl form, or the NaCl form of this compound? (*hint*: calculate the volume per formula unit)
19. Mn_3O_4 and Fe_3O_4 are both mixed-valence oxides. In both cases, there is one M^{2+} ion and two M^{3+} ions per formula unit (M = Fe, Mn).
- (a) One of these is a normal spinel and one is an inverse spinel. Explain which is which, and why. (*hint*: think about CFSE's)
- (b) For Mn_3O_4 , what kind of magnetic ordering (ferri-, ferro-, or antiferromagnetic) would you expect, and why? You can assume that neighboring tetrahedral and octahedral ions in the structure are antiferromagnetically coupled.
- (c) Sketch the approximate form of the χ vs. T and $1/\chi$ vs. T curves for Mn_3O_4 . Label any special values of temperature on your graphs.
20. Predict whether each of the following should form a normal or inverse spinel: MgV_2O_4 , VMg_2O_4 , NiGa_2O_4 , ZnCr_2S_4 , NiFe_2O_4 . Would kind of magnetic ordering (ferro-, ferri-, or antiferromagnetic) would you predict for NiFe_2O_4 ?

This page titled [8.9: Problems](#) is shared under a [CC BY-SA 4.0](#) license and was authored, remixed, and/or curated by [Chemistry 310 \(Wikibook\)](#) via [source content](#) that was edited to the style and standards of the LibreTexts platform; a detailed edit history is available upon request.

8.10: References

1. K. Mizushima, P.C. Jones, P.J. Wiseman, J.B. Goodenough (1980). "Li_xCoO₂(0<x<1): A New Cathode Material for Batteries of High Energy Density". *Materials Research Bulletin* **15**: 783–789. doi:[10.1016/0025-5408\(80\)90012-4](https://doi.org/10.1016/0025-5408(80)90012-4).
 2. Yang Shao-Horn, Laurence Croguennec, Claude Delmas, E. Chris Nelson and Michael A. O'Keefe (July 2003). "Atomic resolution of lithium ions in LiCoO₂". *Nature Materials* **2** (7): 464–467. doi:[10.1038/nmat922](https://doi.org/10.1038/nmat922). PMID [12806387](https://pubmed.ncbi.nlm.nih.gov/12806387/).
 3. M. Stanley Whittingham "Lithium Batteries and Cathode Materials" Chem. Rev., 2004, vol. 104, pp. 4271–4302. DOI: [10.1021/cr020731c](https://doi.org/10.1021/cr020731c)
 4. Kagan, Cherie R.; Mitzi, David B.; Dimitrakopoulos, C. D. (1999). "Organic-inorganic hybrid materials as semiconducting channels in thin-film field-effect transistors". *Science* **286**: 945-947. doi:[10.1126/science.286.5441.945](https://doi.org/10.1126/science.286.5441.945).
 5. Kojima, Akihiro; Teshima, Kenjiro; Shirai, Yasuo; Miyasaka, Tsutomu (6 May 2009). "Organometal Halide Perovskites as Visible-Light Sensitizers for Photovoltaic Cells". *Journal of the American Chemical Society* **131** (17): 6050–6051. doi:[10.1021/ja809598r](https://doi.org/10.1021/ja809598r). PMID [19366264](https://pubmed.ncbi.nlm.nih.gov/19366264/).
 6. Chung, In; Lee, Byunghong; He, Jiaking; Chang, Robert P. H.; Kanatzidis, Mercouri G. (24 May 2012). "All-solid-state dye-sensitized solar cells with high efficiency". *Nature* **485**: 486-489. doi:[10.1038/nature11067](https://doi.org/10.1038/nature11067).
 7. IEEE Spectrum, [Perovskite Solar Cell Bests Bugbears, Reaches Record Efficiency](#), 7 January 2015
 8. W. Zhang et al. (2013), "Unexpected Stable Stoichiometries of Sodium Chlorides." *Science*, vol. 342, no. 6165, pp. 1502-1505. doi: [10.1126/science.1244989](https://doi.org/10.1126/science.1244989)
-

This page titled [8.10: References](#) is shared under a [CC BY-SA 4.0](#) license and was authored, remixed, and/or curated by [Chemistry 310 \(Wikibook\)](#) via [source content](#) that was edited to the style and standards of the LibreTexts platform; a detailed edit history is available upon request.

CHAPTER OVERVIEW

9: Ionic and Covalent Solids - Energetics

Learning Objectives

- Understand the geometric basis of radius ratio rules.
- Understand the chemical basis of structure maps and why they are better predictors of crystal structures than radius ratios.
- Use the Born-Mayer and Kapustinskii equations to calculate lattice energies of known and hypothetical compounds.
- Construct Born-Haber cycles using lattice energies and calculate unknown quantities in the cycles.
- Predict the stabilities of low and high oxidation states using lattice energies.
- Understand the quantum mechanical origin of the extra "resonance" stability of metals.
- Predict trends in the solubility and thermal stability of inorganic compounds using lattice energies.

In Chapter 8, we learned all about crystal structures of **ionic compounds**. A good question to ask is, *what makes a compound choose a particular structure?* In addressing this question, we will learn about the forces that hold crystals together and the relative energies of different structures. This will in turn help us understand in a more quantitative way some of the heuristic concepts we have learned about in earlier chapters, such as hard-soft acid-base theory.

[9.1: Ionic Radii and Radius Ratios](#)

[9.2: Structure Maps](#)

[9.3: Energetics of Crystalline Solids- The Ionic Model](#)

[9.4: Born-Haber Cycles for NaCl and Silver Halides](#)

[9.5: Kapustinskii Equation](#)

[9.6: Discovery of Noble Gas Compounds](#)

[9.7: Stabilization of High and Low Oxidation States](#)

[9.8: Alkalides and Electrides](#)

[9.9: Resonance Energy of Metals](#)

[9.10: Prelude to Ionic and Covalent Solids - Energetics](#)

[9.11: The Strange Case of the Alkali Oxides](#)

[9.12: Lattice Energies and Solubility](#)

[9.13: Discussion Questions](#)

[9.14: Problems](#)

[9.15: References](#)

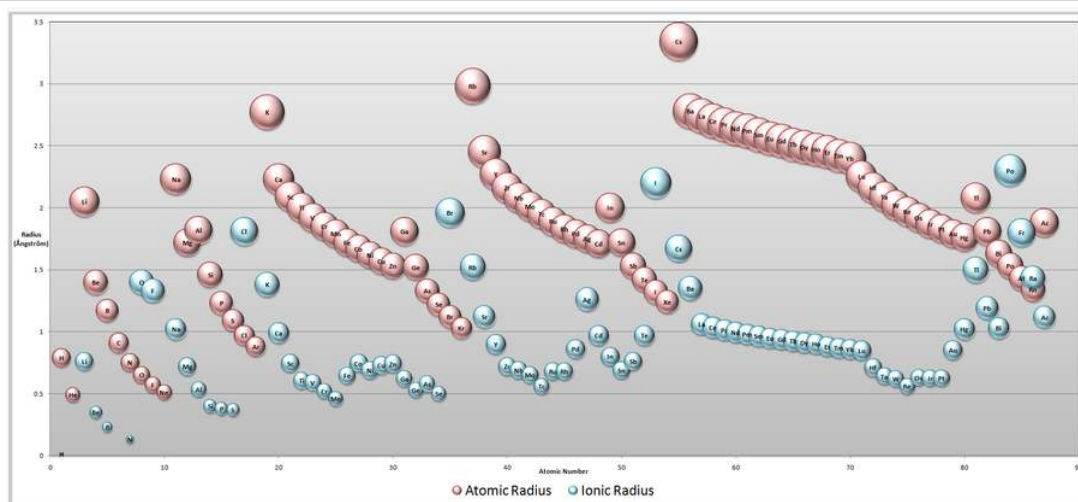
This page titled [9: Ionic and Covalent Solids - Energetics](#) is shared under a [CC BY-SA 4.0](#) license and was authored, remixed, and/or curated by [Chemistry 310 \(Wikibook\)](#) via [source content](#) that was edited to the style and standards of the LibreTexts platform; a detailed edit history is available upon request.

9.1: Ionic Radii and Radius Ratios

Atoms in crystals are held together by electrostatic forces, van der Waals interactions, and covalent bonding. It follows that arrangements of atoms that can maximize the strength of these attractive interactions should be most favorable and lead to the most commonly observed crystal structures.

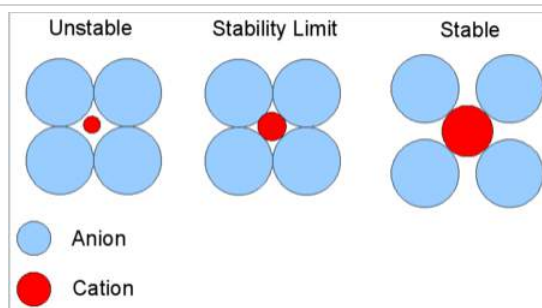
Radius ratio rules

Early crystallographers had trouble solving the structures of inorganic solids using X-ray diffraction because some of the mathematical tools for analyzing the data had not yet been developed. Once a trial structure was proposed, it was relatively easy to calculate the diffraction pattern, but it was difficult to go the other way (from the diffraction pattern to the structure) if nothing was known *a priori* about the arrangement of atoms in the unit cell. It was (and still is!) important to develop some guidelines for guessing the coordination numbers and bonding geometries of atoms in crystals. The first such rules were proposed by Linus Pauling, who considered how one might pack together oppositely charged spheres of different radii. Pauling proposed from geometric considerations that the quality of the "fit" depended on the **radius ratio** of the anion and the cation.



Atomic and Ionic Radii. Note that cations are always smaller than the neutral atom (pink) of the same element, whereas anions are larger. Going from left to right across any row of the periodic table, neutral atoms and cations contract in size because of increasing nuclear charge. (click for larger image)

The basic idea of radius ratio rules is illustrated at the right. We consider that the anion is the packing atom in the crystal and the smaller cation fills interstitial sites ("holes"). Cations will find arrangements in which they can contact the largest number of anions. If the cation can touch all of its nearest neighbor anions, as shown at the right for a small cation in contact with larger anions, then the fit is good. If the cation is too small for a given site, that coordination number will be unstable and it will prefer a lower coordination structure. The table below gives the ranges of cation/anion radius ratios that give the best fit for a given coordination geometry.



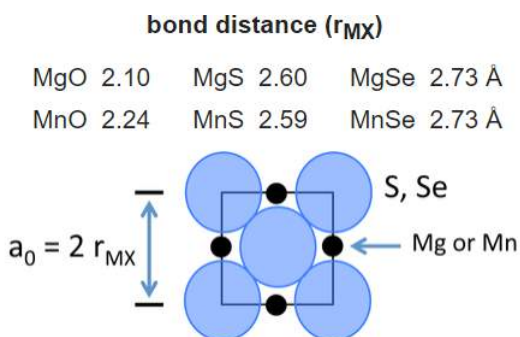
Critical Radius Ratio. This diagram is for coordination number six: 4 anions in the plane are shown, 1 is above the plane and 1 is below. The stability limit is at $r_C/r_A = 0.414$

Coordination number	Geometry	$\rho = r_{\text{cation}}/r_{\text{anion}}$
2	linear	0 - 0.155
3	triangular	0.155 - 0.225
4	tetrahedral	0.225 - 0.414
4	square planar	0.414 - 0.732
6	octahedral	0.414 - 0.732
8	cubic	0.732 - 1.0
12	cuboctahedral	1.0

There are unfortunately several challenges with using this idea to predict crystal structures:

- We don't know the radii of individual ions
- Atoms in crystals are not really ions - there is a varying degree of covalency depending electronegativity differences
- Bond distances (and therefore ionic radii) depend on bond strength and coordination number (remember Pauling's rule $D(n) = D(1) - 0.6 \log n$)
- Ionic radii depend on oxidation state (higher charge => smaller cation size, larger anion size)

We can build up a table of ionic radii by assuming that the bond length is the sum of the radii ($r_+ + r_-$) if the ions are in contact in the crystal. Consider for example the compounds MgX and MnX, where X = O, S, Se. All of these compounds crystallize in the NaCl structure:



For the two larger anions (S^{2-} and Se^{2-}), the unit cell dimensions are the same for both cations. This suggests that the anions are in contact in these structures. From geometric considerations, the anion radius in this case is given by:

$$r_{-} = \frac{r_{MX}}{\sqrt{2}}$$

and thus the radii of the S^{2-} and Se^{2-} ions are 1.84 and 1.93 Å, respectively. Once the sizes of these anions are fixed, we can obtain a self-consistent set of cation and anion radii from the lattice constants of many MX compounds.

How well does this model work? Let's consider the structures of tetravalent metal oxides (MO_2), using Pauling radii and the predictions of the radius ratio model:

Oxide MO_2	Radius ratio	Predicted coord. no.	Observed coord no. (structure)
CO_2	~0.1	2	2 (linear molecule)
SiO_2	0.32	4	4 (various tetrahedral structures)
GeO_2	0.43	4	4 (silica-like structures)
"	0.54	6	6 (rutile)
TiO_2	0.59	6	6 (rutile)
ZrO_2	0.68	6	7 (baddleyite)
"	0.77	8	8 (fluorite)

ThO ₂	0.95	8	8 (fluorite)
------------------	------	---	--------------

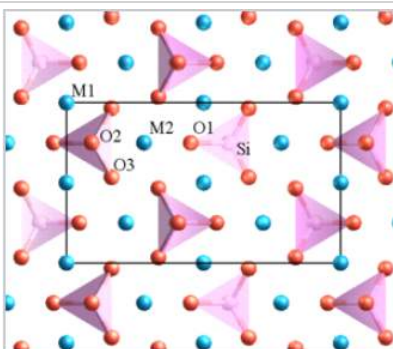
Note that cations have different radii depending on their coordination numbers, and thus different radius ratios are calculated for Ge⁴⁺ with coordination numbers 4 and 6, and for Zr⁴⁺ with coordination numbers 6 and 8.

For this series of oxides, the model appears to work quite well. The correct coordination number is predicted in all cases, and borderline cases such as GeO₂ and ZrO₂ are found in structures with different coordination numbers. The model also correctly predicts the structures of BeF₂ (SiO₂ type), MgF₂ (rutile), and CaF₂ (fluorite).

What about the alkali halides NaCl, KBr, LiI, CsF, etc.? All of them have the NaCl structure except for CsCl, CsBr, and CsI, which have the CsCl (8-8) structure. In this case the radius ratio model fails rather badly. The Li⁺ salts LiBr and LiI are predicted to have tetrahedral structures, and KF is predicted to have an 8-8 structure like CsCl. We can try adjusting the radii (e.g., making the cations larger and anions smaller), but the best we can do with the alkali halides is predict about half of their structures correctly. Since the alkali halides are clearly ionic compounds, this failure suggests that there is something very wrong with the radius ratio model, and its success with MO₂ compounds was coincidental.

In addition to the radius ratio rule, Linus Pauling developed other useful rules that are helpful in rationalizing and also predicting the structures of inorganic compounds. Pauling's rules^[1] state that:

- Stable structures are **locally electroneutral**. For example, in the structure of the double perovskite Sr₂FeMoO₆, MO₆ (M = Fe²⁺, Mo⁶⁺) octahedra share all their vertices, and Sr²⁺ ions fill the cubooctahedral cavities that are flanked by eight MO₆ octahedra.^[2] Each O²⁻ ion is coordinated to one Fe²⁺ and one Mo⁶⁺ ion in order to achieve local electroneutrality, and thus the FeO₆ and MoO₆ octahedra alternate in the structure.
- **Cation-cation repulsion** should be minimized. Anion polyhedra can share vertices (as in the perovskite structure) without any energetic penalty. Shared polyhedral edges, and especially shared faces, cause cation-cation repulsion and should be avoided. For example, in rutile, the most stable polymorph of TiO₂, the TiO₆ octahedra share vertices and two opposite edges, forming ribbons in the structure. In anatase TiO₂, each octahedron shares four edges so the anatase polymorph is less thermodynamically stable.
- **Highly charged cations** in anion polyhedra tend not to share edges or even vertices, especially when the coordination number is low. For example, in orthosilicates such as olivine (M₂SiO₄), there are isolated SiO₄⁴⁻ tetrahedra.



Structure of olivine. M (Mg or Fe) = blue spheres, Si = pink tetrahedra, O = red spheres.

As we will soon see, all of Pauling's rules are justified on the basis of lattice energy considerations. In ionic compounds, the arrangement of atoms that maximizes anion-cation interactions while minimizing cation-cation and anion-anion contacts is energetically the best.

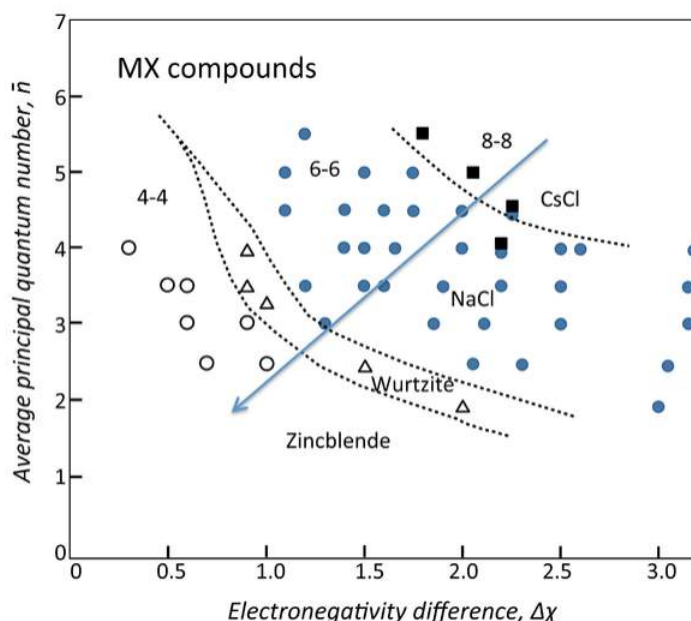
This page titled [9.1: Ionic Radii and Radius Ratios](#) is shared under a [CC BY-SA 4.0](#) license and was authored, remixed, and/or curated by [Chemistry 310 \(Wikibook\)](#) via [source content](#) that was edited to the style and standards of the LibreTexts platform; a detailed edit history is available upon request.

9.2: Structure Maps

Structure maps, which plot structures against properties such as electronegativity, are more consistent than radius ratio rules in correctly predicting coordination numbers and crystal structures. One of the early examples of this approach was published by Mooser and Pearson in 1959.^[3]

A **Mooser-Pearson diagram** maps crystal structures according to the average principal quantum numbers of the atoms and their electronegativity difference. The basic ideas behind such a plot are:

- The greater the electronegativity difference, the more ionic is the compound. Higher ionicity results in higher coordination numbers because anions like to surround cations (and vice versa).
- Higher principal quantum numbers result in less s-p hybridization, less directional bonding, and therefore higher coordination number. We saw this trend before with the structures of elements in group IV: descending the group the coordination number increases progressively from 3-4 (carbon) to 12 (Pb).



The lines in the Mooser-Pearson diagram separate MX compounds with CsCl, NaCl, and tetrahedral (wurtzite and zinblende) structures. Note that wurtzite has higher ionicity than zinblende in the plot, consistent with our discussion of the "boat" and "chair" ring structures in Chapter 8. Diamorphic compounds tend to fall on the boundaries. On the whole, the Mooser-Pearson diagram makes far fewer errors in predicting structures than the radius ratio rule. There are similar diagrams for MX_2 structures, in which the order of ionicity is CaF_2 (8:4 coordination) > rutile (6:3) > silica structures (4:2).

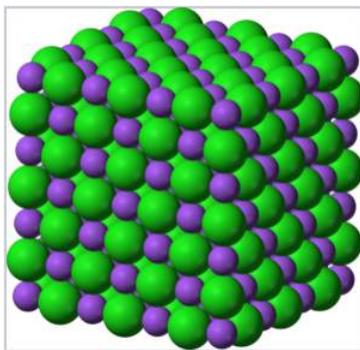
This page titled [9.2: Structure Maps](#) is shared under a [CC BY-SA 4.0](#) license and was authored, remixed, and/or curated by [Chemistry 310 \(Wikibook\)](#) via [source content](#) that was edited to the style and standards of the LibreTexts platform; a detailed edit history is available upon request.

9.3: Energetics of Crystalline Solids- The Ionic Model

Many ionic compounds have simple structures. Because the forces holding the atoms together are primarily electrostatic, we can calculate the cohesive energy of the crystal lattice with good accuracy. Interesting questions to ask about these lattice energy calculations are:

- How accurate are lattice energy calculations?
- What do they teach us about the chemical bonds in ionic crystals?
- Can we use lattice energies to predict properties such as solubility, stability, and reactivity?
- Can we use lattice energies to predict the crystal structures of ionic compounds?

Let's start by looking at the forces that hold ionic lattices together. There are mainly two kinds of force that determine the energy of an ionic bond.



The NaCl crystal structure is the archetype for calculating lattice energies and computing enthalpies of formation from Born-Haber cycles.

1) **Electrostatic Force** of attraction and repulsion (Coulomb's Law): Two ions with charges z_+ and z_- , separated by a distance r , experience a force F :

$$\mathbf{F} = -\frac{e^2}{4\pi\epsilon_0} \frac{z_+z_-}{r^2} \quad (9.3.1)$$

where

$$e = 1.6022 \times 10^{-19} \text{ C}$$

$$4\pi\epsilon_0 = 1.112 \times 10^{-10} \text{ C}^2/(\text{J m})$$

This force is attractive for ions of opposite charge.

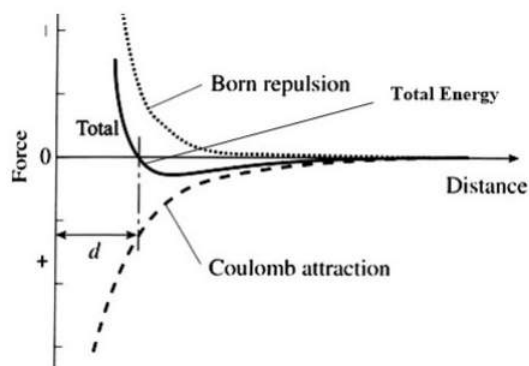
The electrostatic potential energy, E_{elec} , is then given by

$$\mathbf{E}_{elec} \int_{\infty}^r \mathbf{F}(r) dr = \frac{e^2}{4\pi\epsilon_0} \frac{z_+z_-}{r} \quad (9.3.2)$$

The sign of E_{elec} is negative for the attractive interaction between a cation and an anion. That is, the closer oppositely charged ions approach each other, the lower the potential energy.

2) **Closed-shell repulsion.** When electrons in the closed shells of one ion overlap with those of another ion, there is a repulsive force comes from the Pauli exclusion principle. A third electron cannot enter an orbital that already contains two electrons. This force is short range, and is typically modeled as falling off exponentially or with a high power of the distance r between atoms. For example, in the Born approximation, B is a constant and ρ is a number with units of length, which is usually empirically determined from compressibility data. A typical value of ρ is 0.345 \AA .

$$\mathbf{E}_{repulsion} = B \exp\left(\frac{-r}{\rho}\right) \quad (9.3.3)$$



The energy of the ionic bond between two atoms is then calculated as the combination of net electrostatic and the closed-shell repulsion energies, as shown in the figure at the right. Note that for the moment we are ignoring the attractive van der Waals energy between ions, which we will explain below. For a pair of ions, the equilibrium distance between ions is determined by the minimum in the total energy curve. At this distance, the net force on each ion is zero.

Electrostatic energy of a crystal lattice

We can use these equations to calculate the lattice energy of a crystal by summing up the interactions between all pairs of ions. Because the closed-shell repulsion force is short range, this term is typically calculated only for interactions between neighboring ions. However, the Coulomb force is long range, and must be calculated over the entire crystal. This problem was first solved in 1918 by Erwin Madelung, a German physicist.^[4]

Consider an ion in the NaCl structure labeled "O" in the diagram at the right. We can see that the nearest neighbor interactions (+ -) with ions labeled "1" are attractive, the next nearest neighbor interactions (- - and + +) are repulsive, and so on. In the NaCl structure, counting from the ion in the center of the unit cell, there are 6 nearest neighbors (on the faces of the cube), 12 next nearest neighbors (on the edges of the cube), 8 in the next shell (at the vertices of the cube), and so on. Their distances from ion "O" increase progressively: r_o , $\sqrt{2} r_o$, $\sqrt{3} r_o$, and so on, where r_o is the nearest neighbor distance.

We can now write the electrostatic energy at ion "O" as:

$$\mathbf{E}_{elec} = -6 \frac{e^2}{4\pi\epsilon_0} \frac{z_+z_-}{r_o} + 12 \frac{e^2}{4\pi\epsilon_0} \frac{z_+z_-}{\sqrt{2}r_o} - 8 \frac{e^2}{4\pi\epsilon_0} \frac{z_+z_-}{\sqrt{3}r_o} + \dots \quad (9.3.4)$$

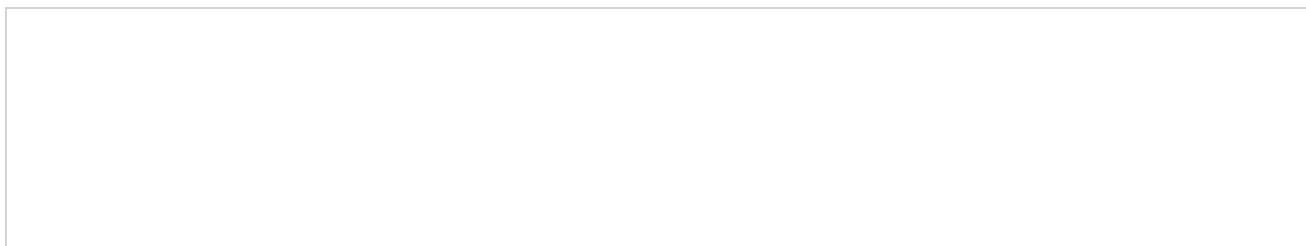
Factoring out constants and the nearest-neighbor bond distance r_o we obtain:

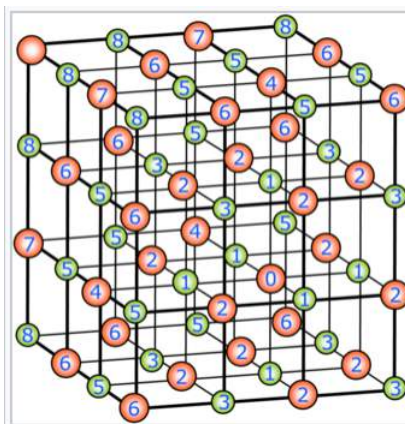
$$\mathbf{E}_{elec} = \frac{e^2}{4\pi\epsilon_0} \frac{z_+z_-}{r_o} \left(6 - \frac{12}{\sqrt{2}} + \frac{8}{\sqrt{3}} - \frac{6}{\sqrt{4}} + \dots \right) \quad (9.3.5)$$

Where the sum in parentheses, which is unitless, slowly converges to a value of $A = 1.74756$. Generalizing this formula for any three-dimensional ionic crystal we get a function:

$$\mathbf{E}_{elec} = \frac{e^2}{4\pi\epsilon_0} \frac{z_+z_-}{r_o} NA \quad (9.3.6)$$

where N is Avogadro's number (because we are calculating energy per mole of ions) and A is called the *Madelung constant*. The **Madelung constant** depends only on the geometrical arrangement of the ions and so it varies between different types of crystal structures, but within a given structure type it does not change. Thus MgO and NaCl have the same Madelung constant because they both have the NaCl structure





The Madelung constant is calculated by summing up electrostatic interactions with ion labeled 0 in the expanding spheres method. Each number designates the order in which it is summed. For example, ions labeled 1 represent the six nearest neighbors (attractive interaction), ions labeled 2 are the 12 next nearest neighbors (repulsive interaction) and so on. Note that if the sum is carried out over shells 1-2-3..., it converges very slowly, but there are mathematical methods for summing it which give a rapidly converging series.

The table below lists Madelung constants for some common structures. The **reduced Madelung constant** is obtained by normalizing the values to the number of ions in the formula unit. It can be seen from the table that the reduced Madelung constants are quite similar for different structures. This makes it hard to determine on the basis of electrostatic energy calculations which structure will be most stable for a given compound. It is interesting to note that the trend in reduced Madelung constants roughly follows the trend in ionicity (cf. the Mooser-Pearson diagram in Section 9.2). For example, wurtzite has a slightly higher Madelung constant than zincblende, consistent with our earlier conclusion that the wurtzite structure is favored by more polar compounds.

Structure	Madelung Constant, A	Reduced Madelung Constant, 2A/n
NaCl (halite)	1.7476	1.7476
CsCl	1.7627	1.7627
ZnS (zincblende)	1.6381	1.6381
ZnS (wurtzite)	1.6413	1.6413
CaF ₂ (fluorite)	2.5194	1.6796
TiO ₂ (rutile)	2.4080	1.6053
Al ₂ O ₃ (corundum)	4.172	1.6688

Total lattice energy of a crystal

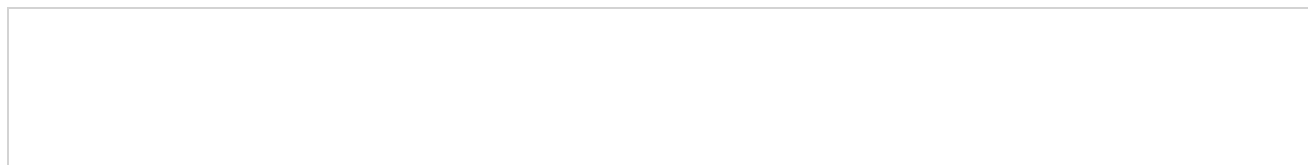
Having in hand a formula for the electrostatic energy, we can now add in the closed-shell repulsion term to obtain an equation that gives us the total lattice energy.

$$E_L = \frac{e^2}{4\pi\epsilon_0} \frac{z_+z_-}{r_o} NA + NB \exp\left(\frac{-r}{\rho}\right) \quad (9.3.7)$$

At the equilibrium bond distance, the forces on all the ions are zero, and we can use this fact to eliminate the constant B:

$$\left[\frac{dE}{dr}\right]_{r=r_o} = 0 \quad (9.3.8)$$

Expressed this way, E_L is a negative number (because z_+ and z_- have opposite signs). It represents the energy change for forming one mole of solid salt from one mole of the gaseous ions, separated initially at an infinite distance.





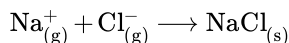
Lithium fluoride (shown here as a large single crystal in a beaker of water) is the only alkali halide that is not freely soluble in water. The lattice energy of LiF is the most negative of the alkali fluorides because Li^+ and F^- are both small ions and E_L is proportional to $1/r_0$.

This page titled [9.3: Energetics of Crystalline Solids- The Ionic Model](#) is shared under a [CC BY-SA 4.0](#) license and was authored, remixed, and/or curated by [Chemistry 310 \(Wikibook\)](#) via [source content](#) that was edited to the style and standards of the LibreTexts platform; a detailed edit history is available upon request.

9.4: Born-Haber Cycles for NaCl and Silver Halides

Now that we have an equation for the lattice energy of an ionic crystal, we can ask the question of how accurate it is. Remember, we made several approximations in arriving at this formula. We assumed that the lattice was completely ionic, we ignored the van der Waals attractive energy of the ions, and we assumed that there was no covalent contribution to the bonding.

Let's consider the lattice energy of table salt (NaCl)



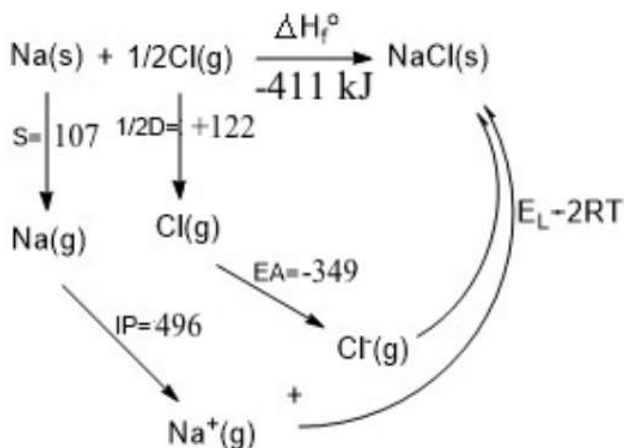
To calculate the lattice energy, we lump together the physical constants:

$$E_L \left(\frac{\text{kJ}}{\text{mol}} \right) = (1389.3) \frac{Aq_1q_2}{r_o} \left(1 - \frac{.345}{r_o} \right) \quad (9.4.1)$$

where r_o is expressed in Å. Now we can calculate the lattice energy for NaCl using $r_o = 2.814$ Å, as:

$$E_L = -(1389.3) \frac{1.7476}{2.814} \left(1 - \frac{.345}{2.814} \right) = -766.5 \frac{\text{kJ}}{\text{mol}} \quad (9.4.2)$$

We can alternatively construct a **Born-Haber cycle** for the formation of NaCl from the elements and calculate the lattice energy as the "missing" term in the cycle.



S= Sublimation energy of Na(s)

IP= Ionization potential of Na(g)

D= Bond dissociation energy of $\text{Cl}_2(\text{g})$

EA= Electron affinity of Cl(g)

E_L =Lattice energy of NaCl

R= Gas constant

T= Absolute temperature

From **Hess' Law**: $\Delta H_f = s + \frac{1}{2}D + IP + EA + E_L - 2RT = -396 \frac{\text{kJ}}{\text{mol}}$

Here we have to subtract $2RT$ to convert our cycle of energies to a cycle of enthalpies, because we are compressing two moles of gas in making $\text{NaCl}(\text{s})$ and $P\Delta V = \Delta nRT$, where $\Delta n = -2$.

Experimentally ΔH_f for NaCl is **-411 kJ/mol**

Because all the other numbers in the cycle are known accurately, the error in our calculation is only about 15 kJ (about 2% of E_L). The result is promising because we neglected the van der Waals term.

But....how did we get away with neglecting the van der Waals term?

This is because we used **energy minimization** to obtain the repulsion energy in the Born-Mayer equation. If we underestimate the attractive energy of the crystal lattice, the energy minimization criterion ensures that the repulsion energy is underestimated as well. The two errors partially compensate, so the overall error in the calculation is small.

We can do better by explicitly including the short-range van der Waals attractive energy between ions. The table below shows results of more detailed lattice energy calculations for ionic fluorides in which the van der Waals term is explicitly included. The errors in this case are only about 1% of E_L .

Compound	Calculated Lattice Energy (kJ/mol)	Experimental E_L from Born-Haber Cycle
MgF ₂ (rutile structure)	-2,920	-2,908
CaF ₂ (fluorite structure)	-2,586	-2,611
BaF ₂ (fluorite structure)	-2,326	-2,368

Silver Halides

It is interesting to repeat this exercise for the silver halides, which have either the NaCl structure (AgF, AgCl, AgBr) or zincblende structure (AgI).

Silver Halide	Calculated	Cycle	Difference (kJ/mol)
AgF	-920	-954	34
AgCl	-833	-908	75
AgBr	-816	-900	84
AgI	-778	-883	105

Looking at the table, we see that the error is small for AgF and becomes progressively larger for the heavier silver halides. However we are still obtaining answers within about 12% error even for AgI. Should we interpret the good agreement with values calculated from the ionic model to mean that these compounds are ionic? Clearly, this description is inappropriate for AgI, where the electronegativity difference $\Delta\chi$ is only 0.6 (compare this value to 0.4 for a C-H bond, which we typically view as non-polar).



A drop of silver nitrate solution, when added to a dilute hydrochloric acid solution, results in the immediate formation of a white silver chloride precipitate. This reaction is used as a qualitative test for the presence of halide ions in solutions. The covalent bonding contribution to the lattice energies of AgCl, AgBr, and AgI makes these salts sparingly soluble in water.

Again, we can interpret the fortuitous agreement between the calculated and experimentally obtained energies in terms of compensating errors. Our lattice energy calculation *overestimates* the ionic contribution in the case of the heavier silver halides, but *underestimates* the covalent contribution. Of these compounds, only AgF is soluble in water and should be thought of as an ionic compound. The others are progressively more insoluble in water (K_{sp} is 10^{-10} , 10^{-13} , and 10^{-16} for AgCl, AgBr, and AgI), reflecting increasing covalency as $\Delta\chi$ decreases.

The moral of the story is that simple lattice energy calculations based on the ionic model work well, but *they do not necessarily imply that the compounds are ionic!*

This page titled [9.4: Born-Haber Cycles for NaCl and Silver Halides](#) is shared under a [CC BY-SA 4.0](#) license and was authored, remixed, and/or curated by [Chemistry 310 \(Wikibook\)](#) via [source content](#) that was edited to the style and standards of the LibreTexts platform; a detailed edit history is available upon request.

9.5: Kapustinskii Equation

From the discussion above, it is clear that the lattice energy, E_L , of an ionic crystal can be calculated with reasonable accuracy if the structure is known. But how can we calculate E_L for a new or hypothetical compound of unknown structure? Recall that the reduced Madelung constant is about the same for different crystal structures. Russian chemist A. F. Kapustinskii recognized this fact and devised a formula that allows one to calculate E_L for any compound if we know the univalent radii of the constituent ions. [5]

The Madelung constant, A , is proportional to the number of ions (n) in formula unit, so dividing by the n gives similar values as shown in the table below:

$A/n \sim$ invariant

Structure	A/n
NaCl	0.874
CsCl	0.882
Rutile	0.803
Fluorite	0.800

Kapustinskii noticed that the difference in ionic radii between M^+ and M^{2+} (the monovalent vs. divalent radius) largely compensates for the differences in A/n between monovalent (NaCl, CsCl) and divalent (rutile, CaF_2) structures. He thus arrived at a lattice energy formula using an average Madelung constant, corrected to monovalent radii. In the **Kapustinskii formula**, the lattice energy (kJ/mol) is given by:

$$E_L = \frac{1213.8z_+z_-n}{r_+ + r_-} \left(1 - \frac{0.345}{r_+ + r_-}\right) \quad (9.5.1)$$

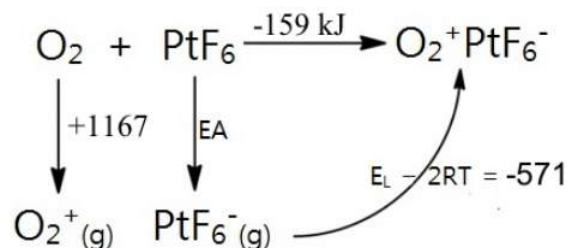
Here the sum of the monovalent radii is used in place of r_0 , the bond distance in the Born-Mayer equation. The beauty of this formula is that it requires no knowledge of the structure of the compound. Therefore it can be used, in combination with Born-Haber cycles, to predict the stability of unknown compounds. As we show below, this is a broadly useful tool in guiding syntheses and predicting the reactivity of inorganic solids.

This page titled [9.5: Kapustinskii Equation](#) is shared under a [CC BY-SA 4.0](#) license and was authored, remixed, and/or curated by [Chemistry 310 \(Wikibook\)](#) via [source content](#) that was edited to the style and standards of the LibreTexts platform; a detailed edit history is available upon request.

9.6: Discovery of Noble Gas Compounds

In 1962 at the University of British Columbia, Neil Bartlett was working with the powerful oxidizer PtF_6 and, because of an accidental leak in his vacuum line, noticed the compound's reaction with O_2 to generate a solid with formula " PtF_6O_2 ." The formula suggested Pt in the +10 oxidation state, which was clearly unreasonable because PtF_6 was known to be a more powerful oxidizer than either molecular fluorine (F_2) or molecular oxygen (O_2). Bartlett noticed that the X-ray powder diffraction pattern of the compound was similar to that of $\text{Cs}^+\text{AsF}_6^-$, a salt with the CsCl structure in which octahedral AsF_6^- ions occupy the chloride ion sites. This led Bartlett to propose a formulation of $\text{O}_2^+\text{PtF}_6^-$ for his new compound.^[6] Magnetic susceptibility data subsequently confirmed the presence of the paramagnetic O_2^+ cation, which (see Chapter 2) has a bond order of 2.5. This formulation implies that PtF_6 was a strong enough oxidizing agent to oxidize molecular oxygen.

But just how strong an oxidizer is PtF_6 ? Its electron affinity could be estimated by using a Born-Haber cycle, filling in the lattice energy of $\text{O}_2^+\text{PtF}_6^-$ by means of Kapustinskii's formula:



The electron affinity (EA) for PtF_6 can be calculated as $\text{EA} = -159 - 1167 + 571 = -751 \text{ kJ/mol}$. To put it in perspective, this is 417 kJ/mol more exothermic than the electron affinity of atomic fluorine (334 kJ). PtF_6 was by far the strongest oxidizer that had ever been made!



Crystals of xenon difluoride (XeF_2), which is made by photolysis of a gas mixture of Xe and F_2 . XeF_2 is used as a selective etchant for SiO_2 in certain microelectronic fabrication processes. Prior to Neil Bartlett's discovery of the first xenon compound in 1962, it was believed that elements in group VIII (He, Ne, Ar, Kr, Xe) could not form chemical compounds. Since then chemists have discovered a rich family of noble gas compounds containing Xe, Kr, or Ar.

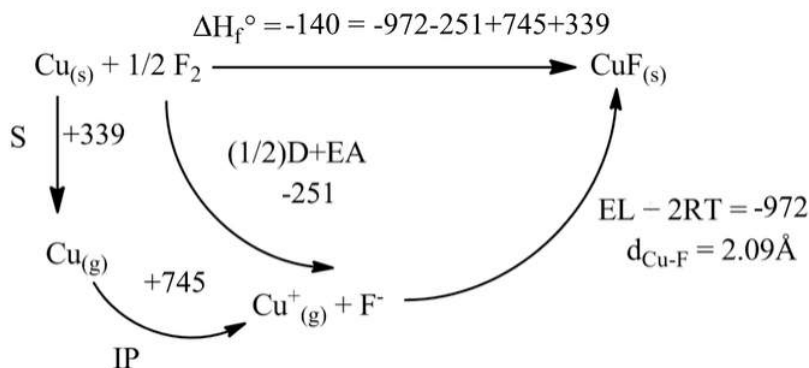
Bartlett recognized that Xe has ionization energy of +1170 kJ, which is very close to the ionization energy of O_2 . Since Xe^+ should be about the same size as O_2^+ , the lattice energy should be about the same with Xe^+ in the cation site of the $\text{O}_2^+\text{PtF}_6^-$ structure. Since all of the other terms in the Born-Haber cycle for the reaction of Xe with PtF_6 are the same, Bartlett concluded that $\text{Xe}^+\text{PtF}_6^-$, like $\text{O}_2^+\text{PtF}_6^-$, should be a stable compound. He purchased a lecture bottle of xenon gas and reacted the two compounds, producing an orange solid.^[7] While the product initially formed in the reaction may in fact be $\text{Xe}^+\text{PtF}_6^-$, the Xe^+ free radical is a powerful Lewis acid and reacts further with excess PtF_6 . The ultimate product of the reaction is formulated $[\text{XeF}^+][\text{Pt}_2\text{F}_{11}^-]$, a salt which contains Xe in the +2 oxidation state and Pt in the +5 oxidation state. This was an important discovery because it shattered the dogmatic notion, which derived from the octet rule, that elements in group VIII could not form bonds with other elements. The name of this group was changed from the "inert gases" to the "noble gases." Subsequently, many compounds of Xe and a few of Kr and even Ar (which is much harder to oxidize) were synthesized and characterized.

This page titled [9.6: Discovery of Noble Gas Compounds](#) is shared under a [CC BY-SA 4.0](#) license and was authored, remixed, and/or curated by [Chemistry 310 \(Wikibook\)](#) via [source content](#) that was edited to the style and standards of the LibreTexts platform; a detailed edit history is available upon request.

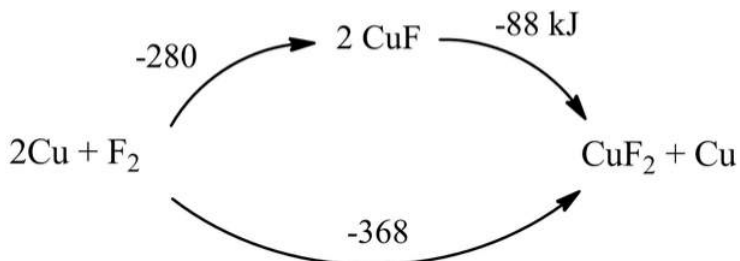
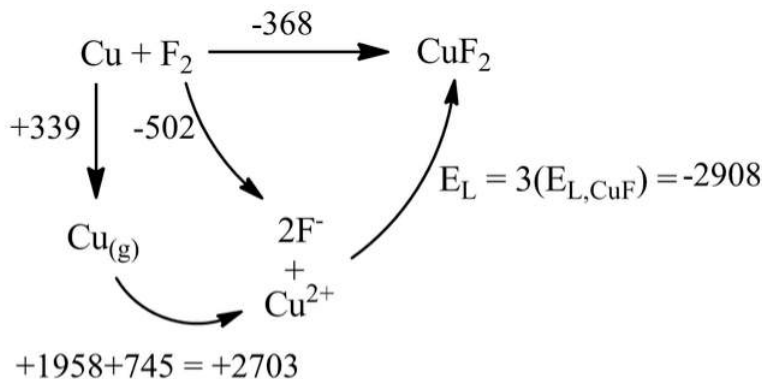
9.7: Stabilization of High and Low Oxidation States

Lattice energies, in addition to guiding the discovery of unknown compounds, are useful in explaining the absence (i.e., the thermodynamic instability) of **non-existent compounds**.^[8] For example, CuF and AuF are unknown compounds, whereas CuF₂, AuF₃, and AuF₅ are stable. In contrast AgF is a known, stable compound.

From the Born Haber cycle for CuF, the compound should be marginally stable ($\Delta H_f^\circ = -140$ kJ/mol) with respect to the elements. Why then is CuF unknown?



To gain insight into this question, we first construct a Born-Haber cycle for the formation of CuF₂ from the elements. This compound is stable with respect to the elements by -368 kJ/mol.



Combining the two cycles we see that the **disproportionation** of CuF to Cu and CuF₂ is spontaneous. From similar cycles, we can also predict that the reaction $3\text{AuF} \rightarrow \text{AuF}_3 + 2\text{Au}$ should be spontaneous.

Why is the lowest oxidation state unstable for these fluorides? The key point is that the large difference in E_L values ($2908 - 972 = 1926$ kJ in the case of copper fluorides) drives their disproportionation reactions. Note that when we use the Kapustinskii equation, we calculate that E_L for CuF₂ is approximately **three times** that of CuF. We use the same univalent radii in both calculations, but Cu has a 2+ charge in CuF₂ (doubling the lattice energy relative to CuF), and contains 3/2 as many ions. The product z_+z_-n is thus three times larger for CuF₂. The difference in E_L values will thus increase as E_L for the monovalent salt

increases. We know that fluorides, having a small anion radius, will give larger E_L values than iodides, which have larger anions. Thus the disproportionation reaction becomes more favorable for CuF than it is for CuI .

The stability of the lower vs. higher oxidation state thus depends on the **size of the anion**. For example, in fluorides, CuF is unstable but CuF_2 is stable. However, in iodides, CuI is stable whereas CuI_2 is unstable. From this we can develop a broad conclusion: **small anions (O,F) tend to stabilize higher oxidation states, whereas large anions (S, Br, I...) stabilize lower oxidation states**. Note that this trend has to do with the **size** and not with the electronegativity of the anion. Coincidentally, F and O are electronegative elements, but it is really their small size that has consequences for the lattice energy and their stabilization of higher oxidation states.



Cuprous iodide (CuI) is a crystalline compound used in organic synthesis and cloud seeding. This compound can be made in the laboratory by reacting soluble Cu^{2+} salts with a solution of sodium or potassium iodide. Because CuI_2 is thermodynamically unstable, the reaction liberates I_2 and a CuI precipitate forms.

Remember that the **hard-soft acid-base rules** could be interpreted in terms of the dominance of ionic vs. covalent interactions. Here we have put the hard-hard interaction in quantitative terms, based on (electrostatic) lattice energies.

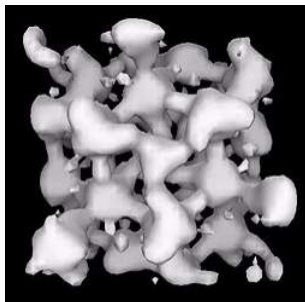
Ag appears to buck the periodic trend. Why is AgF stable? This is because the second IP is very high (2071 kJ vs. 1958 kJ for Cu, 1979 for Au). Thus both AgF and AgF_2 are known fluorides of Ag.

This page titled [9.7: Stabilization of High and Low Oxidation States](#) is shared under a [CC BY-SA 4.0](#) license and was authored, remixed, and/or curated by [Chemistry 310 \(Wikibook\)](#) via [source content](#) that was edited to the style and standards of the LibreTexts platform; a detailed edit history is available upon request.

9.8: Alkalides and Electrides

Another interesting consequence of lattice energies involves the formation of certain salts containing Na^- and e^- anions. These compounds are known as **alkalides** and **electrides**, respectively.^[9] Most of these compounds have been discovered by Prof. James Dye at Michigan State University.

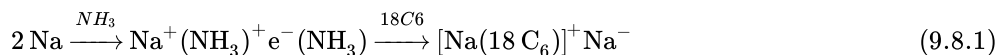
The alkali metals have one electron in their valence shell. For example, the electronic configurations of Na and K are $[\text{Ar}]3s^1$ and $[\text{Kr}]4s^1$, respectively. Although we are accustomed to seeing these very electropositive elements give up their electrons when they make compounds with electronegative elements, they can also gain an electron to achieve a $[\text{noble gas}]ns^2$ configuration. This is possible with strong electron donors such as alkali metals, especially when the cation that is formed is stabilized by coordination to a crown ether. Typically, these compounds are synthesized by combining the alkali metal and the appropriate crown ether in liquid ammonia, and then evaporating the ammonia.



Cavities and channels in an electride

Electride salts are formed under similar conditions, except in this case the anion is simply an electron that exists in an anion "cavity" in the crystal. The crystal structures are clearly salt-like, with the cations (alkali cations stabilized by crown or cryptand ligands) alternating in the structure with electrons.

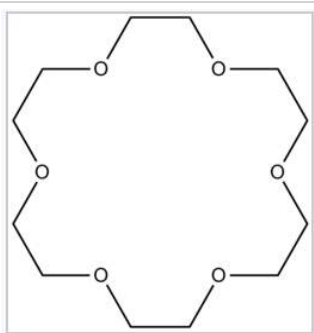
Alkalide Salt



Electride Salt



Complexing Na^+ (K^+ , Rb^+ , Cs^+) with crown ether ligands stabilizes the M^+ form of the metal ("salt" form). Because the metal cation with its ligand shell is rather large, the lattice energy of these salts is rather low.



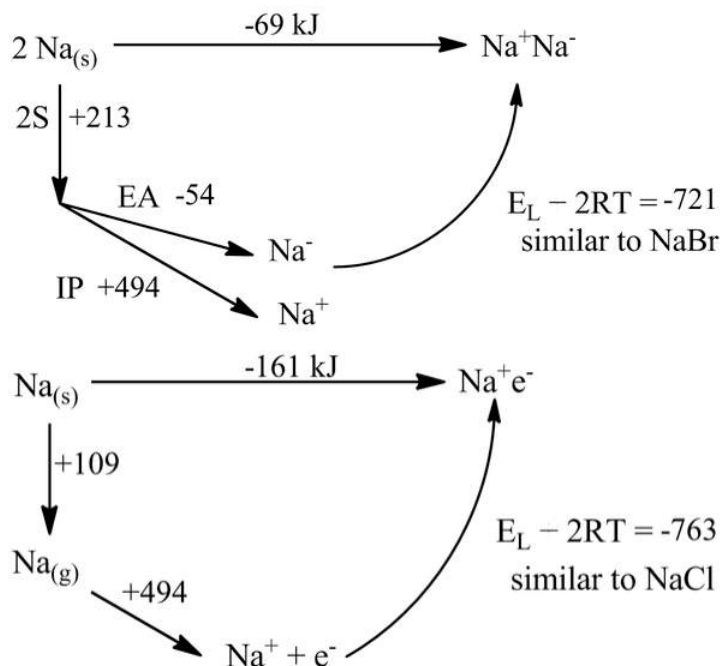
18-Crown-6, a crown ether that strongly complexes Na^+ cations

Solutions of electride salts are powerful reducing agents, as demonstrated by their use in the Birch reduction, in which aromatic compounds are hydrogenated to produce dienes. Electrides are also useful for reducing metal ions to metals. Evaporation of blue electride solutions in anhydrous ammonia affords a mirror of Na. Such solutions slowly lose their color as the electrons reduce ammonia to the amide anion:



It is interesting to consider, in the context of lattice energies and Born-Haber cycles, what might happen without these ligands present. That is, we can ask the question of whether sodium metal would prefer to exist in the metallic form as $\text{Na}(\text{s})$, or to form the sodide salt Na^+Na^- , or the electrider salt $\text{Na}^+ \text{e}^-$. Of course, we already know the answer to this question. Elemental sodium is clearly a metal (it is shiny, conducts electricity, and has a bcc crystal structure) and has never been observed in either of the "salt" forms. But how far away are these forms energetically?

We can calculate the energetics by assuming that the Na^- ion is about the same size as Br^- , and that the e^- anion is about the same size as Cl^- . Then the lattice energies in the cycles become the same as those of NaBr and NaCl :



The rather surprising result from these calculations is that sodium would be marginally stable as a sodide salt and very stable (by 161 kJ) as an electrider. All the terms in these simple cycles are known precisely. But we must be doing something wrong here, because $\text{Na}(\text{s})$ is clearly metallic.

The key, subtle point here is that Born-Haber cycles consider only the *potential energy* (rather than the total energy) of the substances in the cycle. Normally we can ignore the *kinetic energy* part of the total energy, but in this case we cannot because of the quantum mechanical effect of *resonance*.

This page titled [9.8: Alkalides and Electrides](#) is shared under a [CC BY-SA 4.0](#) license and was authored, remixed, and/or curated by [Chemistry 310 \(Wikibook\)](#) via [source content](#) that was edited to the style and standards of the LibreTexts platform; a detailed edit history is available upon request.

9.9: Resonance Energy of Metals

The solution to the problem above must consider the quantum mechanical nature of the electron. The valence electrons in Na metal are in orbitals that are delocalized over the entire crystal. However in the $\text{Na}^+ \text{e}^-$ "salt" form, the electrons are localized on specific anion sites. This localization imparts an additional kinetic energy (via the "**particle in a box**" effect) that adds to the total energy. From the quantum mechanical result for a particle in a one-dimensional box, we obtain

$$KE = \frac{h^2 n^2}{8mL^2} \quad (9.9.1)$$

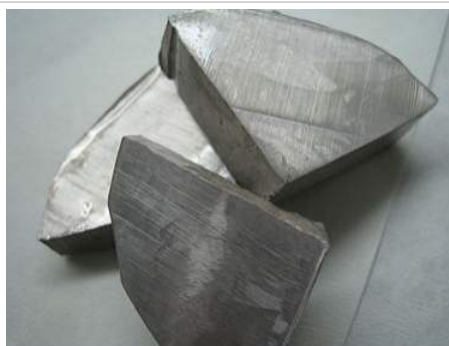
where:

- h = Planck's constant = 6.626×10^{-34} J s
- n = energy level, assumed to be the lowest, $n = 1$
- m = electron mass = 9.109×10^{-31} kg
- L = size of the box

If we approximate the size of the electron "box" as 3 \AA (3×10^{-10} m), we obtain:

$$KE = \frac{(6.626 \cdot 10^{-34})^2 (6.022 \cdot 10^{23})}{8 \cdot (9.1 \cdot 10^{-31}) (3 \cdot 10^{-10})^2} = 4.04 \cdot 10^5 \frac{\text{J}}{\text{mol}} = +404 \frac{\text{kJ}}{\text{mol}} \quad (9.9.2)$$

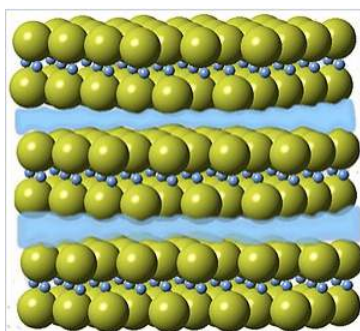
This extra kinetic energy makes the $\text{Na}^+ \text{e}^-$ "salt" unstable relative to the electron-delocalized metal.



Sodium owes its metallic properties to the resonance stabilization of its delocalized valence electrons.

The calculation is not very accurate because the electron kinetic energy is not zero in the metal, and because the "box" size is not so well defined. However, it does illustrate that electron delocalization has a substantial effect in thermodynamically stabilizing metals. The situation is entirely analogous to the stabilization of aromatic molecules by electron delocalization. In molecules like benzene, resonance is also a quantum-mechanical kinetic energy effect. In general, the resonance stabilization energy is significantly larger in metals than it is in π -delocalized organic molecules. For example, the resonance energy of the six π -electrons in benzene is approximately 151 kJ/mol, less than half of the value we have calculated (per electron) in sodium metal.

Interestingly, several of the alkali metals (and other metallic elements) transform at ultrahigh pressures to optically transparent, insulating phases in which the valence electrons are localized.^{[10][11]} These high pressure electrified phases defy the general rule (which we will encounter in Chapter 10) that insulators transform to metals at sufficiently high density. They illustrate how the stable structure of an element can depend on the trade-off between the lattice energy of an ionic electrified structure and the resonance energy of an electron-delocalized metal.



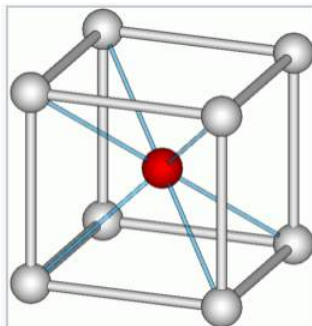
Crystal structure of Ca₂N, with 2D electron layers shown schematically in blue.

In addition to the salt-like electrides that are formed by complexing alkali metals with crown ether ligands, there are a number of recently discovered solid state nitrides and oxides, such as Ca₂N and Ca₂₄Al₂₈O₆₄, that are more properly formulated as electrides, i.e. as [Ca₂N⁺](e⁻)^[12] and [Ca₂₄Al₂₈O₆₄]⁴⁺(e⁻)₄.^[13] In these compounds the Ca, Al, O, and N atoms have their ordinary octet oxidation states (+2, +3, -2, and -3, respectively), and electrons act as anions, filling in cage-like voids or layers in the crystal. For example, Ca₂N adopts the anti-CdCl₂ structure, as shown at the right, with void spaces between layers that are occupied by a 2D gas of electrons. Like other layered materials, Ca₂N can be easily delaminated into thin nanosheets while retaining its structure and properties as an electride.^[14] These compounds are powerful reducing agents and also have interesting activity as catalysts.^[15]

This page titled [9.9: Resonance Energy of Metals](#) is shared under a [CC BY-SA 4.0](#) license and was authored, remixed, and/or curated by [Chemistry 310 \(Wikibook\)](#) via [source content](#) that was edited to the style and standards of the LibreTexts platform; a detailed edit history is available upon request.

9.10: Prelude to Ionic and Covalent Solids - Energetics

In Chapter 8, we learned all about crystal structures of **ionic compounds**. A good question to ask is, *what makes a compound choose a particular structure?* In addressing this question, we will learn about the forces that hold crystals together and the relative energies of different structures. This will in turn help us understand in a more quantitative way some of the heuristic concepts we have learned about in earlier chapters, such as hard-soft acid-base theory.



At ordinary pressures, the CsCl structure is adopted by only three of the alkali halides, CsCl, CsBr, and CsI. Under high pressure however, other alkali halides transform from the NaCl to the CsCl structure because of the higher Madelung constant of CsCl.

This page titled [9.10: Prelude to Ionic and Covalent Solids - Energetics](#) is shared under a [CC BY-SA 4.0](#) license and was authored, remixed, and/or curated by [Chemistry 310 \(Wikibook\)](#) via [source content](#) that was edited to the style and standards of the LibreTexts platform; a detailed edit history is available upon request.

9.11: The Strange Case of the Alkali Oxides

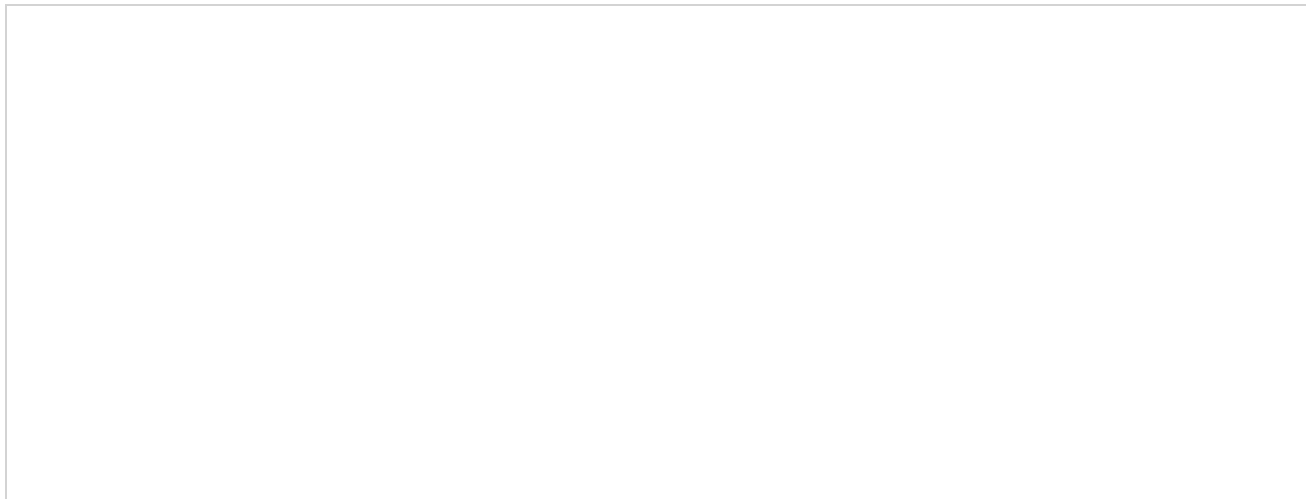
The alkali oxides, made by reacting alkali metals (Li, Na, K, Rb, Cs) with oxygen, show an unusual trend. When lithium reacts with oxygen we obtain the binary oxide Li_2O , as expected from combining an element in group I with one in group VI. Curiously, the oxide that forms most readily when sodium metal is oxidized is not Na_2O , but is instead the peroxide Na_2O_2 , which we can formulate as $(\text{Na}^+)_2(\text{O}_2^{2-})$. With potassium, rubidium, and cesium we obtain the superoxides MO_2 , which contain the superoxide radical anion (O_2^-) and should be formulated as $(\text{M}^+)(\text{O}_2^-)$. While it is possible to make Na_2O , K_2O , Rb_2O , and Cs_2O by reaction of the appropriate metal nitrate (MNO_3) with elemental alkali metal M ,^[16] it is curious that these "normal valent" compounds do not form by direct reaction of the metal with oxygen.

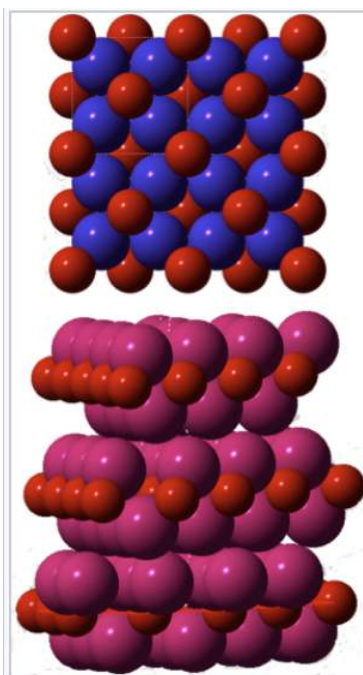


Sodium metal is oxidized in air to sodium peroxide, Na_2O_2

Because the alkali metals are all very electropositive ($\chi = 0.8-1.0$), and oxygen is very electronegative ($\chi = 3.5$), we expect all the compounds we make by combining them to be reliably ionic. Consistent with this picture we find that Li_2O (along with Na_2O , K_2O , and Rb_2O) adopts the antifluorite structure (8:4 coordination - see problem 8.8.2), which we expect to find with relatively ionic M_2X compounds. Strangely however, Cs_2O crystallizes in the anti- CdCl_2 structure. This is odd because CdCl_2 has a layered structure that we normally associate with polar covalent MX_2 compounds (see section 8.4). In Cs_2O , six Cs^+ cations surround each O^{2-} anion in an octahedron. Each Cs^+ is coordinated to three O^{2-} ions, and the Cs^+ ions contact each other across a van der Waals gap. The juxtaposition of Cs^+ ions near each other is clearly electrostatically unfavorable, so why does Cs_2O prefer the anti- CdCl_2 structure to antifluorite?

The answer has to do with the crowding of alkali ions around oxygen, as illustrated for K_2O at the right. Because eight large K^+ ions surround each O^{2-} ion in the structure, the cations are essentially in contact. Indeed, the metal-oxygen bonds are "stretched" in Na_2O , K_2O , and Rb_2O relative to M-O bonds with the same bond order in other structures.^[17] The situation is so extreme for Cs_2O that it finds an (electrostatically unfavorable) structure in which the coordination is lowered to 6:3. This packing problem is relieved somewhat in the peroxides, where the coordination is still 8:4 but the anion is larger, and especially in the superoxides where the cation:anion ratio is 1:1 and the coordination is 6:6. Thus the larger alkali ions (K^+ , Rb^+ , Cs^+) tend to form superoxides.

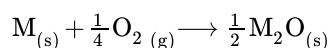




Space-filling models of the crystal structures of K_2O (top) and Cs_2O (bottom). Oxygen atoms are red, potassium ions are blue, and cesium ions are magenta

Another way that we can rationalize this trend is through the energetics of forming the oxides, peroxides, and superoxides.

Let's calculate the enthalpy change (per mole of metal) for forming a metal oxide M_2O from the metal and oxygen:

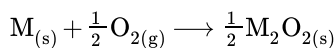


We can use Hess' law to write this as a sum of reactions:

Reaction	ΔH
$M_{(s)} \longrightarrow M_{(g)} \longrightarrow M_{(g)}^+$	$\Delta_s + IE = \Delta_{f,M^+(g)}$
$\frac{1}{4} O_{2(g)} \longrightarrow \frac{1}{2} O_{(g)} \longrightarrow \frac{1}{2} O^{2-}$	$\frac{1}{4} \Delta H_d + \frac{1}{2} EA_1 + \frac{1}{2} EA_2 = \frac{1}{2} \Delta H_{f,O^{2-}(g)}$
$M_{(g)}^+ + \frac{1}{2} O^{2-} \longrightarrow \frac{1}{2} M_2O_{(s)}$	$\frac{1}{2} E_{L,M_2O} - \frac{3}{2} RT$
Overall:	
$M_{(s)} + \frac{1}{4} O_{2(g)} \longrightarrow \frac{1}{2} M_2O_{(s)}$	$\Delta H_{f,M^+(g)} + \frac{1}{2} \Delta H_{f,O^{2-}(g)} + \frac{1}{2} E_{L,M_2O} - \frac{3}{2} RT$

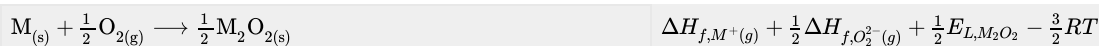
To get the enthalpy change for the overall reaction (the heat of formation of 1/2 mole of M_2O) we will need the heats of formation of $M^+(g)$ and $O^{2-}(g)$, which are available from tabulated values, and E_L , which we can calculate from Kapustinskii's equation.

Similarly, we can write for the formation of the alkali peroxides:

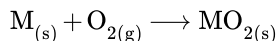


Reaction

Reaction	ΔH
$M_{(s)} \longrightarrow M_{(g)} \longrightarrow M_{(g)}^+$	$\Delta H_{(f,M^+(g))}$
$\frac{1}{2} O_{2(g)} \longrightarrow \frac{1}{2} O_{2(g)}^{2-}$	$\frac{1}{2} \Delta H_{f,O_2^{2-}(g)}$
$M_{(g)}^+ + \frac{1}{2} O_{2(g)}^{2-} \longrightarrow \frac{1}{2} M_2O_{2(s)}$	$\frac{1}{2} E_{L,M_2O_2} - \frac{3}{2} RT$
Overall:	



and for the superoxides:



Reaction	ΔH
$M_{(s)} \longrightarrow M_{(g)} \longrightarrow M_{(g)}^+$	$\Delta H_{f,M^+(g)}$
$O_{2(g)} \longrightarrow O_{2(g)}^-$	$\Delta H_{f,O_2^-(g)}$
$M_{(g)}^+ + O_{2(g)}^- \longrightarrow MO_{2(s)}$	$E_{L,MO_2} - 2RT$
Overall:	
$M_{(s)} + O_{2(g)} \longrightarrow MO_{2(s)}$	$\Delta H_{f,M^+(g)} + \Delta H_{f,O_2^-(g)} + E_{L,MO_2} - 2RT$

For the gaseous anions and cations, we have the following heats of formation and ionic radii (CN=6):

Ion	ΔH_f , kJ	ionic radius, Å
Li ⁺	678	0.76
Na ⁺	602	1.02
K ⁺	506	1.38
Rb ⁺	485	1.52
Cs ⁺	473	1.67
O ²⁻	500	1.20
O ₂ ²⁻	519	1.59
O ₂ ⁻	-88	1.49

Now using Kapustinskii's equation, we can calculate the lattice energies for each compound; these have been converted to lattice enthalpies by subtracting 2 RT or 3 RT as appropriate:

$$E_L = \frac{1213.8z_+z_-n}{r_+ + r_-} \left(1 - \frac{0.345}{r_+ + r_-}\right) \quad (9.11.1)$$

Metal	$\Delta H_{L,M_2O}$	$\Delta H_{L,M_2O_2}$	$\Delta H_{L,MO_2}$
Li	-3,065 kJ	-2,651 kJ	-918 kJ
Na	-2,776	-2,433	-838
K	-2,454	-2,178	-751
Rb	-2,345	-2,090	-721
Cs	-2,241	-2,007	-678

As expected, the lattice energies for M₂O and M₂O₂ are comparable, the latter being somewhat smaller in magnitude because of the larger size of the O₂²⁻ anion. The lattice energies of the superoxides, MO₂, are about 1/3 those of the corresponding peroxides because both the anion and cation are singly charged, and there are only two ions per formula unit.

Now, putting it all together, we can use the lattice energies and heats of formation of the individual ions to compare the heats of formation (per mole of metal) of each of the oxides:

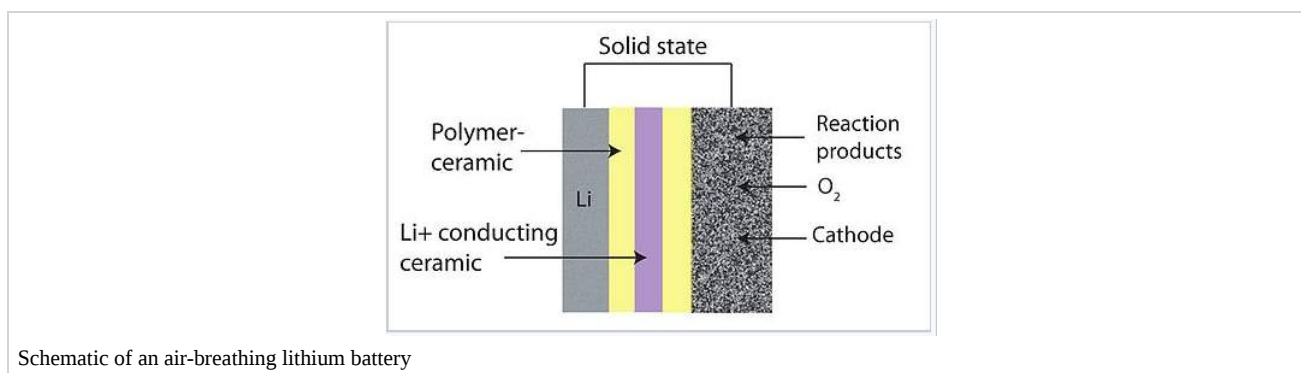
Metal	1/2 $\Delta H_{f,M_2O}$	1/2 $\Delta H_{f,M_2O_2}$	$\Delta H_{f,MO_2}$
Li	-404 kJ	-388 kJ	-328 kJ

Na	-338	-354	-324
K	-271	-321	-328
Rb	-241	-300	-324
Cs	-53	-70	-81

We can see that for Li, the formation of Li_2O is favored over Li_2O_2 or LiO_2 because of the very favorable lattice energy of Li_2O . As the lattice energy becomes less negative with increasing cation size, the peroxide becomes the most stable at Na. For the heavier alkalis, M_2O becomes quite unstable and the superoxides MO_2 are the most stable. This is consistent with our observations of the chemistry of the group I oxides.

Metal-air batteries

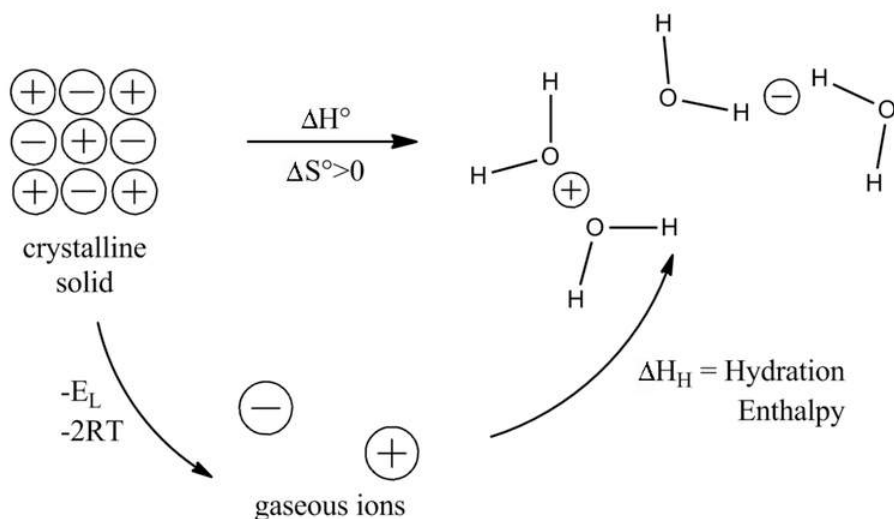
The alkali oxides are quite interesting in the context of metal-air batteries because of their potential for extremely high energy storage on a mass basis. Such batteries have alkali metal (typically Li) or Zn anodes and utilize oxygen from the air at the cathode. Although lithium is the lightest and therefore the most energy-dense alkali metal, there are materials problems associated with the formation of Li dendrites when the battery is recharged, and also with the slow kinetics of the four-electron interconversion between $\text{O}_2(\text{g})$ and 2O^{2-} at the cathode. For this reason, superoxide batteries are currently being studied as alternatives. The one-electron cathode reaction $\text{O}_2 + \text{e}^- = \text{O}_2^-$ is kinetically fast, and potassium^[18] and sodium^[19] represent potentially viable alternatives to lithium for the anode of these air-breathing batteries. Recently, it has been shown that LiO_2 can be kinetically stabilized by template growth on iridium nanoparticles, potentially opening the door to very high energy density lithium-air batteries.^[20]



This page titled [9.11: The Strange Case of the Alkali Oxides](#) is shared under a [CC BY-SA 4.0](#) license and was authored, remixed, and/or curated by [Chemistry 310 \(Wikibook\)](#) via [source content](#) that was edited to the style and standards of the LibreTexts platform; a detailed edit history is available upon request.

9.12: Lattice Energies and Solubility

Lattice energies can also help predict compound solubilities. Let's consider a Born-Haber cycle for dissolving a salt in water. We can imagine this as the sum of two processes: (1) the vaporization of the salt to produce gaseous ions, characterized by the lattice enthalpy, and (2) the hydration of those ions to produce the solution. The enthalpy change for the overall process is the sum of those two steps. We know that the entropy change for dissolution of a solid is positive, so the solubility depends on the enthalpy change for the overall process.



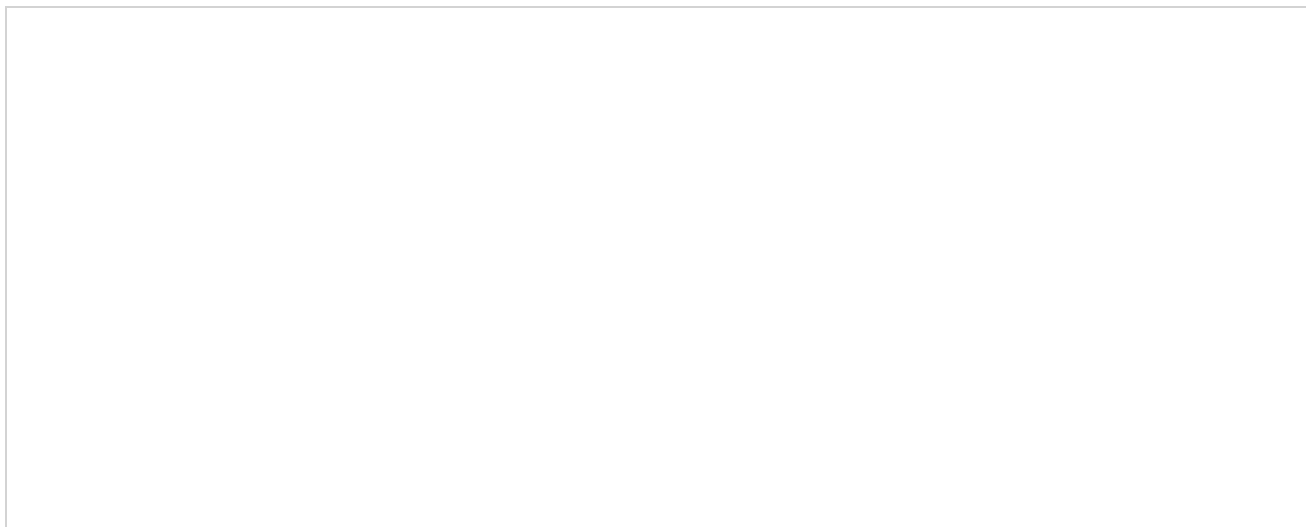
Here we need to consider the trends in both the lattice energy E_L and the hydration energy E_H . The lattice energy depends on the sum of the anion and cation radii ($r_+ + r_-$), whereas the hydration energy has separate anion and cation terms. Generally the solvation of small ions (typically cations) dominates the hydration energy because of the $1/r^2$ dependence.

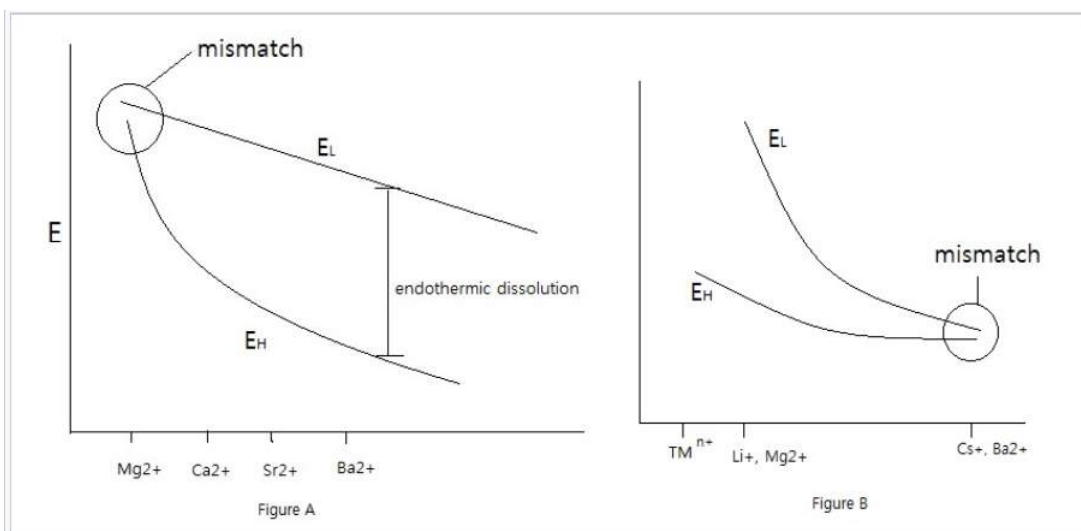
$$E_L \propto \frac{1}{r_+ + r_-} \quad (9.12.1)$$

$$E_H \propto \frac{1}{r_+^2} + \frac{1}{r_-^2} \quad (9.12.2)$$

For salts that contain large anions, E_L doesn't change much as r_+ changes. That is because the anion dominates the $r_+ + r_-$ term in the denominator of the formula for E_L . On the other hand, E_H changes substantially with r_+ , especially for small cations.

As a result, sulfate salts of small divalent cations, such as MgSO_4 (epsom salts), are soluble, whereas the lower hydration energy of Ba^{2+} in BaSO_4 makes that salt insoluble ($K_{sp} = 10^{-10}$).

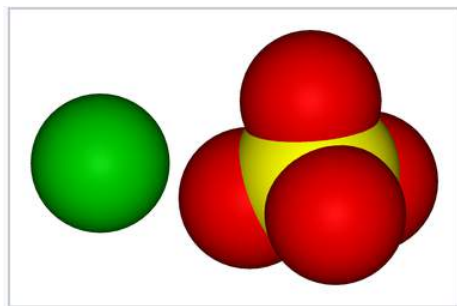




Left: E_L diagram for sulfate salts. The large SO_4^{2-} ion is size-mismatched to small cations such as Mg^{2+} , which have large hydration energies, resulting soluble salts. With larger cations such as Ba^{2+} , which have lower E_H , the lattice energy exceeds the solvation enthalpy and the salts are insoluble. Right: In the case of small anions such as F^- and OH^- , the lattice energy dominates with small cations such as transition metal ions (TM^{n+}), Mg^{2+} , and Li^+ . Anion-cation size mismatch occurs with larger cations, such as Cs^+ and Ba^{2+} , which make soluble fluoride salts.

For small anions, E_L is more sensitive to r_+ , whereas E_H does not depend on r_+ as strongly. For fluorides and hydroxides, LiF is slightly soluble whereas CsF is very soluble, and $\text{Mg}(\text{OH})_2$ is insoluble whereas $\text{Ba}(\text{OH})_2$ is very soluble.

Putting both trends together, we see that **low solubility** is most often encountered when the **anion and cation match well in their sizes**, especially when one or both are **multiply charged**.



Space-filling models showing the van der Waals surfaces of Ba^{2+} and SO_4^{2-} . The similarity in size of the two ions contributes to the low solubility of BaSO_4 in water.

Combining all our conclusions about solubility, we note the following trends:

- 1) Increasing **size mismatch** between the anion and cation leads to greater solubility, so CsF and LiI are the most soluble alkali halides.
- 2) Increasing **covalency** leads to lower solubility in the salts (due to larger E_L). For example, AgF , AgCl , AgBr , and AgI exhibit progressively lower solubility because of increasing covalency.
 $\text{AgF} > \text{AgCl} > \text{AgBr} > \text{AgI}$
- 3) Increasing the **charge on the anion** lowers the solubility because the increase in E_L is large relative to the increase in E_H .
- 4) Small, polyvalent cations (having large E_H) make **soluble salts with large, univalent anions** such as I^- , NO_3^- , ClO_4^- , PF_6^- , and acetate.

Examples: Salts of transition metal and lanthanide ions

- Ln^{3+} : Nitrate salts are soluble, but oxides and hydroxides are insoluble.
- Fe^{3+} : Perchlorate is soluble, but sulfate is insoluble.

5) Multiple charged anions such as O^{2-} , S^{2-} , PO_4^{3-} , and SO_4^{2-} make insoluble salts with most M^{2+} , M^{3+} , and M^{4+} metals.

This page titled [9.12: Lattice Energies and Solubility](#) is shared under a [CC BY-SA 4.0](#) license and was authored, remixed, and/or curated by [Chemistry 310 \(Wikibook\)](#) via [source content](#) that was edited to the style and standards of the LibreTexts platform; a detailed edit history is available upon request.

9.13: Discussion Questions

- Explain why lattice energy calculations are very accurate for NaCl and CaCl₂, but less accurate (by about 10%) for AgCl and PbCl₂. Does the Born-Mayer equation under- or overestimate the latter values?
 - Fluorine is more electronegative than oxygen. However, for many transition metals, we can make higher oxidation states in oxides than we can in fluorides. For example, Mn(IV) is stable in an oxide (MnO₂), but MnF₄ is unstable relative to MnF₃ and fluorine.^[21] Can you explain this in terms of lattice energies?
-

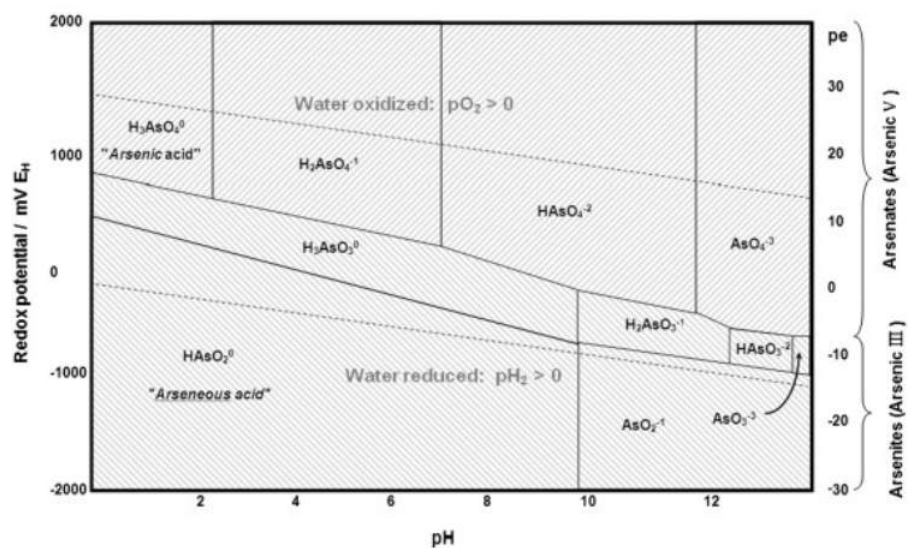
This page titled [9.13: Discussion Questions](#) is shared under a [CC BY-SA 4.0](#) license and was authored, remixed, and/or curated by [Chemistry 310 \(Wikibook\)](#) via [source content](#) that was edited to the style and standards of the LibreTexts platform; a detailed edit history is available upon request.

9.14: Problems

- Use lattice energies to explain why MgSO_4 decomposes to magnesium oxide and SO_3 at a much lower temperature than does BaSO_4 .
- Solid MgO might be formulated as Mg^+O^- or $\text{Mg}^{2+}\text{O}^{2-}$. Use the thermochemical data below (some of which are irrelevant) and Kapustinskii's formula to determine which is more stable. The lattice constant for MgO (NaCl structure) is 4.213 \AA . While the idea of an O^- ion might seem strange, note that the second electron affinity of O and the second ionization potential of Mg (in the table below) are both quite endothermic.

Reaction	ΔH° , kJ/mol
$\text{Mg(s)} = \text{Mg(g)}$	148
$\text{Mg(g)} = \text{Mg}^+(\text{g}) + \text{e}^-$	739
$\text{Mg}^+(\text{g}) = \text{Mg}^{2+}(\text{g}) + \text{e}^-$	1,452
$\text{O}_2(\text{g}) = 2 \text{O}(\text{g})$	498
$\text{O}(\text{g}) + \text{e}^- = \text{O}^-(\text{g})$	-141
$\text{O}^-(\text{g}) + \text{e}^- = \text{O}^{2-}(\text{g})$	790

- From the heat of formation of solid NH_4Cl (-315 kJ/mol) and gaseous NH_3 (-46), the bond dissociation energies of H_2 (436) and Cl_2 (244), the ionization potential of atomic hydrogen ($1,311$), and the electron affinity of atomic chlorine (-349), calculate the gas-phase proton affinity of NH_3 . The lattice energy of NH_4Cl may be estimated from Kapustinskii's formula using $r_{\text{N-Cl}} = 3.50 \text{ \AA}$.
- Bottles of aqueous ammonia are often labeled "ammonium hydroxide." We will test this idea by using a lattice energy calculation to determine whether the salt NH_4^+OH^- can exist.
The heats of formation of gaseous OH^- and H_2O are respectively -141 and -242 kJ/mol . Assuming that NH_4^+ is about the same size as Rb^+ , and OH^- about the same size as F^- , using Kapustinskii's formula, ionic radii, and the NH_3 proton affinity calculated in problem 3, determine whether NH_4^+OH^- should be a stable salt relative to NH_3 and H_2O . At what temperature should NH_4^+Cl^- be unstable relative to NH_3 and HCl , if ΔH_f° for HCl is -92 kJ/mol and $\Delta S^\circ (\text{NH}_4\text{Cl} \rightarrow \text{NH}_3 + \text{HCl}) = 280 \text{ J/mol K}$?
- Lithium metal burns in nitrogen to make the nitride Li_3N . The heavier alkali metals (K , Rb , Cs) can form stable azides (MN_3), but not M_3N nitrides. Explain why this is so.
- (a) Do you expect BaSO_4 or MgSO_4 to be more soluble in water? (b) Is LiF more soluble than LiClO_4 ? Explain.
- Which polymorph of ZnS (zincblende or wurzite) would you expect to be more stable on the basis of electrostatic energy?
- Arsenic contamination of ground water is a serious problem in Bangladesh, Chile, Argentina, and other parts of the world including the western United States. Arsenic poisoning been widespread in the Ganges river delta, where tube wells bring contaminated water up from 20-100 meters below the surface. One simple treatment that has been proposed is to precipitate the arsenic by aeration of the well water, which also contains high concentrations of Fe^{2+} . Referring to the Pourbaix diagram of arsenic below and the Pourbaix diagram of iron in Chapter 4, identify the iron and arsenic species that are present in aerated water at neutral pH. What insoluble compound precipitates to lower the concentration of arsenic? (Hint: which compound would have the largest lattice energy?)



This page titled [9.14: Problems](#) is shared under a [CC BY-SA 4.0](#) license and was authored, remixed, and/or curated by [Chemistry 310 \(Wikibook\)](#) via [source content](#) that was edited to the style and standards of the LibreTexts platform; a detailed edit history is available upon request.

9.15: References

1. Pauling, L. (1929). "The principles determining the structure of complex ionic crystals". *J. Am. Chem. Soc.* **51** (4): 1010–1026. doi:[10.1021/ja01379a006](https://doi.org/10.1021/ja01379a006).
2. K.-I. Kobayashi, T. Kimura, H. Sawada, K. Terakura, and Y. Tokura, Room-temperature magnetoresistance in an oxide material with an ordered double-perovskite structure, *Nature* (1998) **395**, 677–680. DOI:[10.1038/27167](https://doi.org/10.1038/27167)
3. E. Mooser and W. B. Pearson, On the Crystal Chemistry of Normal Valence Compounds, *Acta. Cryst.* **12**, 1015 (1959).
4. Madelung E (1918). "Das elektrische Feld in Systemen von regelmäßig angeordneten Punktladungen". *Phys. Zs.* **XIX**: 524–533.
5. A. F. Kapustinskii: *Lattice energy of ionic crystals*, *Quart. Rev. Chem. Soc.* Nr. 10, **1956**, pp. 283–294. DOI:[10.1039/QR9561000283](https://doi.org/10.1039/QR9561000283)
6. Neil Bartlett and D. H. Lohmann (March 1962). "Dioxygenyl hexafluoroplatinate (V), $O_2^+[PtF_6]^-$ ". *Proceedings of the Chemical Society* (London: Chemical Society) (3): 115. doi:[10.1039/PS9620000097](https://doi.org/10.1039/PS9620000097).
7. Bartlett, N. (June 1962). "Xenon hexafluoroplatinate (V) $Xe^+[PtF_6]^-$ ". *Proceedings of the Chemical Society* (London: Chemical Society) (6): 218. doi:[10.1039/PS9620000197](https://doi.org/10.1039/PS9620000197).
8. W. E. Dasent, Non-Existent Compounds, *J. Chem. Educ.*, **1963**, *40*, p 130, DOI: [10.1021/ed040p130](https://doi.org/10.1021/ed040p130)
9. Dye, J. L. (2003). "Electrons as Anions". *Science* **301** (5633): 607–608. doi:[10.1126/science.1088103](https://doi.org/10.1126/science.1088103). PMID [12893933](https://pubmed.ncbi.nlm.nih.gov/12893933/).
10. Ma, Y.; Eremets, M.; Oganov, A. R.; Xie, Y.; Trojan, I.; Medvedev, S.; Lyakhov, A. O.; Valle, M.; Prakapenka, V., "Transparent Dense Sodium," *Nature* 2009, 458, 182–183. doi:[10.1038/nature07786](https://doi.org/10.1038/nature07786)
11. M.-S. Miao and R. Hoffmann, "High Pressure Electrides: A Predictive Chemical and Physical Theory," *Acc. Chem. Res.* 2014, *47*, 1311–1317. DOI: [10.1021/ar4002922](https://doi.org/10.1021/ar4002922)
12. K. Lee, et al., "Dicalcium nitride as a two-dimensional electride with an anionic electron layer," *Nature*, 2013, 494, 336–340. DOI:[10.1038/nature11812](https://doi.org/10.1038/nature11812)
13. S. Matsuishi, et al., "High-Density Electron Anions in a Nanoporous Single Crystal: $[Ca_{24}Al_{28}O_{64}]^{4+}(e^-)_4$," *Science*, 2003, 301, 626–629. DOI: [10.1126/science.1083842](https://doi.org/10.1126/science.1083842)
14. D. L. Druffel et al., "Experimental Demonstration of an Electride as a 2D Material," *J. Am. Chem. Soc.*, 2016, 138, 16089–16094. DOI: [10.1021/jacs.6b10114](https://doi.org/10.1021/jacs.6b10114)
15. Y. Inoue et al., "Highly Dispersed Ru on Electride $[Ca_{24}Al_{28}O_{64}]^{4+}(e^-)_4$ as a Catalyst for Ammonia Synthesis," *ACS Catal.*, 2014, 4, 674–680. DOI: [10.1021/cs401044a](https://doi.org/10.1021/cs401044a)
16. Holleman, A.F.; Wiberg, E., eds (2001). *Inorganic Chemistry*. San Diego: Academic Press. ISBN [978-0-12-352651-9](https://doi.org/10.1016/0022-4596(84)90129-4).
17. N. K. McGuire and M. O'Keeffe, "Bond lengths in alkali metal oxides," *J. Solid State Chem.* **1984**, *54*, 49–53. DOI:[10.1016/0022-4596\(84\)90129-4](https://doi.org/10.1016/0022-4596(84)90129-4)
18. X. Ren and Y. Wu, "A low-overpotential potassium–oxygen battery based on potassium superoxide," *J. Am. Chem. Soc.* **2013**, *135*, 2923–2926. DOI:[10.1021/ja312059q](https://doi.org/10.1021/ja312059q)
19. P. Hartmann, et al., "A rechargeable room-temperature sodium superoxide (NaO_2) battery," *Nature Materials* **2012**, *12*, 228–232. DOI:[10.1038/nmat3486](https://doi.org/10.1038/nmat3486)
20. Lu et al., "A lithium–oxygen battery based on lithium superoxide," *Nature* **2016**, *529*, 377–382. DOI:[10.1038/nature16484](https://doi.org/10.1038/nature16484)
21. K. O. Christe, "Chemical synthesis of elemental fluorine," *Inorg. Chem.* **1986**, *25*, 3721–3722. DOI: [10.1021/ic00241a001](https://doi.org/10.1021/ic00241a001)

This page titled [9.15: References](#) is shared under a [CC BY-SA 4.0](#) license and was authored, remixed, and/or curated by [Chemistry 310 \(Wikibook\)](#) via [source content](#) that was edited to the style and standards of the LibreTexts platform; a detailed edit history is available upon request.

CHAPTER OVERVIEW

10: Electronic Properties of Materials - Superconductors and Semiconductors

Learning Objectives

- Explain the physical basis of the Hubbard and Mott models of metal-insulator transitions.
- Understand why good superconductors derive from bad metals.
- Know the structures and the periodic trends in band gaps and colors of semiconductors.
- Obtain the band gap of an intrinsic semiconductor from the temperature dependence of the conductivity.
- Predict the doping type when impurities or defects are introduced into a semiconductor.
- Correlate the band picture and Fermi level with n- or p-type doping.
- Understand the physical principles of operation of diodes, LEDs, solar cells, and FETs.
- Explain the differences in structures and electronic properties of crystalline and amorphous semiconductors.

The band model (like MO theory) is based on a *one-electron* model. This was an approximation we made at the very beginning of our discussion of MO theory: we used hydrogen-like (one-electron) solutions to the Schrödinger equation to give us the shapes of s, p, d, and f atomic orbitals. In a one-electron atom, these orbitals are degenerate within a given shell, and the energy differences between, e.g., 2s and 2p orbitals arise only when we consider the energy of an electron in the field of other electrons in the atom. Moving from atoms to molecules, we made linear combinations to generate one-electron molecular orbitals (and, in solids, one-electron energy bands). But as in multi-electron atoms, life is not so simple for real molecules and solids that contain many electrons. Electrons repel each other and so their movement in molecules and in solids is **correlated**.

[10.1: Prelude to Electronic Properties of Materials - Superconductors and Semiconductors](#)

[10.2: Metal-Insulator Transitions](#)

[10.3: Superconductors](#)

[10.4: Periodic Trends- Metals, Semiconductors, and Insulators](#)

[10.5: Semiconductors- Band Gaps, Colors, Conductivity and Doping](#)

[10.6: Semiconductor p-n Junctions](#)

[10.7: Diodes, LEDs and Solar Cells](#)

[10.8: Amorphous Semiconductors](#)

[10.9: Discussion Questions](#)

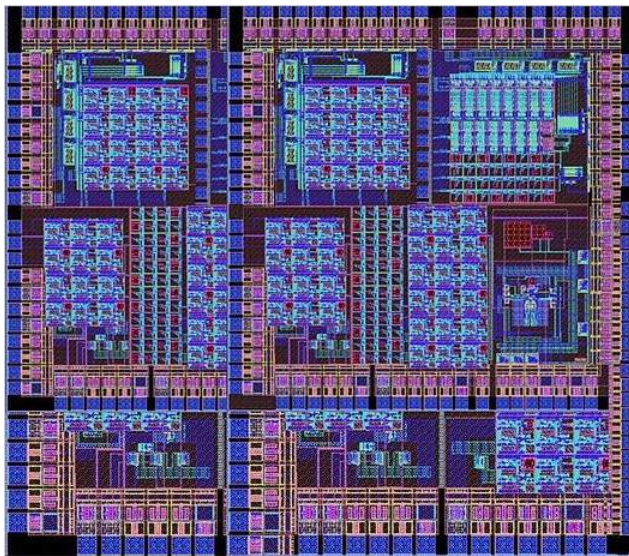
[10.10: Problems](#)

[10.11: References](#)

This page titled [10: Electronic Properties of Materials - Superconductors and Semiconductors](#) is shared under a [CC BY-SA 4.0](#) license and was authored, remixed, and/or curated by [Chemistry 310 \(Wikibook\)](#) via [source content](#) that was edited to the style and standards of the LibreTexts platform; a detailed edit history is available upon request.

10.1: Prelude to Electronic Properties of Materials - Superconductors and Semiconductors

In Chapter 6 we developed an energy band picture for metals, starting from atomic orbitals and building up the molecular orbitals of the solid metallic crystal. This treatment gave us a useful picture of how electrons behave in metals, moving at very fast speed between scattering events, and migrating in an electric field at a slow drift velocity. It also taught us that a metal is something with a partially filled band, meaning that the Fermi level cuts through one of its bands of orbitals. An insulator or a semiconductor has a similar band picture, except that the bands are either completely full or completely empty. In this case the Fermi level lies in the gap between fully occupied and unoccupied bands. We will see in this chapter that the properties of semiconductors (along with their useful electronic applications) depend on the addition of small amounts of impurities ("dopants") that change the position of the Fermi level, resulting in conduction by electrons or "holes."



Modern integrated circuits contain billions of nanoscale transistors and diodes that are essential for logic and memory functions. Both kinds of devices rely on junctions between crystalline silicon regions that contain a few parts per million of boron or phosphorus impurities.

While the band picture works well for most crystalline materials, it does not tell us the whole story of conduction in solids. That is because the band model (like MO theory) is based on a *one-electron* model. This was an approximation we made at the very beginning of our discussion of MO theory: we used hydrogen-like (one-electron) solutions to the Schrödinger equation to give us the shapes of s, p, d, and f atomic orbitals. In a one-electron atom, these orbitals are degenerate within a given shell, and the energy differences between, e.g., 2s and 2p orbitals arise only when we consider the energy of an electron in the field of other electrons in the atom. Moving from atoms to molecules, we made linear combinations to generate one-electron molecular orbitals (and, in solids, one-electron energy bands). But as in multi-electron atoms, life is not so simple for real molecules and solids that contain many electrons. Electrons repel each other and so their movement in molecules and in solids is **correlated**. While this effect is weak in a "good" metal such as sodium - where the wavefunctions are highly delocalized - it can be quite important in other materials such as transition metal oxides. Correlated electron effects give rise to **metal-insulator transitions** that are driven by small changes in temperature, pressure, or composition, as well as to **superconductivity** - the passage of current with zero resistance at low temperatures. In this chapter we will develop some simple models to understand these interesting and important electronic properties of solids.

This page titled [10.1: Prelude to Electronic Properties of Materials - Superconductors and Semiconductors](#) is shared under a [CC BY-SA 4.0](#) license and was authored, remixed, and/or curated by [Chemistry 310 \(Wikibook\)](#) via [source content](#) that was edited to the style and standards of the LibreTexts platform; a detailed edit history is available upon request.

10.2: Metal-Insulator Transitions

In Chapter 6 we learned that metals and insulators not only have different electrical properties but also have very different crystal structures. Metals tend to have high coordination numbers (typically 8 or 12) whereas insulators have low coordination numbers that can be rationalized as "octet" bonding arrangements. For example, in crystalline Si or Ge (diamond structure), each atom has four nearest neighbors. There are two electrons per bond, and thus each atom has eight electrons in its valence shell. Sn, the element below Ge, exists in two different forms, one (gray tin) with the diamond structure that is a brittle narrow-gap semiconductor, and the other (white tin) with a body-centered tetragonal structure that is a malleable metal. These two forms are very close in energy, and in fact metallic white tin transforms to the brittle semiconducting gray form at low temperature. Extremely cold weather in 18th century Europe caused many tin organ pipes to break and eventually turn to dust. This transformation has been called tin blight, tin disease, tin pest or tin leprosy. The dust is actually grey tin, which lacks the malleability of its metallic cousin white tin.

Under experimentally accessible temperatures and pressures, Si and Ge are always semiconducting (i.e., insulating), and Pb is always metallic. Why is Sn different? The reason has to do with orbital overlap. Theory tells us in fact that any (and all) insulators should become metallic at high enough pressure, or more to the point, at high enough density. For most insulators, however, the pressures required are far beyond those that we can achieve in the laboratory.

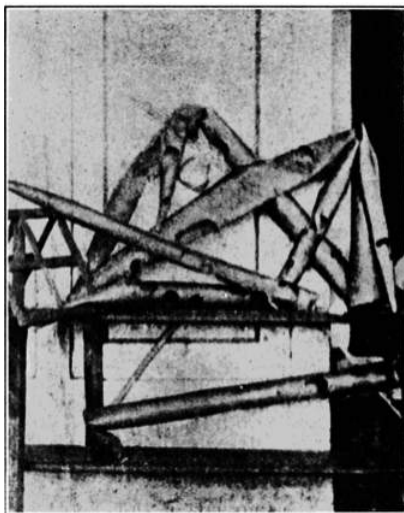
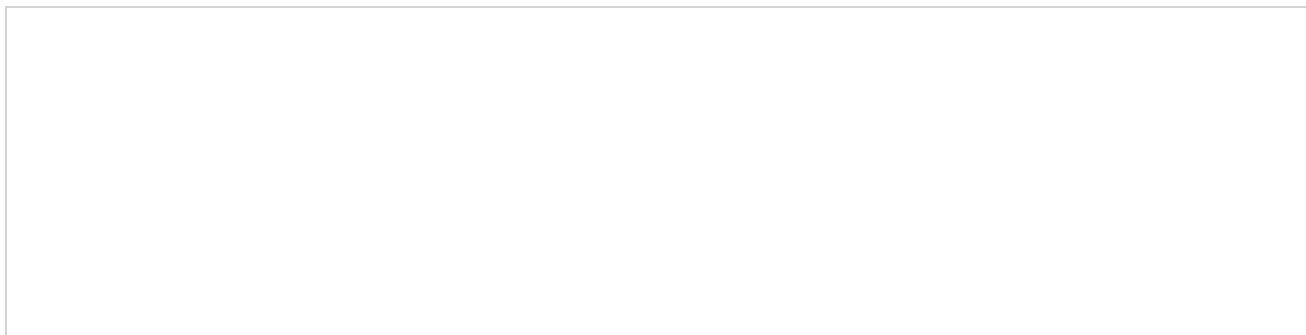


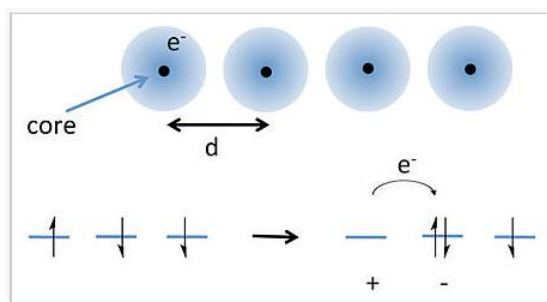
Figure 10.2.1: Organ pipes destroyed by "tin blight"

How can we rationalize the transition of insulators to the metallic state? Indeed, how can we understand the existence of insulators at all?

The Hubbard Model

Let's consider a chain of a large number (N) of atoms as we did in Chapter 6. For convenience, we can say that these are atoms such as H, Na, or Cs that have one valence electron. The simple band model we developed earlier suggests that the chain should be metallic, because N atoms combine to make N orbitals, and the N valence electrons only fill the band of orbitals halfway. But this conclusion doesn't depend on the density, which creates a paradox. If atoms in the chain are very far apart, we suspect that the electrons should localize on the atoms.



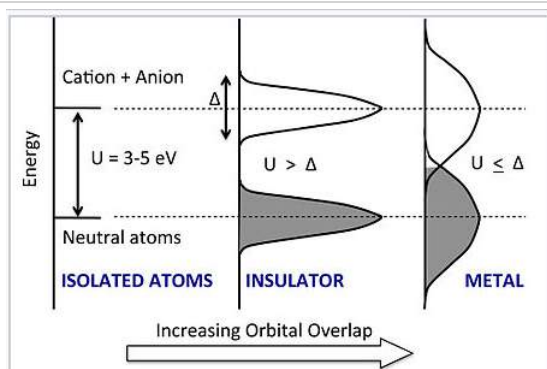


Electron hopping in a 1-D chain of atoms.

A solution to this problem was proposed by J. Hubbard in 1963.^[1] Hubbard considered the energy required to transfer an electron from an atom to its nearest neighbor, as shown in the picture at the right. Because each atom already has one electron (with random spin), moving an electron over by one atom requires overcoming the energy of electron-electron repulsion to make a cation-anion pair. For well-separated atoms this energy (U) is given by:

$$U = IP - Ea - \frac{e^2}{4\pi\epsilon_0 d} \quad (10.2.1)$$

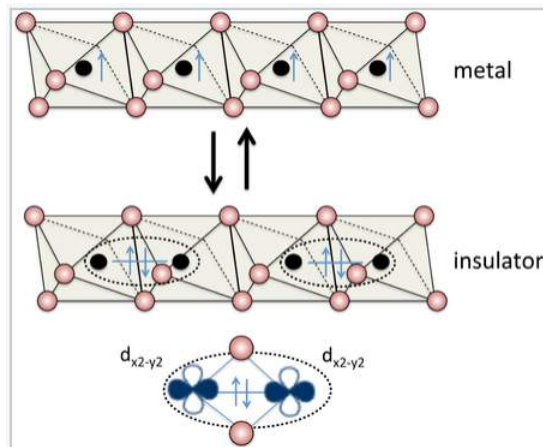
where IP and EA are the ionization energy and electron affinity, ϵ_0 is the permittivity of free space, and the last term in the equation represents the coulombic attraction between the cation and the anion. For atoms such as alkali metals, U is on the order of 3–5 eV, which is much larger than the thermal energy kT . Thus we expect there to be very few anion-cation pairs at room temperature, and the chain of atoms should be insulating.



Energy vs. DOS for the chain of atoms as the density and degree of orbital overlap between atoms increases. Increasing overlap broadens the neutral atom and anion-cation states into bands, each of which has a bandwidth Δ . A transition to the metallic state occurs abruptly when Δ exceeds the Hubbard gap U .

What happens when we squeeze the atoms together? In the Hubbard model, as the distance between atoms decreases, the energies of both the neutral atom states and the anion-cation states broaden into bands, each of which has a band width Δ . The lower band can accommodate exactly N electrons (not $2N$ as in the MO picture we developed earlier) because each orbital can only take one electron without spin-pairing. Thus for small Δ the lower band is full and the upper band is empty. However, as we continue to compress the chain, the orbital overlap becomes so strong that $\Delta \approx U$. At this point, the bands overlap and some of the electrons fill the anion-cation states. The chain then becomes conducting and the material is metallic.

Some materials, such as Sn and VO_2 , happen to have just the right degree of orbital overlap to make the Hubbard transition occur by changing the temperature or pressure. Such materials can be very useful for electrical switching, as illustrated at the right for rutile structure VO_2 . Most materials are far away from the transition, either on the metallic or insulating side. An interesting periodic trend that illustrates this concept can be seen among the transition metal monoxides, MO ($M = \text{Ti}, \text{V}, \text{Cr}, \text{Mn}, \text{Fe}, \text{Co}, \text{Ni}$), all of which have the NaCl structure. TiO and VO are metallic, because the 3d orbitals have significant overlap in the structure. However, CrO , MnO , FeO , CoO , and NiO are all insulators, because the 3d orbitals contract (and therefore $\Delta < U$) going across the transition metal series. In contrast, the analogous sulfides (TiS , VS , ..., NiS) are all metallic. The sulfides have the NiAs structure, in which all the metal atoms are eclipsed along the stacking axis (the hexagonal c -axis). The short metal-metal distances along that axis result in strong orbital overlap, making $\Delta > U$.



Vanadium dioxide has the rutile structure, and in its undistorted form it is metallic, with one valence electron per V atom. Distortion of the lattice makes pairs of V atoms, resulting in an electronically insulating state. The metal-insulator transition can be driven reversibly by changing the temperature, pressure, or orbital occupancy. Electrical switching of this transition in VO_2 is being studied for applications in high performance thin film transistors^[2]

The Mott Model

A simpler, less atomistic model of the metal-insulator transition was formulated by Neville Mott.^[3] The Mott model considers the behavior of an electron in a material as a function of the density of all the other valence electrons. We know for a one-electron hydrogen-like atom (H, Na, Cs, etc.) the Schrödinger equation contains a potential energy term:

$$V(r) = -\left(\frac{e^2}{4\pi\epsilon_0 r}\right) \quad (10.2.2)$$

This potential energy function gives rise to familiar ladder of allowed energy levels in the hydrogen atom. However, in a metal, this Coulomb potential must be modified to include the screening of nuclear charge by the other electrons in the solid. In this case there is a **screened Coulomb potential**:

$$V(r) = -\left(\frac{e^2}{4\pi\epsilon_0 r}\right)\exp(-qr) \quad (10.2.3)$$

where q , which is the inverse of the **screening length**, is given by:

$$q^2 = 4m_e^2 \left(\frac{3n}{\pi}\right)^{\frac{1}{3}} \left(\frac{2\pi}{h}\right) \quad (10.2.4)$$

Here n is the density of atoms (or valence electrons), m_e is the electron mass, and h is Planck's constant. At distances much larger than the screening length q^{-1} , the electron no longer "feels" the charge on the nucleus. Mott showed that there is a critical density of electrons n_c above which the valence electrons are no longer bound by individual nuclei and are free to roam the crystal. This critical density marks the transition to the metallic state, and is given by the Mott criterion:

$$n_c^{\frac{1}{3}} a_H \approx 0.26 \quad (10.2.5)$$

In this equation, a_H is an effective Bohr radius for the valence electrons in the low-density limit, e.g. the average orbital radius of electrons in the 6s shell of a Cs atom when computing the value for Cs metal.



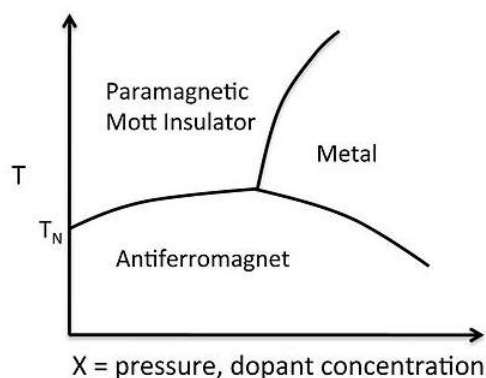
Solutions of lithium metal in liquid ammonia at low (top, ionic conductor) and higher (bottom, metal) Li concentration. From a [video](#) by Joshua Judkins

The important concept from the Mott model is that the metal-insulator transition depends very strongly on the **density of valence electrons**. This is consistent with the orbital overlap model of Hubbard, but also more general in the sense that it does not depend on a periodic structure of atoms. The Mott model is thus applicable to such diverse systems as metal atoms dissolved in liquid ammonia, metal atoms trapped in frozen gas matrices, and dopants in semiconductors.^[4] In some systems, it is possible to continuously tune the density of valence electrons with rather striking results. For example, dissolving alkali metal (Li, Na, ...) in liquid ammonia (bp $-33\text{ }^{\circ}\text{C}$) produces a blue liquid. The solvated alkali cations and negatively charged electrons impart ionic conductivity (as in a salt solution) but not electronic conductivity to the blue liquid ammonia solution. But as the concentration of electrons increases, a reflective, bronze-colored liquid phase forms that floats over the blue phase. This bronze phase is metallic and highly conducting. Eventually, with enough alkali metal added, the entire liquid is converted to the electronically conducting bronze phase.

The electrical switching of VO_2 between insulating and metallic phases (see above) can also be rationalized in terms of the Mott transition. Adding more electron density (by chemical or electric field doping) increases the concentration of valence electrons, driving the phase transition to the metallic state.

Thermodynamics and phase transitions

Thermodynamically, the metal-insulator transition is a **first-order phase transition**. In such a transition, the structure and properties change abruptly (think of the breakfast-to-lunch transition at McDonalds - there is just no way to get pancakes after, or hamburgers before 10:30 AM!^[5]). Thus in the case of Sn metal, the changes in structure (from four- to eight-coordination) and in electronic conductivity (insulator to metal) occur simultaneously. As in other first order phase transitions such as ice to water to steam, there is a latent heat associated with the transition and a discontinuity in derivative properties such as the heat capacity.



A typical phase diagram for a metal-insulator transition is shown at the right for V_2O_3 . The octahedrally coordinated V^{3+} ion has a d^2 electron count, so there are two unpaired spins per atom, and at low temperature the spins in the lattice order

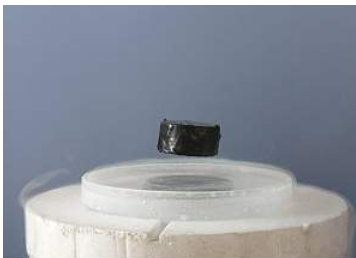
antiferromagnetically. As we learned in Chapter 8, above the Néel temperature an antiferromagnet becomes a paramagnet, which is also a Mott insulator. Increasing the pressure, or doping with electrons (e.g., by substituting some $d^3 \text{Cr}^{3+}$ for V^{3+}) pushes the electron density over the Mott transition, the spins pair, and the solid becomes metallic.

This page titled [10.2: Metal-Insulator Transitions](#) is shared under a [CC BY-SA 4.0](#) license and was authored, remixed, and/or curated by [Chemistry 310 \(Wikibook\)](#) via [source content](#) that was edited to the style and standards of the LibreTexts platform; a detailed edit history is available upon request.

10.3: Superconductors

Superconductivity refers to the flow of electrical current in a material with zero resistance. Such materials are very important for use in electromagnets, e.g., in magnetic resonance imaging (MRI) and nuclear magnetic resonance (NMR) machines, because once the current starts flowing in the coils of these magnets it doesn't stop. Magnetic levitation using superconductors - which, below a critical field strength, are perfect diamagnets that are not penetrated by magnetic flux lines - is also potentially relevant to future technologies such as magnetically levitated trains.

The phenomenon of superconductivity, first discovered in Hg metal in 1911 by Onnes, continues to be only partially understood. It is of great interest to physicists as a macroscopic quantum phenomenon, and to chemists and materials scientists who try to make better superconductors (especially those that superconduct at higher temperatures) and devices derived from them, such as superconducting quantum interference devices (SQUIDs), which are extremely sensitive magnetometers.

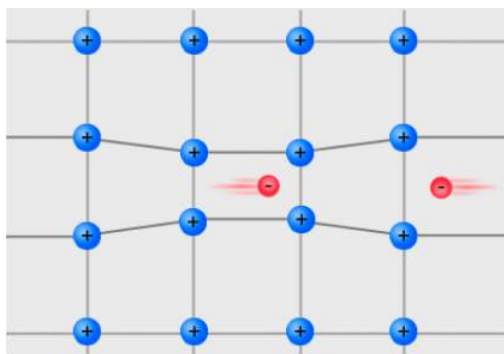


A magnet levitating above a high-temperature superconductor, cooled with liquid nitrogen. Persistent electric current flows on the surface of the superconductor, excluding the magnetic field of the magnet. This current effectively forms an electromagnet that repels the magnet.

Spin pairing and zero resistance

The transition from the metallic to the superconducting state is related to the quantum phenomena of Bose-Einstein condensation and superfluidity. Individual electrons have spin = 1/2, and as such are fermions (particles with half-integer spin). Because of the Pauli exclusion principle, no more than two fermions can occupy the same quantum state (such as an orbital in a molecule or a solid). The familiar consequence of this rule is the aufbau filling of orbitals with spin-paired electrons in each energy level. In contrast, particles with integer spins - which are called bosons - do not have this restriction, and any number of bosons can occupy the same quantized energy level.

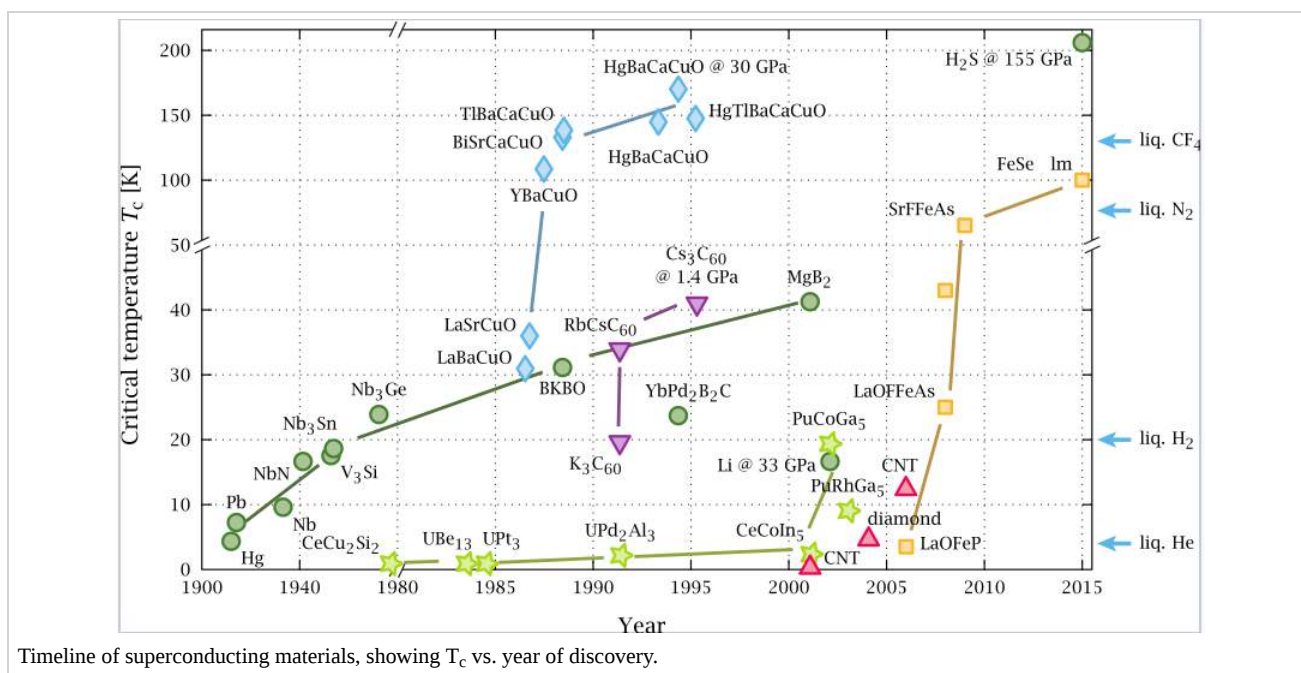
Superconductivity occurs when electrons spin pair into so-called Cooper pairs, which can travel through the lattice together. The electrons in a Cooper pair, although spin-paired, have a long-distance relationship: the spatial extent of a Cooper pair is a few nanometers in cuprate superconductors, and up to one micron in low T_c superconductors such as aluminum. Because its overall spin angular momentum is zero, a Cooper pair is a boson. When the temperature is low enough, the Cooper pairs "condense" into the lowest energy level. The second lowest energy level - which is typically a few meV above the ground state - is not accessible to them as long as the energy gap is larger than the thermal energy, kT . The scattering of electrons by the lattice then becomes forbidden by energy conservation because scattering dissipates energy, and the Cooper pairs cannot change their energy state. Thus the resistance (which arises from scattering, as we learned in Ch. 6) drops abruptly to zero below T_c . However, the Cooper pairs can be broken apart when they move fast, and thus superconductors turn back into normal metals (even below T_c) above some critical current density j_c . This phenomenon is also related to the critical magnetic field, H_c , that quenches superconductivity.



A trampoline for electrons

What causes electrons, which repel each other because of their negative charge, to pair up and travel together in superconductors? The mechanism - which must involve some kind of attractive interaction between electrons - is well understood for "conventional" superconductors which have relatively low transition temperatures, but is not yet known with certainty for high temperature oxide superconductors. In conventional, or BCS superconductors, the spin pairing is mediated by the lattice as shown in the figure at the left. A strong electron-lattice interaction causes a distortion in the lattice as an electron moves through. This elastic deformation is felt as an attractive force by a second electron moving in the opposite direction. This can be thought of as analogous to the interaction of two people jumping on a trampoline. The weight of the first person on the trampoline creates a "well" that attracts the second one, and they tend to move together (even if they don't like each other). Strange as this interaction seems, it is supported experimentally by isotope effects on T_c and by quantitative predictions of T_c values in conventional superconductors.

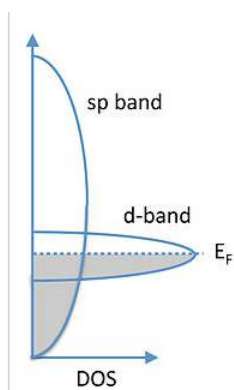
Bad metals make good superconductors. All superconductors are "normal" metals - with finite electrical resistance - above their critical transition temperature, T_c . If you ask where in the periodic table one might look for superconductors, the answer is surprising. The most conductive metals (Ag, Au, Cu, Cs, etc.) make the worst superconductors, i.e., they have the lowest superconducting transition temperatures, in many cases below 0.01 K. Conversely "bad" metals, such as niobium alloys, certain copper oxides, $K_xBa_{1-x}BiO_3$, MgB_2 , FeSe, and alkali salts of C_{60}^{n-} anions, can have relatively high transition temperatures.



We observe that most good superconductors appear in composition space very **near a metal-insulator transition**. In terms of our microscopic picture, orbital overlap in superconductors is poor, just barely enough to make them act as metals ($\Delta \approx U$) above T_c . In the normal state, superconductors with high T_c - which can be as high as 150 K - are typically "bad" metals. An important characteristic of such metals is that the **mean free path** of electrons (in the normal state, above T_c) is on the order of the lattice spacing, i.e., **only a few Å**. In contrast, we learned in Ch. 6 that good metals such as Au, Ag, and Cu have electron mean free paths that are two orders of magnitude longer (ca. 40 nm). In a bad metal, the electron "feels" the lattice rather strongly, whereas in a good metal, the electrons are insensitive to small changes in the distance between metals atoms.

What does the band picture look like for a bad metal? The key point is that because orbital overlap is poor, the metal has a **high density of states** at the Fermi level. This is a universal property of high temperature superconductors and provides a clue of where to look for new and improved superconducting materials. Recall that transition elements in the middle of the 3d series (Cr, Fe, Co, Ni) were magnetic because of poor orbital overlap and weak d-d bonding. The elements below these - especially Nb, Ta, and W - have just barely enough d-d orbital overlap to be on the metallic side of the metal-insulator transition and to be "bad" metals. Carbides and nitrides of these elements are typically superconducting, with the carbon and nitrogen atoms serving to adjust the valence electron density, as illustrated in the table below.

--	--	--



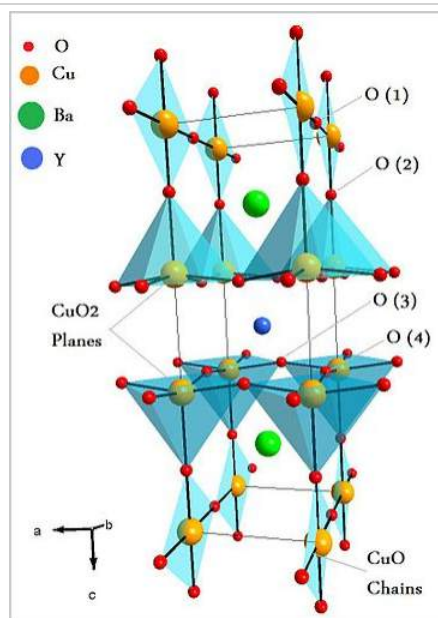
Generic E vs. DOS for a bad metal.

Compound	NbC	Mo ₂ N	TaC	VN	NbN	TaN	Nb ₃ Ge
T _c (K)	11.1	5.0	9.7	7.5	15.2	17.8	22.3

High T_c superconductors

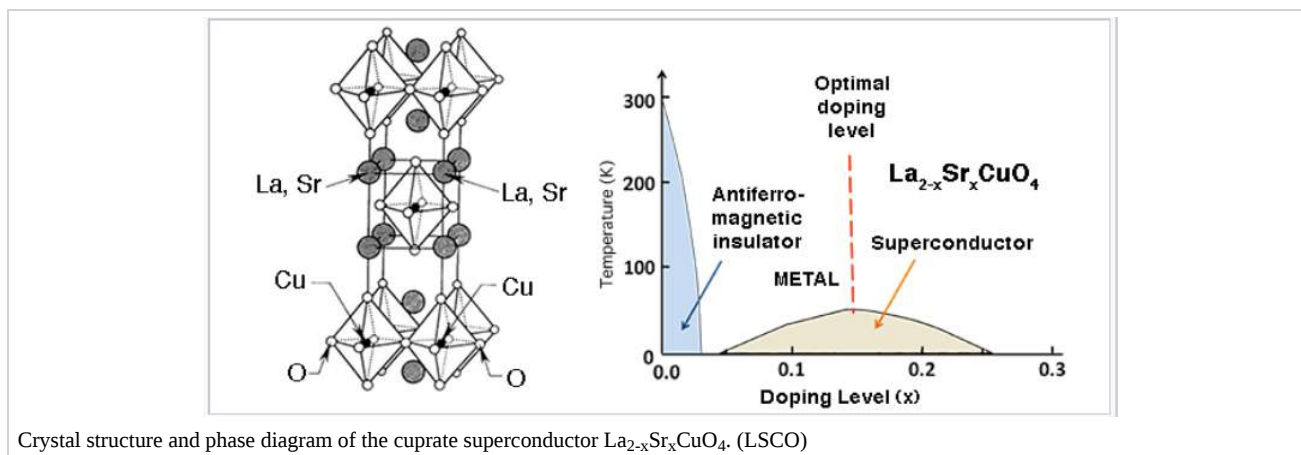
In addition to having weak orbital overlap in the metallic state - which results in a high DOS at E_F - high temperature superconductors also typically contain elements in mixed oxidation states (for example, Cu^{2+/3+} or Bi^{3+/5+}) that are close in energy to the O^{2-/O-} couple in the lattice. At ambient pressure, cuprate superconductors have the highest known T_c values, ranging between about 35 and 150 K. The crystal structures of these materials are almost all variants of the perovskite lattice, as shown at the right for the 1-2-3 superconductor YBa₂Cu₃O_{7-δ}. An ideal perovskite lattice would have formula ABO₃ = A₃B₃O₉. In YBa₂Cu₃O_{7-δ}, Y and Ba occupy the A cation sites, Cu occupies the B sites, and two of the nine O atoms are missing.

The YBa₂Cu₃O_{7-δ} lattice consists of mixed-valent copper(II/III) oxide sheets capped by oxygen atoms to form CuO₅ square pyramids. These sheets encapsulate the Y³⁺ cations. Copper(II) oxide ribbons that share the apical oxygen atoms of the square pyramids run in one direction through the structure. In YBa₂Cu₃O_{7-δ} and related materials, one component of the structure (here the Cu-O ribbons) acts as a **charge reservoir** to control the doping of the planar CuO₂ sheets, which are the elements of the structure that carry the supercurrent. Cuprate superconductors with Bi, Tl, or Hg-containing charge reservoir layers and multiple, eclipsed CuO₂ sheets in the unit cell tend to have the highest T_c values.



Crystal structure of YBa₂Cu₃O_{7-δ} (YBCO), the first superconductor with T_c above the boiling point of liquid nitrogen.

The connection between the metal-insulator transition and superconductivity is nicely illustrated in the phase diagram of $\text{La}_{2-x}\text{Sr}_x\text{CuO}_4$, the first cuprate superconductor, which was discovered in 1986 by Georg Bednorz and K. Alex Müller. This compound has a rather simple structure in which rocksalt $\text{La}(\text{Sr})\text{O}$ layers are intergrown with perovskite $\text{La}(\text{Sr})\text{CuO}_3$ layers. Undoped La_2CuO_4 contains only Cu^{2+} ions and is an antiferromagnetic insulator. As a small amount of Sr^{2+} is substituted for La^{3+} , some of the Cu^{2+} is oxidized to Cu^{3+} , and the lattice is doped with holes. As the doping level increases, the antiferromagnetic phase undergoes a first-order phase transition to a "bad" metal, and at slightly higher doping density the superconducting phase appears. The proximity of the superconducting phase to the metal-insulator transition is a hallmark of cuprate superconductors. A maximum T_c of 35K is observed at $x = 0.15$. Doping at higher levels moves the Fermi level beyond the point of highest DOS in the d-band of Cu and the superconducting phase then gradually disappears. It is interesting to compare this phase diagram with that of V_2O_3 (above), which also undergoes an antiferromagnetic insulator to "bad" metal transition as it is doped.



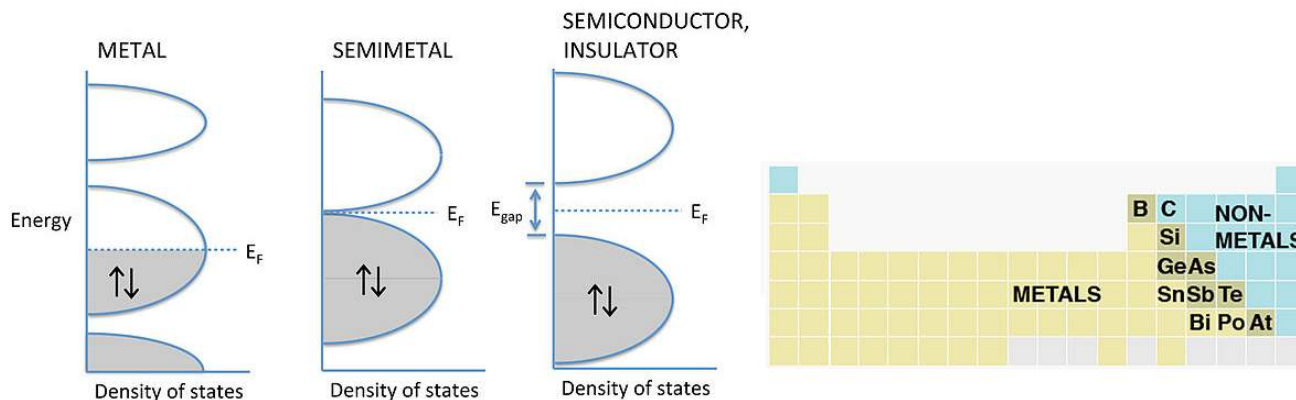
This page titled [10.3: Superconductors](#) is shared under a [CC BY-SA 4.0](#) license and was authored, remixed, and/or curated by [Chemistry 310 \(Wikibook\)](#) via [source content](#) that was edited to the style and standards of the LibreTexts platform; a detailed edit history is available upon request.

10.4: Periodic Trends- Metals, Semiconductors, and Insulators

As we consider periodic trends in the electronic properties of materials, it is important to review some of the key bonding trends we have learned in earlier chapters:

- Going down the periodic table, atoms in solids tend to adopt structures with higher coordination numbers.
- The second row of the periodic table is special, with strong s-p hybridization and π -bonding between atoms.
- Electrons in higher quantum shells are less strongly bound, so the energy difference between bonding and antibonding orbitals becomes smaller for heavier atoms.

We also know that most of the elements in the periodic table are metals, but the elements in the top right corner are insulating under ordinary conditions (1 atm. pressure) and tend to obey the octet rule in their compounds.



At the transition between metals and non-metals in the periodic table we encounter a crossover in electronic properties, as well as in other properties such as the acidity of the oxides (see Ch. 3). The group of elements at the border is loosely referred to as the metalloids. Several of these elements (such as C, Sn, and As) can exist as different allotropes that can be metals, insulators, or something in between.

A more rigorous delineation of the electronic properties of these elements (and of many compounds) can be made by considering their band structures and the **temperature dependence of the electronic conductivity**. As we have previously discussed, metals have partially filled energy bands, meaning that the Fermi level intersects a partially filled band. With increasing temperature, metals become poorer conductors because lattice vibrations (which are called phonons in the physics literature) scatter the mobile valence electrons. In contrast, semiconductors and insulators, which have filled and empty bands, become better conductors at higher temperature, since some electrons are thermally excited to the lowest empty band. The distinction between insulators and semiconductors is arbitrary, and from the point of view of metal-insulator transitions, all semiconductors are insulators. We typically call an insulator a semiconductor if its band gap (E_{gap}) is less than about 3 eV. A semimetal is a material that has a band gap near zero, examples being single sheets of sp^2 -bonded carbon (graphene) and elemental Bi. Like a narrow gap semiconductor, a semimetal has higher conductivity at higher temperature.

This page titled [10.4: Periodic Trends- Metals, Semiconductors, and Insulators](#) is shared under a [CC BY-SA 4.0](#) license and was authored, remixed, and/or curated by [Chemistry 310 \(Wikibook\)](#) via [source content](#) that was edited to the style and standards of the LibreTexts platform; a detailed edit history is available upon request.

10.5: Semiconductors- Band Gaps, Colors, Conductivity and Doping

Semiconductors, as we noted above, are somewhat arbitrarily defined as insulators with **band gap energy** ≤ 3.0 eV (~ 290 kJ/mol). This cutoff is chosen because, as we will see, the conductivity of undoped semiconductors drops off exponentially with the band gap energy and at 3.0 eV it is very low. Also, materials with wider band gaps (e.g. SrTiO₃, $E_{\text{gap}} = 3.2$ eV) do not absorb light in the visible part of the spectrum

There are a number of places where we find semiconductors in the periodic table:

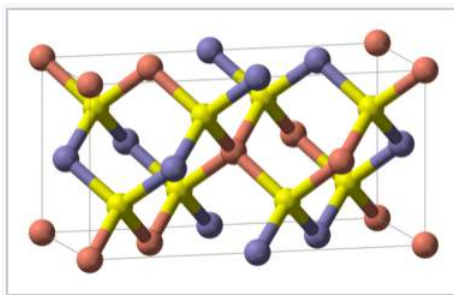
- Early transition metal oxides and nitrides, especially those with d^0 electron counts such as TiO₂, TaON, and WO₃
- Oxides of later 3d elements such as Fe₂O₃, NiO, and Cu₂O
- Layered transition metal chalcogenides with d^0 , d^2 and d^6 electron counts including TiS₂, ZrS₂, MoS₂, WSe₂, and PtS₂
- d^{10} copper and silver halides, e.g., CuI, AgBr, and AgI
- Zincblende- and wurtzite-structure compounds of the p-block elements, especially those that are isoelectronic with Si or Ge, such as GaAs and CdTe. While these are most common, there are other p-block semiconductors that are not isoelectronic and have different structures, including GaS, PbS, and Se.



A 2" wafer cut from a GaAs single crystal. GaAs, like many p-block semiconductors, has the zincblende structure.

The **p-block octet semiconductors** are by far the most studied and important for technological applications, and are the ones that we will discuss in detail.

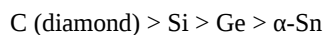
Zincblende- and wurtzite-structure semiconductors have 8 valence electrons per 2 atoms. These combinations include 4-4 (Si, Ge, SiC,...), 3-5 (GaAs, AlSb, InP,...), 2-6 (CdSe, HgTe, ZnO,...), and 1-7 (AgCl, CuBr,...) semiconductors. Other variations that add up to an octet configuration are also possible, such as Cu^IIn^{III}Se₂, which has the **chalcopyrite** structure, shown at the right.



The **chalcopyrite structure** is adopted by ABX₂ octet semiconductors such as Cu^IIn^{III}Se₂ and Cd^{II}Sn^{IV}P₂. The unit cell is doubled relative to the parent **zincblende structure** because of the ordered arrangement of cations. Each anion (yellow) is coordinated by two cations of each type (blue and red).

How does the **band gap energy** vary with **composition**? There are two important trends

(1) Going **down a group** in the periodic table, the gap **decreases**:



E_{gap} (eV): 5.4 1.1 0.7 0.0

This trend can be understood by recalling that E_{gap} is related to the **energy splitting between bonding and antibonding orbitals**. This difference decreases (and bonds become weaker) as the principal quantum number increases.

(2) For isoelectronic compounds, **increasing ionicity** results in a **larger band gap**.

Ge < GaAs < ZnSe
0.7 1.4 2.8 eV

Sn < InSb < CdTe < AgI
0.0 0.2 1.6 2.8 eV

This trend can also be understood from a simple MO picture, as we discussed in Ch. 2. As the electronegativity difference $\Delta\chi$ increases, so does the energy difference between bonding and antibonding orbitals.

The band gap is a very important property of a semiconductor because it determines its color and conductivity. Many of the applications of semiconductors are related to band gaps:

- Narrow gap materials ($\text{Hg}_x\text{Cd}_{1-x}\text{Te}$, VO_2 , InSb , Bi_2Te_3) are used as infrared photodetectors and thermoelectrics (which convert heat to electricity).
- Wider gap materials (Si , GaAs , GaP , GaN , CdTe , $\text{CuIn}_x\text{Ga}_{1-x}\text{Se}_2$) are used in electronics, light-emitting diodes, and solar cells.

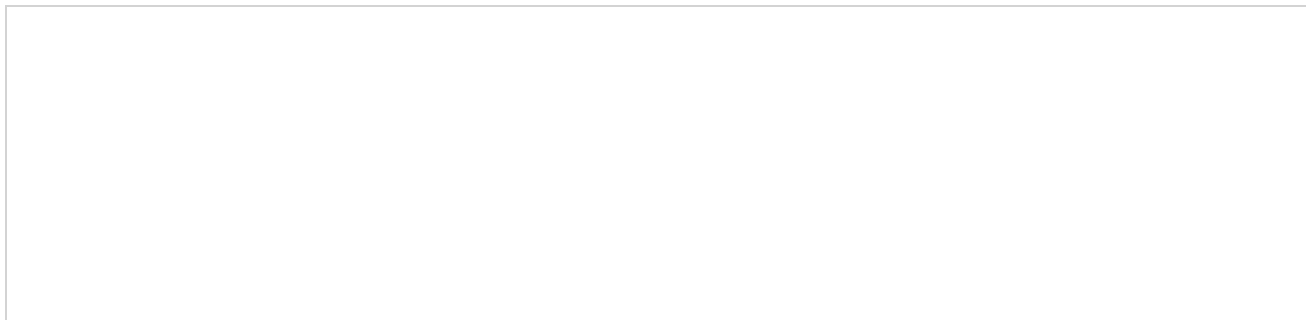


Color wheel showing the colors and wavelengths of emitted light.

Semiconductor solid solutions such as $\text{GaAs}_{1-x}\text{P}_x$ have band gaps that are intermediate between the end member compounds, in this case GaAs and GaP (both zincblende structure). Often, there is a linear relation between composition and band gap, which is referred to as **Vegard's Law**. This "law" is often violated in real materials, but nevertheless offers useful guidance for designing materials with specific band gaps. For example, red and orange light-emitting diodes (LED's) are made from solid solutions with compositions of $\text{GaP}_{0.40}\text{As}_{0.60}$ and $\text{GaP}_{0.65}\text{As}_{0.35}$, respectively. Increasing the mole fraction of the lighter element (P) results in a larger band gap, and thus a higher energy of emitted photons.

Colors of semiconductors

The color of absorbed and emitted light both depend on the band gap of the semiconductor. Visible light covers the range of approximately 390-700 nm, or 1.8-3.1 eV. The **color of emitted light** from an LED or semiconductor laser corresponds to the band gap energy and can be read off the color wheel shown at the right.





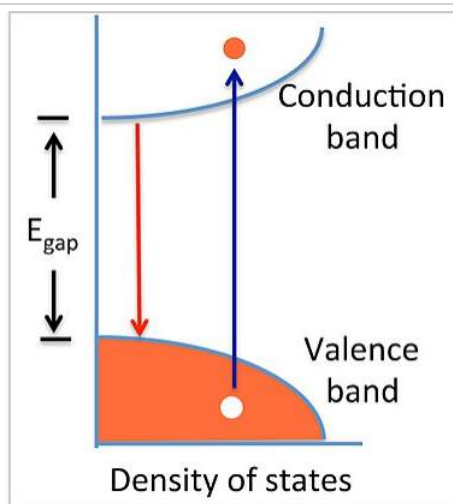
Fe₂O₃ powder is reddish orange because of its 2.2 eV band gap

The color of **absorbed light** includes the band gap energy, but also all colors of higher energy (shorter wavelength), because electrons can be excited from the valence band to a range of energies in the conduction band. Thus semiconductors with band gaps in the infrared (e.g., Si, 1.1 eV and GaAs, 1.4 eV) appear black because they absorb all colors of visible light. Wide band gap semiconductors such as TiO₂ (3.0 eV) are white because they absorb only in the UV. Fe₂O₃ has a band gap of 2.2 eV and thus absorbs light with $\lambda < 560$ nm. It thus appears reddish-orange (the colors of light reflected from Fe₂O₃) because it absorbs green, blue, and violet light. Similarly, CdS ($E_{\text{gap}} = 2.6$ eV) is yellow because it absorbs blue and violet light.

Electrons and holes in semiconductors

Pure (undoped) semiconductors can conduct electricity when electrons are promoted, either by heat or light, from the valence band to the conduction band. The promotion of an **electron** (e⁻) leaves behind a **hole** (h⁺) in the valence band. The hole, which is the absence of an electron in a bonding orbital, is also a mobile charge carrier, but with a positive charge. The motion of holes in the lattice can be pictured as analogous to the movement of an empty seat in a crowded theater. An empty seat in the middle of a row can move to the end of the row (to accommodate a person arriving late to the movie) if everyone moves over by one seat. Because the movement of the hole is in the opposite direction of electron movement, it acts as a positive charge carrier in an electric field.

The opposite process of excitation, which creates an electron-hole pair, is their recombination. When a conduction band electron drops down to recombine with a valence band hole, both are annihilated and energy is released. This release of energy is responsible for the emission of light in LEDs.



An electron-hole pair is created by adding heat or light energy $E \geq E_{\text{gap}}$ to a semiconductor (blue arrow). The electron-hole pair recombines to release energy equal to E_{gap} (red arrow).

At equilibrium, the creation and annihilation of electron-hole pairs proceed at equal rates. This dynamic equilibrium is analogous to the dissociation-association equilibrium of H⁺ and OH⁻ ions in water. We can write a mass action expression:

$$n \times p = K_{eq} = n_i^2$$

where n and p represent the number density of electrons and holes, respectively, in units of cm^{-3} . The intrinsic carrier concentration, n_i , is equal to the number density of electrons or holes in an undoped semiconductor, where $n = p = n_i$.

Note the similarity to the equation for water autodissociation:

$$[H^+][OH^-] = K_w$$

By analogy, we will see that when we increase n (e.g., by doping), p will decrease, and vice-versa, but their product will remain constant at a given temperature.

Temperature dependence of the carrier concentration. Using the equations $K_{eq} = e^{(\frac{-\Delta G^o}{RT})}$ and $\Delta G^o = \Delta H^o - T\Delta S^o$, we can write:

$$n \times p = n_i^2 = e^{(\frac{\Delta S^o}{R})} e^{(\frac{-\Delta H^o}{RT})} \quad (10.5.1)$$

The entropy change for creating electron hole pairs is given by:

$$\Delta S^o = R \ln(N_V) + R \ln(N_C) = R \ln(N_C N_V) \quad (10.5.2)$$

where N_V and N_C are the effective density of states in the valence and conduction bands, respectively.

and thus we obtain

$$n_i^2 = N_C N_V e^{(-\Delta H^o / RT)} \quad (10.5.3)$$

Since the volume change is negligible, $\Delta H^o \approx \Delta E^o$, and therefore $\frac{\Delta H^o}{R} \approx \frac{E_{gap}}{k}$, from which we obtain

$$n_i^2 = N_C N_V e^{(\frac{-E_{gap}}{kT})} \quad (10.5.4)$$

and finally

$$n = p = n_i = (N_C N_V)^{\frac{1}{2}} e^{(\frac{-E_{gap}}{2kT})} \quad (10.5.5)$$

For pure Si ($E_{gap} = 1.1 \text{ eV}$) with $N \approx 10^{22}/\text{cm}^3$, we can calculate from this equation a carrier density n_i of approximately $10^{10}/\text{cm}^3$ at 300 K. This is about 12 orders of magnitude lower than the valence electron density of Al, the element just to the left of Si in the periodic table. Thus we expect the conductivity of pure semiconductors to be many orders of magnitude lower than those of metals.

Conductivity of intrinsic semiconductors

The conductivity (σ) is the product of the number density of carriers (n or p), their charge (e), and their mobility (μ). Recall from Chapter 6 that μ is the ratio of the carrier drift velocity to the electric field and has units of $\text{cm}^2/\text{Volt-second}$. Typically electrons and holes have somewhat different mobilities (μ_e and μ_h , respectively) so the conductivity is given by:

$$\sigma = ne\mu_e + pe\mu_h \quad (10.5.6)$$

For either type of charge carrier, we recall from Ch. 6 that the mobility μ is given by:

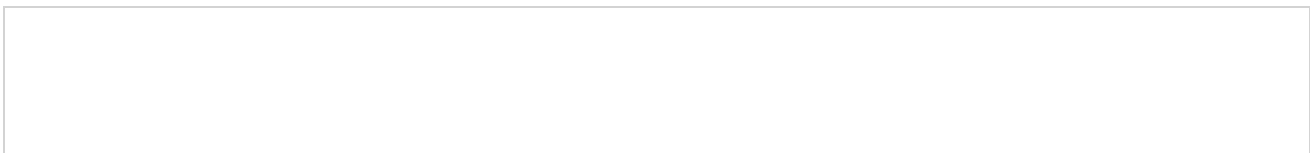
$$\mu = \frac{v_{drift}}{E} = \frac{e\tau}{m} \quad (10.5.7)$$

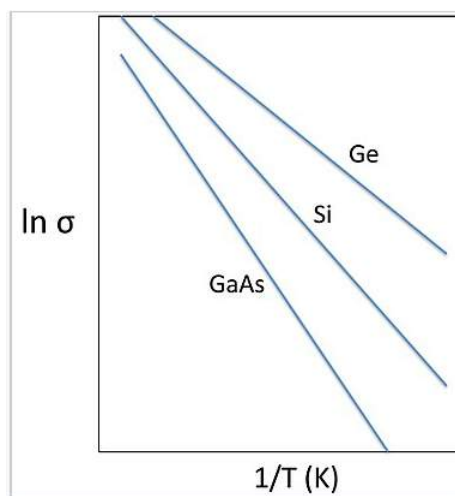
where e is the fundamental unit of charge, τ is the scattering time, and m is the effective mass of the charge carrier.

Taking an average of the electron and hole mobilities, and using $n = p$, we obtain

$$\sigma = \sigma_o e^{(\frac{-E_{gap}}{2kT})}, \text{ where } \sigma_o = 2(N_C N_V)^{\frac{1}{2}} e\mu \quad (10.5.8)$$

By measuring the conductivity as a function of temperature, it is possible to obtain the activation energy for conduction, which is $E_{gap}/2$. This kind of plot, which resembles an Arrhenius plot, is shown at the right for three different undoped semiconductors. The slope of the line in each case is $-E_{gap}/2k$.



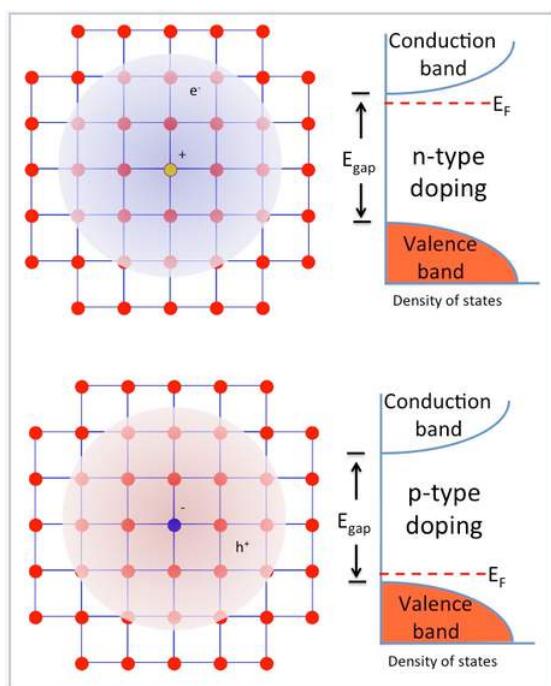


Plots of $\ln(\sigma)$ vs. inverse temperature for intrinsic semiconductors Ge ($E_{\text{gap}} = 0.7$ eV), Si (1.1 eV) and GaAs (1.4 eV). The slope of the line is $-E_{\text{gap}}/2k$.

Doping of semiconductors. Almost all applications of semiconductors involve controlled **doping**, which is the substitution of impurity atoms, into the lattice. Very small amounts of dopants (in the parts-per-million range) dramatically affect the conductivity of semiconductors. For this reason, very pure semiconductor materials that are carefully doped - both in terms of the concentration and spatial distribution of impurity atoms - are needed.

n- and p-type doping. In crystalline Si, each atom has four valence electrons and makes four bonds to its neighbors. This is exactly the right number of electrons to completely fill the valence band of the semiconductor. Introducing a phosphorus atom into the lattice (the positively charged atom in the figure at the right) adds an extra electron, because P has five valence electrons and only needs four to make bonds to its neighbors. The extra electron, at low temperature, is bound to the phosphorus atom in a hydrogen-like molecular orbital that is much larger than the 3s orbital of an isolated P atom because of the high dielectric constant of the semiconductor. In silicon, this "expanded" Bohr radius is about 42 \AA , i.e., 80 times larger than in the hydrogen atom. The energy needed to ionize this electron - to allow it to move freely in the lattice - is only about 40–50 meV, which is not much larger than the thermal energy (26 meV) at room temperature. Therefore the Fermi level lies just below the conduction band edge, and a large fraction of these extra electrons are promoted to the conduction band at room temperature, leaving behind fixed positive charges on the P atom sites. The crystal is **n-doped**, meaning that the majority carrier (electron) is negatively charged.

Alternatively, boron can be substituted for silicon in the lattice, resulting in **p-type** doping, in which the majority carrier (hole) is positively charged. Boron has only three valence electrons, and "borrows" one from the Si lattice, creating a positively charged hole that exists in a large hydrogen-like orbital around the B atom. This hole can become delocalized by promoting an electron from the valence band to fill the localized hole state. Again, this process requires only 40–50 meV, and so at room temperature a large fraction of the holes introduced by boron doping exist in delocalized valence band states. The Fermi level (the electron energy level that has a 50% probability of occupancy at zero temperature) lies just above the valence band edge in a p-type semiconductor.



n- and p-type doping of semiconductors involves substitution of electron donor atoms (light orange) or acceptor atoms (blue) into the lattice. These substitutions introduce extra electrons or holes, respectively, which are easily ionized by thermal energy to become free carriers. The Fermi level of a doped semiconductor is a few tens of mV below the conduction band (n-type) or above the valence band (p-type).

As noted above, the doping of semiconductors dramatically changes their conductivity. For example, the intrinsic carrier concentration in Si at 300 K is about 10^{10} cm^{-3} . The mass action equilibrium for electrons and holes also applies to doped semiconductors, so we can write:

$$n \times p = n_i^2 = 10^{20} \text{ cm}^{-6} \text{ at } 300\text{K} \quad (10.5.9)$$

If we substitute P for Si at the level of one part-per-million, the concentration of electrons is about 10^{16} cm^{-3} , since there are approximately $10^{22} \text{ Si atoms/cm}^3$ in the crystal. According to the mass action equation, if $n = 10^{16}$, then $p = 10^4 \text{ cm}^{-3}$. There are three consequences of this calculation:

- The density of carriers in the doped semiconductor (10^{16} cm^{-3}) is much higher than in the undoped material ($\sim 10^{10} \text{ cm}^{-3}$), so the conductivity is also many orders of magnitude higher.
- The activation energy for conduction is only 40–50 meV, so the conductivity does not change much with temperature (unlike in the intrinsic semiconductor)
- The minority carriers (in this case holes) do not contribute to the conductivity, because their concentration is so much lower than that of the majority carrier (electrons).

Similarly, for p-type materials, the conductivity is dominated by holes, and is also much higher than that of the intrinsic semiconductor.

Chemistry of semiconductor doping. Sometimes it is not immediately obvious what kind of doping (n- or p-type) is induced by "messing up" a semiconductor crystal lattice. In addition to substitution of impurity atoms on normal lattice sites (the examples given above for Si), it is also possible to dope with vacancies - missing atoms - and with interstitials - extra atoms on sites that are not ordinarily occupied. Some simple rules are as follows:

- For substitutions, adding an **atom to the right** in the periodic table results in **n-type** doping, and an atom to the **left** in **p-type** doping.

For example, when TiO_2 is doped with Nb on some of the Ti sites, or with F on O sites, the result is n-type doping. In both cases, the impurity atom has one more valence electron than the atom for which it was substituted. Similarly, substituting a small amount of Zn for Ga in GaAs, or a small amount of Li for Ni in NiO, results in p-type doping.

- **Anion vacancies** result in **n-type** doping, and **cation vacancies** in **p-type** doping.

Examples are anion vacancies in CdS_{1-x} and WO_{3-x} , both of which give n-type semiconductors, and copper vacancies in Cu_{1-x}O , which gives a p-type semiconductor.

- **Interstitial cations** (e.g. Li) donate electrons to the lattice resulting in **n-type** doping. Interstitial anions are rather rare but would result in p-type doping.

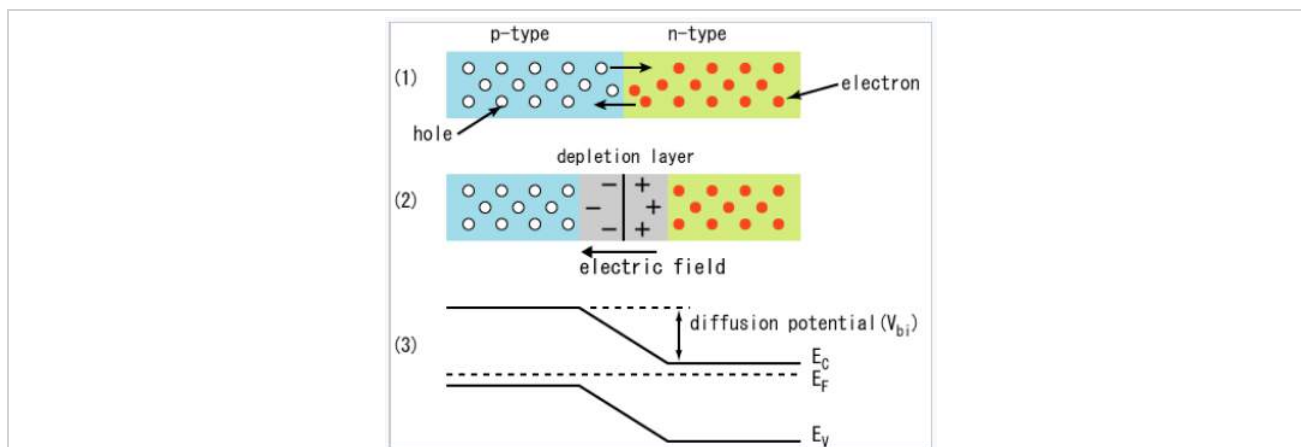
Sometimes, there can be both p- and n-type dopants in the same crystal, for example B and P impurities in a Si lattice, or cation and anion vacancies in a metal oxide lattice. In this case, the two kinds of doping **compensate** each other, and the doping type is determined by the one that is in higher concentration. A dopant can also be present on more than one site. For example, Si can occupy both the Ga and As sites in GaAs, and the two substitutions compensate each other. Si has a slight preference for the Ga site, however, resulting in n-type doping.

This page titled [10.5: Semiconductors- Band Gaps, Colors, Conductivity and Doping](#) is shared under a [CC BY-SA 4.0](#) license and was authored, remixed, and/or curated by [Chemistry 310 \(Wikibook\)](#) via [source content](#) that was edited to the style and standards of the LibreTexts platform; a detailed edit history is available upon request.

10.6: Semiconductor p-n Junctions

Semiconductor p-n junctions are important in many kinds of electronic devices, including diodes, transistors, light-emitting diodes, and photovoltaic cells. To understand the operation of these devices, we first need to look at what happens to electrons and holes when we bring p-type and n-type semiconductors together. At the junction between the two materials, mobile electrons and holes annihilate each other, leaving behind the fixed + and - charges of the electron donor and electron acceptor dopants, respectively. For example, on the n-side of a silicon p-n junction, the positively charged dopants are P^+ ions and on the p-side the negatively charged dopants are B^- . The presence of these uncompensated electrical charges creates an electric field, the **built-in field** of the p-n junction. The region that contains these charges (and a very low density of mobile electrons or holes) is called the **depletion region**.

The electric field, which is created in the depletion region by electron-hole recombination, repels both the electrons (on the n-side) and holes (on the p-side) away from the junction. The concentration gradient of electrons and holes, however, tends to move them in the opposite direction by diffusion. At equilibrium, the flux of mobile carriers is zero because the field-driven migration flux is equal and opposite to the concentration-driven diffusion flux.



When p-type and n-type semiconductors are joined, electrons and holes are annihilated at the interface, leaving a depletion region that contains positively and negatively charged donor and acceptor atoms, respectively. At equilibrium, the Fermi level (E_F) is uniform throughout the junction. E_F lies just above the valence band on the p-type side of the junction and just below the conduction band on the n-type side.

The width of the depletion layer depends on the screening length in the semiconductor, which in turn depends on the dopant density. At high doping levels, the depletion layer is narrow (tens of nanometers across), whereas at low doping density it can be as thick as $1\ \mu\text{m}$. The depletion region is the only place where the electric field is nonzero, and the only place where the bands bend. Elsewhere in the semiconductor the field is zero and the bands are flat.

In the middle of p-n junction, the Fermi level energy, E_F , is halfway between the valence band, VB, and the conduction band, CB, and the semiconductor is intrinsic ($n = p = n_i$)

This page titled [10.6: Semiconductor p-n Junctions](#) is shared under a [CC BY-SA 4.0](#) license and was authored, remixed, and/or curated by [Chemistry 310 \(Wikibook\)](#) via [source content](#) that was edited to the style and standards of the LibreTexts platform; a detailed edit history is available upon request.

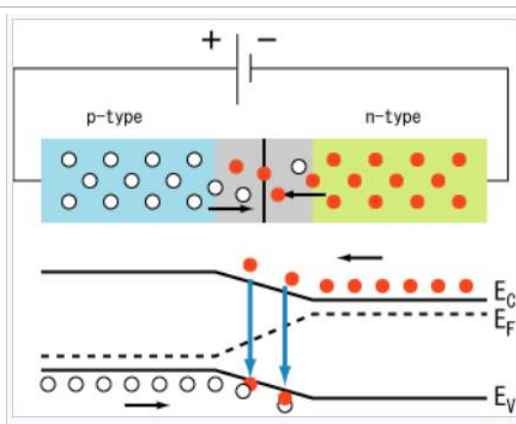
10.7: Diodes, LEDs and Solar Cells

Diodes are semiconductor devices that allow current to flow in only one direction. Diodes act as rectifiers in electronic circuits, and also as efficient light emitters (in LEDs) and solar cells (in photovoltaics). The basic structure of a diode is a junction between a p-type and an n-type semiconductor, called a p-n junction. Typically, diodes are made from a single semiconductor crystal into which p- and n- dopants are introduced.



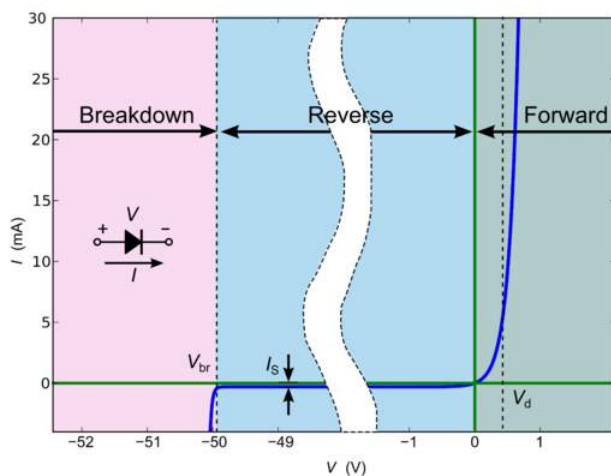
Closeup of a diode, showing the square-shaped semiconductor crystal (*black object on left*) (John Maushammer, [Wikipedia](#), CC-BY-SA)

If the n-side of a diode is biased at positive potential and the p-side is biased negative, electrons are drawn to the n-side and holes to the p-side. This reinforces the built-in potential of the p-n junction, the width of the depletion layer increases, and very little current flows. This polarization direction is referred to as "back bias." If the diode is biased the other way, carriers are driven into the junction where they recombine. The electric field is diminished, the bands are flattened, and current flows easily since the applied bias lowers the built-in potential. This is called "forward bias."



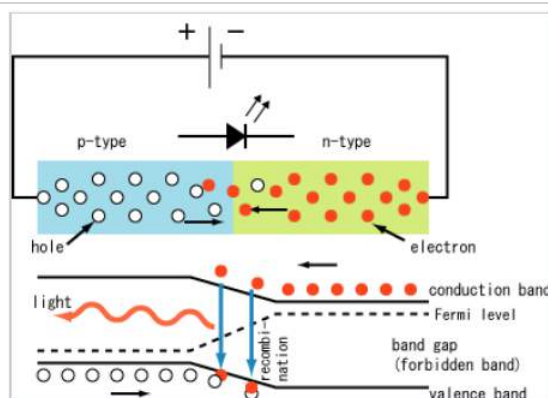
Electrons (red) and holes (white) in a forward-biased diode. (S-kei, [Wikipedia](#), CC-BY-SA)

The figure on the left illustrates a forward-biased diode, through which current flows easily. As electrons and holes are driven into the junction (black arrows in lower left figure), they recombine (downward blue arrows), producing light and/or heat. The Fermi level in the diode is indicated as the dotted line. There is a drop in the Fermi level (equal to the applied bias) across the depletion layer. The corresponding diode i-V curve is shown on the right. The current rises exponentially with applied voltage in the forward bias direction, and there is very little leakage current under reverse bias. At very high reverse bias (typically tens of volts) diodes undergo avalanche breakdown and a large reverse current flows.



Diode i-V curve

A **light-emitting diode** or **LED** is a kind of diode that converts some of the energy of electron-hole recombination into light. This radiative recombination process always occurs in competition with non-radiative recombination, in which the energy is simply converted to heat. When light is emitted from an LED, the photon energy is equal to the bandgap energy. Because of this, LED lights have pure colors and narrow emission spectra relative to other light sources, such as incandescent and fluorescent lights. LED lights are energy-efficient and thus are typically cool to the touch.



Light-emitting diode (LED). (S-kei. [Wikipedia](#), CC-BY-SA)

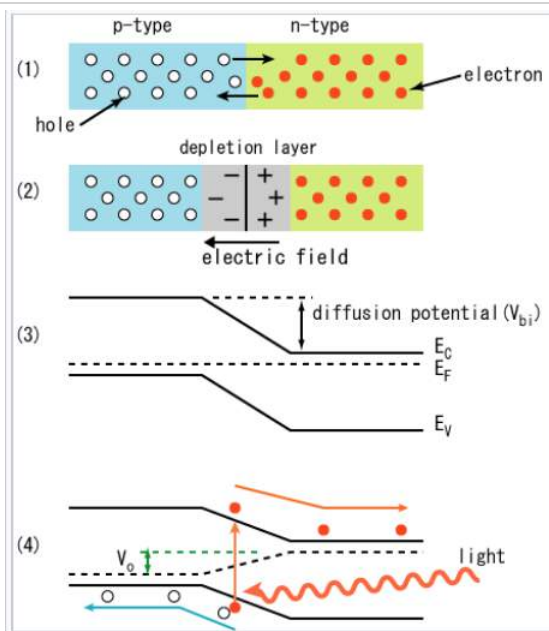
Direct-gap semiconductors such as GaAs and GaP have efficient luminescence and are also good light absorbers. In direct gap semiconductors, there is no momentum change involved in electron-hole creation or recombination. That is, the electrons and holes originate at the same value of the momentum wavevector \mathbf{k} , which we encountered in Ch. 6. \mathbf{k} is related to the momentum (also a vector quantity) by $\mathbf{p} = \hbar\mathbf{k}/2\pi$. In a direct-gap semiconductor, the top of the valence band and the bottom of the conduction band most typically both occur at $\mathbf{k} = 0$. Since the momentum of the photon is close to zero, photon absorption and emission are strongly allowed (and thus kinetically fast). Polar semiconductors such as GaAs, GaN, and CdSe are typically direct-gap materials. **Indirect-gap** semiconductors such as Si and Ge absorb and emit light very weakly because the valence band maximum and conduction band minimum do not occur at the same point in k -space. This means that a lattice vibration (a phonon) must also be created or annihilated in order to conserve momentum. Since this "three body" (electron, hole, phonon) process has low probability, the radiative recombination of electrons and holes is slow relative to non-radiative decay - the thermalization of electron-hole energy as lattice vibrations - in indirect-gap semiconductors. The momentum selection rule thus prevents light absorption/emission and there are no pure Si LEDs or Si-based lasers.



Prof. Shuji Nakamura holding a blue LED.

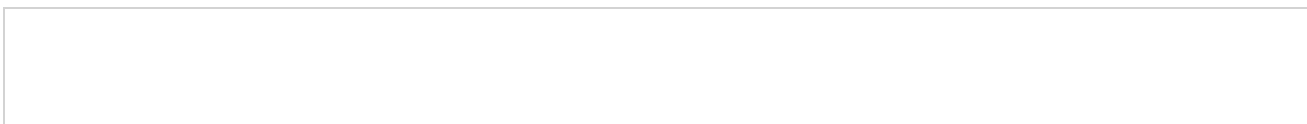
While red, orange, yellow, and green LEDs can be fabricated relatively easily from AlP-GaAs solid solutions, it was initially very difficult to fabricate blue LEDs because the best direct gap semiconductor with a bandgap in the right energy range is a nitride, GaN, which is difficult to make and to dope p-type. Working at Nichia Corporation in Japan, Shuji Nakamura succeeded in developing a manufacturable process for p-GaN, which is the basis of the blue LED. Because of the importance of this work in the development of information storage (Blu-Ray technology) and full-spectrum, energy-efficient LED lighting, Nakamura shared the 2014 Nobel Prize in Physics with Isamu Asaki and Hiroshi Amano, both of whom had made earlier contributions to the development of GaN diodes.

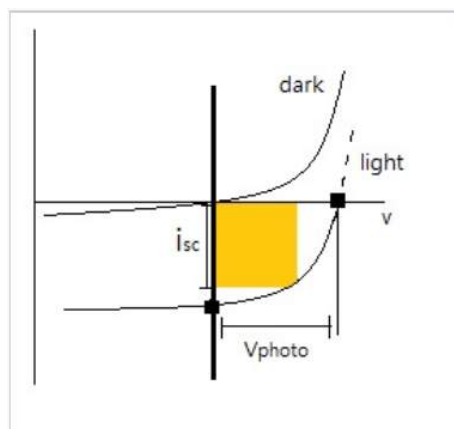
A **Solar cell**, or photovoltaic cell, converts light absorbed in a p-n junction directly to electricity by the photovoltaic effect. Photovoltaics is the field of technology and research related to the development of solar cells for conversion of solar energy to electricity. Sometimes the term solar cell is reserved for devices intended specifically to capture energy from sunlight, whereas the term photovoltaic cell is used when the light source is unspecified.



Photovoltaic effect in a semiconductor p-n junction. (S-kei. Wikipedia, CC-BY-SA)

Photocurrent in p-n junction solar cells flows in the diode reverse bias direction. In the dark, the solar cell simply acts as a diode. In the light, the photocurrent can be thought of as a constant current source, which is added to the i-V characteristic of the diode. The relationship between the dark and light current in a photovoltaic cell is shown in the diagram at the left.

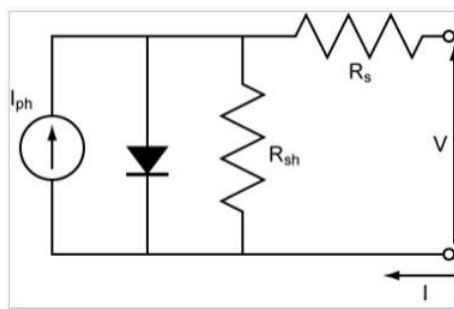




Current-voltage characteristic of a solar cell in the dark and under illumination with band gap light. The short-circuit photocurrent is indicated as i_{sc} , and the open-circuit photovoltage is V_{photo} . The maximum power generated by the solar cell is determined by the area of the orange box.

The built-in electric field of the p-n junction separates $e^- h^+$ pairs that are formed by absorption of bandgap light in the depletion region. The electrons flow downhill, towards the n-type side of the junction, the holes flow uphill towards the p-side. If $h\nu \geq E_{gap}$, light can be absorbed by promoting an electron from the valence band to the conduction band. Any excess energy is rapidly thermalized. Light with $h\nu > E_g$ thus can store only E_g worth of energy in an $e^- h^+$ pair. If light is absorbed outside of depletion region, i.e., on the n- or p-side of the junction where there is no electric field, minority carriers must diffuse into the junction in order to be collected. This process occurs in competition with electron-hole recombination. Because impurity atoms and lattice defects make efficient recombination centers, semiconductors used in solar cells (especially indirect-gap materials such as Si, which must be relatively thick in order to absorb most of the solar spectrum) must be very pure. Most of the cost of silicon solar cells is associated with the process of purifying elemental silicon and growing large single crystals from the melt.

In the photodiode i-V curve above, V_{photo} is typically only about 70% of the bandgap energy E_{gap} . The photocurrent is limited by the photon flux, the recombination rate, and the re-emission of absorbed light.^[6] The area of the orange rectangle indicates the power generated by the solar cell, which can be calculated as $P = i \times V$. In good single crystal or polycrystalline solar cells made of Si, GaAs, CdTe, $CuIn_xGa_{1-x}Se_2$, or $(CH_3NH_3)PbI_3$ the quantum yield (the ratio of short circuit photocurrent to photon flux) is close to unity.

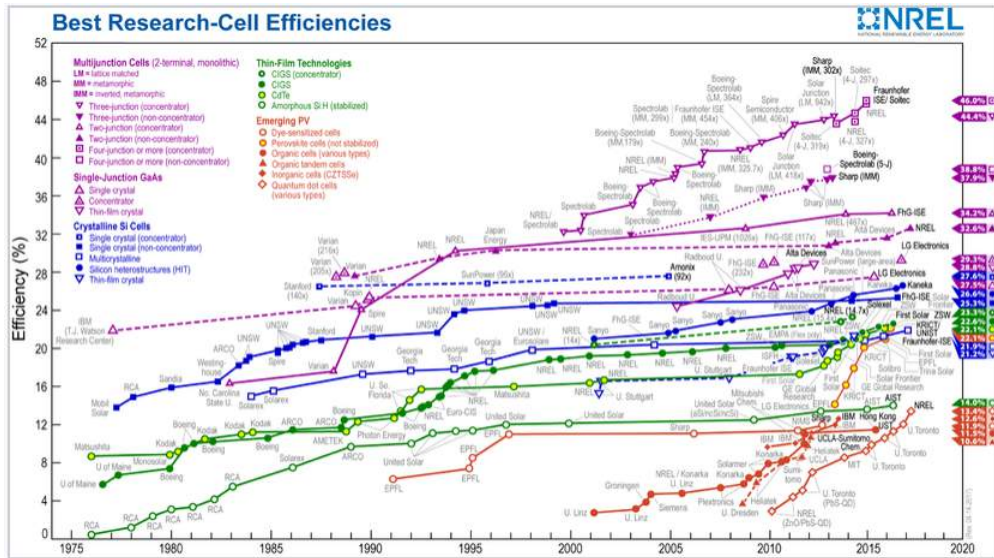


The equivalent circuit of a p-n junction solar cell, which results in the "light" i-V curve shown in the figure above. The solar cell is effectively a diode with a reverse-bias current source provided by light-generated electrons and holes. The shunt resistance (R_{sh}) in the equivalent circuit represents parasitic electron-hole recombination. A high shunt resistance (low recombination rate) and low series resistance (R_s) are needed for high solar cell efficiency.

Solar cells have many current applications. Individual cells are used for powering small devices such as electronic calculators. Photovoltaic arrays generate a form of renewable electricity, particularly useful in situations where electrical power from the grid is unavailable such as in remote area power systems, Earth-orbiting satellites and space probes, remote radio-telephones and water pumping applications. Photovoltaic electricity is also increasingly deployed in grid-tied electrical systems.

The cost of installed photovoltaics (calculated on a per-watt basis) has dropped over the past decade at a rate of about 13% per year, and has already reached grid parity in Germany and a number of other countries.^[7] Photovoltaic grid parity is anticipated in U.S. power markets in the 2020 timeframe.^[8] A major driver in the progressively lower cost of photovoltaic power is the steadily

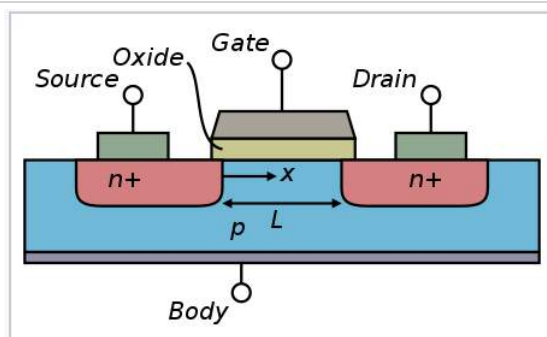
increasing efficiency of solar cells, which is shown in the graphic at the right. Higher efficiency solar cells require less area to deliver the same amount of power, and this lowers the "balance of system" costs such as wiring, roof mounting, etc., which scale as the area of the solar panels. Progress towards higher efficiency reflects improved processes for making photovoltaic materials such as silicon and gallium arsenide, as well as the discovery of new materials. Silicon solar cells are a mature technology, so they are now in the flat part of the learning curve and are approaching their maximum theoretical efficiencies. Newer technologies such as organic photovoltaics, quantum dot solar cells, and lead halide perovskite cells are still in the rising part of the learning curve.



Reported timeline of solar cell energy conversion efficiencies since 1976 (National Renewable Energy Laboratory)

A **field effect transistor (FET)** is a transistor that uses an electric field to control the width of a conducting channel and thus the current in a semiconductor material. It is classified as unipolar transistor, in contrast to bipolar transistors.

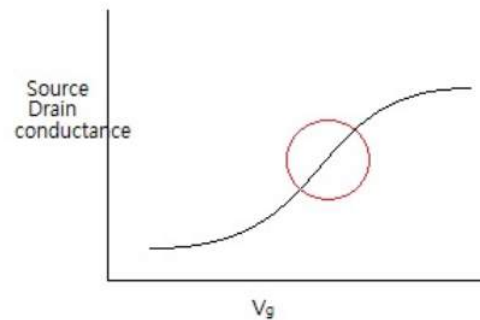
Field effect transistors function as current amplifiers. The typical structure of Si-based FETs is one in which two n-type regions (the source and the drain) are separated by a p-type region. An oxide insulator over the p-type region separates a metal gate lead from the semiconductor. This structure is called a metal-oxide-semiconductor FET (or MOSFET). When voltage is applied between source and drain, current cannot flow because either the n-p or the p-n junction is back-biased. When a positive potential is applied to the gate, however, electrons are driven towards the gate, and locally the semiconductor is "inverted" to n-type. Then the current flows easily between the n-type source and drain through the n-channel. The current flow between the source and drain is many times larger than the current through the gate, and thus the FET can act as an amplifier. Current flow can also represent a logical "1," so FETs are also used in digital logic.



Cross section of an n-type MOSFET

In electronic devices such as microprocessors, field-effect transistors are kept in the off-state most of the time in order to minimize background current and power consumption. The FET shown above, which has n-type source and drain regions, is called an NMOS transistor. In a PMOS transistor, the source and drain regions are p-type and the gate is n-type. In CMOS (complementary metal-oxide semiconductor) integrated circuits, both NMOS and PMOS transistors are used. CMOS circuits are constructed in such a way

that all PMOS transistors must have either an input from the voltage source or from another PMOS transistor. Similarly, all NMOS transistors must have either an input from ground or from another NMOS transistor. This arrangement results in low static power consumption.

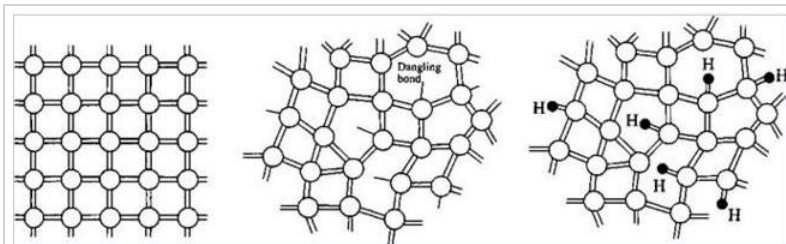


Transistors are most useful in the range of gate voltage (indicated by the red circle in the figure at the left) where the source-drain current changes rapidly. In this region it is possible to effect a large change in current between source and drain when a small signal is applied to the gate. An important figure of merit for FETs is the **subthreshold slope**, which is the slope a plot of $\log(\text{current})$ vs. V_{gate} . An ideal subthreshold slope is one decade of current per 60 mV of gate bias. Typically, a decade change in source-drain current can be achieved with a change in gate voltage of ~ 70 mV. The performance of FETs as switches and amplifiers is limited by the subthreshold slope, which in turn is limited by the capacitance of the gate. It is desirable to have a very high gate capacitance, which requires a thin insulating oxide, but also to have a small leakage current, which requires a thick oxide. A current challenge in the semiconductor industry is to continue to scale FETs to even smaller nanoscale dimensions while maintaining acceptable values of these parameters. This is being done by developing new gate insulator materials that have higher dielectric constants than silicon oxide and do not undergo redox reactions with silicon or with metal gate leads. Only a few known materials (such as hafnium oxynitride and hafnium silicates) currently meet these stringent requirements.

This page titled [10.7: Diodes, LEDs and Solar Cells](#) is shared under a [CC BY-SA 4.0](#) license and was authored, remixed, and/or curated by [Chemistry 310 \(Wikibook\)](#) via [source content](#) that was edited to the style and standards of the LibreTexts platform; a detailed edit history is available upon request.

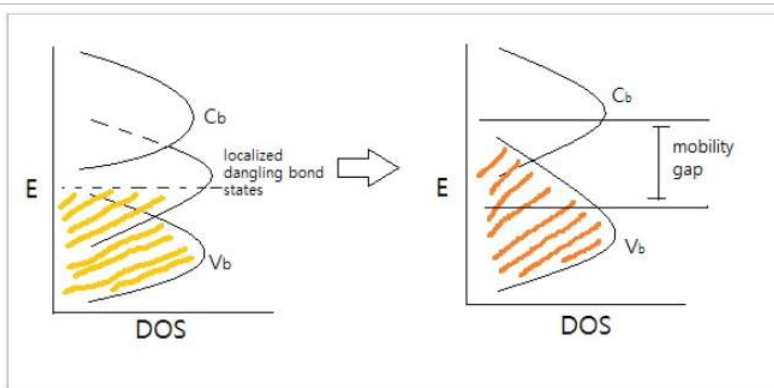
10.8: Amorphous Semiconductors

Amorphous semiconductors are disordered or glassy forms of crystalline semiconductor materials. Like non-conducting glasses, they are network structures with primarily covalent bonding. Crystalline silicon, which has the diamond structure, is an ordered arrangement of fused six-membered silicon rings, all in the "chair" conformation, as we saw in Ch. 8. The local bonding environment of the silicon atoms is tetrahedral. The silicon atoms in amorphous silicon (a-Si) are also predominantly tetrahedrally coordinated, but there is no long-range order in the structure. In addition to six-membered rings, there are five- and seven-membered rings, as well as some "dangling bond" sites in which Si atoms have only three nearest neighbors.



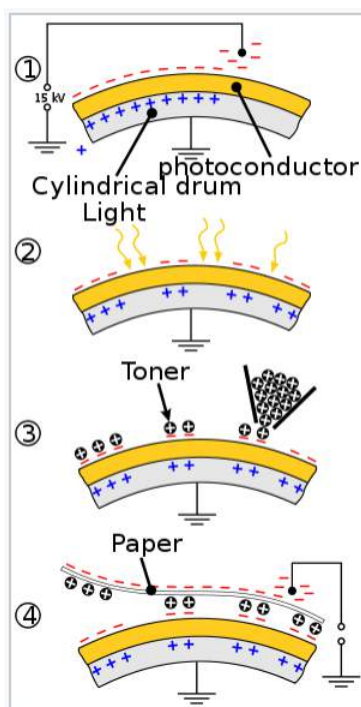
Schematic illustration of the structures of crystalline silicon (left), amorphous silicon (middle), and amorphous hydrogenated silicon (right)

Two of the most widely studied amorphous semiconductors are a-Si and amorphous selenium, a-Se. Si and Se can both be made in glassy form, usually by sputtering or evaporation at relatively low temperature. In a-Se, as in a-Si, locally, most of the atoms have their "normal" valence, but there are many defects and irregularities in the structure. Dangling bonds in amorphous semiconductors have orbital energies in the middle of gap, and electrons in these states are effectively non-bonding. Because these dangling bond sites are far apart from each other, there is little orbital overlap between them, and they also exist over a range of energies. Electrons in these mid-gap states are therefore **localized**, a phenomenon known as Anderson localization. Amorphous Si is insulating because electrons the Fermi level (in the middle of the gap) are not mobile in the lattice. These localized states create a mobility gap, and only electrons in states that are strongly bonding or antibonding are delocalized. Therefore, unmodified a-Si is not very useful as a semiconductor. However, by hydrogenating the material as it is formed (typically in a plasma of H atoms), the under-coordinated Si atoms are bonded to hydrogen atoms. This generates filled bonding and empty antibonding orbitals, the energies of which are outside the mobility gap. Hydrogenation thus lowers the density of states in the mobility gap. Hydrogenated amorphous silicon (a-Si:H) is insulating in the dark, but is a good photoconductor because light absorption creates electrons and holes in mobile states that are outside the mobility gap.



Energy vs. DOS for an amorphous semiconductor. Disorder and dangling bonds result in localized mid-gap states.

The photoconductivity of **amorphous Se** is exploited in xerography. A conductive drum coated with a-Se, which is insulating, is charged with static electricity by corona discharge from a wire. When the drum is exposed to a pattern of light and dark (the image to be duplicated), the illuminated a-Se areas become conductive and the static charge is dissipated from those parts of the drum. Carbon-containing toner particles then adhere via static charge to the areas that were not exposed to light, and are transferred and bonded to paper to make the copy. The speed of the process and the high resolution of pattern transfer depend on the very low conductivity of a-Se in the dark and its high conductivity under illumination.



Charging of amorphous Se and pattern transfer in the xerographic cycle.

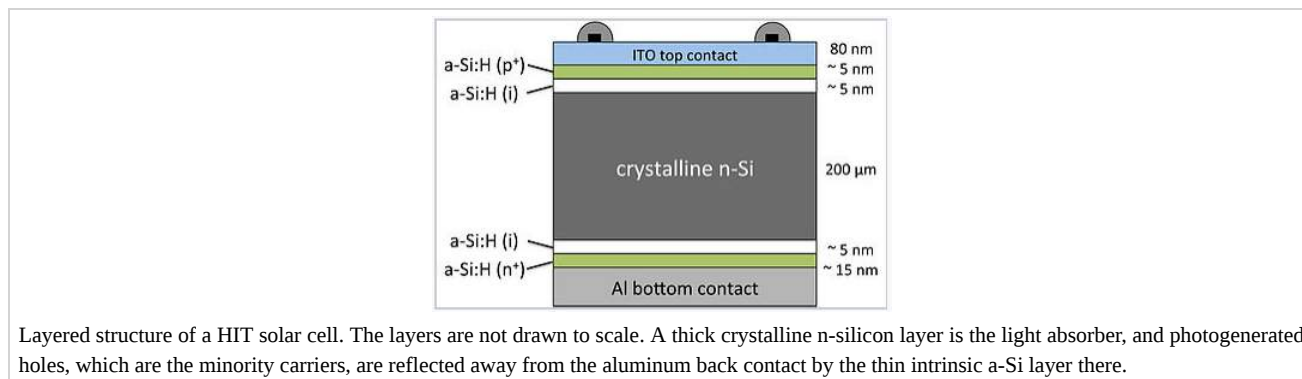
Amorphous hydrogenated Si is used in inexpensive thin film solar cells. The mobility gap is about 1.7 eV, which is larger than the bandgap crystalline of Si (1.1 eV). a-Si:H is a direct-gap material, and therefore thin films are good light absorbers. a-Si:H solar cells can be vapor-deposited in large-area sheets. p⁺Si-a-Si:H-n⁺Si cells have around 10% power conversion efficiency. However amorphous Si solar cells gradually lose efficiency as they are exposed to light. The mechanism of this efficiency loss, called the Staebler-Wronski effect,^[9] involves photogenerated electron-hole pairs which have sufficient energy to cause chemical changes in the material. While the exact mechanism is still unclear, it has been proposed that the energy of electron-hole recombination breaks a weak Si-Si bond, and that one of the resulting dangling bonds abstracts a H atom, leaving a passivated Si-H center and a permanent dangling bond. The effect is minimized by hydrogenating a-Si and can be partially reversed by annealing.



A calculator that runs on solar and battery power

Thin layers of amorphous silicon are used in conjunction with crystalline silicon in heterojunction intrinsic thin-layer (HIT) solar cells.^[10] Because the mobility gap of a-Si is wider than the bandgap of c-Si, there is a potential energy barrier at the amorphous-crystalline interface that reflects electrons and holes away from that interface. At the p⁺ contact, only holes can tunnel through the

barrier, whereas only electrons can tunnel through the barrier to the n^+ contact. The passivation of surface defects that are sites of electron-hole recombination prevents a major loss mechanism in solar cells, increasing both the photovoltage and the photocurrent relative to conventional c-Si p-n junction cells. Panasonic and Sanyo have announced the production of HIT cells with power conversion efficiencies as high as 23%.



This page titled [10.8: Amorphous Semiconductors](#) is shared under a [CC BY-SA 4.0](#) license and was authored, remixed, and/or curated by [Chemistry 310 \(Wikibook\)](#) via [source content](#) that was edited to the style and standards of the LibreTexts platform; a detailed edit history is available upon request.

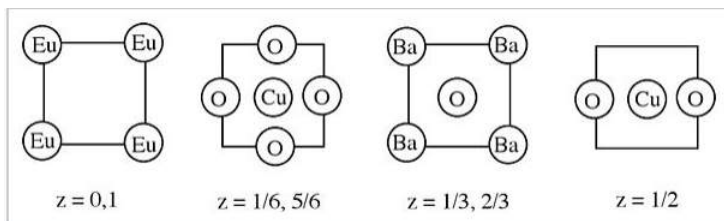
10.9: Discussion Questions

- How is magnetic ordering in the 3d transition metals (Fe, Co, Ni) and the absence of magnetism in the elements just below them (Ru, Ir, Pd) related to the metal-insulator transition?
 - Why are good metals bad superconductors and vice-versa?
 - Discuss why semiconducting oxides of early transition metals such as TiO_2 and Nb_2O_5 can be doped n-type but not p-type. Conversely, semiconducting late transition metal oxides such as NiO and Cu_2O can be doped p-type but not n-type.
-

This page titled [10.9: Discussion Questions](#) is shared under a [CC BY-SA 4.0](#) license and was authored, remixed, and/or curated by [Chemistry 310 \(Wikibook\)](#) via [source content](#) that was edited to the style and standards of the LibreTexts platform; a detailed edit history is available upon request.

10.10: Problems

1. The structure of a high temperature superconductor containing barium, europium, copper, and oxygen is shown below. What are the coordination environments of Cu in this compound? This structure is actually closely related to perovskite, ABO_3 . Explain the relationship between this structure and the ideal perovskite structure.



2. VO_2 can exist in insulating or metallic form, depending on temperature and pressure. Which form would be stabilized by increasing the temperature? Explain your answer.

3. Explain briefly how and why the bandgaps for octet p-block semiconductors vary (1) with the average principal quantum number, and (2) with the electronegativity difference between anion and cation.

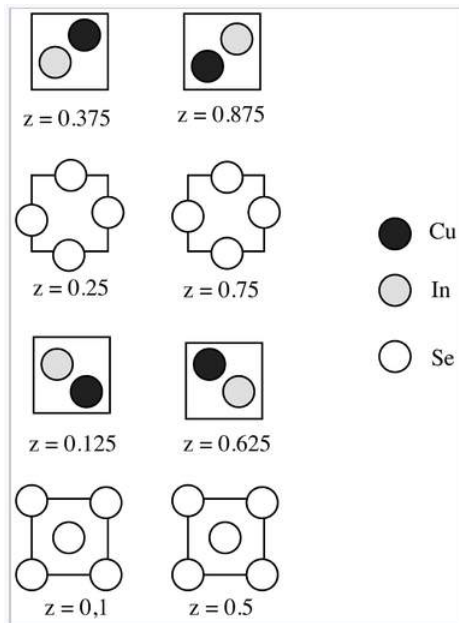
4. Indicate the type of conduction (n or p) in the following: (a) Se-doped GaAs, (b) $InAs_{1-x}$, where $x \ll 1$, (c) $Li_{0.05}Ni_{0.95}O$, (d) Li_xWO_3 , where $x \ll 1$.

5. The structure of copper indium selenide, a semiconductor used in thin film solar cells, is shown below in sections.

(a) What is the stoichiometry of the compound?

(b) What kind of doping (n or p) will occur if a small amount of iodine is substituted for selenium?

(c) What kind of doping (n or p) will occur if a small fraction of the indium sites are occupied by copper atoms?

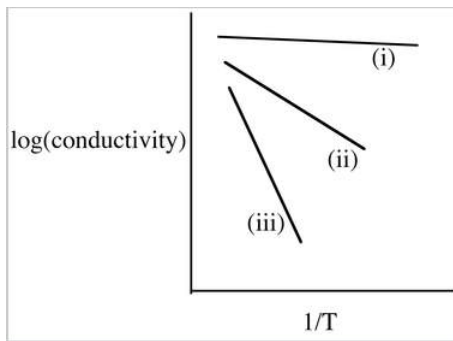


6. Using $1 \text{ eV} = 1240 \text{ nm}$, predict the colors of anatase TiO_2 ($E_g = 3.1 \text{ eV}$), SiC (2.0 eV), $ZnSnP_2$ (1.7 eV), $ZnGeP_2$ (1.9 eV), and InP (1.27 eV).

7. The conductivity of a certain intrinsic (undoped) semiconductor increases by a factor of two when the temperature is raised from 300 to 330 K. What is the bandgap (in eV)? $R = 8.314 \text{ J/mol-K}$, $1 \text{ eV/atom} = 96.52 \text{ kJ/mole}$.

8. Pure Ge is much more conductive than pure Si. Given their bandgaps (0.74 and 1.15 eV , respectively), estimate the ratio of their conductivities at room temperature.

9. The figure below illustrates the trends in conductivity vs. inverse temperature for Si, Ge, and As-doped Ge. Identify lines (i), (ii), and (iii) with the appropriate materials. Explain why the slope of line (i) is close to zero.



10. Sketch a silicon p-n junction, showing the depletion region, band bending, and the Fermi level in the absence of light or applied potential. In the dark, the p-n junction acts as a rectifier. (a) Which way do electrons and holes flow most easily in the dark? (b) Does the built in electric field increase or decrease under forward bias? (c) In the light, the junction acts as a photodiode. In this case, under short circuit conditions, do electrons flow in the same direction or in the opposite direction as in (a)? Explain.

This page titled [10.10: Problems](#) is shared under a [CC BY-SA 4.0](#) license and was authored, remixed, and/or curated by [Chemistry 310 \(Wikibook\)](#) via [source content](#) that was edited to the style and standards of the LibreTexts platform; a detailed edit history is available upon request.

10.11: References

1. Hubbard, J. (1963). "Electron Correlations in Narrow Energy Bands". *Proceedings of the Royal Society of London* **276** (1365): 238–257. doi:10.1098/rspa.1963.0204. Bibcode: [1963RSPSA.276..238H](#).
2. T. Mizokawa, Metal-insulator transitions: orbital control, *Nature Physics* **9**, 612–613 (2013), doi: [doi:10.1038/nphys2769](#)
3. N. F. Mott, (1961) "The Transition to the Metallic State," *Phil. Mag.* **6**, 287. DOI: [10.1080/14786436108243318](#).
4. P. P. Edwards and M. J. Sienko (1982) "The Transition to the Metallic State," *Acc. Chem. Res.* **15**, 87-93. DOI: [10.1021/ar00075a004](#)
5. Recent data have disproven this assertion; MacDonalds has finally responded to public opinion and is offering breakfast after 10:30 AM. But the laws of thermodynamics remain immutable and eternal
6. E. Yablonovitch, O. Miller, and S. Kurtz, "Strong Internal and External Luminescence as Solar Cells Approach the Shockley–Queisser Limit," *IEEE Journal of Photovoltaics*, vol. 2, no. 3, pp. 303-311, July 2012.
7. "[Recent facts about photovoltaics in Germany](#)". Fraunhofer ISE. 7 January 2015. Retrieved 17 February 2015.
8. Energy Information Administration, (November 2010). Levelized Cost of New Generation Resources in the Annual Energy Outlook 2011.
9. Staebler, D. L. and Wronski, C. R. Optically induced conductivity changes in discharge-produced hydrogenated amorphous silicon. *J. Appl. Physics.* **51**(6), June 1980.
10. Mishima, T., Taguchi, M., Sakata, H., Maruyama, E., 2011. Development status of high efficiency HIT solar cells. *Sol. Energy Mater. Sol. Cell.* **95**, 18–21. doi:10.1016/j.solmat.2010.04.030

This page titled [10.11: References](#) is shared under a [CC BY-SA 4.0](#) license and was authored, remixed, and/or curated by [Chemistry 310 \(Wikibook\)](#) via [source content](#) that was edited to the style and standards of the LibreTexts platform; a detailed edit history is available upon request.

CHAPTER OVERVIEW

11: Basic Science of Nanomaterials

Learning Objectives

- Understand the physical basis of mesoscopic behavior in nanoscale semiconducting and magnetic particles.
- Describe how the particle-in-a-box equation applies to electrons in quantum wells.
- Use the Brus formula to calculate the band gap energy of nanoscale semiconductor particles.
- Use the surface energy concept to calculate changes in the melting point and vapor pressure of nanoparticles.
- Describe the methods used to make semiconducting and metal nanocrystals of uniform size.
- Explain the origin of the localized surface plasmon resonance effect in metal nanoparticles.
- Describe the emerging analytical and biomedical applications of metal nanoparticles.

Nanomaterials describe materials of which a single unit is sized (in at least one dimension) between 1 and 1000 nanometers, but is usually 1—100 nm. Nanomaterials research takes a materials science-based approach to nanotechnology, leveraging advances in materials metrology and synthesis which have been developed in support of microfabrication research. Materials with structure at the nanoscale often have unique optical, electronic, or mechanical properties. In this chapter we will learn about the basic science of nanomaterials, i.e., what it is about their size that makes them different.

[11.1: Prelude to Basic Science of Nanomaterials](#)

[11.2: Physics and Length Scales- Cavity Laser, Coulomb Blockade, Nanoscale Magnets](#)

[11.3: Semiconductor Quantum Dots](#)

[11.4: Synthesis of Semiconductor Nanocrystals](#)

[11.5: Surface Energy](#)

[11.6: Nanoscale Metal Particles](#)

[11.7: Applications of Nanomaterials](#)

[11.8: Discussion Questions](#)

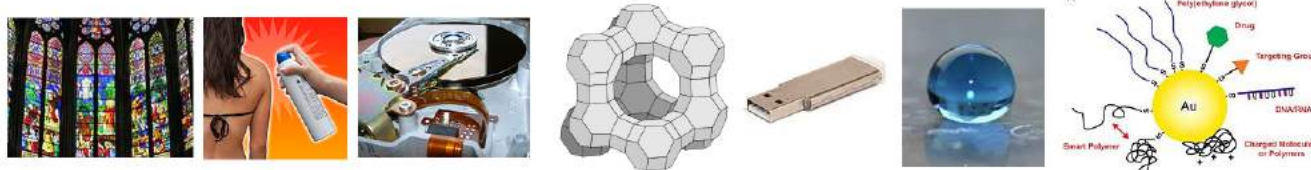
[11.9: Problems](#)

[11.10: References](#)

This page titled [11: Basic Science of Nanomaterials](#) is shared under a [CC BY-SA 4.0](#) license and was authored, remixed, and/or curated by [Chemistry 310 \(Wikibook\)](#) via [source content](#) that was edited to the style and standards of the LibreTexts platform; a detailed edit history is available upon request.

11.1: Prelude to Basic Science of Nanomaterials

What do stained glass, sunscreen, magnetic hard drives, heterogeneous catalysts, consumer electronics, stain-resistant clothing, self-cleaning glass, and medical diagnostics all have in common? All of them derive some special property and utility from **nanoscale materials**: ordinary elements and inorganic compounds such as gold, silver, TiO_2 , chromium, SiO_2 , and silicon that acquire different properties when their characteristic dimensions are somewhere between **1 and 100 nm**. In this chapter we will learn about the basic science of nanomaterials, i.e., what it is about their size that makes them different.



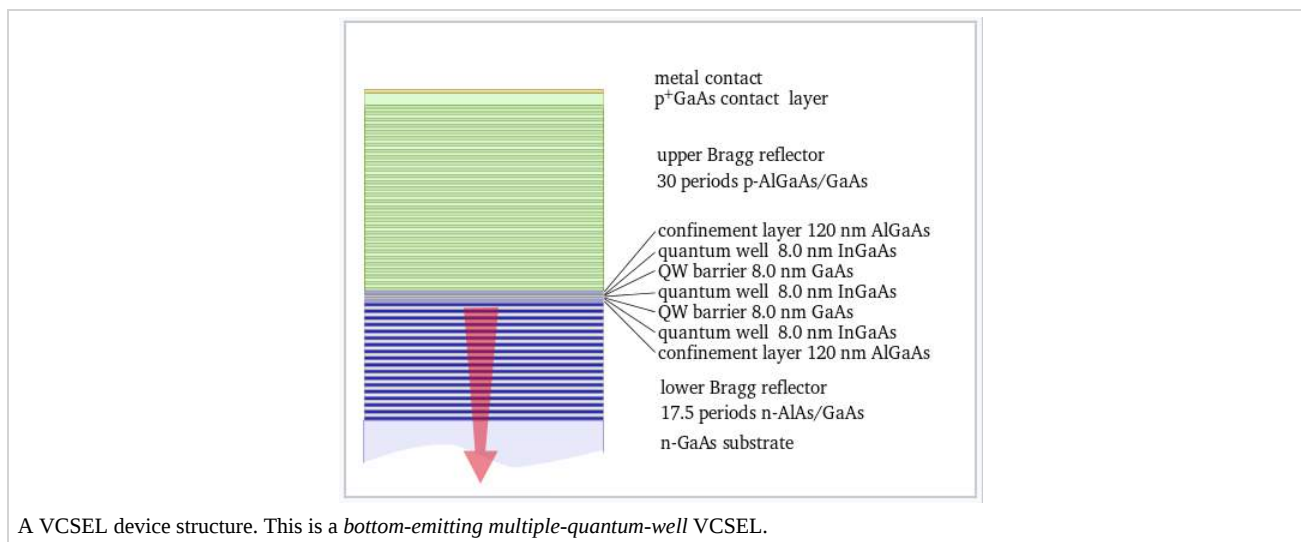
This page titled [11.1: Prelude to Basic Science of Nanomaterials](#) is shared under a [CC BY-SA 4.0](#) license and was authored, remixed, and/or curated by [Chemistry 310 \(Wikibook\)](#) via [source content](#) that was edited to the style and standards of the LibreTexts platform; a detailed edit history is available upon request.

11.2: Physics and Length Scales- Cavity Laser, Coulomb Blockade, Nanoscale Magnets

The special properties of nanomaterials do not derive from different laws of physics, which are the same for objects large and small. For example, Newton's second law ($F = ma$), Coulomb's law ($E = \frac{q_1 q_2}{4\pi\epsilon_0 r}$), and the laws of energy and momentum conservation are the same for buckyballs (C_{60}) and full-size soccer balls. Nevertheless, the physics of electrons, atoms, and photons naturally produce **characteristic length scales**, some of which we have already seen. For example, in Chapter 6 we discovered that the mean free path of an electron in a good metal is about 40 nm. In Chapter 10, we learned that the Bohr radius of an electron or hole in doped Si is about 4 nm, and that the coherence length of Cooper pairs in semiconductors is somewhere between a few nm and 1 μm . When objects become small relative to these characteristic lengths, their physical properties change in interesting ways. Materials that exist at the relevant length scale are called **mesoscopic** (meso = "between," scopic = "size") meaning that they cross over from one kind of behavior - the bulk behavior of large objects - to another. This length scale is different for different kinds of properties, but for many it happens between 1 and 100 nm. We illustrate this point with a few examples.

The cavity laser

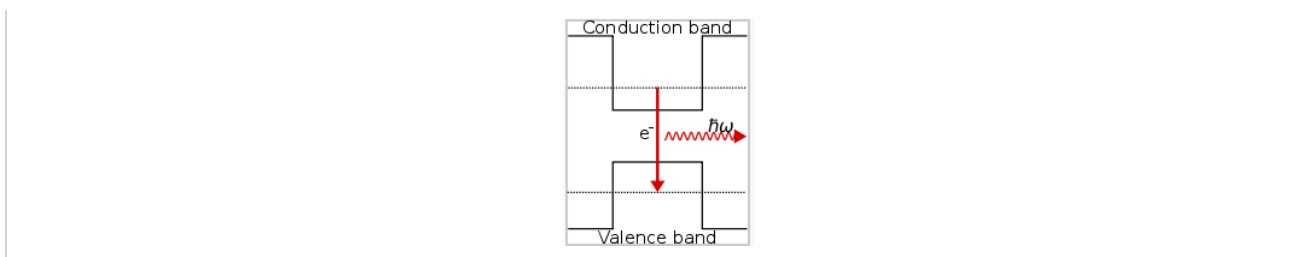
A vertical cavity surface-emitting laser (or VCSEL) is a semiconductor-based device that emits light in the vertical direction relative to the plane of the chip. These devices are being developed and used for high power applications such as laser surgery, infrared illumination for military surveillance, and laser cutting tools. The basic design of a VCSEL is shown at the right. The VCSEL is basically a light-emitting diode, incorporating p-type and n-type regions of the III-V semiconductor (Al,Ga)As. However, it has two special features. First, the refractive index of the semiconductor is modulated above and below the junction to make Bragg mirrors. These mirrors reflect light emitted in the junction, so that the photon density becomes very high there, a necessary condition for stimulated emission and lasing. The Bragg mirror stack is asymmetric (thinner on the bottom), so that light can escape from the junction in one direction only. Second, the junction itself consists of a thin "quantum well" layer of (In,Ga)As, a III-V semiconductor with a smaller band gap than the surrounding (Al,Ga)As layers.



The **quantum well** structure, the band diagram of which is illustrated at the left, is the nanoscale part of the laser. The energies of the conduction and valence bands of (Al,Ga)As flank those of the thin (In,Ga)As layer. Therefore, electrons and holes injected into that layer cannot escape: electrons in (In,Ga)As do not have enough energy to climb "up" to the conduction band of (Al,Ga)As and holes cannot climb "down." Electrons confined to such a small well behave as a particle-in-a-box (as we learned in the context of electrified in Chapter 9).

The electron has a kinetic energy defined by the equation:

$$KE = \frac{h^2 n^2}{8mL^2} \quad (11.2.1)$$



We can calculate the energy difference between the lowest ($n=1$) and next lowest ($n=2$) levels, which is inversely proportional to the square of the thickness (L) of the (In,Ga)As layer. In this calculation we need to use the effective mass of the electron in (In,Ga)As, which is about 7% of the electron rest mass^[1]. With an 8 nm thick layer, this energy is:

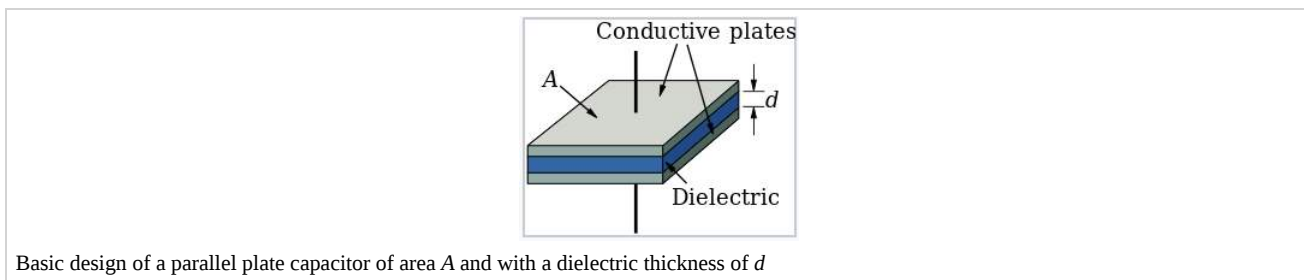
$$E = \frac{(2^2 - 1^2)(6.626 \cdot 10^{-34} \text{ Js})^2}{8 \cdot 0.07 \cdot (9.1 \cdot 10^{-31} \text{ kg})(8 \cdot 10^{-9} \text{ m})^2} = 4.0 \cdot 10^{-20} \text{ J} = 0.25 \text{ eV} \quad (11.2.2)$$

The VCSEL cavity will thus have a resonant energy of 0.25 eV and emit photons at this energy in the infrared ($\lambda \approx 5000 \text{ nm}$). Note that because of the inverse square dependence of the cavity energy on layer thickness, lasers based on this design can only function at nanoscale dimensions. When the cavity is three times thicker, its resonant energy becomes comparable to the thermal energy at room temperature ($kT = 0.026 \text{ eV}$), and the lasing effect is thermally "washed out."

Coulomb blockade

A capacitor is a (macroscopic) device that stores electrical charge. The basic structure of a capacitor is shown at the right. When a voltage is applied to such a device, it develops a charge ($\pm Q$) on the two plates that is proportional to the voltage:

$$C = \frac{Q}{V} \quad (11.2.3)$$



Basic design of a parallel plate capacitor of area A and with a dielectric thickness of d

The magnitude of the capacitance C is determined by the permittivity ϵ and the dimensions of the dielectric layer, A and d .

$$C = \frac{\epsilon A}{d} \quad (11.2.4)$$

We can also calculate the work done in charging the capacitor up (i.e., the energy stored by charging the capacitor) by integrating the voltage times the charge:

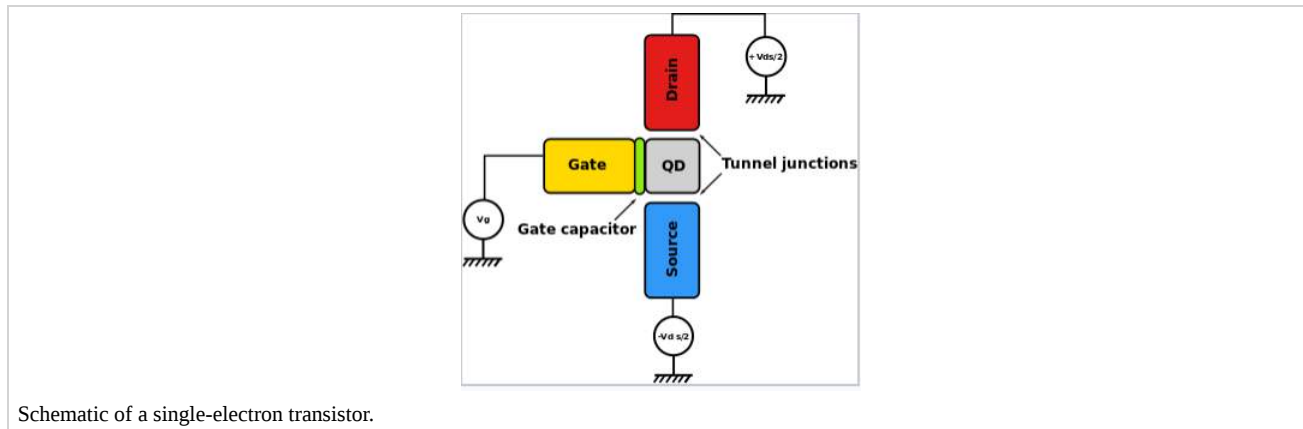
$$E = \int_0^Q V(q) dq = \int_0^Q \frac{q}{C} dq = \frac{1}{2} \frac{Q^2}{C} = \frac{1}{2} CV^2 = \frac{1}{2} VQ \quad (11.2.5)$$

Now it is interesting to ask, what happens to a capacitor when we make it very small? This is of particular interest in a device called a **single electron transistor**, a schematic diagram of which is shown at the right. The metallic gate lead is separated from a "quantum dot," which can be a metal or semiconductor particle, by a thin dielectric layer. This metal-dielectric-metal sandwich acts as a capacitor, and from the equation above, the energy needed to charge it by a single electron ($Q = e$) is:

$$E = \frac{e^2}{2C} \quad (11.2.6)$$

where e is the charge of the electron, $1.602 \times 10^{-19} \text{ Coulomb}$. If the gate width and lateral dimensions are very small - say 2 nm as is readily achievable in self-assembled Coulomb blockade devices^{[2][3]} - then for a typical insulating dielectric, a voltage of about 200 mV is needed to charge the quantum dot by a single electron. Again, this effect is unique to the nanoscale, because a 10 times

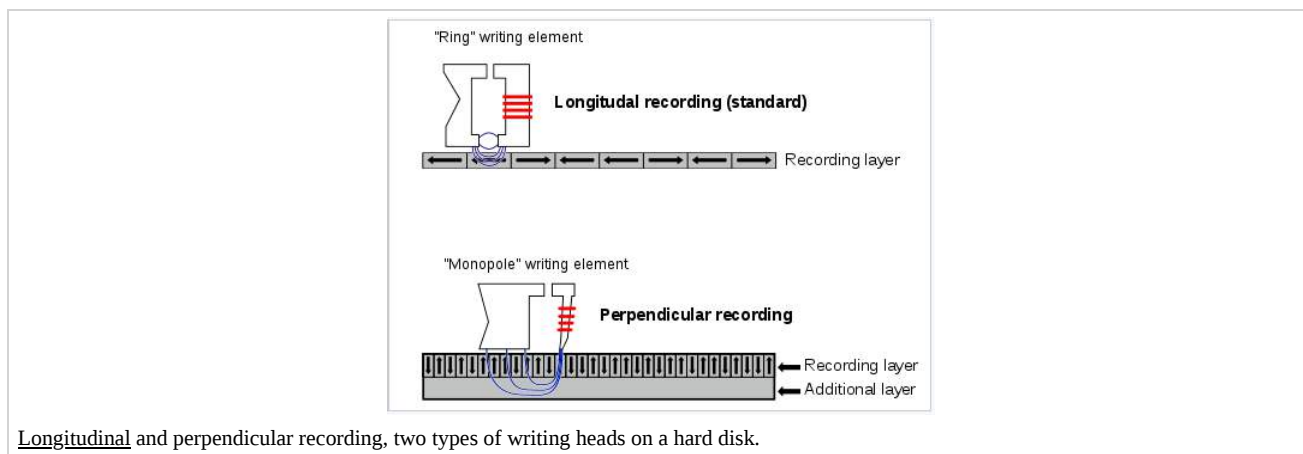
larger device area would make the single-electron charging voltage about 20 mV, which is smaller than the thermal energy kT (26 meV). Thus for devices larger than about 5-6 nm, individual electron charging events are washed out at room temperature by thermal fluctuations.



How can a **nanoscale capacitor** like this act as a **transistor**, which functions as a switch in an electrical circuit? The effect comes from the mutual repulsion of electrons. An electron on the quantum dot repels any other electron that would be forced onto it by applying a small voltage between the source and the drain. Hence the conductance of the quantum dot is very low at a gate bias of zero volts, or at any gate bias (200, 400, 600 mV...) that places an integer number (1, 2, 3,...) of electrons on the dot. But halfway in between these voltages (e.g., at 100, 300, 500 mV) the energy is the same whether there are n or $n+1$ electrons on the dot. This means that electrons can hop on and off without changing their energy, i.e., they can tunnel through the dot from source to drain. This effect gives peaks in the conductance of the dot at regular steps in the gate voltage. In effect, the gate can act as a switch, as in a conventional field-effect transistor. Single-electron transistors are being researched as ultra-sensitive electrometers and single-molecule chemical sensors, since a tiny change in the electrostatic environment of the dot can switch the device on or off.

Nanoscale magnets

Ferro- and ferrimagnetic materials such as iron and chromium oxide are used for digital storage of information in hard disks. The individual memory bits, which can be oriented perpendicular or parallel to the plane of the disk as shown at the right, store a logical "0" or "1" depending on the orientation of their magnetic dipole. To be useful, this information must be non-volatile, i.e., the magnetic bit must retain its polarization in the absence of an applied field from the read/write head.



The storage density of such magnetic memories is impressive. A 2.5" hard drive can now store 1 TB of information, using rod-shaped magnetic grains that are approximately 0.5 μm long. We now have good synthetic methods for making these same materials as crystals with dimensions of only a few nanometers. Why aren't those nanocrystals used to make even more dense memory disks?

The reason is that the energy needed to flip the magnetization (i.e., to turn a "0" into a "1" and vice-versa) is strongly size-dependent. For a ferro- or ferrimagnet this energy is equal to Mr^3 , where M is the magnetic energy per unit volume and r is the characteristic dimension (e.g., the length of the edge of a cube, or the diameter of a sphere) of the magnetic grain. For typical

materials such as iron, this energy becomes comparable to kT when r is about 3-5 nm. Such small particles are superparamagnetic, meaning that they still have a large magnetic moment because of the ordering of their spins, but they do not retain a permanent polarization in the absence of an applied magnetic field. Superparamagnetic particles are thus not useful for magnetic memories, but they are interesting and practical in other ways, for example in ferrofluids, magnetic resonance imaging (MRI), and some emerging medical diagnostic and therapeutic applications.



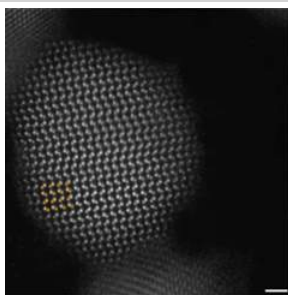
A ferrofluid containing superparamagnetic Fe_3O_4 nanoparticles, which are coated with oleic acid and suspended in oil, in the field of a strong permanent magnet.

In these three illustrative examples (involving light emission, electronic conduction, and magnetic behavior), the transition to new properties involves a crossover in which the characteristic energy of the system is comparable to the thermal energy kT . It just so happens that for many physical phenomena, this crossover occurs on the length scale of nanometers.

This page titled [11.2: Physics and Length Scales- Cavity Laser, Coulomb Blockade, Nanoscale Magnets](#) is shared under a [CC BY-SA 4.0](#) license and was authored, remixed, and/or curated by [Chemistry 310 \(Wikibook\)](#) via [source content](#) that was edited to the style and standards of the LibreTexts platform; a detailed edit history is available upon request.

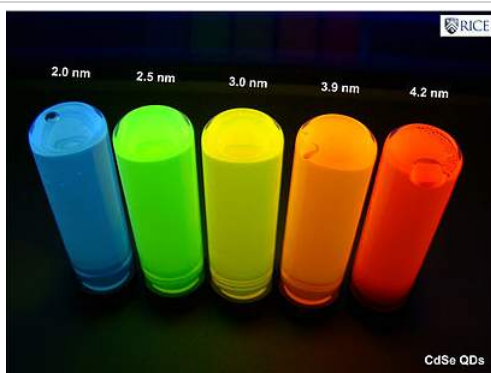
11.3: Semiconductor Quantum Dots

One of the most fascinating and well-studied mesoscopic effects occurs with semiconductor particles of various shapes when one or more of their dimensions is in the range of a few nanometers. These so-called "quantum dots" (0D), "quantum rods" (1D) and "nanosheets" (2D) acquire striking new electronic and optical properties.



Atomic resolution image of a CdSe nanoparticle.

The synthesis of semiconductor quantum dots, which is discussed in more detail below, is sufficiently well controlled to give essentially perfect crystals of a few thousand atoms, something that is statistically impossible in a macroscopic crystal. An image of such a crystal is shown at the right. In the synthesis, these crystals can be capped with an epitaxial layer of ligands or by a shell of a wider bandgap semiconductor (such as ZnS in the case of CdSe), so that the inner core is effectively a quantum well. Electron-hole pairs formed by excitation of the core semiconductor are confined there and cannot reach the external surface of the particle, where they might otherwise be trapped and recombine thermally. Consequently, the quantum yield for bandgap emission of semiconductor quantum dots is typically high, giving rise to the bright emission colors shown at the right for CdSe particles of different sizes. Because of their strong and narrow emission bands, quantum dots are of interest as luminescent tags for biological imaging applications, and also as light absorbers and emitters in solar cells and LEDs.



Emission colors of CdSe nanoparticles of different sizes. Smaller particles emit blue light because the exciton energy increases as the size decreases.

The size-dependence of the emission color comes primarily from a particle-in-a-box effect. The electron and hole that are created when the quantum dot absorbs light are bound together as an **exciton** by the confines of the "box". Louis Brus used first-order perturbation theory to determine that the bandgap of a semiconductor quantum dot is given approximately by:^[4]

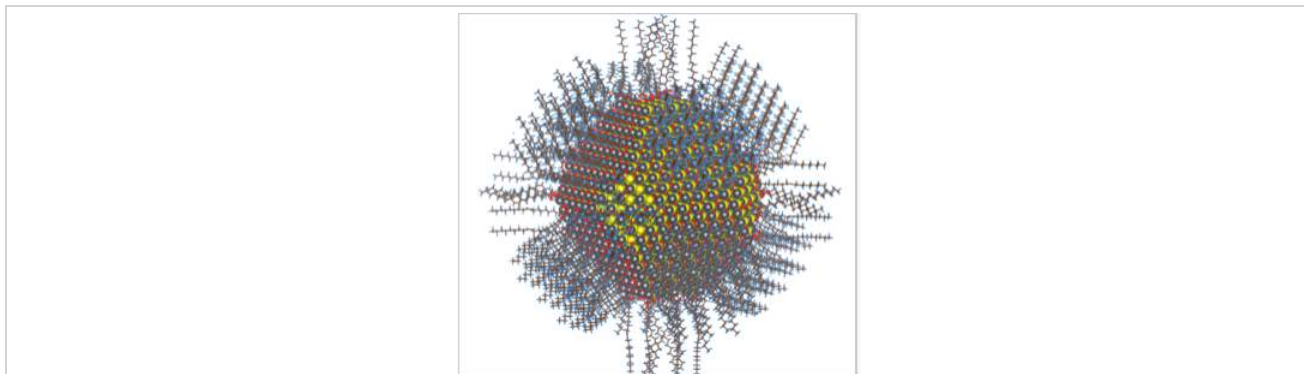
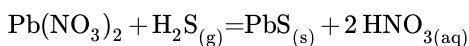
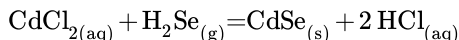
$$E_{gap} = E_{gap,bulk} + \frac{h^2}{8\mu R^2} - \frac{1.8e^2}{4R\pi\epsilon\epsilon_0} + \dots \quad (11.3.1)$$

where R is the particle radius, μ is the electron-hole reduced mass ($1/\mu = 1/m_e^* + 1/m_h^*$), m_e^* and m_h^* are the electron and hole effective masses, and ϵ is the dielectric constant of the semiconductor. In this equation, the first term after the bulk bandgap is the kinetic energy due to confinement of the exciton, and the second term represents the electrostatic attractive energy between the confined electron and hole. Because the energy is a function of R^2 , it can be widely tuned across the visible spectrum by changing the size of the quantum dot.

This page titled [11.3: Semiconductor Quantum Dots](#) is shared under a [CC BY-SA 4.0](#) license and was authored, remixed, and/or curated by [Chemistry 310 \(Wikibook\)](#) via [source content](#) that was edited to the style and standards of the LibreTexts platform; a detailed edit history is available upon request.

11.4: Synthesis of Semiconductor Nanocrystals

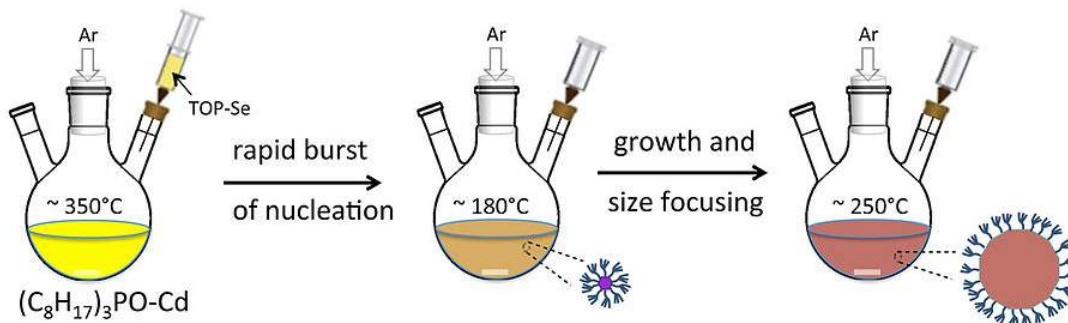
Early work on the quantum size effect in semiconductor nanoparticles used simple metathesis reactions in the synthesis. For example, CdSe and PbS can be precipitated at ambient temperature by the reactions:



Complete atomistic model of a 5 nm diameter colloidal lead sulfide nanoparticle with surface passivation by oleic acid, oleyl and hydroxyl groups.

The growth of the particles was restricted by carrying out these reactions in different matrices, such as in polymer films or the silicate cages of zeolites, and capping ligands were also sometimes used to limit particle growth. While these reactions did produce nanoparticles, in general a broad distribution of particle sizes was obtained. The particles were also unstable to **Ostwald ripening** - in which large particles grow at the expense of smaller ones in order to minimize the total surface energy - because of the reversibility of the acid-forming synthetic reactions in aqueous media. The lack of good samples prevented detailed studies and the development of applications for semiconductor quantum dots.

A very important development in nanoparticle synthesis came in the early 1990's, when Murray, Norris, and Bawendi introduced the first non-aqueous, controlled growth process for II-VI semiconductor quantum dots.^[5] The keys to this synthesis were (1) to use non-aqueous solvents and capping ligands to stabilize the products against ripening, (2) to carry out the reaction at high temperature to ensure good crystallinity, and (3) to separate the steps of particle **nucleation** and **growth**, and thereby obtain particles of uniform size. This procedure is illustrated below:

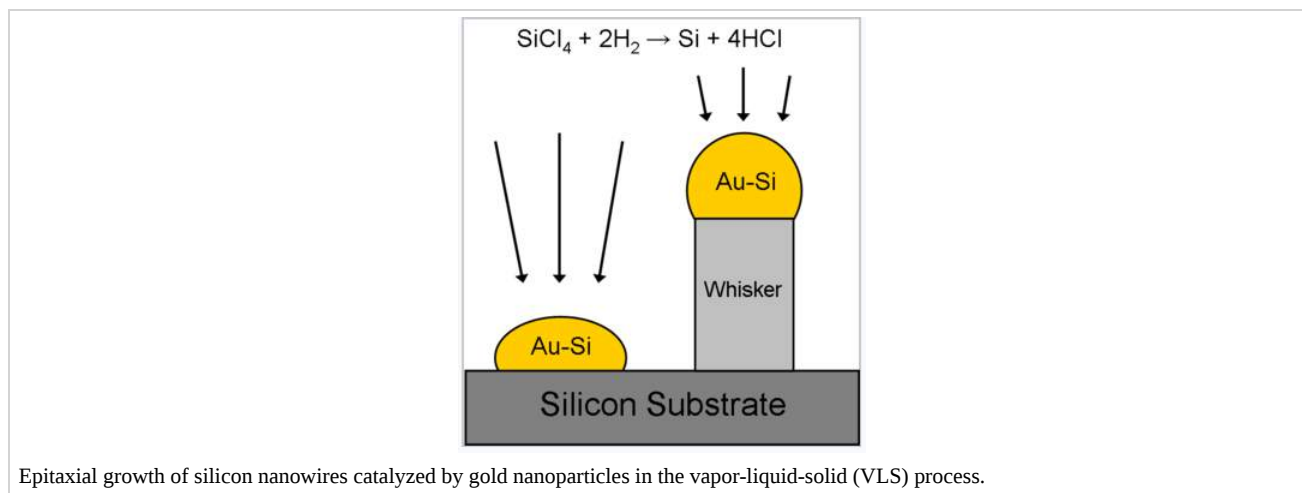


The synthesis is carried out in a coordinating, high boiling solvent that is a mixture of trioctylphosphine (**TOP**) and trioctylphosphine oxide (**TOPO**). In early experiments, organometallic cadmium compounds such as diethylcadmium were used as the metal source, but it was later found that these highly toxic and pyrophoric compounds could be replaced by CdO. At the start of the reaction, a selenium source, typically bis(trimethylsilyl)selenium, $[(\text{CH}_3)_3\text{Si}]_2\text{Se}$, dissolved in TOP is rapidly injected into the hot (350 °C) reaction mixture. The reaction causes a rapid burst of nanoparticle nucleation, but the temperature also drops as the cold solvent is injected and so the nucleation event ends quickly. The cooled solution now contains nanocrystal seeds. It is supersaturated in TOPO-Cd and TOP-Se, but particle growth proceeds slowly until the solution is heated again to the growth temperature, ca. 250°C. Particle growth and **size-focusing** occurs because small particles require less added material to grow by an amount ΔR than larger particles. This is because the volume of an added shell around a spherical seed is $4\pi R^2\Delta R$, so for larger R,

ΔR is smaller. Very narrow particle size distributions can be obtained under conditions of high supersaturation, where the rate of nanoparticle growth is fast relative to particle dissolution and Ostwald ripening.^[6] The size distribution can then be narrowed further by adding a non-solvent such as hexane to the cooled reaction mixture. The largest particles precipitate first, followed by smaller particles. Because the nanoparticles are capped with a ligand shell of TOP, they can be re-suspended in organic solvents once they are size-separated.

The high temperature synthesis of semiconductor quantum dots has been applied to a broad variety of materials including II-VI, III-V, and IV-VI semiconductors. Monodisperse nanoparticles of **controlled shapes** can be made by variants of this method. For example, it is possible to adjust the conditions so that CdSe nucleates in the zincblende polymorph as tetrahedrally shaped seeds, and then grow polar wurtzite "arms" onto each triangular face, resulting in nanocrystal tetrapods. Numerous other nanocrystal shapes such as rods, arrowheads, rice (tapered rods), and polar structures such as Janus rods can be made by variants of this technique. These shape-control strategies often involve the use of ligands that adsorb specifically to certain crystal faces and inhibit their growth. For example, hexylphosphonic acid ligands adsorb selectively to Cd-rich crystal faces and thus lead to the growth of prismatic wurtzite-phase CdSe nanocrystals.

A second widely used method of semiconductor nanocrystal synthesis involves growth from molecular precursors and molten metal droplets, as shown in the figure at the right. The **vapor-liquid-solid (VLS)** and related **solution-liquid-solid (SLS)** growth processes rely on the fact that semiconductors such as Si, Ge, GaAs, InP, and others are soluble at high temperatures in liquid metals such as Au and Cu. The catalytic reduction of a molecule such as silicon tetrachloride (SiCl_4) at the surface of a gold nanocrystal liberates HCl gas and creates a solid solution of Si in Au. The presence of Si lowers the melting point of Au, and as more SiCl_4 reacts, a liquid **eutectic** droplet of the Si-Au alloy is formed. When this droplet becomes supersaturated in Si, a silicon nanocrystal nucleates and grows. This reaction can be performed on the surface of a macroscopic Si crystal, in which case nanocrystal "whiskers" grow from the surface, typically as single crystals and with an epitaxial orientation that is determined by the Si crystal face of the substrate. The diameter of the whiskers is controlled by the radius of the Au drops, which can be as small as a few nanometers and as large as several microns. Using this technique, "forests" of nanowires or microwires can be grown. Because the composition of the nanowire depends on the precursor being fed to the Au droplets, it is possible to make "totem pole" structures with varied compositions along the nanowire axis. Semiconductor shells can also be grown around the wires by **chemical vapor deposition (CVD)**. The VLS process can also be adapted to complex compositions for which no molecular precursor is available by using a laser to ablate the semiconductor from a solid target.

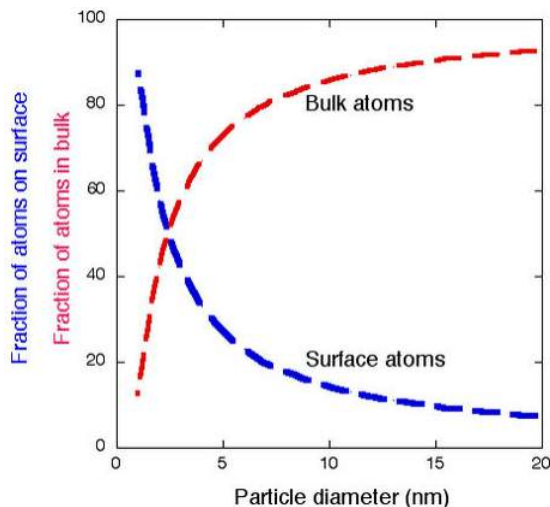


Semiconductor nanowires made by this method are the basis of extremely sensitive **biosensors**, in which a molecular binding event anywhere along the wire strongly affects its electrical conductivity.^[7] Nanowire and microwire arrays are also being studied as **solar cell** and **lithium battery** materials, as well as nanoscale electronic and optoelectronic devices.

This page titled [11.4: Synthesis of Semiconductor Nanocrystals](#) is shared under a [CC BY-SA 4.0](#) license and was authored, remixed, and/or curated by [Chemistry 310 \(Wikibook\)](#) via [source content](#) that was edited to the style and standards of the LibreTexts platform; a detailed edit history is available upon request.

11.5: Surface Energy

Nanoparticles have a substantial fraction of their atoms on the surface, as shown in the plot at the right.^[8] This high surface area to volume ratio is an important factor in many of the physical properties of nanoparticles, such as their **melting point** and **vapor pressure**, and also in their **reactivity**. Heterogeneous catalysts, for example, are often based on nanoparticles because the catalytically reactive atoms are those that are on the surface of the particle.



The surface energy is always positive. A key quantity that is connected with the chemistry of all surfaces is the **surface energy**. This is the (thermodynamically unfavorable) energy of making "dangling bonds" at the surface. Atoms at the surface are under-coordinated, and because breaking bonds costs energy, surface atoms always have higher energy than atoms in the bulk. This happens regardless of whether the bonding is covalent (as in a metal), ionic (in a salt), or non-covalent (in a liquid such as water). We see this effect, for example, in water droplets that bead up on a waxy surface. The droplet contracts into a sphere (against the force of gravity that works to flatten it) in order to minimize the number of dangling hydrogen bonds at the surface.

In the case of metal or semiconductor particles, strong covalent bonds are broken at the surface. For example, a gold atom in bulk face-centered cubic Au has 12 nearest neighbors, but a gold atom on the (111) surface of the crystal (the most dense crystal plane of gold) has six nearest neighbors in-plane and three underneath, for a total of 9. We might expect the surface energy of this crystal face to be a little less (because the remaining bonds will become slightly stronger) than $3/12 = 1/4$ of the **bonding energy** of bulk Au, and this is in fact a fairly good rule of thumb for many materials. When translated into energy per unit area, the surface energy of metals and inorganic salts is usually in the range of 1-2 J/m².

Example: The sublimation energy of bulk gold is 334 kJ/mol, and the surface energy is 1.5 J/m². What percentage of the bulk bonding energy is lost by atoms at the (111) surface of a gold crystal?

To solve this problem, we need to know the surface area per Au atom. Gold has the face-centered cubic structure, and the unit cell edge length is 4.08 Å. From this we can determine that the Au-Au distance is $4.08/1.414 = 2.88$ Å. In a hexagonal array of gold atoms with this interatomic spacing, the surface area per atom is $(2.88 \text{ Å})^2 \times 0.866 = 7.2 \text{ Å}^2$. Multiplying by Avogadro's number, we find that the area per mole of Au surface atoms on the (111) crystal face is $4.3 \times 10^4 \text{ m}^2$.

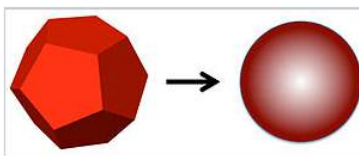
Now we multiply this area by the surface energy:

$$(4.3 \times 10^4 \frac{\text{m}^2}{\text{mol}}) \times (1.5 \frac{\text{J}}{\text{mol}}) \times (\frac{1\text{kJ}}{1000\text{J}}) = +\mathbf{65\text{kJ}}$$
 per mole of Au surface atoms.

$$\frac{65\text{kJ}}{334\text{kJ}} \times 100\% = \mathbf{19\%}$$
 of the bulk bonding energy is lost by atoms at the surface.

It is clear from this example that the surface energy of nanoparticles can have a major effect on their physical properties, since a large fraction of the atoms in a nanoparticle are on the surface. A good example of this is the dramatic depression of the **melting point**.

Solid nanocrystals are in general faceted, whereas liquid droplets made by melting nanocrystals adopt a spherical shape to minimize the surface area.



A faceted solid nanocrystal melts into a spherical droplet in order to minimize its surface energy.

Let's consider melting a silver nanocrystal that is 2 nm in diameter, meaning that about 1/2 of the atoms are on the surface. The spherical liquid droplet has lower surface area than the faceted crystal. For example, a cube has 1.24 times the surface area of a sphere of the same volume. If the decrease in surface area is about 20% upon melting, and the surface energy is about 1/4 of the bulk bonding energy of the atoms, then for a 2 nm diameter nanocrystal we would estimate that:

$$\Delta H_{fusion}^{\circ} \approx \Delta H_{fusion, bulk}^{\circ} - \left(\frac{1}{2}\right)(0.25)\left(\frac{1}{4}\right)\Delta H_{vap}^{\circ} = \Delta H_{fusion, bulk}^{\circ} - 0.025\Delta H_{vap, bulk}^{\circ} \quad (11.5.1)$$

where $\Delta H_{vap, bulk}^{\circ}$, the heat of vaporization, is the total bonding energy of atoms in a bulk crystal. For silver, $\Delta H_{fusion, bulk}^{\circ} = 11.3$ kJ/mol and $\Delta H_{vap, bulk}^{\circ} = 250$ kJ/mol. From this we can calculate the heat of fusion of a 2 nm Ag nanocrystal:

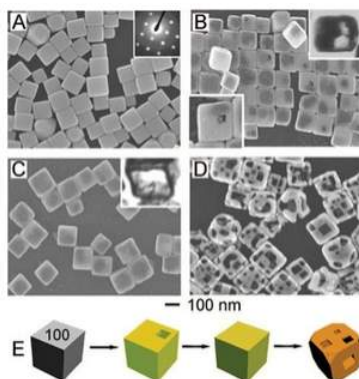
$$\Delta H_{fusion}^{\circ} \approx 11.3 - (0.025)(250) = 5.1 \frac{kJ}{mol} \quad (11.5.2)$$

The melting point of bulk silver is $962^{\circ}\text{C} = 1235\text{ K}$. Assuming that the entropy of fusion is the same in the bulk and in the nanocrystal, the melting point of the nanocrystal should be $1234\text{ K} \times \left(\frac{5.1}{11.3}\right) = 557\text{ K} = 284^{\circ}\text{C}$, a drop of almost 700 degrees from the bulk value. Experimentally, the melting point of a 2 nm diameter silver nanocrystal drops about **800 degrees below that of the bulk**, to 127°C .^[9] This is a whopping big change in the melting point, which is in reasonable agreement with our rough estimate.

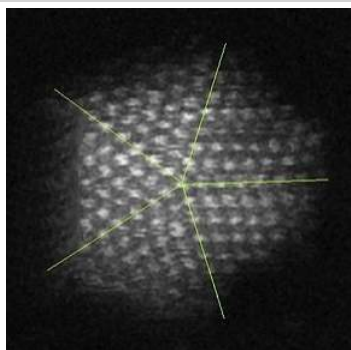
The same effect - energetic destabilization of the surface atoms relative to bulk atoms - results in the **lower boiling point, higher vapor pressure, higher solubility, and higher reactivity** of nanocrystals relative to microcrystals (or larger crystals) of the same material.

This page titled [11.5: Surface Energy](#) is shared under a [CC BY-SA 4.0](#) license and was authored, remixed, and/or curated by [Chemistry 310 \(Wikibook\)](#) via [source content](#) that was edited to the style and standards of the LibreTexts platform; a detailed edit history is available upon request.

11.6: Nanoscale Metal Particles



Nanoscale metal particles have been the subject of intense research over the past 20 years, especially because of their unusual **optical**, **magnetic**, and **catalytic** properties. The synthesis of metal nanocrystals in various shapes has become increasingly sophisticated and rational, like the synthesis of semiconductor nanocrystals described above. By controlling the separate phases of nucleation and growth, and by using ligands that cap specific crystal faces during growth, it is possible to make metal nanocrystals of uniform size in a variety of interesting and useful shapes including cubes, truncated cubes, octahedra, triangular prisms, and high aspect ratio rods. By exploiting displacement reactions that replace one metal with another, complex hollow shapes such as nanocages (as shown at the left) can be made starting with other shapes. In this case, solid silver nanocubes are transformed to gold nanocages.



Five-fold twinning in a gold nanoparticle

The interesting optical properties of nanocrystalline Au, Ag, Cu, and a number of other metals, derive from the collective oscillation of their valence electrons, a phenomenon known as **plasmon resonance**. Remember that in these metals, the electron mean free path is long (about 100 times larger than the size of the atoms), so the valence electrons feel only the average positive charge of the atomic cores as they zoom around the crystal. Light impinging on the metal acts as an oscillating electric field, pushing and pulling on the valence electrons at the characteristic frequency of the light wave. The situation is very much like a pendulum or a weight on a spring. The electrons, pushed away from their equilibrium positions, feel a restoring force that is proportional to their displacement. Their motion can be described by **Hooke's Law**:

$$F = kx \quad (11.6.1)$$

where the spring constant k determines the "stiffness" of the spring. In the case of the plasmon resonance, k is proportional to the number density of valence electrons n , and the square of the electronic charge e :

$$k = \frac{ne^2}{\epsilon_0} \quad (11.6.2)$$

The **resonant frequency** of the plasma oscillation is given by:

$$\omega_p = \left(\frac{k}{m}\right)^{\frac{1}{2}} = \left(\frac{n e^2}{m_e \epsilon_0}\right)^{\frac{1}{2}} \quad (11.6.3)$$

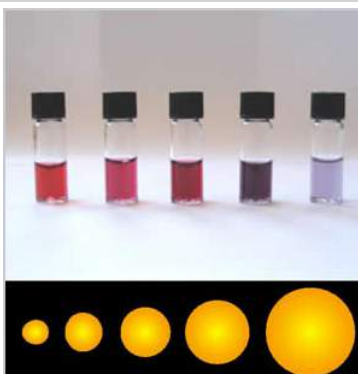
where m_e is the electron mass. For most metals, the plasmon resonance is in the ultraviolet part of the spectrum, but for a few metals like Au, Ag, and Cu it is in the visible.



The Lycurgus cup (4th century Roman glass) derives its unique coloration from noble metal nanoparticles. The cup is red in transmitted light and green in scattered (reflected) light.

For metal particles that are much smaller than the wavelength of light, this effect is called the **localized surface plasmon resonance**, or LSPR. There are three important consequences of the LSPR effect:

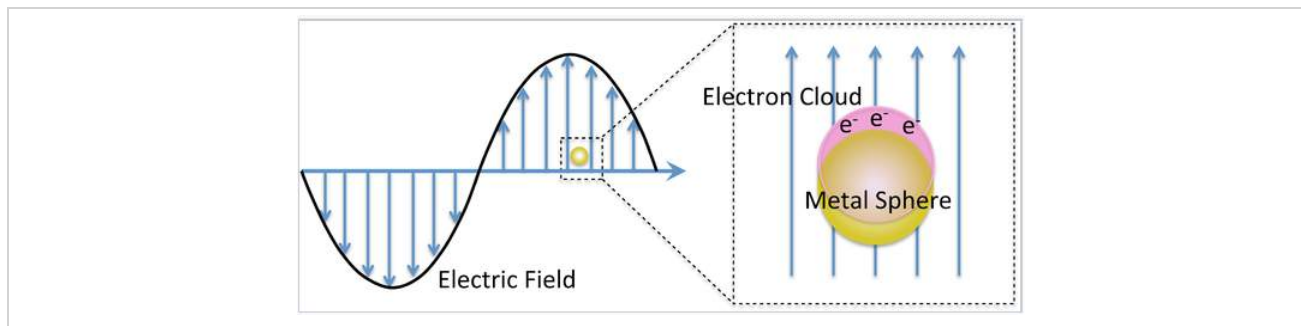
- The **local electric field** of the incoming light wave is greatly **enhanced** at the particle surface. This gives rise to huge enhancement factors in optical processes such as **Raman scattering** and **fluorescence**. Thus, certain analytical spectroscopic techniques are greatly enhanced by LSPR.
- Near the plasmon resonance frequency, metal nanocrystals **absorb** and **scatter light** very strongly. This makes them brightly reflective, and the strong light absorption can be exploited for light-induced local heating. These properties are being applied in medical diagnostics and therapy, e.g., for detection and photothermal destruction of cancer cells. By adjusting the size and shape of the gold nanoparticles, which are more stable than Ag and Cu in biological media, the plasmon frequency can be tuned to the tissue-transparent near-IR region of the spectrum between 700 and 900 nm. Small quantities of plasmonic Ag and Au particles also make brightly colored and strongly scattering pigments, e.g. in stained glass as shown above at the right.
- The plasmon frequency is sensitive to the refractive index of the particle's surroundings, i.e., its chemical environment. This makes metal nanoparticles of special interest for **sensing and biosensing** applications.



The colors of plasmonic gold nanoparticles depend on their size and shape.

Theory of light scattering and absorption by metal nanoparticles

The valence electrons in metal nanoparticles oscillate in the electric field of a light wave. While the nature of these oscillations is somewhat complex in metal particles that are non-spherical, the theory for spherical particles is relatively simple and in fact was worked out over 100 years ago by German physicist Gustav Mie.



Mie considered the interaction of a spherical particle with a **uniform electric field, E** , oscillating at angular frequency ω ($= 2\pi f$). This is a good approximation when the particle diameter is much smaller than the wavelength of light, as shown on the left. The particle is embedded in a uniform, insulating material (e.g. a solvent) that has a dielectric constant ϵ_{diel} . For insulators, ϵ_{diel} is a positive real number.

The dielectric constant ϵ of a metal is actually a complex number:

$$\epsilon = \epsilon' + i\epsilon'' \quad (11.6.4)$$

Here the real part, ϵ' , is related to the refraction of light, and the imaginary part, ϵ'' , is related to light absorption. Both ϵ' and ϵ'' are dependent on the frequency of the light. For metals near the plasmon resonance frequency, ϵ' is typically a *negative number*.

The **cross-section for absorption** of the light wave by the particle is:

$$\sigma_{\text{absorption}} = \frac{9\omega}{c} \epsilon_{\text{diel}}^{\frac{3}{2}} V \frac{\epsilon''_{\text{metal}}}{(\epsilon'_{\text{metal}} + 2\epsilon_{\text{diel}})^2 + (\epsilon''_{\text{metal}})^2} \quad (11.6.5)$$

and the **cross-section for scattering** is:

$$\sigma_{\text{scattering}} = \frac{3}{2\pi} \left(\frac{\omega}{c}\right)^4 \epsilon_{\text{diel}}^2 V^2 \frac{(\epsilon'_{\text{metal}} - \epsilon_{\text{diel}})^2 + (\epsilon''_{\text{metal}})^2}{(\epsilon'_{\text{metal}} + 2\epsilon_{\text{diel}})^2 + (\epsilon''_{\text{metal}})^2} \quad (11.6.6)$$

The sum of these two is the **cross-section for extinction**:

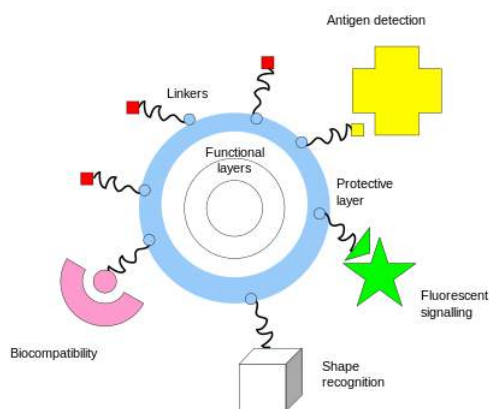
$$\sigma_{\text{extinction}} = \sigma_{\text{absorption}} + \sigma_{\text{scattering}} \quad (11.6.7)$$

These cross-sections become large when the $(\epsilon'_{\text{metal}} + 2\epsilon_{\text{diel}})$ term in the denominator becomes small. This occurs when

$$\epsilon'_{\text{metal}} \simeq -2\epsilon_{\text{diel}} \quad (11.6.8)$$

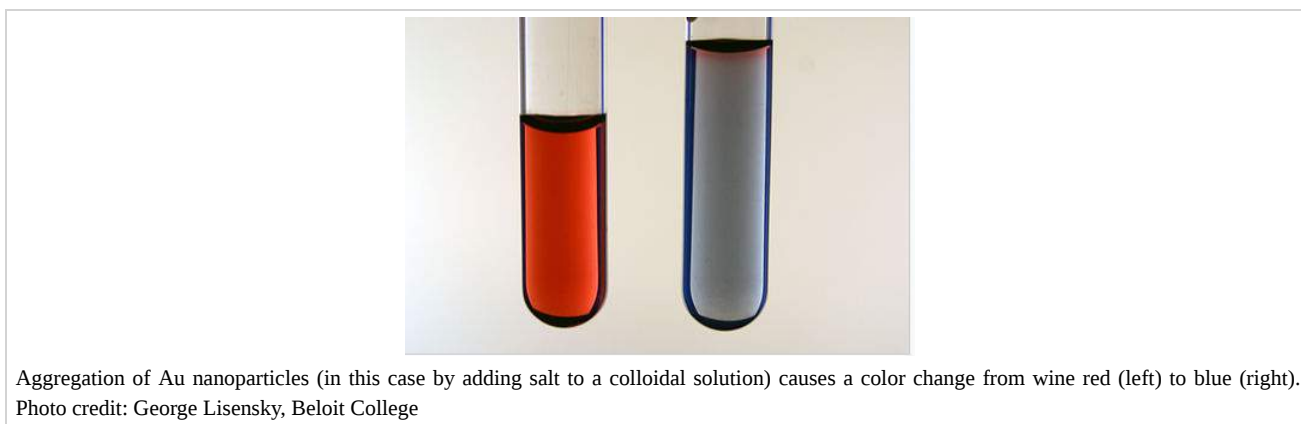
For 15 nm diameter gold nanoparticles in water, this happens at about 580 nm, resulting in the characteristic wine-red color of colloidal gold solutions. Changing the solution environment (e.g., by adsorbing a molecule onto the gold surface) changes ϵ_{diel} and thus alters the color slightly.

It is important to note that the cross-section for **scattering** is proportional to the **square of the volume** of the particle, V^2 , whereas the absorption is proportional to V . This means that very small gold particles (< 5 nm) are strongly absorbing but not strongly scattering. Larger particles (> 30 nm) scatter light very strongly. Depending on the application, therefore, we choose larger or smaller particles.

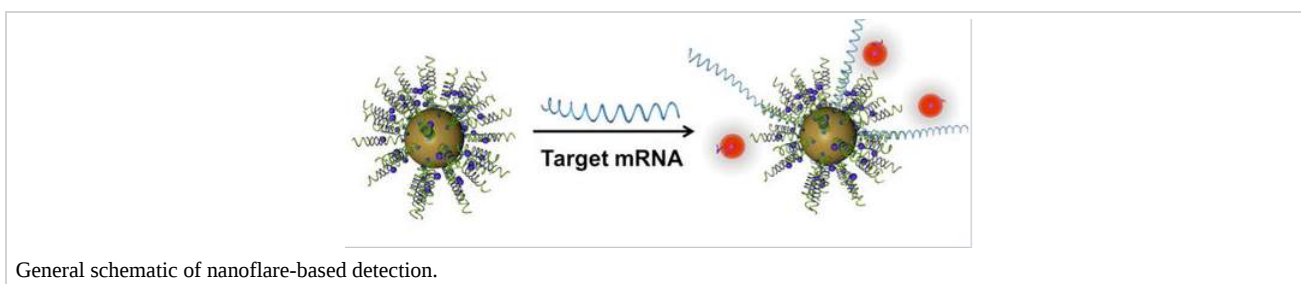


One of the key complementary properties of noble metal nanoparticles that is important to their use in biomedicine is the ease with which they can be **covalently conjugated** with polymers or small molecules, typically via thiol or amine bonds at their surface. This imparts biological recognition properties to the particles that enables them to bind to specific biomolecular targets. The figure at the left illustrates some of the functionality that can be imparted to nanoparticles through surface functionalization.

Functionalization of gold nanoparticles with thiol-terminated single-stranded DNA was the basis of one of the first nanoparticle sensors, developed by the Mirkin group at Northwestern University. **DNA-coated nanoparticles** have the characteristic wine-red plasmonic color of spherical nano-gold. However, when these particles are linked together by a complementary DNA strand, the resonance frequency shifts, resulting in a blue color. This color change, illustrated in the figure at the right, provides a "litmus test" for the presence of the target DNA sequence.^[10] "Melting" of the DNA - heating it to the temperature at which double stranded DNA dissociates to make single strands - reverses the color change. The DNA hybridization/melting transition is highly **cooperative** because of the aggregation of many gold particles, so the transition temperature is very sharp. With proper temperature control, the color change can be sensitive to a **single base mismatch** in the target DNA that is detected by this method.



Subsequent research has developed sophisticated diagnostic and therapeutic ("theranostic") applications for these **spherical nucleic acid**^[11] particles. These particles easily penetrate cell membranes and can report on the chemistry happening inside living cells.



An important property of gold nanoparticles in these applications is their ability to **quench** the **fluorescence** of reporter molecules that are near their surface. Nucleic acid strands that contain a hairpin loop can position fluorescent molecules near the gold surface,

where their fluorescence is turned off by nanoparticle quenching. Hybridization of these sequences to target RNA or DNA causes the fluorescence to turn on by moving the fluorescent molecule away from the nanoparticle surface. These so called "nanoflares" can thus signal the up- or down-regulation of specific genes inside cells. Nanoflares are the basis of the Verigene System, developed and commercialized by Nanosphere, Inc. to detect markers for infectious diseases and cancers.

This page titled [11.6: Nanoscale Metal Particles](#) is shared under a [CC BY-SA 4.0](#) license and was authored, remixed, and/or curated by [Chemistry 310 \(Wikibook\)](#) via [source content](#) that was edited to the style and standards of the LibreTexts platform; a detailed edit history is available upon request.

11.7: Applications of Nanomaterials

PowerPoint slides for this section

This page titled [11.7: Applications of Nanomaterials](#) is shared under a [CC BY-SA 4.0](#) license and was authored, remixed, and/or curated by [Chemistry 310 \(Wikibook\)](#) via [source content](#) that was edited to the style and standards of the LibreTexts platform; a detailed edit history is available upon request.

11.8: Discussion Questions

- Explain how separating the nucleation and growth steps leads to nanoparticles of uniform size.
 - A recent paper by Delia Milliron and coworkers (*Nature*, 2013, 500, 323–326, doi:10.1038/nature12398) describes plasmonic indium-tin-oxide (ITO) nanoparticles that can control the infrared transparency of windows. Explain how the plasmon resonance wavelength of the nanoparticles can be tuned by electrochemical doping, and how the invention could save some of the energy used to heat and cool buildings.
-

This page titled [11.8: Discussion Questions](#) is shared under a [CC BY-SA 4.0](#) license and was authored, remixed, and/or curated by [Chemistry 310 \(Wikibook\)](#) via [source content](#) that was edited to the style and standards of the LibreTexts platform; a detailed edit history is available upon request.

11.9: Problems

1. Consider a spherical gold nanoparticle that contains 500 atoms. If the diameter of an atom is approximately 3 Å, what fraction of the gold atoms in the particle are on the surface?
2. Now consider small droplets of mercury that contains 500 atoms. Mercury atoms are also about 3 Å in diameter. The heat of vaporization of bulk mercury is 64.0 kJ/mol, and the vapor pressure of mercury is 0.00185 torr = 2.43×10^{-6} atm. The surface tension of mercury (γ_{Hg}) is 0.518 N/m, and the surface excess energy can be calculated as $\gamma_{\text{Hg}}A$, where A is the surface area. Using this information and the Clausius-Clapyron equation ($P = \text{const} \cdot \exp(-\Delta H_{\text{vap}}/RT)$), calculate the vapor pressure of these small droplets of mercury.
3. James Heath and coworkers (Phys. Rev. Lett. 1995, 75, 3466) have observed Ostwald ripening in thin films of gold nanoparticles at room temperature. Starting with an uneven distribution of particle sizes, they find that the large particles grow at the expense of smaller ones. Can you explain this observation, based on your answers to problems (1) and (2)?
4. The bandgap of bulk germanium is 0.67 eV. What bandgap would you expect for a 4 nm diameter Ge nanocrystal? Use the Brus formula,

$$\Delta E_{\text{gap}} \approx \frac{h^2}{8\mu R^2} - \frac{1.8e^2}{4R\pi\epsilon\epsilon_0} + \dots \quad (11.9.1)$$

where R is the particle radius, $\epsilon_{\text{Ge}} = 16.2$, $h = 6.6 \times 10^{-34}$ J s, $1 \text{ eV} = 1.6 \times 10^{-19}$ J, $1 \text{ J} = 1 \text{ kg m}^2/\text{s}^2$. and $e^2/4\pi\epsilon_0 = 1.44 \times 10^{-9}$ eV m. Assume that the electron-hole reduced mass μ is approximately 40% of the free electron mass, $m_e = 9.1 \times 10^{-31}$ kg.

5. Grecian Formula (a hair coloring product) until recently contained lead acetate, which reacts with the cysteine in hair to make PbS. In bulk form, PbS is a semiconductor with a band gap of 0.3 eV (1 eV = 1240 nm). The particles are initially very small but grow as more Grecian Formula is applied and reacts with cysteine. As the particles grow, they change progressively from colorless to yellow to black. Explain why the particles are initially colorless and why their color changes. (Grecian formula now uses Bi, which is less toxic than Pb, and works by the same mechanism)

This page titled [11.9: Problems](#) is shared under a [CC BY-SA 4.0](#) license and was authored, remixed, and/or curated by [Chemistry 310 \(Wikibook\)](#) via [source content](#) that was edited to the style and standards of the LibreTexts platform; a detailed edit history is available upon request.

11.10: References

1. C.T. Liu, S. Y. Lin, D. C. Tsui, H. Lee, and D. Ackley, *Appl. Phys. Lett.* 1988, 53, 2510. DOI: 10.1063/1.100409.
2. D. L. Feldheim, K. C. Grabar, M. J. Natan, and T. E. Mallouk, "Electron Transfer in Self-Assembled Inorganic Polyelectrolyte/Metal Nanoparticle Heterostructures," *J. Am. Chem. Soc.*, 118, 7640-1 (1996)
3. S. Chen, R. W. Murray, and S. W. Feldberg, "Quantized Capacitance Charging of Monolayer-Protected Au Clusters," *J. Phys. Chem. B* 1998, 102, 9898-9907.
4. Brus, Louis E. (1984). "[Electron–electron and electron-hole interactions in small semiconductor crystallites: The size dependence of the lowest excited electronic state](#)". *J. Chem. Phys.* 80, 4403. DOI: 10.1063/1.447218.
5. C. B. Murray, D. J. Norris, and M. G. Bawendi, "Synthesis and characterization of nearly monodisperse CdE (E = sulfur, selenium, tellurium) semiconductor nanocrystallites," *J. Am. Chem. Soc.* 1993, 115, 8706–8715. DOI: 10.1021/ja00072a025.
6. Y. Yin and A. P. Alivisatos, "Colloidal nanocrystal synthesis and the organic–inorganic interface," *Nature* 2005, 437, 664-670. DOI: 10.1038/nature04165
7. G. Zheng, F. Patolsky, Y. Cui, W. U. Wang and C. M. Lieber, "Multiplexed electrical detection of cancer markers with nanowire sensor arrays," *Nature Biotechnol.* 2005, 23, 1294 - 1301. DOI:10.1038/nbt1138.
8. K. J. Klabunde, J. Stark, O. Koper, C. Mohs, D. G. Park, S. Decker, Y. Jiang, I. Lagadic, and D. Zhang, "Nanocrystals as Stoichiometric Reagents with Unique Surface Chemistry," *J. Phys. Chem.* 1996, 100, 12142–12153. DOI: 10.1021/jp960224x.
9. S. A. Little, T. Begou, R. W. Collins, and S. Marsillac, *Appl. Phys. Lett.* 2012, 100, 051107. DOI: 10.1063/1.3681367
10. Mirkin, C. A., et al., A DNA-based method for rationally assembling nanoparticles into macroscopic materials. *Nature* 1996, 382 (6592), 607-609.
11. Cutler, J. I., et al., Spherical Nucleic Acids. *J Am Chem Soc* 2012, 134 (3), 1376-1391.

This page titled [11.10: References](#) is shared under a [CC BY-SA 4.0](#) license and was authored, remixed, and/or curated by [Chemistry 310 \(Wikibook\)](#) via [source content](#) that was edited to the style and standards of the LibreTexts platform; a detailed edit history is available upon request.

CHAPTER OVERVIEW

12: Resources for Students and Teachers

Powerpoint slides to accompany the chapters of this book will be provided to instructors upon request (tem5@psu.edu)

Additional resources:

12.1: VIPER- Virtual Inorganic Pedagogical Electronic Resource- A Community for Teachers and Students of Inorganic Chemistry

12.2: Beloit College/University of Wisconsin Video Lab Manual

12.3: Atomic and Molecular Orbitals (University of Liverpool)

12.4: Interactive 3D Crystal Structures (University of Liverpool)

12.5: Appendix 1- Periodic Tables

12.6: Appendix 2- Selected Thermodynamic Values

12.7: Appendix 3- Bond Enthalpies

This page titled [12: Resources for Students and Teachers](#) is shared under a [CC BY-SA 4.0](#) license and was authored, remixed, and/or curated by [Chemistry 310 \(Wikibook\)](#) via [source content](#) that was edited to the style and standards of the LibreTexts platform; a detailed edit history is available upon request.

12.1: VIPeR- Virtual Inorganic Pedagogical Electronic Resource- A Community for Teachers and Students of Inorganic Chemistry

IONIC VIPeR is a cyber-interface that facilitates collaborative development of learning materials and their dissemination to the wider inorganic community. This website, VIPeR (Virtual Inorganic Pedagogical Electronic Resource), serves both as a repository and as a user-friendly platform for social networking tools that facilitate virtual collaboration and community building. The VIPeR community seeks to develop and disseminate best practices for teaching inorganic chemistry.

[IONIC VIPeR website](#)

This page titled [12.1: VIPeR- Virtual Inorganic Pedagogical Electronic Resource- A Community for Teachers and Students of Inorganic Chemistry](#) is shared under a [CC BY-SA 4.0](#) license and was authored, remixed, and/or curated by [Chemistry 310 \(Wikibook\)](#) via [source content](#) that was edited to the style and standards of the LibreTexts platform; a detailed edit history is available upon request.

12.2: Beloit College/University of Wisconsin Video Lab Manual

The video lab manual provides a broad range of videos of laboratory experiments in inorganic nanoscience and materials chemistry. This is an especially useful resource for teachers who would like to develop laboratory experiments for their classes in inorganic chemistry.

Video Lab Manual website

This page titled [12.2: Beloit College/University of Wisconsin Video Lab Manual](#) is shared under a [CC BY-SA 4.0](#) license and was authored, remixed, and/or curated by [Chemistry 310 \(Wikibook\)](#) via [source content](#) that was edited to the style and standards of the LibreTexts platform; a detailed edit history is available upon request.

12.3: Atomic and Molecular Orbitals (University of Liverpool)

The University of Liverpool website shows animations of atomic orbitals, selected molecular orbital diagrams, and the VSEPR shapes of selected molecules.

[Structure and Bonding website](#)

This page titled [12.3: Atomic and Molecular Orbitals \(University of Liverpool\)](#) is shared under a [CC BY-SA 4.0](#) license and was authored, remixed, and/or curated by [Chemistry 310 \(Wikibook\)](#) via [source content](#) that was edited to the style and standards of the LibreTexts platform; a detailed edit history is available upon request.

12.4: Interactive 3D Crystal Structures (University of Liverpool)

The University of Liverpool website also provides a menu of inorganic structures (both molecules and extended solids) that can be visualized and manipulated in 3D. This is a valuable tool that supplements the descriptions of structures in Chapters 5-8 of this book.

[3D Crystal Structure website](#)

This page titled [12.4: Interactive 3D Crystal Structures \(University of Liverpool\)](#) is shared under a [CC BY-SA 4.0](#) license and was authored, remixed, and/or curated by [Chemistry 310 \(Wikibook\)](#) via [source content](#) that was edited to the style and standards of the LibreTexts platform; a detailed edit history is available upon request.

12.5: Appendix 1- Periodic Tables

Interactive Periodic Table (Wikipedia)

ОПЫТЪ СИСТЕМЫ ЭЛЕМЕНТОВЪ.

ОСНОВАННОЙ НА ИХЪ АТОМНОМЪ ВѢСѢ И ХИМИЧЕСКОМЪ СХОДСТВѢ.

	Ti = 50	Zr = 90	? = 180.
	V = 51	Nb = 94	Ta = 182.
	Cr = 52	Mo = 96	W = 186.
	Mn = 55	Rh = 104,4	Pt = 197,4.
	Fe = 56	Ru = 104,4	Ir = 198.
	Ni = 59	Pd = 106,8	Os = 199.
H = 1	Cu = 63,4	Ag = 108	Hg = 200.
Be = 9,4	Mg = 24	Zn = 65,2	Cd = 112
B = 11	Al = 27,4	? = 68	Ur = 116 Au = 197?
C = 12	Si = 28	? = 70	Sn = 118
N = 14	P = 31	As = 75	Sb = 122 Bi = 210?
O = 16	S = 32	Se = 79,4	Te = 128?
F = 19	Cl = 35,4	Br = 80	I = 127
Li = 7	Na = 23	K = 39	Rb = 85,4 Cs = 133 Tl = 204.
	Ca = 40	Sr = 87,6	Ba = 137 Pb = 207.
	? = 45	Ce = 92	
	?Er = 56	La = 94	
	?Yt = 60	Di = 95	
	?In = 75,6	Th = 118?	

Д. Менделѣевъ

Mendeleev's periodic table (1869)

		Group																	
		I	II											III	IV	V	VI	VII	VIII
Period	1	1 H																	2 He
	2	3 Li	4 Be											5 B	6 C	7 N	8 O	9 F	10 Ne
	3	11 Na	12 Mg											13 Al	14 Si	15 P	16 S	17 Cl	18 Ar
	4	19 K	20 Ca	21 Sc	22 Ti	23 V	24 Cr	25 Mn	26 Fe	27 Co	28 Ni	29 Cu	30 Zn	31 Ga	32 Ge	33 As	34 Se	35 Br	36 Kr
	5	37 Rb	38 Sr	39 Y	40 Zr	41 Nb	42 Mo	43 Tc	44 Ru	45 Rh	46 Pd	47 Ag	48 Cd	49 In	50 Sn	51 Sb	52 Te	53 I	54 Xe
	6	55 Cs	56 Ba	* La	72 Hf	73 Ta	74 W	75 Re	76 Os	77 Ir	78 Pt	79 Au	80 Hg	81 Tl	82 Pb	83 Bi	84 Po	85 At	86 Rn
	7	87 Fr	88 Ra	** Ac	104 Rf	105 Db	106 Sg	107 Bh	108 Hs	109 Mt	110 Ds	111 Rg	112 Cn	113 Nh	114 Fl	115 Mc	116 Lv	117 Ts	118 Og
	8	119 Uun																	

* Lanthanides	57 La	58 Ce	59 Pr	60 Nd	61 Pm	62 Sm	63 Eu	64 Gd	65 Tb	66 Dy	67 Ho	68 Er	69 Tm	70 Yb	71 Lu
** Actinides	89 Ac	90 Th	91 Pa	92 U	93 Np	94 Pu	95 Am	96 Cm	97 Bk	98 Cf	99 Es	100 Fm	101 Md	102 No	103 Lr

Alkali metals	Alkaline earth metals	Lanthanides	Actinides	Transition metals
Poor metals	Metalloids	Nonmetals	Halogens	Noble gases

State at standard temperature and pressure

Atomic number in red: gas
 Atomic number in blue: liquid
 Atomic number in black: solid

solid border: at least one isotope is older than the Earth (Primordial elements)
 dashed border: at least one isotope naturally arise from decay of other chemical elements and no isotopes are older than the earth
 dotted border: only artificially made isotopes (synthetic elements)
 no border: undiscovered

18-column periodic table

		Group																															
		1	2															3	4	5	6	7	8	9	10	11	12	13	14	15	16	17	18
Period	1	1 H																	2 He														
	2	3 Li	4 Be											5 B	6 C	7 N	8 O	9 F	10 Ne														
	3	11 Na	12 Mg											13 Al	14 Si	15 P	16 S	17 Cl	18 Ar														
	4	19 K	20 Ca											21 Sc	22 Ti	23 V	24 Cr	25 Mn	26 Fe	27 Co	28 Ni	29 Cu	30 Zn	31 Ga	32 Ge	33 As	34 Se	35 Br	36 Kr				
	5	37 Rb	38 Sr											39 Y	40 Zr	41 Nb	42 Mo	43 Tc	44 Ru	45 Rh	46 Pd	47 Ag	48 Cd	49 In	50 Sn	51 Sb	52 Te	53 I	54 Xe				
	6	55 Cs	56 Ba	57 La	58 Ce	59 Pr	60 Nd	61 Pm	62 Sm	63 Eu	64 Gd	65 Tb	66 Dy	67 Ho	68 Er	69 Tm	70 Yb	71 Lu	72 Hf	73 Ta	74 W	75 Re	76 Os	77 Ir	78 Pt	79 Au	80 Hg	81 Tl	82 Pb	83 Bi	84 Po	85 At	86 Rn
	7	87 Fr	88 Ra	89 Ac	90 Th	91 Pa	92 U	93 Np	94 Pu	95 Am	96 Cm	97 Bk	98 Cf	99 Es	100 Fm	101 Md	102 No	103 Lr	104 Rf	105 Db	106 Sg	107 Bh	108 Hs	109 Mt	110 Ds	111 Rg	112 Cn	113 Nh	114 Fl	115 Mc	116 Lv	117 Ts	118 Og

A 32-column periodic table with Sc, Y, Lu and Lr in group 3

This page titled [12.5: Appendix 1- Periodic Tables](#) is shared under a [CC BY-SA 4.0](#) license and was authored, remixed, and/or curated by [Chemistry 310 \(Wikibook\)](#) via [source content](#) that was edited to the style and standards of the LibreTexts platform; a detailed edit history is available upon request.

12.6: Appendix 2- Selected Thermodynamic Values

Selected Thermodynamic Values (at 298.15 K)

Substance	ΔH_f° (kJ/mol)	S° (J/K·mol)	ΔG_f° (kJ/mol)
Aluminum			
Al(s)	0	28.3	0
AlCl ₃ (s)	-704.2	110.67	-628.8
Al ₂ O ₃ (s)	-1675.7	50.92	-1582.3
Barium			
BaCl ₂ (s)	-858.6	123.68	-810.4
BaCl ₂ · 2 H ₂ O (s)	-1460.1	203	-1296.5
BaO(s)	-553.5	70.42	-525.1
Ba(OH) ₂ · 8 H ₂ O (s)	-3342	427	-2793
BaSO ₄ (s)	-1473.2	132.2	-1362.2
Beryllium			
Be(s)	0	9.5	0
Be(OH) ₂ (s)	-902.5	51.9	-815
Bromine			
Br(g)	111.884	175.022	82.396
Br ₂ (liq)	0	152.2	0
Br ₂ (g)	30.907	245.463	3.11
BrF ₃ (g)	-255.6	292.53	-229.43
HBr(g)	-36.4	198.695	-53.45
Calcium			
Ca(s)	0	41.42	0
Ca(g)	178.2	158.884	144.3
Ca ₂ ⁺ (g)	1925.9		
CaC ₂ (s)	-59.8	69.96	-64.9
CaCO ₃ (s; calcite)	-1206.92	92.9	-1128.79
CaCl ₂ (s)	-795.8	104.6	-748.1
CaF ₂ (s)	-1219.6	68.87	-1167.3
CaH ₂ (s)	-186.2	42	-147.2
CaO(s)	-635.09	39.75	-604.03
CaS(s)	-482.4	56.5	-477.4
Ca(OH) ₂ (s)	-986.09	83.39	-898.49
Ca(OH) ₂ (aq)	-1002.82	-74.5	-868.07
CaSO ₄ (s)	-1434.11	106.7	-1321.79
Carbon			
C(s, graphite)	0	5.74	0

C(s, diamond)	1.895	2.377	2.9
C(g)	716.682	158.096	671.257
CCl ₄ (liq)	-135.44	216.4	-65.21
CCl ₄ (g)	-102.9	309.85	-60.59
CHCl ₃ (liq)	-134.47	201.7	-73.66
CHCl ₃ (g)	-103.14	295.71	-70.34
CH ₄ (g, methane)	-74.81	186.264	-50.72
C ₂ H ₂ (g, ethyne)	226.73	200.94	209.2
C ₂ H ₄ (g, ethene)	52.26	219.56	68.15
C ₂ H ₆ (g, ethane)	-84.68	229.6	-32.82
C ₃ H ₈ (g, propane)	-103.8	269.9	-23.49
C ₄ H ₁₀ (g, butane)	-888.0		
C ₆ H ₆ (liq, benzene)	49.03	172.8	124.5
C ₆ H ₁₄ (liq)	-198.782	296.018	-4.035
C ₈ H ₁₈ (liq)	-249.952	361.205	6.707
CH ₃ OH(liq, methanol)	-238.66	126.8	-166.27
CH ₃ OH(g, methanol)	-200.66	239.81	-161.96
C ₂ H ₅ OH(liq, ethanol)	-277.69	160.7	-174.78
C ₂ H ₅ OH(g, ethanol)	-235.1	282.7	-168.49
CH ₃ COOH(liq)	-276.981	160.666	-173.991
CO(NH ₂) ₂ (s, urea)	-333.5	104.6	-197.4
CO(g)	-110.525	197.674	-137.168
CO ₂ (g)	-393.509	213.74	-394.359
CS ₂ (g)	117.36	237.84	67.12
COCl ₂ (g)	-218.8	283.53	-204.6
Cesium			
Cs(s)	0	85.23	0
Cs ⁺ (g)	457.964		
CsCl(s)	-443.04	101.17	-414.53
Chlorine			
Cl(g)	121.679	165.198	105.68
Cl ⁻ (g)	-233.13		
Cl ₂ (g)	0	223.066	0
HCl(g)	-92.307	186.908	-95.299
HCl(aq)	-167.159	56.5	-131.228
Chromium			
Cr(s)	0	23.77	0
Cr ₂ O ₃ (s)	-1139.7	81.2	-1058.1
CrCl ₃ (s)	-556.5	123	-486.1

Copper			
Cu(s)	0	33.15	0
CuO(s)	-157.3	42.63	-129.7
CuCl ₂ (s)	-220.1	108.07	-175.7
Fluorine			
F ₂ (g)	0	202.78	0
F(g)	78.99	158.754	61.91
F ⁻ (g)	-255.39		
F ⁻ (aq)	-332.63	-13.8	-278.79
HF(g)	-271.1	173.779	-273.2
HF(aq)	-332.63	-13.8	-278.79
Hydrogen			
H ₂ (g)	0	130.684	0
H(g)	217.965	114.713	203.247
H ⁺ (g)	1536.202		
H ₂ O(liq)	-285.83	69.91	-237.129
H ₂ O(g)	-241.818	188.825	-228.572
H ₂ O ₂ (liq)	-187.78	109.6	-120.35
Iodine			
I ₂ (s)	0	116.135	0
I ₂ (g)	62.438	260.69	19.327
I(g)	106.838	180.791	70.25
I ⁻ (g)	-197		
ICl(g)	17.78	247.551	-5.46
Iron			
Fe(s)	0	27.78	0
FeO(s)	-272		
Fe ₂ O ₃ (s, hematite)	-824.2	87.4	-742.2
Fe ₃ O ₄ (s, magnetite)	-1118.4	146.4	-1015.4
FeCl ₂ (s)	-341.79	117.95	-302.3
FeCl ₃ (s)	-399.49	142.3	-344
FeS ₂ (s, pyrite)	-178.2	52.93	-166.9
Fe(CO) ₅ (liq)	-774	338.1	-705.3
Lead			
Pb(s)	0	64.81	0
PbCl ₂ (s)	-359.41	136	-314.1
PbO(s, yellow)	-217.32	68.7	-187.89
PbS(s)	-100.4	91.2	-98.7
Lithium			

Li(s)	0	29.12	0
Li ⁺ (g)	685.783		
LiOH(s)	-484.93	42.8	-438.95
LiOH(aq)	-508.48	2.8	-450.58
LiCl(s)	-408.701	59.33	-384.37
Magnesium			
Mg(s)	0	32.68	0
MgCl ₂ (g)	-641.32	89.62	-591.79
MgO(s)	-601.7	26.94	-569.43
Mg(OH) ₂ (s)	-924.54	63.18	-833.51
MgS(s)	-346	50.33	-341.8
Mercury			
Hg(liq)	0	29.87	0
HgCl ₂ (s)	-224.3	146	-178.6
HgO(s, red)	-90.83	70.29	-58.539
HgS(s, red)	-58.2	82.4	-50.6
Nickel			
Ni(s)	0	29.87	0
NiO(s)	-239.7	37.99	-211.7
NiCl ₂ (s)	-305.332	97.65	-259.032
Nitrogen			
N ₂ (g)	0	191.61	0
N(g)	472.704	153.298	455.563
NH ₃ (g)	-46.11	192.45	-16.45
N ₂ H ₄ (liq)	50.63	121.21	149.34
NH ₄ Cl(s)	-314.43	94.6	-202.87
NH ₄ Cl(aq)	-299.66	169.9	-210.52
NH ₄ NO ₃ (s)	-365.56	151.08	-183.87
NH ₄ NO ₃ (aq)	-339.87	259.8	-190.56
NO(g)	90.25	210.76	86.55
NO ₂ (g)	33.18	240.06	51.31
N ₂ O(g)	82.05	219.85	104.2
N ₂ O ₄ (g)	9.16	304.29	97.89
NOCl(g)	51.71	261.69	66.08
HNO ₃ (liq)	-174.1	155.6	-80.71
HNO ₃ (g)	-135.06	266.38	-74.72
HNO ₃ (aq)	-207.36	146.4	-111.25
Oxygen			
O ₂ (g)	0	205.138	0

O(g)	249.17	161.055	231.731
O ₃ (g)	142.7	238.93	163.2
Phosphorus			
P ₄ (s, white)	0	164.36	0
P ₄ (s, red)	-70.4	91.2	-48.4
P(g)	314.64	163.193	278.25
PH ₃ (g)	5.4	310.23	13.4
PCl ₃ (g)	-287	311.78	-267.8
P ₄ O ₁₀ (s)	-2984	228.86	-2697.7
H ₃ PO ₄ (s)	-1279	110.5	-1119.1
Potassium			
K(s)	0	64.18	0
KCl(s)	-436.747	82.59	-409.14
KClO ₃ (s)	-397.73	143.1	-296.25
KI(s)	-327.9	106.32	-324.892
KOH(s)	-424.764	78.9	-379.08
KOH(aq)	-482.37	91.6	-440.5
Silicon			
Si(s)	0	18.83	0
SiBr ₄ (liq)	-457.3	277.8	-443.8
SiC(s)	-65.3	16.61	-62.8
SiCl ₄ (g)	-657.01	330.73	-616.98
SiH ₄ (g)	34.3	204.62	56.9
SiF ₄ (g)	-1614.94	282.49	-1572.65
SiO ₂ (s, quartz)	-910.94	41.84	-856.64
Silver			
Ag(s)	0	42.55	0
Ag ₂ O(s)	-31.05	121.3	-11.2
AgCl(s)	-127.068	96.2	-109.789
AgNO ₃ (s)	-124.39	140.92	-33.41
Sodium			
Na(s)	0	51.21	0
Na(g)	107.32	153.712	76.761
Na ⁺ (g)	609.358		
NaBr(s)	-361.062	86.82	-348.983
NaCl(s)	-411.153	72.13	-384.138
NaCl(g)	-176.65	229.81	-196.66
NaCl(aq)	-407.27	115.5	-393.133
NaOH(s)	-425.609	64.455	-379.484

NaOH(aq)	-470.114	48.1	-419.15
Na ₂ CO ₃ (s)	-1130.68	134.98	-1044.44
Sulfur			
S(s, rhombic)	0	31.8	0
S(g)	278.805	167.821	238.25
S ₂ Cl ₂ (g)	-18.4	331.5	-31.8
SF ₆ (g)	1209	291.82	-1105.3
H ₂ S(g)	-20.63	205.79	-33.56
SO ₂ (g)	-296.83	248.22	-300.194
SO ₃ (g)	-395.72	256.76	-371.06
SOCl ₂ (g)	-212.5	309.77	-198.3
H ₂ SO ₄ (liq)	-813.989	156.904	-690.003
H ₂ SO ₄ (aq)	-909.27	20.1	-744.53
Tin			
Sn(s, white)	0	51.55	0
Sn(s, gray)	-2.09	44.14	0.13
SnCl ₄ (liq)	-511.3	248.6	-440.1
SnCl ₄ (g)	-471.5	365.8	-432.2
SnO ₂ (s)	-580.7	52.3	-519.6
Titanium			
Ti(s)	0	30.63	0
TiCl ₄ (liq)	-804.2	252.34	-737.2
TiCl ₄ (g)	-763.2	354.9	-726.7
TiO ₂ (s)	-939.7	49.92	-884.5
Zinc			
Zn(s)	0	41.63	0
ZnCl ₂ (s)	-415.05	111.46	-369.398
ZnO(s)	-348.28	43.64	-318.3
ZnS(s, sphalerite)	-205.98	57.7	-201.29
Aqueous Ions and Molecules			
Ca ²⁺ (aq)	-542.96	-55.2	-553.04
CO ₃ ²⁻ (aq)	-676.26	-53.1	-528.1
CO ₂ (aq)	-413.8	117.6	-386.0
Cl ⁻ (aq)	-167.16	56.5	-131.26
H ⁺ (aq)	0		0
HCO ₂ ⁻ (aq)	-410	91.6	-335
HCO ₂ H(aq)	-410	164	-356
HCO ₃ ⁻ (aq)	-691.11	95	-587.06
H ₂ CO ₃ (aq)	-698.7	191	-623.42

$\text{NH}_3(\text{aq})$	-80.29	111	-26.6
$\text{OH}^-(\text{aq})$	-229.94	-10.54	-157.3
$\text{Ag}^+(\text{aq})$	105.58	72.68	77.124

This page titled [12.6: Appendix 2- Selected Thermodynamic Values](#) is shared under a [CC BY-SA 4.0](#) license and was authored, remixed, and/or curated by [Chemistry 310 \(Wikibook\)](#) via [source content](#) that was edited to the style and standards of the LibreTexts platform; a detailed edit history is available upon request.

12.7: Appendix 3- Bond Enthalpies

Average single bond enthalpies (kJ/mol)

H-H 436	C-H 413	N-H 391	O-H 483	F-F 155
H-F 567	C-C 348	N-N 163	O-O 146	
H-Cl 431	C-N 293	N-O 201	O-F 190	Cl-F 253
H-Br 366	C-O 358	N-F 272	O-Cl 203	Cl-Cl 242
H-I 299	C-F 485	N-Cl 200	O-I 234	
	C-Cl 328	N-Br 243		Br-F 237
	C-Br 276		S-H 339	Br-Cl 218
	C-I 240	P-H 322	S-F 327	Br-Br 193
	C-S 259	P-F 490	S-Cl 253	
			S-Br 218	I-Cl 208
	Si-H 323		S-S 266	I-Br 175
	Si-Si 226			I-I 151
	Si-C 301			
	Si-O 368			
	Si-F 565			
	Si-Cl 464			

Average double bond enthalpies (kJ/mol)

C=C 614	N=N 418	O=O 495
C=N 615	N=O 607	S=O 523
C=O 799		S=S 418

Average triple bond enthalpies (kJ/mol)

C≡C 839	C≡N 891	N≡N 941	C≡O 1072
---------	---------	---------	----------

This page titled [12.7: Appendix 3- Bond Enthalpies](#) is shared under a [CC BY-SA 4.0](#) license and was authored, remixed, and/or curated by [Chemistry 310 \(Wikibook\)](#) via [source content](#) that was edited to the style and standards of the LibreTexts platform; a detailed edit history is available upon request.

CHAPTER OVERVIEW

13: Metals and Alloys - Mechanical Properties

13.1: Prelude to Metals and Alloys - Mechanical Properties

Thumbnail: Microstructure of rolled and annealed brass (400× magnification). Public Domain via [Wikipedia](#)

This page titled [13: Metals and Alloys - Mechanical Properties](#) is shared under a [CC BY-SA 4.0](#) license and was authored, remixed, and/or curated by [Chemistry 310 \(Wikibook\)](#) via [source content](#) that was edited to the style and standards of the LibreTexts platform; a detailed edit history is available upon request.

13.1: Prelude to Metals and Alloys - Mechanical Properties

How much do the mechanical properties of metals and alloys vary with processing? The answer is, a great deal. Consider the following hypothetical situation: Upon graduation, you go to work as an engineer for Boeing. Your job is to work with aluminum companies to help them produce high strength alloys. Why? A large jet airplane weighs a total of 500 tons. Of that total, 50 tons is cargo, 150 tons is the plane structure, and the remainder is fuel. If you can triple the strength of the materials in the structure (aluminum), you can reduce the mass of the structure to 50 tons and increase the cargo to 150 tons. Look at what has been done already:

Material	Tensile strength yield (psi)
pure (99.45%) annealed Al	4×10^3
pure (99.45%) cold drawn Al	24×10^3
Al alloy - precipitated, hardened	50×10^3

By chemical and physical manipulation we have already increased the yield strength 12 times over annealed Al. Yet the yield strength of a "perfect" single crystal of pure Al is ca. 10^6 psi. We still have 3 orders of magnitude to go. This just shows that there will still be plenty to do on this project between now and graduation!

This page titled [13.1: Prelude to Metals and Alloys - Mechanical Properties](#) is shared under a [CC BY-SA 4.0](#) license and was authored, remixed, and/or curated by [Chemistry 310 \(Wikibook\)](#) via [source content](#) that was edited to the style and standards of the LibreTexts platform; a detailed edit history is available upon request.

Index

A

alkalides

[9.8: Alkalides and Electrides](#)

B

Berry pseudorotation

[5.12: Ligand Substitution Reactions](#)

birefringence

[8.3: Structures Related to NaCl and NiAs](#)

C

chelate effect

[5.10: Stability of Transition Metal Complexes](#)

coordinate covalent bonds

[5: Coordination Chemistry and Crystal Field Theory](#)

crystal field stabilization energy

[5.10: Stability of Transition Metal Complexes](#)

D

Diode

[10.7: Diodes, LEDs and Solar Cells](#)

[10.8: Amorphous Semiconductors](#)

[10.9: Discussion Questions](#)

[10.10: Problems](#)

[10.11: References](#)

E

electrides

[9.8: Alkalides and Electrides](#)

F

fluorite (structure)

[8.4: Tetrahedral Structures](#)

H

Hubbard model

[10.2: Metal-Insulator Transitions](#)

K

Kapustinskii equation

[9.5: Kapustinskii Equation](#)

L

ligand

[5: Coordination Chemistry and Crystal Field Theory](#)

P

plasmons

[11.6: Nanoscale Metal Particles](#)

Pourbaix diagrams

[4.6: Pourbaix Diagrams](#)

pyrite structure

[8.6: Bonding in TiS₂, MoS₂, and Pyrite Structures](#)

S

spectrochemical series

[5.4: Spectrochemical Series](#)

superconductor

[10.3: Superconductors](#)

Glossary

Sample Word 1 | Sample Definition 1

Detailed Licensing

Overview

Title: Book: Introduction to Inorganic Chemistry (Wikibook)

Webpages: 150

All licenses found:

- [CC BY-SA 4.0](#): 98% (147 pages)
- [Undeclared](#): 2% (3 pages)

By Page

- [Book: Introduction to Inorganic Chemistry \(Wikibook\) - CC BY-SA 4.0](#)
 - [Front Matter - CC BY-SA 4.0](#)
 - [TitlePage - CC BY-SA 4.0](#)
 - [InfoPage - CC BY-SA 4.0](#)
 - [Table of Contents - Undeclared](#)
 - [Licensing - Undeclared](#)
 - [1: Review of Chemical Bonding - CC BY-SA 4.0](#)
 - [1.1: Prelude to Chemical Bonding - CC BY-SA 4.0](#)
 - [1.2: Valence Bond Theory- Lewis Dot Structures, the Octet Rule, Formal Charge, Resonance, and the Isoelectronic Principle - CC BY-SA 4.0](#)
 - [1.3: The Shapes of Molecules \(VSEPR Theory\) and Orbital Hybridization - CC BY-SA 4.0](#)
 - [1.4: Bond Polarity and Bond Strength - CC BY-SA 4.0](#)
 - [1.5: Discussion Questions - CC BY-SA 4.0](#)
 - [1.6: Problems - CC BY-SA 4.0](#)
 - [1.7: References - CC BY-SA 4.0](#)
 - [2: Molecular Orbital Theory - CC BY-SA 4.0](#)
 - [2.1: Prelude to Molecular Orbital Theory - CC BY-SA 4.0](#)
 - [2.2: Constructing Molecular Orbitals from Atomic Orbitals - CC BY-SA 4.0](#)
 - [2.3: Orbital Symmetry - CC BY-SA 4.0](#)
 - [2.4: \$\sigma\$, \$\pi\$, and \$\delta\$ orbitals - CC BY-SA 4.0](#)
 - [2.5: Diatomic Molecules - CC BY-SA 4.0](#)
 - [2.6: Orbital Filling - CC BY-SA 4.0](#)
 - [2.7: Periodic Trends in \$\pi\$ Bonding - CC BY-SA 4.0](#)
 - [2.8: Three-center Bonding - CC BY-SA 4.0](#)
 - [2.9: Building up the MOs of More Complex Molecules- \$\text{NH}_3\$, \$\text{P}_4\$ - CC BY-SA 4.0](#)
 - [2.10: Homology of \$\sigma\$ and \$\pi\$ orbitals in MO diagrams - CC BY-SA 4.0](#)
 - [2.11: Chains and Rings of \$\pi\$ -Conjugated Systems - CC BY-SA 4.0](#)
 - [2.12: Discussion Questions - CC BY-SA 4.0](#)
 - [2.13: Problems - CC BY-SA 4.0](#)
 - [2.14: References - CC BY-SA 4.0](#)
 - [3: Acid-Base Chemistry - CC BY-SA 4.0](#)
 - [3.1: Prelude to Acid-Base Chemistry - CC BY-SA 4.0](#)
 - [3.2: Brønsted and Lewis Acids and Bases - CC BY-SA 4.0](#)
 - [3.3: Hard and Soft Acids and Bases - CC BY-SA 4.0](#)
 - [3.4: The Electrostatic-Covalent \(ECW\) Model for Acid-Base Reactions - CC BY-SA 4.0](#)
 - [3.5: Frustrated Lewis Pairs - CC BY-SA 4.0](#)
 - [3.6: Discussion Questions - CC BY-SA 4.0](#)
 - [3.7: Problems - CC BY-SA 4.0](#)
 - [3.8: References - CC BY-SA 4.0](#)
 - [4: Redox Stability and Redox Reactions - CC BY-SA 4.0](#)
 - [4.1: Prelude to Redox Stability and Redox Reactions - CC BY-SA 4.0](#)
 - [4.2: Balancing Redox Reactions - CC BY-SA 4.0](#)
 - [4.3: Electrochemical Potentials - CC BY-SA 4.0](#)
 - [4.4: Latimer and Frost Diagrams - CC BY-SA 4.0](#)
 - [4.5: Redox Reactions with Coupled Equilibria - CC BY-SA 4.0](#)
 - [4.6: Pourbaix Diagrams - CC BY-SA 4.0](#)
 - [4.7: Discussion Questions - CC BY-SA 4.0](#)
 - [4.8: Problems - CC BY-SA 4.0](#)
 - [4.9: References - CC BY-SA 4.0](#)
 - [5: Coordination Chemistry and Crystal Field Theory - CC BY-SA 4.0](#)
 - [5.1: Prelude to Coordination Chemistry and Crystal Field Theory - CC BY-SA 4.0](#)
 - [5.2: Counting Electrons in Transition Metal Complexes - CC BY-SA 4.0](#)
 - [5.3: Crystal Field Theory - CC BY-SA 4.0](#)
 - [5.4: Spectrochemical Series - CC BY-SA 4.0](#)
 - [5.5: \$\pi\$ -Bonding between Metals and Ligands - CC BY-SA 4.0](#)
 - [5.6: Crystal Field Stabilization Energy, Pairing, and Hund's Rule - CC BY-SA 4.0](#)
 - [5.7: Non-octahedral Complexes - CC BY-SA 4.0](#)
 - [5.8: Jahn-Teller Effect - CC BY-SA 4.0](#)
 - [5.9: Tetrahedral Complexes - CC BY-SA 4.0](#)

- 5.10: Stability of Transition Metal Complexes - *CC BY-SA 4.0*
- 5.11: Chelate and Macrocyclic Effects - *CC BY-SA 4.0*
- 5.12: Ligand Substitution Reactions - *CC BY-SA 4.0*
- 5.13: Discussion Questions - *CC BY-SA 4.0*
- 5.14: Problems - *CC BY-SA 4.0*
- 5.15: References - *CC BY-SA 4.0*
- 6: Metals and Alloys- Structure, Bonding, Electronic and Magnetic Properties - *CC BY-SA 4.0*
 - 6.1: Prelude to Metals and Alloys - *CC BY-SA 4.0*
 - 6.2: Unit Cells and Crystal Structures - *CC BY-SA 4.0*
 - 6.3: Bravais Lattices - *CC BY-SA 4.0*
 - 6.4: Crystal Structures of Metals - *CC BY-SA 4.0*
 - 6.5: Bonding in Metals - *CC BY-SA 4.0*
 - 6.6: Conduction in Metals - *CC BY-SA 4.0*
 - 6.7: Atomic Orbitals and Magnetism - *CC BY-SA 4.0*
 - 6.8: Ferro-, Ferri- and Antiferromagnetism - *CC BY-SA 4.0*
 - 6.9: Hard and Soft Magnets - *CC BY-SA 4.0*
 - 6.10: Discussion Questions - *CC BY-SA 4.0*
 - 6.11: Problems - *CC BY-SA 4.0*
 - 6.12: References - *CC BY-SA 4.0*
- 7: Metals and Alloys - Mechanical Properties - *CC BY-SA 4.0*
 - 7.1: Defects in Metallic Crystals - *CC BY-SA 4.0*
 - 7.2: Work Hardening, Alloying, and Annealing - *CC BY-SA 4.0*
 - 7.3: Malleability of Metals and Alloys - *CC BY-SA 4.0*
 - 7.4: Iron and Steel - *CC BY-SA 4.0*
 - 7.5: Amorphous Alloys - *CC BY-SA 4.0*
 - 7.6: Discussion Questions - *CC BY-SA 4.0*
 - 7.7: Problems - *CC BY-SA 4.0*
 - 7.8: References - *CC BY-SA 4.0*
- 8: Ionic and Covalent Solids - Structures - *CC BY-SA 4.0*
 - 8.1: Prelude to Ionic and Covalent Solids - Structures - *CC BY-SA 4.0*
 - 8.2: Close-packing and Interstitial Sites - *CC BY-SA 4.0*
 - 8.3: Structures Related to NaCl and NiAs - *CC BY-SA 4.0*
 - 8.4: Tetrahedral Structures - *CC BY-SA 4.0*
 - 8.5: Layered Structures and Intercalation Reactions - *CC BY-SA 4.0*
 - 8.6: Bonding in TiS_2 , MoS_2 , and Pyrite Structures - *CC BY-SA 4.0*
 - 8.7: Spinel, Perovskite, and Rutile Structures - *CC BY-SA 4.0*
 - 8.8: Discussion Questions - *CC BY-SA 4.0*
 - 8.9: Problems - *CC BY-SA 4.0*
- 8.10: References - *CC BY-SA 4.0*
- 9: Ionic and Covalent Solids - Energetics - *CC BY-SA 4.0*
 - 9.1: Ionic Radii and Radius Ratios - *CC BY-SA 4.0*
 - 9.2: Structure Maps - *CC BY-SA 4.0*
 - 9.3: Energetics of Crystalline Solids- The Ionic Model - *CC BY-SA 4.0*
 - 9.4: Born-Haber Cycles for NaCl and Silver Halides - *CC BY-SA 4.0*
 - 9.5: Kapustinskii Equation - *CC BY-SA 4.0*
 - 9.6: Discovery of Noble Gas Compounds - *CC BY-SA 4.0*
 - 9.7: Stabilization of High and Low Oxidation States - *CC BY-SA 4.0*
 - 9.8: Alkalides and Electrides - *CC BY-SA 4.0*
 - 9.9: Resonance Energy of Metals - *CC BY-SA 4.0*
 - 9.10: Prelude to Ionic and Covalent Solids - Energetics - *CC BY-SA 4.0*
 - 9.11: The Strange Case of the Alkali Oxides - *CC BY-SA 4.0*
 - 9.12: Lattice Energies and Solubility - *CC BY-SA 4.0*
 - 9.13: Discussion Questions - *CC BY-SA 4.0*
 - 9.14: Problems - *CC BY-SA 4.0*
 - 9.15: References - *CC BY-SA 4.0*
- 10: Electronic Properties of Materials - Superconductors and Semiconductors - *CC BY-SA 4.0*
 - 10.1: Prelude to Electronic Properties of Materials - Superconductors and Semiconductors - *CC BY-SA 4.0*
 - 10.2: Metal-Insulator Transitions - *CC BY-SA 4.0*
 - 10.3: Superconductors - *CC BY-SA 4.0*
 - 10.4: Periodic Trends- Metals, Semiconductors, and Insulators - *CC BY-SA 4.0*
 - 10.5: Semiconductors- Band Gaps, Colors, Conductivity and Doping - *CC BY-SA 4.0*
 - 10.6: Semiconductor p-n Junctions - *CC BY-SA 4.0*
 - 10.7: Diodes, LEDs and Solar Cells - *CC BY-SA 4.0*
 - 10.8: Amorphous Semiconductors - *CC BY-SA 4.0*
 - 10.9: Discussion Questions - *CC BY-SA 4.0*
 - 10.10: Problems - *CC BY-SA 4.0*
 - 10.11: References - *CC BY-SA 4.0*
- 11: Basic Science of Nanomaterials - *CC BY-SA 4.0*
 - 11.1: Prelude to Basic Science of Nanomaterials - *CC BY-SA 4.0*
 - 11.2: Physics and Length Scales- Cavity Laser, Coulomb Blockade, Nanoscale Magnets - *CC BY-SA 4.0*
 - 11.3: Semiconductor Quantum Dots - *CC BY-SA 4.0*
 - 11.4: Synthesis of Semiconductor Nanocrystals - *CC BY-SA 4.0*
 - 11.5: Surface Energy - *CC BY-SA 4.0*
 - 11.6: Nanoscale Metal Particles - *CC BY-SA 4.0*
 - 11.7: Applications of Nanomaterials - *CC BY-SA 4.0*

- 11.8: Discussion Questions - *CC BY-SA 4.0*
- 11.9: Problems - *CC BY-SA 4.0*
- 11.10: References - *CC BY-SA 4.0*
- 12: Resources for Students and Teachers - *CC BY-SA 4.0*
 - 12.1: VIPEr- Virtual Inorganic Pedagogical Electronic Resource- A Community for Teachers and Students of Inorganic Chemistry - *CC BY-SA 4.0*
 - 12.2: Beloit College/University of Wisconsin Video Lab Manual - *CC BY-SA 4.0*
 - 12.3: Atomic and Molecular Orbitals (University of Liverpool) - *CC BY-SA 4.0*
 - 12.4: Interactive 3D Crystal Structures (University of Liverpool) - *CC BY-SA 4.0*
- 12.5: Appendix 1- Periodic Tables - *CC BY-SA 4.0*
- 12.6: Appendix 2- Selected Thermodynamic Values - *CC BY-SA 4.0*
- 12.7: Appendix 3- Bond Enthalpies - *CC BY-SA 4.0*
- 13: Metals and Alloys - Mechanical Properties - *CC BY-SA 4.0*
 - 13.1: Prelude to Metals and Alloys - Mechanical Properties - *CC BY-SA 4.0*
- Back Matter - *CC BY-SA 4.0*
 - Index - *CC BY-SA 4.0*
 - Glossary - *CC BY-SA 4.0*
 - Detailed Licensing - *Undeclared*